Parallel cerebello-cerebral pathways and their involvement in implicit learning

Romain William Sala

Sorbonne Université

Ecole doctorale Cerveau Cognition Comportement (ED3C)

IBENS / Neurophysiology of Brain Circuits

Parallel cerebello-cerebral pathways and their involvement in implicit learning

Par Romain William Sala

Thèse de doctorat en Neurosciences

Dirigée par Daniela Popa et Clément Léna

Présentée et soutenue publiquement le : 11 décembre 2023

Président:

Dr FAURE Philippe	DRCE, Université Paris Sciences et Lettres (PSL)

Rapporteurs:

Pr SILLITOE Roy	Professeur, Baylor College of Medicine (Texas)
Dr EGO-STENGEL Valérie	DR, Université de Neurosciences Paris-Saclay

Examinateurs:

Dr ISOPE Philippe	DR, Université de Strasbourg
Dr GALLEA Cécile	CR, Sorbonne Université
Dr WOLFF Mathieu	DR, Université de Bordeaux

Membre invité:

Dr HERVE Denis	DR, Sorbonne Université

Acknowledgements

First of all I would like to dedicate this PhD thesis to my parents, especially to my late father, who passed away few years ago. It is safe to say that I wouldn't have been able to face the challenge of a PhD without their love, appreciation and unconditional support. Thank you to both of you, I love you very much.

Now that the emotionally loaded paragraph is out of the way, we can go to much lighter acknowledgements.

I would like to thank Clément and Daniela, my PhD supervisors, who supported me and manage to tolerate me during the past years. Thank you for believing in me and giving me the freedom of mind to explore different projects and several questions. You made this PhD a really enjoyable experience for me. I am truly happy about the relationship that we built over these years, at it is deeper than a work relationship. I will never forget our project meetings with my never-ending Jupyter notebooks, without any legend or labels, which would have driven crazy any other supervisor, but not you! You have been there for me in the most difficult moments of my life, and I am honoured to have you as my PhD supervisors.

When I joined the team, I had the chance to be welcomed by the smartest and craziest people around. Thank you to Andres, who transformed me, going from a Master 2 intern to a fully fledged PhD student. I would like to take the time to thank Ioana for the years that we spent together, as they profoundly changed me and gave me incredibly fond memories. And in addition, we were pretty good collaborators! Thank you to Jimena, Berenice, Aurélie, Thibault, Idriss, Nolwenn, Sami for the good moments that we had together! Special mention to Hind, with which I collaborated on God knows how many projects, to the extent that PubMed might start considering that we are the same author.

Who could forget the babies that I had the chance to see grow up, Julie (from which I am still not able to write the last name without doing a typo) and Stefano (aka "doing a pub crawling wasn't a good idea").

Speaking of babies, big shout-out to my two incredible Master 1 interns, Alexandre and Pauline. I am extremely happy to see that both of you decided to carry on with a PhD, I can't wait to see the beautiful things that you will come up with! I have a kind thought for the next generation of the lab. Ines, Marie, Margarida, Marion, Maria, Sarah, Maud, Roman, Ahsan. Special thanks to Daisy, who subtly

and consistently reinforced my decision to go do a postdoc in Champalimaud. Muito obrigado Margarida. Big thanks to Guillaume, which was always up to give me good guidance and have a beer together (except when his family duties were calling). To all the members of the team, both past and present, I will dearly miss how our time was bi-modally distributed between mind-churning discussions about data and setups, and having the most absurd and outrageous laughs one could imagine. You guys are truly amazing and I am happy I had the occasion to be in the lab with you (although I wished we had more time together). Keep up the good work!

In the IBENS I had the chance to create beautiful relationships with people outside of the team. This includes the Barbour team, which consistently provided insane people that were a pleasure to hang out with, namely Victor (professional over-thinker), Alan (the man who dragged me into being a vice-president), Flavien (aka "the butt-scratcher"), Aurélien (the spike-sorting master) and of course Boris himself (whose lectures made me scratch my head a couple of times). This also includes the team of Cécile Charrier, in which I was able to sequentially meet Nora (the best president an association can dream about), Joseph (that I interestingly met in the L2), Eirini (a tiny greek girl who changed forever my perspective on how greek letters are meant to be pronounced), Marine (THE vice-president) and Doris (or maybe Dori, I am never sure). Big thanks to two people who are very dear to me, Marie and Caroline (who are so inseparable that it is tough to acknowledge them separately). Both of them were always there to guide me from the start of my Master 2 to the end of my PhD.

A huge shout-out to SPIBENS (for those who don't know, the association of Students and Postdocs of the IBENS), which I had the chance to be a part of since the start of my PhD. Special mention to Nicolas, my crazy party-buddy who acquired the status of "bébou", and to Margaux and Michella who had the braveness to constantly push the association further!

Now it is time to go out of the IBENS! Starting with the unforgettable, the one, the only, Youcef! Along with Mangala, Sami and Ameur, truly supported my PhD form across the street, and that I am happy to consider my friends. Let's not forget the Youcef's drinking buddy that I had met these years, with Nadia, Arnaud, Lucia, Jerome, Thomas, Tom, but of course the recent Andres, Vasco, Cathal and Mikaelis!

Although not everyone cares about the cerebellum, the people who do happen to be amazing (coincidence? I don't think not). I would like to thank Cécile, Beetsi

and Vinh with who I co-organized the Cerebellum Days in 2023, but also the rest of the France Cerebellum Club and the rest of the french cerebellum community with Philippe, Fekrije, David (yes I still consider you as french), Michael, Alex,...I had the chance to meet incredible students from this community, including Maxime, Ludo (my God man, the drinks that we had), Fede, Theo, but also Capucine, Leonardo, Melika... Of course the cerebellum is not a french-limited research thematics. Thank you to Roy, Megan, Javier, Michael,... Can't wait to see all of you in the next cerebello-centric conference!

As we are going further and further away from my research topic, I have to mention the ICM crew, as I met some of my best friends in this Institute. I will have to thank Nunzio and Marcel (the people who welcomed me in the lab and turned me into a man), Taddy (r-square = 1), Javier ("you send the manuscript, I start cooking"), Filipa (our favourite introvert), Joana, Giulia, Lucie, Marie, Florian, Emmanuelle, Lucien, Sofia, Cibele, Yann,... Also, I have to give a special thank you to Nelson for being my first mentor in science, I am truly honoured to have been one of your students, and that we remained close during these years.

I would like to thank the people that I stayed close during all these years. Guillaume ("Drap-Sala Industires, on le fait"), Louis ("I know Romain since kindergarten"), Kévin ("je suis un grand malade"), Laurie (aka "Totote"), their little "chocbar"-faced Mathis, Maelle, Lucas, Mathilde, Valentin, Yin ka,... Of course I have to mention, La BaZz! The people I unlikely met through Guillaume and with which I shared amazing moments, with the titular Zizou, Simon, David, Lenny, Antoine, Thomas, NajNaj, Sheppard (I am trying very hard to not say Yohann). You guys are amazing, I hope that we will stay friends for the longest time possible!

I especially thank my family, in particular with my parents but also my brother Mathieu, his wife Frédérique and their children Maël, Mattéo and Iliana, but also my uncle Frédéric, my aunt Corinne, my cousins Adrien, Alexandre and Sébastien and my cousins Michel and Stéphanie.

Ultimately, I would like to thank the members of the jury for accepting the heavy task of reviewing my work and sitting through a lengthy presentation on cerebello-forebrain coupling! In particular to Roy and Valérie who accepted to be my referees, but also to Philippe, Philipe, Cécile, Mathieu, and Denis (which always had been a close collaborator).

Contents

Table of Acronyms

ALM Antero Lateral Motor cortex

ALS Amyotrophic Lateral Sclerosis

BLA Basolateral Amygdala

CeA Central Amygdala

CF Climbing Fiber

CL Centrolateral thalamus

CN Cerebellar Nuclei

CNO Clozapine N Oxide

CS Complex spike (in the first section of the introduction)

CS Conditioned stimulus

cTBS continous Theta Burtst Stimualtion

dlPAG dorso-lateral Periaqueductal Gray

DLS Dorso-Lateral Striatum

dmPFC dorso-medial Prefrontal Cortex

DMS Dorso-Medial Striatum

DN Dentate Nucleus

EPSC Excitatory Post Synaptic Current

EZ Excitatory zone of the motor thalamus

FN Fastigial Nucleus

GPe external Globus Pallidus

GPi internal Globus Pallidus

HFS High Ferquency Stimulation

IL Infra-Limbic cortex

IN Interposed Nucleus

iTBS intermittent Theta Burtst Stimualtion

IPSC Inhibitory Post Synaptic Current

IZ Inhibitory zone of the motor thalamus

LFP Local Field Potential

LFS Low Ferquency Stimulation

LTD Long Term Depression

LTP Long Term Potentiation

M1 Primary Motor Cortex

MD Medio-Dorsal Thalamus

MEP Movement evoked Potential

MF Mossy Fiber

MLI Molecular Layer Interneurons

MSN Medium Spiny Neurons

NREM Non-Rapid Eye Movement sleep

PAG Periaqueductal Gray

PC Purkinje Cell

PF Parallel Fiber (in the first section of the introduction)

PF Prafascicular thalamus

PFC Pre-Frontal Cortex

PL Pre-Limbic cortex

PMA Pre-Motor Area

REM Rapid Eye Movement sleep

rTMS repetitive Transcranial Magnetic Stimualtion

SAL Saline

SCA Spino Cerebellar Ataxia

SMA Supplementary Motor Area

SNc Substantia Nigra pars compacta

SNr Substantia Nigra pars reticulata

STN Sub-Thalamic Nucleus

TBS Theta Burtst Stimualtion

TMS Transcranial Magnetic Stimualtion

UBC Unipolar Brush Cells

US Unconditioned stimulus

VAL Ventro-Lateral (motor) thalamus

vlPAG ventro-lateral Periaqueductal Gray

vmPFC ventro-medial Prefrontal Cortex

WT Wild Type

Abstract

The cerebellum is mostly known to be a key structure in the regulation of movements. However, its high degree of inter-connectivity with various cortical and subcortical structures brings the question of its involvement in regulating other brain functions, such as cognitive processes. In particular, the tight links between the cerebellum, the motor circuits and the limbic circuits suggest a contribution of the cerebellum to both motor learning and emotional learning. Using anatomical tracing, extracellular electrophysiology and behavior, the aim of this thesis is to unravel the involvement of the cerebellum in the extinction of fear memory through the control of thalamo-cortical synchrony of fear-related oscillations. Then, this thesis will investigate the differential contributions of cerebello-cortical and cerebello-striatal networks to the acquisition and the consolidation of a complex motor skill. Ultimately, it will focus on the integrity of cerebello-thalamic networks and the functionality of cerebello-thalamic plasticity in a mouse model of DYT25, a genetic form of dystonia.

"Everything in nature is a cause from which there flows some effect".

Baruch Spinoza

1 Introduction

1.1 Cerebellar networks and function

1.1.1 Anatomical description

The cerebellum is a brain structure part of the rhombencephalon and located at the posterior part of the encephalon, inside the posterior cranial fossa. Although the encephalon displays wide inter-species variability, the gross anatomy of the cerebellum is relatively well preserved among mammals. Although this thesis will focus on the murine cerebellum, most of the principles described here should be shared by mammalian cerebelli.

Due to its location in the posterior cranial fossa, the cerebellum is encased by the occipital bone, and is surrounded by different anatomical structures. In particular, the superior part of the cerebellum is delimited by the tentorium cerebelli, a layer of dura matter hosting the straight sinus at its midline. The cerebellum has several anterior relationships, including the brainstem at the level of the pons, the medullary vela covering the fourth ventricule, but also the foramen of Magendie and the medulla oblongata.

In terms of structural organization, the cerebellum is composed of deep cerebellar nuclei, being the main output of the cerebellum towards other regions of the

central nervous system, around which a formation of folded three-layer laminar gray matter named the cerebellar cortex is distributed. The cerebellar cortex is formed by two hemispheres, connected on their medial parts to the cerebellar vermis. Thus, the cortex displays a medio-lateral organization, with the vermis at the midline, continued by an intermediate zone of the hemisphere, and lateral hemispheres at its extremities.

The cerebellar cortex is partitioned in three anatomical lobes along the antero-posterior axis, separated by horizontal grooves called fissures. The most superior lobe of the cerebellum is called the anterior lobe, and is separated from the posterior lobe of the cerebellum by the primary fissure. The remaining lobe of the cerebellum is called the flocculonodular lobe and is anterior to the posterolateral fissure, separating it from the posterior lobe. Deep cerbellar nuclei come into four pairs, with a medio-lateral distribution. From the most medial to the most lateral, they are composed of the fastigial nuclei (or medial nuclei), the globose nuclei, the emboliform nuclei and the dentate nuclei (or lateral nuclei). Although separated by fiber bundles (Voogd, and Ruigrok 2012), the globose and emboliform nuclei are not distinguishable in the cerebellum of some mammals (including humans and rodents) and are fused in a single nucleus named the interpositus nucleus (or intermediate), with its anterior and posterior parts respectively corresponding to the emboliform and globose nuclei (Moini et al. 2020). The cerebellar cortex also sends substantial projections to the vestibular and parabrachial nuclei, which are not counted as part of the cerebellum but share functional similarities with the cerebellar nuclei.

The cerebellum is anchored to the brainstem by three processes called peduncles, segregating the different input and output pathways of the cerebellum. The superior cerebellar peduncles host the main output pathways to the mesencephalon, hosting the cerebello-thalamic pathways allowing for information transfer between the cerebellum and the forebrain. Also, the superior peduncles provide a pathway for afferences from the ventral spinocerebellar tract carrying proprioceptive information, the trigeminal nucleus and the locus coeruleus. The middle cerebellar peduncles host afferences from the pons, representing the main inputs of the cerebellum. Ultimately, the inferior cerebellar peduncles connects to the spinal cord and the medulla oblongata. It contains two different pathways, the restiform body carrying afferences from the dorsal spinocerebellar, the olivocerebellar and the cuneocerebellar tracts, and the juxtarestiform body that carries both vestibulocerebellar and cerebellovestibular tracts.

1.1.2 Functions

Historically, the function of the cerebellum was first described through the characterization of syndromes associated to cerebellar lesions. Indeed, patients suffering from lesions of the cerebellum tended to consistently display a range of symptoms which taken altogether constitute the cerebellar syndrome. This syndrome includes:

- **Ataxia**, which is a deficit in coordination in voluntary movements
- **Dysmetria**, or the inability to finely tune the timing of a movement
- **Dysarthria**, a speech disorder leading to an altered articulation
- **Nystagmus**, an abnormal rhythmic eye movement
- **Intention tremor**, an involuntary oscillatory and high-amplitude movement during voluntary movements
- **Hypotonia**, which is a deficit in coordination of a voluntary movement
- **Paralysis** (although less frequent)

The ensemble of symptoms reported in this syndrome highlights the importance of the cerebellum in motor control, as lesions of the cerebellum induce a strong deficit in motor coordination and movement timing. However, more recent studies have revealed the possibility that the cerebellum could be involved in non-motor functions. Indeed, clinical studies have revealed that patients suffering from cerebellar degeneration or stroke would display cognitive dysfunctions, including learning deficits, difficulties with paired-associations and generalized intellectual slowing (Kish et al. 1988; Bracke-Tolkmitt et al. 1989), but also impaired executive functions (Grafman et al. 1992) and visual spatial deficits (Wallesch et al. 1990). In addition, linguistic deficits were also observed in patient in cerebellar patients, ranging from agrammatism (Silveri et al. 1994) to mutism (Kingma et al. 1994) with a possible association to regressive personality changes and emotional lability (Pollack et al. 1995). These prior observations lead Schamhmann and Sherman to describe a set of non-motor symptoms associated to cerebellar lesions, defined as the "cerebellar cognitive affective syndrome" (Schmahmann et al. 1998). The association of deficits observed in this syndrome suggests a role of the cerebellum in modulating higher brain functions through its connections with the forebrain, particularly with the prefrontal cortex.

These clinical observations were later supported by many animal studies, further cementing the contribution of the cerebellum to non-motor functions (Strick et al.

2009), such as spatial navigation (Rochefort et al. 2013) and reward prediction (Wagner et al. 2017; Kostadinov et al. 2019).

1.1.3 Cerebellar circuits

During my PhD, I studied mostly the deep cerebellar nuclei and their interactions with the forebrain. In this chapter, I will first briefly describe the structure and cellular types of the cerebellar cortex, and then present more in details the cerebellar nuclei.

1.1.3.1 Cerebellar cortex

As described earlier, the cerebellum is composed of deep cerebellar nuclei, surrounded by an extensively folded cerebellar cortex. This cerebellar cortex has a very stereotypical laminar structure, including three layers: the granular layer (deepest), the Purkinje cell layer (intermediate) and the molecular layer (the most superficial) (Braitenberg et al. 1958). Each of the previously mentioned layer hosting specific types of neurons. This laminar structure of the cerebellar cortex follows a modular compartmentalization, with parallel modules organized in the sagittal axis (Voogd 1967). Each of these module can be subdivided in micro-zones, defining the functional processing unit of the cerebellar cortex (Apps, Hawkes, et al. 2018).

Granule cells

The granular layer hosts the most prevalent neuronal type of the cerebellar cortex (and of the brain), the granule cells. Granule cells represent more than 90% of the neurons in the cerebellum. They are glutamatergic neurons with a particularly small soma (< 5 μm in diameter) surrounded by few 'club-like' dendrites (4 on average), and a long and thin ascending axon projecting towards the molecular layer of the cerebellar cortex (Ramo et al. 1911; Palay et al. 1974).

The dendrites of granule cells receive glutamatergic excitatory inputs from the mossy fibers, but also receive inhibitory inputs from Golgi cells (Eccles 1967). In addition, granule cells dendrites receive excitatory inputs from glutamatergic interneurons of the granular layer called unipolar brush cells (Mugnaini, Di˜o, et al. 1997; Mugnaini, Sekerková, et al. 2011), as well as excitatory inputs coming from glutamatergic neurons of the deep cerebellar nuclei through collaterals (Houck et al. 2015). However, the synaptic inputs of the granule cells have a peculiar structure. Indeed, a single mossy fiber axon will terminate in multiple contacts surrounded by a glial sheet, forming a "cerebellar glomerulus" (Palay et al. 1974). Dendrites from

many granule cells (up to 50 different dendrites) will be encased in a single glomerulus, along with inputs from Golgi cells, unipolar brush cells and deep cerebellar nuclei projections.

The ascending axon stemming from granule cells projects in the direction of the molecular layer, is unmyelinated (Palay et al. 1974), and bifurcates in the molecular layer to form a "parallel fiber". Indeed, this axons splits in the molecular layer in a 'T-shape' manner, forming two branches perpendicular to the ascending axon and running parallel with the branches from the other granule cells . These parallel fibers will notably form varicosities to make synaptic contacts on dendritic spines of many different Purkinje cells. Because parallel fibers are oriented orthogonally to the sagittal micro-zones of the cerebellar cortex, a single fiber will contact Purkinje cells from different zones, allowing for communication between different modules (Valera et al. 2016; Spaeth, Bahuguna, et al. 2022). Reciprocally, a single Purkinje cell will be contacted by many different parallel fibers, with a wide variability in terms of synaptic weights (Isope et al. 2002). This strong divergence of mossy fibers signals to many granule cells then to many Purkinje cells and the convergence of many parallel fibers to a single Purkinje cells reflect the computational richness of the cerebellar cortex, and contributes to the emergence of broad connectivity maps between granule cells and Purkinje cells (Valera et al. 2016; Spaeth, Bahuguna, et al. 2022), which were hypothesized to contribute to the implementation of internal models within the cerebellum (Spaeth, and Isope 2023).

Purkinje cells

The Purkinje cells layer is populated by an eponym GABAergic projection neuron, the Purkinje cell. Purkinje cells are compolocal sed of a large pear-shaped soma (around 25µm in diameter) laying in the Purkinje cell layer, a massive dendritic arbor protruding towards the molecular layer, and a thin axon projecting towards the deep cerebellar nuclei (Golgi 1874; Ramo et al. 1911), also emitting collaterals to other Purkinje cells and local interneurons (Witter et al. 2016).

The dendritic arbors of the Purkinje cells are disposed in a parallel fashion in the sagittal plane, and are not overlapping between cells. The tree has a complex morphology, with proximal dendrites stemming out of the cell's soma, being the site where synaptic inputs from the climbing fibers are distributed; and distal dendrites receiving inputs from the parallel fibers. Strikingly, the morphology of their dendritic arbor has been shown to be more complex in humans compared to rodents.

Indeed, while the majority of human Purkinje cells display multiple branches in their dendritic arbor, this phenomenon is much more rare in mice (Busch et al. 2023). This wide distribution of dendritic arbor allows for the integration of a staggering amount of inputs from the parallel fibers, with more than 175 000 different synapses for a single Purkinje cell (Napper et al. 1988), most of them being electrically silent (Isope et al. 2002; Ho et al. 2021).

When isolated, Purkinje cells exhibit a tonic spiking pattern at ~50Hz in a pacemaker fashion (Häusser et al. 1997; Nam et al. 1997; Raman, and Bean 1997). They receive two main excitatory inputs: parallel fibers from granule cells and the climbing fibers coming from olivary neurons, each of these two having different effect on the spiking pattern of the Purkinje cell. Indeed, an impluse from the parallel fibers releases glutamate in the synaptic cleft, leading to a small depolarizing synaptic potential, which is generally too weak to induce an action potential from the Purkinje cell. However, if these depolarizing synaptic potentials are spatially and temporally summed at the level of the proximal axon, the Purkinje cell will emit an action potential in the form of a simple spike (SS) (Palmer et al. 2010). In contrary to the parallel fibers, a single impulse of activity coming from the climbing fiber releases a tremendous amount of glutamate along the dendritic arbor of the Purkinje cell, causing a burst-like activity of the Purkinje cell called a complex spike (CS). Interestingly, a strong enough stimulation of parallel fibers could induce complex spike activity in Purkinje cell, suggesting that the mechanism underlying the generation of complex spikes is directly dependent on the magnitude of the excitation bestowed upon the Purkinje cell.

In vivo studies on anesthetized animals revealed that Purkinje cells activity is composed of a tonic discharge of simple spikes at frequencies ranging between 50Hz and 120Hz, and a much less frequent discharge of complex spikes at 1Hz (Latham et al. 1971). Complex spikes may exert an antagonistic effect on simple spikes discharge, as in some regions of the cerebellum, a complex spike will be followed by a pause in simple spike discharge, lasting for roughly 100ms (Latham et al. 1971).

Interneurons

The cerebellar cortex is composed of a plethora of types of interneurons, which are inhibitory for the most part or excitatory. Depending on their types, these interneurons can be located in the molecular layer, in the Purkinje cell layer or in the granular layer of the cerebellar cortex.

The molecular layer of the cerebellar cortex is populated by two classes of morphologically distinct inhibitory interneurons, the stellate cells and the basket cells, usually considered as belonging to the same category of interneurons, named "molecular layer interneurons", or MLI.

Stellate cells are small GABAergic interneurons located in the upper two thirds of the molecular layer. They receive excitatory inputs directly from both parallel fibers and climbing fibers, and exert an inhibitory effect over local Purkinje cells at the level of their dendrites. Basket cells are small GABAergic interneurons located in the basal third of the molecular layer, which exert an inhibitory effect of Purkinje cells by sending an axon terminating directy on the soma and axon (initial segment) of the Purkinje cells(Somogyi et al. 1976; Iwakura et al. 2012).

This particular network configuration empowers molecular layer interneurons to perform feed-forward inhibition on the Purkinje cells (Mittmann et al. 2005). Because this inhibition is delayed in time compared to the initial excitatory signal of the parallel fibers (by approximately 1ms), it restricts the excitation window of the Purkinje cells, thus allowing to increase the temporal contrast of the signal carried by the parallel fibers and contributes to shaping the output of the Purkinje cells (Mittmann et al. 2005; Blot et al. 2016).

Although basket cells and stellate cells were originally considered as two completely different neuronal classes, recent evidence suggest that they represent a neuronal continuum (Zhang, and Goldman 1996; Sultan et al. 1998; Schilling et al. 2008). In addition, a recent theory proposes the molecular layer interneurons to be divided in two different categories based on their physiological properties: MLI1 and MLI2 (Kozareva et al. 2020).

The granular layer of the cerebellar cortex hosts several types of interneurons, including inhibitory and excitatory neurons. Golgi cell are the main inhibitory interneurons of the granular layer (Eccles et al. 1964), and the sole inhibitory output provided directly to the granule cells through their terminals located in the cerebellar glomeruli. They receive excitatory inputs directly from mossy fibers (Palay et al. 1974; Cesana et al. 2013), but also from the ascending axon of the granule cells (Cesana et al. 2013) and finally by terminals in the molecular layers between the apical dendrite of the Golgi cell and the parallel fibers (Cesana et al. 2013). This triple source of excitation allows the Golgi cells to perform feedback inhibition on the granule cells. They also receive an inhibitory input from nearby Lugaro cells.

Lugaro cells are inhibitory interneurons of the top of the granular layer, just below the Purkinje cell layer (Lugaro 1894). They are both GABAergic and glycin-

ergic, and typically inhibit nearby Golgi cells (Dieudonné et al. 2000; Dumoulin et al. 2001), as well as molecular layer interneurons (Lainé et al. 1998) through their ascending axon projected towards the molecular layer (Palay et al. 1974; Lainé et al. 1996). Given that a single Lugaro cell can inhibit up to 150 Golgi cells (Dieudonné et al. 2000; Dumoulin et al. 2001), it has been hypothesized that Lugaro cells contribute to synchronize the local population of Golgi cells.

An excitatory type of interneuron can be found in the granular layer, called unipolar brush cells (UBCs). They have been extensively characterized in the vestibulo-cerebellum (UBCs type I and type II), but can also be observed in non-vestibular areas of the cerebellum (UBCs type II only) (Sekerková et al. 2013). UBCs receive strong excitatory inputs from a single extra-cerebellar mossy fiber (also called extrinsic) or from a vestibular afference, and will in turn create excitatory synapses with local granule cells as well as other UBCs (Mugnaini, Sekerková, et al. 2011). These UBCs to granule cells and UBCs to UBCs projections are called "intrisinc mossy fibers", and contribute to the feed-forward amplification of the extra-cerebellar signal provided to the cerebellar granule cells (Mugnaini, Sekerková, et al. 2011).

The Purkinje cell layer hosts one type of inhibitory interneurons, the candelabrum cells. They form a class of GABAergic interneurons, located near the soma of Purkinje cells. Candelabrum cells receive excitatory inputs from mossy fibers, granule cells and climbing fibers (Osorno et al. 2022). They are inhibited by Purkinje cells and molecular layer interneurons (Osorno et al. 2022). Candelabrum cells project an ascending axon to the molecular layer, where they inhibit molecular layer interneurons, potentially disinhibitting Purkinje cells (Osorno et al. 2022).

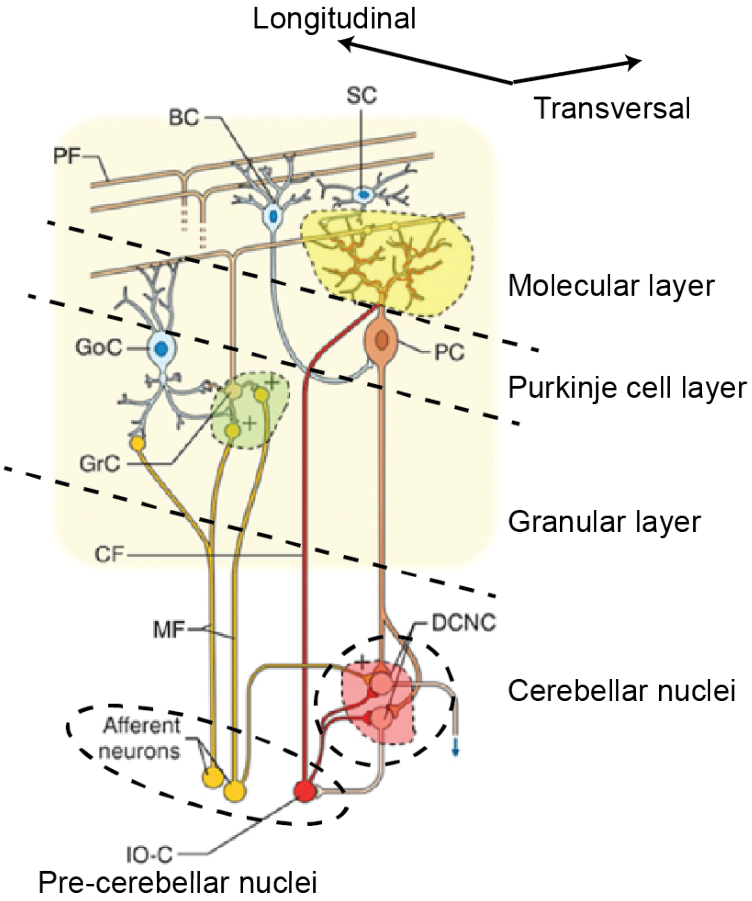

Figure 1.1: Neuronal circuits of the cerebellum. Simplified schematic of the cerebellar cortex, its afferenced and efference to the cerebellar nuclei. This circuit includes mossy fiber (MF), parallel fiber (PF), climbing fiber (CF), granule cell (GrC), Golgi cell (GoC), Purkinje cell (PC), stellate cell/basket cell (SC/BC), deep cerebellar nuclei cell (DCNC), and inferior olive cell (IO-C). The cerebellar cortex is indicated by a color graded area, and its different layers are delimited by straight dashed lines. Adapted from D'Angelo 2014

1.1.3.2 Cerebellar nuclei

The deep cerebellar nuclei are the sole output of the cerebellum, with the exception of the Purkinje cells of the vestibulo-cerebellum directly inhibiting the vestibular nuclei (Novello et al. 2022), and the medial parabrachial nucleus being inhibited by vermal Purkinje cells (Hashimoto, Yamanaka, et al. 2018).

Structure

The cerebellar nuclei seem to be arranged to maintain parallel olivo-cortico-nuclear loops, corresponding to the different zones of the cerbellar cortex (Apps,

Hawkes, et al. 2018). Indeed, the inputs of the cerebellar nuclei coincide with cortico-olivary networks, as each of the 14 identified longitudinal zones of the mouse cerebellar cortex (Apps, and Hawkes 2009; Apps, Hawkes, et al. 2018) would project to a particular sub-division of the cerebellar nuclei, which will also receive inputs from the region of the olivary inputs projecting to the corresponding cortical zone (Kebschull, Casoni, et al. 2023).

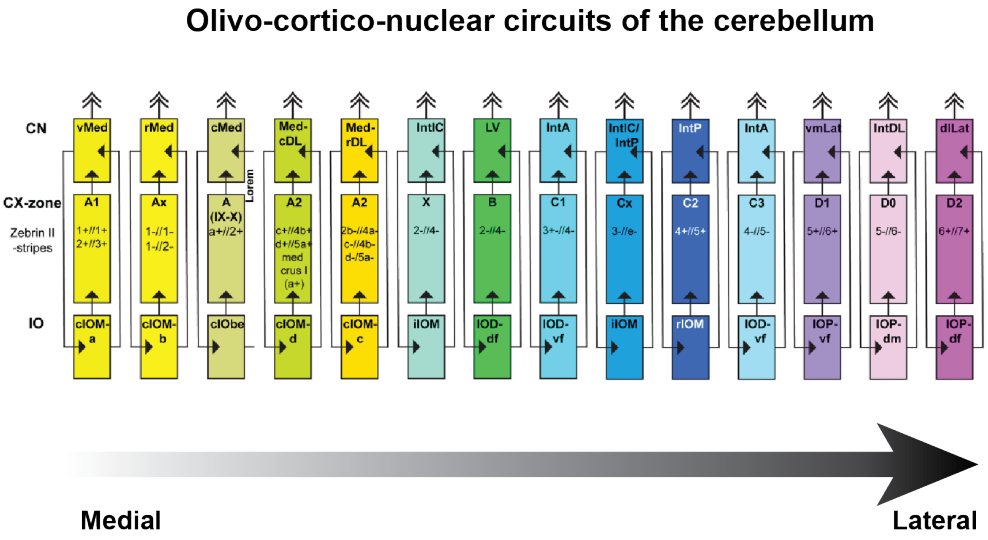

Figure 1.2: Parallel olivo-cortico-nuclear circuits. Schematic representation of the different olivo-cortico-nuclear loops, including cerebellar nuclei (top row), modules of the cerebellar cortex (middle row) and territories of the inferior olive (bottom row). This parralel loops are represented from their medial (left) to lateral (right). Adapted from Kebschull, Casoni, et al. 2023.

Although the knowledge related to the characterization of cerebellar nuclei neurons is quite modest, specially compared to the neurons of the cerebellar cortex. Typically, the different categories of neurons in the cerebellar nuclei are defined by their neurotransmitter expression, their morphology and their projection patterns. This classification leads to the characterization of 5 different types of neurons, preserved across amniotes (Kebschull, Richman, et al. 2020). These classes are composed of 4 types of projection neurons, with 2 types of excitatory neurons and 2 types of inhibitory neurons, as well as a local inhibitory interneuron (Kebschull, Casoni, et al. 2023).

Glutamatergic projection neurons

The 2 classes of excitatory projection neurons, Class-A and Class-B, share some characteristics. They are large glutamatergic neurons (Uno et al. 1970; Kebschull,

Richman, et al. 2020) originating from the rostral rhombic lip (Wang, Rose, et al. 2005), sending axons projecting to extra-cerebellar targets including numerous thalamic nuclei, brainstem nuclei and spinal cord (Fujita et al. 2020). These neurons also emit collaterals to Golgi cells and granule cells of the cerebellar cortex (Houck et al. 2015), thus providing feedback inhibition to the Purkinje cells through the excitation of inhibitory interneurons. This excitatory nucleocortical feedback has been shown to bi-directionally contribute to cerebellar associative learning, as its stimulation and inhibition respectively induced an increase and a decrease in the conditioned response during eyeblink conditioning (Gao, Proietti-Onori, et al. 2016).

In a recent study, the contribution of these glutamatergic projection neurons to an excitatory nucleo-olivary pathway was discovered (Wang, Liu, et al. 2023). Indeed, several cerebellar nuclei neurons projecting to both motor and non motor regions will emit collaterals to the inferior olive. This excitation is strong enough to trigger the emission of feedback complex spikes in the cerebellar cortex (Wang, Liu, et al. 2023), and the photostimulation of these projection can elicit saccadic and upper body movements (Wang, Liu, et al. 2023).

They receive direct excitatory inputs from the mossy fibers and climbing fibers, but are also strongly inhibited by Purkinje cells of the cerebellar cortex, and local interneurons (Uusisaari, and Knöpfel 2010).

Class-A and Class-B neurons are present in all cerebellar nuclei, with some local variations in density (Kebschull, Richman, et al. 2020). The dentate nucleus of the human is known to be critically expanded compared to rodents with more than half of cerebellar nuclei neuron being in the dentate nucleus (Kebschull, Richman, et al. 2020), but quite interestingly, this expansion was shown to be population specific, as the human dentate nucleus is almost exclusively composed of Class-B neurons (Kebschull, Richman, et al. 2020).

This bias in population during the expansion of the dentate nucleus in human brings the question of a the involvement of Class-A and Class-B neurons in different circuits. To answer this question, Kebschull et al performed retrograde tracings coupled with a sequencing analysis (Kebschull, Richman, et al. 2020). This experimental design allowed them to observed that while Class-A and Class-B would have broad and overlapping projections patterns, the contralateral zona incerta would predominantly receive inputs from Class-A neurons, and the contralateral reticular nucleus of the brainstem would receive more inputs from Class-B neurons.

Nucleo-cortical inhibitory neurons

They are inhibited by Purkinje cells (Uusisaari, and Knöpfel 2012; Ankri et al. 2015), and project to the granule cell layer of the cerebellar cortex (Uusisaari, and Knöpfel 2010; Ankri et al. 2015), where they inhibit Golgi cells (Ankri et al. 2015).

However, it is important to note that the nature and function of this inhibitory nucleo-cortical feedback pathways are not well known as of today, highlighting the necessity to study them more thoroughly in the future.

Olive-projecting inhibitory neurons

A population of small GABAergic neurons was shown to project to the inferior olive (Fredette et al. 1991; Angaut, and Sotelo 1987; Angaut, and Sotelo 1989). These neurons are mainly found in the dentate nucleus as well as in the interposed nucleus, with fewer of them in the fastigial nucleus (Fredette et al. 1991). The synapses of these neurons in the inferior olive are located nearby gap junctions of olivary neurons, suggesting that these cerebellar nuclei neuron could influence the electrical coupling of the inferior olive (Fredette et al. 1991; Angaut, and Sotelo 1987). Although these neurons represent a small population within the cerebellar nuclei, specially compared to the glutamatergic projection neurons (Batini et al. 1992), they account for the vast majority of the inhibitory inputs of the inferior olive (Fredette et al. 1991).

They receive direct excitatory inputs from the climbing fibers, suggesting a role of these neurons in feedback inhibition of the inferior olive, and are also inhibited by Purkinje cells of the cerebellar cortex (Uusisaari, and Knöpfel 2012).

This inhibition of the inferior olive has been proposed to play a role in the regulation of cerebellar associative learning (Rasmussen et al. 2014), as the inhibition of the climbing fiber response by these neurons was enough to trigger the extinction of a previously learned conditioned response (Medina, Nores, et al. 2002; Kim, Ohmae, et al. 2020).

Inhibitory interneurons

The cerebellar nuclei have a recurrent inhibition system, supported by a local population of small GABAergice and/or glycinergic interneurons (Chen, and Hillman 1993). They receive direct excitatory inputs from the mossy fibers and climbing fibers, and are also inhibited by Purkinje cells of the cerebellar cortex (Uusisaari,

and Knöpfel 2012).

Cerebellar nuclei neurons recurrent connectivity is not only done locally within a given cerebellar nucleus. Indeed, the fastigial nucleus has been shown to emit GABAergic projections to the contralateral fastigial nucleus (Gómez-González et al. 2021), which suggests a potential inter-nuclear communication.

Glutamatergic neurons are overwhelmingly more prevalent in the cerebellar nuclei than GABAergic neurons (Batini et al. 1992). However, the proportion of large neurons (putative glutamatergic projection neurons) and small neurons has been shown to be variable in the different cerebellar nuclei, the fastigial nucleus having around twice the amount of large neurons compared to small neurons, while the interposed and dentate nuclei displaying a more balanced distribution in mice (Heckroth 1994).

Recent technical advances using genetic targeting provide a better classification of cerebellar nuclei neurons (Kebschull, Casoni, et al. 2023). Indeed, a single-cell transcriptomic approach revealed 14 different classes of excitatory neurons in the cerebellar nuclei, derived from the rhombic lip, as well as 3 GABAergic and/or glycineric cell types, and one glycinergic neuron found only in the fastigial nucleus and showing a stunning morphological and physiological resemblance to glutamatergic projection neurons (Kebschull, Richman, et al. 2020; Kebschull, Casoni, et al. 2023).

Physiological properties

Ex-vivo studies from cerebellar slices demonstrated that deep cerebellar neurons (CN) display specific physiological properties. Typically, CN neurons spontaneously exhibit regular spiking (Jahnsen 1986) at several tens of Hz in slices (Raman, Gustafson, et al. 2000). While CN neurons are tonically inhibited by many Purkinje cells, they receive strong excitatory inputs from the mossy fibers and from the inferior olive.

Glutamatergic neurons of the cerebellar nuclei display a higher firing rate than GABAergic and glycinergic neurons (Uusisaari, and Knöpfel 2010). In addition, it has been shown that action potential waveform could be used to discriminate between neuronal types in the cerebellar nuclei (Uusisaari, Obata, et al. 2007; Uusisaari, and Knöpfel 2010). Indeed, glutamatergic neurons display faster action potentials, with a more pronounced hyperpolarization (Uusisaari, Obata, et al. 2007). On the other hand, GABAergic and glycinergic neurons will display larger wave-

forms, with slower hyperpolarizations (Uusisaari, Obata, et al. 2007; Uusisaari, and Knöpfel 2010). These two properties can allow to tentatively identify glutamatergic-like and GABAergic-like neurons in in-vivo extracellular recordings based on their average firing rate and the characteristics of their action potential waveforms (Özcan et al. 2020).

A peculiar property of CN neurons is the ability to perform rebound burst firing following an hyperpolarization (Jahnsen 1986; Llinás et al. 1988; Aizenman, and Linden 1999). During the phase of resting tonic discharge of CN neurons, T-type calcium channels are partially inactivated. However, a subsequent hyperpolarization of CN neurons driven by IPSCs from Purkinje cells may alleviate the inactivation of T-type calcium channels, as well as directly activate the hyperpolarization-activated cyclic nucleotide-gated channels (HCN). The return to resting membrane potential will then trigger a large calcium current from the T-type channels (Molineux, McRory, et al. 2006; Molineux, Mehaffey, et al. 2008; Alviña, Ellis-Davies, et al. 2009), in coordination with the HCN driven current (Engbers et al. 2011), resulting in a strong depolarization of the CN neuron. This rebound firing is typically bi-phasic, with a fast increase in firing rate during the first 100ms following the end of hyperpolarization, and a later increase that can last for seconds (Sangrey et al. 2010). While the fast component of rebound has been shown to extensively depend on T-type channels and HCN channels, the later phase of rebound firing was hypothesized to be mediated by different conductances, including sodium channels with slow inactivation (Aman et al. 2007; Sangrey et al. 2010). Similarily to T-type channels, these Na channels are inactivated during resting tonic discharge of CN neurons, and will recover from their inactivation during hyperpolarization. The return to resting membrane potential will then trigger a long-lasting depolarizing Na current which will slowly be inactivated during rebound firing. In addition, the balance between tonic firing and rebound firing in the CN neurons has been linked with voltage-gated and calcium-gated potassium channels (Joho et al. 2009; Pedroarena 2011).

While the functional role of CN neurons rebound firing is not fully known, it has been hypothesized that this mechanism allows for CN neurons to non-linearly process sustained activation of mossy fibers and olivary neurons (Hoebeek et al. 2010), and plays a role in synaptic plasticity in CN neurons. Indeed, the synapse formed between the mossy fibers inputs in the deep cerebellar nuclei and the recipient CN neurons can undergo long term potentiation (LTP) in the case where the activation of the mossy fibers is followed by an hyperpolarization of the CN neuron by Purkinje cells and a rebound firing, otherwise this synapse will undergo long term depression

(LTD) (Pugh et al. 2008; Zheng et al. 2010).

Similarly, the synaptic plasticity between the Purkinje cell and the CN neuron was shown to be bidirectionally affected by rebound firing (Aizenman, Manis, et al. 1998). Indeed, a high frequency train of stimulation (100Hz) of the Purkinje cells with enough IPSPs to induce a rebound firing of the CN neurons leads to LTP of the Purkinje cell to CN neuron synapse, while shorter trains of stimulation without a subsequent rebound would tend to elicit LTD. In addition, a dampening of the rebound firing by decreasing the excitability of the CN neuron may shift the plasticity elicited by the LTP-inducing trains of stimulation to an LTD, further suggesting that rebound firing of CN neurons also drives synaptic plasticity at the level of the Purkinje cell to CN neuron synapse.

These observations suggest a contribution of CN rebound firing to the computation performed by the cerebellum and to cerebellar learning. However, we should take into consideration that the study of rebound firing in-vivo has revealed that this phenomenon is not commonly observed (Alviña, Walter, et al. 2008), thus showing the need to reconsider the importance of CN neuron rebound firing in-vivo.

1.1.4 Cerebellar inputs

The cerebellum receives a wide variety of inputs from many extra-cerebellar sources. However, most of these inputs are ultimately provided by two different systems, the mossy fiber system and the climbing fiber system. These two systems originate from structures called precerebellar nuclei, which comes into six pairs of nuclei located in the hindbrain nearby the cerebellum (Rodriguez et al. 2000; Hoshino et al. 2019). This set of nuclei is composed of the pontine gray nuclei, the reticulotegmental nuclei, the vestibular nuclei, the lateral reticular nuclei, the external cuneate nuclei and the inferior olive nuclei. While the inferior olive nuclei are the sole known contributor of the climbing fiber system, all the other 5 nuclei mentioned before contribute to the mossy fibers system.

1.1.4.1 Mossy fibers

The mossy fibers originate mainly from precerebellar nuclei, in particular the pontine, reticulotegmental, and lateral reticular nuclei (Léna et al. 2016). Neurons in these precerebellar nuclei send projecting axons, gathering in forms of bundles, entering the cerebellum through the cerebellar peduncles. Then, they ascend towards the cerebellar cortex, emitting collateral axons to the cerebellar nuclei along the way,

and terminate in the granular layer of the cerebellar cortex, in a structure called cerebellar glomerulus (Sillitoe, Fu, et al. 2012). Each axon emit several collaterals in the granular layer, thus innervating a wide population of granule cells (Sillitoe, Fu, et al. 2012). Depending on their origin, the mossy fibers can predominantly project to the ipsilateral cerebellar cortex (for example if they originate from the external cuneate nuclei), or to the controlateral cerebellar cortex (in the case of the pontine gray nuclei). A large portion of the brain contributes to the mossy fiber systems, either through projections to the precerebellar nuclei, or direct projections to the granular layer of the cerebellar cortex and cerebellar nuclei.

Cerebro-cerebellar pathways

The cerebrum projects to the cerebellum through oligosynaptic pathways, by sending inputs to precerebellar nuclei, contributing to both mossy fiber and climbing fiber systems (Léna et al. 2016).

For the longest time, the cerebellum was considered as solely acting on motor functions. The classical view was that the cerebellum provided a potential substrate for different cerebral areas to influence movement control in the primary motor cortex. However, while investigating cerebellar afferences potentially coming from the primary motor cortex, Kelly and Strick observed that the parts of the cerebellum receiving from these areas were mainly restricted to the anterior lobe and to some extent present in lobule VII and VIII (Kelly et al. 2003). This observation suggests that, for the most part, the cerebellum receives inputs from non-motor cortical areas.

Strikingly, Kelly and Strick observed that the injection of anterograde trans-synaptic viral tracers in the area 46 of the cerebral cortex in monkeys leads to a robust labeling in the Crus II region and lobule VII of the cerebellar cortex, with little to no overlap with the regions receiving inputs from the primary motor cortex (Kelly et al. 2003). Knowing that the area 46 is a non-motor area of the prefrontal cortex involved in cognition and memory (Friedman et al. 2022), this not only was compatible with a functional organization of the cerebellum, but also brought additional anatomical evidences supporting the idea that the cerebellum could influence cognitive functions (Middleton et al. 1994; Schmahmann et al. 1998).

And indeed, most cortical regions were shown to contribute to cerebro-cerebellar pathways, with the strongest contributors being the frontal and parietal cortices (Legg et al. 1989; Leergaard et al. 2007; Léna et al. 2016).

Despite the profuse interplay between non-motor areas of the brain and the

cerebellum, how the cerebellum participates to cognitive and affective functions as to yet to be properly described.

Spinocerebellar pathways

Although the precerebellar nuclei are major providers of the mossy fibers system, they are not its sole contributor. Indeed, the spinal cord remains a strong contributor to cerebellar inputs reaching the cerebellar cortex through the mossy fibers, either through direct or indirect spinocerebellar tracts (Ruigrok 2016). There are four distinguishable direct spinocerebellar tracts: the dorsal spinocerebellar tract, the ventral spinocerebellar tract, the spino-cuneo-cerebellar tract and the rostral spinocerebellar tract (Ruigrok 2016).

The dorsal spinocerebellar tract, originating from the column of Clarke in the lamina VII of the thoracic and lumbar spinal cord, relays proprioceptive information from the ipsilateral part of the body (mainly hindlimbs) to the cerebellar cortex through the inferior cerebellar peduncle. Interestingly, the dorsal spinocerebellar tract is also populated by fibers from Stiling's nucleus and from the central cervical tract, conveying information about the contralateral side of the body to the cerebellar cortex through the superior cerebellar peduncle (Matsushita et al. 1995; Kitamura et al. 1989).

The ventral spinocerebellar tract, also known as Gower's tract, includes fibers from spinal neurons located in many parts of the ventral and dorsal spinal cord. They converge in the contralateral ventral spinocerebellar tract and recross to enter the ipsilateral cerebellum though the superior cerebellar peduncle (Kitamura et al. 1989). They relay proprioceptive information as well as motor and premotor signals (Bosco et al. 2001; Arshavsky, Berkinblit, et al. 1972; Arshavsky, Gelfand, Orlovsky, and Pavlova 1978; Arshavsky YuI et al. 1984) mainly for the hindlimb. The rostral spinocerebellar tract is the equivalent of the ventral spinocerebellar tract for the forelimb (Ruigrok 2016).

The spino-cuneo-cerebellar tract relays proprioceptive information related to the ipsilateral forelimb to the cerebellum, entering through the inferior cerebellar peduncle (Ruigrok 2016). It can thus be considered as an equivalent of the dorsal spinocerebellar tract for the forelimbs.

In addition to the four direct spinocerebellar tracts mentioned previously, the spinal cord also projects to the cerebellum through indirect tracts involving the precerebellar nuclei (Ruigrok 2016). In particular, the lateral reticular nucleus has

been shown to be the site of convergence of proprioceptive informations from both lower limbs, as well as from the ipsilateral forelimb (Pivetta et al. 2014; Azim et al. 2014).

1.1.4.2 Climbing fibers

Climbing fibers arise from the inferior olive. The inferior olive is subdivided into different compartments (Ruigrok, de Zeeuw, et al. 1990). Axons emitted by olivary neurons gather in bundles of fibers and reach the cerebellum through the inferior cerebellar peduncle. Then, they will ascend towards the cerebellar cortex, where they form many synapses with the dendritic tree of the Purkinje cells. The terminals of the climbing fibers in the cerebellar cortex are known to be arranged in narrow sagittal bands, matching the zonal organization of the cerebellar cortex (Groenewegen, and Voogd 1977; Sugihara, Wu, et al. 1999; Sugihara, Wu, et al. 2001). This comes as a stark contrast with the mossy fibers which display a broad extension in the medio-lateral axis. A single olivo-ceerbellar axon will innervate from 1 to 10 different Purkinje cells, parallely distributed in the same parasagittal plane.

Climbing fibers also emit collaterals during their ascension towards the cerebellar cortex, which will directly innervate the deep cerebellar nuclei (Ruigrok 1997; Ruigrok, and Voogd 2000). They form excitatory synapses with cerebellar nuclei neurons inhibited by the Purkinje cells which are innervated by climbing fiber collaterals from the same parent fibers (van der Want et al. 1987; Van der Want et al. 1989; Sugihara, Wu, et al. 1999), effectively forming a olivo-cortico-nuclear loop.

During pre-natal development, olivo-cerebellar axons come into contact with the soma of Purkinje cells (around E18) (Watanabe et al. 2011; Hashimoto, and Kano 2013). At this stage and until P3, many axons from different olivary neurons will create terminals on the soma of a single Purkinje cell, these synapses will be considered immature (Watanabe et al. 2011). In-between P3 and P7, one (or few) olivary input will be selected and reinforced, which will lead to its translocation on the dendritic branch of the Purkinje cell. Then, a non-selective synaptic elimination of olivary inputs on the soma of the Purkinje cell will occur from P7 to P17, preserving only the olivary axon(s) that developed alongside the dendritic branch of the Purkinje cell, forming a fully mature climbing fiber (Watanabe et al. 2011; Hashimoto, and Kano 2013). This synaptic elimination has been shown to be dependent on parallel fibers inputs to Purkinje cells, as the deletion of GluD2 resulted in an impaired synapse formation between parallel fibers originating from the inferior olive and Purkinje

cells, which lead to to a defect in synaptic elimination of olivary inputs (Hashimoto, Yoshida, et al. 2009).

This synaptic elimination mechanism ensures to preserve only one climbing fiber input per dendritic branch. However, as mentioned before, the Purkinje cell can have a single straight branch in their dendritic arbor (most prevalent morphology observable in mice), or can have either a split dendritic branch, or multiple branches (main morphology observable in humans) (Busch et al. 2023). It was shown recently that split branches or multiples branches could be innervated by inputs from different climbing fibers (Busch et al. 2023), suggesting that a single Purkinje cell could integrate information from multiple olivary neurons.

Similarly to climbing fibers inputs on Purkinje cells, the convergence of many synaptic inputs from olivary neurons to cerebellar nuclei neurons seems to undergo a refinement. Indeed, the number of different olivary inputs to a single cerebellar nuclei neuron was reduced from ~40 in juvenile mice to ~8 in adults (Najac et al. 2017), suggesting that these inputs may play different roles during development, initially shaping cerebellar microcircuits in juvenile animals (Najac et al. 2017; Pickford et al. 2017).

1.1.5 Cerebellar outputs

The cerebellum projects to a wide variety of extra-cerebellar targets, with different projections sites in the medulla oblongata, in the brainstem and in the diencephalon (Novello et al. 2022).

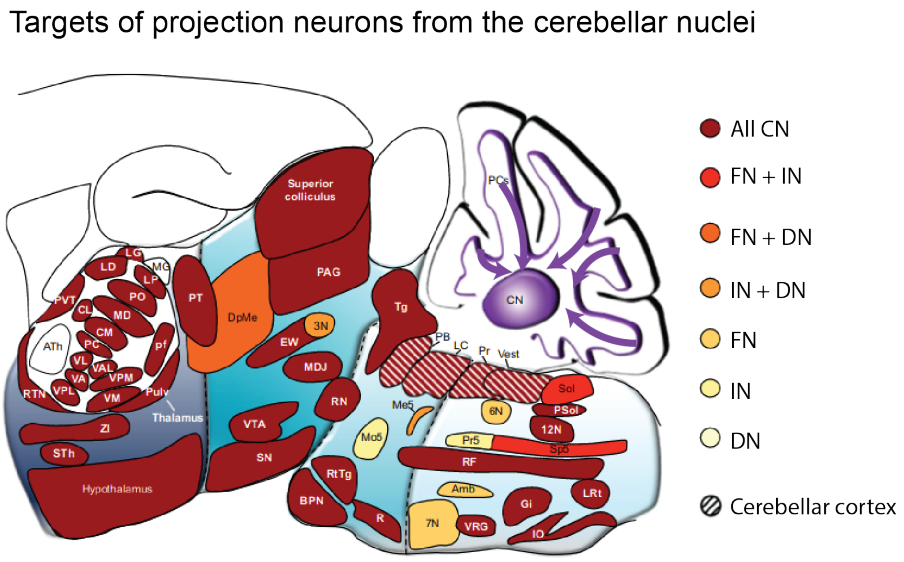

Figure 1.3: Identified projection targets of the cerebellar nuclei. Scheme of a saggital slice of mouse brain, with the monosynaptic projection targets of the cerebellar nuclei. Adapted from Novello et al. 2022.

1.1.5.1 Cerebellar descending pathways

For the longest time, the functional role of the cerebellum was tightly related to motor control. Thus, a particular interest was given to cerebellar projections to the descending motor pathways described by Hans Kuypers (Kuypers 1964). While all the cerebellar nuclei take part in these pathways (Ruigrok 2013), the contribution of the fastigial nucleus is the most well-documented.

Notably, the caudal part of the fastigial nucleus projects to the contralateral medial pontomedullary reticular formation (Gonzalo-Ruiz et al. 1988; Teune et al. 2000), known to be involved in the control of eye saccades (Enderle 2002). Consistently with this, both cerebellar vermis and fastigial nucleus have been shown to exert control over this function (Noda 1991; Ohtsuka et al. 1991; Ohtsuka et al. 1995). Indeed, the stimulation of the occulomotor part of the cerebellar vermis resulted in ipsilateral eye saccades in opposition to the stimulation of the fastigial nucleus leading to controlateral eye saccades, suggesting that vermal Purkinje cells inhibit fastigial neurons controlling the eye saccade (Noda 1991). Furthermore, the onset of eye saccades were shown to be preceded by a burst activity of neurons in the fastigial nucleus controlateral to the saccade direction (Dean 1995; Ohtsuka et al. 1991), in coordination with a pause in Purkinje cell activity (Ohtsuka et al. 1995). In addition to eye saccade control, these fastigial projections were also proposed to contribute to head orientation and spinal-related motor control (Sugihara, and

Shinoda 2007).

The interposed nucleus also contributes to ipsilateral descending cerebellar pathways, mainly through projections to the pontomedullary reticular formation and to the deepest the deepest layers of the spinal trigeminal nucleus (Teune et al. 2000). These regions were shown to be substantially involved in feeding behaviour, as they contain pre-oromotor neurons either rhythmically entrained by licking, or tuned to oral sensorimotor state (Travers et al. 2000), and can even be involved in the control of jaw muscles during mastication (Luo et al. 2001). Consistently with a role in food manipulation, the stimulation of the interposed nucleus induced movement of the lips, neck and forelimbs (Angaut, and Cicirata 1990).

Many studies revealed projections of the dentate nucleus in the controlateral pontomedullary reticular formation (Tolbert et al. 1980; Teune et al. 2000). However, the actual functional role of these descending pathways is still not well known, although they were proposed to be involved in the control of rhythmical movements (Arshavsky, Gelfand, and Orlovsky 1983). Similarily to the interposed, stimulating the dentate nucleus elicits movement of the upper-body, including forelimb and digits (Angaut, and Cicirata 1990; Angaut, and Cicirata 1994).

1.1.5.2 Cerebellar ascending pathways

In the light of the many functions in which the cerebellum is involved in, it becomes clear that the its functional connectivity with the encephalon is broader than what predicted. And indeed, cerebellar projections reach many metencephalic, mesencephalic and diencephalic structures monosynaptically (Fujita et al. 2020; Novello et al. 2022), which are themselves embedded in larger networks.

While a modulation of the cerebral cortex by the cerebellum was suggested by a myriad of functional connectivity and electrophysiological studies, it is only thanks to the development and perfection of trans-synaptic tracing that oligosynaptic pathways towards the cerebral cortex and subcortical structures could be revealed (Kelly et al. 2000; Ugolini 2010).

The thalamus is a set of diencephalic nuclei, often regarded as a prime relay between subcortical and cortical structures. However, the thalamus has been shown to support several cerebral functions through its interactions with the cortex, being necessary to maintain cortical activity (Reinhold et al. 2015), driving cortical dynamics during movement (Sauerbrei et al. 2020), and sustaining brain rhythms through an interplay between the thalamus and the cerebral cortex (Buzsáki 2006; Steriade 2000; Steriade 2006).

The cerebellum is known to have broad projection patterns within the thalamus (Léna et al. 2016; Fujita et al. 2020; Novello et al. 2022), with the main cerebellar targets being the ventro-lateral thalamus, the intralaminar thalamus, the ventro-medial nucleus and the zona incerta (Angaut, Cicirata, and Serapide 1985; Aumann, Rawson, et al. 1994; Teune et al. 2000). Although the density of cerebellar inputs in the thalamus can be lower than for cortical inputs, they remain extremely potent (Sawyer et al. 1994; Gornati et al. 2018). In addition, they have been shown to display plastic changes (Aumann 2002), as a LTP of cerebello-thalamic synapses was inducible in slices (Aumann, Redman, et al. 2000), and ultrastructural changes were observed in these synapses following motor adaptation training (Aumann, and Horne 1999).

Quite strikingly, a subset of cerebello-thalamic neurons also display a degree of collateralization to the ispi-lateral medulla oblongata (Bentivoglio, and Molinari 1986; Sathyamurthy et al. 2020)and to contralateral spinal circuits (Sathyamurthy et al. 2020). These neurons have been shown to be required for locomotor skill learning (Sathyamurthy et al. 2020), suggesting potential synergy between cerebellar ascending and descending pathways during motor learning.

1.1.6 Cerebellar algorithms

As described in a previous section of this introduction, the cerebellar networks display a high level of uniformity in their structure (Sillitoe, and Joyner 2007), with many cortico-nucleo-olivary loops and a modular organization. This particular organization has led many researchers to investigate the existence of a uniform 'cerebellar algorithm', allowing the cerebellum to perform a transform on its input signal according to some general computational rules.

1.1.6.1 From Marr-Albus-Ito to adaptative filters

The first descriptions of cerebellar circuits highlighted few key features (Eccles 1967): 1) the Purkinje cells are the sole output of the cerebellar cortex, projecting to the cerebellar nuclei 2) each Purkinje cell receives a single climbing fibre inputs (although recent evidence reveal that multiple inputs are possible (Busch et al. 2023)), 3) a given Purkinje cell receives inputs from thousands of granule cells.

In the light of these network properties, Marr proposed a model of the cerebellum relying on the analogy of structure between the cerebellar cortex and a perceptron (Rosenblatt 1958), suggesting the cerebellum to be a supervised learning machine

able to perform pattern recognition (Marr 1969). This theory critically relied on the PF-PC synapse and its ability to undergo plastic changes driven by a concomitant activation of parallel fibers. Marr predicted that a simultaneous activation of PF and CF input will lead to a long term potentiation of the PF-PC synapse, considering the CF input as a teaching signal responsible for the update of the synaptic weight. However, Albus shifted this concept towards an anti-Hebbian form of learning, suggesting that simultaneous activation will lead to LTD rather than LTP. This conceptual change in the direction of plasticity was later corroborated by physiological studies performed by Ito, who observed a decreased response of Purkinje cells to stimulation the parallel fibers inputs induced by a conjunctive stimulation of the same fibers along with the climbing fiber (Ito 1982; Ito, and Kano 1982; Ito 1989). These results were consistent with the LTD predicted by Albus, and cemented the Marr-Albus-Ito theory as the main framework to understand cerebellar computation.

Additionally, Ito proposed the climbing fiber input to represent an error signal, provided to the Purkinje cell in order to decrease the synaptic weight of parallel fiber inputs associated to sub-optimal situations, thus achieving optimal movement control.

Ito's view allowed to place cerebellar computation in the context of a network. Indeed, Marr and Albus' view on the role of the cerebellum in motor control was independent of other brain structures, suggesting that the cerebellum could control movement by itself in an holistic fashion (Kawato et al. 2021). In contrary, Ito acknowledged potential interactions with other brain regions, proposing the cerebellum to have a complementary modulating role of both motor and non-motor functions.

However, these models do not necessarily consider that the input signals from the mossy fiber are continuous and rate modulated, rather than relying on sparse spike timing (which is the case for the climbing fiber input). Thus, Fujita proposed to create a new model based on the theory of adaptive filters (Sakrison 1963; Widrow et al. 1967) and integrate it to the Marr-Albus-Ito framework to enrich it (Fujita 1982). In an adaptive filter, a continuous input signal is de-multiplexed by a transducer into multiple channels which will be linearly transformed and integrated with different weights. This integrated signal will then be compared to a reference signal by a comparator, and the output of this comparator will be used to iteratively adjust the different weights of the integrator.

As evidenced by Fujita, the circuits of the cerebellar cortex bear some resem-

blance with the architecture of an adaptive filter (Fujita 1982), with the granular layer contributing to the transduction and amplification of the input signal, the Purkinje cell integrating direct excitatory inputs from the parallel fibers and inhibitory inputs from the molecular layer interneurons, the climbing fiber being the reference error signal and the Golgi cells potentially introducing a phase lag transform in the input. In this particular situation, the aim of this adaptive filter model of the cerebellum is to decorrelate the mossy fibers input signal from the climbing fiber reference signal.

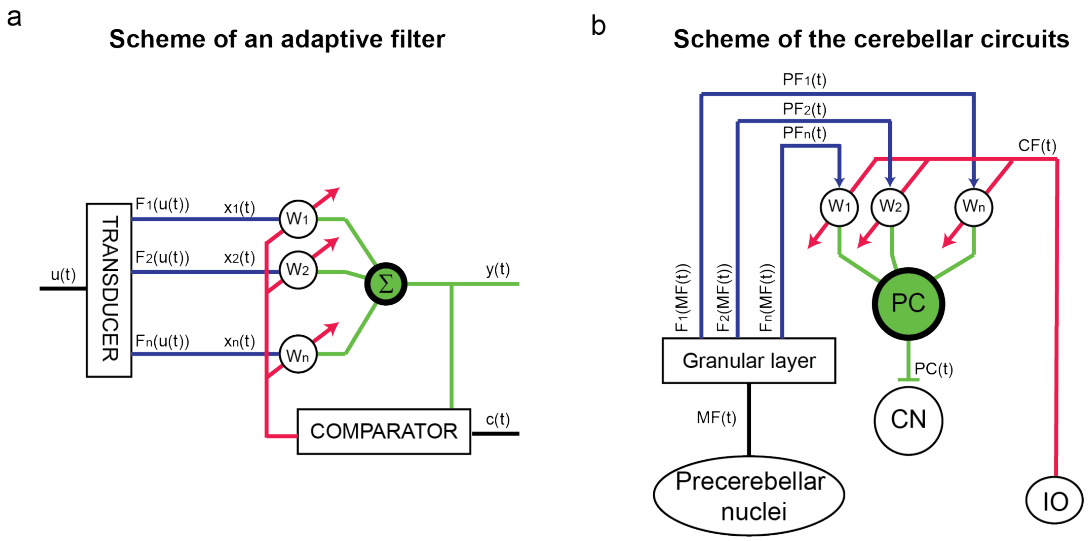

Figure 1.4: Similarities between the structure of an adaptive filter and the cerebellar cortex. **(a)** Schematic representation of a typical adaptive filter. Adapted from Fujita 1982. **(b)**. Simplified schematic representation of the cerebellar circuits, where a parallel is drawn between the input signal of the filter ($u(t)$) and the mossy fiber inputs ($MF(t)$), conveyed to the granular layer which acts as a transducer applying different transforms ($Fn(MF(t))$) to the input signal, each of them carried through separated parallel fibers ($PFn(t)$) to the Purkinje cell (PC) with wich they form synapses with adjustable weights (Wn). The weight of each of these synapse is calibrated using a teaching signal ($CF(t)$) coming from the inferior olive (IO). The Purkinje cell integrates the signal from the parallel fibers and exerts an inhbitiory action ($PC(t)$) over the cerebellar nuclei (CN).

A key advantage of these models is that since their learning strategy is based on covariance between analog signals, they allow to dynamically adjust synaptic weights while also being resilient to intrinsic noise (Dean, and Porrill 2008; Porrill, and Dean 2008). Implementing such adaptive filters could serve a wide variety of functions, including dynamic denoising, suppression of the sensory consequences of an action, and optimal motor control through the computation of an internal forward model (Porrill, Dean, and Anderson 2013).

1.1.6.2 Internal forward model

A critical aspect of motor control is the ability to dynamically tune the motor command in order to maximize the success of an action. This process requires to integrate sensory information about the state of the body in motion. However, afferent sensory signals possibly used as feedback have a temporal delay before reaching brain structures, which is variable depending on the sensory modality and the target structure. For example, a visual stimulus presented to a macaque will elicit a response in the primary visual cortex with a delay of 30ms, and reach the parietal cortex nearly 80ms after the onset of the stimulus (Schmolesky et al. 1998), which in essence correspond to the timing of rapid eye movements. Because the latency of feedback signaling can be in the same order of magnitude as the timing necessary to execute motor actions, solely relying on this delayed sensory feedback will lead to unstable motion control (Wolpert et al. 1996). Thus, the central nervous system needed to implement a compensation mechanism for this delayed signaling in order to finely tune motor commands.

A potential solution for this problem is to predict the future state of the system based on its current state and on an efferent copy of the motor command, and then use this predicted state for feedback control. In the context of motor control, this means that the network implements a function able to solve the differential equation expressing the future state of the body induced by a movement. The ability to anticipate the perturbations induced by an action allows to quickly update the motor plan if any variation from the predicted state is detected.

The most striking physiological evidences of the cerebellum encoding internal model for feed forward motor control come from studies of manual pursuit tracking task in monkeys (Coltz et al. 1999; Roitman et al. 2005; Pasalar et al. 2006; Ebner et al. 2008). In these studies, the discharge rate of Purkinje cell simple spikes was tuned to movement kinematics, such as position of the arm, direction and velocity of movement rather than movement dynamics. Interestingly, Coltz et al showed that Purkinje cells tuned to movement speed were selectively responsive to a particular direction, and conversely (Coltz et al. 1999). These evidences suggest that Purkinje cell population can encode complex movement kinematics through the combination of multiple parameters, consistently with the hypothesis of the internal model.

Strikingly, a recent study showed that the future activity of the mossy fiber could be robustly predicted by the activity of the cerebellar nuclei in a sensory motor task (Tanaka et al. 2019). This predictive power of the cerebellar nuclei activity remained

high even with lags of more than 100ms, supporting the idea that the cerebellum can implement an internal forward model to predict a future state, which can be used to compensate for delayed sensory input.

1.1.6.3 Limitations of the current models of cerebellar function

The models do not take into account the complexity of the actual cerebellar networks

The previously mentioned computational models of the cerebellum were established with their contemporary knowledge of the wiring in the cerebellar cortex, which was incomplete to say the least. Indeed, while the feedforward excitation of both mossy and climbing fibers was described, along with feedforward and feedback inhibition, we now know that the degree of recurrent connectivity in the cerebellum is much higher than envisioned in the models of Marr, Albus and Ito (De Zeeuw et al. 2021). A striking example of these newly discovered connections is the presence of feedback inhibition in the Purkinje cells population, with collaterals sent to other Purkinje cells and molecular layer interneurons (Witter et al. 2016). Similarly, recurrent inhibition was discovered in Golgi cells and molecular layer interneurons (Hull et al. 2012; Rieubland et al. 2014). In addition, an excitatory nucleo-cortical pathway has been recently discovered, providing feedback excitation to the cerebellar cortex and amplifying associative learning (Gao, Proietti-Onori, et al. 2016). These newly discovered feedback pathways could be a support for the participation of the cerebellum to movement sequences (Khilkevich et al. 2023).

Plasticity in cerebellar networks is more diverse than in models

The typical models of cerebellar processing and learning heavily rely on the ability of the synapse between parallel fibers and Purkinje cells to be altered by climbing fiber inputs. For many decades, the idea that synapses associated to the error signal carried by the climbing fibers will undergo long term depression (Ito, and Kano 1982; Ito 1983) was considered as the key mechanism underlying cerebellar learning. Because of this, these models usually operate under the assumption that plasticity is restricted to PF-PC synapses (see prediction b in (Marr 1969)). Moreover, since Purkinje cells are spontaneously active, the reduction of firing (as obseved in eyeblink conditioning) may require an increased inhibitory drive, possibly by a LTP at the parallel-fiber to molecular-layer-interneuron controlled by the climbing fiber

[Jorntell 2002]]. However, we now know that many forms of plasticity occur in the cerebellum, including synaptic plasticity and intrinsic plasticity (De Zeeuw et al. 2021), and that the rules underlying the CF dependent PF-PC plasticity are more complex, as it is bidirectional and dependent on intra-cellular calcium concentration (Coesmans et al. 2004).

Many more sites of plasticity have been discovered in the cerebellum. Nearly every synapse type has been shown to be able to undergo plastic changes (Hansel, Linden, and D'Angelo 2001; D'Angelo et al. 2016; De Zeeuw et al. 2021). In addition, long term changes in excitability have been observed in granule cells (Armano et al. 2000), but also Purkinje cells (Schreurs et al. 1998; Belmeguenai et al. 2010) and cerebellar nuclei neurons (Aizenman, and Linden 2000; Zhang, Shin, et al. 2004). Evidences of intrinsic plasticity correlated to learning were observed. Notably, an increased dendritic excitability was observed in Purkinje cells after classical conditioning (Belmeguenai et al. 2010), leading to a prolonged after-hyperpolarization, potentially alleviating the inhibition of PC on cerebellar nuclei neurons.

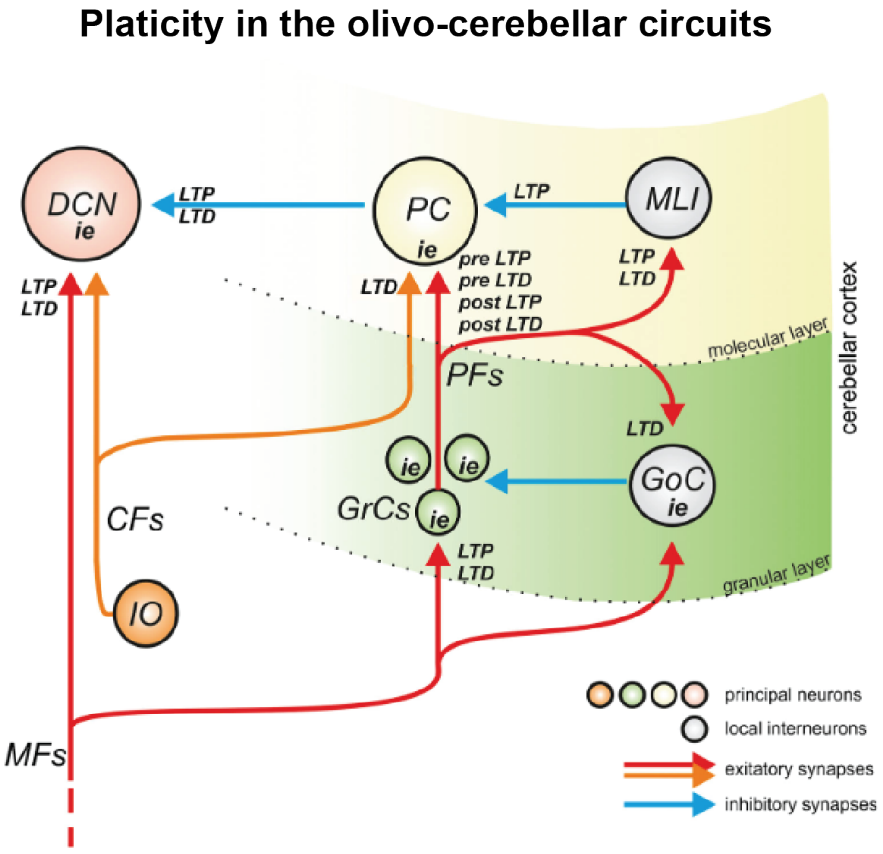

Figure 1.5: Identified sites of plasticity in the olivo-cerebellar circuits. Simplified schematic of the cerebellar cortex and cerebellar nuclei (DCN). This circuit includes mossy fibers (MFs), parallel fibers (PFs), climbing fibers (CFs), granule cells (GrCs), Golgi cell (GoC), Purkinje cell (PC), molecular layer interneurons (MLI), and the inferior olive (IO). Within this network, different forms of plasticity have been identified, including changes in intrisic excitability (ie), synaptic long term potentiation (LTP) and synaptic long term depression (LTD), which can be pre-synaptic (pre) or post-synaptic (post). The different layers of cerebellar cortex is indicated by a color graded area, and its different layers are delimited by straight dashed lines, excitatory projections are represented by red and orange arrows, and inhibitory projections are represented by blue arrows. Adapted from D'Angelo et al. 2016.

The climbing fiber inputs to Purkinje cells were initially believed to be invariant, justifying their role as an external signal to fine-tune the more plastic parallel fibers to Purkinje cells synapse. However, this input can undergo long term depression (Hansel, and Linden 2000; Ohtsuki et al. 2009) and long term potentiation (Ohtsuki et al. 2009). The long term depression of CF-PC synapses can be obtained by performing 5 Hz tetanic stimulations of the climbing fibers, and is associated to an altered shape of the spikelets in the complex spike induced by CF stimulation (Hansel, and Linden 2000). Other factors can alter CF-PC inputs, as the numbers of spikelets in the complex spike is positively correlated to the simple spike rate prior the occurrence of the complex spike (Burroughs et al. 2017), and the length

of a complex spike increases with its frequency of occurrence (Warnaar et al. 2015). These synaptic and non-synaptic changes reflect the non-uniformity of climbing fibers inputs, representing a graded input signal rather than an invariant teaching input. Knowing that both complex spike duration and frequency were associated to trial-to-trial learning (Yang et al. 2017), this indicates that the dynamic tuning of CF-PC inputs can contribute to cerebellar learning.

In addition, recent studies have suggested a contribution of synaptic plasticity in the cerebellar nuclei to cerebellar learning. Indeed, transient engrams initially formed in the cerebellar cortex are thought to be transferred in the cerebellar nuclei to be maintained (Medina, and Lisberger 2008; Masuda et al. 2008). This nuclear plasticity was speculated to potentially play a role in the persistence of memory within cerebellar networks, and its resilience to background activity (Medina, and Mauk 1999).

Mismatch between models and in-vivo learning

Typically in the Marr-Albus-Ito framework, learned motor control is assumed to be dictated by the simple spike output of Purkinje cells. Situations where the measured sensory state does not match the prediction generate an error signal manifesting as an action potential in the climbing fiber. This triggers a complex spike in the Purkinje cell receiving the climbing fiber input and depresses the parallel fibers synapses which excited the Purkinje cell prior. This long term depression reduces the weight of synapses associated to an erratic outcome, thus reducing the simple spike rate of this Purkinje cell and optimizing the motor output. This hypothesis predicts a reduction of Purkinje cells spiking output, allowing for a disinhibition of the deep cerebellar nuclei, driving the motor activity and the expression of the conditioned response.

Although a compatible process was observed in-vivo during eye-blink conditioning (ten Brinke et al. 2017), many in-vivo studies do not necessarily reveal a reduction of simple spikes output associated to learning. For example, Romano et al. observed that an increase in simple spike output was correlated with a stronger whisker protraction following sensori-motor learning (Romano et al. 2018), suggesting that a potentiation of the PF-PC synapse could also be involved in cerebellar learning and movement adaptation. However, this observation was still consistent with the previoulsy established learning rules of the cerebellum, as the Purkinje cell undergoing an increased simple spike activity also had lower rates of complex spikes.

In contrary, Lisberger and Raymond reported that, in a vestibulo-occular reflex task, the effect of vestibular signals on Purkinje cells was potentiated in situations were it should have underwent LTD (Lisberger et al. 1996).

We previously mentioned studies showing that Purkinje cells encode movement kinematics, thus potentially predicting the sensory outcome of an action. However, a force field task study revealed a population of Purkinje cells tuned to movement dynamics, and not movement kinematics (Yamamoto et al. 2007). The authors of this study points towards that fact that this observation conflicts with the idea that the cerebellum performs a forward-model computation in the kinematic space and is more in favor of an inverse-model computation in the dynamic space. Nonetheless, the encoding of both movement kinematics and dynamics in the context of an internal forward model remains a possibility (Miall et al. 1993).

As we know, the mossy fibers input of the cerebellum are originating from many regions of the brain, including motor, sensory and cognitive regions. Similarly, the cerebellar nuclei have a wide variety of outputs, with both descending pathways and ascending pathways towards cerebral structures. In addition, the cerebellum has been shown to be involved in a myriad of functions, including both motor and non motor. Thus, it is unlikely for the cerebellum to operate under an uniform computation explaining all of its functions.

1.2 Motor circuits, motor learning and motor pathologies

1.2.1 Motor circuits

1.2.1.1 Motor cortex

The motor cortex is the telencephalic structure, part of the neocortex, with a strong ability to plan and execute motor commands. Historically, our understanding of both structures and functions of the motor cortex came from human studies (Penfield et al. 1937; Woolsey et al. 1952; Woolsey 1963), which revealed that the motor cortex was functionally separated into two areas: the primary motor cortex (M1) and the pre-motor area (PMA).

Primary motor cortex

More importantly, M1 has a peculiar structure, being an agranular cortex (devoid of cytoarchitecturally visible layer IV), which in primates hosts gigantic pyramidal neurons named Betz cells (Meyer 1987; Bhattacharjee et al. 2021). These cells directly participate to cortico-spinal pathways, as they send downstream projections to the spinal cord and thus can directly excite the spinal neurons responsible for muscle contraction (Porter et al. 1995). This direct control over spinal circuits gives the ability to M1 to generate movements, as suggested by the experiments of Penfield, in which the motor activity induced by the electrical stimulation of different areas of M1 allowed to identify a topographical organization of the M1, with a representation of each part of the body (Penfield et al. 1937; Catani 2017), named homunculus. The ability to generate motion, as well as the somatotopical organization of M1, lead to the conclusion that the primary motor cortex mainly has an executive role in the control of motor actions (Bhattacharjee et al. 2021).

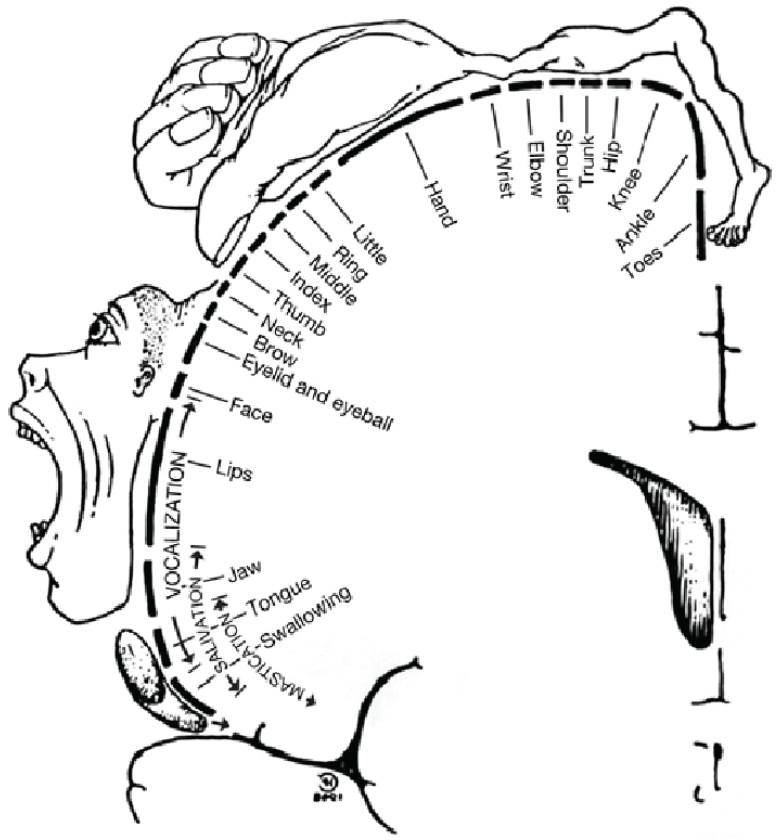

Figure 1.6: Somatic representation of the body in the motor cortex. Schematic representation of the homunculus of the human motor cortex drawn by Penfield, affecting regions of the motor cortex to the control of a specific body region. Adapted from Gordon et al. 2023.

Supplementary motor areas

In contrast, the PMA, altogether with the other secondary motor areas located in the frontal cortex; the supplementary motor area (SMA) and the cingulate motor area (CMA), share more cognitive roles over the regulation of motor actions (Picard et al. 2001; Chouinard et al. 2006). These roles include action planning, coordination and action selection (Nachev et al. 2008; Rizzolatti, Fadiga, et al. 1996; Rizzolatti, Fogassi, et al. 2002). While these areas can also project to spinal neurons, the local density of cortico-spinal neurons is lower compared to the primary motor cortex (He et al. 1995; Wise 1996; Dum et al. 1991). However, these secondary motor cortices display a high degree of reciprocal connections with M1 (Nachev et al. 2008), which

suggest that they are involved in modulating neuronal dynamics in M1.

Strikingly, PMA neurons undergo an activation anticipating the movement and ceasing at onset, which was proposed to be preparatory (Li, Daie, et al. 2016). Consistently with this, the perturbation of this activity leads to decreased performances in a sensory-motor task, but only if this perturbation is performed bilaterally on both hemispheres (Li, Daie, et al. 2016), suggesting a modular organization of these premotor networks, with enough redundancy to support a stable and robust motor output (Li, Daie, et al. 2016; Yu 2016).

Motor planning not only concerns the execution of a single movement, but can also encompass the production of a sequence of actions. Interestingly, the anticipatory activation observed in secondary motor areas before the onset of a movement was demonstrated to be possibly sequence specific (Tanji et al. 1994; Shima et al. 2000). Indeed, subsets of neurons in SMA display preparatory activity only when a particular sequence is performed (Tanji et al. 1994; Shima et al. 2000), or on the opposite at a particular index in the sequence (i.e. third movement of the sequence) regardless of the sequence actually expressed (Shima et al. 2000). This suggests that supplementary motor areas play a critical role in movement sequences generation. Similar patterns of activity have not yet been discovered in M1, further supporting the executive role of M1.

M1 connectivity

As evidenced previously, the primary motor cortex receives inputs from many structures, including other cortical areas such as the supplementary motor areas (Hira et al. 2013; Hooks et al. 2013; Peters et al. 2017), but also from sensory cortices (Mao et al. 2011; Peters et al. 2017)[. Interestingly, the projections from other cortices are distributed in a layer specific manner (Peters et al. 2017). Indeed, while the somatosensory cortex projects mainly to layers II/III and Va (Mao et al. 2011), frontal area As evidenced previously, the primary motor cortex receives inputs from many structures, including other cortical areas such as the supplementary motor areas (Hira et al. 2013; Hooks et al. 2013; Peters et al. 2017), but also from sensory cortices (Mao et al. 2011; Peters et al. 2017). Interestingly, the projections from other cortices are distributed in a layer specific manner (Peters et al. 2017). Indeed, while the somatosensory cortex projects mainly to layers II/III and Va (Mao et al. 2011), frontal area rather project to layer V and VI (Hira et al. 2013; Hooks et al. 2013; Peters et al. 2017). These later patterns of projection, mainly targeting deep layers, may play a direct modulatory role over the motor command, bypassing the

integration of more superficial layers.

The primary motor cortex also receives a strong drive from subcortical structures, mainly from the basal ganglia and the cerebellum. However, these input pathways are not direct, as they rely on the thalamus as a relay, using separated thalamic compartments (Hooks et al. 2013; Kuramoto, Furuta, et al. 2009; Kuramoto, Ohno, et al. 2015). The strongest provider of thalamic inputs to M1 is the motor thalamus, also referred to as the ventro-lateral (VAL), which is roughly segregated in two compartments, the inhibitory zone and the excitatory zone. This naming convention refers to the types of input that these compartments receive and not to the different types of neuronal populations that they contain. Indeed, the VAL contains an immense majority of glutamtergic neurons, and very few inhibitory interneurons in mice (Jager et al. 2023). types present, as the Glutamatergic neurons from the cerebellar nuclei project to the excitatory zone of the VAL, which projects to the layer II/III and layer V of M1. On the other hand, inhibitory output neurons of the basal ganglia, located in the internal segment of the globus pallidus (GPi) and in the substantia nigra pars reticulata (SNr), project to the inhibitory zone of the VAL, which mainly sends projections to layer I of M1 (Kuramoto, Furuta, et al. 2009). This heavily suggest a differential contribution of cerebellar and striatal inputs to regulation of M1 neuronal dynamics.

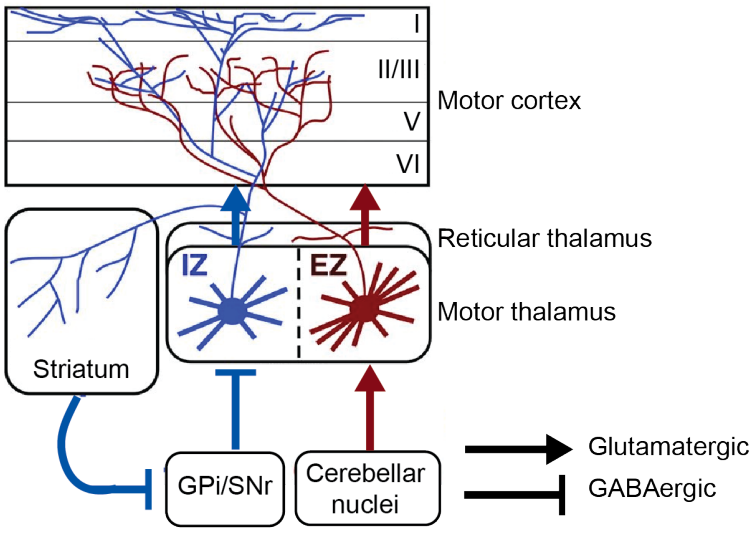

Figure 1.7: Segregated striato-cortical and cerebello-cortical pathways displaying distinct projection patterns in the motor cortex. The striatum projects to the output nuclei of the basal ganglia (GPi/SNr) which projects to the inhibitory zone of the motor thalamus (IZ). The inhibitory zone of the motor thalamus preferentially targets superficial layers of the motor cortex. On the other hand, the cerebellar nuclei projects to the excitatory zone of the motor thalamus (EZ), which targets deeper layers of the motor cortex. The striato-cortical pathway is represented in blue, the cerebello-cortical pathway is represented in red. Adapted from Kuramoto, Furuta, et al. 2009.

The output pathways of the primary motor cortex also exhibit a layer specific distribution (Weiler et al. 2008; Peters et al. 2017), with cortico-cortical communication occurring mainly at layers Va and VI, the pyramidal tract (cortico-spinal) at layer Vb and the cortico-thalamic neurons located in layer VI (Harris, and Shepherd 2015). It should be noted that cortical output neurons can project to multiple cortical and subcortical structure simultaneously, as they can exhibit a high degree of collateralization (Kita, and Kita 2012), suggesting a divergence of information at the output of the primary motor cortex.

M1 functions

Although the experiments of Penfield revealed a potential for the primary motor cortex to both initiate and drive movement through electrical stimulations applied on anaesthetized patients (Penfield et al. 1937), the investigation of the actual functional role of M1 required to study the consequences of its perturbations in-vivo.

Localized lesions of the motor cortex in humans, for example with strokes or focal traumas, have dramatic consequences on the ability of the patient to execute actions, with localized weakness and loss of movement.

1.2.1.2 Basal ganglia

The basal ganglia are a set of teleencephalic nuclei involved in voluntary motor control. Although the structure of these nuclei individually seems less organized than the laminar layout of the motor cortex or the modular organization of the cerebellum, the basal ganglia has very segregated input and output pathways. In terms of nuclei, it is composed of the striatum, the internal Globus Pallidus (GPi), he external Globus Pallidus (GPe), the subthalamic nucleus (STN), the substantia nigra pars compacta (SNc) and the substantia nigra pars reticulata (SNr).

Input nucleus: the striatum

The main input structure of the basal ganglia is the striatum, which receives inputs from many cortical and subcortical structures, and projects to intrinsic and output nuclei of the basal ganglia (Lanciego et al. 2012).

In terms of neuronal populations, the striatum is composed of two different categories of neurons, the Medium-sized Spiny Neurons (MSNs) representing 90-95% of striatal neurons, and local interneurons (Lanciego et al. 2012).

MSNs are relatively small projection neurons using GABA as a neurotransmitter, with a profuse dendritic arborization completely covered by dendritic spines, giving these neurons their name (Graybiel 1990). However, MSNs themselves are not an homogeneous population, and can be further separated into at least two groups based on their projection patterns and their molecular expression.

On one hand, striatal MSNs which express the dopamine receptor subtype 1 (D1R) project to the GPi and to the SNr and thus participate to the "direct" pathway (discussed in a later paragraph). The binding of dopamine on D1R activate an intracellular adenylate cyclase, leading to an increased cellular excitability (Kawaguchi 1997; Castro et al. 2013; Lanciego et al. 2012). Interestingly, these D1Rs are coupled to Golf rather than Gs (Corvol, Studler, et al. 2001). Mutations of the Golf-encoding gene can lead to a particular motor disorder (Pelosi et al. 2017) which will be discussed more in details in a later section of this thesis.

On the other hand, MSNs expressing the dopamine receptor subtype 2 (D2R)

participate to the "indirect" pathway and project to the GPe (Kawaguchi 1997; Lanciego et al. 2012). In opposition to D1R, the activation of D2R leads to the inhibition of adenylate cyclase activity, decreasing neuronal excitability. Thus, increased levels of striatal dopamine will have an opposite effect on both MSN populations. A third small population of MSNs expressing both D1R and D2R has also been identified (e.g. (Gagnon et al. 2017)) but its characterization is still underway.

Besides the previously described MSNs, the striatum also hosts different types of local interneurons. Typically, they are separated in four different classes (Kawaguchi, Wilson, Augood, et al. 1995), the most prevalent class being the large aspiny cholinergic interneurons, also known as tonically active neurons. Other interneurons types include GABAergic calretinin-positive interneurons, GABAergic parvalbumin-positive interneurons and the nitregic interneurons, a subclass of GABAergic neurons also using nitric oxide as a neurotransmitter. These later classes of interneurons are rather fast-spiking, in opposition to MSNs and cholinergic interneurons.

Although the striatum seems to be homogenous under most histological characterizations, the use of techniques such as acetylcholine esterase (AChE) staining, opiod receptor immunocytochemical detection and calbindin staining reveal two particular compartments within the striatum, the striosomes and the matrix (Lanciego et al. 2012). While matrix striatum displays strong AChE activity, parvalbumin and calbindin labelling (Graybiel, and Ragsdale 1978; Prensa et al. 1999; Gerfen, Baimbridge, et al. 1985), the characteristics of the striosome are weaker AChE activity, immunoreactivity against enkephalin, substance P, GABA and neurotensin (Graybiel, and Ragsdale 1978; Graybiel, Ragsdale, et al. 1981; Gerfen 1984), as well as μ opiod receptors (Pert et al. 1976).

Typically, the dendritic arbor of MSNs is restricted to their respective striosome or matrix (Penny et al. 1988; Kawaguchi, Wilson, and Emson 1989; Fujiyama et al. 2011), suggesting that their is little to no cross-talk between striatal compartments. Consistently with this segregation of integrative properties, striosomes and matrices receive different types of inputs. Sensory and motor cortices, thalamostriatal projections and dopaminergic neurons from the SNc tend to project preferentially to the matrix, while structures from the limbic circuits such as BLA, PFC preferentially target striosomes (Graybiel 1984; Graybiel 1990; Donoghue et al. 1986; Gerfen, Staines, et al. 1982; Sadikot et al. 1992; Kincaid et al. 1996).

Moreover, while MSNs present in the matrix project to the GPi, GPe and SNr, the MSNs from the striosomes sends most of their projections to the SNc, with some axonal collaterals going towards the GPi, GPe and SNr (Gerfen 1984; Bolam et al.

1988; Kawaguchi, Wilson, and Emson 1989; Giménez-Amaya et al. 1990; Fujiyama et al. 2011).

Despite the clear compartmentalization of the striatum between striosomes and matrix which express distinct genetic markers and receive different sets of inputs, the functional difference between these two compartments is still not fully understood.

Intrinsic nuclei: GPe, STN and SNc

The globus pallidus is separated in two compartments the GPi and GPe. Although these two structures share many similarities, the GPe only being separated from the GPi by a thin layer of white fiber, both of these nuclei have a very different contribution to basal ganglia circuits, both in terms of inputs and outputs (Lanciego et al. 2012). The GPe receives inputs from two main sources, the D2 MSNs from the striatum (Rosin et al. 1998; Bogenpohl et al. 2012), and the STN that shares reciprocal connections with the GPe (Shink et al. 1996; Joel et al. 1994). However, the Gpe also receives inputs from the intralaminar thalamus, and is reciprocally connected with the GPi (Marini et al. 1999). This complex connectivity leads to the proposition that basal ganglia functions are supported by a dynamical interplay between its different pathways (Nambu 2004).

The STN can be considered as the second relay of the indirect pathway; it receives massive amounts of inhibitory projections from the GPe (Nambu 2004; Castle et al. 2005; Lanciego et al. 2012). But interestingly, the STN also receives an extensive amount of glutamatergic projections from different areas of the cerebral cortex (Nambu 2004), as well as from the intralaminar thalamic nuclei (Sugimoto et al. 1983; Royce et al. 1985; Castle et al. 2005), and thus participates to a "hyperdirect" pathway (Nambu 2004). In terms of outputs, the STN hosts glutamatergic neurons projecting to a wide variety of targets in the basal ganglia, including the GPi, the SNr and the GPe to which it sends feedback projections (Van Der Kooy et al. 1980; Kita, Chang, et al. 1983; Kita, and Kitai 1987). Strikingly, the STN also outputs projection axons to thalamic nuclei, mainly to the ventral thalamic nuclei (Nauta et al. 1978; Rico et al. 2010) and to the parafascicular nucleus (Gerfen, Staines, et al. 1982; Castle et al. 2005). Knowing that the VAL projects to the primary motor cortex and can modulate its activity (Kuramoto, Furuta, et al. 2009), this is a parallel pathway through which the basal ganglia can influence neuronal dynamics in the motor cortex. Similarly, the parafascicular nucleus is a strong provider of inputs to the striatum, suggesting that the STN exerts an excitatory feedback on striatal cir-

cuits. A retrograde tracing study has revealed that the basal ganglia-projecting and thalamus-projecting neurons in the STN are different neuronal populations, with no collateralization between these outputs (Rico et al. 2010).

The substantia nigra pars compacta is a set of dopaminergic midbrain neurons, along with the neurons from the ventral tegmental area (VTA) and retrorubral field (Dahlström et al. 1964; Fu et al. 2012). They mainly receive inputs from the STN, and send dopaminergic projections to the striatum, regulating the local levels of dopamine and influencing the activity of both direct and indirect pathways.

Output nuclei: GPi and SNr

The substantia nigra pars compacta (SNr), often functionally grouped with the internal globus pallidus (GPi), are the main output nuclei of the basal ganglia and effectively the convergence point between both direct and indirect pathways (Lanciego et al. 2012). The inhibitory projection neurons of these structures then inhibit several thalamic territories and brainstem areas.

Although many similarities exits between the SNr and GPi, their thalamic projections seem to target different territories, particularly in the VAL (Ilinsky et al. 1987; Percheron et al. 1996). In contrast, the parafascicular nucleus of the thalamus seems to mainly receive inputs from the GPi.

Direct, indirect and hyperdirect pathways

The hypothesis of segregated parallel pathways in the basal ganglia is relatively recent (Albin et al. 1989; DeLong 1990), and stems from the observation that both hyperkinetic and hypokinetic disorders could arise from basal ganglia dysfunction. Albin et al proposed that this heterogeneity could be due to the existence of different sub-populations of striatal MSNs, having either a prokinetic or an antikinetic effect (Albin et al. 1989). One population of MSN would solely project to the SNr and GPi, inhibiting the output nuclei of the basal ganglia and thus disinhibit the thalamus, leading to a prokinetic effect, while the other population would send inhibitory inputs to the GPe, projecting indirectly to the SNr through the STN, leading to a disinhibition of the output nuclei, and thus increasing the inhibitory tonus that they exert over the thalamus, leading to an antikinetic effect (Calabresi, Picconi, et al. 2014).

These two different pathways were labelled as direct and indirect pathways, re-

ferring to the number of intermediate relays between the striatum and the ouput of the basal ganglia. Later, this dichotomy between direct and indirect pathways having different projections targets has been complemented by the discovery that the striatal MSN express different genes, particularly in terms of dopamine receptors (Gerfen, and Surmeier 2011). Thus, MSNs participating to the direct and indirect pathway respectively express D1 and D2 receptors, which exert opposite effect on the regulation of excitability.

However, in-vivo studies have revealed that both direct and indirect pathways are activated during locomotion, particularly during action initiation (Cui et al. 2013), leading to the need to reconsider the functional contribution of both pathways to voluntary locomotion. Thus, the new models of striatal functions revolve around the ability of the direct pathway to promote one selected motor plan, whereas the indirect pathway is simultaneously activated in order to suppress concurrent motor plans (Gerfen, and Surmeier 2011; Calabresi, Picconi, et al. 2014; Cui et al. 2013).

More recently, an alternative pathway has been described within the basal ganglia. This pathway provides direct excitation from the cerebral cortex to the STN, leading to an excitation of the output nuclei of the basal ganglia, thus inhibiting the thalamus (Lanciego et al. 2012; Rocha et al. 2023). Thus, this "hyperdirect" pathway provides a short latency inhibition of the thalamus, contributing to the suppression of motor action (Chen, de Hemptinne, et al. 2020).

Consistently with the existence of these three parallel pathways with different numbers of relays and neurotransmitters, the stimulation of the motor cortex elicits a compound response in the pallidum (Nambu 2004). Indeed, three components can be observed while recording pallidal neurons following an electrical stimulation of the cortex: a short latency excitation, a subsequent inhibition and a longer latency excitation (Nambu, Yoshida, et al. 1990; Yoshida et al. 1993; Nambu, Tokuno, et al. 2000).

While an excitation of the pallidum could arise from an activation of the indirect pathway, the exquisitely short latency of the first excitatory volley is incompatible with the length of the indirect pathway, where an excitation of D2 MSNs in the striatum can cause an inhibition of the GPe, leading to a disinhibition of the STN and ultimately an excitation of the GPi. Instead, this response was proposed to be carried by the hyperdirect pathway (Nambu, Takada, et al. 1996), where cortical projections directly excites the STN, leading to an activation of the GPi. Thus, the hyperdirect pathway acts in parallel of the indirect pathway, with a shorter latency for information transfer.

The subsequent inhibition of the pallidum has been proposed to be mediated by the direct pathway, both being consistent with the existence of a cortico-striato-pallidal pathway, and with the fact that the latency observed is compatible with cortico-striatal conduction time (Yoshida et al. 1993). This idea is supported by the fact that blocking cortico-striatal transmission is sufficient to abolish this inhibition (Maurice et al. 1999), further suggesting that the striatum is required for this pattern of activity to occur.

However, the late pallidal excitation observed following cortical stimulation may originate from multiple parallel pathways. Indeed, it could very well be mediated by the indirect pathway, as suggested by the late increase in SNr neurons firing observed in these conditions (Maurice et al. 1999), but also involve the hyperdirect pathway (Nambu, Tokuno, et al. 2000). Altogether, these observations suggest a parallel contributions of the hyperdirect, direct and indirect pathways to the regulation of basal ganglia functions.

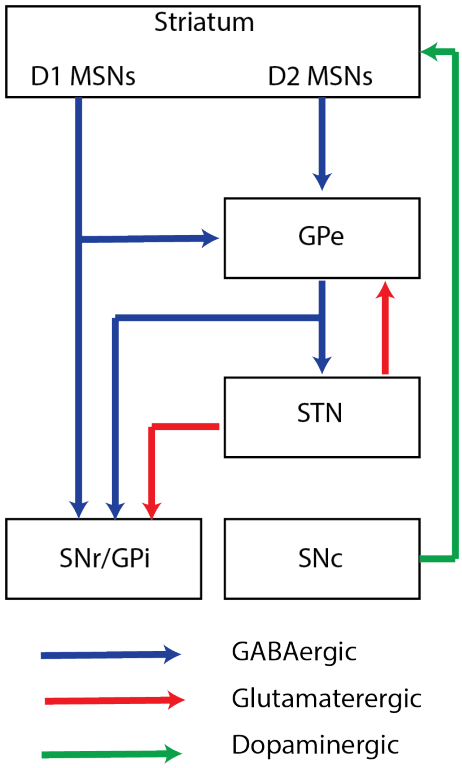

Figure 1.8: Neuronal circuits in the basal ganglia. Simplified schematic of the basal ganglia, with the striatum containing D1R expressing medium spiny neurons (D1 MSNs) and D2R expressing medium spiny neurons (D2 MSNs), the external globus pallidus (GPe), the internal globus pallidus (GPi), the subthalamic nucleus (STN), the substantia nigra pars reticulata (SNr) and pars compacta (SNc). GABAergic projections are represented by blue arrows, glutamatergic by red arrows and dopaminergic by green arrows.

Functions of the basal ganglia

The idea that the basal ganglia contribute to motor control dates as far back as the first histological descriptions of the lesions associated to Parkinson's Syndrome, where the Snpc is completely devoid of its natural pigmentation, suggesting that the neuronal degeneration in this region contributes to the physiopathology of this motor disorder.

Most models of the basal ganglia rely on the duality between the direct and the indirect pathways and claim that the direct pathways promotes a motor plan while the indirect pathway inhibits competing motor programs, thus producing the focused release of the selected motor program (Mink, and Thach 1993; Mink 1996).

Not only do the the basal ganglia participate to the process of action selection, but their activity is also necessary for movement execution (Park et al. 2020). Indeed, many studies have shown that neuronal activity of both D1 and D2 MSNs correlate with movement speed, which could be relatively well decoded from population activity (Barbera et al. 2016). Moreover, the neurons in the basal ganglia, particularly in the striatum, display a degree of tuning to the kinematics of the movement, and perturbing its activity during movement alter the parameters of the movement (Pimentel-Farfan et al. 2022). This suggests that the basal ganglia not only contribute to action selection, but also to the tuning of an ongoing action through the modulation of movement parameters such as vigor.

Similarly, the basal ganglia also play a critical role in the organization of sequences of actions (Jin et al. 2015), further indicating that the basal ganglia contribute to voluntary motor control at different timescales, being involved in the organization of motor sequences, in the initiation of an action and in the tuning of the ongoing movement.

The discovery of the hyperdirect pathway has led to an incentive to reconsider the functions of cortical projections to the basal ganglia (Nambu 2004). Indeed, cortico-striatal transmission is deemed to be slow, which in addition to the number of intermediate relays comprised in both direct and indirect pathway results in tremendous transmission latencies between the cortex and the output of the basal ganglia. However, the hyperdirect pathway can activate the STN with short latencies, which directly excites the output nuclei of the basal ganglia. Thus, an updated model of the interactions between the cortex and the basal ganglia was proposed (Nambu 2004).

In this model, the preparation of a voluntary movement leads to a corollary

transmission of the motor plan to the STN, which excites the GPi. Simultaneously, this motor plan is sent to a particular population of D1 MSN, allowing the selection of the optimum motor plan, and the repression of competing motor plans through the indirect pathway. Thus, the convergence of these three pathways at the level of the GPi/SNr leads to the robust selection, execution and termination of one motor plan.

However, it should be noted that these models heavily rely on interactions between the motor cortex and the basal ganglia, without considering other actors such as the cerebellum and other subcortical motor centers.

1.2.1.3 Cerebellar interactions with the motor cortex and the basal ganglia

Cerebello-basal ganglia interactions

For an extended period of time, the potential drive of the cerebellum on the basal ganglia was neglected, as little to no evidence was associated to a short latency modulation of the basal ganglia by cerebellar stimulations. Instead, the stimulation of the dentate nucleus of the cerebellum in anaesthetized cats produces a long latency responses in the pallidum, in the range of 50 to 300ms (Li, and Parker 1969), even suggesting that the cerebellum could have an indirect modulation of the activity in the basal ganglia.

However, the development of trans-synaptic viral tracing has allowed for the identification of disynaptic communication pathways between the cerebellum and the basal ganglia (Hoshi et al. 2005; Bostan, Dum, et al. 2010). Indeed, the dentate nucleus projects to the striatum using the centro-lateral nucleus (part of the intralaminar thalamus) as a synaptic relay (Hoshi et al. 2005; Ichinohe et al. 2000), while the STN sends projections to neurons in the pontine nuclei innervating the cerebellar cortex via the mossy fiber system (Bostan, Dum, et al. 2010). This confirms that the cerebellum and basal ganglia are reciprocally interconnected through relatively short oligo-synaptic pathways.

The existence of these anatomical connections suggests that the cerebellum could exert a short latency modulation of the activity in the basal ganglia, which has been later confirmed by extracellular recordings in the dorsolateral striatum performed along stimulations of the dentate nucleus of the dentate nucleus (Chen, Fremont, et al. 2014). In this study, both electrical and optogenetic stimulation of neurons in the dentate nucleus elicited short latency responses in DLS neurons, including excitation,

inhibition and sequential excitation followed by a pause (Chen, Fremont, et al. 2014). The disynaptic nature of these responses was confirmed by local infusions of TTX in the CL and in the cerebral cortex, which respectively abolished and did not alter the responses (Chen, Fremont, et al. 2014), suggesting that they were mediated by a cerebello-thalamo-striatal pathway using CL as a relay. Strikingly, while the application of high frequency stimulations (HFS) to the motor cortex mainly induces a LTD in cortico-striatal transmission, the pairing of cerebellar HFS (in the dentate nucleus) with cortical HFS leads to a LTP of cortico-striatal transmission. This is consistent with the recent discoveries revealing that striatal plasticity can be directed by the interactions between cortical and thalamic inputs (Mendes et al. 2020), and suggests that the cerebellum can not only modulate the activity in the DLS, but also alter its plasticity.

More recent evidence suggests that the parafascicular nucleus of the thalamus is a strong relay in cerebello-striatal communication, in conjunction with the centrolateral nucleus (Xiao et al. 2018) and possibly the VAL (Contreras-López et al. 2023).

Cerebello-cortical interactions

As described previously on the section regarding cerebellar outputs, the most direct pathways originating from the cerebellum and reaching the cortex mainly rely on thalamic nuclei as relays. In the case of the primary motor cortex and the secondary motor areas, the main nuclei contributing to these pathways are the contralateral ventrolateral thalamus (Teune et al. 2000; Middleton et al. 1997; Alonso-Martínez et al. 2023) and the ventromedian thalamus (Gao, Davis, et al. 2018; Zhu et al. 2023).

Glutamatergic projection neurons from the cerebellar nuclei send dense projections to the excitatory zone of the VAL (Alonso-Martínez et al. 2023), which projects to the layer II/III and layer V of M1 (Kuramoto, Furuta, et al. 2009).

Strikingly, a recent study demonstrated that the cerebellar nuclei also innervates the inhibitory part of the VAL (Alonso-Martínez et al. 2023), suggesting it to be a potential interaction point between basal ganglia and cerebellar inputs. Thus, the cerebellum could support or override the inhibitory control that the pallidum exerts over the motor thalamus.

While the ventrolateral thalamus preferentially targets motor, premotor and so-

matosensory regions (Hunnicutt et al. 2014), the ventromedian thalamus targets a wider set of cortical areas, including frontal and prefrontal areas (Kuramoto, Ohno, et al. 2015), with which it can form reciprocal connections (Gao, Davis, et al. 2018; Guo, Yamawaki, et al. 2018). Critically, it targets the anterior lateral motor cortex (ALM), a secondary motor area, and supports the existence of a communication pathway between the fastigial nucleus (FN) of the cerebellum and the ALM (Gao, Davis, et al. 2018). Both the FN and the ALM have been shown to be involved in motor planning, as preparatory activity could be observed in these structures prior to movement onset (Gao, Davis, et al. 2018). More importantly, generating an optogenetic perturbation of FN activity during the preparatory phase of the movement leads to a decrease in performance in a sensorimotor discrimination task without altering the movement itself, and is associated to altered neural dynamics in the ALM (Gao, Davis, et al. 2018), suggesting that cerebellar activity is critical for the persistence of cortical activity before movement onset.

Interestingly, cerebello-cortical and striato-cortical circuits may not be completely independent, as it was shown that the cerebellar nuclei and the pallidum target similar cortical areas using VAL as a relay (Jinnai et al. 1993). Although the lamination projections patterns of the excitatory and inhibitory zone of the VAL differ in the cortex (Kuramoto, Furuta, et al. 2009), it suggests potential interactions between cerebellar and basal ganglia inputs at the level of the motor cortex, where they are integrated.

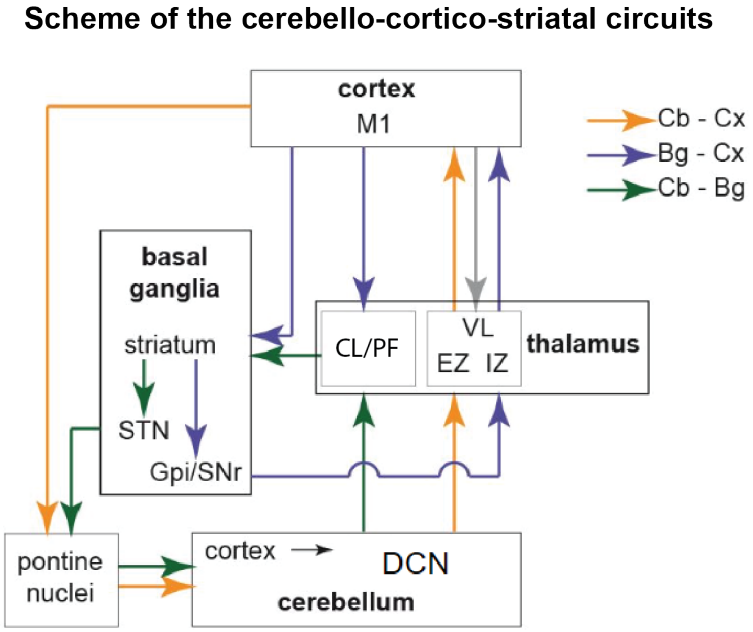

Figure 1.9: Cerebellum, striatum and motor cortex are connected through oligosynaptic loops. Schematic representation of the neuronal circuits linking the cerebellum, striatum and motor cortex through segregated thalamic compartments. The cerebello-cortical loop is represented by orange arrows, the striato-cortical loop by purple arrows and the cerebello-striatal loop by green arrows.

1.2.2 Motor learning

Motor learning can be defined as the ensemble of processes related to the repetition of an action that lead to long-lasting changes in the ability to perform this action (Seidler 2010). The support of volontary motor function requires not only a functional motor system, but perceptive and proprioceptive abilities are essential as well. However, the concept of motor learning focuses on the optimization of the motor output, which is what sets it apart from more sensory-driven tasks (Krakauer et al. 2019).

When a situation urges a subject to perform an action, the motor system will sequentially create a motor goal, then select the proper sequence of movement to perform, and finally execute the action (Krakauer et al. 2019). Any motor learning process is likely to act on one or more of these components in order to optimize the motor output (Krakauer et al. 2019).

1.2.2.1 The different components of motor learning

Most motor skill learning tasks will engage two different components: sequence learning and motor adaptation (Seidler 2010; Krakauer et al. 2019).

Sequence learning

Sequence learning refers to the process through which single isolated actions are concatenated into a continuous, smooth motor output (Seidler 2010) necessary to achieve the motor goal. If we were to make a sports-related analogy, this process is needed to acquire the ability to serve in a tennis match. Although the tennis serve movement seems smooth and almost unitary, it is constituted of several smaller movement units, pieced together into a seamless action.

The contribution of cerebellum to sequence learning is much less clear than its contribution to motor adaptation (Krakauer et al. 2019). Although several studies have shown an activation of the cerebellum during sequence learning tasks (Jenkins et al. 1994; Grafton et al. 2001; Orban et al. 2010), the extent to which cerebellum contributes to sequence learning remains disputed (Krakauer et al. 2019).

Motor adaptation

In contrast, motor adaptation refers to the modifications of the original motor plan based on the occurrence of external events. These events induce changes in sensory inputs, which are integrated and lead to an update of the motor output (Seidler 2010). The need for adaptation arises from the inability to reach the motor goal by expressing an already well-learned sequence. Thus, instead of building a completely new motor controller from scratch, a previously learned sequence is adapted on the fly (Krakauer et al. 2019). To use the previous tennis serve analogy, changing tennis racket with a lighter or a heavier one will lead to an erroneous position of the tennis racket during the movement, which will trigger a fast and smooth recalibration in order to reach the movement goal.

Experimentally, motor adaptation is usually investigated by introducing a perturbation in a goal directed task (King et al. 2013), which can be made in form of visuomotor distortions (Kagerer et al. 1997) or mechanical perturbations (Shadmehr, and Mussa-Ivaldi 1994). These perturbation induce a deviation from the predicted sensory state of the system, and urge the subject to provide an adapted answer

to correct its movement. A implicit assumption in motor adaptation is that the motor program remains intact and that the adaptation is performed by a separate, subsidiary system.

In opposition to sequence learning, the contribution of the cerebellum to motor adaptation is very well characterized (Krakauer et al. 2019), particularly through the study of visuomotor adaptation (Bernard et al. 2013; Tzvi et al. 2022).

Inducing lesions of the cerebellum in monkeys impairs the ability to adapt eye saccades during a visuomotor adaptation task (Barash et al. 1999). This phenomenon is also visible in patients suffering from cerebellar alterations, as they display tremendous deficits in visuomotor adaptation (Morehead et al. 2017). Disruptions of the cerebellum not only creates deficits in visuomotor tasks, but also in other forms of motor adaptation, such as force-field adaptation (Criscimagna-Hemminger et al. 2010; Gibo et al. 2013; Maschke et al. 2004) and locomotor adaptation (Morton et al. 2006). Moreover, these phenomena are highly consistent with the idea that the cerebellum implements internal forward models, used to predict the sensory consequences of motor actions at short timescales in order to achieve optimal motor control (Krakauer et al. 2019).

In contrast, the motor cortex and the basal ganglia are relatively less involved in motor adaptation (Krakauer et al. 2019). Indeed, perturbing the motor cortex during motor adaptation tasks usually doesn't impair motor adaptation per se, but seems to rather influence its retention (Krakauer et al. 2019; Galea et al. 2011; Herzfeld, Pastor, et al. 2014). Similarly, patients suffering from pathologies altering basal ganglia functions tend to display normal motor adaptation (Krakauer et al. 2019) but reduced retention (Marinelli et al. 2009; Bédard et al. 2011).

1.2.2.2 Dynamics of motor learning

Different algorithms for motor learning

While the cerebellum, the motor cortex and the basal ganglia contribute to both motor control and motor learning, they were theorized to implement vastly different learning algorithms (Doya 1999).

In the case of the cerebellum, the modular organization of the cerebellar cortex, coupled with the fact that the climbing fiber signal seems to drive error-driven learning in Purkinje cells lead to models stating that the cerebellum primarily implements a supervised learning algorithm (Marr 1969; Ito 1983; Albus 1971; Doya

1999)[. This aspect of cerebellar function as been extensively studied, specially in the context of eye-blink conditioning (Ito 1983; ten Brinke et al. 2017), and is consistent with the involvement of the cerebellum in motor adaptation where the climbing fibers propagate a directional error routed to the Purkinje cells suitable to correct the error (Herzfeld, Vaswani, et al. 2014; Herzfeld, Pastor, et al. 2014; Yang et al. 2017).

The cerebral cortex, on the other hand, has a high degree of recurrent connectivity (Douglas et al. 1991; Douglas et al. 2004; Harris, and Shepherd 2015), primarily uses Hebbian rules to update synaptic weights (Artola et al. 1990), and receives a wide variety of inputs. This suggests that the cortex can refine its representation of the outside world using an unsupervised learning algorithm (Doya 1999).

On the other hand, the basal ganglia are thought to implement a reinforcement learning algorithm (Doya 1999). This is supported by the neuronal dynamics of dopaminergic neurons in the substantia nigra, which show a phasic increase in firing at the delivery of an unexpected reward, or during the presentation of a stimulus associated to the reward, and a phasic decrease at the omission of an expected reward (Schultz et al. 1993; Schultz 1998). Thus, the dopaminergic inputs of the striatum originating from the substantia nigra encode reward prediction error (Montague et al. 1996; Schultz 1997).

The multiple timescales of motor learning

Motor learning is an heterogeneous process, occurring at different timescales (Krakauer et al. 2019; Karni et al. 1998). Indeed, the study of functional activity related to motor learning reveals that there is a dynamic representation of the learned task, involving different brain areas depending on the timing.

Thus, motor learning sequentially involves the acquisition of a skill, which occurs relatively fast and is followed by a longer lasting consolidation.

1.2.2.3 Neural basis of motor learning consolidation

Among the many factors influencing the consolidation of motor learning, sleep seems to be of a great importance. Indeed, sleeping between training sessions affects both savings (a form of motor memory which allows for faster re-learning in later attempts) and offline gains in motor learning (King et al. 2013). This sleep-dependent phenomenon can be triggered by night-time sleep, as well as by a day-time nap,

inducing a significant increase in offline learning and in the resistance to potential interferences (Walker, Brakefield, Hobson, et al. 2003; Walker 2008; Walker, Brakefield, Morgan, et al. 2002; Walker, and Stickgold 2006; Korman et al. 2007; Nishida et al. 2007; Doyon, Korman, et al. 2009). Several neuronal mechanisms have been proposed to explain this process, including particular rhythms occurring during sleep, and synchronous reactivations of patterns associated to the learned task, called "replays".

Sleep spindles

Functionally, these offline gains in motor learning seem to be related to the stage II of sleep, also referred to Non Rapid Eye Movement sleep (NREM) (Fogel et al. 2007), as well as to the occurrence of sleep spindles (Nishida et al. 2007; Morin et al. 2008; Barakat, Doyon, et al. 2011). Sleep spindles are activity patterns manifesting as short bursts of oscillatory activity in the range of 12 to 16Hz (Steriade 2006; Buzsáki 2006; Timofeev, and Chauvette 2013), occurring during NREM sleep, and thought to involve an interplay between the cerebral cortex and the thalamus (Buzsáki 2006; Bonjean et al. 2011; Fernandez et al. 2020), notably involving the reticular thalamus to create an inhibitory volley following the sequences of activations (Timofeev, and Chauvette 2013).

Although the functional role of sleep spindles is still not clearly understood, they have been associated to motor learning in different occasions (Fernandez et al. 2020). Indeed, the frequency of occurrence of sleep spindles, as well as their duration, increase following motor learning (Fogel et al. 2007; Morin et al. 2008; Barakat, Doyon, et al. 2011). This increase in spindle density was shown to be directly correlated to overnight improvement in performances following motor sequence learning (Barakat, Doyon, et al. 2011).

Interestingly, the correlation between spindle density and learning rate is not only observable during night-time sleep, but also during naps performed in daytime (Nishida et al. 2007), suggesting that the role of sleep spindles in memory consolidation doesn't require a full night of sleep, and can be engaged even during resting periods in-between training.

In addition, the amplitude of sleep spindles was revealed to be correlated with the overnight learning gain (Barakat, Carrier, et al. 2013), and to be associated with increased BOLD signals in motor areas such as the M1 and the striatum (Barakat, Carrier, et al. 2013). This suggests that sleep spindles can activate several motor-

related brain regions. Strikingly, a recent study revealed that spindles recorded in M1 propagate to the striatum, where they can entrain local neuronal activity (Lemke et al. 2021). More importantly, pairs of cortical and striatal neurons entrained by cortical spindles would display maintained connectivity, whereas pairs that were not entrained would rather display a decreased connectivity (Lemke et al. 2021). This, in addition to the fact that spindle entrainment was also linked to an overnight increase in coherence in the theta band (Lemke et al. 2021) suggests that sleep spindles influence functional connectivity in the motor network during motor learning.

Although spindles are oftentimes detected in cortical areas and have been shown to propagate the striatum, the mechanism underlying their generation and maintenance is still under debate. In the classical model of spindle generation, an hyperpolarized reticular thalamus receives an excitatory volley leading to a low threshold calcium channel-dependent burst of activity, creating a succession of inhibition and rebound bursting in thalamo-cortical neurons (Timofeev, and Chauvette 2013). In this framework, spindles are purely initiated and maintained in the thalamus, and just propagate to cortical network through thalamo-cortical projections. However, the involvement of cortical areas doesn't seem to be restricted to a passive modulation by the thalamus, as they have been proposed to drive the onset of the spindle activity through cortico-thalamic projections (Timofeev, Bazhenov, et al. 2001), and to even be able to potentiate spindle activity (Contreras et al. 1996) and determine the spindle duration (Bonjean et al. 2011).

Knowing that the cerebellum is heavily connected to the thalamus through which it can affect the activity in the cerebral cortex, and that it receives inputs from the cortex through the pontine nuclei, the cerebellum could very well be entrained by spindle activity and in return modulate it through cerebello-thalamic projections. However, to this day little is known on the relationship between the cerebellum and cortico-thalamic spindles. A recent study in monkeys revealed dynamic interactions between the cerebellum and the motor cortex during cortical spindles (Xu, De Carvalho, Clarke, et al. 2021). Indeed, not only the spiking activity from cerebellar Purkinje cells displays high spike-field coherence with the LFP from M1 in the spindle range (10-16Hz), but spikes from M1 also display high spike-field coherence with cerebellar LFP in the same range (Xu, De Carvalho, Clarke, et al. 2021), which reveals a potential mutual entrainment of the cerebellum and M1 during spindle-like activity. Furthermore, the directed coherence between the local field potentials of M1 and cerebellar cortex is higher in the direction from cerebellum to M1 in the spindle range compared to the M1 to cerebellum direction, suggesting

that the frequency of spindle activity of the cortex is controlled to some extent by the cerebellum through the thalamus (Xu, De Carvalho, Clarke, et al. 2021)].

Replays

In the context of his memory formation model, Buzsaki predicted that sharp-wave ripples would be associated to sequential replay of neuronal activity after training (Buzsáki 1989). Subsequently, the first observations of the replay of neuronal firing sequences during sleep was performed in the hippocampus of rats, where place cells that underwent concomitant firing during wake were reactivated during sleep in a similar fashion (Wilson et al. 1994; Skaggs et al. 1996). These reactivations of ensembles reflect changes in the functional connectivity in the hippocampal network (Wilson et al. 1994; Skaggs et al. 1996).

Knowing that the population of place cells in the hippocampus exhibit attractor dynamics where individual neurons fire when the animal is at a particular position during spatial exploration, these sequences of activation reflect the different trajectories that the animal explored before sleep (Lee, and Wilson 2002), and where even shown to mimic relatively long trajectories, being then labelled as "extended replays" (Davidson et al. 2009).

In the hippocampus, replays of activity arise concomitantly with events called sharp wave ripples (Wilson et al. 1994; Davidson et al. 2009), which corresponds to bursts of high frequency oscillations ($>$ 100Hz) in the local field potential. Nested within sharp wave ripples, these replays of neuron firing can occur in the same order as the sequence experienced during wake ("forward replays") or occur in reverse order (Foster, and Wilson 2006), being called "reverse replays".

Strikingly, the selective disruption of hippocampal ripple activity during sleep, which is known to be associated to replays of neuronal activity in the hippocampus following spatial learning, was shown to reduce the learning rate in a spatial learning task (Ego-Stengel et al. 2010; Girardeau, Benchenane, et al. 2009). During episodes of sharp wave ripple activity, the electrical stimulation of the ventral hippocampal commissure, containing afferences from the CA3 to the CA1 region of the hippocampus, leads to a transient interruption of neuronal activity in the CA1 as well as a perturbation of the ripple activity (Ego-Stengel et al. 2010). Indeed, both the amplitude of the ripple and the frequency of subsequent ripples is decreased, together with a complete nullification of the firing rate during the following hundreds of milliseconds (Ego-Stengel et al. 2010). Because neuronal activity is silenced during sharp-wave ripples, the occurrence of subsequent sequential replays of neuronal

activity is prevented. The fact that this perturbation leads to a decreased learning rate is an indication that replays occurring during sharp wave ripples directly contribute to the consolidation of memory.

Although discovered in the hippocampus, replays of activity are not restricted to hippocampal networks. Indeed, coordinated replays have been observed between the hippocampus and other structures, such as sensory cortices (Ji, and Wilson 2007), the amygdala (Girardeau, Inema, et al. 2017). During a spatial exploration task, not only replays could be observed in the visual cortex (Ji, and Wilson 2007), they could happen simultaneously in the cortex and in the hippocampus, reflecting similar trajectories. Similarly, following the exposure to a task combining spatial navigation and the delivery of an aversive stimulus at a given place, pairs of neurons in the hippocampus and in the basolateral amygdala which were activated during the task tend to be reactivated, mostly during hippocampal ripples (Girardeau, Inema, et al. 2017).

Replays can also arise in motor areas, as Xu et al observed that neurons in the primary motor cortex of non-human primates would undergo patterns of reactivation similar to the neuronal sequences expressed during freely moving behaviour (Xu, de Carvalho, et al. 2019). The fact that replays of sequences associated to previously performed motor actions occur in the motor cortex during sleep raises the question of the involvement of such reactivations in the consolidation of a motor skill.

And indeed, sequential reactivations of neurons during resting were observed following the learning of motor sequences (Eichenlaub et al. 2020; Rubin et al. 2022). Recent studies performed in humans revealed that the neuronal activity corresponding to previously learned sequences would be replayed in the motor cortex during sleep (Eichenlaub et al. 2020; Rubin et al. 2022). These replays are nested in cortical ripples, and were shown to potentially occur in a compressed manner, with sequences 1 to 4 faster than during wake (Rubin et al. 2022). Interestingly, a recent study has observed that not only replays can arise during inter-trials resting periods, but also that their frequency was positively correlated to inter-trials change in performance (Buch et al. 2021).

All together, these results suggest that replays of neuronal activity are present in the motor cortex in the resting periods following motor learning, and that they could contribute to the offline consolidation of a motor skill. However, whether these replays have functional consequences on the motor networks remains unknown. Similarly, the mechanisms through which they can actively contribute to motor learning remains a mystery.

The contribution of the cerebellum to offline consolidation

The evidence suggesting that the cerebellum could be involved in memory consolidation of motor skill learning are scarce. A recent study revealed that muscimol infusion in the ventro-medial cerebellum after exposing rats to a Morris water maze task induced an impairment during the following days, suggesting that the cerebellum could play a role in the consolidation of spatial memory (Andre et al. 2019). However, little evidence suggest that the cerebellum contributes to the offline consolidation of motor learning, although cerebellar-dependent motor skills are shown to undergo offline consolidation (Shadmehr, and Holcomb 1997; Cohen et al. 2005; Doyon, Korman, et al. 2009; Muellbacher et al. 2002; Nagai et al. 2017). Strikingly, cerebellar transcranial direct current stimulation was shown to be able to improve the offline consolidation of a motor learning (Samaei et al. 2017).

Interestingly, a wide body of literature suggest that the offline consolidation of motor learning is supported by multi-structures coordinated events, such as sleep spindles and activity replays. However, as of today, little is known on the extent to which replays could arise in broad systems such as the motor network. Indeed, although the cerebellum is reciprocally connected to the motor cortex, in which replays were observed, no evidence of activity replays in the cerebellum during sleep was observed before. In addition, although sleep spindles were observed in the cerebellum, the role of these cerebellar spindles and whether they can affect cerebellar connectivity with the motor network remains unknown.

In conclusion, even though the cerebellum has the potential to be involved in many mechanisms underlying the consolidation of a learned motor sequence, little is known on whether it is the case and to which extent the cerebellum is necessary for it.

Thus, we sought to determine whether the cerebellum could contribute to the learning and the offline consolidation of a complex motor skill, the accelerating rotarod.

1.2.3 Pathologies of the motor system

Dysfunctions of the motor system can arise at different nodes of the network, leading to the expression of various motor disorders depending on the pathophysiological mechanisms associated with them. Thus, these motor disorders can appear in a wide variety.

1.2.3.1 The hypothesis of focal pathophysiology

For the most part, the study of the pathophysiology of a motor disorder starts by the search for a visible alteration in the brain tissue of a particular area. This approach was critical for the early functional characterizations of many brain areas, such as the motor cortex or the basal ganglia.

However, this oftentimes leads to the belief that the site of neuronal degeneration was the sole contributor to the pathology. Thus, most motor disorder are classically associated to one particular brain region.

Cerebellar pathologies

Pathologies arising from alterations of cerebellar networks are numerous (KOEPPEN 2018), however their symptomatology share characteristics which can be attributed to the more general "cerebellar syndrome" (Bodranghien et al. 2016). Indeed, cerebellar dysfunction causes a myriad of symptoms, mainly motor-related, the characterization of which significantly contributed to our understanding of cerebellar functions. This includes ataxia, dysmetria, dysarthria, nystagmus and intention tremor.

The cerebellar cortex can undergo degeneration, either from hereditary causes or sporadically (KOEPPEN 2018). This is the case in spinocerebellar ataxia (SCA), a group of hereditary neurodegenerative disorders displaying autosomal dominant inheritance (Sullivan et al. 2019).

Many forms of SCA, in particular the heavily prevalent SCA1, SCA2, SCA3, SCA6 and SCA7, involve the erroneous expansion of CAG triplets within a gene. These mutations lead to the expression of a toxic polyglutamine protein (Paulson et al. 2017), a mechanism shared with Hungtington's chorea. Each of these mutations causes neurodegeneration in different targets (Paulson et al. 2017). For example, while degeneration of the Purkinje cells, cerebellar nuclei, pontine nuclei and inferior olive can be observed in SCA1 and SCA3, SCA6 mainly targets Purkinje cells (KOEPPEN 2018). Patients suffering from SCAs mainly exhibit a typical association of symptoms including gait ataxia, poor coordination in movement execution, nystagmus and dysarthria (Paulson et al. 2017). However, depending on the SCA form, additional symptoms have been observed, including pyramidal and extrapyramidal syndromes, as well as cognitive impairments (Paulson et al. 2017), which indicates that certain symptoms of SCA can involve extra-cerebellar alterations.

Similarly to SCAs, Friedreich ataxia is a common neurodegenerative disorder with a strong impact on the cerebellum and the spinal cord (Koeppen 2011; Bürk 2017). This ataxia is caused by the mutation of the frataxin gene, coding for a mitochondrial protein involved in iron metabolism (Clark et al. 2018). A deficiency in this protein leads to an iron overload within the mitochondria, which in terms alters energy production and promotes neuronal degeneration through the accumulation of reactive oxygen species (Koeppen 2011)(Koeppen 2011; Bürk 2017; Clark et al. 2018). This neurodegeneration primarily targets the dentate nucleus of the cerebellum and the superior cerebellar (Koeppen 2011), suggesting that many symptoms are due to an aberrant cerebellar output. Consistently with this, patients suffering from Friedreich ataxia usually exhibit typical cerebellar symptoms such as dysarthrian, progressive limb and gait ataxia, but also absence of tendon reflexes, sensory neuropathy, weakness, spasticity and alterations of proprioception and pallesthesia (Clark et al. 2018).

In addition, the cerebellum can be the target of many lesions, including traumatic lesions, vascular embolism or haemorrhage, or can degenerate in the context of paraneoplasic cerebellar degeneration (KOEPPEN 2018). Similarly, the cerebellum is sensitive to hypoxia during development, hypoglycemia, and toxins such as ethanol and mercury (KOEPPEN 2018).

Motor cortex pathologies

Studying the effect of lesions in the motor cortex allows to highlight strong differences between species. Indeed, while lesions in the motor cortex in humans lead to dramatic consequences, the results are more mitigated in other species (Lopes et al. 2023).

In humans, strokes or injuries located in the motor areas of the neocortex are followed by weakness or paralysis in the limbs controlled by the injured territory, corresponding to the matching body part on the motor cortex homunculus on the contralateral side of the lesion (Louis 1994). These symptoms are long lasting, even though a partial recovery is possible (Laplane et al. 1977; Kwakkel et al. 2003; Lopes et al. 2023). Most of the time, the paralysis and flaccidity of the affected limb will remain (Kwakkel et al. 2003).

In the case of non-human primates, the acute effects of cortical lesions also include weakness and paralysis, but they are usually transient and undergo fast recovery (Leyton et al. 1917; Travis 1955). The only type of movement impaired in

the long-term are the precise movements of distal limbs, particularly involving dexterous finger motions (Leyton et al. 1917), whereas walking, climbing and grasping are recovered (Leyton et al. 1917).

The differences with humans become even deeper when comparing the effect of cortical lesions in non-primates mammals, such as rodents. Indeed, long-lasting effects of such lesions are usually not reported, and only impairments of motor learning are observed (Kawai et al. 2015).

These diverging observations between species suggest that the organization and function of motor circuits may be different in humans compared to other mammals, with the human heavily relying on the cortical functions needed for dexterous movements, while other primates and rodents can rely more on subcortical circuits in order to achieve voluntary motor control.

Amongst the motor pathologies associated to anomalies of the motor cortex, the case of the amyotrophic lateral sclerosis (ALS) is particularly interesting. Patient suffering from ALS exhibit a variety of symptoms, including twitching, cramps, loss of motor control, fatigue, and may worsen to reach muscular paralysis (Masrori et al. 2020). Often-times, the onset of the disease is focal but becomes generalized later.

Although cortical alterations are consistently described in the ALS (Eisen et al. 2001), the contribution of these alterations to the pathophysiology of the disease is not fully elucidated, as they have been proposed to be either causal to the onset of the disease or just a mere consequence of the degeneration of spinal neurons that would propagate retrogradely to the cortex. In the ALS, the primary motor cortex is found to be hyper-excitable (Eisen et al. 2001), which is proposed to trigger glutamate-induced excitotoxicity in downstream neurons and to lead to the cortico-spinal degeneration (Eisen et al. 2001). Given the early appearance of increased cortical excitability and the late spinal degeneration, this anterograde cortic-spinal propagation hypothesis is favoured over the retrograde propagation.

Alzheimer's disease, a pathology associated to alterations in the cerebral cortex, is mainly known for its non-motor symptoms affecting cognitive functions. However, physiological alterations of the motor cortex have also been observed in this disease, with an higher excitability of the motor cortex, correlated with the severity of the cognitive symptoms (Zadey et al. 2021). Strikingly, there is increasing evidence of subtle motor dysfunctions associated to this pathology (Vidoni et al. 2012; Koppelmans et al. 2022), further highlighting the contribution of alterations of the motor cortex to pathological motor control.

Pathologies of the basal ganglia

Dysfunction of the basal ganglia has been associated to multiple motor disorders, including the parkinsonian syndrome, chorea-ballism and dystonia (Lanciego et al. 2012).

The parkinsonian syndrome is probably the best characterized disorder of the basal ganglia. Patients suffering from this syndrome exhibit a key set of symptoms, which includes hypokinesia, bradykinesia, extrapyramidal rigidity and resting tremors (Lanciego et al. 2012; Williams et al. 2013; Poewe et al. 2017). While hypokinesia corresponds to a defect in movement initiation, bradykinesia is related to a decreased movement speed. Thus, besides the resting tremors, parkinsonian syndrom is characterized by a poverty in voluntary movements execution. In its most prevalent form, Parkinson's disease, the lack of movement initiation and slowness are linked to a depletion of striatal dopamine following the degeneration of the nigro-striatal dopaminergic neurons in the substantia nigra (Poewe et al. 2017). This neurodegeneration in the basal ganglia is thought to be caused by a cytotoxic accumulation of α-synuclein, which aggregates with other proteins and form Lewy bodies.

Knowing that dopamine exerts an opposite control on the activity of striatal MSNs, this depletion of dopaminergic inputs is believed to decrease the activity of the D1R expressing MSNs, while increasing the activity of the D2R expressing MSNs. This creates an imbalance between the direct and indirect pathways, promoting the movement-suppressing indirect pathway leading to the hypokinesia and the bradykinesia (McGregor et al. 2019). Interestingly, MSNs from the indirect pathway have been shown to be entrained by beta oscillations, a pattern of brain oscillations known to be excessively expressed in Parkinson's disease and correlated with immobility (Sharott et al. 2017).

The imbalance of activity in striatal MSNs propagates downstream and leads to an erratic neuronal activity reported in the GPe (Soares et al. 2004), STN (Bergman et al. 1994; Benazzouz et al. 2002), GPi (Miller et al. 1988; Muralidharan et al. 2016) and finally to the motor cortex (Pasquereau, and Turner 2011; Pasquereau, DeLong, et al. 2016; McCairn et al. 2015) where the activity and the tuning to movement are altered. This suggests that even though the core of the physiopathology of Parkinson's disease is due to a degeneration of the basal ganglia, the resultant aberrant activity is propagated in the rest of the motor network.

1.2.3.2 Network disorders: the example of dystonia

As discussed before, most of the motor disorders are usually associated to the dysfunction of one particular structure, as it is the case for the previously mentioned parkinsonian syndrome and dystonia for instance. However, the case of dystonia is particularly interesting, as even though it is mainly presented as a pathology originating from a dysfunction of the basal ganglia, it is highly heterogeneous, in terms of aetiology and characteristics of the disease (Balint et al. 2018).

Dystonia is a group of motor disorders characterized by excessive involuntary muscle contractions leading to abnormal postures and repetitive movements (Jinnah 2015).

Plurality of dystonic phenotypes

Strikingly, the possible phenotypes of dystonia are many, as these pathologies can be described regarding several criteria, including their body distribution, the temporal distributions of the dystonic attacks, the age of onset, and their aetiology.

In terms of body distribution, dystonia can be deemed generalized if it affects the multiple body parts, or otherwise focal. In the case of the latter, few body regions are most frequently described, including cervical dystonia targeting the neck, laryngeal dystonia affecting the vocal chords leading to impaired vocalizations, the relatively frequent blepharospasm leading to eyelid spasms, oromandibular forms of dystonia affecting the muscles of the jaw (Balint et al. 2018). In addition, focal forms of dystonia can also target the limbs, specifically in their distal parts. Focal dystonia is often-times reported to evolve, with some forms progressing towards a generalization of the symptoms, while some remain focal (Jinnah 2015).

Although the previously described forms of focal dystonia display persistent episodes of dystonic attacks, some forms of dystonia display different short-term variations (Jinnah 2015; Balint et al. 2018). Indeed, some forms of dystonia are action-specific, and their episodes of dystonic attacks are triggered only during the execution of particular actions (Quartarone, Siebner, et al. 2006; Jinnah 2015; Balint et al. 2018). Notably, this is the case for musician's dystonia (Sheehy et al. 1982; Conti et al. 2008; Horisawa, Taira, et al. 2013) and for writer's cramp (Sheehy et al. 1982; Tinazzi et al. 2005; Fukaya et al. 2007; Meunier et al. 2012). The main characteristic of these two forms of dystonia is that they arise from the over-training for one particular action, in these case playing a piano piece or writing with a pen. Once the pathology has set in, a simple attempt at executing this action or a simi-

lar movement triggers involuntary muscle contractions. This is consistent with the more recent view on dystonia, suggesting that this disorder involves an abnormal plasticity in the motor network (Quartarone, and Hallett 2013).

Maladaptive plasitcity

Altered plasticity is a common feature of hyperkinetic disorders, as long term depression seems to be absent or at least dysfunctional in pathologies such as Hungtington's disease, levodopa-induced dyskinesias and dystonia (Calabresi, Pisani, et al. 2016; Quartarone, Bagnato, et al. 2003; Quartarone, Rizzo, Bagnato, et al. 2005; Quartarone, Morgante, et al. 2008).

Specifically, a transcranial stimulation study has revealed that cortical plasticity is impaired in focal hand dystonia (Quartarone, Rizzo, Bagnato, et al. 2005). Healthy subject may display both signs of potentiation and depression following plasticity-inducing protocols, whereas patients suffering from cervical dystonia can only display signs of potentiation, suggesting that synaptic downscaling could be impaired in this dystonia. Moreover, healthy subjects display signs of homeostatic plasticity, which is the ability to revert a plastic change, and which is also impaired in dystonic patients (Quartarone, Rizzo, Bagnato, et al. 2005). Interestingly, this feature seems to be a hallmark of task-specific dystonia (Quartarone, Bagnato, et al. 2003; Quartarone, Siebner, et al. 2006), which is also associated with signs of abnormal potentiation, a lack of potential depression, as well as an impaired homeostatic plasticity. This may suggest that task-specific dystonia arises from a maladaptive plasticity following an over-training for a particular motor sequence (Quartarone, and Hallett 2013).

Genetic forms of dystonia

Although most cases of dystonia are classified as idiopathic, with no apparent cause underlying the apparition of the symptoms, patients can develop dystonia from different etiologies. This includes mutations of several key genes, leading to hereditary dystonia. To this day, many different hereditary dystonia have been discovered (Balint et al. 2018), each being caused by a mutation of a different gene.

The genes affected in these forms of dystonia are various and affect different cellular functions, and as consequence can lead to very different phenotypes, with variable ages of onsets, localization of dystonia and mode of hereditary transmission

(Balint et al. 2018).

Interestingly, as oftentimes described in the genealogical trees of families suffering from hereditary dystonia, being a carrier of a mutation does not necessarily result in the development of a dystonic phenotype (Hutchinson et al. 2013). This phenomenon is called incomplete penetrance, and highlights the fact that sub-threshold alterations can exist in absence of the full expression of the phenotype. Such alterations often provide cues on the direct functional consequences of the genetic mutations, which may be obscured once the pathology has set in and has produced multiple cascadic effects.

DYT25: an adult-onset hereditary dystonia

While most genetic causes of dystonia involve genes which can only be remotely linked to motor function, this is less the case for the DYT25 dystonia which is linked to mutations in the GNAL gene. The GNAL gene codes for the alpha subunit of a G-protein named Golf, an homologous protein to Gs, coupled to an adenylate cyclase stimulating the production of cyclic Adenosine MonoPhosphate (cAMP) (Jones, and Reed 1989; Zhuang et al. 2000; Corvol, Studler, et al. 2001; Hervé et al. 2001; Pelosi et al. 2017). While the Gs counterpart is widely distributed in the nervous system, the expression of Golf is more focal in the brain. It was originally observed in the neuro-epithelium of the olfactory system (Jones, and Reed 1989; Belluscio et al. 1998). However, its presence is not restricted to the olfactory bulb, and substantial expression is observed in other brain structures including mainly the striatum (and pyriform cortex), but also the cerebellum, where some sparse expression is present in the Purkinje cells of the cerebellar cortex (Belluscio et al. 1998; Vemula et al. 2013).

In the striatum, Golf is enriched in MSNs belonging to both direct and indirect pathways, where it completely replaces its homologous Gs (Drinnan et al. 1991; Herve et al. 1993; Hervé et al. 2001). Although it is evenly distributed between the two categories of MSNs, it is coupled to different receptors in these two populations. Indeed, MSNs belonging to the direct pathway express D1 dopamine receptors, to which Golf is coupled (Herve et al. 1993; Hervé et al. 2001; Corvol, Studler, et al. 2001). On the other hand, Golf is coupled to adenosine A2A receptors in MSNs from the indirect pathway, where it stimulates adenylate cyclase activity in response to adenosine (Hervé et al. 2001; Corvol, Studler, et al. 2001). Golf is also present in cholinergic interneurons of the striatum, along its homologous Gs (Hervé et al. 2001), where it may contribute to the signaling of D5 dopamine receptors and adenosine

A2A receptors (Yan et al. 1997; Tozzi et al. 2011). Thus, Golf is heavily involved in the regulation of striatal excitability, specially in the context of dopaminergic and adenosine signalling.

Recently, heterozygous knockout mutation of the GNAL gene in mice (Gnal+/-) was proposed to replicate the alterations observed in DYT25 patients (Pelosi et al. 2017). In this model, the heterozygous knockout mutation leads to an altered expression of Golf in the striatum, with only 50% of its normal protein levels (Corvol, Valjent, et al. 2007). This heavily impairs intracellular signalling in the striatum, and although no dystonic phenotype is visible in Gnal+/- adult mice before old age, the administration of a muscarinic cholinergic agonist (oxotremorine M) triggers dystonic symptoms, either when administered systemically or locally in the striatum (Pelosi et al. 2017). This suggests that increased cholinergic activation participates to dystonic attacks in DYT25.

The pharmacologically-nduced dystonic phenotype seems fully reversible, as the observable motor symptoms disappear after some time, suggesting that the washout of the cholinergic agonist is sufficient to end the dystonic attack and that the network then recovers its full function.

However, the potential persistence of functional alterations in the motor network following the elimination of oxotremorine, even in absence of motor symptoms, remains possible. Indeed, the initial exposure to oxotremorine could be the necessary trigger to induce lasting changes facilitating the switch to the next pathological state. This switch could hinder the resilience of the motor system, and make it more susceptible to dystonic attacks in the future. Similarly, the existence of subthreshold functional alterations in the motor network before the first administration of oxotremorine remains a possibility. This would be consistent with the notions of incomplete penetrance and mediational endophenotypes (Hutchinson et al. 2013).

1.2.3.3 Cerebellar involvement in dystonia

Although dystonia has long been believed to arise from a dysfunction of the basal ganglia, it has been linked to cerebellar alterations in many occasions.

Cerebellar loci for lesion-induced dystonia

Interestingly, even though cerebellar lesions typically result in the expression of a cerebellar syndrome, patients have been reported to exhibit dystonic symptoms in some cases (Bologna et al. 2017). Indeed, tumors affecting the cerebellum, including

infra-tentorial tumors, tumors of the posterior fossa, were shown to be related to the expression of cervical dystonia (Boisen 1979; Krauss et al. 1997; Kumandaş et al. 2006; Fafara-Leś et al. 2014).

Similarly, vascular lesions in the cerebellum can induce several forms of dystonia, including cervical dystonia (O'Rourke et al. 2006; Zadro et al. 2008; Usmani et al. 2011), oromandibular dystonia (Waln et al. 2010; Bana et al. 2015), blepharospasm (Khooshnoodi et al. 2013), and hemidystonia (Rumbach et al. 1995).

Cerebellar atrophia, a known cause of ataxia, has been reported to be associated to a broad dystonic symptomatology, with focal, multifocal and generalized dystonia (Le Ber et al. 2006), targeting the upper limbs (Baik 2012), but also the cranium and the cervical areas (Batla 2018).

Cerebellar dysfunction in dystonia

The previously mentioned studies suggest that dystonia can arise from an aberrant cerebellar function. Consistently with this idea, several mice models of dystonia have been engineered by performing cerebellar perturbations.

This category notably contains two mice models of dystonia: the infusion of kainate in the cerebellar vermis (Pizoli et al. 2002; Georgescu, Georgescu, et al. 2018; Georgescu Margarint et al. 2020), and the application of ouabain on the cerebellar cortex, modelling DYT12 (Calderon et al. 2011; Fremont, and Khodakhah 2012; Fremont, Calderon, et al. 2014).

As initially described by Pizoli et al, the micro-injection of kainic acid in the cerebellar vermis leads to the expression of a robust dystonic phenotype (Pizoli et al. 2002). Kainic acid is an agonist for the kainate receptor, a specific type of glutamate receptor heavily expressed in the granular layer of the cerebellar cortex (Foster, Mena, et al. 1981; Hampson et al. 1998; Straub et al. 2011). In the span of the 10 to 20 minutes following injection of kainate, mice start displaying dystonic symptoms mainly affecting the hindlimbs at first, which then get generalized to the four limbs and trunk (Pizoli et al. 2002). In this model, the severity of the phenotype is directly correlated to the dose injected (Pizoli et al. 2002). Recent studies revealed that cortico-cortical interactions are altered in this mouse model, with a lower coherence between the primary motor and primary sensory cortices on the controlateral side to the cerebellar injection of kainate (Georgescu, Georgescu, et al. 2018), and between the primary motor cortices in both hemispheres (Georgescu, Popa, et al. 2020).

Similarly, affecting cerebellar metabolism by infusing ouabain, a blocker of the

Na/K ATPase pump, partially impairs its activity and leads to a dystonic phenotype (Calderon et al. 2011; Fremont, and Khodakhah 2012; Fremont, Calderon, et al. 2014). This pharmacological model is proposed to mimic the alteration induced by the mutation of the gene ATP1A3 in patients suffering from DYT12, which induces a loss of function in a particular isomere of the sodium pump. The infusion of ouabain dramatically affects the activity of Purkinje cells, which switch from a regular firing rate to an irregular firing displaying an increased bursting activity (Fremont, Calderon, et al. 2014). This, in-vivo, leads to an altered activity in the cerebellar nuclei, which similarly to the Purkinje cells of the cerebellar cortex display more irregular firing patterns with an increased bursting behaviour (Fremont, Calderon, et al. 2014).

As described before, mice models of hereditary dystonia induced by introducing mutations in the genes of interest altered in the human form of the pathology do exist. This is the case for the mouse model of DYT1, created by inducing a loss of function mutation in torsinA, the gene involved in the human DYT1 (Dang et al. 2005; Shashidharan et al. 2005). However, most mice of this model do not display a strong dystonic phenotype (Fremont, and Khodakhah 2012; Fremont, Tewari, et al. 2017), which is potentially in line with the notion of incomplete penetrance present in hereditary dystonia, but impairs the ability of studying the mechanisms underlying dystonia in the pathological state of DYT1.

Although the complete knockout of torsinA is lethal in mice (Goodchild et al. 2005), a recent study using acute knockout of torsinA in the cerebellum revealed the critical role of the cerebellum in the pathophysiology of DYT1 (Fremont, Tewari, et al. 2017). Not only the local knockout of torsinA in the cerebellum is sufficient to trigger robust and persistent dystonic episodes, but the depth of the cerebellar knockout is correlated with the severity of the phenotype (Fremont, Tewari, et al. 2017), further suggesting that the cerebellum is a key element of the pathophysiology of DYT1. Moreover, similarly to what was observed in the pharmacologically induced model of DYT12, the firing patterns of both Purkinje cells and cerebellar nuclei neurons were altered in this model of DYT1, with an overall decrease in average firing rate, but an increase irregularity, leading to the expression of more bursts (Fremont, Tewari, et al. 2017). This is consistent with the other observations suggesting a correlation between an altered cerebellar output and dystonia.

Strikingly, cerebello-thalamic tracts were shown to be affected in DYT1 (Argyelan et al. 2009; Uluğ et al. 2011). A tractography and functional imaging study revealed that the integrity of cerebello-thalamo-cortical pathways was reduced in

DYT1 mutation carrier, regardless of if they were expressing symptoms or not (Argyelan et al. 2009). While the integrity of fiber tracts was altered in both cerebellar and thalamo-cortical tracts of DYT1 mutation carriers, what differentiates symptomatic from asymptomatic carriers is the difference in connectivity between these two pathways (Argyelan et al. 2009). Indeed, while non-manifesting carriers display a stronger alteration of thalamo-cortical tract, manifesting carriers display an even stronger alteration of cerebellar tract, in addition with the thalamo-cortical (Argyelan et al. 2009). This suggests that the penetrance of DYT1 is linked to the depth of the alteration in cerebello-thalamo-cortical networks.

These observations were later corroborated by the study of mutant DYT1 mice, which do not display a dystonic phenotype, and thus may reflect alterations found in non-manifesting human carriers (Uluğ et al. 2011). Mutant mice display structural alterations in multiple areas of the brain, including cerebellar tracts, thalamo-cortical tracts and white fiber tracts in the brainstem (Uluğ et al. 2011). While the metabolic activity of the cortex is positively correlated to the trophicity of thalamo-cortical tracts, it is anti-correlated to the trophicity of cerebellar tracts (Uluğ et al. 2011), consistently with an inhibition of the cerebral cortex by the cerebellar cortex, and an excitation of the cerebral cortex by thalamo-cortical neurons. Similarly to non-manifesting human carriers of DYT1, mutant mice display a stronger alteration of thalamo-cortical tracts compared to cerebellar tracts (Uluğ et al. 2011).

Altogether, these result suggest that the integrity of cerebello-thalamic tracts is correlated to the expression of dystonic symptoms in DYT1, and that the cerebellum could potentially contribute to compensatory mechanisms in non-manifesting mutation carriers, thus potentially explaining incomplete penetrance of hereditary dystonia.

Consistently with the notion that dystonia could arise from altered cerebellar activity, a recent mouse model of dystonia was engineered by genetically silencing synapses from the climbing fiber to the Purkinje cells of the cerebellar cortex (White et al. 2017). This is performed by specifically removing the vesicular glutamate transporter 2 (Vglut2) from the olive under the control of Ptf1a, which is expressed only in inhibitory neurons, as well as excitatory projection neurons of the inferior olive (White et al. 2017). Thus, removing Vglut2 from Ptf1a expressing neuron mainly affects the function of olivo-cerebellar neurons.

In this model, because the climbing fiber to the Purkinje cells synapses are silenced, the olivo-cerebellar signalling is completely disrupted and Purkinje cells do not exhibit complex spike activity (White et al. 2017). This leads to an aberrant

activity of Purkinje cells and cerebellar nuclei neurons, with juvenile mice displaying slower and more regular simple spike activity, with an heightened firing rate of cerebellar nuclei neurons, while cerebellar nuclei neurons of adult mice exhibit an opposite behaviour, being slower and more irregular (White et al. 2017).

Both juvenile and adult mice of this model exhibit strong dystonic phenotypes, with symptoms including hyperextension of the limbs and twisting of the trunk, as well as varied dystonic postures and tremors (White et al. 2017). However, this model does not only display motor symptoms (van der Heijden et al. 2021; Leon et al. 2023), as a recent study revealed that although the circadian rythm of these mice was unaltered, the balance between sleep stages was perturbed (Leon et al. 2023). Indeed, the time spent awake and in NREM sleep is increased in these mice, and conversely the time spent in REM sleep is decreased (Leon et al. 2023). In addition, the temporal structure of the different sleep stages is altered, as the average duration of wake episodes, as well as the number of episodes of NREM sleep are drastically increased, in opposition to a decreased number of REM episodes (Leon et al. 2023). These observations not only suggest that sleep-dependent processes may be altered in dystonia (Salazar Leon et al. 2022), but also that cerebellar activity may be critical in maintaining normal sleep.

Since the dystonic phenotype associated to this model arises from an aberrant cerebellar activity, it brings the question of a potential to mitigate dystonic symptoms by affecting cerebellar activity. Strikingly, the local infusion of lidocaine, a sodium channel blocker, in the interposed nucleus of these mice reduces tremors and improves the overall locomotor activity of these dystonic mice (White et al. 2017). In addition, the administration of electrical deep brain stimulations (DBS) in the interposed nucleus of the cerebellum in these mice drastically improves their dystonic phenotype (White et al. 2017; Brown, van der Heijden, et al. 2023). These observations, altogether with the previous discovery that altering the propagation of cerebellar activity to the basal ganglia in a DYT12 mouse model could alleviate dystonic symptoms (Calderon et al. 2011), strongly suggest that the cerebellum can be a potent therapeutic target in the treatment of dystonia.

1.2.3.4 Cerebellum as a therapeutic target for dystonia

Cerebellar lesions

The cerebellum has been proposed to be a potential site for therapeuticmanipulations in the context of motor disorders (Hitchcock 1973; Fremont, and Khodakhah 2012). For example, the surgical lesion of the dentate nucleus of the cerebellum,

also called dentatectomy, was shown to improve symptoms in various kind of disorders with a wide range of efficiency, ranging from subtle to critical improvements (Hitchcock 1973; Heimburger 1967; Zervas et al. 1967; Fraioli et al. 1975). This includes a reduction of symptoms in chorea (Hitchcock 1973), parkinsonism (Zervas et al. 1967) and particularly striking results in dystonia (Zervas et al. 1967; Fraioli et al. 1975). These observations suggest an involvement of the cerebellum in the physiopathology of dystonia and shines light on the possibility that manipulating cerebellar output can contribute to mitigate symptoms of motor disorders.

Cerebellar stimulations

Multiple studies revealed an improvement of dystonic symptoms by the administration of DBS, either in the cerebellar nuclei, or in the cerebellar peduncules (Tai et al. 2022). Indeed, cerebellar DBS in the dentate nucleus did alleviate dystonic symptoms in idiopathic generalized dystonia (Horisawa, Kohara, et al. 2021), cerebral palsy (Lin et al. 2019) and in secondary dystonia following a stroke (Brown, Bledsoe, et al. 2020). In addition, cerebellar DBS in the dentate nucleus was also reported to reduce tremors along with dystonic symptoms (Horisawa, Kohara, et al. 2021).

However, DBS is a highly invasive procedure with an incomplete success rate and potential iatrogenic effects due to the surgical procedure. Thus, a particular attention was brought on the use of non-invasive stimulations procedures in order to treat dystonia.

Transcranial stimulations is a non-invasive way of affecting neuronal activity in superficial brain structures, and can be used for both the investigation of network function and for the treatment of neurological diseases. They are usually delivered in two different ways, either magnetically using an electro-magnet placed over the area of interest, or electrically using cutaneous electrodes [(Classen 2013).

Transcranial magnetic stimulations (TMS) relies on electro-magnetic induction (Chail et al. 2018), occurring when an alternating electric current passes through an inductor (primary), inducing an alternating magnetic field around the primary, which can create an alternating current (and an electric field) in an other inductor (secondary). In the case of TMS, the primary is the coil of the stimulation machine, and the secondary is the neuronal tissue of the stimulated area (Klomjai et al. 2015).

TMS was extensively used to investigate the cortico-spinal tract, as performing a single pulse of stimulation over the motor cortex leads to its transient excitation,

inducing a muscle twitch at the periphery (Huang, Edwards, et al. 2005). The magnitude of this response can be measure through electromyography (EMG) as the amplitude of the peak to peak EMG response, called motor-evoked potential (MEP) which is thought to reflect the excitability of the cortico-spinal tract (Klomjai et al. 2015).

On the other hand, lower intensity pulses delivered in patterns have been shown to be able to induce plastic changes (Berardelli et al. 1998; Iyer et al. 2003; Huang, Edwards, et al. 2005; Klomjai et al. 2015). Typically, low frequency (< 1Hz) repetitive TMS (rTMS) is believed to have a depressing effect, as it induces a decreased MEP when applied over the motor cortex (Iyer et al. 2003). In opposition, higher frequency (> 5Hz) rTMS over the motor cortex tends to increase MEP, which suggests a potentiating effect (Berardelli et al. 1998).

Strikingly, a particularly potent stimulation protocol known to induce plastic changes is the theta-burst stimulation (TBS) protocol (Huang, Edwards, et al. 2005; Huang, Chen, et al. 2007), where stimulations are delivered in short bursts administered in the theta frequencies (5-10Hz). The plastic changes induced by this protocol are long-lasting, and dependent on NMDA receptors (Huang, Chen, et al. 2007). Variations of the TBS exist, with differences in the structure of the stimulations. Typically, TBS can be delivered continuously over the span of several tens of seconds, which will correspond to the continuous TBS (cTBS), or through short blocks of stimulations lasting few seconds, corresponding to intermittent TBS (iTBS), displaying opposite results on plasticity (Huang, Edwards, et al. 2005).

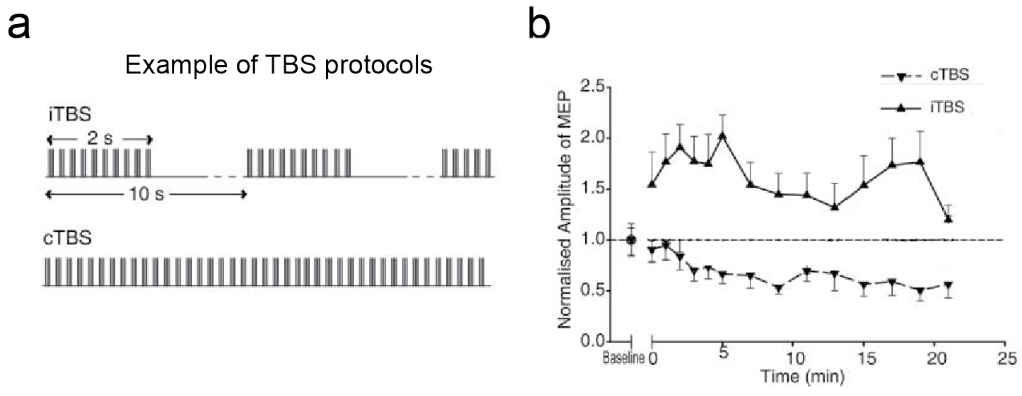

Figure 1.10: Typical protocols of theta burst stimulations applied over the motor cortex and their effects on cortical excitability. **(a)** Schematic representation of the stimulation patterns for intermittent theta burst stimulation (iTBS) and continous theta burst stimulation (cTBS). **(b)** Opposite effect of cortical cTBS and iTBS on the amplitude of movement evoked potential (MEP) induced by cortical trasncranial magnetic stimulation (TMS), reflecting cortical excitability. Adapted from Huang, Edwards, et al. 2005.

Interestingly, cerebellar TBS has been shown to be able to induce similar plastic changes (Koch, Mori, et al. 2008). This highlights cerebellar TBS as a potential treatment for motor disorders. And indeed, cerebellar TBS can induce an improvement of gait and balance in patients suffering from hemiparesis following a stroke affecting the cerebral cortex (Koch, Bonnì, et al. 2019). In this study, the application of iTBS over the cerebellum allowed for a progressive recovery of balance, as evidenced by an increased Berg Balance Scale, coupled to a reduction of the step with during walk (Koch, Bonnì, et al. 2019). This suggests that cerebellar TBS can heavily influence cerebello-cortical plasticity and thus can contribute to the treatment of motor disorders linked to an erratic activity of the motor cortex.

Similarly, the repetitive administration of cerebellar cTBS on patients suffering from levodopa-induced dyskinesias, a well known side-effect of the long term treatment of Parkinson's disease by levodopa, increased intracortical inhibition and lead to a reduction of dyskinesias following administration of levodopa (Koch, Brusa, et al. 2009). Consistently with this, a recent study on an animal model of levodopa-induced dyskinesias revealed that the preventive application of optogenetic theta-burst stimulation on Purkinje cells of the cerebellar cortex can contribute to reduce the apparition of levodopa-induced dyskinesias, normalize the activity in the network and promote LTD at the cortico-striatal synapse of D1R expressing MSNs (Coutant et al. 2022).

Strikingly, studies investigating the potential use of cerebellar TBS in the treatment of dystonia showed a potential to relieve patients from their dystonic symptoms, at least partially. Indeed, the daily administration of bilateral cerebellar cTBS in patients suffering from cervical dystonia revealed an improvement of the Toronto Western Spasmodic Torticollis Rating Scale (TWSTRS), suggesting a decreased dystonic phenotype (Koch, Porcacchia, et al. 2014). In addition, the cTBS protocol induced plastic changes in the network, as evidenced by the variations in Cerebellar Brain Inhibition (inhibition of M1-evoked EMG responses by cerebellar TMS delivered a few milliseconds before the M1 TMS) after the delivery of the TBS session (Koch, Porcacchia, et al. 2014). Interestingly, an other study revealed that daily sessions of cerebellar iTBS on patients suffering from cervical dystonia lead to a decrease in symptoms assessed by the TWSTRS score, as well as a (moderate) improvement in quality of life and hand dexterity (Bradnam, McDonnell, et al. 2016). Another approach of non-invasive cerebellar stimulation consist in applying continuous currents, which is thought to shift the excitability of neuronal tissue. Such approach has also been attempted in dystonia but has shown limited success

(Benninger et al. 2010; Buttkus et al. 2011; Ferrucci et al. 2016; Bradnam, Graetz, et al. 2015).

Considering the similarities between DYT25 and DYT1, an hereditary dystonia heavily associated to a cerebellar dysfunctions and to alterations of cerebello-thalamo-cortical networks, we sought to investigate the presence of such dysfunctions in the motor network of Gnal+/- mice by optogenetically probing the functionality of cerebello-thalamic pathways. In addition, knowing that rodent models of DYT25 display an altered plasticity which cerebellar TBS was shown to influence, we explored the potential use of cerebellar TBS in the rescue of an aberrant plasticity in Gnal+/- mice, which could contribute to the treatment of DYT25.

1.3 Limbic circuits and emotional processing

1.3.1 Neuro-anatomy

The name of the limbic circuits stems from latin and means "border". This comes from the initial documentation of a cortical border surrounding the human brainstem by Thomas Willis in 1664, corresponding to the cyngulate cortex. However, as we now know, the networks responsible for emotional processing and learning are much more distributed, and include many other brain structures. Later, Broca proposed the olfactory structures to be included in the limbic system (Broca 1878). It is only in 1906 that Christopher Jakob emits the idea that the limbic system is composed of an ensemble of both cortical and subcortical brain structures (Jakob 1906). This idea was later supported by James Wenceslaus Papez, who identified a network involved in emotional processing and memory (Papez 1937).

This network, named Papez circuit, starts from the hippocampus, traverses through the fornix, the mammillary bodies, and then through the mammillothalamic tract, towards the anterior thalamic nucleus. Then, it reaches the cingulate cortex, courses round the entorhinal cortex and returns to the hippocampus (Herrick 1933; Papez 1937; Shah et al. 2012). Later, Paul Yakovlev then proposed a parallel basolateral circuit including the thalamus, particularly the mediodorsal thalamus, and the orbitofrontal cortex (Yakovlev 1948). Our modern view of the limbic system truly appeared when Paul MacLean decided to integrate both models from Papez and Yakovlev into a unique system and added the prefontal cortex, the septum and the amygdala (MacLEAN 1949; Maclean 1952). However, even then, the knowledge of the extent of limbic circuit was definitely not complete, as evidenced by the late inclusion of the midbrain (Nauta et al. 1978) This suggests that many more brain structures could be part of the limbic circuit.

Despite the fact that the cerebellum displays a high degree of interconnectivity with the structures of the limbic system, it is not canonically considered as being part of it. In fact, the cerebellum was shown to project to these structures, either monosynaptically as it is the case for the ventro-lateral Peri-Aqueducal Gray (vlPAG, (Frontera, Baba Aissa, et al. 2020)) the mediodorsal thalamus (MD, (Groenewegen 1988; Fujita et al. 2020; Frontera, Sala, et al. 2023)) and the hypothalamus (Haines, May, et al. 1990; Haines, Dietrichs, et al. 1997; Cavdar et al. 2001), or through oligosynaptic pathways in the case of the prefrontal cortex (Frontera, Sala, et al. 2023) and the basolateral amygdala (Jung et al. 2022). Conversely, the cerebellum also receives inputs from these structures through the precerebellar nuclei

like the inferior olive (Watson et al. 2009; Kostadinov et al. 2019) or through the pontine nuclei (Farley et al. 2016). These observations highlight the wide projections patterns of the cerebellum, and is an incentive for us to investigate the role of the cerebellum as a potential modulator of limbic circuits-mediated functions.

1.3.2 Fear and fear conditioning

Studies have demonstrated the engagement of the different nodes of the limbic circuit during tasks involving memory and/or emotions.

Although important breakthroughs about limbic systems and emotions were made in the first half of the twentieth century, the interest of neuroscientists for the neural basis of emotion then plummeted in favor of the study of other cognitive processes such as memory (LeDoux n.d.). The rational was that studying emotions required the measure of a conscious feeling, which wasn't the case for a wide range of cognitive processes who are mainly subconscious. However, not only emotional responses involve unconscious mechanisms, but conscious feelings are not even required to shape some of these responses (Öhman 1993; LeDoux n.d.). This realization sparked an interest for the study of the neural mechanisms underlying such emotional processes, particularly for in the context of fear (LeDoux n.d.).

Fear can be defined as an ensemble of responses caused by the presence of an external stimulus, leading to an unpleasant sensation. Fear response is multidimensional, as it is presented through behavioral, physiological and hormonal changes, leading to defensive behaviors, autonomic arousal, hypoalgesia, reflex potentiation and release of stress hormones (LeDoux n.d.; Blanchard, Blanchard, et al. 2008; Tovote et al. 2015). These changes allow for the identification of a potential danger and the expression of an appropriate response. Thus, fear is paramount for survival.

The study of mechanisms underlying fear required the design of an experimental paradigm yielding an objective and measurable output, solely corresponding to fear behaviour. For the most part, this was made possible by Pavlovian fear conditioning (Pavlov (1927) 2010; LeDoux n.d.; Tovote et al. 2015; Urrutia Desmaison et al. 2023). This paradigm is based in a form of associative learning described by Pavlov in 1927, in which an initially neutral stimulus, also named conditioned stimulus (CS), will develop similar properties as another event called unconditioned stimulus (US) upon the repeated temporal pairing of both CS and US (Pavlov (1927) 2010).

1.3.2.1 Fear acquisition during fear conditioning

In fear conditioning, an innocuous stimulus corresponding to the CS is presented together with an aversive event corresponding to the US. When such experiment is performed with rodents, the CS is typically a sensory cue (usually a tone, a light or an odour) or a given context (in the case of contextual fear conditioning), the US is an electrical shock delivered to the limbs using a conductive grid under the animal called footshock (although an air puff can also be used), and the variable used to quantify the fear response is the percentage of time spent immobile, also called freezing. Thus, this paradigm brings a simple framework to study fear network, with a measurable outcome and reproducible results among the population of animals studied (Tovote et al. 2015).

The presentation of the US elicits a fear response (also called unconditioned fear response), which is not the case initially for the CS. However, the repetition of the CS in association with the US will induce a fear response triggered by CS presentation, effectively creating an anticipation of the subsequent US. Thus, the fear network overrides the fear response induced by the US, and is now controlled by the CS. This phenomenon is referred to as fear acquisition, and results in a gradual increase in fear response induced by the presentation of the CS, now called conditioned fear response. The fear memory created during this pairing is long-lasting and consolidated over time, as it can be retrieved at a later point in time, either by presenting the CS without the US in a new context (following cued fear conditioning) or by presenting the animal in the same context as during fear acquisition in contextual fear conditioning (Tovote et al. 2015).

This process of fear conditioning has all the hallmarks of an associative learning triggered by the initial unexpectedness of observing an US following a CS, which forms a long-lasting association between the two stimuli. In 1972, Rescorla and Wagner proposed that an associative learning process, such as fear conditioning, could be modelled by an estimated probability of observing an US following a CS (Rescorla 1972). This probability, or expectancy, is discretely updated by each CS presentation, either increased if it was paired to the US or decreased otherwise. Thus, the unexpected contingency between stimuli acts as a teaching signal, bi-directionally controlling the estimated probability of observing a CS-US pair.

$$\Delta V = ab(\lambda - V)$$

In this equation, the term ΔV represents the variation in predictive value induced

by the CS presentation, a corresponds to the saliency of the conditioned stimulus and acts as a variable gain in the learning process, b is the actual learning rate, and V is the estimated probability of an CS-US pair occurring. Conventionally, the value of λ is considered as 1 if the presented CS was followed by an US, 0 otherwise. Thus, the level of unexpectedness heavily influences the probability update, as the variation of predictive value directly depends on the deviation between the observed event and the prediction, causing unexpected events to induce dramatic changes in probability, and expected events to mildly alter it.

1.3.2.2 Freezing as an indicator of fearful state

As described earlier, the variable typically used to measure fear expression in rodents is freezing (Johansen et al. 2010; Dejean et al. 2016; Pasquet et al. 2016; Frontera, Baba Aissa, et al. 2020). However, it needs to be mentioned that some pitfalls are related to its sole use to quantify fear responses. Indeed, freezing corresponds to a lack of motion during the presentation of a previously conditioned stimulus or in a conditioned context, which could be widely mistaken for immobility.

In addition, freezing is not the only possible fear response expressed by rodents, as they can also exhibit fight or flight reactions (Lang et al. 2000). Actually, fear response was hypothesized to vary depending on the arousal state of the animal, with freezing being favoured at lower arousal levels, and a switch to fight or flight responses occurring at extremes levels of arousal (Lang et al. 2000). Thus, the emotional intensity associated to the fearful state of the animal could bias the expression of fear toward high mobility, and lead to an underestimation of the actual fear response if only freezing is considered.

To overcome these issues, alternative measures of fearful state were envisioned. For example, the measure of freezing can be combined with physiological variables such as heart rate (Signoret-Genest et al. 2023) or body temperature (Liu, Lee, et al. 2021) in order to help disambiguating between freezing and immobility. Also, fear conditioning was shown to alter other behavioral parameters, inducing an increased startle response to the presentation of a sound (VanElzakker et al. 2014; Tovote et al. 2015), as well as changes in the vocalization patterns of animals (Wöhr et al. 2005; Olszyński et al. 2021), an increased probability of urination and defecation (Blanchard, and Blanchard 1988), although these later behaviors are much more inconsistent than freezing.

1.3.3 Fear extinction

1.3.3.1 Suppression of conditioned fear response

Following the acquisition of fear conditioning, the repeated presentation of the CS unpaired with the US will ultimately lead to a gradual decrease in fear response induced by the CS, in a process called extinction of fear memory. Initially, extinction was proposed to be a form of "unlearning" of the previously learned association based on the violation of the CS-US contingency established during acquisition (Rescorla 1972), leading to a decreased expectancy of receiving an US after a CS.

However, evidence lead to challenge this conception of extinction. Indeed, the engram associated to fear conditioning is known to be highly resistant to loss, injury and to the passage of time (McAllister et al. 1986; Myers et al. 2002). In contrary, the expression of extinction learning was shown to weaken over time, leading to a phenomenon named spontaneous recovery (Robbins 1990). In addition, if CS presentation occurs after extinction learning but in a different context than the one where extinction took place, a strong conditioned response will be expressed, in a process called renewal (Bouton et al. 1979). Both notions of spontaneous recovery and renewal highlight the resilience of fear conditioning engram, and reveal that the CS still retains control over fear expression even after the occurrence of extinction learning. Therefore, we now conceptualize extinction as a new learning, and not just a simple forgetting of the engram associated to fear conditioning.

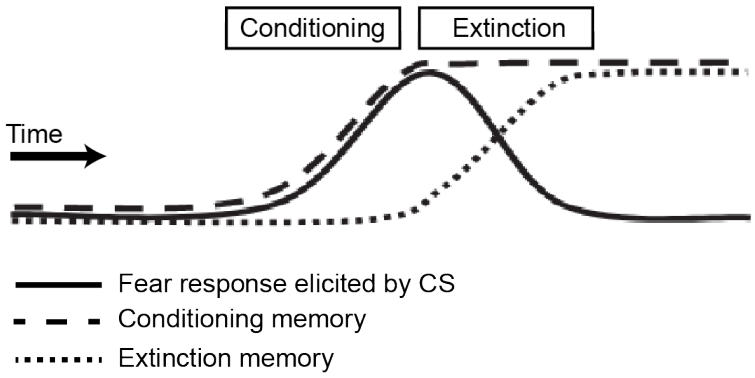

Figure 1.11: Relationship between the expression of conditioned behaviour, conditioning memory and extinction memory. While the initial fear response elicited by the CS is low, it is increased as fear conditioning occurs and the memory associated to the conditioning is strengthened. However, the occurrence of extinction doesn't alter the memory associated to the conditioning, but creates a competing extinction memory, allowing for the fear response to decrease. Adapted from Quirk, Garcia, et al. 2006.

During extinction learning, a new memory which suppresses the expression of

fear behaviour in the previously conditioned context is created, while the consolidated engram associated to fear conditioning still promotes fear expression. Thus, extinction of fear memory engages different networks having an antagonistic effect on fear networks (Myers et al. 2002; Tovote et al. 2015; Urrutia Desmaison et al. 2023), and the behavioural response is a resultant of both competing networks.

1.3.3.2 Neuronal basis of fear extinction

The neuronal networks supporting fear extinction involve many brain structures, including some important for fear conditioning, with a particularly strong contribution of the amygdala, the medial prefrontal cortex, the hippocampus (Tovote et al. 2015; Urrutia Desmaison et al. 2023).

Hippocampus

The hippocampus is proposed to be involved in both the encoding and the retrieval of fear learning (Ji, and Maren 2007), in particular through the storage of the engrams related to fear conditioning and fear extinction (Zaki et al. 2022; Lacagnina et al. 2019). Indeed, a recent study showed that the activity dependent reactivations of hippocampal neurons associated to conditioning and extinction could bi-directionally control the expression of conditioned fear behaviour (Lacagnina et al. 2019). While the stimulation of fear conditioning related neurons promotes fear expression, both the inhibition of this population or the stimulation of extinction related neurons suppresses fear behaviour.

Amygdala

Critically, perturbing the activity in the basolateral amygdala (BLA) during the acquisition of extinction was shown to lead to a sustained expression of fear response, putting forward the BLA as a key player in the acquisition of fear extinction. Indeed, the antagonization of NMDA transmission in the BLA impairs the extinction of conditioned fear (Sotres-Bayon, Bush, et al. 2007; Falls et al. 1992), suggesting that NMDA-dependent plasticity is required for extinction learning. This idea was further cemented by a study revealing that the inhibition of MAPK/ERK pathway, an intra-cellular phosphorylation cascade involved in neuronal plasticity, also impaired extinction (Herry, Trifilieff, et al. 2006).

Prefrontal cortex

The prefrontal cortex is also considered as one of the main contributor to fear extinction, particularly the medial prefrontal cortex in rodents. Interestingly, there seem to be a dichotomy between the ventral part of the mPFC (vmPFC) corresponding to the infra-limbic cortex (IL) and the dorsal part of the mPFC (dmPFC) corresponding to the pre-limbic cortex (PL) and the anterior cingulate cortex (Acc). Although they are contiguous in space, the PL and the IL are different in terms of connectivity and functions (Heidbreder et al. 2003; Vidal-Gonzalez et al. 2006; Sierra-Mercado et al. 2011). In particular, study of the activity in PL and IL during extinction learning showed different dynamics. While neurons in IL display CS-evoked activity, it is initially weak after fear conditioning, and is increased following extinction learning (Milad et al. 2002). In addition, an increased excitability and metabolic activity was observed in IL neurons following extinction learning (Herry, and Garcia 2002; Barrett et al. 2003). Consistently with this, lesions studies in IL revealed that although a decrease of freezing during the extinction session was visible, the recall of extinction the next days was impaired (Quirk, Russo, et al. 2000; Lebrón et al. 2004), which was supported by a similar effect of the inhibition of protein synthesis in IL (Santini et al. 2004).

Interestingly, the reversible inactivation of IL using local injections of muscimol lead to an impaired extinction, with higher levels of freezing both during the session where muscimol was injected and during the next session (Sierra-Mercado et al. 2011). This may suggest a wider role of IL, both in the acquisition and consolidation of extinction learning.

Consistently with a contribution of IL in promoting extinction learning, the electrical stimulation of IL at the onset of the CS lead to a long lasting decrease in the levels of freezing during CS (Vidal-Gonzalez et al. 2006). All together, these results suggesting that IL is involved in suppressing conditioned fear following extinction learning.

In contrast, the PL cortex is proposed to exert control over the production of fear responses (Sotres-Bayon, and Quirk 2010) with a critical role in the expression of fear behaviour following conditioning (Blum et al. 2006; Vidal-Gonzalez et al. 2006). Indeed, in contrast to IL, neurons in PL initially display strong CS-evoked activity after conditioning, which decreases along extinction learning (Milad et al. 2002).

Moreover, the reversible inactivation of PL during extinction using muscimol leads to lower levels of freezing during the session of the inactivation (Laurent et al.

2009). Interestingly, this decrease in freezing induced by a perturbation of PL is specific to conditioned fear and cannot suppress innate fear (Corcoran et al. 2007). Conversely, the electric stimulation of PL during extinction leads to increased levels of freezing (Vidal-Gonzalez et al. 2006).

The functional differences observed between IL and PL during extinction were proposed to arise from an heterogeneity in their downstream projections (Brown, van der Heijden, et al. 2022), particularly in their targets within the amygdala (Vertes 2004; Gabbott et al. 2005).

However, despite the different roles of IL and PL in fear extinction, an increased synchrony during was observed between these structures during fear conditioning and extinction, particularly in the theta range (4-10Hz) (Wang, Stratton, et al. 2022), suggesting an interplay between IL and PL during the process of learning.

Fear-related oscillations in the prefrontal cortex

Interestingly, the expression of conditioned fear behaviour is associated to theta-range oscillations in the local field potential (LFP) of the dmPFC (Dejean et al. 2016; Karalis et al. 2016b; Bagur et al. 2021). These oscillations have a dominant frequency of 4Hz in mice, they are olfactory driven as they originate from sensory inputs related to the breathing of the animal during freezing (Bagur et al. 2021), and share a strong temporal relationship with the structure of freezing episodes (Karalis et al. 2016b). Indeed, the appearance of such activity pattern in the LFP of the dmPFC is predictive of the onset of a freezing episode, and a decreasing power of 4Hz oscillations precedes the offset of the freezing episode (Karalis et al. 2016b). Not only their presence correlates with freezing behaviour, but Karalis et al showed that the induction of 4Hz oscillations in the dmPFC through optogenetic stimulations was sufficient to induce freezing (Karalis et al. 2016b).

Strikingly, the induction of 4Hz oscillations in the dmPFC increased the levels of freezing during the stimulation, but also lead to a higher expression of freezing in the same context at a later point in time (Karalis et al. 2016b). This result suggests that in addition to being causal in the apparition of fear response, 4Hz oscillations in the dmPFC can also be involved in fear learning. Knowing that these oscillations propagate to the BLA where they can organise neuronal activity (Karalis et al. 2016b), their contribution to fear learning may be due to a modulation of the activity in the amygdala.

Prefronto-amygdalar circuits

Consistently with a modulation of the amygdala by the prefrontal cortex, both of these structures have been shown to be reciprocally interconnected (Arruda-Carvalho et al. 2015). Critically, the projections from the prefrontal cortex to the BLA were shown to contribute to fear extinction (Bloodgood et al. 2018). Indeed, the projection from IL to BLA undergo plastic changes during extinction, with an increased excitability of BLA-projecting IL neurons following extinction learning (Bloodgood et al. 2018). Interestingly, this increased excitability was specific to BLA-projecting IL neurons and absent in BLA-projecting PL neurons, consistently with the IL cortex promoting fear extinction in opposition to PL controlling fear response (Bloodgood et al. 2018). Moreover, the chemogenetic inhibition of BLA-projecting dmPFC neurons during fear extinction lead to increased levels of freezing during a later session of fear recall (Bloodgood et al. 2018). In addition, the optogenetic activation of these projections during extinction lead to lower levels of freezing during the extinction session and during a later retrieval session (Bukalo et al. 2021). These results suggest that cortico-amygdalar projections contribute to the acquisition of fear extinction, as well as to the stabilization of its engram.

Conversely, segregated pathways exist between the BLA and both PL and IL (Senn et al. 2014). Indeed, separated populations in the BLA will project either to IL or PL, and were shown to have an opposite control on the expression of conditioned fear. While the inhibition of PL-projecting BLA neurons leads to a decreased freezing during CS administration, the inhibition of IL-projecting BLA neurons induces higher levels of freezing (Senn et al. 2014). Furthermore, the CS-evoked activity of these two populations evolves along extinction learning, with an initially stronger activation of PL-projecting neurons decreasing over time, and a milder activation of IL-projecting neurons during early extinction increasing in late extinction. This is consistent with the role of PL in fear expression and IL being rather involved in the acquisition of extinction learning. Taken all-together, these results suggest that extinction learning is supported by a switch in balance of activity between two populations of neurons in the BLA with different control over cortical activity. Interestingly, while the acquisition and consolidation of extinction learning seems to require both prefrontal cortex and basolateral amygdala, the acquisition and consolidation of re-extinction following retrieval of fear conditioning seem to depend more on IL cortex than on the BLA (Lingawi et al. 2019), which could suggest a parallel storage of the engram associated to fear extinction in both the prefrontal cortex and the amygdala.

Thalamus

In addition to the previously mentioned structures, a particular attention was brought on the thalamus and its role in regulating extinction of fear memory (Lee, Ahmed, et al. 2012; Penzo et al. 2015; Marek et al. 2019; Furlong et al. 2016; Ramanathan et al. 2019; Tao et al. 2020; Silva et al. 2021). Notably, the thalamic nuclei mainly involved in the regulation of extinction are the medio-dorsal thalamus (MD, (Lee, Ahmed, et al. 2012), the nucleus reuniens (Ramanathan et al. 2019; Silva et al. 2021), the paraventral nucleus (Penzo et al. 2015; Tao et al. 2020), the reticular nucleus (Lee, Latchoumane, et al. 2019) and the parafascicular (Jeon et al. 2010).

The nucleus reuniens is a key player in the regulation of the oscillatory synchrony between the prefrontal cortex and the hippocampus (Roy et al. 2017; Ferraris et al. 2018), two structures heavily involved in various cognitive processes, emotional processing and fear extinction learning. Thus, this nucleus can have the ability to regulate these functions. Strikingly, increased levels of C-fos expressions were observed in the nucleus reuniens following extinction learning compared to mice that didn't undergo extinction (Ramanathan et al. 2019), which suggests that neuronal activity was particularily increased in this nucleus during learning. Moreover, the injection local inhibition of the nucleus reuniens through local injections of muscimol just prior extinction learning lead to increased levels of freezing during the session and also at a later point in time during retrieval, further suggesting an involvement of the nucleus reuniens in both the acquisition and consolidation of fear extinction (Ramanathan et al. 2019).

The reticular thalamus stands out among thalamic regions, as it a nucleus located at the outer border of the thalamus, profusely populated by GABAergic neurons which provide an inhibition to other thalamic nuclei (Jones 1975; Pinault et al. 1998). It receives inputs from a wide range of cortices, and was proposed to gate transthalamic information transfer between cortices through its thalamic inhibitory projections (Takata 2020). In a recent study, it has been shown to regulate extinction learning (Lee, Latchoumane, et al. 2019), with the optogenetic stimulation and inhibition of the reticular thalamus held a bi-directional control over extinction learning, respectively inducing a facilitation and an impairment of extinction (Lee, Latchoumane, et al. 2019). The rostro-ventral reticular thalamus sends inhibitory projections to the dorsal midline thalamus, a CeA-projecting thalamic nuclei, which were shown to be necessary for extinction learning (Lee, Latchoumane, et al. 2019). Interestingly, the rostral reticular thalamus receives inputs from the

cerebellum (Çavdar et al. 2002), which may suggest an alternative pathway through which the cerebellum could influence fear extinction.

The paraventricular nucleus of the thalamus has also been shown to influence fear extinction, mainly through its projections to the CeA (Tao et al. 2021; Penzo et al. 2015; Chen, and Bi 2019).

Medio-dorsal thalamus

However, particular attention was brought on the role of the medio-dorsal thalamus (MD) in fear extinction. Indeed, the MD has a high degree of connectivity with structures of the limbic circuits (Georgescu, Popa, et al. 2020), including reciprocal connections with the prefrontal cortex (Morceau et al. 2019; Collins et al. 2018) and the amygdala (Aggleton et al. 1984; Krettek et al. 1977), which are structures known to be involved in fear extinction.

Consistently with reciprocal connectivity between the MD and the PFC, the electrical stimulation of the MD leads to both short and long latency responses in the PFC (Herry, Vouimba, et al. 1999; Gioanni et al. 1999; Pirot et al. 1994). Similarly, the optogenetic activation of the MD terminals in the PFC leads to strong depolarizing currents, particularly in layer II/III pyramidal cells, and to a lesser extent in the layer V (Collins et al. 2018). Reciprocally, stimulating cortical terminals from the PFC in the MD leads to strong EPSCs in MD neurons, facilitated by paired pulses (Collins et al. 2018). This suggests a strong anatomical and functional interplay between the MD and the PFC, potentially involved in fear extinction.

Strikingly, not only plastic changes in thalamo-cortical transmission between the MD and the PFC can be induced by periodic electrical stimulations of the MD (Herry, Vouimba, et al. 1999), but the exposition to extinction learning itself induces changes in coupling between the MD and PFC (Herry, Vouimba, et al. 1999; Herry, and Garcia 2002). Indeed, the first day of extinction is associated to a decreased transmission between MD and prefrontal cortex, which is converted to a potentiation during the following extinction sessions (Herry, Vouimba, et al. 1999). Moreover, inducing long-term depression or potentiation of this thalamo-cortical axis bi-directionally influences extinction learning (Herry, and Garcia 2002), respectively impairing or stabilizing it, suggesting that thalamo-cortical LTP is required for the extinction of fear memory.

Although plastic changes in this thalamo-cortical network can be induced experimentally and seems to also occur physiologically during learning, the actual

mechanism supporting the increased coupling observed following extinction learning has yet to be determined. Thalamic patterns of activity could contribute to these plastic changes, in particular thalamic bursts who were proposed to be able to drive thalamo-cortical plasticity (Hu et al. 2016; Langberg 2016).

Interestingly, the patterns of activity in the MD have been shown to exert a bi-directional control over fear extinction (Lee, Ahmed, et al. 2012; Lee, and Shin 2016). Indeed, the induction of either tonic firing or burst firing in the MD during CS using a bipolar stimulation electrode altered the time-course of extinction. While the induction of tonic firing (100Hz) during CS induced a drastic and long-lasting facilitation of extinction learning, inducing burst firing (416Hz during 12ms) had an opposite effect, yielding a long lasting impairment in extinction (Lee, Ahmed, et al. 2012). Consistently with this, there is a negative correlation between the frequency of tonic firing in the MD during extinction and the amount of freezing expressed by the animal (Lee, Ahmed, et al. 2012), and the blockade of T-type calcium channels participating to MD bursting facilitates extinction (Lee, Ahmed, et al. 2012).

It is interesting to note that while the potentiation of GABAergic transmission in the MD leads to persistent freezing during extinction, its antagonization facilitates extinction learning (Paydar et al. 2014). This is consistent with the fact that MD activity directly affects extinction, and may suggest that MD GABAergic transmission is required to provide the hyperpolarization necessary to aleviate the inactivation of the T-type calcium channels participating to MD bursting.

Thus, not only the thalamus can heavily influence the extinction of fear memory via its particular position as a major relay between the different structures of the limbic circuit, but also seems to have a leverage over extinction learning through its patterns of neuronal activity (Lee, Ahmed, et al. 2012; Lee, and Shin 2016). This suggests that the thalamus, and more particularly the MD, can have integrative properties involved in the regulation of fear learning. Interestingly, the cerebellum remains a strong provider of thalamic inputs.

1.3.4 Cerebellar contribution to fear learning

Although the role of the cerebellum was mainly understood in the scope of motor control, it both receives inputs from and exerts control over many non-motor areas of the brain (Léna et al. 2016). Interestingly, the cerebellum has been shown to be able to modulate the activity of most of the previously mentioned structures. Indeed, the cerebellum project to a wide variety of thalamic nuclei (Novello et al.

2022; Fujita et al. 2020), on which it can exert a "driver" or "modulator" control on thalamic activity (Gornati et al. 2018).

These observations, taken together with the fact that the cerebellum is heavily involved in sensory prediction error, suggest a contribution of the cerebellum in the acquisition and consolidation of both fear conditioning and fear extinction. However, little attention was brought on the role of cerebellum in emotional processing.

1.3.4.1 Cerebellum in fear in Human studies

Although being a rare occurrence in the literature, some functional studies in humans revealed a potential involvement of the cerebellum in fear conditioning (Ploghaus et al. 1999; Frings et al. 2002; Utz et al. 2015) and fear extinction (Kattoor et al. 2014; Utz et al. 2015). While the cerebellar cortex undergoes an activation induced by painful stimuli (mainly bilaterally in the anterior cerebellum), the anticipation of a painful stimulus leads to the activation of a different region of the cerebellar cortex, in the ipsilateral posterior cerebellum (Ploghaus et al. 1999), suggesting separated cerebellar networks for the processing of nociceptive inputs and for sensory associative learning related to them. In accordance with an involvement in associative learning, both cerebellar vermis and lobule VI were shown to be activated during the process of fear conditioning (Lange et al. 2015; Utz et al. 2015). The anterior part of the vermis seems to also be involved in fear extinction, as it is activated by the presentation of the CS following fear conditioning and in the absence of the US (Utz et al. 2015).

1.3.4.2 Cerebellar activity is required for fear conditioning and extinction in rodents

However, the previously mentioned study mainly assess correlation between cerebellar activity and the presentation of the CS during or after conditioning, without unravelling a causal contribution of the cerebellum to these learning processes. The first indications that the cerebellum could be necessary for fear conditioning and fear extinction were obtained thanks to rodent studies allowing for the manipulation of cerebellar networks during learning.

Indeed, the inactivation of the cerebellar vermis in rats using local TTX infusion induced an impairment in the retrieval of both contextual and cued fear memory (Sacchetti, Baldi, et al. 2002). A similar effect was obtained by inactivating the

interposed nucleus using TTX, which caused a deficit in the retrieval of cued fear memory (Sacchetti, Baldi, et al. 2002). In contrast, the chemogenetic activation of Purkinje cells in lobule V and VI of the cerebellar cortex induces a deficit in the consolidation of fear memory (Dubois, Fawcett-Patel, et al. 2020).

Similarly, altering cerebellar plasticity impairs fear conditioning and fear extinction (Hwang et al. 2022; Otsuka et al. 2016; Sacchetti, Scelfo, et al. 2004). The genetic deletion Cerebellin1, a critical gene for the formation and function of the synapse between the parallel fibers and the Purkinje cells, creates a deficit in the acquisition of fear conditioning (Otsuka et al. 2016). In addition, the deletion of GluD2, a subunit of NMDA receptor present at the same synapse induce lower levels of freezing during the following session, suggesting a role of this subunit in the creation of a strong fear conditioning engram (Sacchetti, Scelfo, et al. 2004). In opposition, another study observed that the deletion of GluD2 lead to higher levels of freezing during the session following fear conditioning, and impaired fear extinction (Dubois, and Liu 2021).

1.3.4.3 Cerebellar targets during fear learning

Although the previously mentioned studies highlight a role of the cerebellum in fear conditioning and fear extinction by showing that cerebellar activity is required for these functions, the downstream pathways, and in particular the targets integrating cerebellar activity remain unclear.

In a recent study, the cerebellar projections to the vlPAG were shown to be critical for the creation of maintenance of a proper association between the CS and the US (Frontera, Baba Aissa, et al. 2020). Indeed, the chemogenetic modulation of FN-vlPAG projections during fear conditioning was able to exert a bidirectional control over extinction learning, with the inhibition of these projections leading to a facilitated extinction, and the stimulation impairing extinction learning (Frontera, Baba Aissa, et al. 2020). Interestingly, the optogenetic stimulation of these projections during CS-US pairing facilitated extinction learning, similarly to the chemogenetic activation (Frontera, Baba Aissa, et al. 2020). However, the vlPAG isn't the only target of the cerebellum which can be involved in fear conditioning and fear extinction.

Notably, the fastigial nucleus was shown to profusely project to the medio-dorsal thalamus (Fujita et al. 2020). Knowing that activity patterns in MD can bidirectionally influence fear extinction (Lee, Ahmed, et al. 2012; Lee, and Shin 2016), that

reciprocal connections exist between the MD and both prefrontal cortex and amygdala (Morceau et al. 2019; Collins et al. 2018; Georgescu, Popa, et al. 2020), and considering that the MD exerts a control over PFC plasticity (Herry, Vouimba, et al. 1999) which is important for the maintenance of extinction learning (Herry, and Garcia 2002), this brings the question of a potential contribution of the cerebellum to extinction learning through its projections to the MD. However, this question was never investigated. Thus, we sought to determine whether FN-MD projections could modulate the extinction of fear memory and regulate thalamo-cortical dynamics.

2

Dual contributions of cerebello-cortical and cerebello-striatal networks to learning and offline consolidation of a complex motor task.

In this study, we used a combination of pathway-specfic chemogenetic inhibition of cerebello-thalamic pathways and multi-site extracellular recordings in the cerebellar nuclei (CN), ventro-lateral thalamus (VAL), centro-lateral thalamus (CL), primary motor cortex (M1) and dorsolateral striatum (DLS) during a complex motor skill learning, the accelerating rotarod, in order to investigate the differential contribution of cerebello-cortical and cerebello-striatal networks to the execution and the offline consolidation of the accelerating rotarod.

My contribution to this study included the development of a rotarod device allowing for multi-focal video acquisition of the behaviour and the development of a new electrode design allowing to record simultaneously CN, VAL, CL, M1 and DLS bilaterally while performing optogenetic actuations of the CN. Then, I performed accelerating rotarod learning on the implanted mice, and analyzed the electrophysiological and behavioural data acquired. I did not participate to the experiments in-

volving chemogenetic inhibitions, which were performed before I joined this project.

I observed short latency increases of firing rate in the CL, VAL, M1 and DLS following optogenetic stimulations of CN neurons. Moreover, I revealed that the cerebello-cortical and cerebello-striatal couplings were increased during learning. Strikingly, while cerebello-cortical was maintained during resting periods, cerebello-striatal coupling was altered, which suggested an involvement of cerebello-cortical pathways during resting periods following learning. Consistently with this, I discovered that, cerebellar spindle activity during NREM sleep following trials selectively entrains cortical neurons which were engaged with the cerebellum during trials, and observed that being entrained by cerebellar spindle activity promoted a maintained cerebello-cortical connectivity.

Ultimately, I discovered strategy-specific replays of neuronal activity in the motor network during resting periods following learning, which were predictive of the trial-to-trial refinement of motor strategy.

Dual contributions of cerebello-cortical and cerebello-striatal networks to learning and offline consolidation of a complex motor task.

Romain W Sala [1#], Andres P Varani[1#], Caroline Mailhes-Hamon[1], Jimena L Frontera[1], Daniela Popa[1*], Clément Léna[1*]

(1) Institut de biologie de l'Ecole normale supérieure (IBENS), Ecole normale supérieure, CNRS, INSERM, PSL Research University, 75005 Paris, France
* these authors jointly directed the work
# these authorscontributed equally to this work

ABSTRACT

The contribution of the cerebellum to motor learning is often considered to be limited to adaptation, a short-timescale tuning of reflexes and learned skills. Yet, the cerebellum is reciprocally connected to two main players of motor learning, the motor cortex and the basal ganglia, via the ventral and intralaminar thalamus respectively. Here, we evaluated the functional changes occurring in the cerebello-cortical and cerebello-striatal networks, as well as the neural mechanisms underlying the offline consolidation of a learned skilled locomotor task in mice. Using multisite extracellular recordings in the motor networks, we found that the coupling between the dentate nucleus of the cerebellum (DN) and both primary motor cortex (M1) and dorsolateral striatum (DLS) was increased along learning the task, and that the connectivity between DN and M1 was maintained during the resting periods in between the rotarod trials. Using pathway-specific inhibition, we confirmed that cerebellar nuclei neurons projecting to the intralaminar thalamus contribute to learning and retrieval, and that cerebellar nuclei neurons projecting to the ventral thalamus contribute to the offline consolidation of a motor skill. Ultimately, we found that offline replays of neuronal activity in the motor network contributed to the refinement of the motor strategy used by the mice during the task. Our results thus show that cerebello-cortical and cerebello-striatal networks support distinct computations operating on different timescales in motor learning.

INTRODUCTION

Learning to execute and automatize certain actions is essential for survival and, indeed, animals have the ability to learn complex patterns of movement with great accuracy to improve the outcomes of their actions {Krakauer, 2019 #53}. Two categories of learning are often engaged in motor skill acquisition {Seidler, 2010 #26;Krakauer, 2019 #53}: 1) sequence learning, which is needed when series of distinct actions are required, and 2) adaptation which corresponds to learning a variation of a previous competence, and typically takes place when motor actions yield unexpected sensory outcomes. The neurobiological substrate of motor skills involves neurons distributed in the cortex, basal ganglia and cerebellum, each structure implementing a distinct learning algorithm {Doya, 1999 #62}. On one hand, the cerebellum is a site where supervised learning takes place {Raymond, 2018 #59}. The cerebellum has been shown to be central for the adaptation of skills such as oculomotor movements {Yang, 2014 #60;Herzfeld, 2018 #61;Nguyen-Vu, 2013 #65}, reaching {Hewitt, 2015 #63}, locomotion {Morton, 2006 #27;Darmohray, 2019 #66}, as well as conditioned reflexes {Longley, 2014 #64;Clopath, 2014 #75}. The cerebellum is thought to form associations between actions and predicted sensory outcome at short-time scale (typically under one second), which are seen as internal models {Ito, 2008 #39}. On the other hand, reinforced learning takes place in the basal ganglia, which are usually linked to learning complex actions involving sequences of movements, for which the involvement of the cerebellum is far less well understood and still controversial {Bernard, 2013 #32;Krakauer, 2019 #53;Seidler, 2002 #44;Baetens, 2020 #30}.

Motor skills are generally progressively acquired {e.g. \Karni, 1998 #57} and their final encoding in the brain may rely on different sets of brain structures compared to the initial training {e.g. \Brashers-Krug, 1996 #58;Korman, 2003 #49;Muellbacher, 2002 #3}. Strikingly, motor skills consolidation is not simply occurring during repetitions of the task, but also takes place offline during resting periods {Brashers-Krug, 1996 #58;Cohen, 2005 #4;Doyon, 2009 #1;Muellbacher, 2002 #3}, which may even be sufficient to change the recruitment of brain regions in the task execution {Shadmehr, 1997 #6}. Motor memories may also persist in the form of savings, which facilitate relearning of the task at a later time {Huang, 2011 #67;Mauk, 2014 #68}. Overall, motor learning is a dynamical process distributed in time and across brain regions.

Understanding the contribution of the cerebellum to motor learning thus requires taking into account its integration in brain-scale circuits including the cortex and basal ganglia {Caligiore, 2017 #56}. In the mammalian brain, both cerebellum and basal ganglia receive the majority of their inputs from the cerebral cortex (via the pontine nuclei for the cerebellum) and send projections back to the cortex via anatomically and functionally segregated channels, which are relayed by predominantly non-overlapping thalamic regions {Bostan, 2013 #101;Hintzen, 2018 #103;Proville, 2014 #102}. Furthermore, anatomical and functional reciprocal di-synaptic connections have been demonstrated between the basal ganglia and the cerebellum {Bostan, 2010 #71;Carta, 2019 #72}. The projections from the cerebellum to the striatum and to the motor cortex are relayed through distinct thalamic regions, respectively the intralaminar thalamus and ventral thalamus {Steriade, 1995 #73;Chen, 2014 #74}, suggesting distinct contributions of these cerebello-diencephalic projections.

In the present study, we hypothesized that the cerebellum may contribute to some phases of learning in a complex motor task via its projections to thalamic nuclei embedded in thalamo-cortical and thalamo-striatal networks. We thus focused on the cerebellar nuclei (CN) Dentate and Interposed and their projections to the centrolateral (intralaminar) thalamus and ventral anterior lateral complex (motor thalamus), which respectively relay their activity to the striatum and the motor cortex {Chen, 2014 #74;Proville, 2014 #102;Gornati, 2018 #104}. First, we examined the contribution of CN and cerebello-thalamic pathways to learning using chemogenetic disruptions either during or after the learning sessions and revealed a differential contribution of the different pathways to online learning and offline consolidation. Then, we investigated the presence of changes of connectivity between the cerebellar nuclei, the motor cortex and the striatum along learning using chronic *in vivo* extracellular recordings. Ultimately, we examined the modulation of neuronal activity in the motor network during the different possible strategies that mice could use during the rotarod task, and investigated the presence of offline replays of neuronal activities as well as their consequences on the strategy used on the rotarod.

RESULTS

In the present study, we used the paradigm of the accelerating rotarod, where the animals walk on an accelerating rotating horizontal rod; over multiple repetitions of the tasks, the rodents develop locomotion skills to avoid falling from the rod. This paradigm allows to study the neurobiological basis of motor skill learning {e.g. \Costa, 2004 #76;Rothwell, 2014 #77;Yang, 2009 #78}. It is notably suitable to investigate the multiple time scales of motor learning: when repeated over multiple days, distinct phases of learning, with different rate of performance improvement and organization of locomotion strategies, can be distinguished {Buitrago, 2004 #79} and selectively disrupted {Hirata, 2016 #80}.

To examine the involvement of the cerebellum in the accelerating rotarod task along the different phases of learning, we first used a chemogenetic approach {Roth, 2016 #94} in order to inhibit neurons from the cerebellar nuclei, using the inhibitory DREADD (hM4D-Gi) activated by the synthetic drug Clozapine-N-Oxide (CNO). In order to validate this approach, mice were injected with AAV5-hSyn-hM4D(Gi)-mCherry (DREADD mice) or AAV5-hSyn-EGFP (Sham mice) and implanted with microelectrode arrays in the CN (Fig. 1a-d). Post-hoc histology confirmed the position of the electrodes (Fig. 1e) and showed that the expression of hM4D(Gi)-mCherry was confined to the CN and restricted to the neuronal membrane, with 78% of the cells expressing hM4D(Gi)-DREADD in the CN (Fig. 1b-d). A week after surgery, the neuronal activity was recorded in the CN in an open-field arena before and after accelerating rotarod sessions. Neither saline (SAL) in DREADD mice nor CNO injection (1 mg/kg) in Sham mice affected the firing rate, while the same dose of CNO induced a significant decrease of the firing rate in DREADD mice during Initial (day 1), Refinement (day 4) and Maintenance (day 7) phases (Fig. 1g and h).

We then examined whether the reduction of CN firing impacted spontaneous motor activity, strength and motor coordination. The average velocity of open-field locomotion was not altered by CNO or SAL injection in DREADD or Sham mice (Fig. Sup1a). In addition, no significant differences were observed between the experimental groups in the fixed speed rotarod (Fig. Sup1b), footprint patterns (Fig. Sup1c), grid test (Fig. Sup1d), horizontal bar (Fig. Sup1e) and vertical pole (Fig. Sup1f) indicating that fatigue, coordination and strength were not affected by the reduction of CN firing induced by 1mg/kg CNO**.** These results thus indicate that the reduction of the CN firing induced by the CNO had a limited impact on the basic motor abilities of the mice.

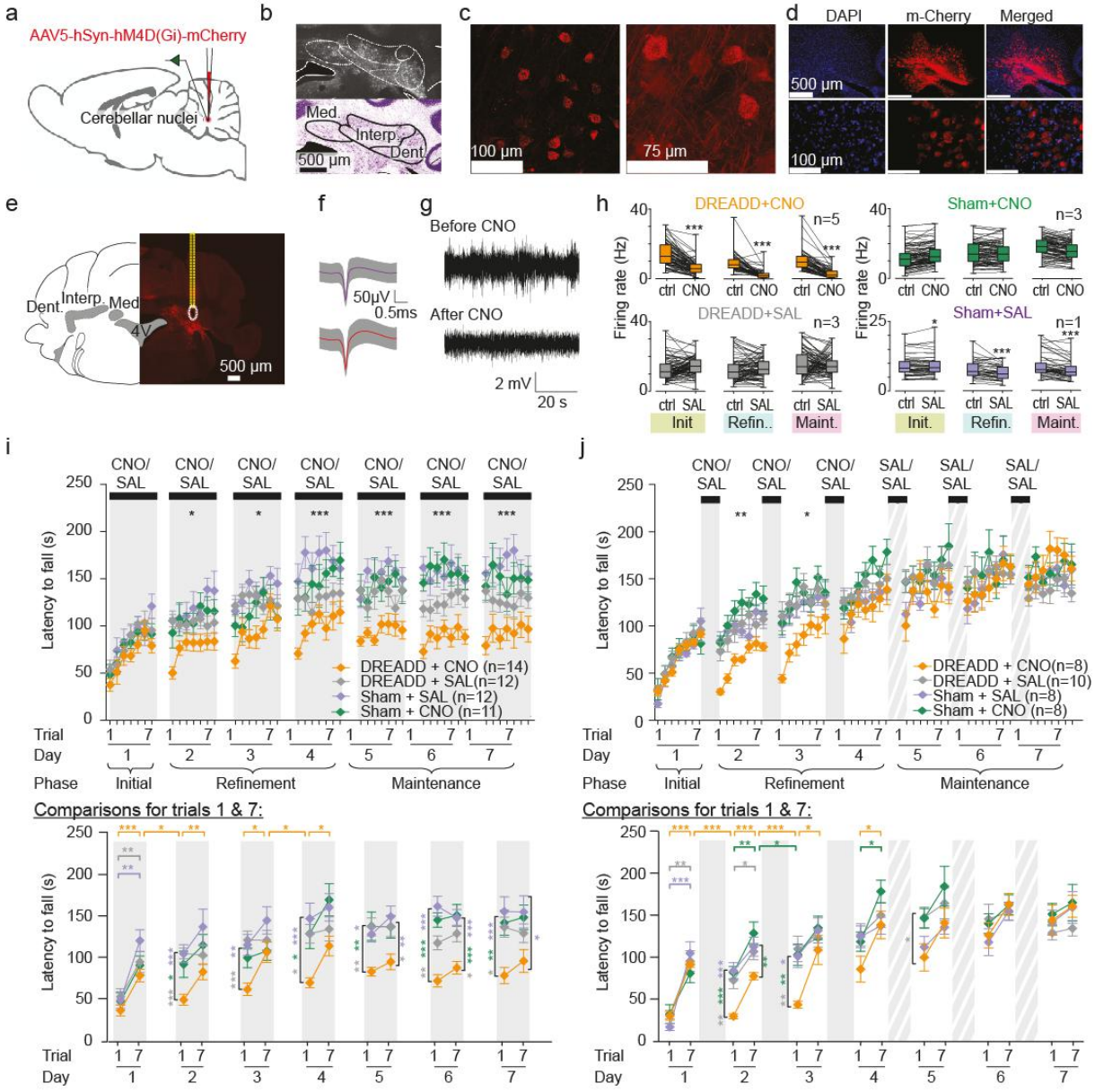

Figure 1. Cerebellar inactivation impairs the performance in the Refinement and Maintenance but not Initial phases of motor learning task. a) Scheme of the implantation and injection. **b**) Coronal section of the cerebellum showing hM4Di-DREADD expression in the three CN. **c**) Representative confocal image showing hM4Di-DREADD expression on neuronal membranes. **d**) DAPI positive neurons expressing hM4Di-DREADD. **e**) Electrode placement close to cells expressing hM4Di-DREADD (red: lesion site, yellow: electrode track). **f**) Examples of spike shapes obtained from spike sorting in CN (mean +/- SD). **g**) Examples of high-pass filtered traces of CN recordings before and after CNO injection. **h**) Boxplots (box: quartiles, whiskers: min/max) of the mean firing rate of neurons recorded in DREADD and non-DREADD injected mice after CNO or SAL injection during Initial (Init.), Refinement (Refin.) and Maintenance (Maint.) phases. CN firing rate was reduced after 1 mg/kg of CNO injection in DREADD injected mice (***p<0.001 paired t-test). Small variations were observed in a Sham+SAL mouse (*p<0.05, ***p<0.001 paired t-test). **i**) Impact of daily of injections of CNO before trial 1 on accelerating rotarod performance. *Top*: summary of the performance for each trial/day (*p<0.05, ***p<0.001; repeated measure ANOVA Group effect). *Bottom*: Latencies to fall in trial 1 and 7 and post-hoc comparisons for only these trials. Horizontal comparison lines correspond to trial 1 versus next trial 7, and trial 7 versus next trial 1, comparisons (*p<0.05, **p<0.01, ***p<0.001 paired t-test). Vertical comparison lines report trial 1 and trial differences to controls (*p<0.05, **p<0.01, ***p<0.001 t-test). **j**) Impact of daily of injections of CNO after the task (30 min after trial 7). All treatment is switched to

saline in the Maintenance phase. Same presentation as in i). Data represents mean ± S.E.M. *n* indicates the number of mice.

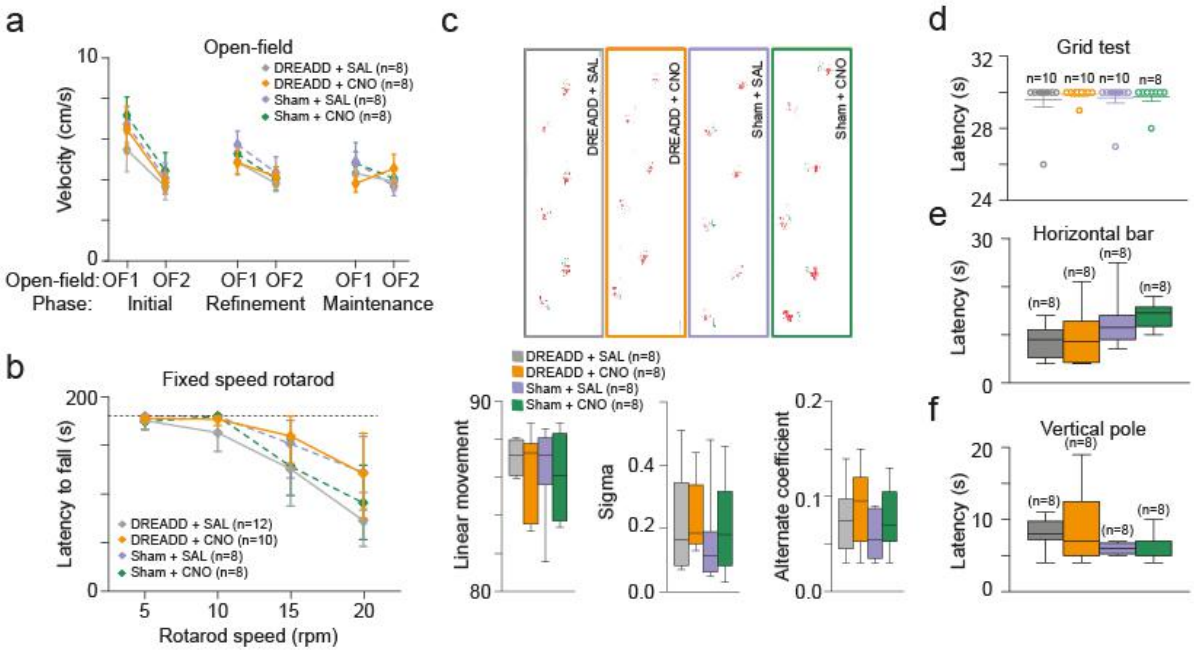

Supplementary Figure 1. Cerebellar nuclei inhibition did not affect execution and fatigue, locomotion, motor coordination, balance and strength. a) Locomotor activity (Velocity) in DREADD and non-DREADD (Sham) injected mice after CNO or SAL injection during open-field sessions before (OF1) and after (OF2) rotarod for Initial, Refinement and Maintenance (**p<0.01 t-test OF1 vs OF2). **b**) Latency to fall during fixed speed rotarod (5, 10, 15, 20r.p.m.) for all experimental groups. One way repeated measure ANOVA was performed on averaged values for all the speed steps in each experimental group followed by a Tukey Posthoc pairwise comparison. **c**) Footprint patterns were quantitatively assessed for 3 parameters as shown on representative footprint patterns (top) for all experimental groups. Three parameters are represented graphically: linear movement (bottom left), sigma (bottom middle) and alternation coefficient (bottom right). **d**) Latency reflecting the time before falling from the grid. 30 seconds of cut-off of was established as the maximum latency (dotted line on figure). **e**) Latency to cross the horizontal bar (balance beam test) for all experimental groups. **f**) Latency to reach home cage in vertical pole test for all experimental groups. *p<0.05 One Way ANOVA followed by a Posthoc Tukey test. *n* indicates the number of mice.

Partial CN inhibition during or after the task has a different impact on motor learning.

To test the effect of a reduction of CN activity on motor learning, we first examined the impact of CN inhibition by injecting CNO (1 mg/kg) each day before the first trial of an accelerating rotarod session (Fig. 1i). This treatment did not affect significantly the learning of DREADD-expressing mice on the first day, but reduced their performance on the following days compared to the control groups: Sham mice which received either SAL or CNO (respectively referred to as Sham+SAL, Sham+CNO), and DREADD mice which received SAL (referred to as DREADD+SAL). During the Refinement phase, the performance in the initial trial of each day was reduced in DREADD+CNO mice compared to the control groups. These poor performances were associated with a significant loss of performance overnight

between the last trial of one day and the first trial of the following day, indicating an impairment in the consolidation of motor learning in the DREADD+CNO mice. Yet, within each daily session, these mice learned fast enough to compensate for their poor initial performance. However, during the Maintenance phase, the performance of the DREADD+CNO group remained lower than the control groups both for the first and last trials of the task, and no further improvement of the performance of this group was observed during this phase. Thus, these results show that the inhibition of the CN impacts on learning consolidation in the Refinement phase, and on the maximal performance reached in the Maintenance phase.

The effect of systemic CNO administration lasted longer than the duration of the learning trials; therefore the results above do not distinguish the action of cerebellar inhibition during the learning trials or after training (offline consolidation). We therefore injected another set of mice with CNO after the training sessions (Fig. 1j). CN inhibition after learning in the Initial and Refinement phases reduced the performance on the first trials of the next day, but did not prevent learning within days, indicating an impairment in the offline consolidation. The performance on the last day of the Refinement phase of DREADD+CNO mice was not different from the mice of the control groups indicating that the lack of overnight consolidation was overcome by training the next day. We then shifted the treatment of all mice to SAL during the Maintenance phase, and this did not reveal any further difference between the groups. Thus, these results indicate that the cerebellum participates to the offline consolidation of the accelerating rotarod learning.

Selective inhibition of cerebello-thalamic pathways differentially impacts motor learning.

Since the CN project to a wide array of targets {Teune, 2000 #118}, we specifically examined whether Interposed and Dentate cerebellar neurons projecting to VAL and CL differentially contribute to the rotarod learning and execution. For this purpose, an AAV5-hSyn-DIO-hM4D(Gi)-mCherry virus expressing an inhibitory DREADD conditioned to the presence of Cre-recombinase was injected either into the Dentate and Interposed CN, while a retrograde CAV-2 virus expressing the Cre recombinase was injected either in the CL or in the VAL, which respectively relay cerebellar activity to the striatum and cerebral cortex. In both cases, we found an expression of hM4D(Gi)-mCherry throughout the CN mostly in the Interposed and Dentate for the CL injections (Supplementary Figure 2). Since there was no

effect of CNO in Sham mice (Fig. 3), we only compared DREADD-injected animals receiving either CNO or SAL.

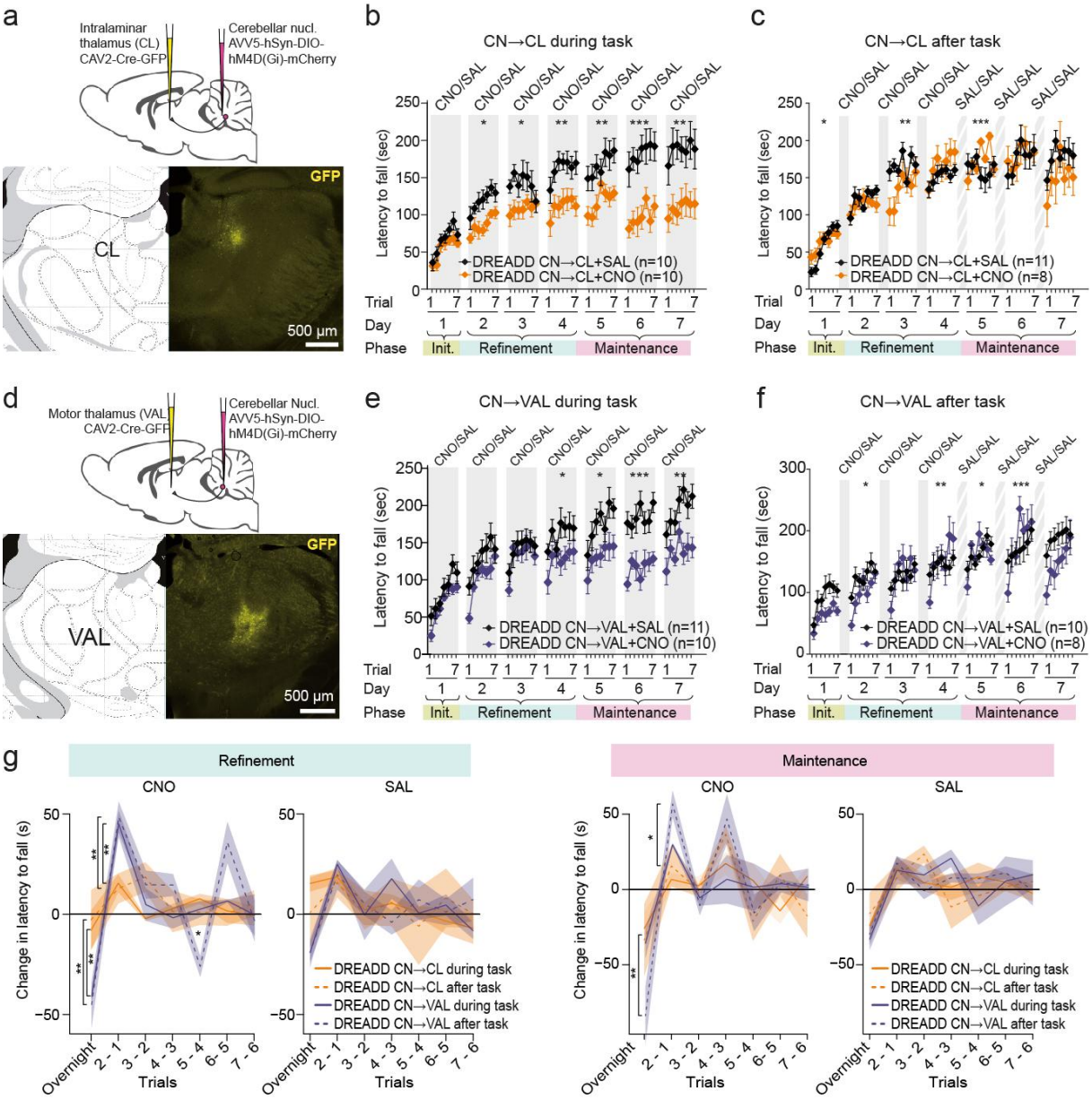

Figure 2. Inhibition of cerebellar nuclei (CN) neurons projecting to the centrolateral thalamus (CL) and to the ventral anterior lateral (VAL) thalamus during and after the training sessions differentially impairs motor learning. a) combined viral injections targeting the CN->CL neurons using a retrograde virus expressing the Cre in the thalamus and a virus inducing Cre-dependent expression of inhibitory DREADD in the CN. *Top*: schematic of the viral injections. *Bottom*: GFP fluorescence revealing the site of injection of the CAV viruses. **b**) Daily of injections of CNO before trial 1 in mice described in panel A reduce performance during Maintenance phase but not earlier phases (*Top*: *p<0.05, **p<0.01, ***p<0.001; repeated measure ANOVA Group effect. **c**) Same as B for daily CNO injections 30 minutes after trial 7 during the Initial and Refinement phases. **d**) combined viral injections targeting the CN->VAL neurons using a retrograde virus expressing the Cre in the thalamus and a virus inducing Cre-dependent expression of inhibitory DREADD in the CN. **e**) same as B for mice described in panel d. **f**) same as panel c for mice described in panel d. **g)** Change of latency to fall in successive trials pooled for the Refinement and Maintenance phases. (comparison between groups during vs after session: p<0.05, **p<0.01, ***p<0.001 Sidak-adjusted)CN: cerebellar nuclei, VAL: ventral anterior lateral thalamus, CL: central lateral thalamus. Data represents mean ± S.E.M, *n* indicates the number of mice.

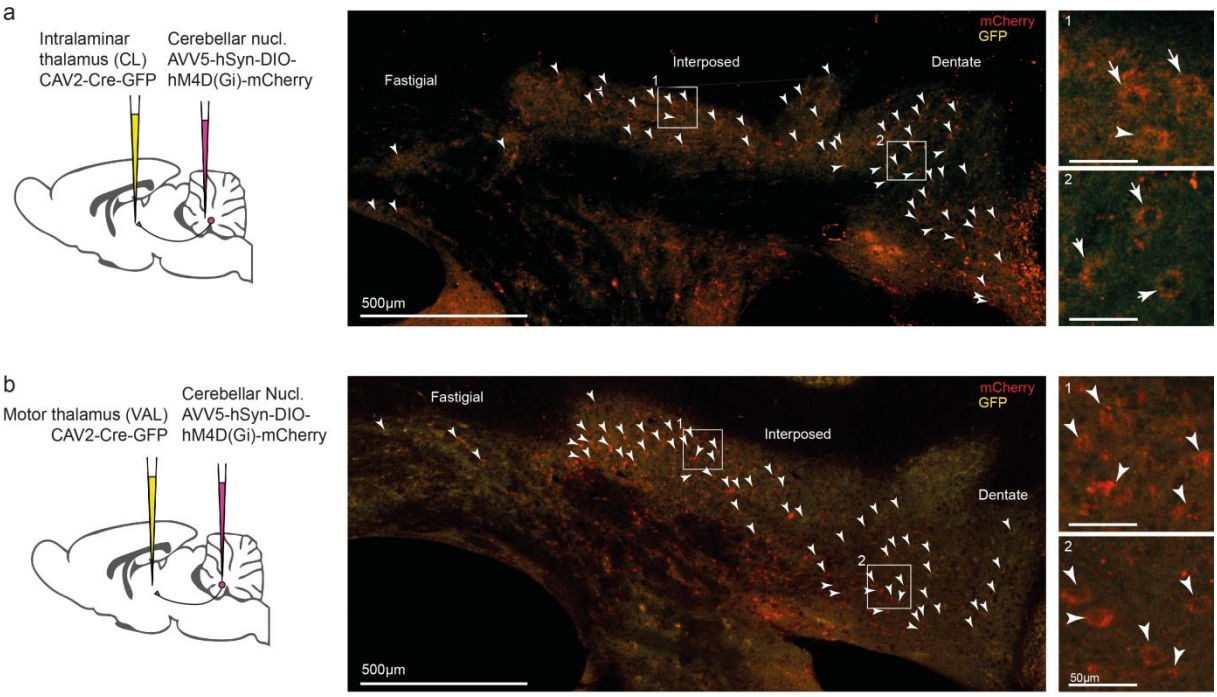

Supplementary Figure 2. Expression of hM4D(Gi)-mCherry in the cerebellar nuclei following CL and VAL injections. a) left: schematics of the experiment for CN-CL groups, right: distribution of labeled neurons. Identified soma expressing mCherry are indicated by arrow-heads. b) same as a for CN-VAL groups.

To examine the impact of the inhibition of cerebello-thalamic neurons on spontaneous locomotion, motor coordination and strength, we first examined locomotor activity in open-field experiments (Fig. Sup3a). Analysis of the open-field locomotor activity revealed that velocity was generally not affected by CNO injection in DREADD or Sham mice (Fig. Sup3a); CNO-injected CN-VAL and CN-CL mice respectively exhibited slightly higher velocity in day 1 and lower velocity in day 4 in the first open field session compared to control group. No significant differences were observed between Saline- vs. CNO-treated CN-CL mice in the fixed speed rotarod test (Fig. Sup3b). We found however a decrease in the latency to fall for 15 and 20 r.p.m. in the CN-VAL+CNO group. No significant differences were observed between the experimental groups for footprint patterns (Fig. Sup3c), grid test (Fig. Sup3d), horizontal bar (Fig. Sup3e) and vertical pole (Fig. Sup3f) indicating that coordination and strength are not affected by the inhibition of cerebellar-thalamic pathways induced by 1mg/kg CNO.

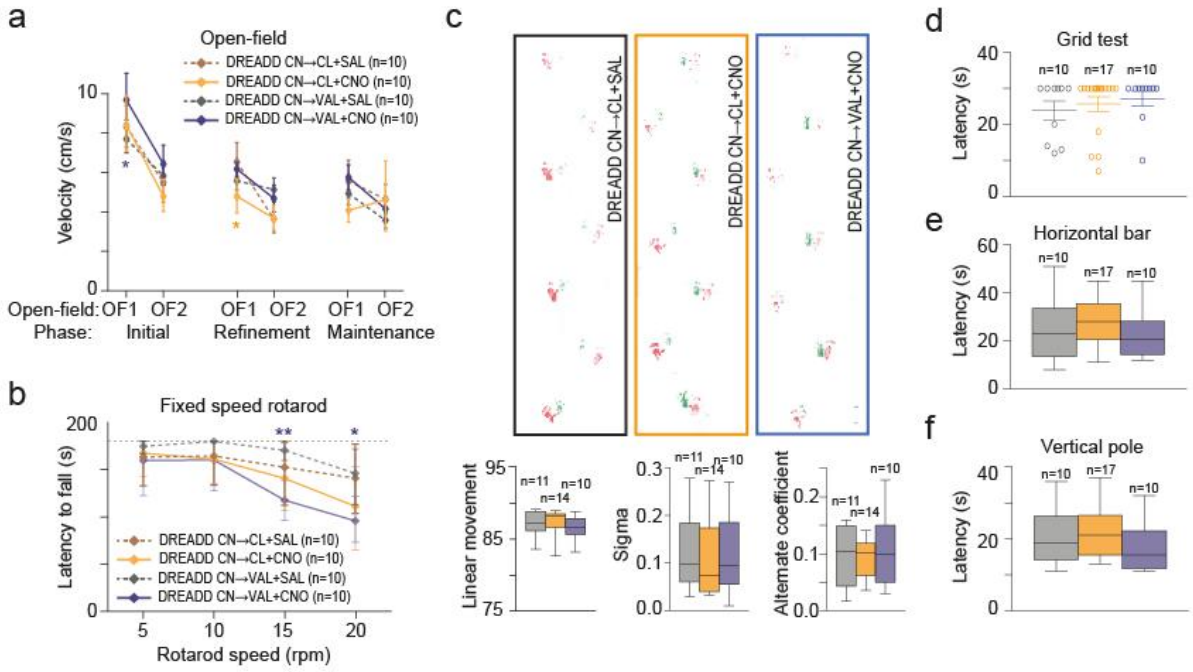

Supplementary Figure 3. Inhibition of CN-CL or CN-VAL by 1mg/kg CNO does not affect execution and fatigue, locomotion, motor coordination, balance and strength. **a**) Locomotor activty (Velocity) in DREADD injected mice after CNO or SAL injection during open-fields sessions before (OF1) and after (OF2) rotarod for Initial, Refinement and Maintenance (**p<0.01 paired t-test OF1 vs OF2). **b**) Latency to fall during fixed speed rotarod (5, 10, 15, 20 r.p.m.) for all experimental groups. One way repeated measure ANOVA was performed on averaged values for all the speed steps in each experimental group followed by a Tukey Posthoc pairwise comparison. **c**) Footprint patterns were quantitatively assessed for 3 parameters as shown on representative footprint patterns (top) for all experimental groups. Three parameters are represented graphically: linear movement (bottom left), sigma (bottom middle and alternation coefficient (bottom right). **d**) Latency reflecting the time before falling from the grid. 30 seconds of cut-off of was established as the maximum latency (dotted line on figure). **e**) Latency to cross the horizontal bar (balance beam test) for all experimental groups. **f**) Latency to reach home cage in vertical pole test for all experimental groups. *p<0.05 One Way ANOVA followed by a PostHoc Tukey test. CN, cerebellar nuclei, CL, centrolateral thalamus; VAL, ventral anterior lateral thalamus. *n* indicates the number of mice.

We then examined how the accelerating rotarod learning was impaired by the inhibition of cerebello-thalamic pathways during (Fig. 2b, e) and after (Fig. 2c, f) the task. Inhibition of the CN-CL pathway during the task (Fig. 2b) did not affect the performance in the Initial phase, but produced a progressive deviation from the performance of the control group during the Refinement phase, yielding to a strong reduction of performance in the Maintenance phase. In contrast, when the inhibition took place after the task during days 1, 2 and 3 (Fig. 2c), the performances remained similar to the control group. This suggests that the CN-CL neurons mostly contribute to the learning during training, and not significantly to offline consolidation.

In contrast, the inhibition of the CN-VAL pathway yielded another pattern of evolution of performances. First, when inhibition took place during the task (Fig. 2e), there was a

strong loss of performance from the last trial of one day to the first trial of the following day (Fig. 2g). This overnight loss was compensated by a fast relearning up to similar levels as the control mice during the Refinement phase. However, despite the fast relearning following the overnight loss, the performances saturated at lower level than control mice during the Maintenance phase. Second, when inhibition took place after the task during days 1, 2 and 3 (Fig. 2f), a similar overnight decrease of performance was observed during the Refinement phase (Fig. 2g). These results are consistent with a contribution of offline activity of the CN-VAL pathway to the prevention of an overnight loss of the motor learning (as observed for full cerebellar nuclei inhibition, Fig. 1j). Interestingly, when the mice previously treated with CNO after the task in the Initial and Refinement phases were injected with SAL during the Maintenance phase, they continued to exhibit a strong reduction in performance on the first trial of each day, but the performances then raised up to similar levels of the control group within each day (associated with significant within-day learning during the Maintenance phase, Fig. 2c, f). This indicates that the mice still failed to consolidate new learning in the Maintenance phase, even in the absence of cerebellar inhibition, suggesting that the overnight consolidation depending on CN-VAL neurons is only possible in the earliest phases of learning.

Overall, this shows on one hand that CL-projecting CN neurons are involved in the task learning and/or execution during the late stages of learning; on the other hand, VAL-projecting CN neurons have a distinct contribution in the offline consolidation of the learning, although their inhibition does not prevent the preservation of a memory trace allowing fast relearning on the next day.

Reversal of the inhibition of the cerebello-thalamic neurons after learning yields dramatic impairments in performances

Mice that learned the task while either CN-CL or CN-VAL neurons were inhibited showed reduced performance compared to controls after 7 days of training. To examine to which extent the reduced performance was associated to a deficit of execution versus a reduced learning, we switched the treatment in each group (Fig. 3): mice that received SAL during 7 previous days were then administered with CNO and *vice versa*. In both groups, mice that received CNO during learning did not exhibit a sudden improvement of performance upon replacement by SAL. In the case of the CN-CL (Fig. 3a), the performances

only mildly improved during the two days of reverse treatment. In the case of CN-VAL (Fig. 3b), CNO-treated mice switched to SAL treatment continued to show a pattern of overnight performance loss and relearning, reaching similar final values at the end of each day as under CNO. Reciprocally, in both groups, SAL-treated mice switched to CNO treatment exhibited a sudden drop in performance in the first day of reverse treatment. In the case of the CN-CL (Fig. 3a), no improvement within days was observed, while for the CN-VAL pathway (Fig. 3b), mice exhibited the same alternation of within-day increases and overnight decreases of performance, as observed in the CNO-treated CN-VAL mice before the reversal of treatment. These results show that the impact of cerebellar-thalamic inhibition during learning cannot be readily reversed by alleviating the inhibition. Cerebellar-thalamic inhibition after learning under SAL reduces the performance and prevents relearning, but with different patterns for each pathway, the CN-VAL inhibition showed a pattern of within-day improvement and overnight decline in performance that was absent following CN-CL pathway inhibition.

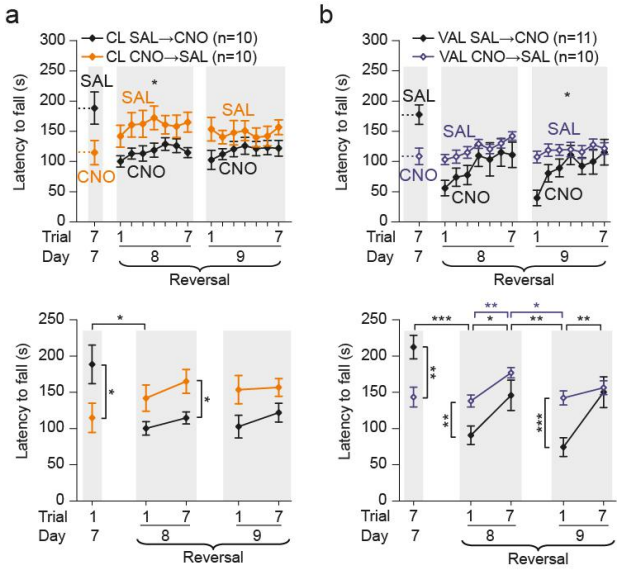

Figure 3. Reversal of the inhibition of the cerebello-thalamic neurons in the late Maintenance phase yields lasting impairments. a) Performance of mice with DREADD expression in CL-projecting CN neurons, which learned the task under respectively CNO and Saline treatment (Figure 4b) during 7 days and then receive respectively Saline and CNO treatment during a Reversal phase. *Top*: time course of the average performance (repeated-measure ANOVA group effect: *: p<0.05). *Bottom*: summary of post-hoc comparisons limited to first and last trials of each day: horizontal comparison lines indicate differences between successive trials 1 and 7; *p<0.05, **p<0.01, ***p<0.001 paired t-test; vertical comparison lines indicate differences between groups of trial 1 and trial 7; *p<0.05, **p<0.01, ***p<0.001 t-test. **b**) same as panel a for mice with DREADD expression in VAL-projecting CN neurons. CN: cerebellar nuclei, VAL: ventral anterior lateral thalamus, CL: central lateral thalamus. Data represents mean ± S.E.M, *n* indicates the number of mice.

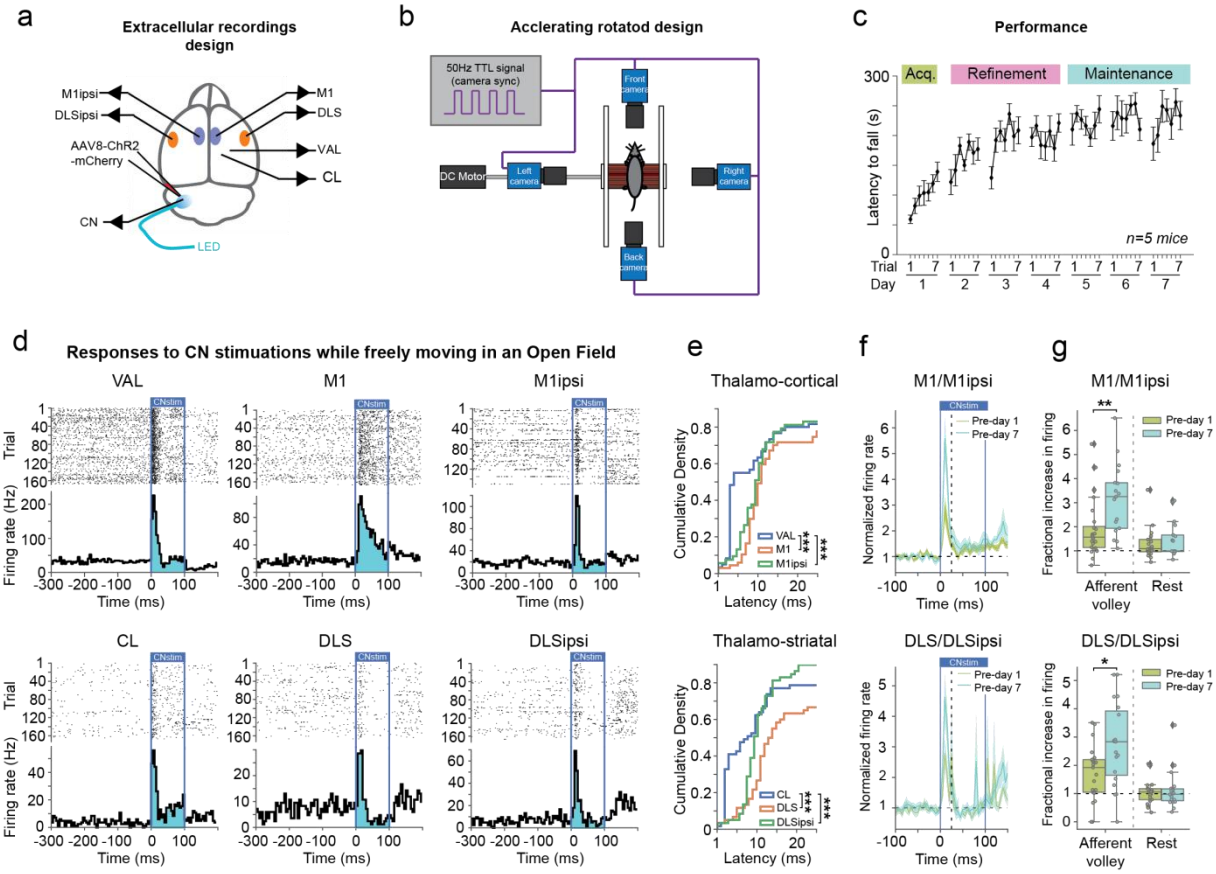

Figure 4. Cerebellar nuclei neurons can bilaterally modulate the activity of the motor cortex and the dorsolateral striatum. a) Experimental design for the extracellular recording of the cerebellar nuclei, thalamus, motor cortex and striatum, and viral strategy for the optogenetic activation of the cerebellar nuclei. **b**) Scheme of the accelerating rotarod setup. **c**) Latency to fall during the accelerating rotarod across trials along days in mice recorded over the 7 days. **d**) Example of peristimulus time histogram (PSTH, 5ms bins) and corresponding raster plots, centred on the onset of the CN stimulation for neurons in the VAL, M1, M1ipsi, CL, DLS, DLSipsi. **e**) Cumulative histograms showing the latency of neuronal response of neurons in the VAL, M1, M1ipsi, CL, DLS, DLSipsi responsive to CN stimulations. **p<0.01, ***p<0.001, Kolmogorov-Smirnoff test. **f**) PSTH (5ms bins, centred on stimulation onset) displaying the change in normalized firing rate (average ± SEM) of responsive neurons in the M1, M1ipsi, DLS and DLSipsi, before the start of the first day of accelerating rotarod training, and before the day 7 (vertical dashed line represents the limit of the afferent volley, 25ms). **g**) Average fractional increase in firing of responsive neurons in the M1, M1ipsi, DLS and DLSipsi, before the start of the first day of accelerating rotarod training, and before the day 7, during the afferent volley (0 to 25ms) and during the rest of the stimulation (25 to 100ms). *p<0.05, **p<0.01, Mann-Whitney U test.

Thalamic, cortical and striatal responses to cerebellar nuclei sitmulations

In order to investigate neuronal dynamics in cerebello-cortical and cerebello-striatal networks during accelerating rotarod learning, we designed an extracellular recording electrode (Fig. 4a) able to simultaneously record neuronal activity in the motor thalamus (VAL), the centro-lateral nucleus of the thalamus (CL), bilaterally record the primary motor cortex (M1 and M1ispi) and dorsolateral striatum associated to hindlimbs (DLS and DLSispi), and to both record and perform optogenetic manipulations of the Dentate and Interposed nuclei of the cerebellum (CN). We also built an accelerating rotarod device, allowing for the acquisition of multiple point of views while the animal is performing the task (Fig. 4b), in

order to better characterize the motor strategies used by the mice on the rotarod, potentially explaining the increase in performances observed during learning (Fig. 4c).

Performing 100ms optogenetic stimulations of the CN during the Open Field sessions preceeding the rotarod training elicited an excitation of neurons in the thalamo-cortical tract, with short latency responses observed in VAL, M1 and M1ispi (Fig. 4de). Latencies of response were significantly shorter in the VAL compared to M1 and M1ispsi (Fig. 4e). Similarly, we observed short latency responses in the thalamo-striatal tract with faster responses in CL compared to DLS and DLSipsi (Fig. 4de). This is consistent with the deep cerebellar nuclei projecting to thalamic nuclei, which then project to cortical and striatal targets.

To examine whether learning induced a change in cerebello-cortical or cerebello-striatal coupling, we compared the magnitude of response to cerebellar stimulations in the cortex and the striatum before starting the accelerating rotarod learning (Day1) and before starting the last day of protocol (Day7). We observed that the increase of firing elicited by the stimulation was greater in M1, M1ipsi, DLS and DLSipsi at the end of the protocol (Fig. 4fg). Interestingly, this increased was mainly present during a short time period corresponding to the afferent volley following cerebellar stimulation (from 0 to 25ms of stimulation, Fig. 4fg). All together, these results suggest that deep cerebellar nuclei neurons can affect the neuronal activity in the motor cortex and the striatum, and that cerebello-cortical and cerebello-striatal couplings are increased as a consequence of motor learning.

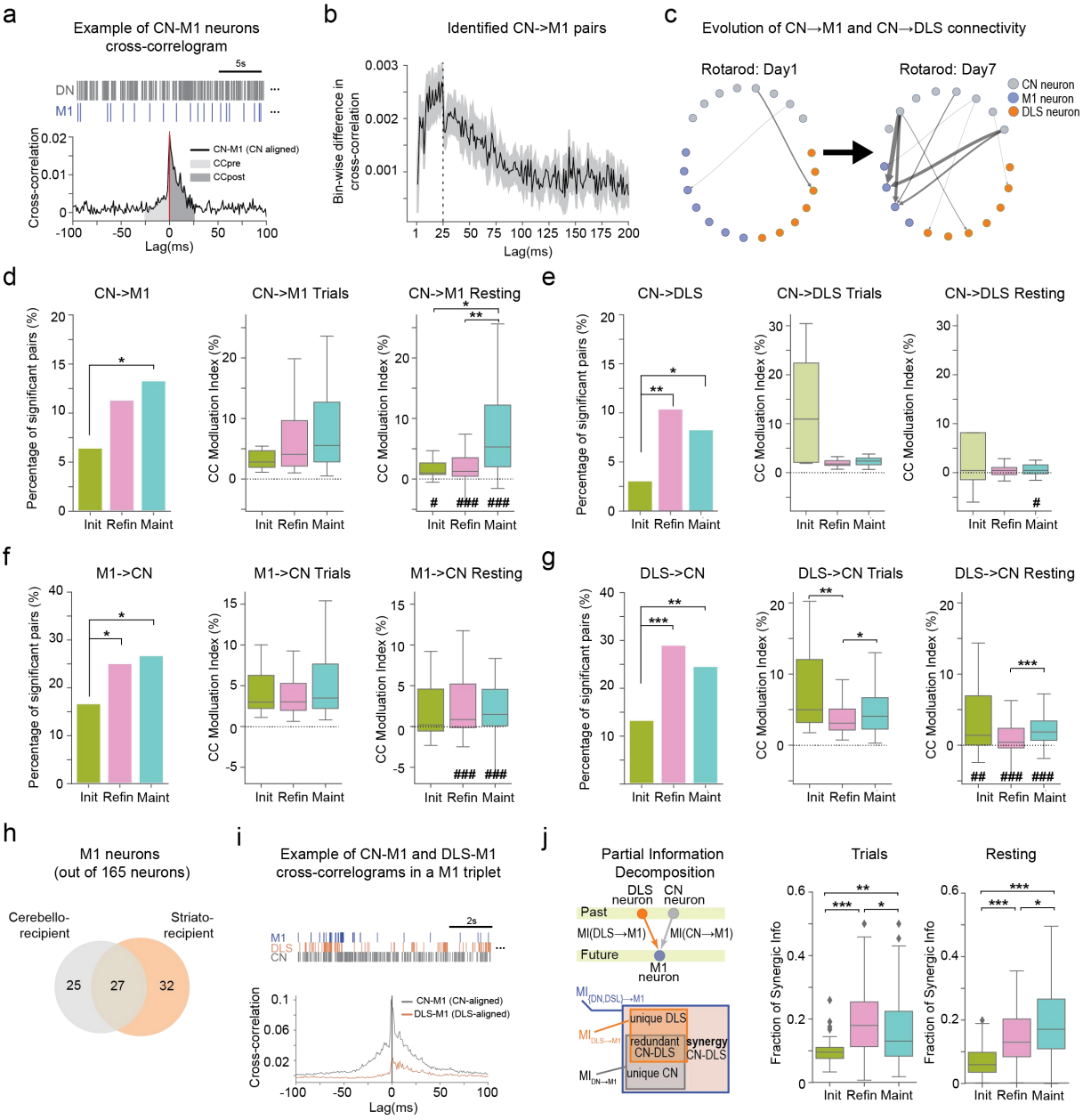

Figure 5. Cerebellar connectivity with the motor cortex and the striatum increases along learning and is partially maintained during resting. a) Example cross-correlogram of a CN neuron and a M1 neuron, and example of associated spiketrains (top). **b**) Measure of bin-wise asymmetry in cross-correlograms of CN and M1 neurons directionally connected. The dotted line represents the limit of the considered zone for asymmetry detection (25ms) **c**) Ascending connectivity map of neurons in the CN, M1 and DLS for a mouse during the first day of rotarod training (left) and for the same mouse during the last day of rotarod training (right). Significant connectivity during trials is represented by arrows, the thickness of the arrow is proportional to the asymmetry index. **d) e) f) g)** Percentage of significantly connected pairs in a given direction during trials. *p<0.05 **p<0.01, ***p<0.001, Fischer exact test. (left). Distributions of asymmetry indices during trials of pairs of neurons significantly connected in a given direction during trials. *p<0.05 **p<0.01, ***p<0.001, Dunn posthoc test following a Kruskal Wallis test.(middle). Distributions of asymmetry indices during resting of pairs of neurons significantly connected in a given direction during trials. *p<0.05 **p<0.01, ***p<0.001, Dunn posthoc test following a Kruskal Wallis test. #p<0.05, ##p<0.01, ###p<0.001, Wilcoxon test for the difference to 0.(right). **h**) Venn diagram showing the proportions of targets neurons in M1 significantly connected with the CN, DLS or both. **i**) Example cross-correlograms of a CN, DLS and M1 triplet, and example of associated spiketrains (top). **j**) Schematics of the partial information decomposition used to characterize information transfer in M1 triplets (left). Distributions of the fraction of synergy between CN and DLS neurons towards M1 neurons during trials (middle) and during resting (right). *p<0.05 **p<0.01, ***p<0.001, Dunn posthoc test following a Kruskal Wallis test.

Cerebellar connectivity with the motor cortex and striatum is enhanced during motor learning.

We then investigated the previously observed increase in cerebello-cortical and cerebello-striatal coupling by analyzing single neurons connectivity between CN, M1 and DLS. We computed the cross-correlograms of spiketrains from pairs of single neurons recorded during rotarod trials, allowing us to observe an enrichment of correlation distributed in a short period following the discharge of the reference neuron (Fig. 5a) . This asymmetry in cross-correlogram suggests that sequences of neuronal activities are propagated in the motor network, and reveals the presence of a directional connectivity between CN, M1 and DLS. Thus, we defined 25ms time windows following (CCpost) and preceding (CCpre) the discharge of the reference neuron, and pairs of neurons displaying a distribution of bin-wise difference in correlation (CCpost-CCpre) significantly different from 0 during these 25ms time windows were considered connected (Wilcoxon rank test, $p<0.05$). The sign of this difference was indicative of the direction of the connectivity, as a difference greater than 0 would suggest that the activity of the reference neuron was preceding the one of the target neuron. For example, a pair of neuron composed of a CN neuron as the reference and a M1 neuron as the target with a difference significantly greater than 0 would be categorized as a CN->M1 pair (Fig. 5b).

This analysis revealed that the connectivity between the cerebellm and the striatum was initially low during the initial phase of learning, but greatly increased during the maintenance phase (Fig. 5c). Indeed, we observed that the percentage of CN->M1 pairs was significantly higher during the maintenance phase compared to the initial phase (Fig. 5d). The percentage of CN->DLS pairs increased during learning, but in contrast to CN->M1 pairs, it was higher during both refinement and maintenance phase compared to during the initial phase (Fig. 5e). This result suggests that the coupling between the cerebellum and both motor cortex and striatum increasse during motor learning, with a rapid increase in cerebello-striatal connectivity, and a more progressive increase in cerebello-cortical connectivity. We also identified M1->CN and DLS->CN pairs, which were significantly more frequent during both refinement and maintenance phase compared to initial phase (Fig. 5fg). However, the strength of coupling between CN, M1 and DLS neurons during rotarod trials remained stable during learning, as evidenced by the stationarity of the asymmetry modulation index along learning phases for CN->M1, CN->M1, M1->CN pairs (Fig. 5def),

although DLS->CN pairs displayed a lower modulation index during the refinement phase compared to both initial and maintenance phase (Fig. 5g).

These results suggest that the degree of connectivity between the cerebellum and both motor cortex and striatum is increased during motor learning in both ascending and descending directions, more rapidly with the striatum than with the cortex.

Cerebello-cortical coupling is vastly maintained during the resting periods in-between rotarod trials, while cerebello-striatal coupling is decreased.

Knowing that the offline consolidation of a learned task is paramount for the ability of maintaining its memory trace, we explored the coupling between connected pairs during the resting periods in-between the rotarod trial. We observed that the modulation index of CN->M1 pairs was significantly greater than 0 during all the learning phases (Fig. 5d), and that it was increased during maintenance phase compared to initial and refinement phase, suggesting that cerebello-cortical coupling is not only maintained during resting periods, but is also increasing during learning. Similarily, the modulation indices of M1->CN and DLS->CN pairs were signifcanlty greater than 0 during resting periods, although the modulation indices of M1->CN pairs wasn't different from 0 during the initial phase (Fig. 5fg). The modulation indices of M1->CN and DLS->CN pairs remains stable during learning, with the exception of DLS->CN pairs having a lower modulation index during refinement compared to maintenance phase.

In contrast, the modulation index of DN->DLS pairs was not different from 0 during resting periods, except for the maintenance phase. These results reveal that while cerebello-cortical connectivity is maintained during resting periods, the cerebello-striatal connectivity is reduced, suggesting an engagement of cerebello-cortical networks during the offline consolidation of a the accelerating rotarod learning.

Increased interactions between cerebellar and striatal inputs to the motor cortex during accelerating rotarod learning.

Because the striatum exerts a modulation of the motor cortex and its cortico-spinal output, we investigated the potential interactions between cerbellar and striatal inputs to the motor cortex during motor learning. Indeed, DLS also exhibits directional connectivity with M1, and we were able to record neurons in M1 simultaneously being connected with

one or more CN neurons and one or more DLS neurons (Fig. 5hi). In a total population of 165 M1 neurons, 52 neurons were categorized as cerebello-recipient, 59 were striato-recipient, and 27 were receiving from both cerebellum and striatum simultaneously (Fig. 5h), suggesting that a substantial amount of M1 neurons are integrating information from both CN and DLS.

In order to delineate the contributions of CN neurons and DLS neurons over M1 in triplets, we used the Partial Information Decomposition technique (PID) derived from information theory (Fig. 5j). This technique allows to quantify the amount of information carried uniquely by the CN neuron, the information carried uniquely by the DLS neuron, the information carried by both (redundancy) and the interactions between CN and DLS neurons (synergy). We observed that, during trials, the fraction of synergic information was increased during refinement and maintenance phase compared to the initial phase (Fig. 5j), suggesting a greater collaboration between CN and DLS neurons during the execution of the task. Strikingly, the the fraction of synergic information during resting periods also underwent a progressive increase during learning (Fig. 5j).

These results reveal the fact that cerebellar and striatal inputs to the motor cortex are not independent, and that the cooperation between these inputs becomes greater during the later phases of learning, both during the execution of the task and during resting periods. Overall, our findings suggests that the functional coupling between the cerebellum, the striatum and the motor cortex is increased during motor learning, with cerebello-cortical networks being strongly engaged during the resting periods after the task.

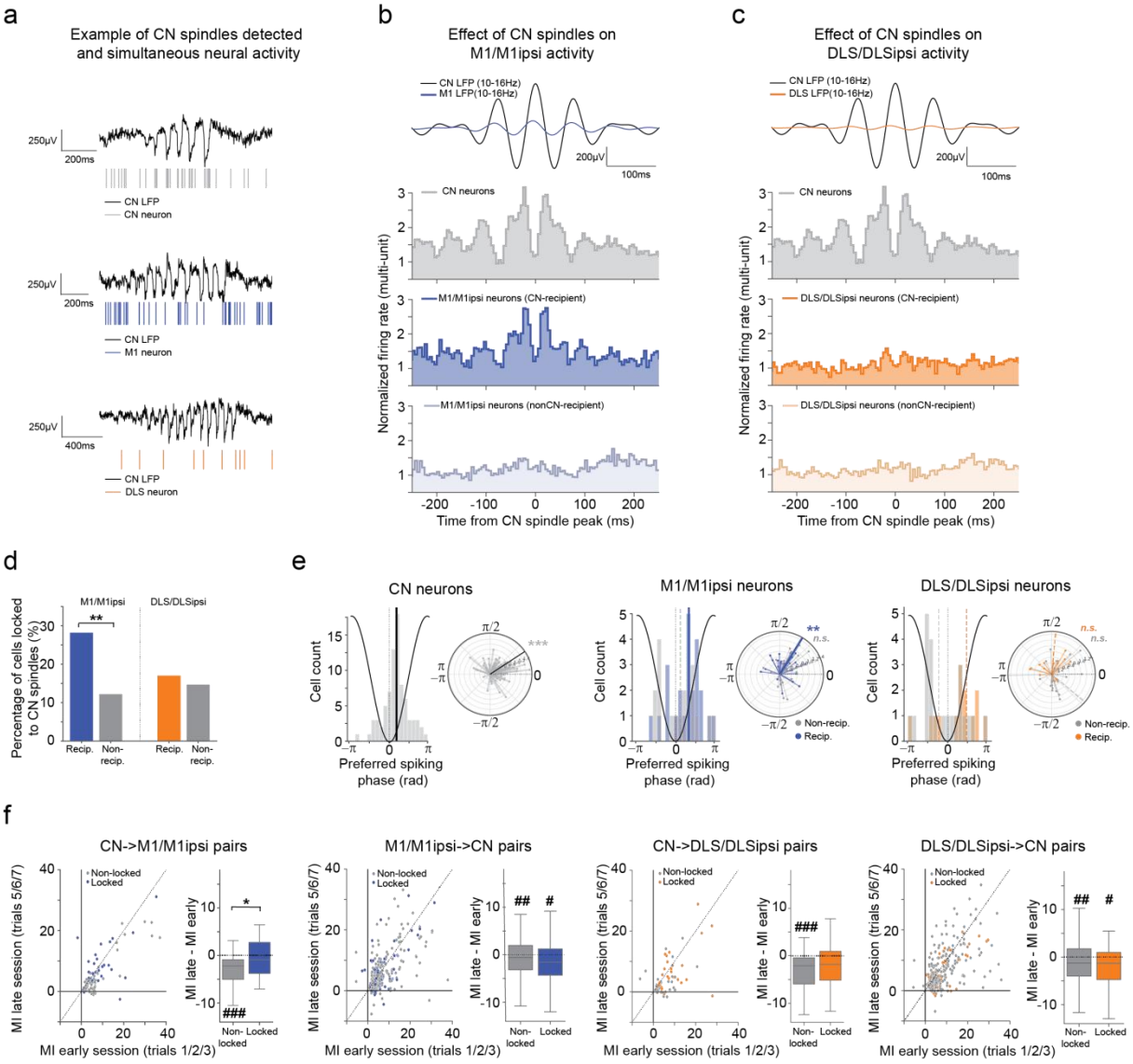

Figure 6. Cerebellar spindles activity during NREM sleep selectively reactivates cortical neurons engaged with the cerebellum during trials and shapes cerebello-cortical connectivity. a) Examples of spindles detected in the LFP of the CN and simultaneous spiketrains of a CN neuron (top), M1 neuron (centre) and DLS neuron (bottom). **b**) Average filtered LFP (10-16Hz) in the CN and M1 centered on CN spindles peak (top), corresponding normalized multi-unit activity of neurons in the CN, M1 and M1ipsi depending on their relationship with CN neurons during trial (bottom). **c**) Average filtered LFP (10-16Hz) in the CN and DLS centered on CN spindles peak (top), corresponding normalized multi-unit activity of neurons in the CN, DLS and DLSipsi depending on their relationship with CN neurons during trial (bottom). **d**) Proportions of neurons in M1/M1ipsi and DLS/DLSipsi locked to cerebellar spindles, depending on their relationship with CN neurons during trial. **p<0.01, Fischer exact test. **e**) Histogram and polar plot of preferred firing phase within cerebellar spindles for neurons significantly locked to cerebellar spindles, depending on their relationship with CN neurons during trial. Vertical lines represent the populational circular mean, plain line if there was a significant populational locking, dashed otherwise (left). **p<0.01,***p<0.001 Rayleigh test. **f**) Scatterplot showing the evolution of the asymmetry modulation index of connected pairs during a training session (left) and the distribution of the difference in modulation index (right) for different directions of connectivity and depending on their locking to cerebellar spindles. *p<0.05, Mann-Whitney U test. #p<0.05, ##p<0.01, ###p<0.001, Wilcoxon test for the difference to 0.

Cerebellar spindle activity during NREM sleep entrains cortical neurons and is associated to a preserved cerebello-cortical connectivity

The maintained cerebello-cortical connectivity during resting periods and the effect of CN-VAL inhibition after the task support the involvement of the cerebello-cortical loop in offline consolidation of a motor skill. Memory consolidation is known to be supported by different mechanisms, including patterns of activity occurring during sleep. Particularly, sleep spindles were demonstrated to play a role in shaping functional connectivity in neuronal networks. Recent studies have demonstrated the presence of such patterns of activity in the cerebellum, but little is known on the functional consequences of cerebellar spindles on long-range connectivity.

Therefore, we classified sleep cycles during resting period using M1 Local Field Potential then detected cerebellar sleep spindles using DN LFP based on the methods proposed by Lemke et al (see Material and Methods). We were able to observed spindle like activity in the deep cerebellar nuclei during NREM sleep (Fig. 6a). We observed that cerebellar spindles strongly entrained neuronal activity in the DCN (Fig. 6ab), but also in M1 bilaterally (Fig. 6b). In contrast, neurons in DLS and DLSispi displayed little entrainement by cerebellar spindles (Fig. 6ab), consistently with the alteration of cerebello-striatal coupling during resting periods in-between trials.

Interestingly, M1 and M1ispi neurons considered as cerebello-recipient on the rotarod were more often significantly phase locked to cerebellar spindles than neurons non considered as cerebello-recipient on the rotarod (Fig. 6d), suggesting that cortical neurons engaged in the rotarod task were more consistently activated by cerebellar spindles than other cortical neurons. However, this was not the case for DLS and DLSipsi neurons (Fig. 6d). The vast majority of DN neurons were phase-locked to the troughs of cerebellar spindles (Fig. 6e), however, only cortical neurons considered as cerebello-recipient on the rotarod were consistently locked to the troughs of cerebellar spindles, with a preferred spiking phase lagging behind the preferred spiking phase of CN neurons (Fig. 6e), consistently with these neurons being entrained by cerebellar activity. Non cerebello-recipient cortical neurons didn't display consistent phase locking, which was also the case for striatal neurons, regardless of them being considered as cerebello-recipient are not (Fig. 6e).

Then, we investigated whether being entrained by cerebellar spindles had an effect on the functional connectivity of cortical and striatal neurons with the cerebellum. We

calculated the cross-correlogram modulation index of both cerebello-recipient and cerebello-projecting cortical and striatal neurons during the first three trials (early) and during the last three trials (late) of each session. Comparing early and late modulation indices revealed that modulation indices of such pairs were significantly decreased during each session, with the exception of cerebello-recipient cortical cells significantly locked to cerebellar spindles (Fig. 6f). Interestingly, cerebello-recipient striatal cell locked to cerebellar spindles did not display a decrease in modulation index, but the difference in modulation index was not significantly different from non-locked striatal cells. Overall, these result suggest that cerebellar spindles are able to entrain cortical activity bilaterally, and may be involved in preserving the functional coupling between cerebellar and motor cortex neurons during the execution of the task

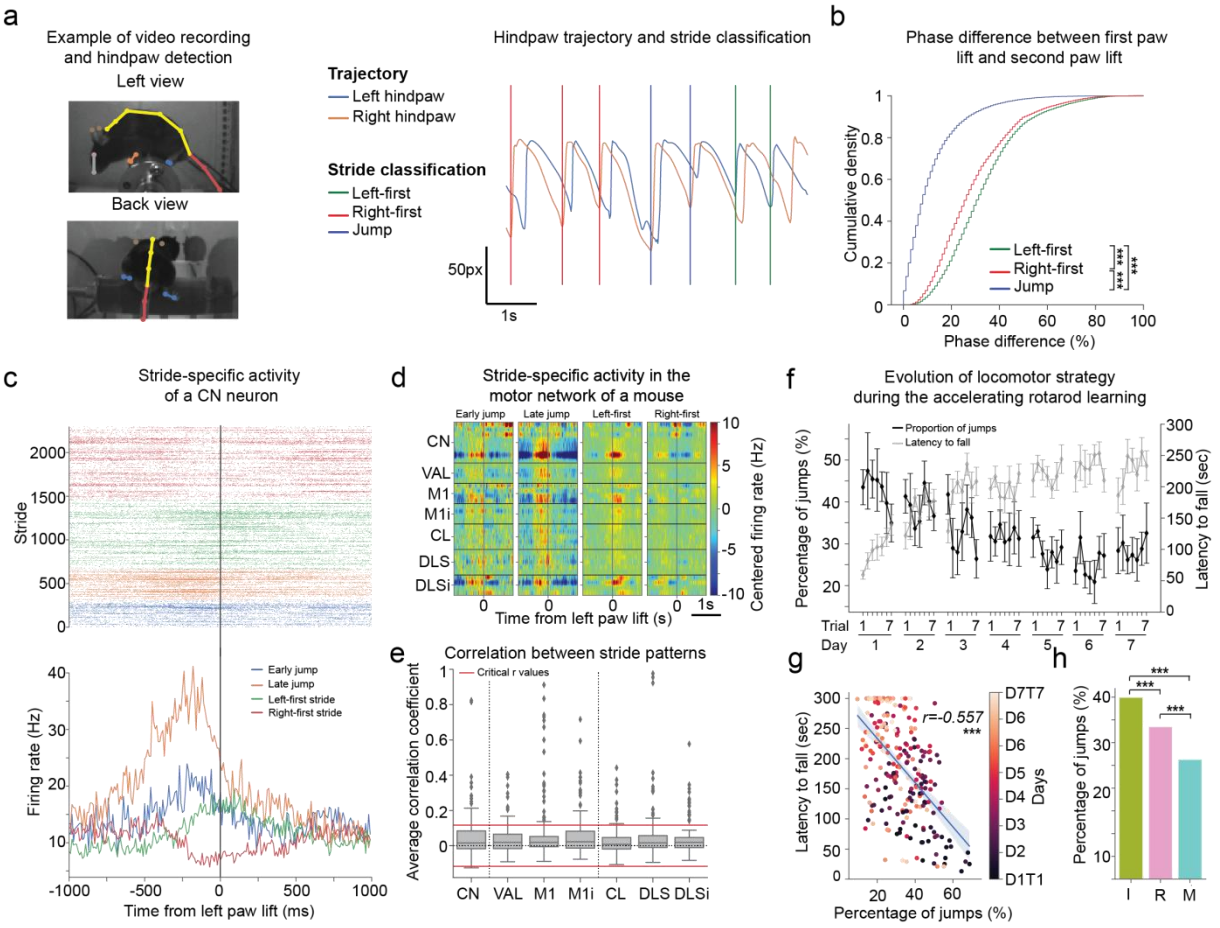

Figure 7. The motor strategies used by mice on the rotarod differentially modulates the activity in the cerebello-cortico-striatal network and evolves during learning. a) Examples of frame and detection from the left view and back view camera (left). Example traces for the y positions of the hind-paws in time, as well as the associated stride classification (right). Coloured vertical lines represent the different stride types. **b**) Cumulative histogram of phase difference between the lift of the first hind-paw and the lift of the second hind-paw. ***p<0.001, Kolmogorov-

Smirnoff test. **c**) Example of PSTH 10ms bins and corresponding raster plots, centred on the lift of the left paw for a neuron in the CN during the different types of strides. **d**) Example of PSTH 10ms bins and corresponding raster plots, centred on the lift of the left paw for neurons recorded simultaneously in a same mouse in the CN, VAL, M1, M1ipsi, CL, DLS, DLSipsi during the different types of strides. **e**) Distributions of average pairwise cross-correlations between the average activity observed during the different types of strides for single neurons. Red bars represent the critical values for significant correlation. p>0.05 Wilcoxon test for the difference to 0. **f**) Evolution of the percentage of jump during the learning protocol (black line), along with the evolution of latency to fall (gray line). Data are represented in average+/-SEM. **g**) Scatterplot and associated linear regression showing the latency to fall as a function of the percentage of jumps during trial. The colours of the dots reflect the timepoint at which the trial occurred ***p<0.001, Pearson's correlation test. **h**) Percentage of jump during each phases of learning. ***p<0.001, Fischer exact test.

The motor strategies used by mice on the rotarod differentially modulates the activity in the cerebello-cortico-striatal network.

The latency to fall is classically used as an indicator of performances during the accelerating rotarod task. However, the latency to fall strictly reflects the time spent before doing a critical error causing the fall, and thus bears little information on the motor sequences chosen by the mice on the rotarod or on the behavioural correlates of the increased performances during learning. In order to furher understand the changes in motor strategy used by mice during learning, we built a custom rotarod with transparent walls allowing for video acquisition and tracking of mice limbs during the task using DeeplabCut (Fig. 7a). Based on the tracking of their hindpaws, mice seem to express a discrete set of motor strategies (Fig. 7a). They would either express a sequential stride, with a full swing of a paw occuring before starting the swing of the contra-lateral hindpaw, this type of stride would be called 'left-first' if the swing of the left hindpaw started before the right hindpaw, and 'right-first' otherwise. In some case, the mice would initiate swings of both hindpaws simultaneously, this was considered as a 'jump' (Fig. 7b).

While investigating the average neuronal response around the lift of the left paw, we observed that the neurons we recorded were modulated during the stride. However, the modulation of neuronal activity varied depending on the type of stride that was expressed, in terms of magnitude, polarity and temporal sequence (Fig. 7c). Interestingly, while the strides characterized as jumps displayed similar characteristics and kinematics behaviourally, the neuronal activity associated to their expression wasn't stationary. Particularly, jumps occurring early during a trial (first half of the trial) lead to a different modulation of neuronal activity than jumps occurring later during the trial (Fig Xcd).

This differential modulation of neuronal activity by the different stride types could be observed in every structure of the cerebello-cortico-striatal network (Fig. 7d), and most recorded neurons displayed poor correlations between their modulation during the different

stride types (Fig. 7e). This suggest that the different motor strategies used by the mouse on the rotarod have a specific neuronal signature.

The motor strategies used by mice on the rotarod evolves along learning

Jumps are overall sub-optimal, as they require a propulsion intense enough to allow for both hindpaws to be lifted from the rod at the same time, and thus are both energy demanding and induce a risk of loss of balance. Interestingly, the proportion of jumps expressed by the mice on the rotarod decreased during learning (Fig. 7fh), along with the increase in latency to fall (Fig. 7f). Indeed, the proportion of jumps was anti-correlated to the latency to fall (Fig. 7fg), suggesting that jumps were more frequently expressed by naive mice than expert mice.

Thus, the evolution of the motor strategy used on the rotarod may be a behavioural correlate of learning. Initially, the strategy is biased towards jumping, and along learning, gradually shifts and promotes the use of left-first and right-first strides. However, the mechanisms underlying this gradual decrease in jumping on the rotarod remain unknown.

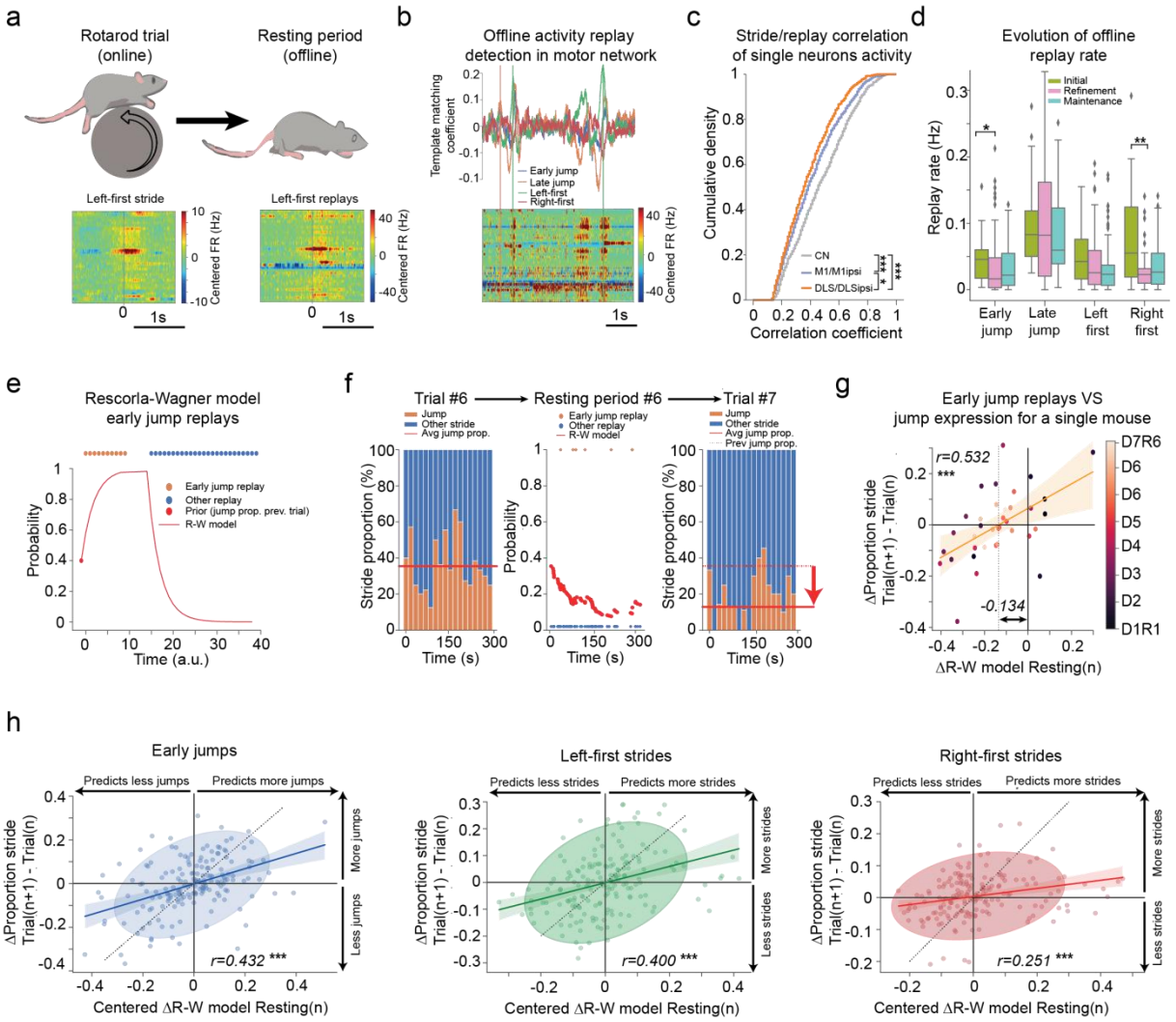

Figure 8. Mice perform strategy-specific replays of neuronal activity in the motor network during resting, which predict changes in motor strategy. a) Conceptualization of the detection of strategy-specific replays of activity during resting periods. **b**) Example of template matching analysis (top) detecting the replays of different types of stride from the neuronal activity of a mouse during resting period (bottom). **c**) Cumulative histogram of the Pearson's correlation coefficient between average activity during a stride type and during a replay for neurons significantly correlated. *p<0.05, ***p<0.001, Kolmogorov-Smirnoff test. **d**) Distributions of the frequencies of offline replay detection during each phase, for the different stride types. *p<0.05 **p<0.01, Dunn posthoc test following a Kruskal Wallis test. **e**) Scheme explicating the learning model used to predict trial-to-trial change in stride proportion based on the temporal structure of the replay during a resting period. **f**) Example of the learning model prediction a trial-to-trial change in stride proportion based on the temporal structure of the replay during a resting period. **g**) Scatterplot and associated linear regression showing the actual variation in stride proportion between trial-to-trial as a function of the predicted variation. The colours of the dots reflect the timepoint at which the resting period occurred. **h**) Scatterplots and associated linear regressions showing the actual variation in stride proportion between trial-to-trial as a function of the predicted variation for different stride types. Covariance ellipses of 2SD are represented. ***p<0.001, Pearson's correlation test.

Stride-specific replays of neuronal activity in the cerbello-cortico-striatal network during resting periods is predictive of inter-trial refinement of motor strategy

Knowing that offline replays of neuronal activity were shown to be involved in the offline consolidation of a learned task, we assessed the presence of strategy-specific replays of activity during the resting periods in-between rotarod trials (Fig. 8a). We used a template

matching approach to detect the presence of events displaying a strong similarity to the sequence of activity induced by a given type of stride during resting periods (Fig. 8b). We were able to observe replays associated to each motor strategy, with a reactivation of neurons in the cerebellum, thalamus, motor cortex and striatum. However, the consistency of the relationship between the replay and the stride-related activity varied between structures (Fig. 8c). Indeed, the cerebellum displayed the highest consistency of reactivation, suggesting a strong engagement of the cerebellum in offline replays. In contrast, the striatum displayed the lowest correlation between stride related activity and reactivation, consistently with a lower connectivity with the striatum during resting periods.

Interestingly, little changes were observed in the replay rate of the different strategies along learning (Fig. 8d), which strongly contrasts with the dramatic decrease in percentage of jumps expressed during learning. Regardless, we hypothesized that the structure and content of the replays during resting period could be linked to the triat-to-trial changes in motor strategy expressed by the mouse on the rotarod. We defined a simple learning model trying to predict the probability of expressing a type of stride on a given trial based on the content of replays during the resting period preceding this trial and the probability of expressing this stride during the previous trial (Fig. 8e). In this model, while replaying the activity associated to this given stride will increase the probability of expressing this stride, replaying the activity associated to an other type of stride will decrease the probability of expressing it (Fig. 8e). The model reached good performances in predicting changes in the probability of expressing a stride (Fig. 8f). Indeed, only fitting a learning rate per mouse allowed the model to perform predictions significantly correlated to the variation in stride expression (Fig. 8g), suggesting that for single mice, the structure of replay activity was predictive of the trial-to-trial variation in stride expression. However, the model tended to generally overestimate the occurrence of reduction in proportion of strides, as evidences by the negative offset in the model prediction corresponding to a steady proportion of strides (Fig. 8g). This offset varies between mice, and its subtraction allows to assess the relationship between prediction and actual variation in behaviour in the entire population of mice (Fig. 8h).

We observed that the model prediction was positively correlated to the variation in stride proportion in-between trials, for jumps, left-first strides and right-first strides (Fig. 8j).

These results support the role of offline replays of neuronal activity in refining the motor strategy used by the mice on the rotarod in a trial-to-trial basis.

MATERIAL AND METHODS

1. Behavioral experiments

1.1. Accelerated rotarod task

The rotarod apparatus (mouse rotarod, Ugo Basile) consisted of a plastic roller with small grooves running along its turning axis (Bearzatto et al., 2005). One week after injections, mice were trained with seven trials per day during seven consecutive days. This training protocol was chosen in order to distinguish the three different phases (Acquisition, Consolidation and Maintenance). During each trial, animals were placed on the rod rotating at a constant speed (4 r.p.m.), then the rod started to accelerate continuously from 4 to 40 r.p.m. over 300 s. The latency to fall off the rotarod was recorded. Animals that stayed on the rod for 300 s were removed from the rotarod and recorded as 300 s. Mice that clung to the rod for two complete revolutions were removed from the rod and time was recorded. Between each trial, mice were placed in their home cage for a 5-minutes interval.

1.2. Open-field activity

Mice were placed in a circle arena made of plexiglas with 38 cm diameter and 15 cm height (Noldus, Netherlands) and video recorded from above. Each mouse was placed in the open-field for a period of 10 minutes before and after the accelerated rotarod task with the experimenter out of its view. The position of center of gravity of mice was tracked using an algorithm programmed in Python 3.5 and the OpenCV 4 library. Each frame obtained from the open fields videos were analyzed according to the following process: open-field area was selected and extracted in order to be transformed into a grayscale image. Then, a binary threshold was applied on this grayscale image to differentiate the mouse from the white background. To reduce the noise induced by the recording cable or by particles potentially present in the Open-field, a bilateral filter and a Gaussian blur were sequentially applied, since those components are supposed to have a higher spatial frequency compared to the mouse. Finally, the OpenCV implementation of Canny algorithm was applied to detect the contours of the mouse, the position of the mouse was computed as mouse's center of mass.

The trajectory of the center of mass were interpolated in x and y using scipy's Univariate Spline function (with smoothing factor s=0.2 x length of the data), allowing the extraction of a smoothed trajectory of the mouse. The distance traveled by the mouse between two consecutive frames was calculated as the variation of position of the mouse multiplied by a scale factor, to allow the conversion from pixel unit to centimeters. The total distance traveled was obtained by summing the previously calculated distances over the course of the entire open-field session. The speed was computed as the variation of position of center points on two consecutive frames divided by the time between these frames (the inverse of the number of frames per seconds). This speed was then averaged by creating sliding windows of 1 second. After each session, fecal boli were removed and the floor was wiped clean with a damp cloth and dried after the passing of each mouse. Active and quiet state was determined by using a bi-threshold method in which two consecutive thresholded and filtered frames were subtracted one from each other. In order to have a proper recognition of both active and quiet state, lower and upper threshold of the changed pixels were arbitrarily set to 0.04% and 0.12%, respectively. The both thresholds were based on the video acquisition conditions (camera resolution, focal distance of the objective and distance from the objective) and the size of the animal detected. For each time point, every percentage of changed pixels below the lower or above the upper threshold was considered as quiet or active state, and percentages placed between both thresholds were considered as a continuity of the previous state.

1.3. Horizontal bar

Motor coordination and balance were estimated with the balance beam test which consists of a linear horizontal bar extended between two supports (length: 90 cm, diameter: 1.5 cm, height: 40 cm from a padded surface). The mouse is placed in one of the sides of the bar and released when all four paws gripped it. The mouse must cross the bar from one side to other and latencies before falling are measured in a single trial session with a 3-minutes cut-off period.

1.4. Vertical pole

Motor coordination was estimated with the vertical pole test. The vertical pole (51 cm in length and 1.5 cm in diameter) was wrapped with white masking tape to provide a firm grip.

Mice were placed heads up near the top of the pole and released when all four paws gripped the pole. The bottom section of the pole was fixated to its home-cage with the bedding present but without littermates. When placed on the pole, animals naturally tilt downward and climb down the length of the pole to reach their home cage. The time taken before going down to the home-cage with all four paws was recorded. A 20 seconds habituation was performed before placing the mice at the top of the pole. The test was given in a single trial session with a 3-minutes cut-off period.

1.5. Footprint patterns

Motor coordination was also evaluated by analysing gait patterns. Mouse footprints were used to estimate foot opening angle and hindbase width, which reflects the extent of muscle loosening. The mice crossed an illuminated alley, 70 cm in length, 8 cm in width, and 16 cm in height, before entering a dark box at the end. Their hindpaws were coated with nontoxic water-soluble ink and the alley floor was covered with sheets of white paper. To obtain clearly visible footprints, at least 3 trials were conducted. The footprints were then scanned and examined with the Dvrtk software (Jean-Luc Vonesch, IGBMC). The stride length was measured with hindbase width formed by the distance between the right and left hindpaws.

1.6. Grid test

The grid test is performed to measure the strength of the animal. It consists of placing the animal on a grid which tilts from a horizontal position of 0° to 180°. The animal is registered by the side and the time it drops is measured. The time limit for this experiment is 30 seconds. In those cases where the mice climbed up to the top of grid, a maximum latency of 30 seconds was applied.

1.7. Fixed speed rotarod

Motor coordination, postural stability and fatigue were estimated with the rotorod (mouse rotarod, Ugo Basile). Facing away from the experimenters view, the mice placed on top of the plastic roller were tested at constant speeds (5, 10, 15 and and 20 r.p.m). Latencies before falling were measured for up to 3 minutes in a single trial session.

2. Chronic in vivo extracellular recordings

2.1 Electrode design

In order to record neuronal activity in the motor network during the accelerating rotarod learning, we designed a custom made microwire electrode array coupled with an optrode destined to be implanted in the deep cerebellar nuclei (CN). The bundles of electrodes were manufactured by folding in six and twisting a nichrome wire with a 0.005- inch diameter (Kanthal RO-800). Each bundle was then placed inside guide cannulas (10 mm length and 0.16–0.18 mm inner diameter, Coopers Needle Works Limited, UK), glued (Loctite universal glue) to a 3D-printed holder. Individual wires of the bundles were then connected to the electrode interface board (EIB-36; Neuralynx, Boze- man, MT) with one wire for each channel and four channels for each brain region (CL, VAL, M1, M1ipsi, DLS, DLSipsi), extending 0.5 mm below the tube tip and fixed using gold pins (Neuralynx). In order to perform optogenetic manipulations and recording of the cerebellar nuclei (CN), an optrode was built by associating the bundles destined to be implanted in the CN (eight channels) to an optic fiber (200µm, 0.22NA) housed in a stainless steel ferrule (Thor labs). Finally, the EIB was secured in place by dental cement. A gold solution (cyanure-free gold solution, Sifco, France) was used for gold plating, and the impedance of each electrode was set to 200–500 kΩ.

Recordings were performed in awake freely moving mice during the Open field as well as the accelerating rotarod sessions. A custom-made pulley system balanced the weight and torque of the wires during running and allowed the wires to accompany the mouse during the accelerating rotarod task. Signal was acquired using a headstage and amplifier from TDT (32 channels headstage, RZ2, Tucker-Davis Technologies, USA) and analyzed with Python 3.7. The spike sorting was performed using MountainSort4.

2.2 Surgeries

Mice were anesthetized using a mixture of isoflurane and O2 (4% for induction, 1.5% for maintenance). Injections with buprenorphine (0.05 mg/kg, s.c.) were performed to control pain, and core temperature (37°C) was kept with a heating pad. The mice were then fixed in a stereotaxic apparatus (David Kopf Instruments, USA). After a local subcutaneous injection of lidocaine under the scalp (2%, 1 ml), a medial incision was performed, exposing the skull. Small craniotomies were drilled above the recording sites and above the optic fiber location

(above the virus injection site). Then, AAV8.hSyn.ChR2(H134R)-mCherry (400 nl) was injected into the cerebellar nuclei (CN), followed by a descent of the optrode in the CN, and by the descent of the remaining electrodes in the brain. This procedure allowed us, in one experimental set, to record in the motor cortex bilaterally (M1) (AP 0 mm and –1 mm ML from the Bregma, DV = 0.8 mm depth from the dura), ventrolateral thalamus (VAL) (–1.34 mm AP, ML = 1.00 mm, and DV = 3.6 mm depth from the dura), centrolateral thalamus (CL) (AP at –1.58 mm, ML = 0.9 mm, DV = 3.00 mm depth from the dura), dorsolateral striatum bilaterally (DLS, 0 mm AP,±2.7 mm ML, 2.5 mm depth from dura) and the cerebellar nuclei (CN, 6 mm AP, ±2.3 mm ML, 2.4 mm depth from dura). The ground screw was placed on the surface of the right parietal bone. Super Bond cement (Dental Adhesive Resin Cement, Sun Medical CO, Japan) was applied on the surface of the skull to strengthen the connection between the bone and the cement.

2.3 Optogenetic stimulation of the Deep Cerebellar Nuclei

The injection of an AAV expressing ChR2 coupled with the implantation of an optic fiber in the left CN allowed for the optogenetic activation of local neurons. Illumination was performed using a LED driver and a 470nm LED (Mightex Systems). Light transmission from the LED output to the implanted optic fiber was done through a 200µm diameter flexible optic fiber. The coupling between the flexible fiber and the implanted optic fiber was allowed by a ceramic mating sleeve. The intensity of current provided to the LED was calibrated in order to obtain an illuminance of 40mW/mm² at the tip of the optic fiber. Optogenetic stimulations of the DN were performed during 100 ms at a frequency of 0.25 Hz during 10 minutes in an Open Field arena, before the start of the rotarod session. The average increase in firing rate during the stimulation was determined by computing the peristimulus time histogram (10 ms bins) of the spikes during the stimulation; the spike count in the histogram was divided by the duration of the bin and the number of stimulations administered to yield a firing rate. The response to stimulation was only analyzed in neurons where at least one bin during the stimulation was 3.5 times larger than the SD of the values of firing rate during baseline (300ms before the onset of stimulation, 10ms bins).

2.4 Connectivity analysis

Spiketrains of single cells were used to compute cross-correlograms of neuronal pairs. Spiketrains were binned (1ms), then timeseries cross-correlation was applied on the binned spiketrains using the cross_correlation_histogram function from the package elephant in order to obtain the cross-correlation of neuronal activity. Then, the asymetry of cross-correlogram was established using the lag-wise difference in cross-correlation coefficient on a short time window (25ms) preceeding and folowing the spiking of the reference neuron.

$$dcc^t = cc^t - cc^{-t}$$

Where dcc is the difference in cross-correlation for a given lag value t , cc is the value of cross-correlation at the lag value t, with t in the range [1ms, 25ms].
Pairs of neurons showing a distribution of lag-wise differences significantly different from 0 (Wilcoxon rank test, $p<0.05$) were considered as significantly connected. If the distribution of differences was significantly higher than 0, the reference neuron was considered as a modulator of the target neuron. A modulation index of this asymetry was computed to reflect the strengh of the modulation of the target neuron by the reference neuron, this modulation index was calculated as follows:

$$\mathrm{MI} = 100 \times \frac{(\mathrm{CCpost} - \mathrm{CCpre})}{(\mathrm{CCpost} + \mathrm{CCpre})}$$

Where MI is the modulation index, expressed in percentage, CCpost is the average cross-correlogram value in the [1ms, 25ms] time window and CCpre is the average cross-correlogram value in the [-25ms, -1ms] time window.

Cortical triplets of neurons were defined as combinations of pairs involving a directional connectivity of a DCN neuron and a M1 neuron, and a directional connectivity between a DLS neuron and the same M1 neuron. In order to delineate the respective contributions of the DCN and DLS neurons on the M1 neuron of each triplets, spiketrains were binned using bins of 15ms, then the Partial Information Decomposition (PID) included in the Python package IdtXl was used. PID is based on the bivariate mutual information of two source

timeseries (DCN and DLS binned spiketrains in this case) and a target timeseries (M1 binned spiketrain in this case). The algorithm decomposes this bivariate mutual information into the unique contribution of each sources, the redundant information carried by both, and the residual component of the subtraction of unique contribution and redundancy to the bivariate mutual information, named synergy, represents the information that is only explaining variance of the target by considering both sources at the same time, thus unraveling interactions between these two sources. Each of these components was then divided by the total bivariate mutual information, yielding a value corresponding to the fraction of the mutual information represented by each component.

2.5 Sleep cycle classification and sleep spindles detection

Sleep spindles are known to occur during NREM sleep. Thus, we separated the resting periods into 10s epochs and classified each of these periods using the method described in Lemke et al. The spectrogram of each 10s epochs of M1 LFP was computed with the Welch method, using the welch_psd function from the package scipy. The average power of different frequency bands was then extracted, in the delta band (1-4Hz), in the theta band (5-10Hz) and the average power in the delta-theta-beta band (2-15Hz), then the theta ratio was computed as the average theta power divided by the average power in the delta-theta-beta band (5-10Hz / 2-15Hz). Epochs with high delta power (greater than the average delta power) were considered as NREM sleep, whereas epochs with low delta power and high theta ratio (greater than the average theta ratio) were considered as REM sleep, the remaining epochs were considered as wake.

Then, cerebellar sleep spindles were detected within periods of NREM sleep using the following process. The cerebellar recording site displaying the highest average power in the spindle frequency range (10-16Hz) compared to the average power in the wide-band local field potential (1-100Hz) was selected as the site for spindles in the deep cerebellar nuclei. The signal from this electrode was then filtered in the sleep spindle frequency range (10-16Hz) using a third order bilateral Butterworth filter. An Hilbert's transform was then applied on this filtered signal, allowing to extract the smoothed amplitude of envelope of the 10-16Hz signal. The amplitude of the signal during NREM sleep was then z-scored by subtracting its mean and dividing it by its standard deviation. Events where the spindle envelope

exceeded 2.5 SD above the mean for at least one sample and the spindle power exceeded 1.5 SD above the mean for at least 300 ms were detected as spindles.

2.6 Sleep spindles locking

The Hilbert's transform applied on the CN LFP filtered in the range of sleep spindles (10-16Hz) allowed for the extraction of the instantaneous phase of this signal, which was then used to compute the phase of each spike of a given neuron. In order to assess if a neuron was significant phase-locked to cerebellar spindles, we extracted the spikes of this neuron occurring during spindles and their associated phase which allowed for the computation of the Rayleigh Z of the phase distribution using the function circ_rayleigh of the package pingouin. Then, we iteratively simulated 1000 phase distributions with a number of value equivalent to the number of spikes occurring during spindles, randomly drawn from the instantaneous phase distribution of the signal during spindles, and computed their Rayleigh Z. Neurons displaying a Rayleigh Z higher than the 95th percentile of the distribution of simulated Rayleigh Z were considered as significantly phase-locked to cerebellar spindles.

2.7 Hindpaw tracking and stride classification

During trials, recording was made thought four Imgaging Source DMK 37BUX273 cameras (left, right, front and back) with an acquisition frequency of 50Hz. Afterwards, videos were analysed thanks to a trained neural network on the back view (Deep Lab Cut, Python 3).The position of each hindpaw in the Y axis was considered. The detection of negative peaks in the trajectory of each paw yielded the timing of each paw lift, while the detection of positive peaks yielded the timing of each paw landing. Then, we used the relative timing of lifts and landing of each paw to classify each stride in different category. The left hindpaw was taken as a reference. Each lift of the left paw was either preceded or followed by the lift of right hinpaw. Jumps were event during which the lift of the second hindpaw of the stride was preceeding the landing of the first hindpaw of the stride. Then the jumps were separated in

two categories, the early jumps occurring during the first half of a trial and the late jumps occurring during the second half of a trial. However, if the lift of the second paw was following the landing of the first one, the strides were classified in two other categories. If the closest lift of a right paw was preceding the lift of the left hindpaw, the stride was considered as a right first, otherwise it was a left-first stride.

2.8 Detection of replays associated to strides

In order to detect replays of neuronal activity corresponding to a given type of stride during the offline resting period in-between trials, we used a template-matching approach. The peri-stimuli time histograms (PSTH, 10ms bins, -1s to 1s centered on left-paw lift) previously computed for each stride type during the sessions were used as templates to perform replay detection during the offline resting period between the trials. The neural activity during resting period for each cell of the network was binned (10ms bins) and centered by subtracting the mean firing rate of each neuron during the resting period, creating a 2-dimensional histogram with similar time scaling as the PSTHs. Then, template matching was perform using the Python Package OpenCV, which returned a 1-dimensional timeseries of template-matching coefficients. The detection of replays presenting a significant similarity in terms of temporal sequence was done by applying random vertical shuffling on the templates 100 times and performing template matching using these shuffled templates. Vertical shuffling was chosen as a way to detect replays, as it allows for the randomization of the temporal sequence of activity, while preserving co-activation in the network. These shuffled template matchings yielded a mean template-matching coefficient as well as a standard deviation for each timepoint during the resting period. Peaks which were locally higher than 5 SD above the mean were considered as significant replays.

Since patterns of activity may display a degree of covariance between stride types, coincidental replays were detected. If replays of different stride type were detected in a time period of 500ms, they were considered coincidental. They were then disambiguated by retaining the replay displaying the highest template-matching coefficient, as it will represent the stride type sharing the highest covariance with the offline activity.

2.9 Replay-based learning model for motor strategy

The content of different types of replays within a given resting period is varigated. Thus, we fitted a learning model in order to predict the variations in motor strategy based on the content of replay activity during a resting period. The model was elaborated as follows:

$$P_{n+1}^{strideA} = P_{n}^{strideA} + \Delta P_{n+1}^{strideA}$$

with $\Delta P_{n+1}^{strideA} = \rho \times (H_{n}^{replay} - P_{n}^{strideA})$

and $P_{n=0}^{strideA}$ = proportion of stride A during the previous trial

Where is the predicted probability of performing a stride A at the replay n, is the learning rate fitted for each mouse, is the updating component, equal to 1 if the replay n was a replay of stride A or equal to 0 otherwise.

$$\Delta P_{resting}^{strideA} = \sum_{n=1}^{k} \Delta P_{n}^{strideA}$$

Where is the variation of proportion of stride predicted by the model during one resting period. This value was then compared to the difference of stride proportion between the trial following the resting period and the preceding trial. This model was fitted separately for each mouse and each stride type.

3. Chemogenetic

3.1. Cerebellar outputs inactivation

We used evolved G-protein-coupled muscarinic receptors (hM4Di) that are selectively activated by the pharmacologically inert drug Clozapine-N-Oxide (CNO) (Alexander et al.,

2009). In our study, non-cre and cre dependent version of the hM4Di receptor packaged into an AAV were used in order to facilitate the stereotaxic-based delivery and regionally restricted the expression of hM4Di. As demonstrated previously (Anaclet et al., 2018; Anaclet et al., 2014; Anaclet et al., 2015; Pedersen et al., 2017; Venner et al., 2016). hM4Di receptor and ligand are biologically inert in the absence of ligand. Moreover, at the administered dose of 1 mg/kg, CNO injection induces a maximum effect during the 1–3 h postinjection period (Anaclet et al., 2018; Anaclet et al., 2014) which enables us to confirm that during the whole duration of our protocols the CNO was still effective. We are therefore confident that the findings described in our study result from specific inhibition of the targeted neuronal population and not from a nonspecific effect of CNO or its metabolite clozapine (Gomez et al., 2017).

In order to globally inactivate the cerebellar outputs, stereotaxic surgeries were used to inject DREADD viral constructs bilaterally into the Dentate, Interposed and Fastigial nucleus. Mice were anesthetized with isoflurane for induction (3% in closed chamber during 4-5 minutes) and placed in the Kopf stereotaxic apparatus (model 942; PHYMEP, Paris, France) with mouse adapter (926-B, Kopf), and isoflurane vaporizer. Anesthesia was subsequently maintained at 1–2% isoflurane. A longitudinal skin incision and removal of pericranial connective tissue exposed the bregma and lambda sutures of the skull. The coordinates for the Dentate nucleus injections were: 6.2 mm posterior to bregma, +/-2.3 mm lateral to the midline and -2.4 mm from dura while the Interposed injections were placed anteroposterior (AP) -6.0 mm, mediolateral (ML) = +/-1.5 mm in respect to bregma and dorsoventral (DV) -2.1 mm depth from dura. Finally, the Fastigial injections were placed -6.0 AP, +/-0.75 ML in respect to bregma and -2.1 depth from dura. Small holes were drilled into the skull and DREADD (AAV5-hSyn-hM4D(Gi)-mCherry, University of North Carolina Viral Core, 7.4 × 1012 vg per ml, 0.2 µl) or control (AAV5-hSyn-EGFP, UPenn Vector Core, the same concentration and amount) virus were delivered bilaterally via quartz micropipettes (QF 100-50-7.5 ,Sutter Instrument, Novato, USA) connected to an infusion pump (Legato 130 single syringe, 788130-KDS, KD Scientific, PHYMEP, Paris, France) at a speed of 100 nl/minutes. The micropipette was left in place for an additional 5 minutes to allow viral dispersion and prevent backflow of the viral solution into the injection syringe. The scalp wound was closed

with surgical sutures, and the mouse was kept in a warm environment until resuming normal activity. All animals were given analgesic and fluids before and after the surgery.

In a separate set of mice, non-DREADD or DREADD (Dentate, Fastigial and Interposed) bundles of electrodes were implanted into the cerebellar nuclei, as described above. Both non-DREADD or DREADD injections and electrodes implantation were performed the same day. This experiment was performed in order to evaluate and validate that hM4D(Gi) receptors decrease the activity within the three cerebellar nuclei. Surgery, virus injections (AAV5-hSyn-hM4D(Gi)-mCherry or AAV5-hSyn-EGFP), coordinates (Fastigial: -6.0 AP, +/-0.75 ML, -2.1 depth from dura; Interposed: -6.0 AP, +/-1.5 ML, -2.1 depth from dura; Dentate: -6.2 AP, +/-2.3 ML, -2.4 depth from dura), chronic in vivo extracellular recordings and analysis were performed as we previously described above. One week following stereotaxic surgery to allow for virus expression, recordings at open-field were performed before and after CNO or saline (SAL) injection at the day 1, 4 and 7 of the accelerated rotarod task protocol. Mice were recorded for a 10 minutes baseline period followed by intraperitoneal injections of CNO 1mg/kg or SAL which were performed in a random sequence using a crossover design. After CNO or SAL injection, mice were recorded during 30 minutes before and 15 minutes after the accelerated rotarod task protocol.

3.2. Cerebellar-thalamic outputs inactivation

In order to inhibit specifically cerebellar outputs to the centrolateral (CL) and/or ventral anterior lateral (VAL) thalamus we applied a chemogenetic pathway-specific approach (Boender et al., 2014). The technique comprises the combined use of a CRE-recombinase expressing canine adenovirus-2 (CAV-2) and an adeno-associated virus (AAV-hSyn-DIO-hM4D(Gi)-mCherry) that contains the floxed inverted sequence of the DREADD hM4D(Gi)-mCherry. It entails the infusion of these two viral vectors into two sites that are connected through direct neuronal projections and represent a neuronal pathway. AAV-hSyn-DIO-hM4D(Gi)-mCherry is infused in the site where the cell bodies are located, while CAV-2 is infused in the area that is innervated by the corresponding axons. After infection of axonal terminals, CAV-2 is transported towards the cell bodies and expresses CRE-recombinase (Kremer et al., 2000; Hnasko et al., 2006). AAV-hSyn-DIO-hM4D(Gi)-mCherry contains the floxed inverted sequence of hM4D(Gi)-mCherry, which is reoriented in the presence of CRE, prompting the expression of hM4D(Gi)-mCherry. This ensures that hM4D(Gi)-mCherry is not

expressed in all AAV-hSyn-DIO-hM4D(Gi)-mCherry infected neurons, but exclusively in those that are also infected with CAV-2. Using the same procedures described above, 0.4 µl of the retrograde canine adeno-associated cre virus (CAV-2-cre, titter ≥ 2.5 × 108) (Plateforme de Vectorologie de Montpellier, Montpellier, France) was bilaterally injected in the CL (from bregma: AP -1.70 mm, ML ±0.75 mm, DV −3.0 mm) and VAL (from bregma: AP -1.4 mm, ML ±1.0 mm, DV −3.5 mm). In addition, 0.2 µl of AAV-hSyn-DIO-hM4D(Gi)-mCherry (UNC Vector Core, Chapel Hill, NC, USA) was bilaterally injected one week later into the cerebellar nuclei, focusing on the Dentate (from bregma: AP −6.2 mm, ML ±2.3 mm, DV −2.4 mm) and Interposed (from bregma: AP −6.0 mm, ML ±1.5 mm, DV −2.1 mm) nucleus. Based on anatomical and functional evidences (Hintzen et ., 2018; Chen et al., 2014; Teune et al., 2000; Sakai 2000), in a group of mice we decided to inhibit those neurons that project from Dentate to CL and in another group we targeted those neurons that project from Interposed to VAL. All the stereotactic coordinates were determined based on The Mouse Brain Atlas (Paxinos and Franklin, 2004).

4. Behavioral experiments design

Behavioral tests were performed one week following stereotaxic surgery to allow for virus expression. Balance beam, vertical pole, footprint patterns, grid test and fixed speed rotarod experiments were performed 30 minutes after CNO (1 mg/kg, ip) or SAL injections. Two different strategies were used for the accelerating rotarod motor learning task experiments: 1) CNO (1 mg/kg, ip) or SAL was injected every day 30 minutes before the 1st trial of the accelerated rotarod task. Four days later to ensure a proper CNO washout, mice were retested by receiving 7 trials for two consecutive daily sessions. Drug-free mice received CNO (1mg/kg) or SAL 30 minutes before the first trial in both days. The treatments were inverted meaning that those animals that received CNO during the preceding 7 days in this case were injected with SAL and the other way around. 2) CNO (1 mg/kg, ip) was injected 30 minutes after last trial at the day 1, 2 and 3; subsequently mice received SAL 30 minutes after last trial at the day 4, 5 and 6 of the accelerated rotarod task.

The DREADD ligand Clozapine-N-Oxide (CNO, TOCRIS, Bristol, UK) was dissolved in SAL (0.9% sodium chloride) and injected intraperitoneally at 1mg/kg.

5. Histology

Mice were anesthetized with ketamine/xylazine (100 and 10 mg/kg, i.p., respectively) and rapidly perfused with ice-cold 4% paraformaldehyde in phosphate buffered SAL (PBS). The brains were carefully removed, postfixed in 4% paraformaldehyde for 24 h at 4 °C, cryoprotected in 20% sucrose in PBS. The whole brain was cut into 40-µm-thick coronal sections on a cryostat (Thermo Scientific HM 560; Waltham, MA, USA). The sections were mounted on glass slides sealed with Mowiol mounting medium (Mowiol® 4-88; Sigma-Aldrich, France). Verification of virus injection site and DREADDs expression was assessed using a wide-field epifluorescent microscope (BX-43, Olympus, Waltham, MA, USA) using a mouse stereotaxic atlas (Paxinos and Franklin, 2004). We only kept mice showing a well targeted viral expression. Representative images of virus expression were acquired a Zeiss 800 Laser Scanning Confocal Microscope (×20 objective, NA 0.8) (Carl Zeiss, Jena, Germany). Images were cropped and annotated using Zeiss Zen 2 Blue Edition software.

DISCUSSION

In this study, we observed that a transient and mild chemogenetic inhibition which reduces the cerebellar nuclei activity preserves the motor abilities but disrupts motor learning in this task. Moreover, we could distinguish two contributions of the cerebellum to learning; one is carried by CN neurons projecting toward the midline thalamus, and is needed for learning and recall. The other is carried by CN neurons projecting toward the motor thalamus and is required to perform an offline consolidation of a latent memory trace into a consolidated, readily available, motor skill.

In addition, we observed that the connectivity between the cerebellum, the motor cortex and the striatum drastically increased while undergoing motor learning. Consistently with an involvement of CN neurons projecting toward the motor thalamus in the offline consolidation of motor skill, we revealed that the connectivity between CN neurons and cortical neurons was maintained during the resting periods in-between rotarod trials. During these resting periods, cerebellar sleep spindles concomitantly reactivate cerebellar and cortical neurons engaged during the task, and contributes shaping cerebello-cortical connectivity.

Thus, our results suggest that learning a complex motor task involves the coupling of the cerebellum with the basal ganglia, which is needed during the learning and execution, and the coupling of the cea rebellum with the cortex which plays a critical role in the offline consolidation of the task.

A role for the cerebellum in the multi-nodal network of motor skill learning

By showing an involvement of the cerebellar nuclei neurons in the accelerating rotarod task, our results complement the previous results which demonstrated that the basal ganglia and motor cortex are recruited and required to complete the task {Cao, 2015 #81;Costa, 2004 #76;Kida, 2016 #82}. Our chemogenetic experiments also indicate that the involvement of the cerebellum changes along the multiple phases of motor learning, ranging from a minimal contribution in the Initial phase to a stronger contribution in the later phases. The differential modulation of CN and thalamic firing during the rotarod task across the different phase also likely reflect changes in the engagement of these structures along the task. These observations parallel the converging evidence indicating that the areas of the basal ganglia involved in the accelerating rotarod evolve along the phases of learning {Yin, 2009 #84;Cao, 2015 #81;Durieux, 2012 #85}. Therefore, the three main central nodes of motor function (cortex, basal ganglia and cerebellum) are differentially recruited along the multiple phases of the accelerating rotarod task.

Nonetheless, our observations that cerebello-cortical and cerebello-striatal connectivities are increased in expert mice, along with an enhaced cooperation between cerebellar and striatal inputs to the motor cortex suggests that the different actors of this multi-nodal motor learning network, although being differentially recruited during learning, participate to a coordinated interplay in order to achieve the proper execution of a learned motor skill.

The impact of cerebellar defects or manipulations on accelerating rotarod learning have previously been examined in too many studies to be listed exhaustively here, but the reported effects range from ataxia and disruption of the ability to run on a rod {Sausbier, 2004 #86}, to normal learning {Galliano, 2013 #92}, defects in learning {Groszer, 2008 #90;Galliano, 2013 #92}, defects in consolidation {Sano, 2018 #87} and even increase in learning {Iscru, 2009 #91}. However, the cerebellum is critical for inter-limb coordination {Machado, 2015 #18;Sathyamurthy, 2020 #119}, and many studies lack proper motor

controls to test the ability to walk on a rotating rod: a lack of improvement in performance with training may thus simply result from problems of running on the rod rather than problems of learning. Moreover studies often involve genetic mutations which leave room from variable compensations along development and adult life, as exemplified by the diversity of the motor phenotypes of mice with degeneration of Purkinje cells {Porras-Garcia, 2013 #88}. Finally the multiphasic nature of rotarod learning is often overlooked.

However, studies of cerebellar synaptic plasticity provide support of an involvement of cerebellum in learning. Indeed, the targeted suppression of parallel-fiber to Purkinje cell synaptic long-term depression in the cerebellar cortex disrupts rotarod learning after the Initial phase, without altering any other motor ability {Galliano, 2013 #92}. Consistently, Thyrotropin-releasing hormone (TRH) knock-out mice do not express long-term depression at parallel fiber-Purkinje cell synapses and exhibit impaired performance in the late phase of rotarod learning, while the administration of TRH in the knock-out mice both restores long-term depression and accelerating rotarod learning {Watanave, 2018 #93}. More generally, studies in mutant mice suggest that cerebellar plasticity is required for adapting skilled locomotion {Vinueza Veloz, 2015 #97}. This suggests that cerebellar plasticity is involved in accelerating rotarod learning and thus contributes to learning and not simply to the execution of the task.

A specific impact on learning of CL-projecting CN neurons.

In our study, we found that the chemogenetic inhibition of CN-CL neurons during the task reduces the performances of the mice in the late phases of learning. This effect unlikely results from basic motor deficits: we found that the chemogenetic modulation did not significantly alter 1) limb motor coordination in footprint analysis, 2) strength in the grid test, 3) speed in spontaneous locomotion in the open-field test, 4) locomotion speed and balance required to complete the horizontal bar test and 5) body-limb coordination and balance required in the vertical pole test. Since all these motor parameters may be affected by cerebellar lesions, this suggests that CN-CL neurons are not necessary to maintain those functions, which might thus be relayed by other cerebellar nuclei neurons; indeed focal lesions in the intermediate cerebellum (thus projecting to the Interposed nuclei) has been reported to induce ataxia without altering rotarod learning {Stroobants, 2013 #13}. Alternatively, the effect of the partial inhibition induced by CNO (typically ~50% reduction in

firing rate) may be compensated at other levels in the motor system to ensure normal performances in these tasks; indeed, the selective ablation of CN-CL neurons has been reported to yield locomotor deficits in the initial performances on the accelerating rotarod {Sakayori, 2019 #11}, which contrasts with the lack of significant deficit in the Initial phase following CN-CL (partial) inhibition in our study. A possible explanation for this discrepancy could be that our intervention, being milder than a full ablation, selectively disrupted the advanced patterns of locomotion only needed at the higher speeds of the rotarod and thus did not impact on the slow rotarod locomotion typically performed in the Initial phase. However, the highest speeds reached on the rotarod correspond to the average locomotion speed in the open-field, which is unaffected by the chemogenetic inhibition. Moreover, in our conditions, the inhibition of the CN-CL neurons did not produce significant deficits in the fixed speed rotarod; CNO-treated animals ran in average for about two minutes at 20 r.p.m. while they fell in average after the same amount of time on the accelerating rotarod, corresponding to a rotarod speed below 20 r.p.m. at the time of the fall. This rules out a contribution of weakness or fatigue to the latency to fall in the accelerating rotarod, the CNO-treated animals being able to run on the fixed speed rotarod more than twice the distance, at a higher speed, than the distance they run on the accelerating rotarod before falling. Overall, this indicates that the partial inhibition of the CN-CL neurons does not disrupt the elementary motor abilities needed in the task.

The inhibition of CN-VAL neurons during the task also yielded lower levels of performance in the Maintenance stage, and the degree of connectivity between the cerebellum and the motor cortex is increased during the Maintenance phase, suggesting that cerebello-cortical networks contribute to the learning and the retrieval of motor skills, although the mild defect in fixed speed rotarod could indicate the presence of a locomotor deficit, only visible at high speed. Interestingly, both Dentate and Interposed nuclei contain some neurons with collaterals in both VAL and CL thalamic structures {Sakayori, 2019 #11;Aumann, 1996 #12}, suggesting that the effect on learning could be mediated by a combined action on the learning process in the striatum (via the CL thalamus) and in the cortex (via the VAL thalamus); however, consistent with {Sakayori, 2019 #11}, we found that the manipulations of cerebellar neurons retrogradely targeted either from the CL or from the VAL produced different effects in the task. This indicates that either the distinct functional roles of VAL-projecting of CL-projecting neurons reported in our study is carried

by a subset of pathway-specific neurons without collaterals, or that our retrograde infections in VAL and CL effectively targeted different cerebello-thalamic populations even if these populations had axon terminals in both thalamic regions.

Contribution of VAL-projecting CN neurons to offline consolidation.

While in control mice, the final performance at the end of a session could be reproduced at the beginning of the next session, this preservation of performance across night was lost when CN-VAL neurons were inhibited after the task, suggesting an impairment of offline consolidation. However, in this group of mice, the daily gain of performance increased across days, instead of decreasing, and compensated the overnight loss. We therefore interpret this faster relearning as the presence of "savings". Therefore, if the inhibition of CN-VAL neurons alters the offline consolidation, a latent trace of the learning remains unaltered by CN-VAL inhibition and allows for a faster relearning on the next day.

The effect of CNO peaks in less than an hour and lasts for several hours afterwards {Alexander, 2009 #95}; therefore the disruption of offline consolidation reported above is produced by a disruption of the cerebellar activity in the few hours that follow the learning session. In agreement with this, we found in normal conditions that the connectivity between the cerebellum and the motor cortex was maintained during the resting periods in-between the rotarod trials. These results suggest that an activity-dependent offline consolidation of motor skill learning starts readily when the animals are resting. This falls in line with a number of evidence indicating that cerebellar-dependent learning is consolidated by the passage of time, even in the awake state {Shadmehr, 1997 #6;Cohen, 2005 #4;Doyon, 2009 #1;Muellbacher, 2002 #3;Nagai, 2017 #55}, although very few studies in the Human have examined the impact of offline cerebellar stimulations on motor learning {Samaei, 2017 #40}.

In the case of rotarod, it has been noted that sleep is not required for the overnight preservation of performance {Nagai, 2017 #55}; however sleep may still be required for the change of cortical {Cao, 2015 #81;Li, 2017 #54} or striatal neuronal substrate of the accelerating rotarod skill {Yin, 2009 #84}. Moreover, the previously mentionned study investigated the effect of sleep deprivation on accelerating rotarod learning, and observed little effect on performances {Nagai, 2017 #55}. However, we observed that even during the short periods of time in-between trials, mice undergo short cycles of sleep during which

cerebellar sleep spinldes could be observed. Furthermore, replays of neuronal activity specific to behavioural patterns were measurable during these periods, and the fact that their presence correlates with trial-to-trial refinement of motor strategy suggests that the little amount of time between trials is enough to create substanital changes in the consolidation of accelerating rotarod learning, and may explain why a completely unperturbed sleep is not necessary to observe decent learning.

These results are consistent with the fact that sleep-dependent learning processes were shown to occur even during day-time naps, as sleep spindles can happen during naps [[Nishida and Walker 2007]]], and replays of activity can even happen during wakefulness [[Karlsson et al 2009, Durbin et al 2022]].

The existence of multiple timescales for consolidation has already been described in Human physiology where the movements could be consolidated without sleep while consolidation of goals {Cohen, 2005 #4} or sequences {Doyon, 2009 #1} would require sleep. It is indeed difficult, as for most real-life skills, to classify the accelerating rotarod as a pure adaptive learning, or a pure sequence learning: on one hand, the shape of the rod and its rotation induce a change in the correspondence between steps and subsequent body posture and thus require some locomotor “adaptation”. On the other hand, the acceleration of the rod introduces sequential aspects: 1) the same step executed a few seconds or tens of seconds apart in a trial result in different consequences on body position, and 2) asymptotic performances require to use successively multiple types of gaits as the trial progresses {Buitrago, 2004 #79}. Following offline inhibition of CN-VAL neurons, which aspect of the accelerating rotarod skill would be maintained and which would be lost? Faster relearning has been proposed to reflect an improved performance at selecting successful strategies {Ruitenberg, 2018 #69;Morehead, 2015 #70}. In addition, recent studies revealed cerebellar mechanisms which could serve sequence learning {Khilkevich, 2018 #42;Ohmae, 2015 #43} and the offline inhibition of CN-VAL neurons could disrupt the consolidation of these sequences via the feedback collaterals of CN-VAL neurons to the cerebellar cortex {Houck, 2015 #96}. However, our study does not allow us to conclude on the nature of savings remaining after the offline inhibition of CN-VAL neurons.

An internal model in the output of the cerebellum?

Improving the rotarod performance requires the mice to match their locomotion speed to the accelerating speed of the rod. In the cerebellar nuclei, we observed that neurons exhibited substantial modulation during each rotarod stride, with a modulation of activity specific to the type of stride pattern that was expressed. It is well established that a number of neurons in the Interposed nucleus exhibit a modulation along the stride {Armstrong, 1984 #20;Sarnaik, 2018 #19}, and a transient optogenetic manipulation of this activity results in an alteration of the gait {Sarnaik, 2018 #19}. Indeed, the optogenetic activation of genetically-defined Interposed nucleus neurons projecting mainly to the ventral lateral thalamus and the red nucleus produced higher strides {Low, 2018 #21}. Stride-related signals are also found in the Dentate nucleus, which is more clearly recruited in response to perturbations {Schwartz, 1987 #22} or during skilled locomotion such as on a ladder {Marple-Horvat, 1999 #23}; this is consistent with the selective impact of lateral cerebellum lesion to obstacle stepping while preserving overground locomotion {Aoki, 2013 #24}**.** The changes of firing rate in the Dentate and Interposed units reported in our study thus likely reflect the integrated representation of the stride {Sauerbrei, 2015 #99}.

In conclusion, our results provide clear evidence for the existence of online contributions of the cerebello-thalamic pathways to the formation and retrieval of motor memories distributed in a cerebello-striato-cortical network. They also show a contribution to the offline consolidation of savings by cerebello-thalamo-cortical networks. Thus, our work highlights the importance of studying the contribution to learning of single nodes in the brain motor network from an integrated perspective {Caligiore, 2017 #56;Krakauer, 2019 #53}.

FIGURE LEGENDS

Figure 1. Cerebellar inactivation impairs the performance in the Refinement and Maintenance but not Initial phases of motor learning task. a) Scheme of the implantation and injection. b) Coronal section of the cerebellum showing hM4Di-DREADD expression in the three CN. c) Representative confocal image showing hM4Di-DREADD expression on neuronal membranes. d) DAPI positive neurons expressing hM4Di-DREADD. e) Electrode placement close to cells expressing hM4Di-DREADD (red: lesion site, yellow: electrode track). f) Examples of spike shapes obtained from spike sorting in CN (mean +/- SD). g) Examples of high-pass filtered traces of CN recordings before and after CNO injection. h) Boxplots (box: quartiles, whiskers: min/max) of the mean firing rate of neurons recorded in DREADD and non-DREADD injected mice after CNO or SAL injection during Initial (Init.), Refinement (Refin.) and Maintenance (Maint.) phases. CN firing rate was reduced after 1 mg/kg of CNO injection in DREADD injected mice (***p<0.001 paired t-test). Small variations were observed in a Sham+SAL mouse (*p<0.05, ***p<0.001 paired t-test). i) Impact of daily of injections of CNO before trial 1 on accelerating rotarod performance. Top: summary of the performance for each trial/day (*p<0.05, ***p<0.001; repeated measure ANOVA Group effect). Bottom: Latencies to fall in trial 1 and 7 and post-hoc comparisons for only these trials. Horizontal comparison lines correspond to trial 1 versus next trial 7, and trial 7 versus next trial 1, comparisons (*p<0.05, **p<0.01, ***p<0.001 paired t-test). Vertical comparison lines report trial 1 and trial differences to controls (*p<0.05, **p<0.01, ***p<0.001 t-test). j) Impact of daily of injections of CNO after the task (30 min after trial 7). All treatment is switched to saline in the Maintenance phase. Same presentation as in i). Data represents mean ± S.E.M. n indicates the number of mice.

Figure 2. Inhibition of cerebellar nuclei (CN) neurons projecting to the centrolateral thalamus (CL) and to the ventral anterior lateral (VAL) thalamus during and after the training sessions differentially impairs motor learning. a) combined viral injections targeting the CN->CL neurons using a retrograde virus expressing the Cre in the thalamus and a virus inducing Cre-dependent expression of inhibitory DREADD in the CN. Top: schematic of the viral injections. Bottom: GFP fluorescence revealing the site of injection of the CAV viruses. b) Daily of injections of CNO before trial 1 in mice described in panel A reduce performance during Maintenance phase but not earlier phases (Top: *p<0.05,

**p<0.01, ***p<0.001; repeated measure ANOVA Group effect. c) Same as B for daily CNO injections 30 minutes after trial 7 during the Initial and Refinement phases. d) combined viral injections targeting the CN->VAL neurons using a retrograde virus expressing the Cre in the thalamus and a virus inducing Cre-dependent expression of inhibitory DREADD in the CN. e) same as B for mice described in panel d. f) same as panel c for mice described in panel d. g) Change of latency to fall in successive trials pooled for the Refinement and Maintenance phases. (comparison between groups during vs after session: p<0.05, **p<0.01, ***p<0.001 Sidak-adjusted)CN: cerebellar nuclei, VAL: ventral anterior lateral thalamus, CL: central lateral thalamus. Data represents mean ± S.E.M, n indicates the number of mice.

Figure 3. Reversal of the inhibition of the cerebello-thalamic neurons in the late Maintenance phase yields lasting impairments. a) Performance of mice with DREADD expression in CL-projecting CN neurons, which learned the task under respectively CNO and Saline treatment (Figure 4b) during 7 days and then receive respectively Saline and CNO treatment during a Reversal phase. Top: time course of the average performance (repeated-measure ANOVA group effect: *: p<0.05). Bottom: summary of post-hoc comparisons limited to first and last trials of each day: horizontal comparison lines indicate differences between successive trials 1 and 7; *p<0.05, **p<0.01, ***p<0.001 paired t-test; vertical comparison lines indicate differences between groups of trial 1 and trial 7; *p<0.05, **p<0.01, ***p<0.001 t-test. b) same as panel a for mice with DREADD expression in VAL-projecting CN neurons. CN: cerebellar nuclei, VAL: ventral anterior lateral thalamus, CL: central lateral thalamus. Data represents mean ± S.E.M, n indicates the number of mice.

Figure 4. Cerebellar nuclei neurons can bilaterally modulate the activity of the motor cortex and the dorsolateral striatum. a) Experimental design for the extracellular recording of the cerebellar nuclei, thalamus, motor cortex and striatum, and viral strategy for the optogenetic activation of the cerebellar nuclei. b) Scheme of the accelerating rotarod setup. c) Latency to fall during the accelerating rotarod across trials along days in mice recorded over the 7 days. d) Example of peristimulus time histogram (PSTH, 5ms bins) and corresponding raster plots, centred on the onset of the CN stimulation for neurons in the VAL, M1, M1ipsi, CL, DLS, DLSipsi. e) Cumulative histograms showing the latency of neuronal response of neurons in the VAL, M1, M1ipsi, CL, DLS, DLSipsi responsive to CN stimulations.

**p<0.01, ***p<0.001, Kolmogorov-Smirnoff test. f) PSTH (5ms bins, centred on stimulation onset) displaying the change in normalized firing rate (average ± SEM) of responsive neurons in the M1, M1ipsi, DLS and DLSipsi, before the start of the first day of accelerating rotarod training, and before the day 7 (vertical dashed line represents the limit of the afferent volley, 25ms). g) Average fractional increase in firing of responsive neurons in the M1, M1ipsi, DLS and DLSipsi, before the start of the first day of accelerating rotarod training, and before the day 7, during the afferent volley (0 to 25ms) and during the rest of the stimulation (25 to 100ms). *p<0.05, **p<0.01, Mann-Whitney U test.

Figure 5. Cerebellar connectivity with the motor cortex and the striatum increases along learning and is partially maintained during resting. a) Example cross-correlogram of a CN neuron and a M1 neuron, and example of associated spiketrains (top). b) Measure of bin-wise asymmetry in cross-correlograms of CN and M1 neurons directionally connected. The dotted line represents the limit of the considered zone for asymmetry detection (25ms) c) Ascending connectivity map of neurons in the CN, M1 and DLS for a mouse during the first day of rotarod training (left) and for the same mouse during the last day of rotarod training (right). Significant connectivity during trials is represented by arrows, the thickness of the arrow is proportional to the asymmetry index. d) e) f) g) Percentage of significantly connected pairs in a given direction during trials. *p<0.05 **p<0.01, ***p<0.001, Fischer exact test. (left). Distributions of asymmetry indices during trials of pairs of neurons significantly connected in a given direction during trials. *p<0.05 **p<0.01, ***p<0.001, Dunn posthoc test following a Kruskal Wallis test.(middle). Distributions of asymmetry indices during resting of pairs of neurons significantly connected in a given direction during trials. *p<0.05 **p<0.01, ***p<0.001, Dunn posthoc test following a Kruskal Wallis test. #p<0.05, ##p<0.01, ###p<0.001, Wilcoxon test for the difference to 0.(right). h) Venn diagram showing the proportions of targets neurons in M1 significantly connected with the CN, DLS or both. i) Example cross-correlograms of a CN, DLS and M1 triplet, and example of associated spiketrains (top). j) Schematics of the partial information decomposition used to characterize information transfer in M1 triplets (left). Distributions of the fraction of synergy between CN and DLS neurons towards M1 neurons during trials (middle) and during resting (right). *p<0.05 **p<0.01, ***p<0.001, Dunn posthoc test following a Kruskal Wallis test.

Figure 6. Cerebellar spindles activity during NREM sleep selectively reactivates cortical neurons engaged with the cerebellum during trials and shapes cerebello-cortical connectivity. a) Examples of spindles detected in the LFP of the CN and simultaneous spiketrains of a CN neuron (top), M1 neuron (centre) and DLS neuron (bottom). b) Average filtered LFP (10-16Hz) in the CN and M1 centered on CN spindles peak (top), corresponding normalized multi-unit activity of neurons in the CN, M1 and M1ipsi depending on their relationship with CN neurons during trial (bottom). c) Average filtered LFP (10-16Hz) in the CN and DLS centered on CN spindles peak (top), corresponding normalized multi-unit activity of neurons in the CN, DLS and DLSipsi depending on their relationship with CN neurons during trial (bottom). d) Proportions of neurons in M1/M1ipsi and DLS/DLSipsi locked to cerebellar spindles, depending on their relationship with CN neurons during trial. **p<0.01, Fischer exact test. e) Histogram and polar plot of preferred firing phase within cerebellar spindles for neurons significantly locked to cerebellar spindles, depending on their relationship with CN neurons during trial. Vertical lines represent the populational circular mean, plain line if there was a significant populational locking, dashed otherwise (left). **p<0.01,***p<0.001 Rayleigh test. f) Scatterplot showing the evolution of the asymmetry modulation index of connected pairs during a training session (left) and the distribution of the difference in modulation index (right) for different directions of connectivity and depending on their locking to cerebellar spindles. *p<0.05, Mann-Whitney U test. #p<0.05, ##p<0.01, ###p<0.001, Wilcoxon test for the difference to 0.

Figure 7. The motor strategies used by mice on the rotarod differentially modulates the activity in the cerebello-cortico-striatal network and evolves during learning. a) Examples of frame and detection from the left view and back view camera (left). Example traces for the y positions of the hind-paws in time, as well as the associated stride classification (right). Coloured vertical lines represent the different stride types. b) Cumulative histogram of phase difference between the lift of the first hind-paw and the lift of the second hind-paw. ***p<0.001, Kolmogorov-Smirnoff test. c) Example of PSTH 10ms bins and corresponding raster plots, centred on the lift of the left paw for a neuron in the CN during the different types of strides. d) Example of PSTH 10ms bins and corresponding raster plots, centred on the lift of the left paw for neurons recorded simultaneously in a same mouse in the CN, VAL, M1, M1ipsi, CL, DLS, DLSipsi during the different types of strides. e) Distributions of average

pairwise cross-correlations between the average activity observed during the different types of strides for single neurons. Red bars represent the critical values for significant correlation. p>0.05 Wilcoxon test for the difference to 0. f) Evolution of the percentage of jump during the learning protocol (black line), along with the evolution of latency to fall (gray line). Data are represented in average+/-SEM. g) Scatterplot and associated linear regression showing the latency to fall as a function of the percentage of jumps during trial. The colours of the dots reflect the timepoint at which the trial occurred ***p<0.001, Pearson's correlation test. h) Percentage of jump during each phases of learning. ***p<0.001, Fischer exact test.

Figure 8. Mice perform strategy-specific replays of neuronal activity in the motor network during resting, which predict changes in motor strategy. a) Conceptualization of the detection of strategy-specific replays of activity during resting periods. b) Example of template matching analysis (top) detecting the replays of different types of stride from the neuronal activity of a mouse during resting period (bottom). c) Cumulative histogram of the Pearson's correlation coefficient between average activity during a stride type and during a replay for neurons significantly correlated. *p<0.05, ***p<0.001, Kolmogorov-Smirnoff test. d) Distributions of the frequencies of offline replay detection during each phase, for the different stride types. *p<0.05 **p<0.01, Dunn posthoc test following a Kruskal Wallis test. e) Scheme explicating the learning model used to predict trial-to-trial change in stride proportion based on the temporal structure of the replay during a resting period. f) Example of the learning model prediction a trial-to-trial change in stride proportion based on the temporal structure of the replay during a resting period. g) Scatterplot and associated linear regression showing the actual variation in stride proportion between trial-to-trial as a function of the predicted variation. The colours of the dots reflect the timepoint at which the resting period occurred. h) Scatterplots and associated linear regressions showing the actual variation in stride proportion between trial-to-trial as a function of the predicted variation for different stride types. Covariance ellipses of 2SD are represented. ***p<0.001, Pearson's correlation test.

Supplementary Figure 1. Dentate and Interposed nuclei display a context-dependent sensitivity to speed, with a negative correlation between cerebellar activity and rotarod speed. a) Raster plots showing the activity of representative cells for Dentate (left) and

Interposed (right) during trials for Initial, Refinement and maintenance (same example cells as Figure 1). **b)** Distribution of the number of trials with significant modulation of firing rate between the trial and nearby inter-trial periods during Initial (Init.), Refinement (Refin.) and Maintenance (Maint.) phases for Dentate (top) and Interposed (bottom) (*p<0.05, ***p<0.001 Mann-Whitney test, Holm-Sidak corrected for multiple comparison; trials are compared to the previous and following inter-trial period except the first and last trial which are respectively compared only to the following and to the preceding inter trial period). **c**) Fraction of cerebellar units exhibiting significant positive or negative regression slope of firing rate vs rotarod speed (*p<0.05, **p<0.01, ***p<0.001 chi-square test, Holm-Sidak corrected). **d**) Scatter plot of the slope values for all units in CL (top) and VAL (bottom) thalamic nuclei during Initial (Init.), Refinement (Refin.) and Maintenance (Maint.). Marginal distributions are displayed as in Figure 1e. **e**) Scatter plot of the slope of linear regression on rotarod versus the (dimension-less) associated Pearson correlation coefficient for each neuron for Dentate (top) and Interposed (bottom) nucleus during Initial (Init.), Refinement (Refin.) and Maintenance (Maint.). The lines represent the isotonic regression of the Pearson's r by the slope on rotarod (***p<0.001 Spearman Rank test). **f**) Same as e) for the CL and VAL. **g**) Overlapping index η of the distributions of Pearson's r coefficients for Initial, Refinement and Maintenance phase (*p<0.05, **p<0.01, ***p<0.001 Mann Whitney test).

Supplementary Figure 1. Cerebellar nuclei inhibition did not affect execution and fatigue, locomotion, motor coordination, balance and strength. a) Locomotor activity (Velocity) in DREADD and non-DREADD (Sham) injected mice after CNO or SAL injection during open-field sessions before (OF1) and after (OF2) rotarod for Initial, Refinement and Maintenance (**p<0.01 t-test OF1 vs OF2). **b**) Latency to fall during fixed speed rotarod (5, 10, 15, 20r.p.m.) for all experimental groups. One way repeated measure ANOVA was performed on averaged values for all the speed steps in each experimental group followed by a Tukey Posthoc pairwise comparison. **c**) Footprint patterns were quantitatively assessed for 3 parameters as shown on representative footprint patterns (top) for all experimental groups. Three parameters are represented graphically: linear movement (bottom left), sigma (bottom middle) and alternation coefficient (bottom right). **d**) Latency reflecting the time before falling from the grid. 30 seconds of cut-off of was established as the maximum latency (dotted line on figure). **e**) Latency to cross the horizontal bar (balance beam test) for

all experimental groups. **f**) Latency to reach home cage in vertical pole test for all experimental groups. *p<0.05 One Way ANOVA followed by a Posthoc Tukey test. *n* indicates the number of mice.

Supplementary Figure 2. Expression of hM4D(Gi)-mCherry in the cerebellar nuclei following CL and VAL injections. a) left: schematics of the experiment for CN-CL groups, right: distribution of labeled neurons. Identified soma expressing mCherry are indicated by arrow-heads. b) same as a for CN-VAL groups.

Supplementary Figure 3. Inhibition of CN-CL or CN-VAL by 1mg/kg CNO does not affect execution and fatigue, locomotion, motor coordination, balance and strength. **a**) Locomotor activty (Velocity) in DREADD injected mice after CNO or SAL injection during open-fields sessions before (OF1) and after (OF2) rotarod for Initial, Refinement and Maintenance (**p<0.01 paired t-test OF1 vs OF2). **b**) Latency to fall during fixed speed rotarod (5, 10, 15, 20 r.p.m.) for all experimental groups. One way repeated measure ANOVA was performed on averaged values for all the speed steps in each experimental group followed by a Tukey Posthoc pairwise comparison. **c**) Footprint patterns were quantitatively assessed for 3 parameters as shown on representative footprint patterns (top) for all experimental groups. Three parameters are represented graphically: linear movement (bottom left), sigma (bottom middle and alternation coefficient (bottom right). **d**) Latency reflecting the time before falling from the grid. 30 seconds of cut-off of was established as the maximum latency (dotted line on figure). **e**) Latency to cross the horizontal bar (balance beam test) for all experimental groups. **f**) Latency to reach home cage in vertical pole test for all experimental groups. *p<0.05 One Way ANOVA followed by a PostHoc Tukey test. CN, cerebellar nuclei, CL, centrolateral thalamus; VAL, ventral anterior lateral thalamus. *n* indicates the number of mice.

AUTHOR CONTRIBUTIONS

Conceptualization, A.P.V., D.P. and C.L.; Methodology, A.P.V. and D.P.; Software, R.W.S. and C.L.; Formal Analysis, A.P.V., R.W.S. and C.L.; Investigation, A.P.V., R.W.S., C.M.H and J.L.F.; Data Curation, A.P.V., R.W.S. and C.L.; Writing –Original Draft, A.P.V., C.L. and D.P.; Writing – Review & Editing, D.P. and C.L.; Visualization, A.P.V., R.W.S., J.L.F and C.L.; Supervision, D.P. and C.L.; Funding Acquisition, D.P. and C.L.

ACKNOWLEDGMENTS

This work was supported by Fondation pour la Recherche Medicale (FRM, DPP20151033983) to D.P. and Agence Nationale de Recherche to D.P. (ANR-16-CE37-0003-02 Amedyst, ANR-19-CE37-0007-01 Multimod, Labex Memolife) and to C.L. (ANR-17-CE37-0009 Mopla, ANR-17-CE16-0019 Synpredict) and by the Institut National de la Santé et de la Recherche Médicale (France). The authors thank David Robbe and Philippe Isope for critical reading of the manuscript.

REFERENCES:

1. Krakauer, J.W., Hadjiosif, A.M., Xu, J., Wong, A.L. & Haith, A.M. Motor Learning. *Compr Physiol* 9, 613-663 (2019).
2. Seidler, R.D. Neural correlates of motor learning, transfer of learning, and learning to learn. *Exerc Sport Sci Rev* 38, 3-9 (2010).
3. Doya, K. What are the computations of the cerebellum, the basal ganglia and the cerebral cortex? *Neural Netw* 12, 961-974 (1999).
4. Raymond, J.L. & Medina, J.F. Computational Principles of Supervised Learning in the Cerebellum. *Annu Rev Neurosci* 41, 233-253 (2018).
5. Yang, Y. & Lisberger, S.G. Purkinje-cell plasticity and cerebellar motor learning are graded by complex-spike duration. *Nature* 510, 529-532 (2014).
6. Herzfeld, D.J., Kojima, Y., Soetedjo, R. & Shadmehr, R. Encoding of error and learning to correct that error by the Purkinje cells of the cerebellum. *Nat Neurosci* 21, 736-743 (2018).
7. Nguyen-Vu, T.D*., et al.* Cerebellar Purkinje cell activity drives motor learning. *Nat Neurosci* 16, 1734-1736 (2013).
8. Hewitt, A.L., Popa, L.S. & Ebner, T.J. Changes in Purkinje cell simple spike encoding of reach kinematics during adaption to a mechanical perturbation. *J Neurosci* 35, 1106-1124 (2015).
9. Morton, S.M. & Bastian, A.J. Cerebellar contributions to locomotor adaptations during splitbelt treadmill walking. *J Neurosci* 26, 9107-9116 (2006).
10. Darmohray, D.M., Jacobs, J.R., Marques, H.G. & Carey, M.R. Spatial and Temporal Locomotor Learning in Mouse Cerebellum. *Neuron* 102, 217-231 e214 (2019).

11. Longley, M. & Yeo, C.H. Distribution of neural plasticity in cerebellum-dependent motor learning. *Prog Brain Res* 210, 79-101 (2014).
12. Clopath, C., Badura, A., De Zeeuw, C.I. & Brunel, N. A cerebellar learning model of vestibulo-ocular reflex adaptation in wild-type and mutant mice. *J Neurosci* 34, 7203-7215 (2014).
13. Ito, M. Control of mental activities by internal models in the cerebellum. *Nat Rev Neurosci* 9, 304-313 (2008).
14. Bernard, J.A. & Seidler, R.D. Cerebellar contributions to visuomotor adaptation and motor sequence learning: an ALE meta-analysis. *Front Hum Neurosci* 7, 27 (2013).
15. Seidler, R.D*., et al.* Cerebellum activation associated with performance change but not motor learning. *Science* 296, 2043-2046 (2002).
16. Baetens, K., Firouzi, M., Van Overwalle, F. & Deroost, N. Involvement of the cerebellum in the serial reaction time task (SRT) (Response to Janacsek et al.). *Neuroimage* 220, 117114 (2020).
17. Karni, A*., et al.* The acquisition of skilled motor performance: fast and slow experience-driven changes in primary motor cortex. *Proc Natl Acad Sci U S A* 95, 861-868 (1998).
18. Brashers-Krug, T., Shadmehr, R. & Bizzi, E. Consolidation in human motor memory. *Nature* 382, 252-255 (1996).
19. Korman, M., Raz, N., Flash, T. & Karni, A. Multiple shifts in the representation of a motor sequence during the acquisition of skilled performance. *Proc Natl Acad Sci U S A* 100, 12492-12497 (2003).
20. Muellbacher, W*., et al.* Early consolidation in human primary motor cortex. *Nature* 415, 640-644 (2002).
21. Cohen, D.A., Pascual-Leone, A., Press, D.Z. & Robertson, E.M. Off-line learning of motor skill memory: a double dissociation of goal and movement. *Proc Natl Acad Sci U S A* 102, 18237-18241 (2005).
22. Doyon, J*., et al.* Contribution of night and day sleep vs. simple passage of time to the consolidation of motor sequence and visuomotor adaptation learning. *Exp Brain Res* 195, 15-26 (2009).
23. Shadmehr, R. & Holcomb, H.H. Neural correlates of motor memory consolidation. *Science* 277, 821-825 (1997).
24. Huang, V.S., Haith, A., Mazzoni, P. & Krakauer, J.W. Rethinking motor learning and savings in adaptation paradigms: model-free memory for successful actions combines with internal models. *Neuron* 70, 787-801 (2011).
25. Mauk, M.D., Li, W., Khilkevich, A. & Halverson, H. Cerebellar mechanisms of learning and plasticity revealed by delay eyelid conditioning. *Int Rev Neurobiol* 117, 21-37 (2014).
26. Caligiore, D*., et al.* Consensus Paper: Towards a Systems-Level View of Cerebellar Function: the Interplay Between Cerebellum, Basal Ganglia, and Cortex. *Cerebellum* 16, 203-229 (2017).
27. Bostan, A.C., Dum, R.P. & Strick, P.L. Cerebellar networks with the cerebral cortex and basal ganglia. *Trends Cogn Sci* 17, 241-254 (2013).
28. Hintzen, A., Pelzer, E.A. & Tittgemeyer, M. Thalamic interactions of cerebellum and basal ganglia. *Brain Struct Funct* 223, 569-587 (2018).
29. Proville, R.D*., et al.* Cerebellum involvement in cortical sensorimotor circuits for the control of voluntary movements. *Nat Neurosci* 17, 1233-1239 (2014).
30. Bostan, A.C. & Strick, P.L. The cerebellum and basal ganglia are interconnected. *Neuropsychol Rev* 20, 261-270 (2010).

31. Carta, I., Chen, C.H., Schott, A.L., Dorizan, S. & Khodakhah, K. Cerebellar modulation of the reward circuitry and social behavior. *Science* 363 (2019).
32. Steriade, M. Two channels in the cerebellothalamocortical system. *J Comp Neurol* 354, 57-70 (1995).
33. Chen, C.H., Fremont, R., Arteaga-Bracho, E.E. & Khodakhah, K. Short latency cerebellar modulation of the basal ganglia. *Nat Neurosci* 17, 1767-1775 (2014).
34. Gornati, S.V*., et al.* Differentiating Cerebellar Impact on Thalamic Nuclei. *Cell reports* 23, 2690-2704 (2018).
35. Costa, R.M., Cohen, D. & Nicolelis, M.A. Differential corticostriatal plasticity during fast and slow motor skill learning in mice. *Curr Biol* 14, 1124-1134 (2004).
36. Rothwell, P.E*., et al.* Autism-associated neuroligin-3 mutations commonly impair striatal circuits to boost repetitive behaviors. *Cell* 158, 198-212 (2014).
37. Yang, G., Pan, F. & Gan, W.B. Stably maintained dendritic spines are associated with lifelong memories. *Nature* 462, 920-924 (2009).
38. Buitrago, M.M., Schulz, J.B., Dichgans, J. & Luft, A.R. Short and long-term motor skill learning in an accelerated rotarod training paradigm. *Neurobiol Learn Mem* 81, 211-216 (2004).
39. Hirata, H., Takahashi, A., Shimoda, Y. & Koide, T. Caspr3-Deficient Mice Exhibit Low Motor Learning during the Early Phase of the Accelerated Rotarod Task. *PLoS One* 11, e0147887 (2016).
40. Roth, B.L. DREADDs for Neuroscientists. *Neuron* 89, 683-694 (2016).
41. Teune, T.M., Van Der Burg, J., Van Der Moer, J., Voogd, J. & Ruigrok, T.J.H. Topography of cerebellar nuclear projections to the brain stem in the rat. *Progress in Brain Research* 124, 141-172 (2000).
42. Cao, V.Y*., et al.* Motor Learning Consolidates Arc-Expressing Neuronal Ensembles in Secondary Motor Cortex. *Neuron* 86, 1385-1392 (2015).
43. Kida, H*., et al.* Motor Training Promotes Both Synaptic and Intrinsic Plasticity of Layer II/III Pyramidal Neurons in the Primary Motor Cortex. *Cereb Cortex* 26, 3494-3507 (2016).
44. Yin, H.H*., et al.* Dynamic reorganization of striatal circuits during the acquisition and consolidation of a skill. *Nat Neurosci* 12, 333-341 (2009).
45. Durieux, P.F., Schiffmann, S.N. & de Kerchove d'Exaerde, A. Differential regulation of motor control and response to dopaminergic drugs by D1R and D2R neurons in distinct dorsal striatum subregions. *EMBO J* 31, 640-653 (2012).
46. Sausbier, M*., et al.* Cerebellar ataxia and Purkinje cell dysfunction caused by Ca2+-activated K+ channel deficiency. *Proc Natl Acad Sci U S A* 101, 9474-9478 (2004).
47. Galliano, E*., et al.* Synaptic transmission and plasticity at inputs to murine cerebellar Purkinje cells are largely dispensable for standard nonmotor tasks. *J Neurosci* 33, 12599-12618 (2013).
48. Groszer, M*., et al.* Impaired synaptic plasticity and motor learning in mice with a point mutation implicated in human speech deficits. *Curr Biol* 18, 354-362 (2008).
49. Sano, T*., et al.* Loss of GPRC5B impairs synapse formation of Purkinje cells with cerebellar nuclear neurons and disrupts cerebellar synaptic plasticity and motor learning. *Neurosci Res* 136, 33-47 (2018).
50. Iscru, E*., et al.* Sensorimotor enhancement in mouse mutants lacking the Purkinje cell-specific Gi/o modulator, Pcp2(L7). *Mol Cell Neurosci* 40, 62-75 (2009).

51. Machado, A.S., Darmohray, D.M., Fayad, J., Marques, H.G. & Carey, M.R. A quantitative framework for whole-body coordination reveals specific deficits in freely walking ataxic mice. *Elife* 4 (2015).
52. Sathyamurthy, A.*, et al.* Cerebellospinal Neurons Regulate Motor Performance and Motor Learning. *Cell reports* 31, 107595 (2020).
53. Porras-Garcia, M.E., Ruiz, R., Perez-Villegas, E.M. & Armengol, J.A. Motor learning of mice lacking cerebellar Purkinje cells. *Front Neuroanat* 7, 4 (2013).
54. Watanave, M.*, et al.* Contribution of Thyrotropin-Releasing Hormone to Cerebellar Long-Term Depression and Motor Learning. *Front Cell Neurosci* 12, 490 (2018).
55. Vinueza Veloz, M.F.*, et al.* Cerebellar control of gait and interlimb coordination. *Brain Struct Funct* 220, 3513-3536 (2015).
56. Stroobants, S., Gantois, I., Pooters, T. & D'Hooge, R. Increased gait variability in mice with small cerebellar cortex lesions and normal rotarod performance. *Behav Brain Res* 241, 32-37 (2013).
57. Sakayori, N.*, et al.* Motor skills mediated through cerebellothalamic tracts projecting to the central lateral nucleus. *Mol Brain* 12, 13 (2019).
58. Aumann, T.D. & Horne, M.K. Ramification and termination of single axons in the cerebellothalamic pathway of the rat. *J Comp Neurol* 376, 420-430 (1996).
59. Alexander, G.M.*, et al.* Remote control of neuronal activity in transgenic mice expressing evolved G protein-coupled receptors. *Neuron* 63, 27-39 (2009).
60. Nagai, H.*, et al.* Sleep Consolidates Motor Learning of Complex Movement Sequences in Mice. *Sleep* 40 (2017).
61. Samaei, A., Ehsani, F., Zoghi, M., Hafez Yosephi, M. & Jaberzadeh, S. Online and offline effects of cerebellar transcranial direct current stimulation on motor learning in healthy older adults: a randomized double-blind sham-controlled study. *Eur J Neurosci* 45, 1177-1185 (2017).
62. Li, W., Ma, L., Yang, G. & Gan, W.B. REM sleep selectively prunes and maintains new synapses in development and learning. *Nat Neurosci* 20, 427-437 (2017).
63. Ruitenberg, M.F.L.*, et al.* Neural correlates of multi-day learning and savings in sensorimotor adaptation. *Sci Rep* 8, 14286 (2018).
64. Morehead, J.R., Qasim, S.E., Crossley, M.J. & Ivry, R. Savings upon Re-Aiming in Visuomotor Adaptation. *J Neurosci* 35, 14386-14396 (2015).
65. Spencer, R.M. & Ivry, R.B. Sequence learning is preserved in individuals with cerebellar degeneration when the movements are directly cued. *J Cogn Neurosci* 21, 1302-1310 (2009).
66. Khilkevich, A., Zambrano, J., Richards, M.M. & Mauk, M.D. Cerebellar implementation of movement sequences through feedback. *Elife* 7 (2018).
67. Ohmae, S. & Medina, J.F. Climbing fibers encode a temporal-difference prediction error during cerebellar learning in mice. *Nat Neurosci* 18, 1798-1803 (2015).
68. Houck, B.D. & Person, A.L. Cerebellar Premotor Output Neurons Collateralize to Innervate the Cerebellar Cortex. *J Comp Neurol* 523, 2254-2271 (2015).
69. Caggiano, V.*, et al.* Midbrain circuits that set locomotor speed and gait selection. *Nature* 553, 455-460 (2018).
70. Rueda-Orozco, P.E. & Robbe, D. The striatum multiplexes contextual and kinematic information to constrain motor habits execution. *Nat Neurosci* 18, 453-460 (2015).
71. Armstrong, D.M. & Edgley, S.A. Discharges of nucleus interpositus neurones during locomotion in the cat. *J Physiol* 351, 411-432 (1984).

72. Sarnaik, R. & Raman, I.M. Control of voluntary and optogenetically perturbed locomotion by spike rate and timing of neurons of the mouse cerebellar nuclei. *Elife* 7 (2018).
73. Low, A.Y.T.*, et al.* Precision of Discrete and Rhythmic Forelimb Movements Requires a Distinct Neuronal Subpopulation in the Interposed Anterior Nucleus. *Cell reports* 22, 2322-2333 (2018).
74. Schwartz, A.B., Ebner, T.J. & Bloedel, J.R. Responses of interposed and dentate neurons to perturbations of the locomotor cycle. *Exp Brain Res* 67, 323-338 (1987).
75. Marple-Horvat, D.E. & Criado, J.M. Rhythmic neuronal activity in the lateral cerebellum of the cat during visually guided stepping. *J Physiol* 518 (Pt 2), 595-603 (1999).
76. Aoki, S., Sato, Y. & Yanagihara, D. Lesion in the lateral cerebellum specifically produces overshooting of the toe trajectory in leading forelimb during obstacle avoidance in the rat. *J Neurophysiol* 110, 1511-1524 (2013).
77. Sauerbrei, B.A., Lubenov, E.V. & Siapas, A.G. Structured Variability in Purkinje Cell Activity during Locomotion. *Neuron* 87, 840-852 (2015).

3

Functional abnormalities in the cerebello-thalamic pathways in a mouse model of DYT25 dystonia

In this study, we used a combination of optogenetic activation of neurons in the dentate nucleus of the cerelllum (DN), coupled with multi-site extracellular recordings in the ventro-lateral thalamus (VAL), centro-lateral thalamus (CL), primary motor cortex (M1) and dorsolateral striatum (DLS) in a mouse model of DYT25 dystonia in order to assess the functionality of cerebello-thalamic pathways in this model, and to investigate the potential effect of cerebellar theta bursts stimulations on the motor network.

My contribution to this study was to analyse the extracellular recordings acquired during optogenetic stimulation of the DN, as well as to participate to the surgeries, the recording and the analysis of the optogenetic stimulation of the DN-CL pathway. I discovered a constitutive alteration of the DN-VAL pathway in this model, with an enhanced sensitivity to cerebellar stimulations in presymptomatic mice. Then, I discovered that the first exposition of the model to the cholinergic agonist needed to trigger symptoms lead to long lasting increases in the sensitivity of VAL, CL and M1 to cerebellar stimulations. I observed that cerebellar theta-burst stimulations

could induce plastic changes in VAL, CL, M1 and DLS fast-spiking neurons, which could not be observed in asymptomatic mice of this model, suggesting an abnormal cerbello-thalamic, cerebello-cortical and cerebello-striatal plasticity in DYT25.

Ultimately, I observed that the administration of cerebellar theta-burst stimulations to symptomatic mice lead to a depression of the response to cerebellar stimulations in the VAL, CL and M1.

RESEARCH ARTICLE

Functional abnormalities in the cerebello-thalamic pathways in a mouse model of DYT25 dystonia

Hind Baba Aïssa[1†], Romain W Sala[1†], Elena Laura Georgescu Margarint[1†], Jimena Laura Frontera[1], Andrés Pablo Varani[1], Fabien Menardy[1], Assunta Pelosi[2,3,4], Denis Hervé[2,3,4], Clément Léna[1*‡], Daniela Popa[1*‡]

[1]Neurophysiology of Brain Circuits Team, Institut de biologie de l'Ecole normale supérieure (IBENS), Ecole normale supérieure, CNRS, INSERM, PSL Research University, Paris, France; [2]Inserm UMR-S 1270, Paris, France; [3]Sorbonne Université, Sciences and Technology Faculty, Paris, France; [4]Institut du Fer à Moulin, Paris, France

Abstract Dystonia is often associated with functional alterations in the cerebello-thalamic pathways, which have been proposed to contribute to the disorder by propagating pathological firing patterns to the forebrain. Here, we examined the function of the cerebello-thalamic pathways in a model of DYT25 dystonia. DYT25 (*Gnal*$^{+/-}$) mice carry a heterozygous knockout mutation of the *Gnal* gene, which notably disrupts striatal function, and systemic or striatal administration of oxotremorine to these mice triggers dystonic symptoms. Our results reveal an increased cerebello-thalamic excitability in the presymptomatic state. Following the first dystonic episode, *Gnal*$^{+/-}$ mice in the asymptomatic state exhibit a further increase of the cerebello-thalamo-cortical excitability, which is maintained after θ-burst stimulations of the cerebellum. When administered in the symptomatic state induced by a cholinergic activation, these stimulations decreased the cerebello-thalamic excitability and reduced dystonic symptoms. In agreement with dystonia being a multiregional circuit disorder, our results suggest that the increased cerebello-thalamic excitability constitutes an early endophenotype, and that the cerebellum is a gateway for corrective therapies via the depression of cerebello-thalamic pathways.

***For correspondence:** lena@biologie.ens.fr (CL); dpopa@biologie.ens.fr (DP)

†These authors contributed equally to this work
‡These authors are co-directed to this work

Competing interest: The authors declare that no competing interests exist.

Funding: See page 19

Preprinted: 03 February 2020
Received: 31 March 2022
Accepted: 27 May 2022
Published: 14 June 2022

Reviewing Editor: Megan R Carey, Champalimaud Foundation, Portugal

Editor's evaluation

Baba Aissa et al. provide compelling evidence for a modulatory role of the cerebello-thalamo-striatal pathway in the pathology of DYT25 dystonia. Their results further suggest that cerebellar stimulation holds promise as a therapeutic intervention for treating dystonia.

Introduction

Dystonia is a class of neurological disease whose symptomatology is characterized by involuntary movements and abnormal postures, caused by the co-contraction of antagonistic muscles (***Berardelli et al., 1998***; ***Albanese et al., 2013***). The wide clinical spectrum of dystonia, whether in causes or clinical manifestations, has hampered so far the identification of a common pathophysiological mechanism underlying the disease (***Balint et al., 2018***). If early studies have primarily highlighted the role of the basal ganglia in the onset of the disease, more recent studies have revealed strong dysfunctions in the motor cortex, thalamus, and cerebellum in dystonic patients, questioning which structural impairments are primary or secondary causes of dystonia (***Simonyan, 2018***). Indeed, lesions in the basal

ganglia or in the cerebellum do not systematically induce a dystonic phenotype, and the onset of the disease is usually delayed following the lesions. Moreover, if the basal ganglia and cerebellum have been considered as therapeutic targets, approaches targeting these structures yielded inconsistent outcomes (**Oyama and Hattori, 2021**). These specificities led to the emergence of a new working hypothesis, that dystonia is a circuit disorder that has a diversity of triggering mechanisms but requires the interactions between several nodes of the motor network to reach a symptomatic state (**Lehéricy et al., 2013**; **Prudente et al., 2014**).

In line with the circuit disorder theory, studies of genetic forms of the disease have identified endophenotypes in the form of nonmotor symptoms, such as altered temporal discrimination threshold in nonmanifesting mutation carriers (**Hutchinson et al., 2013**), causing an inability of individuals to consider two subsequent stimuli as asynchronous if those are presented in a short amount of time. Such endophenotypes indicate an altered sensorimotor processing, which after amplification over time or through environmental interactions would lead to motor dysfunction. Anomalies in synaptic plasticity in the cortex and striatum have also been linked to dystonia in genetic forms of dystonia in rodent models (**Calabresi et al., 2016**). Cerebellar dysfunction preexisting to symptoms has also been observed in such models: nonmanifesting DYT6 mice exhibit an aberrant electrophysiological activity in the cerebellar cortex and nuclei, which is further disrupted in manifesting animals (**van der Heijden et al., 2021**). The functional connectivity in motor circuit may play an important role in the expression of symptoms. Indeed, DYT1 mutation carriers exhibit cerebello-thalamic disruptions, and the penetrance of DYT1 dystonia, as well as the severity of symptoms, is regulated by the structural integrity of cerebello-thalamo-cortical tracts (**Argyelan et al., 2009**). This observation has been reproduced in a mouse model of DYT1 (**Uluğ et al., 2011**), as well as a defect in cortico-striatal plasticity (**Yu-Taeger et al., 2020**), supporting the possibility of an inter-dependence of cerebello-thalamic and striatal dysfunctions. Thus, animal models of genetic forms of dystonia support the idea of a circuit disorder, but also offer an opportunity to investigate the network alterations at the level of the cerebellum, basal ganglia, motor cortex, and their reciprocal connections.

DYT25 is a recently identified genetic form of primary torsion dystonia, characterized as an autosomal-dominant adult-onset disorder (**Fuchs et al., 2013**; **Kumar et al., 2014**). It is caused by loss-of-function mutations of the *Gnal* gene encoding Gα(olf), a G-protein stimulating adenylate cyclase activity, mainly expressed in the olfactory bulb and striatum, with a sparse expression in Purkinje cells of the cerebellar cortex (**Belluscio et al., 1998**; **Vemula et al., 2013**). The genetic alterations discovered in DYT25 dystonic patients can be mimicked by heterozygous knockout mutation of the *Gnal* gene ($Gnal^{+/-}$) (**Pelosi et al., 2017**). In this model, cAMP production is reduced in the striatum, disrupting striatal functions, but the mice are devoid of dystonic symptoms in early adulthood. In agreement with a role of increased striatal cholinergic activity in dystonia (**Pisani et al., 2007**), dystonic symptoms are induced by injections of a muscarinic cholinergic agonist (oxotremorine M) administered either systemically or in the striatum, but not in the cerebellum, and were prevented by the muscarinic antagonist, trihexyphenidyl, a drug alleviating symptoms in many dystonic patients. This indicates that an increase in striatal cholinergic tone is critical to the onset of the disorder (**Pelosi et al., 2017**). This is consistent with a primary involvement of *Gnal* in striatal neurotransmission, despite its sparse expression in other brain regions (**Zhuang et al., 2000**; **Corvol et al., 2001**; **Hervé et al., 2001**; **Corvol et al., 2007**; **Vemula et al., 2013**).

Regardless of the heterogeneity in the function and expression of the genes involved in DYT1 and DYT25, these types of dystonia share many similarities. Strikingly, in animal models, similar alterations in cortico-striatal plasticity were observed in DYT1 and DYT25, suggesting common pathophysiological mechanisms (**Martella et al., 2021**). While the alteration of cerebellum or cerebello-thalamic tracts has been linked to the expression of DYT1 in patients and mouse models (**Argyelan et al., 2009**; **Uluğ et al., 2011**; **Fremont et al., 2017**), studies of DYT25 have remained focused on striatal alterations. However, an involvement of cerebello-thalamic tracts in the pathophysiology of DYT25 remains an open question. Moreover, cerebellar stimulations have been shown to be beneficial in idiopathic cervical dystonia (**Koch et al., 2014**; **Bradnam et al., 2016**), and genetic mouse models of dystonia allow a finer dissection of the effects induced by this type of approach (**van der Heijden et al., 2021**). In contrast to the DYT1 mouse, the DYT25 mouse model has the additional advantage of being pharmacologically inducible, allowing the study of the network's state in the presymptomatic and symptomatic states.

In this study, we therefore investigated the functional connectivity and plasticity of cerebello-thalamic tracts in the *Gnal* mouse model. We performed optogenetic stimulations in the cerebellar dentate nucleus (DN) and recorded activity in the ventrolateral thalamus (VAL, which projects to the motor cortex), centrolateral thalamus (CL, which projects to the striatum), primary motor cortex (M1), and dorsolateral striatum (DLS). We investigated the state of this network in the presymptomatic condition, symptomatic state, and asymptomatic state after the induction of the disease. Finally, in line with the therapeutic benefit of cerebellar stimulations in patients, we tested the effect of optogenetic θ-frequency stimulations of the DN on the plasticity of cerebello-thalamo-cortical tracts and on motor symptoms.

Results

Young adult *Gnal*$^{+/-}$ mice do not exhibit constitutive locomotor impairments

3–7-month-old *Gnal*$^{+/-}$ mice have been described as asymptomatic, without dystonic phenotype in control conditions (***Pelosi et al., 2017***). To further examine whether *Gnal*$^{+/-}$ mice exhibit constitutive motor deficit (taking into account gender), we performed a larger set of motor experiments, including vertical pole, horizontal bar, grid test, fixed-speed rotarod, gait test, and an open-field test (***Figure 1***, ***Supplementary file 1a***).

We observed that the motor performance of *Gnal*$^{+/-}$ mice was not impaired in the vertical pole test (***Figure 1A***, ***Supplementary file 1a***), horizontal bar test (***Figure 1B***, ***Supplementary file 1a***), and grid test (***Figure 1C***, ***Supplementary file 1a***). Females exhibited better performances in the horizontal bar test, regardless of their genotype.

Motor coordination was also examined in a fixed-speed rotarod test. We did not find significant differences between *Gnal*$^{+/-}$ and WT mice (***Figure 1D***, ***Supplementary file 1a***), nor when comparing males and females for each speed step (***Figure 1E***, ***Supplementary file 1a***).

In the gait test, we found no significant differences in gait width, alternation coefficient, linear movement, sigma, or length of stride (***Figure 1F***, ***Supplementary file 1a***).

Finally, in spontaneous locomotion in the open field, we observed no significant differences between genotype and gender neither in median instantaneous speed nor in distance traveled (***Figure 1G, J and K***, ***Supplementary file 1a***). Additionally, we included an analysis of the thigmotaxis and time spent exploring the center of the open field and observed no significant differences between genotypes or genders in our mice (***Figure 1H, I***, ***Supplementary file 1a***). In conclusion, motor activity and motor coordination are not impaired in young 3–7-month-old *Gnal*$^{+/-}$ mice; furthermore, no significant differences were observed between male and female *Gnal*$^{+/-}$ mice compared to their WT littermates, allowing us to merge genders in the following physiological experiments.

Thalamo-cortical alteration in *Gnal*$^{+/-}$ mice in presymptomatic and symptomatic states

To assess the functional connectivity of the ascending pathway connecting the cerebellum with the thalamus and motor cortex, we performed extracellular recordings of the VAL and CL thalamic nuclei, as well as M1 in awake freely moving young adult mice of both genotypes (***Figure 2***, ***Figure 2—figure supplement 1***, ***Supplementary file 1b***). Mice were recorded at the age of 3–7 months, at which *Gnal*$^{+/-}$ mice are asymptomatic, before the onset of an abnormality of motor coordination (***Pelosi et al., 2017***). VAL, CL, and M1 neurons presented no differences in firing rate between WT and *Gnal*$^{+/-}$ mice in basal conditions (***Figure 2—figure supplement 2A***, ***Supplementary file 1k and l***).

To induce a dystonic-like phenotype in *Gnal*$^{+/-}$ mice (***Pelosi et al., 2017***), we then injected oxotremorine M (0.1 mg/kg, i.p.), a nonselective cholinergic agonist in both WT and *Gnal*$^{+/-}$ mice. As described previously, this treatment induces in both genotypes a cholinergic shock, which translates into excessive salivation and lacrimation, as well as a persistent immobility. It also induces in *Gnal*$^{+/-}$ mice abnormal dystonic-like movements and postures. Oxotremorine-treated mice, whether WT or *Gnal*$^{+/-}$, presented a significant decrease in the firing rate of VAL and M1 (***Figure 2—figure supplement 2A***, ***Supplementary file 1k and l***). While oxotremorine did not modify the firing properties of CL neurons in WT mice, it decreased the firing rate of CL neurons in *Gnal*$^{+/-}$ mice (***Figure 2—figure supplement 2A***, ***Supplementary file 1k and l***). We then investigated the effect of a first exposure to oxotremorine

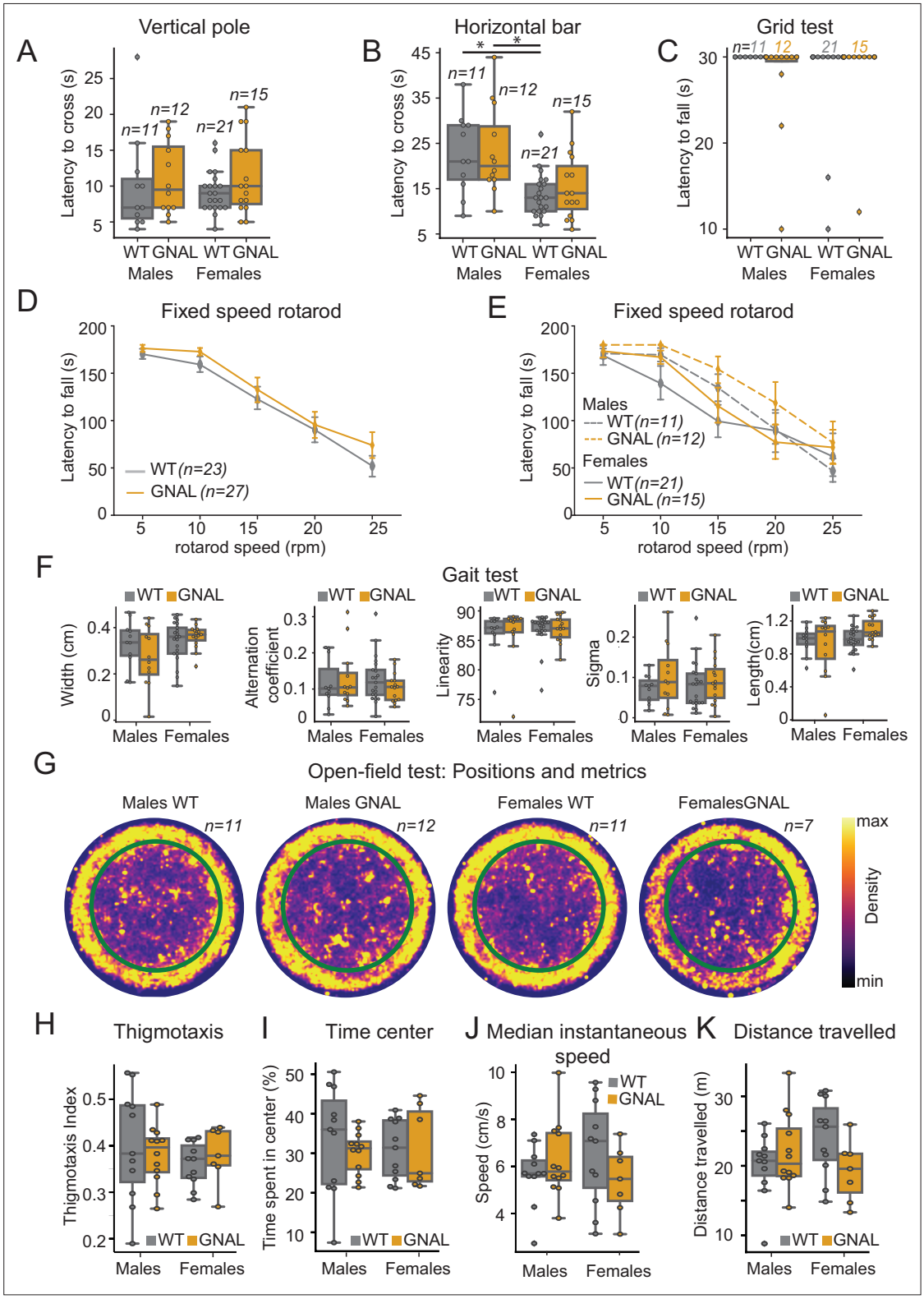

Figure 1. Young male and female *Gnal*$^{+/-}$ mice do not display motor coordination impairments. (**A**) Latency to climb down the vertical pole in male and female *Gnal*$^{+/-}$ (GNAL) and wildtype (WT) mice. (**B**) Latency to cross the horizontal bar. (**C**) Latency to fall during the grid test (30 s cutoff). (**D**) Latency to fall during the fixed-speed rotarod test separated by genotype, and (**E**) by gender and genotype. (**F**) Gait width, alternation coefficient, movement linearity, sigma, and stride length during the gait test. (**G**) Two-dimensional histograms showing the density of position of mice during open-field

Figure 1 continued on next page

Figure 1 continued

sessions, separated by gender and genotype. Thigmotaxis index (**H**), percentage of time spent in center (**I**), median instantaneous speed (**J**), and total distance traveled (**K**) during the open-field test. Reported statistics are the comparison of groups separated by gender and genotype using a Kruskal–Wallis test, followed by a Dunn's post-hoc test corrected using Holm–Sidak method. *p<0.05.

on the regularity of firing patterns in the thalamus. We observed a significant decrease in CV_{isi} of VAL neurons in both WT and *Gnal*$^{+/-}$ mice (***Figure 2—figure supplement 3A***, ***Supplementary file 1o and p***). While oxotremorine did not modify the CV_{isi} of CL neurons in WT mice, it was decreased for CL neurons in *Gnal*$^{+/-}$ mice (***Figure 2—figure supplement 3A***, ***Supplementary file 1o and p***), suggesting an increased regularity of firing.

Overall, these results show no thalamic impairments in *Gnal*$^{+/-}$ mice in the presymptomatic state compared to WT mice but reveal differences between genotypes following the induction of dystonic-like state using oxotremorine injection. Oxotremorine by itself affects VAL-M1 activity, while a sensitivity of the CL was only found in *Gnal*$^{+/-}$ mice compared to WT mice.

First exposure to cholinergic agonist induces long-lasting changes in cerebello-thalamic excitability

The DN is the main output of the cerebellum towards the thalamus and is known to project both to the VAL and CL (***Ichinohe et al., 2000***; ***Teune et al., 2000***). To probe the activity of these cerebello-thalamic pathways, we hence paired recordings of these structures with low-frequency, low-intensity stimulations of the DN in *Gnal*$^{+/-}$ and WT mice not only in the presymptomatic state (saline-injected naive mice) and symptomatic (oxotremorine-injected mice) states, but also in an asymptomatic state (saline-injected mice at least 2 days after oxotremorine injection) (***Figure 2C***, ***Figure 2—figure supplement 2B and C***).

In naive saline-treated mice, we found a significant increase in firing rate for the VAL, CL thalamus and M1 neurons during 100 ms DN stimulations in WT and *Gnal*$^{+/-}$mice (***Figure 2—figure supplement 2B and C***). Responses in the VAL were significantly larger in *Gnal*$^{+/-}$ than in WT mice, suggesting an increased responsiveness of this thalamo-cortical pathway in the presymptomatic state. We verified the absence of plastic changes of the responses in VAL, CL, and M1 induced by our low-frequency stimulation of the DN by showing the absence of significant difference between the average response to the first half of the stimulations ('early') and the second half of the stimulations ('late,' ***Figure 2—figure supplement 2B and D***, ***Supplementary file 1n***).

Then, we examined the effect of acute exposure to oxotremorine on cerebello-thalamo-cortical projections. The naive saline-treated mice were thereafter injected with oxotremorine and subjected again to low-frequency stimulations ('Oxo' condition, ***Figure 2A and C***). We did not observe any significant difference in response to DN stimulation in the VAL, CL, and M1 in comparison to naive condition, for both genotypes (***Supplementary file 1c and d***). This suggests that the first exposure to oxotremorine does not cause significant short-term changes in the cerebellar drive of thalamic nuclei and motor cortex.

In order to investigate a potential long-term effect of the exposure to oxotremorine on cerebello-thalamo-cortical sensitivity, the mice were subjected once more to low-frequency, low-intensity optogenetic stimulations of the DN in saline conditions, 2 days after their first exposition to oxotremorine ('Post-Oxo,' asymptomatic condition, ***Figure 2A***). While the acute exposure to oxotremorine yielded slightly increased responses in VAL neurons and decreased responses in M1 neurons in WT mice, *Gnal*$^{+/-}$ mice in the asymptomatic state presented a significantly larger response to DN stimulations in all recorded structures compared to the changes induced by oxotremorine in WT animals (***Figure 2C***, ***Supplementary file 1c and d***), indicating an increased excitability of the cerebello-thalamic pathways in asymptomatic *Gnal*$^{+/-}$ mice following the first dystonia induction.

Overall, these results show that a single exposure of *Gnal*$^{+/-}$ mice to oxotremorine induces, in the cerebello-thalamic pathways, long-lasting functional alterations that are more pronounced than the mild alterations observed in the presymptomatic state.

Cerebello-thalamic plasticity is altered in asymptomatic *Gnal*$^{+/-}$ mice

The long-lasting increase after oxotremorine treatment in *Gnal*$^{+/-}$mice of the excitability in the cerebello-thalamic connections could be associated with an alteration of their plasticity. To test this

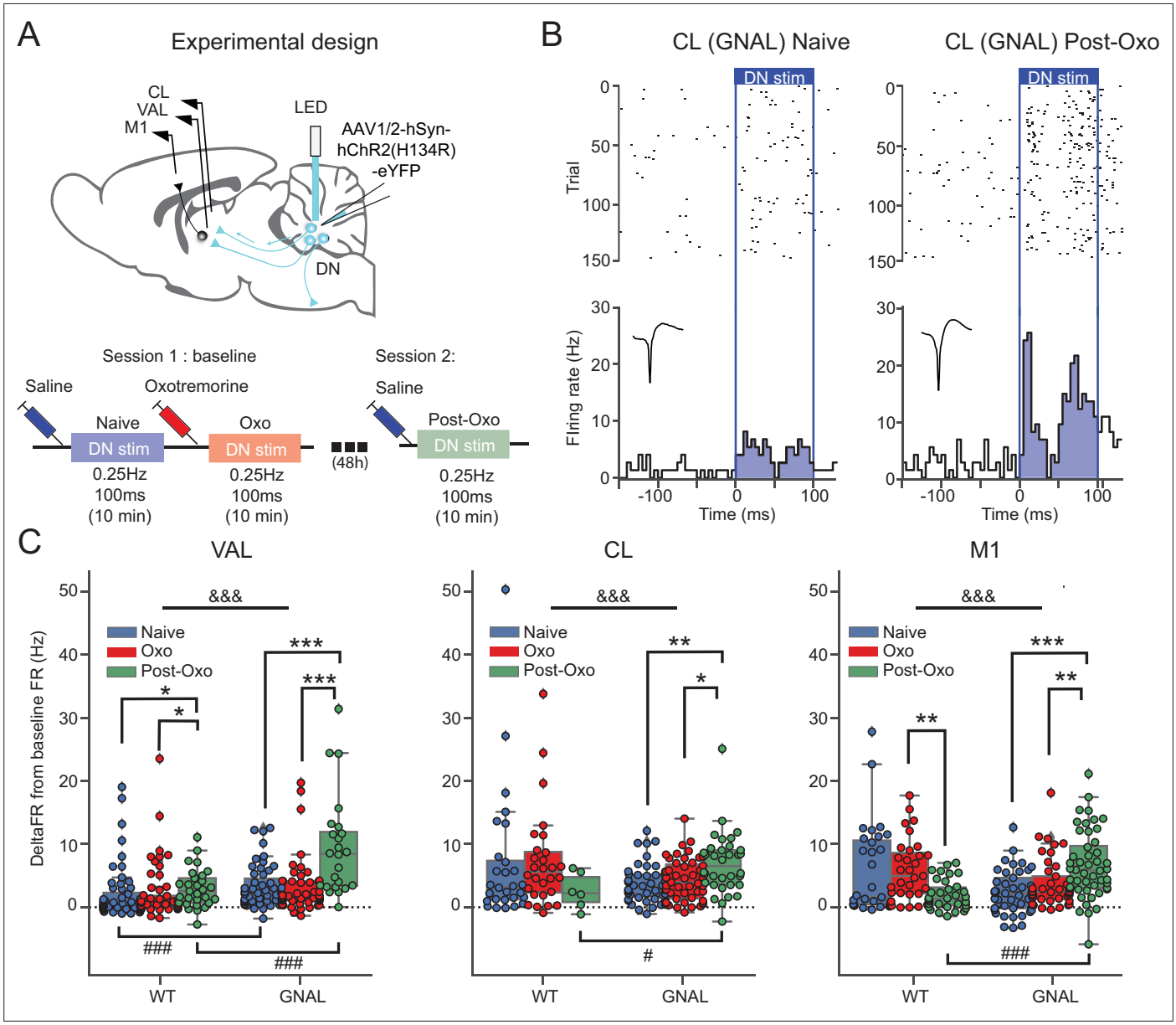

Figure 2. Exposure to oxotremorine causes a long-lasting increase in thalamic and cortical response to dentate nucleus (DN) stimulation in *Gnal*$^{+/-}$ mice. (**A**) Schematics describing the experimental design of thalamo-cortical recordings coupled with DN stimulation (top) and experimental timeline (bottom). (**B**) Examples of peristimulus time histogram (PSTH) and corresponding raster plot, centered on the onset of the cerebellar stimulation, of centrolateral thalamus (CL) neurons from the same recording site in a *Gnal*$^{+/-}$ mouse under saline condition, before being exposed to oxotremorine ('naive,' left) and 48–72 hr after being exposed to oxotremorine ('Post-Oxo,' right). Inset represents the average waveforms of the recorded neuron. (**C**) Distributions of responses to DN stimulations in naive condition (blue), under the acute effect of oxotremorine (red) and in saline post-oxo condition (green). Two-way ANOVA, with state and genotype as factors, followed by a Dunn's post-hoc test corrected using Holm–Sidak method to compare states within genotype. *p<0.05, **p<0.01, ***p<0.001; &&&p<0.001 for ANOVA interaction term between states and genotype.

The online version of this article includes the following figure supplement(s) for figure 2:

Figure supplement 1. Electrophysiology recordings in thalamo-cortical and cerebello-striatal networks.

Figure supplement 2. Effects of initial exposure to oxotremorine and dentate nucleus (DN) stimulation on the thalamo-cortical network in wildtype (WT) and *Gnal*$^{+/-}$ mice.

Figure supplement 3. Effects of initial exposure to oxotremorine on the regularity of thalamic firing patterns in wildtype (WT) and *Gnal*$^{+/-}$ mice.

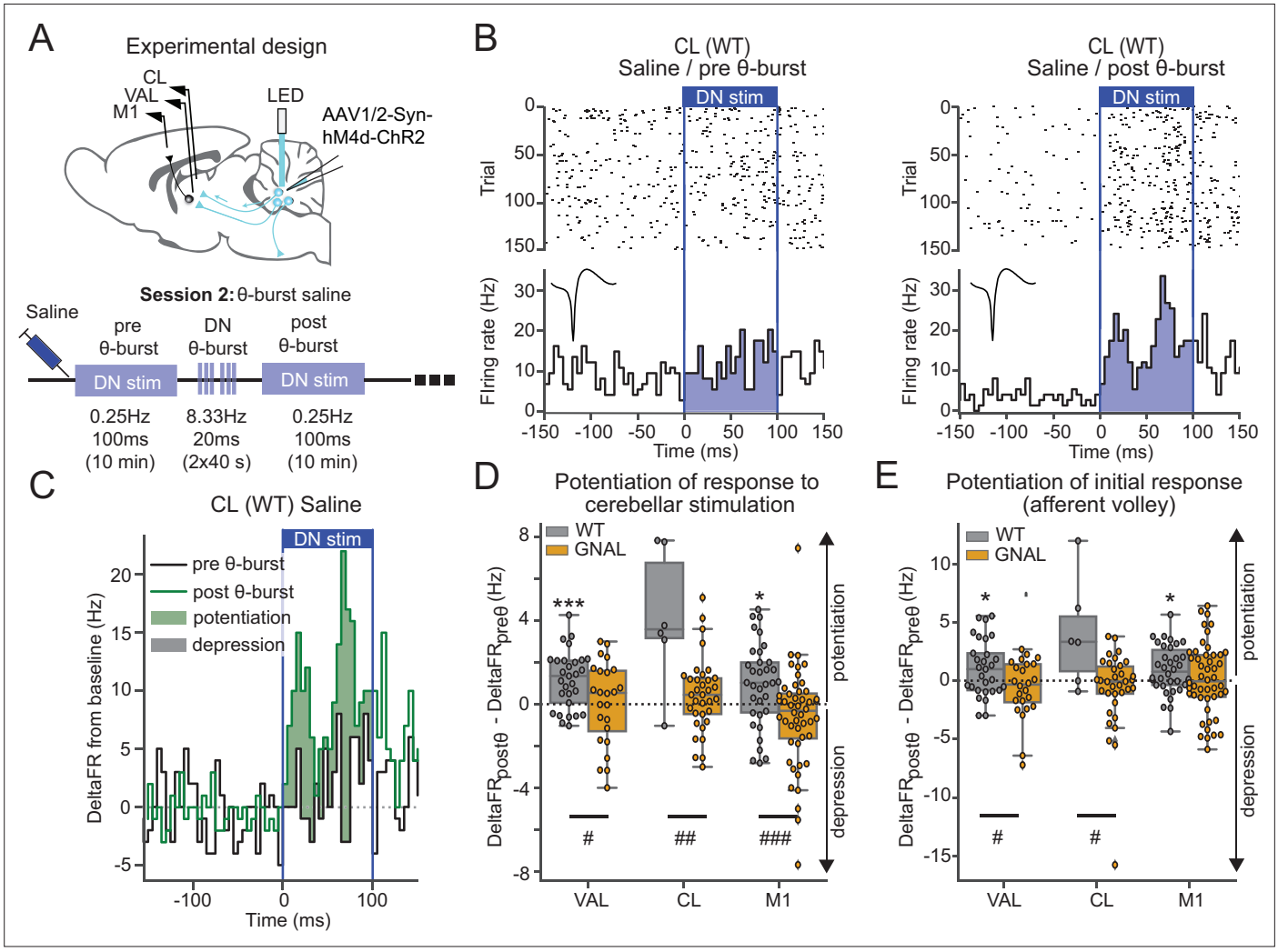

Figure 3. Asymptomatic *Gnal*$^{+/-}$ mice display an abnormal cerebello-thalamic plasticity induced by dentate nucleus (DN) θ -bursts. (**A**) Schematics describing the experimental design of thalamo-cortical recordings coupled with dentate nucleus-centrolateral thalamus (DN-CL) stimulation (top) and experimental timeline (bottom). All the mice received oxotremorine (0.1 mg/kg) in session 1, which took place 2–3 days before. (**B**) Example of peristimulus time histogram (PSTH) and corresponding raster plot, centered on the onset of the cerebellar stimulation, of a CL neuron from a wildtype (WT) mouse under saline condition, before θ -burst (left) and after θ -burst (right). Inset represents the average waveform of the neuron. (**C**) Overlay of PSTHs for the neuron shown in panel (**B**); the difference between the histograms is filled to highlight the potentiation or depression of the responses. (**D**) Impact of θ -burst stimulations administered in saline condition on the response to 100 ms DN stimulations. (**E**) Impact of θ -burst stimulations administered in saline condition on the afferent volley in response to 100 ms DN stimulation. Wilcoxon test for paired samples *p<0.05, **p<0.01, ***p<0.001. Mann–Whitney test for independent samples #p<0.05, ##p<0.01, ###p<0.001 difference between genotypes.

possibility, we performed optogenetic θ-burst stimulations of the DN and examined the changes in thalamic and cortical responses to cerebellar stimulation by subsequently applying low-frequency DN stimulations (***Figure 3***).

In saline-treated WT mice, the comparison of the increase in firing rate induced by DN stimulations before and after θ-burst stimulations (***Figure 3B and C***) revealed a potentiation of the response in VAL and M1 neurons to the low-frequency stimulation (***Figure 3D***, ***Supplementary file 1e***). On the other hand, in *Gnal*$^{+/-}$ mice, θ-burst stimulations failed to induce a significant potentiation in the responses of VAL, CL, or M1 neurons to DN stimulations, yielding significantly smaller θ-burst-induced changes in response to DN stimulations compared to WT mice (***Figure 3D***, ***Supplementary file 1e***). We verified that these effects did not result from the recruitment of other brain structures over the duration of the 100 ms stimulation by quantifying the change in response in a short (10 ms wide) initial window corresponding to the putative afferent volley. This analysis reduced the spikes counts considered and

thus decreased the signal/noise ratio of detection of potentiation. However, a reduction of θ-burst effect was observed in *Gnal*$^{+/-}$ mice compared to WT mice in VAL and CL neurons. In M1, the significant θ-burst-induced potentiation was only observed in WT but not *Gnal*$^{+/-}$ mice (***Figure 3E***). Hence, in the saline condition, θ-burst stimulations of the DN induced a potentiated response for WT mice in motor thalamo-cortical pathways, whereas this potentiation was absent in *Gnal*$^{+/-}$ mice, indicating an impaired plasticity of cerebello-thalamic pathways in the asymptomatic state.

Effect of cerebellar stimulation on the cerebello-striatal pathway

The cerebello-CL-striatal pathway (***Ichinohe et al., 2000***; ***Bostan and Strick, 2010***; ***Chen et al., 2014***; ***Gornati et al., 2018***; ***Xiao et al., 2018***) has been shown to play a central role in certain forms of dystonia (***Chen et al., 2014***). We therefore further investigated the functionality of the cerebello-striatal pathway by recording awake freely moving mice where DN neurons were retrogradely infected from the CL with a ChR2-expressing AAV virus (***Figure 4A***). With the use of an optrode, we recorded the activity of DN neurons while performing optogenetic stimulations in the DN and recorded simultaneously extracellular activity from the DLS.

Using 100 ms low-frequency DN stimulations, we observed in both *Gnal*$^{+/-}$ and WT mice an increased firing rate in DN neurons consistent with the existence of a population of CL-projecting DN neurons (***Figure 4B and C***, ***Supplementary file 1f***). Application of a θ-burst protocol in these mice (***Figure 4—figure supplement 1***, ***Supplementary file 1q***) failed to induce a global potentiation or depression of DN responses to subsequent low-frequency 100 ms stimulations (***Figure 4D***), suggesting that θ-burst stimulations in the DN do not result in a long-lasting change of excitability in the stimulated neurons. Finally, we examined the impact of oxotremorine injections on DN discharge and found, as in other recorded brain regions, a significant decrease in firing rate in DN neurons under oxotremorine conditions in both *Gnal*$^{+/-}$ and WT mice (***Figure 4—figure supplement 2A***, ***Supplementary file 1r***). However, contrarily to the impact of oxotremorine injections on CL discharge (***Figure 2—figure supplement 2A***), we found no such difference between the genotypes in the DN (***Figure 4—figure supplement 2A***, ***Supplementary file 1r***). Interestingly, while dystonia has been associated with irregular cerebellar firing in other models of dystonia (***LeDoux and Lorden, 1998***; ***Chen et al., 2014***; ***Fremont et al., 2014***; ***Fremont et al., 2017***; ***van der Heijden et al., 2021***), the firing irregularity (as measured by the coefficient of variation of the interspike interval, CV_{isi}) was not significantly modified under oxotremorine for WT and *Gnal*$^{+/-}$ mice, although DN neurons in *Gnal*$^{+/-}$ mice exhibited a stronger shift toward regular firing discharge under oxotremorine compared to WT mice (***Figure 4—figure supplement 2B***, ***Supplementary file 1r***).

The impact of these DN stimulations was then examined in the DLS. DLS neurons exhibited a bimodal distribution of firing rate (***Figure 4E***), allowing to separate slow- and fast-spiking neurons corresponding to putative medium spiny neurons and interneurons (***Her et al., 2016***). Neurons from both populations in the DLS displayed significant departure from baseline firing during DN optogenetic stimulations in both WT and *Gnal*$^{+/-}$ mice, but there was no significant increase in the firing rate of the population over the whole stimulation interval (***Figure 4F***, ***Supplementary file 1f***). Θ-burst stimulations of the DN also produced a rhythmic entrainment of the DLS fast-spiking populations (***Figure 4—figure supplement 1B and C***) consistent with a striatal entrainment through CL-projecting DN neurons.

Aberrant striatal plasticity in asymptomatic *Gnal*$^{+/-}$ mice

We then examined the long-lasting effect of θ-burst DN-CL stimulations on DLS responses in the saline condition (***Figure 4G–J***). In WT animals, DLS fast-spiking neurons exhibited increased responses to low-frequency 100 ms DN stimulations after θ-burst protocol, not only when taking into account the whole duration of the DN stimulation (***Figure 4H and I***), but also when focusing on the initial response (***Figure 4J***). This suggests that θ-burst DN stimulations increase the recruitment of DLS fast-spiking units through an oligo-synaptic pathway. In contrast, such change in response to DN low-frequency 100 ms stimulations was absent in *Gnal*$^{+/-}$ mice in either type of units in the DLS following θ-burst stimulations. This observed difference between genotypes is consistent with the impact of θ-burst stimulations in the CL neurons in saline condition (***Figure 3D and E***) and thus indicates an impairment in cerebello-thalamo-striatal plasticity in asymptomatic ('post-Oxo') *Gnal*$^{+/-}$ mice.

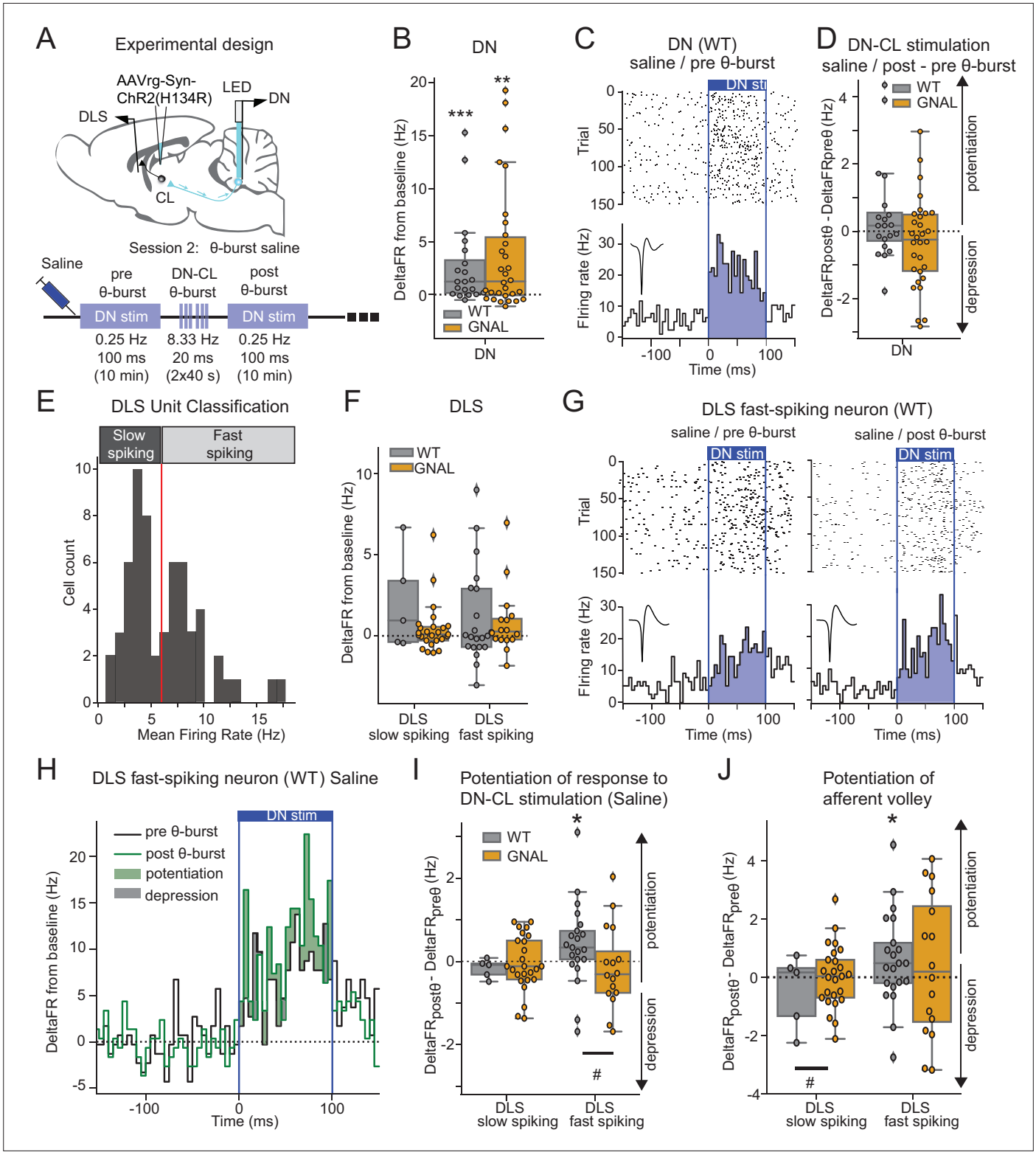

Figure 4. Dentate nucleus-centrolateral thalamus (DN-CL) θ -bursts potentiate the response of fast-spiking dorsolateral striatum (DLS) neurons to DN stimulation in WT wildtype (mice), but not in *Gnal*$^{+/-}$ mice. (**A**) Schematics describing the experimental design of cerebello-striatal recordings coupled with DN-CL stimulation (top) and experimental timeline (bottom). (**B**) Distributions of response amplitude in the DN to optogenetic stimulation in saline condition, before θ -bursts. (**C**) Example of peristimulus time histogram (PSTH) and corresponding raster plot, centered on the onset of the

Figure 4 continued on next page

Figure 4 continued

cerebellar stimulation, of a DN neuron from a WT mouse under saline condition, before θ-bursts. Inset represents the average waveform of the neuron. (**D**) Impact of θ-burst stimulations administered in saline condition on the amplitude of response to 100 ms DN-CL stimulation. (**E**) Illustration of the criteria used to classify DLS neurons as slow spiking and fast spiking based on their mean firing rate using a threshold of 6 Hz (red line). (**F**) Distributions of striatal responses to DN-CL stimulation in saline condition, before θ-burst. (**G**) Example of a PSTH and corresponding raster plot, centered on the onset of the DN-CL stimulation, of a DLS fast-spiking neuron from a WT mouse under saline condition, before θ-burst (left) and after θ-burst (right). Inset represents the average waveform of the neuron. (**H**) Overlay of the PSTHs from panel (**G**); the difference between the histograms is filled to highlight the potentiation or depression of responses. (**I**) Impact of θ-burst stimulations administered in saline condition on the response to 100 ms DN-CL stimulation. (**J**) Impact of θ-burst stimulations administered in saline condition on the afferent volley in response to 100 ms DN-CL stimulation. Wilcoxon test for paired samples *p<0.05, **p<0.01, ***p<0.001. Mann–Whitney test for independent samples #p<0.05, ##p<0.01, ###p<0.001 for differences between genotypes.

The online version of this article includes the following figure supplement(s) for figure 4:

Figure supplement 1. Dentate nucleus-centrolateral thalamus (DN-CL) θ-bursts elicit excitation in DN neurons and dorsolateral striatum (DLS) fast-spiking neurons.

Figure supplement 2. Effect of oxotremorine on the firing of the dentate nucleus (DN).

Aberrant cerebello-thalamic plasticity in *Gnal*$^{+/-}$ mice in the symptomatic state

Since cerebellar θ-burst transcranial stimulation protocols have been shown to produce symptomatic relief in human motor disorders (***Koch et al., 2014***; ***Bradnam et al., 2016***), we then examined the effects on motor circuits and behavior of θ-burst stimulations applied during oxotremorine-induced dystonia in our mice (***Figure 5***). Following oxotremorine administration, the increase in firing rate in response to low-frequency 100 ms DN stimulations in VAL, CL, and M1 neurons was stronger in *Gnal*$^{+/-}$ mice than WT mice (***Figure 5B***), as also found in the asymptomatic condition (***Figure 2C***).

In WT mice, θ-burst stimulations under oxotremorine did not induce lasting changes in the response of VAL and M1 neurons to low-frequency 100 ms DN stimulations, neither when taking into account the whole duration of stimulation (***Figure 5E***, ***Supplementary file 1i***), nor when looking only at the initial response ('afferent volley,' ***Figure 5F***, ***Supplementary file 1i***). In contrast, θ-burst stimulations in *Gnal*$^{+/-}$ mice induced a lasting depression of the response to low-frequency cerebellar stimulations in VAL, CL, and M1 for the whole duration of the stimulation (***Figure 5C–E***, ***Supplementary file 1i***). This depression was also observed in the afferent volley (***Figure 5F***, ***Supplementary file 1i***). Thus, while cerebellar drive of the thalamus and cortex is enhanced in asymptomatic *Gnal*$^{+/-}$ mice, θ-bursts applied in symptomatic (but not asymptomatic, ***Figure 3E and F***) *Gnal*$^{+/-}$ mice induce a decrease in the entrainment of the thalamus and M1 by the cerebellum.

Cerebellar θ-burst stimulations reduce dystonic symptoms in *Gnal*$^{+/-}$ mice

We then evaluated the effect of optogenetic θ-burst stimulations on the motor state of *Gnal*$^{+/-}$ mice compared to WT mice (***Figure 5G–I***). In *Gnal*$^{+/-}$ mice, oxotremorine consistently induced abnormal postures such as the extension of hind limbs from the body axis for >10 s, sustained hunched posture with little movements, slow walking with increased hind limb gait, yielding maximal dystonia scores, while only mild motor signs were observed in WT mice (***Figure 5H***, ***Supplementary file 1j***). These observations are consistent with the previous findings in *Gnal*$^{+/-}$ mice (***Pelosi et al., 2017***) and indicate that the surgical interventions (electrode and optical fiber implantation, AAV infections) did not impact the development of dystonic-type motor abnormalities.

DN optogenetic θ-burst stimulations decreased the abnormal motor state in *Gnal*$^{+/-}$ mice following oxotremorine injection (***Figure 5H***). To confirm these observations, we also evaluated the activity of mice by measuring the percentage of time spent moving in an open field ('active wakefulness') (***Georgescu et al., 2018***). In the saline-treated WT mice, DN optogenetic θ-burst stimulations had no significant effect on the active wake time. Similarly, in the asymptomatic *Gnal*$^{+/-}$ mice, θ-burst stimulations did not significantly change the percentage of time spent in active wake (***Figure 5I***, ***Supplementary file 1j***). In contrast, in the oxotremorine condition, the average active wake time decreased in both WT and *Gnal*$^{+/-}$ mice compared to saline, the effect being more pronounced in the mutant mice (***Figure 5I***). One session of DN optogenetic θ-burst stimulation was sufficient to increase the time

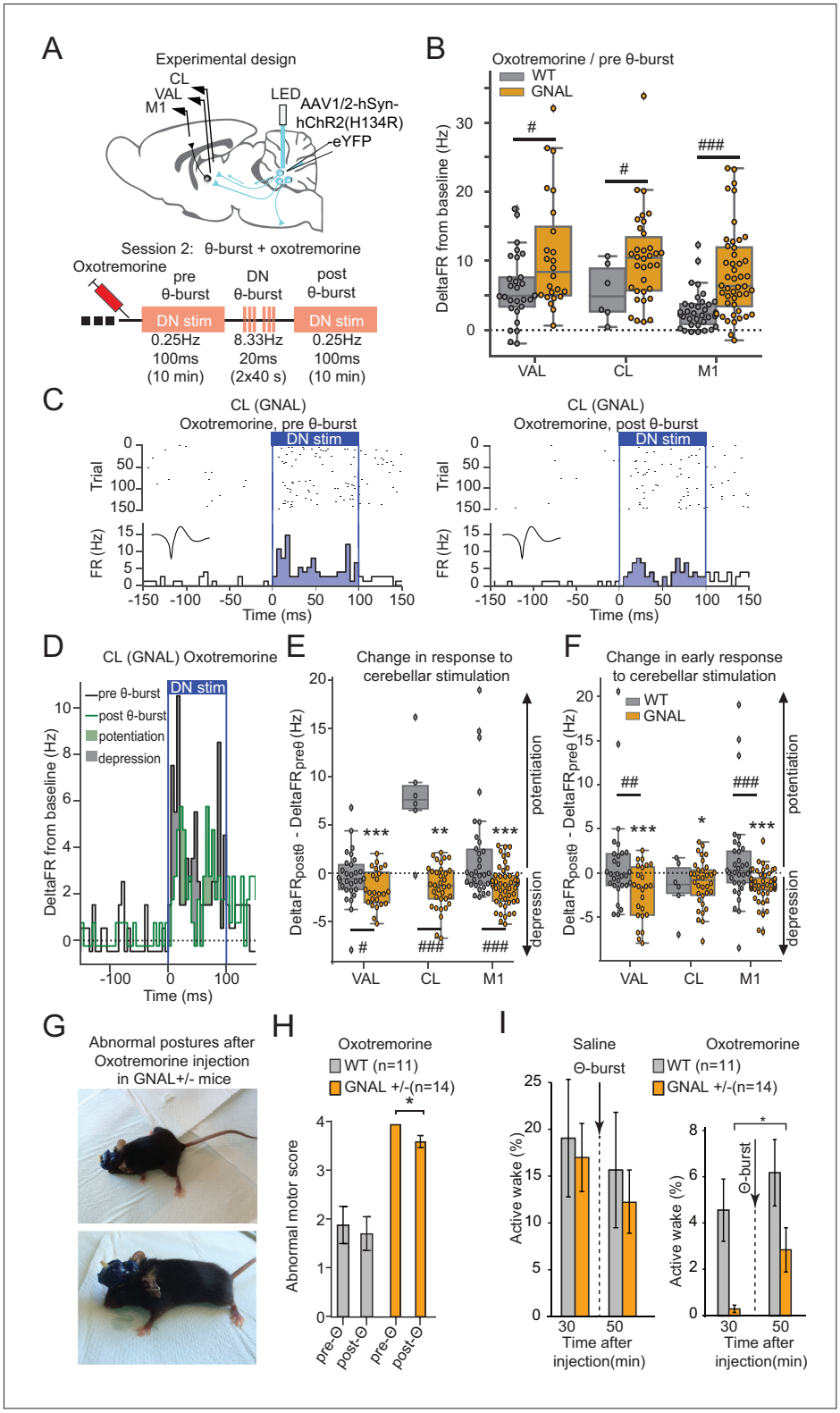

Figure 5. Dentate nucleus (DN) θ -bursts administered to symptomatic *Gnal*$^{+/-}$ mice induce a decreased response to DN stimulation and decrease motor symptoms of dystonia. (**A**) Schematics describing the experimental design of thalamo-cortical recordings coupled with DN stimulation (top) and experimental timeline (bottom). (**B**) Distributions of responses to DN stimulation in oxotremorine condition, before θ -burst. (**C**) Example peristimulus

Figure 5 continued on next page

Figure 5 continued

time histogram (PSTH) and corresponding raster plot, centered on the onset of the cerebellar stimulation of a centrolateral thalamus (CL) neuron from a *Gnal*$^{+/-}$ mouse under oxotremorine condition, before θ -burst (left) and after θ -burst (right). Inset represents the average waveform of the neuron. (**D**) Overlay of the PSTHs from panel (**C**); the difference between the histograms is filled to highlight the potentiation or depression of the responses. (**E**) Impact of θ -burst stimulations administered in oxotremorine condition on the response to +/-ms DN stimulation. (**F**) Impact of θ -burst stimulations administered in oxotremorine condition on the afferent volley in response to 100 ms DN stimulation. Wilcoxon test for paired samples *p<0.05, **p<0.01, ***p<0.001; Mann–Whitney test for independent samples #p<0.05, ##p<0.01, ###p<0.001 difference between genotypes. (**G**) Examples of dystonic postures in *Gnal*$^{+/-}$ mice following oxotremorine administration. (**H**) Average dystonia scores in *Gnal*$^{+/-}$ and wildtype (WT) mice following oxotremorine administration before and after DN θ -burst stimulations. (**I**) Change of average active wake percentage after one session of DN θ -burst stimulations in *Gnal*$^{+/-}$ and WT mice. Wilcoxon test *p<0.05 difference between pre- and post- θ -burst stimulations.

spent in active wake in *Gnal*$^{+/-}$ mice (***Figure 5I***, ***Supplementary file 1j***). Overall, these results indicate that DN optogenetic θ-burst stimulations decrease the dystonic phenotype in symptomatic *Gnal*$^{+/-}$ mice regarding both the abnormal motor scores and active wake deficit.

Discussion

Our results show that young adult *Gnal*$^{+/-}$ mice in the presymptomatic state, that is, without overt motor impairment, already exhibit altered cerebello-thalamic functional connectivity. After the first dystonic episode triggered by a cholinergic agonist, mutant animals, once returned to an asymptomatic state, exhibit further functional alterations of the cerebello-thalamic pathways, with a marked increase in cerebello-thalamic excitability and loss of potentiation of these functional connections by cerebellar θ-burst stimulations, which are also reflected downstream in the motor cortex and striatum. Finally, cerebellar θ-burst stimulations in the symptomatic state induce a functional depression of the cerebello-thalamic pathway absent from control mice, and this effect is accompanied by a reduction of the motor symptoms. This shows that in *Gnal*$^{+/-}$ mice before the first dystonia episode the cerebello-thalamic tract exhibits an increased excitability that is amplified after the first episode and can thus be seen as a functional endophenotype. Indeed, the plasticity induced in this pathway via cerebellar stimulations reducing the cerebello-thalamic excitability exerts an effective therapeutic potential.

DYT25 penetrance and dystonia endophenotypes

Mutations in *Gnal* (DYT25) were first identified in 2012 (***Fuchs et al., 2013***) as a cause of primary torsion dystonia. DYT25 is known to be an adult-onset dystonia, with an age at onset ranging from 7 to 63 years (average of about 30 years), and, although the onset occurs mainly in the neck (about 80%), dystonia can affect various body parts, with generalization in 10% of the cases (***Fuchs et al., 2013***; ***Miao et al., 2013***; ***Vemula et al., 2013***; ***Dufke et al., 2014***; ***Kumar et al., 2014***; ***Ziegan et al., 2014***; ***Saunders-Pullman et al., 2014***; ***Carecchio et al., 2016***; ***Dos Santos et al., 2016***). Interestingly, the immunohistochemistry study in rats of Gα(olf), the protein encoded by *Gnal*, reveals labeling in the olfactory bulb, striatum, substantia nigra, and cerebellar cortex (***Vemula et al., 2013***). In the striatum, Gα(olf) is closely associated with the G protein subunits, Gγ7 and Gβ2, and the type 5 adenylyl cyclase (AC5) to form a multi-molecular complex critical for cAMP production (***Hervé, 2011***; ***Xie et al., 2015***) and mutations of Gγ7 and AC5 cause motor disorders, including dystonia, in animals and humans. Homozygous Gγ7 knockout mice, which have a severe impairment of Gα(olf) signaling in the striatum, display age-dependent dystonia (***Sasaki et al., 2013***). In addition, loss-of-function mutations of ADCY5, the human gene encoding AC5, are responsible for chorea with dystonia (***Carapito et al., 2015***), whereas gain-of-function mutations cause dyskinesia with facial myokymia (***Chen et al., 2015***). Thus, the disruption of the striatal transduction pathway involving Gα(olf) likely plays a central role in the development of dystonia.

In the mouse striatum, expression of Gα(olf) highly increases between postnatal day 7 (P7) and P14 (***Iwamoto et al., 2004***), a period during which motor skills of pups are developing intensely. Moreover, while juvenile rats (P14) displayed intense staining in cell bodies of striatal cholinergic neurons and medium spiny neurons, adult rats displayed a more diffused staining in the striatum, with a weaker staining in cholinergic neurons. Similarly, juvenile rats displayed a staining of the soma and dendrites

of Purkinje cells, while it was restricted to their soma in adult rats. These shifts in expression suggest that Gα(olf) plays a role in shaping neuronal networks and that the mutation of *Gnal* may cause an abnormal neuronal circuit development. DYT25 is inherited in an autosomal-dominant manner, but the penetrance of the disease is only partial (**Fuchs et al., 2013**; **Vemula et al., 2013**), and the higher penetrance and earlier childhood onset in carriers of the homozygous mutation (**Masuho et al., 2016**) is consistent with a contribution of *Gnal* to the maturation of the motor system.

While old (>1 year) *Gnal*$^{+/-}$ adult mice exhibit motor impairments and occasional dystonic-like posture (**Pelosi et al., 2017**), our results in young adult *Gnal*$^{+/-}$ mice failed to evidence motor deficits either in simple activities (locomotion and strength test) or in skilled movements (vertical rod, bar test, rotarod). They indeed provide a model of the presymptomatic stage of dystonia. Identifying presymptomatic alterations may provide insights into the mechanism by which the network activity will shift toward the pathological state (mediational endophenotypes), although these alterations may simply be a side effect of the mutation unrelated to the disease (**Hutchinson et al., 2013**). In humans, several physiological markers were proposed as endophenotypes of primary dystonia. The tactile temporal discrimination threshold (TDT) is increased in different types of isolated dystonia, nonmanifesting DYT1-mutation carriers, and unaffected relatives of both familial and sporadic adult-onset dystonia patients, and the somatotopic representation of fingers in the S1 cortex was disorganized on both sides in unilaterally affected dystonic patients (**Meunier et al., 2001**). Inter-hemispheric inhibition, as assessed by dual-site paired-pulse TMS, is reduced in asymptomatic individuals but with a family history of dystonia (**Bäumer et al., 2016**). A critical issue is that these subclinical physiological alterations may not be specific to dystonia: for example, TDT was found abnormal in Parkinson's disease (**Conte et al., 2016**) and psychogenic dystonia (**Morgante et al., 2011**). Some neuroimaging studies also demonstrated a pattern of hypermetabolism of the basal ganglia, cerebellum, and supplementary motor area linked with DYT1 and DYT6 dystonia even in nonmanifesting gene carriers (**Eidelberg et al., 1998**; **Trost et al., 2002**). While cerebello-thalamic fiber tract integrity in these dystonias is diversely affected in all gene carriers, nonmanifesting subjects exhibit a combination of rather preserved cerebello-thalamic tract and reduced downstream thalamus-motor cortex tract, suggesting that symptom manifestation due to disrupted cerebello-thalamic communication may be prevented by reduced thalamo-cortical interactions, as seen in nonmanifesting carriers (**Argyelan et al., 2009**). Although our data did not reveal significant increases in neuronal activity in naive *Gnal*$^{+/-}$ mice that would compare to the hypermetabolism found in DYT1 or DYT6 patients, we found an anomalously high responsiveness of thalamus VAL neurons to cerebellar stimulations; since we found no difference in DN responsiveness to optogenetic modulations between genotypes, it is likely that this difference results at least in part from an increased synaptic transmission or postsynaptic excitability. The origin of this alteration is unclear but could result from structural defects or homeostatic regulations (i.e., compensatory mechanisms) of the cerebello-thalamic pathway.

Cerebello-thalamic network after dystonia induction in *Gnal*$^{+/-}$ mice

Oxotremorine injections affected both control and *Gnal*$^{+/-}$ mice, but induced dystonic postures in the mutant mice. While these injections induced an overall decrease in firing rate in the DN, VAL, and M1 in both genotypes, the reduction in firing rate in the CL was only visible in mutant mice. Since only *Gnal*$^{+/-}$ mice expressed a strong dystonic phenotype, an oxotremorine-induced reduction of firing may correspond to a rather nonspecific effect of the cholinergic stimulation in the DN, VAL, and M1 while the specific change in the CL of *Gnal*$^{+/-}$ most likely reflects abnormal activity in the thalamo-striatal pathway in relation with dystonic symptoms. We did not observe a difference between genotypes in the reduction of discharge or irregularity of DN neurons under oxotremorine in *Gnal*$^{+/-}$ mice, nor a decreased excitability to optogenetic stimulations. This contrasts with the observations from murine models of DYT1, DYT12, DYT6 dystonia or from dystonic *dt* rats, where increased irregularity of neuronal discharge is observed in the cerebellar nuclei (**LeDoux and Lorden, 1998**; **Chen et al., 2014**; **Fremont et al., 2014**; **Fremont et al., 2017**; **van der Heijden et al., 2021**), as also seen in dystonia caused by cerebellar infusion with kainate (e.g., **Pizoli et al., 2002**). This increased discharge irregularity could therefore be a landmark of dystonia with a primary cerebellar contribution (**LeDoux et al., 1993**; **Fremont et al., 2017**). In contrast to these rodent models, dystonia in *Gnal*$^{+/-}$ mice might mainly result from the action of oxotremorine in the striatum of *Gnal*$^{+/-}$ mice (**Pelosi et al., 2017**) and hence exhibit less fewer abnormalities in the cerebellar nuclei discharge.

The first dystonia episode in *Gnal*$^{+/-}$ mice was followed by strong and lasting increases in cerebello-thalamic excitability and stronger responses to DN stimulations in the motor cortex in the asymptomatic state. Such direct assessment of the cerebello-thalamic functional connectivity cannot be performed in patients. However, integrated measures of connectivity such as cerebellar brain inhibition (CBI, ***Ugawa et al., 1995***), which measures – by subtraction – the tonic excitatory effect exerted by the cerebellar nuclei over the motor cortex, or the covariance of metabolic activity in the brain motor circuits, which reflects inter-regional functional connectivity, have been performed in several cohorts of dystonic patients (for the most part focal hand or cervical dystonia). These studies rather point toward a reduction of the entrainment of the cerebellum over downstream regions (***Brighina et al., 2009***; ***Koch et al., 2014***; ***Filip et al., 2017***; ***DeSimone et al., 2019***; ***Porcacchia et al., 2019***; ***Panyakaew et al., 2020***; but see ***Kita et al., 2021***). So far, the significance of these alterations is unclear: while a reduction of CBI was found in focal hand dystonia, it was either reduced or normal in cervical dystonia (***Brighina et al., 2009***; ***Koch et al., 2014***; ***Porcacchia et al., 2019***). In a rodent model of DYT12 dystonia, the cerebello-thalamic tract propagates pathological activities toward the striatum (***Chen et al., 2014***), suggesting that a decreased cerebello-thalamic functionality could exert a protective effect. Abnormal involvement of the cerebellum in the motor circuits has also been linked to the presence of tremor in dystonia (***DeSimone et al., 2019***), for which accumulating evidence correlates this feature with cerebellar dysfunction (***Antelmi et al., 2017***; ***Martino et al., 2020***). Indeed, dynamic causal modeling of brain activity from patients with dystonic tremor suggests a central contribution of the cerebellum and cerebello-thalamic pathway in this form of tremor (***Nieuwhof et al., 2022***). Overall, the functional state of cerebello-thalamic pathway may thus depend on the type of dystonia. Our results suggest that in a type of dystonia with a primary striatal dysfunction (***Pelosi et al., 2017***) the hyperexcitability of the cerebello-thalamic tract could reveal an increased susceptibility to dystonia, already present in presymptomatic *Gnal*$^{+/-}$ mice and further potentiated after the first dystonic episode; a decrease in functional connectivity could however correspond to a long-term adaptation of the cerebello-forebrain pathways, which did not take place in the timescale of our experiments.

Effects of θ-burst stimulations in *Gnal*$^{+/-}$ mice

Our results showed a differential sensitivity of the ascending cerebello-thalamic pathways to θ-burst stimulations of the DN in *Gnal*$^{+/-}$ and WT mice. In WT mice, these stimulations induce a lasting potentiation of responses in the downstream structures. They do not affect the response in the DN, indicating that their effect occurs downstream either as an increase in thalamic excitability or as a potentiation of cerebello-thalamic synapses (***Aumann et al., 2000***). In contrast, in *Gnal*$^{+/-}$ mice, the θ-burst stimulations failed to evoke a potentiation in saline condition. Since in these experiments the effect of DN stimulations on downstream structures has already been potentiated following the first dystonic episode, the failure to potentiate the responses to DN in the asymptomatic state could result from a saturation of the potentiation. In contrast, θ-burst stimulations administered in the presence of oxotremorine were followed by a depression of the cerebello-thalamic responses only in *Gnal*$^{+/-}$ mice, consistent with an abnormal cerebello-thalamic state or sensitivity to the cholinergic excitation.

Impaired plasticity is a landmark feature at cortico-striatal synapses in hyperkinetic disorders (***Calabresi et al., 2016***) and also found for cortical plasticity in transcranial experiments in focal dystonia patients (***Quartarone et al., 2005***). So far, the effect of the cerebellum on plasticity at the level of the thalamus, cortex, or striatum in dystonia is not well understood. In healthy subjects, cerebellar transcranial θ-burst protocols alter the cerebral cortex responsiveness, intra-cortical inhibition, and propensity to develop sensorimotor plasticity in the cortex (***Koch et al., 2008***; ***Popa et al., 2010***; ***Popa et al., 2013***); these protocols generally fail, in focal dystonia, to restore the influence of the cerebellum on the cerebral cortex (***Hubsch et al., 2013***; ***Koch et al., 2014***; ***Bologna et al., 2016***; ***Bradnam et al., 2016***; ***Porcacchia et al., 2019***). Transcranial cerebellar stimulations are thought to recruit Purkinje cells and thus affect the cerebellar nuclei, but the site where these transcranial protocols elicit plastic changes is not established. Interestingly, daily sessions of θ-burst protocols have been found to mildly improve the condition of dystonic patients (***Koch et al., 2014***; ***Bradnam et al., 2016***). Alternatively, deep brain (high frequency) stimulations in patients indicate an improvement of dystonia, and notably tremor, when performed in the cerebello-thalamic pathway (***Cury et al., 2017***; ***Coenen et al., 2020***). Stimulating the cerebellar nuclei has also been proven beneficial in

the treatment of secondary dystonia associated with palsy (**Sokal et al., 2015**). In all these studies, as in our experiments, the size effects of the treatment remained modest, but their impact on the life quality of patients may be noteworthy (e.g., **Bradnam et al., 2016**). Finally, repeated sessions of θ-burst stimulation might potentiate the effect (**Meunier et al., 2015**). In light of our results and consistent with the 'protective' effect of depressed cerebello-thalamo-cortical connections (**Argyelan et al., 2009**), the depression of the cerebello-thalamic pathway could thus be a mechanism by which cerebellar manipulations improve the condition of patients.

Gnal$^{+/-}$ mice display an abnormal striatal plasticity

We observed short-latency responses in the DLS following stimulations of CL-projecting DN neurons, consistent with the disynaptic cerebello-striatal connection (**Bostan et al., 2013**) primarily relayed through the intralaminar thalamus (**Ichinohe et al., 2000**; **Chen et al., 2014**; **Gornati et al., 2018**) and targeting both interneurons and medium spiny neurons (**Xiao et al., 2018**). Additionally, we found that DN θ-stimulations induce a potentiation of the response of fast-spiking striatal neurons in control mice. This potentiation could result from the potentiation at the level of the CL; however, CL striatal afferents have been shown to be less prone to synaptic plasticity in medium spiny striatal neurons (**Ellender et al., 2013**), so the difference of effect of DN θ-burst between slow- and fast-spiking could also result to the recruitment of synaptic plasticity at the striatal level. In contrast to control mice, θ-burst stimulations did not induce cerebello-thalamo-striatal plasticity in asymptomatic *Gnal*$^{+/-}$ mice.

Defects in striatal plasticity have been found in murine models of primary dystonia DYT25 and DYT1: cortico-striatal synapses in DYT1 mice could undergo LTP but not LTD, and a previously-potentiated synapse could not be depotentiated (**Maltese et al., 2014**). Similarly, a loss of cortico-striatal LTD was observed in a DYT25 rat model. This loss of LTD could be rescued by blocking adenosine A2A receptors (**Yu-Taeger et al., 2020**) or by negatively modulating mGluR5 receptors (**Martella et al., 2021**). Interestingly, the striatal inputs from the CL have been shown to shift the cortico-striatal plasticity in favor of LTP (**Chen et al., 2014**); therefore, the increased excitability of the DN-CL pathway after the first dystonic episode could participate to maintain potentiated cortico-striatal synapses. However, the cortico-striatal plasticity is controlled by many parameters, including notably the striatal acetylcholine (**Deffains and Bergman, 2015**), which is altered in dystonia. Further work clarifying the control of cortico-striatal plasticity by thalamic inputs (**Mendes et al., 2020**) is needed to understand how the cerebello-thalamo-striatal projections contribute to the impairments of cortico-striatal plasticity in dystonia.

In conclusion, our study investigates an original dystonia model that mimics the genetic alterations discovered in patients suffering from the recently identified DYT25 dystonia and demonstrates the benefits of a model with a pharmacological switch between presymptomatic, symptomatic, and asymptomatic states. Although the striatum is likely the primary origin of functional alterations (**Pelosi et al., 2017**), our study reveals the presence of early abnormalities in cerebello-thalamic pathways in *Gnal*$^{+/-}$ mice and thus supports the view that dystonia is a motor network disorder. Furthermore, our results suggest that identifying cerebellar stimulation patterns that maximize the depression of the cerebello-thalamic pathway in patients could help improve therapeutic interventions.

Materials and methods

Animals

Experiments were performed in accordance with the guidelines of the European Community Council Directives. *Gnal*$^{+/-}$ mice were mated with C57BL/6J mice in order to obtain male and female *Gnal*$^{+/-}$ and WT littermates. Animals (males and females *Gnal*$^{+/-}$ and WT aged 3–7 months old) were kept at a constant room temperature and humidity on 12 hr light/dark cycle and with ad libitum access to water and food. All the motor control experiments were performed in males and females, and recordings were performed in freely moving mice.

Open-field activity

Mice were placed in a circular arena made of polyvinyl chloride with 38 cm diameter and 15 cm height (Noldus, Netherlands) and video-recorded from above. Each mouse was placed in the open field for 5 min with the experimenter out of its view. The center of gravity of the mice was tracked using an

algorithm programmed in Python 3.5 and the OpenCV 4 library. Each frame obtained from the open field's videos was analyzed according to the following process: open-field area was selected and extracted in order to be transformed into a grayscale image. A binary threshold was then applied to this grayscale image to differentiate the mouse from the white background. To reduce the noise induced by the recording cable or by particles potentially present in the open field, a bilateral filter and a Gaussian blur were sequentially applied since those components are supposed to have a higher spatial frequency compared to the mouse. Finally, the OpenCV implementation of the Canny algorithm was applied to detect the contours of the mouse; the position of the mouse was computed as the mouse's center of mass. The distance traveled by the mouse between two consecutive frames was calculated as the variation of the position of the mouse center point multiplied by a scale factor to allow the conversion from pixel unit to centimeters. The total distance traveled was obtained by summing the previously calculated distances throughout the entire open-field session. The speed was computed as the variation of position of center points on two consecutive frames divided by the time between these frames (the inverse of the number of frames per second). This speed was then averaged by creating sliding windows of 1 s. After each session, fecal boles were removed and the floor was wiped clean with a damp cloth and dried after the passing of each mouse.

Horizontal bar test

Motor coordination and balance were estimated with the horizontal bar test, which consists of a linear horizontal bar extended between two supports (length: 90 cm; diameter: 1.5 cm; height: 40 cm from a padded surface). The mouse is placed on one of the sides of the bar and released when all four paws gripped it. The mouse must cross the bar from one side to the other, and latencies to cross the bar are measured in a single trial session with a 3 min cutoff period.

Vertical pole test

Motor coordination was estimated with the vertical pole test. The vertical pole (51 cm in length and 1.5 cm in diameter) was wrapped with white masking tape to provide a firm grip. Mice were placed heads up near the top of the pole and released when all four paws gripped the pole. The bottom section of the pole was fixated to its home-cage with the bedding present but without littermates. When placed on the pole, animals naturally tilt downward and climb down the length of the pole to reach their home cage. The time taken before going down to the home-cage with all four paws was recorded. A 20 s habituation was performed before placing mice at the top of the pole. The test was given in a single trial session with a 3 min cutoff period.

Gait test

Motor coordination was also evaluated by analyzing gait patterns. Mouse footprints were used to estimate foot opening angles and hind base width, reflecting the extent of muscle loosening. The mice crossed an illuminated alley, 70 cm in length, 8 cm in width, and 16 cm in height, before entering a dark box at the end. Their hind paws were coated with nontoxic, water-soluble ink, and the alley floor was covered with sheets of white paper. To obtain clearly visible footprints, at least three trials were conducted. The footprints were then scanned and examined with the Dvrtk software (Jean-Luc Vonesch, IGBMC). The stride length was measured with hind base width formed by the distance between the right and left hind paws. The footprint pattern generated was scored for five parameters (***Simon et al., 2004***). Step length, the average distance of forward movement between alternate steps, is defined as the distance of travel divided by the number of steps. Sigma, describing the regularity of step length, is defined as the standard variation of all right-right and left-left step distance. Gait width, the average lateral distance between opposite left and right steps, is determined by measuring the perpendicular distance of a given step to a line connecting its opposite preceding and succeeding steps. Alternation coefficient, describing the uniformity of step alternation, is calculated by the mean of the absolute value of 0.5 minus the ratio of right-left distance to right-right step distance for every left-right step pair. Linearity, average change in angle between consecutive right-right steps is calculated by drawing a line perpendicular to direction of travel, starting at first right footprint. After determining angle between this perpendicular line and each subsequent right footprint, differences in angle were estimated between each consecutive step pair, and the average of absolute values of all angles was calculated.

Grid test

The grid test is performed to measure the animal strength. It consists of placing the animal on a grid that tilts from a horizontal position of 0–180°. The time elapsed until the animal drops is recorded. The time limit for this experiment is 30 s. In those cases where the mice climbed up to the top of the grid, a maximum latency of 30 s was applied.

Fixed-speed rotarod

Motor coordination, postural stability, and fatigue were estimated with the rotarod (mouse rotarod, Ugo Basile). The mice were placed on top of the plastic roller facing away from the experimenter's view and tested at constant speeds (5, 10, 15, 20, and 25 rpm). Latencies before falling were measured for up to 3 min in a single trial session.

Surgery

Two surgeries were performed. During the first surgery, AAV2/1.hSyn.ChR2(H134R)-eYFP.WPRE.hGH (700 nl) was injected into the dentate nucleus of cerebellum (DN) of the *Gnal*$^{+/-}$ and WT mice (−6 mm AP, ±2.3 mm ML, −2.4 mm depth from dura). After 3 weeks, implantation surgery was performed. For both surgeries, the mice were anesthetized either with a mixture of ketamine/xylazine or a mixture of isoflurane and O_2 (3% for induction, 1.7% for maintenance). Injections with buprenorphine (0.05 mg/kg, s.c.) were performed to control pain, and core temperature (37°C) was kept with a heating pad. The mice were fixed in a stereotaxic apparatus (David Kopf Instruments, USA). After a local midline lidocaine injection s.c. (2%, 1 ml), a medial incision was performed, exposing the skull. Small craniotomies were drilled above the recording sites and above the optic fiber location (above the virus injection site), and then the electrodes were stereotaxically lowered inside the brain. This procedure allowed us, in one experimental set, to record in the left motor cortex (M1) (AP +2 mm and –2 mm ML from the Bregma, DV = −0.5 mm depth from the dura), ventrolateral thalamus (VAL) (–1.34 mm AP, ML = −1.00 mm, and DV = −3.4 mm depth from the dura), and centrolateral thalamus (CL) (AP at –1.58 mm, ML = −0.8 mm, DV = −3.00 mm depth from the dura). On a second experimental set, we recorded in the left dorsomedial striatum (DLS, −6 mm AP,±2.3 mm ML, −2.4 mm depth from dura) and dentate nucleus of cerebellum (DN, −6 mm AP, ±2.3 mm ML, −2.4 mm depth from dura). The mice were implanted with bundles of extracellular electrodes for each recording site. The ground wire was placed on the surface of cerebellum. Super Bond cement (Dental Adhesive Resin Cement, Sun Medical CO, Japan) was applied on the surface of the skull to strengthen the connection between the bone and the cement. The cannulas and ground wire were then fixed with dental cement (Pi-Ku-Plast HP 36, Bredent GmbH, Germany). The bundles of eight electrodes were made in-house by folding and twisting the nichrome wire with a 0.005-inch diameter (Kanthal RO-800) (***Menardy et al., 2019***). The bundles were placed inside guide cannulas (8–10 mm length and 0.16–0.18 mm inner diameter, Coopers Needle Works Limited, UK) glued (Loctite universal glue) to an electrode interface board (EIB-16; Neuralynx, Bozeman, MT) with one wire for each channel and four channels for each brain region (M1, CL, VAL), extending 0.5 mm below the tube tip. Wires were then fixed to the EIB with gold pins (Neuralynx), and then the EIB was secured in place by dental cement. A gold solution (cyanure-free gold solution, Sifco, France) was used for gold plating, and the impedance of each electrode was set to 200–500 kΩ.

Manipulations of cerebellar output

Because the cerebellar nuclei send projections in the contralateral thalamus that then connects with the M1 (***Teune et al., 2000***), optogenetic stimulations were performed in the contralateral cerebellar DN (left M1 and right DN). Light-induced excitation of the cerebellar-projection neurons was elicited by using an LED driver (Mightex Systems) through optical fibers radiating blue light (470 nm) unilaterally implanted into the deep cerebellar nuclei (light intensity of 1.5 mW/mm^2). Optogenetic stimulations of the DN were either 100 ms, 0.25 Hz, or θ-burst stimulation, 20 ms, 8.33 Hz, applied for 2 × 40 s with a 2 min pause in between and were performed before and after triggering the dystonic attacks by an oxotremorine methiodide (oxotremorine M) intraperitoneal injection.

Electrophysiological recordings

The recordings began after at least 3 days of recovery and were performed on awake freely moving mice using a 16-channel acquisition system with a sampling rate of 25 kHz (Tucker-Davis Technology System 3, Tucker-Davis Technologies, Alachua, FL). We performed 60 min baseline recording in an open field, followed by a 60 min recording after a saline injection. *Gnal*$^{+/-}$ and WT mice were then injected intraperitoneally with oxotremorine methiodide (0.1 mg/kg, Sigma-Aldrich), dissolved in saline (NaCl 0.9 g/l), and recorded another 60 min with the same protocol as for saline. Optogenetic stimuli were applied to the DN at low-frequency stimuli of 100 ms, 1.5 mW/mm^2, and 0.25 Hz. After 48–72 hr, a second session with θ-burst stimulations was performed. The mice were recorded 60 min after the saline injection and then 60 min after the oxotremorine M1 injection using the same protocol as in baseline day except that after 30 min two θ-burst sessions of 40 s each with 2 min pause in between were applied (a total of 600 pulses for each condition). The stimulations induced small twitches but no major motor effect.

Histological verification of the site of optical fiber in DN and verification of the position of the electrodes

The animals were sacrificed with a single dose of pentobarbital (100 mg/kg, i.p.). Electrolytic lesions were performed to check the position of electrodes, mice were perfused with paraformaldehyde, and the brains were removed and kept in paraformaldehyde (4%). After slicing (using a vibratome at 90 µm thickness), all sites of the recordings were verified by superposing the atlas (Allen Brain Atlas) on slices, with the closest anatomical landmarks from our lesions used as reference points. Injections in the CL usually encompassed the neighboring structures (lateral mediodorsal thalamus, medial posterior thalamus), which have little if any projection to the dorsolateral striatum, but touched also the anterior part of the parafascicular thalamus that may contribute in part to the cerebello-thalamo-striatal pathway (***Xiao et al., 2018***).

Behavioral analysis

Video recordings monitored the motor behavior of *Gnal*$^{+/-}$ and WT mice in the open field. Dystonia severity was estimated using a previously published abnormal movement scoring scale (***Jinnah et al., 2000***; ***Calderon et al., 2011***; ***Pelosi et al., 2017***) for every 10-min-long blocks of the recording after the oxotremorine M injection was given. The assessment was blinded for mouse genotype and was done by two members of the team. The scale uses the following scores: 0 = normal motor behavior; 1 = no impairment, but slightly slowed movements; 2 = mild impairment: occasional abnormal postures and movements; ambulation with slow walk; 3 = moderate impairment: frequent abnormal postures and movements with limited ambulation; 4 = severe impairment: sustained abnormal postures without any ambulation or upright position. In addition, the total time of active wakefulness from the total time of recording (active wake percentages, AW%) was assessed for both states, pre- and post-oxotremorine and pre- and post θ-burst stimulation. Active wake was considered as the state when the mouse is exploring the open field by walking in any direction and is expressed as a percentage of the total time of the recording (***Georgescu et al., 2018***). We evaluated the impact of θ-burst DN stimulation on the onset of dystonic-like symptoms in saline- and oxotremorine-treated *Gnal*$^{+/-}$ mice.

Electrophysiological analysis

Spike sorting was completed using homemade MATLAB scripts (MathWorks, Natick, MA) based on *k-means* clustering on PCA of the spike waveforms (***Paz et al., 2006***). In order to evaluate the activity of the same cells in similar conditions during experiments, we investigated the change of the firing rate probability in the thalamus and M1 motor cortex during cerebellar DN 100 ms stimulations after saline or oxotremorine M administration was done and analyses in one continuous session. The average increase in firing rate during the stimulation was determined by computing the peristimulus time histogram (bin: 10 ms) of the spikes around the stimulation; the spike count in the histogram was divided by the duration of the stimulation and the number of stimulations administered to yield a firing rate. The acceleration of discharge due to the stimulation was taken as the average spike count during the stimulation subtracted by the baseline (taken as the 300 ms that preceded the stimulation onset). The response to stimulation was only analyzed in cells where at least one bin during the stimulation was four times larger than the standard deviation of the baseline values. To isolate in the

responses the part corresponding to the direct excitation (in the same neuron for DN recordings, after one synapse in the thalamus, and after two synapses in the cortex and striatum), we also measured the discharge in 10-ms-long windows: 0–10 ms after illumination onset in the DN, 4–14 ms after illumination onset in the thalamus, and 7–17 ms in the cortex.

Statistics

Figures represent the averages ± standard error of the mean (SEM). We used nonparametric tests: Wilcoxon and Mann–Whitney statistics (depending on whether the measures were paired or unpaired). For factorial analysis, we used repeated-measures ANOVA. The statistical values were computed in Python using the modules SciPy (version 1.5.4), statsmodels (version 0.12.2), and scikit_posthocs (version 0.6.1). Boxplots are composed of a box that extends from the first quartile to the third quartile of the data, with a line at the median. The whiskers extend from the box by 1.5× the interquartile range, and data values falling outside the range of the whiskers are represented individually.

Acknowledgements

This work was supported by the Agence Nationale de Recherche to DP and DH (ANR-16-CE37-0003 Amedyst), CL (ANR-17-CE37-0009 Mopla), the Fondation pour la Recherche Médicale (FRM-EQU202103012770), the Labex Memolife, and the Institut National de la Santé et de la Recherche Médicale (France). The authors declare no competing financial interests. The authors are very grateful to Sabine Meunier and Cecile Gallea for the critical reading of the manuscript.

Additional information

Funding

Funder	Grant reference number	Author
Agence Nationale de la Recherche	ANR-16-CE37-0003 Amedyst	Denis Hervé Daniela Popa
Agence Nationale de la Recherche	ANR-17-CE37-0009 Mopla	Clément Léna
Fondation pour la Recherche Médicale	FRM-EQU202103012770	Clément Léna
Agence Nationale de la Recherche	ANR-19-CE37-0007	Daniela Popa
Labex Memolife		Clément Léna Daniela Popa

The funders had no role in study design, data collection and interpretation, or the decision to submit the work for publication.

Author contributions

Hind Baba Aïssa, Elena Laura Georgescu Margarint, Data curation, Formal analysis, Investigation, Writing – original draft; Romain W Sala, Data curation, Formal analysis, Investigation, Methodology, Software, Visualization, Writing – original draft; Jimena Laura Frontera, Investigation; Andrés Pablo Varani, Conceptualization, Data curation, Formal analysis; Fabien Menardy, Data curation; Assunta Pelosi, Resources; Denis Hervé, Funding acquisition, Resources; Clément Léna, Conceptualization, Formal analysis, Funding acquisition, Supervision, Validation, Visualization, Writing – original draft, Writing – review and editing; Daniela Popa, Conceptualization, Funding acquisition, Supervision, Writing – original draft, Writing – review and editing

Author ORCIDs

Denis Hervé http://orcid.org/0000-0003-1376-1522
Clément Léna http://orcid.org/0000-0002-1431-7717
Daniela Popa http://orcid.org/0000-0002-8389-1122

Ethics

Information on Gnal$^{+/-}$ mice are all provided in the Materials and Methods section. Ethics approval: APAFIS #29793-202102121752192 v3 & APAFIS #1334-2015070818367911.

Decision letter and Author response

Decision letter https://doi.org/10.7554/eLife.79135.sa1
Author response https://doi.org/10.7554/eLife.79135.sa2

Additional files

Supplementary files

- Supplementary file 1. Tables of statistical results for all comparisons reported in the text.
- MDAR checklist

Data availability

All data are available on Dryad repository https://doi.org/10.5061/dryad.p5hqbzkr9. The code for electrophysiological analysis is available on GitHub repository https://github.com/teamnbc/GNAL2022/, (copy archived at swh:1:rev:3ee1122cc220f91529a9d011d965e4ef4b72ed52).

The following dataset was generated:

Author(s)	Year	Dataset title	Dataset URL	Database and Identifier
Baba Aïssa H, Sala R, Georgescu Margarint E, Frontera J, Varani A, Menardy F, Pelosi A, Herve D, Léna C, Popa D	2022	Electrophysiological and behavioral analysis of cerebello-cerebral coupling in GNAL+/- mice	https://dx.doi.org/10.5061/dryad.p5hqbzkr9	Dryad Digital Repository, 10.5061/dryad.p5hqbzkr9

References

Albanese A, Bhatia K, Bressman SB, Delong MR, Fahn S, Fung VSC, Hallett M, Jankovic J, Jinnah HA, Klein C, Lang AE, Mink JW, Teller JK. 2013. Phenomenology and classification of dystonia: A consensus update. *Movement Disorders* **28**:863–873. DOI: https://doi.org/10.1002/mds.25475, PMID: 23649720

Antelmi E, Erro R, Rocchi L, Liguori R, Tinazzi M, Di Stasio F, Berardelli A, Rothwell JC, Bhatia KP. 2017. Neurophysiological correlates of abnormal somatosensory temporal discrimination in dystonia. *Movement Disorders* **32**:141–148. DOI: https://doi.org/10.1002/mds.26804, PMID: 27671708

Argyelan M, Carbon M, Niethammer M, Ulug AM, Voss HU, Bressman SB, Dhawan V, Eidelberg D. 2009. Cerebellothalamocortical connectivity regulates penetrance in dystonia. *The Journal of Neuroscience* **29**:9740–9747. DOI: https://doi.org/10.1523/JNEUROSCI.2300-09.2009, PMID: 19657027

Aumann TD, Redman SJ, Horne MK. 2000. Long-term potentiation across rat cerebello-thalamic synapses in vitro. *Neuroscience Letters* **287**:151–155. DOI: https://doi.org/10.1016/s0304-3940(00)01162-9, PMID: 10854734

Balint B, Mencacci NE, Valente EM, Pisani A, Rothwell J, Jankovic J, Vidailhet M, Bhatia KP. 2018. Dystonia. *Nature Reviews. Disease Primers* **4**:25. DOI: https://doi.org/10.1038/s41572-018-0023-6, PMID: 30237473

Bäumer T, Schmidt A, Heldmann M, Landwehr M, Simmer A, Tönniges D, Münte T, Lohmann K, Altenmüller E, Klein C, Münchau A. 2016. Abnormal interhemispheric inhibition in musician's dystonia - Trait or state? *Parkinsonism & Related Disorders* **25**:33–38. DOI: https://doi.org/10.1016/j.parkreldis.2016.02.018, PMID: 26923523

Belluscio L, Gold GH, Nemes A, Axel R. 1998. Mice deficient in G(olf) are anosmic. *Neuron* **20**:69–81. DOI: https://doi.org/10.1016/s0896-6273(00)80435-3, PMID: 9459443

Berardelli A, Rothwell JC, Hallett M, Thompson PD, Manfredi M, Marsden CD. 1998. The pathophysiology of primary dystonia. *Brain: A Journal of Neurology* **121 (Pt 7)**:1195–1212. DOI: https://doi.org/10.1093/brain/121.7.1195, PMID: 9679773

Bologna M, Paparella G, Fabbrini A, Leodori G, Rocchi L, Hallett M, Berardelli A. 2016. Effects of cerebellar theta-burst stimulation on arm and neck movement kinematics in patients with focal dystonia. *Clinical Neurophysiology* **127**:3472–3479. DOI: https://doi.org/10.1016/j.clinph.2016.09.008, PMID: 27721106

Bostan AC, Strick PL. 2010. The cerebellum and basal ganglia are interconnected. *Neuropsychology Review* **20**:261–270. DOI: https://doi.org/10.1007/s11065-010-9143-9, PMID: 20811947

Bostan AC, Dum RP, Strick PL. 2013. Cerebellar networks with the cerebral cortex and basal ganglia. *Trends in Cognitive Sciences* **17**:241–254. DOI: https://doi.org/10.1016/j.tics.2013.03.003, PMID: 23579055

Bradnam LV, McDonnell MN, Ridding MC. 2016. Cerebellar Intermittent Theta-Burst Stimulation and Motor Control Training in Individuals with Cervical Dystonia. *Brain Sciences* **6**:E56. DOI: https://doi.org/10.3390/brainsci6040056, PMID: 27886079

Brighina F, Romano M, Giglia G, Saia V, Puma A, Giglia F, Fierro B, Romano M, Puma A, Giglia F, Saia V, Giglia G, Saia V, Puma A, Giglia F, Fierro B. 2009. Effects of cerebellar TMS on motor cortex of patients with focal dystonia: A preliminary report. *Experimental Brain Research* **192**:651–656. DOI: https://doi.org/10.1007/s00221-008-1572-9, PMID: 18815775

Calabresi P, Pisani A, Rothwell J, Ghiglieri V, Obeso JA, Picconi B. 2016. Hyperkinetic disorders and loss of synaptic downscaling. *Nature Neuroscience* **19**:868–875. DOI: https://doi.org/10.1038/nn.4306, PMID: 27351172

Calderon DP, Fremont R, Kraenzlin F, Khodakhah K. 2011. The neural substrates of rapid-onset Dystonia-Parkinsonism. *Nature Neuroscience* **14**:357–365. DOI: https://doi.org/10.1038/nn.2753, PMID: 21297628

Carapito R, Paul N, Untrau M, Le Gentil M, Ott L, Alsaleh G, Jochem P, Radosavljevic M, Le Caignec C, David A, Damier P, Isidor B, Bahram S. 2015. A de novo ADCY5 mutation causes early-onset autosomal dominant chorea and dystonia. *Movement Disorders* **30**:423–427. DOI: https://doi.org/10.1002/mds.26115, PMID: 25545163

Carecchio M, Panteghini C, Reale C, Barzaghi C, Monti V, Romito L, Sasanelli F, Garavaglia B. 2016. Novel GNAL mutation with intra-familial clinical heterogeneity: Expanding the phenotype. *Parkinsonism & Related Disorders* **23**:66–71. DOI: https://doi.org/10.1016/j.parkreldis.2015.12.012, PMID: 26725140

Chen CH, Fremont R, Arteaga-Bracho EE, Khodakhah K. 2014. Short latency cerebellar modulation of the basal ganglia. *Nature Neuroscience* **17**:1767–1775. DOI: https://doi.org/10.1038/nn.3868, PMID: 25402853

Chen D-H, Méneret A, Friedman JR, Korvatska O, Gad A, Bonkowski ES, Stessman HA, Doummar D, Mignot C, Anheim M, Bernes S, Davis MY, Damon-Perrière N, Degos B, Grabli D, Gras D, Hisama FM, Mackenzie KM, Swanson PD, Tranchant C, et al. 2015. ADCY5-related dyskinesia: Broader spectrum and genotype-phenotype correlations. *Neurology* **85**:2026–2035. DOI: https://doi.org/10.1212/WNL.0000000000002058, PMID: 26537056

Coenen VA, Sajonz B, Prokop T, Reisert M, Piroth T, Urbach H, Jenkner C, Reinacher PC. 2020. The dentato-rubro-thalamic tract as the potential common deep brain stimulation target for tremor of various origin: an observational case series. *Acta Neurochirurgica* **162**:1053–1066. DOI: https://doi.org/10.1007/s00701-020-04248-2, PMID: 31997069

Conte A, Leodori G, Ferrazzano G, De Bartolo MI, Manzo N, Fabbrini G, Berardelli A. 2016. Somatosensory temporal discrimination threshold in Parkinson's disease parallels disease severity and duration. *Clinical Neurophysiology* **127**:2985–2989. DOI: https://doi.org/10.1016/j.clinph.2016.06.026, PMID: 27458837

Corvol JC, Studler JM, Schonn JS, Girault JA, Hervé D. 2001. Galpha(olf) is necessary for coupling D1 and A2a receptors to adenylyl cyclase in the striatum. *Journal of Neurochemistry* **76**:1585–1588. DOI: https://doi.org/10.1046/j.1471-4159.2001.00201.x, PMID: 11238742

Corvol J-C, Valjent E, Pascoli V, Robin A, Stipanovich A, Luedtke RR, Belluscio L, Girault J-A, Hervé D. 2007. Quantitative changes in Galphaolf protein levels, but not D1 receptor, alter specifically acute responses to psychostimulants. *Neuropsychopharmacology* **32**:1109–1121. DOI: https://doi.org/10.1038/sj.npp.1301230, PMID: 17063155

Cury RG, Fraix V, Castrioto A, Pérez Fernández MA, Krack P, Chabardes S, Seigneuret E, Alho EJL, Benabid A-L, Moro E. 2017. Thalamic deep brain stimulation for tremor in Parkinson disease, essential tremor, and dystonia. *Neurology* **89**:1416–1423. DOI: https://doi.org/10.1212/WNL.0000000000004295, PMID: 28768840

Deffains M, Bergman H. 2015. Striatal cholinergic interneurons and cortico-striatal synaptic plasticity in health and disease. *Movement Disorders* **30**:1014–1025. DOI: https://doi.org/10.1002/mds.26300, PMID: 26095280

DeSimone JC, Archer DB, Vaillancourt DE, Wagle Shukla A. 2019. Network-level connectivity is a critical feature distinguishing dystonic tremor and essential tremor. *Brain* **142**:1644–1659. DOI: https://doi.org/10.1093/brain/awz085, PMID: 30957839

Dos Santos CO, Masuho I, da Silva-Júnior FP, Barbosa ER, Silva SMCA, Borges V, Ferraz HB, Rocha MSG, Limongi JCP, Martemyanov KA, de Carvalho Aguiar P. 2016. Screening of GNAL variants in Brazilian patients with isolated dystonia reveals a novel mutation with partial loss of function. *Journal of Neurology* **263**:665–668. DOI: https://doi.org/10.1007/s00415-016-8026-2, PMID: 26810727

Dufke C, Sturm M, Schroeder C, Moll S, Ott T, Riess O, Bauer P, Grundmann K. 2014. Screening of mutations in GNAL in sporadic dystonia patients. *Movement Disorders* **29**:1193–1196. DOI: https://doi.org/10.1002/mds.25794, PMID: 24408567

Eidelberg D, Moeller JR, Antonini A, Kazumata K, Nakamura T, Dhawan V, Spetsieris P, deLeon D, Bressman SB, Fahn S. 1998. Functional brain networks in DYT1 dystonia. *Annals of Neurology* **44**:303–312. DOI: https://doi.org/10.1002/ana.410440304, PMID: 9749595

Ellender TJ, Harwood J, Kosillo P, Capogna M, Bolam JP. 2013. Heterogeneous properties of central lateral and parafascicular thalamic synapses in the striatum. *The Journal of Physiology* **591**:257–272. DOI: https://doi.org/10.1113/jphysiol.2012.245233, PMID: 23109111

Filip P, Gallea C, Lehéricy S, Bertasi E, Popa T, Mareček R, Lungu OV, Kašpárek T, Vaníček J, Bareš M. 2017. Disruption in cerebellar and basal ganglia networks during a visuospatial task in cervical dystonia. *Movement Disorders* **32**:757–768. DOI: https://doi.org/10.1002/mds.26930, PMID: 28186664

Fremont R, Calderon DP, Maleki S, Khodakhah K. 2014. Abnormal high-frequency burst firing of cerebellar neurons in rapid-onset dystonia-parkinsonism. *The Journal of Neuroscience* **34**:11723–11732. DOI: https://doi.org/10.1523/JNEUROSCI.1409-14.2014, PMID: 25164667

Fremont R, Tewari A, Angueyra C, Khodakhah K. 2017. A role for cerebellum in the hereditary dystonia DYT1. *eLife* **6**:e22775. DOI: https://doi.org/10.7554/eLife.22775, PMID: 28198698

Fuchs T, Saunders-Pullman R, Masuho I, Luciano MS, Raymond D, Factor S, Lang AE, Liang TW, Trosch RM, White S, Ainehsazan E, Hervé D, Sharma N, Ehrlich ME, Martemyanov KA, Bressman SB, Ozelius LJ. 2013. Mutations in GNAL cause primary torsion dystonia. *Nature Genetics* **45**:88–92. DOI: https://doi.org/10.1038/ng.2496, PMID: 23222958

Georgescu EL, Georgescu IA, Zahiu CDM, Şteopoaie AR, Morozan VP, Pană AŞ, Zăgrean A-M, Popa D. 2018. Oscillatory Cortical Activity in an Animal Model of Dystonia Caused by Cerebellar Dysfunction. *Frontiers in Cellular Neuroscience* **12**:1–23. DOI: https://doi.org/10.3389/fncel.2018.00390, PMID: 30459559

Gornati SV, Schäfer CB, Eelkman Rooda OHJ, Nigg AL, De Zeeuw CI, Hoebeek FE. 2018. Differentiating Cerebellar Impact on Thalamic Nuclei. *Cell Reports* **23**:2690–2704. DOI: https://doi.org/10.1016/j.celrep.2018.04.098, PMID: 29847799

Her ES, Huh N, Kim J, Jung MW. 2016. Neuronal activity in dorsomedial and dorsolateral striatum under the requirement for temporal credit assignment. *Scientific Reports* **6**:27056. DOI: https://doi.org/10.1038/srep27056, PMID: 27245401

Hervé D, Le Moine C, Corvol JC, Belluscio L, Ledent C, Fienberg AA, Jaber M, Studler JM, Girault JA. 2001. Galpha(olf) levels are regulated by receptor usage and control dopamine and adenosine action in the striatum. *The Journal of Neuroscience* **21**:4390–4399 PMID: 11404425.,

Hervé D. 2011. Identification of a specific assembly of the G protein golf as a critical and regulated module of dopamine and adenosine-activated cAMP pathways in the striatum. *Frontiers in Neuroanatomy* **5**:48. DOI: https://doi.org/10.3389/fnana.2011.00048, PMID: 21886607

Hubsch C, Roze E, Popa T, Russo M, Balachandran A, Pradeep S, Mueller F, Brochard V, Quartarone A, Degos B, Vidailhet M, Kishore A, Meunier S. 2013. Defective cerebellar control of cortical plasticity in writer's cramp. *Brain* **136**:2050–2062. DOI: https://doi.org/10.1093/brain/awt147, PMID: 23801734

Hutchinson M, Kimmich O, Molloy A, Whelan R, Molloy F, Lynch T, Healy DG, Walsh C, Edwards MJ, Ozelius L, Reilly RB, O'Riordan S. 2013. The endophenotype and the phenotype: temporal discrimination and adult-onset dystonia. *Movement Disorders* **28**:1766–1774. DOI: https://doi.org/10.1002/mds.25676, PMID: 24108447

Ichinohe N, Mori F, Shoumura K. 2000. A di-synaptic projection from the lateral cerebellar nucleus to the laterodorsal part of the striatum via the central lateral nucleus of the thalamus in the rat. *Brain Research* **880**:191–197. DOI: https://doi.org/10.1016/s0006-8993(00)02744-x, PMID: 11033006

Iwamoto T, Iwatsubo K, Okumura S, Hashimoto Y, Tsunematsu T, Toya Y, Hervé D, Umemura S, Ishikawa Y. 2004. Disruption of type 5 adenylyl cyclase negates the developmental increase in Galphaolf expression in the striatum. *FEBS Letters* **564**:153–156. DOI: https://doi.org/10.1016/S0014-5793(04)00333-3, PMID: 15094058

Jinnah HA, Sepkuty JP, Ho T, Yitta S, Drew T, Rothstein JD, Hess EJ. 2000. Calcium channel agonists and dystonia in the mouse. *Movement Disorders* **15**:542–551. DOI: https://doi.org/10.1002/1531-8257(200005)15:3<542::AID-MDS1019>3.0.CO;2-2, PMID: 10830422

Kita K, Furuya S, Osu R, Sakamoto T, Hanakawa T. 2021. Aberrant Cerebello-Cortical Connectivity in Pianists With Focal Task-Specific Dystonia. *Cerebral Cortex* **31**:4853–4863. DOI: https://doi.org/10.1093/cercor/bhab127, PMID: 34013319

Koch G, Mori F, Marconi B, Codecà C, Pecchioli C, Salerno S, Torriero S, Lo Gerfo E, Mir P, Oliveri M, Caltagirone C. 2008. Changes in intracortical circuits of the human motor cortex following theta burst stimulation of the lateral cerebellum. *Clinical Neurophysiology* **119**:2559–2569. DOI: https://doi.org/10.1016/j.clinph.2008.08.008, PMID: 18824403

Koch G, Porcacchia P, Ponzo V, Carrillo F, Cáceres-Redondo MT, Brusa L, Desiato MT, Arciprete F, Di Lorenzo F, Pisani A, Caltagirone C, Palomar FJ, Mir P. 2014. Effects of two weeks of cerebellar theta burst stimulation in cervical dystonia patients. *Brain Stimulation* **7**:564–572. DOI: https://doi.org/10.1016/j.brs.2014.05.002, PMID: 24881805

Kumar KR, Lohmann K, Masuho I, Miyamoto R, Ferbert A, Lohnau T, Kasten M, Hagenah J, Brüggemann N, Graf J, Münchau A, Kostic VS, Sue CM, Domingo AR, Rosales RL, Lee LV, Freimann K, Westenberger A, Mukai Y, Kawarai T, et al. 2014. Mutations in GNAL: A novel cause of craniocervical dystonia. *JAMA Neurology* **71**:490–494. DOI: https://doi.org/10.1001/jamaneurol.2013.4677, PMID: 24535567

LeDoux MS, Lorden JF, Ervin JM. 1993. Cerebellectomy eliminates the motor syndrome of the genetically dystonic rat. *Experimental Neurology* **120**:302–310. DOI: https://doi.org/10.1006/exnr.1993.1064, PMID: 8491286

LeDoux MS, Lorden JF. 1998. Abnormal cerebellar output in the genetically dystonic rat. *Advances in Neurology* **78**:63–78 PMID: 9750904.,

Lehéricy S, Tijssen MAJ, Vidailhet M, Kaji R, Meunier S. 2013. The anatomical basis of dystonia: current view using neuroimaging. *Movement Disorders* **28**:944–957. DOI: https://doi.org/10.1002/mds.25527, PMID: 23893451

Maltese M, Martella G, Madeo G, Fagiolo I, Tassone A, Ponterio G, Sciamanna G, Burbaud P, Conn PJ, Bonsi P, Pisani A. 2014. Anticholinergic drugs rescue synaptic plasticity in DYT1 dystonia: role of M1 muscarinic receptors. *Movement Disorders* **29**:1655–1665. DOI: https://doi.org/10.1002/mds.26009, PMID: 25195914

Martella G, Bonsi P, Imbriani P, Sciamanna G, Nguyen H, Yu-Taeger L, Schneider M, Poli SM, Lütjens R, Pisani A. 2021. Rescue of striatal long-term depression by chronic mGlu5 receptor negative allosteric modulation in distinct dystonia models. *Neuropharmacology* **192**:108608. DOI: https://doi.org/10.1016/j.neuropharm.2021.108608, PMID: 33991565

Martino D, Bonassi G, Lagravinese G, Pelosin E, Abbruzzese G, Avanzino L. 2020. Defective Human Motion Perception in Cervical Dystonia Correlates With Coexisting Tremor. *Movement Disorders* **35**:1067–1071. DOI: https://doi.org/10.1002/mds.28017, PMID: 32199036

Masuho I, Fang M, Geng C, Zhang J, Jiang H, Özgul RK, Yılmaz DY, Yalnızoğlu D, Yüksel D, Yarrow A, Myers A, Burn SC, Crotwell PL, Padilla-Lopez S, Dursun A, Martemyanov KA, Kruer MC. 2016. Homozygous GNAL mutation associated with familial childhood-onset generalized dystonia. *Neurology. Genetics* **2**:e78. DOI: https://doi.org/10.1212/NXG.0000000000000078, PMID: 27222887

Menardy F, Varani AP, Combes A, Léna C, Popa D. 2019. Functional Alteration of Cerebello-Cerebral Coupling in an Experimental Mouse Model of Parkinson's Disease. *Cerebral Cortex* **29**:1752–1766. DOI: https://doi.org/10.1093/cercor/bhy346, PMID: 30715237

Mendes A, Vignoud G, Perez S, Perrin E, Touboul J, Venance L. 2020. Concurrent Thalamostriatal and Corticostriatal Spike-Timing-Dependent Plasticity and Heterosynaptic Interactions Shape Striatal Plasticity Map. *Cerebral Cortex* **30**:4381–4401. DOI: https://doi.org/10.1093/cercor/bhaa024, PMID: 32147733

Meunier S, Garnero L, Ducorps A, Mazières L, Lehéricy S, du Montcel ST, Renault B, Vidailhet M. 2001. Human brain mapping in dystonia reveals both endophenotypic traits and adaptive reorganization. *Annals of Neurology* **50**:521–527. DOI: https://doi.org/10.1002/ana.1234, PMID: 11601503

Meunier S, Popa T, Hubsch C, Roze E, Kishore A. 2015. Reply: A single session of cerebellar theta burst stimulation does not alter writing performance in writer's cramp. *Brain: A Journal of Neurology* **138**:e356. DOI: https://doi.org/10.1093/brain/awu322, PMID: 25395099

Miao J, Wan XH, Sun Y, Feng JC, Cheng FB. 2013. Mutation screening of GNAL gene in patients with primary dystonia from Northeast China. *Parkinsonism & Related Disorders* **19**:910–912. DOI: https://doi.org/10.1016/j.parkreldis.2013.05.011, PMID: 23759320

Morgante F, Tinazzi M, Squintani G, Martino D, Defazio G, Romito L, Albanese A, Di Matteo A, Quartarone A, Girlanda P, Fiorio M, Berardelli A. 2011. Abnormal tactile temporal discrimination in psychogenic dystonia. *Neurology* **77**:1191–1197. DOI: https://doi.org/10.1212/WNL.0b013e31822f0449, PMID: 21900627

Nieuwhof F, Toni I, Dirkx MF, Gallea C, Vidailhet M, Buijink AWG, van Rootselaar AF, van de Warrenburg BPC, Helmich RC. 2022. Cerebello-thalamic activity drives an abnormal motor network into dystonic tremor. *NeuroImage. Clinical* **33**:102919. DOI: https://doi.org/10.1016/j.nicl.2021.102919, PMID: 34929584

Oyama G, Hattori N. 2021. New modalities and directions for dystonia care. *Journal of Neural Transmission* **128**:559–565. DOI: https://doi.org/10.1007/s00702-020-02278-9, PMID: 33389184

Panyakaew P, Cho HJ, Lee SW, Wu T, Hallett M. 2020. The Pathophysiology of Dystonic Tremors and Comparison With Essential Tremor. *The Journal of Neuroscience* **40**:9317–9326. DOI: https://doi.org/10.1523/JNEUROSCI.1181-20.2020, PMID: 33097635

Paz R, Pelletier JG, Bauer EP, Paré D. 2006. Emotional enhancement of memory via amygdala-driven facilitation of rhinal interactions. *Nature Neuroscience* **9**:1321–1329. DOI: https://doi.org/10.1038/nn1771, PMID: 16964249

Pelosi A, Menardy F, Popa D, Girault JA, Hervé D. 2017. Heterozygous Gnal Mice Are a Novel Animal Model with Which to Study Dystonia Pathophysiology. *The Journal of Neuroscience* **37**:6253–6267. DOI: https://doi.org/10.1523/JNEUROSCI.1529-16.2017, PMID: 28546310

Pisani A, Bernardi G, Ding J, Surmeier DJ. 2007. Re-emergence of striatal cholinergic interneurons in movement disorders. *Trends in Neurosciences* **30**:545–553. DOI: https://doi.org/10.1016/j.tins.2007.07.008, PMID: 17904652

Pizoli CE, Jinnah HA, Billingsley ML, Hess EJ. 2002. Abnormal cerebellar signaling induces dystonia in mice. *The Journal of Neuroscience* **22**:7825–7833 PMID: 12196606.,

Popa T, Russo M, Meunier S. 2010. Long-lasting inhibition of cerebellar output. *Brain Stimulation* **3**:161–169. DOI: https://doi.org/10.1016/j.brs.2009.10.001, PMID: 20633445

Popa T, Velayudhan B, Hubsch C, Pradeep S, Roze E, Vidailhet M, Meunier S, Kishore A. 2013. Cerebellar processing of sensory inputs primes motor cortex plasticity. *Cerebral Cortex* **23**:305–314. DOI: https://doi.org/10.1093/cercor/bhs016, PMID: 22351647

Porcacchia P, Álvarez de Toledo P, Rodríguez-Baena A, Martín-Rodríguez JF, Palomar FJ, Vargas-González L, Jesús S, Koch G, Mir P, Chen R. 2019. Abnormal cerebellar connectivity and plasticity in isolated cervical dystonia. *PLOS ONE* **14**:e0211367. DOI: https://doi.org/10.1371/journal.pone.0211367

Prudente CN, Hess EJ, Jinnah HA. 2014. Dystonia as a network disorder: what is the role of the cerebellum? *Neuroscience* **260**:23–35. DOI: https://doi.org/10.1016/j.neuroscience.2013.11.062, PMID: 24333801

Quartarone A, Rizzo V, Bagnato S, Morgante F, Sant'Angelo A, Romano M, Crupi D, Girlanda P, Rothwell JC, Siebner HR. 2005. Homeostatic-like plasticity of the primary motor hand area is impaired in focal hand dystonia. *Brain* **128**:1943–1950. DOI: https://doi.org/10.1093/brain/awh527, PMID: 15872016

Sasaki K, Yamasaki T, Omotuyi IO, Mishina M, Ueda H. 2013. Age-dependent dystonia in striatal Gγ7 deficient mice is reversed by the dopamine D2 receptor agonist pramipexole. *Journal of Neurochemistry* **124**:844–854. DOI: https://doi.org/10.1111/jnc.12149, PMID: 23311775

Saunders-Pullman R, Fuchs T, San Luciano M, Raymond D, Brashear A, Ortega R, Deik A, Ozelius LJ, Bressman SB. 2014. Heterogeneity in primary dystonia: lessons from THAP1, GNAL, and TOR1A in Amish-Mennonites. *Movement Disorders* **29**:812–818. DOI: https://doi.org/10.1002/mds.25818, PMID: 24500857

Simon D, Seznec H, Gansmuller A, Carelle N, Weber P, Metzger D, Rustin P, Koenig M, Puccio H. 2004. Friedreich ataxia mouse models with progressive cerebellar and sensory ataxia reveal autophagic neurodegeneration in dorsal root ganglia. *The Journal of Neuroscience* **24**:1987–1995. DOI: https://doi.org/10.1523/JNEUROSCI.4549-03.2004, PMID: 14985441

Simonyan K. 2018. Neuroimaging Applications in Dystonia. *International Review of Neurobiology* **143**:1–30. DOI: https://doi.org/10.1016/bs.irn.2018.09.007, PMID: 30473192

Sokal P, Rudaś M, Harat M, Szylberg Ł, Zieliński P. 2015. Deep anterior cerebellar stimulation reduces symptoms of secondary dystonia in patients with cerebral palsy treated due to spasticity. *Clinical Neurology and Neurosurgery* **135**:62–68. DOI: https://doi.org/10.1016/j.clineuro.2015.05.017, PMID: 26038278

Teune TM, van der Burg J, van der Moer J, Voogd J, Ruigrok TJ. 2000. Topography of cerebellar nuclear projections to the brain stem in the rat. *Progress in Brain Research* **124**:141–172. DOI: https://doi.org/10.1016/S0079-6123(00)24014-4, PMID: 10943123

Trost M, Carbon M, Edwards C, Ma Y, Raymond D, Mentis MJ, Moeller JR, Bressman SB, Eidelberg D. 2002. Primary dystonia: is abnormal functional brain architecture linked to genotype? *Annals of Neurology* **52**:853–856. DOI: https://doi.org/10.1002/ana.10418, PMID: 12447944

Ugawa Y, Uesaka Y, Terao Y, Hanajima R, Kanazawa I. 1995. Magnetic stimulation over the cerebellum in humans. *Annals of Neurology* **37**:703–713. DOI: https://doi.org/10.1002/ana.410370603, PMID: 7778843

Uluğ AM, Vo A, Argyelan M, Tanabe L, Schiffer WK, Dewey S, Dauer WT, Eidelberg D. 2011. Cerebellothalamocortical pathway abnormalities in torsinA DYT1 knock-in mice. *PNAS* **108**:6638–6643. DOI: https://doi.org/10.1073/pnas.1016445108, PMID: 21464304

van der Heijden ME, Kizek DJ, Perez R, Ruff EK, Ehrlich ME, Sillitoe RV. 2021. Abnormal cerebellar function and tremor in a mouse model for non-manifesting partially penetrant dystonia type 6. *The Journal of Physiology* **599**:2037–2054. DOI: https://doi.org/10.1113/JP280978, PMID: 33369735

Vemula SR, Puschmann A, Xiao J, Zhao Y, Rudzińska M, Frei KP, Truong DD, Wszolek ZK, LeDoux MS. 2013. Role of Gα(olf) in familial and sporadic adult-onset primary dystonia. *Human Molecular Genetics* **22**:2510–2519. DOI: https://doi.org/10.1093/hmg/ddt102, PMID: 23449625

Xiao L, Bornmann C, Hatstatt-Burklé L, Scheiffele P. 2018. Regulation of striatal cells and goal-directed behavior by cerebellar outputs. *Nature Communications* **9**:3133. DOI: https://doi.org/10.1038/s41467-018-05565-y, PMID: 30087345

Xie K, Masuho I, Dessauer CW, Xie K, Lai CWJ, Xu B, Martemyanov KA, P-l H, Ueda H, Sasaki K, Ehrlich ME, Cao Y, Willardson BM. 2015. Stable G protein-effector complexes in striatal neurons: mechanism of assembly and role in neurotransmitter signaling. *eLife* **4**:e10451. DOI: https://doi.org/10.7554/eLife.10451

Yu-Taeger L, Ott T, Bonsi P, Tomczak C, Wassouf Z, Martella G, Sciamanna G, Imbriani P, Ponterio G, Tassone A, Schulze-Hentrich JM, Goodchild R, Riess O, Pisani A, Grundmann-Hauser K, Nguyen HP. 2020. Impaired dopamine- and adenosine-mediated signaling and plasticity in a novel rodent model for DYT25 dystonia. *Neurobiology of Disease* **134**:104634. DOI: https://doi.org/10.1016/j.nbd.2019.104634, PMID: 31678405

Zhuang X, Belluscio L, Hen R. 2000. G(OLF)alpha mediates dopamine D1 receptor signaling. *The Journal of Neuroscience* **20**:RC91. DOI: https://doi.org/10.1523/JNEUROSCI.20-16-j0001.2000, PMID: 10924528

Ziegan J, Wittstock M, Westenberger A, Dobričić V, Wolters A, Benecke R, Klein C, Kamm C. 2014. Novel GNAL mutations in two German patients with sporadic dystonia. *Movement Disorders* **29**:1833–1834. DOI: https://doi.org/10.1002/mds.26066, PMID: 25382112

RESEARCH ARTICLE

Figures and figure supplements

Functional abnormalities in the cerebello-thalamic pathways in a mouse model of DYT25 dystonia

Hind Baba Aïssa *et al*

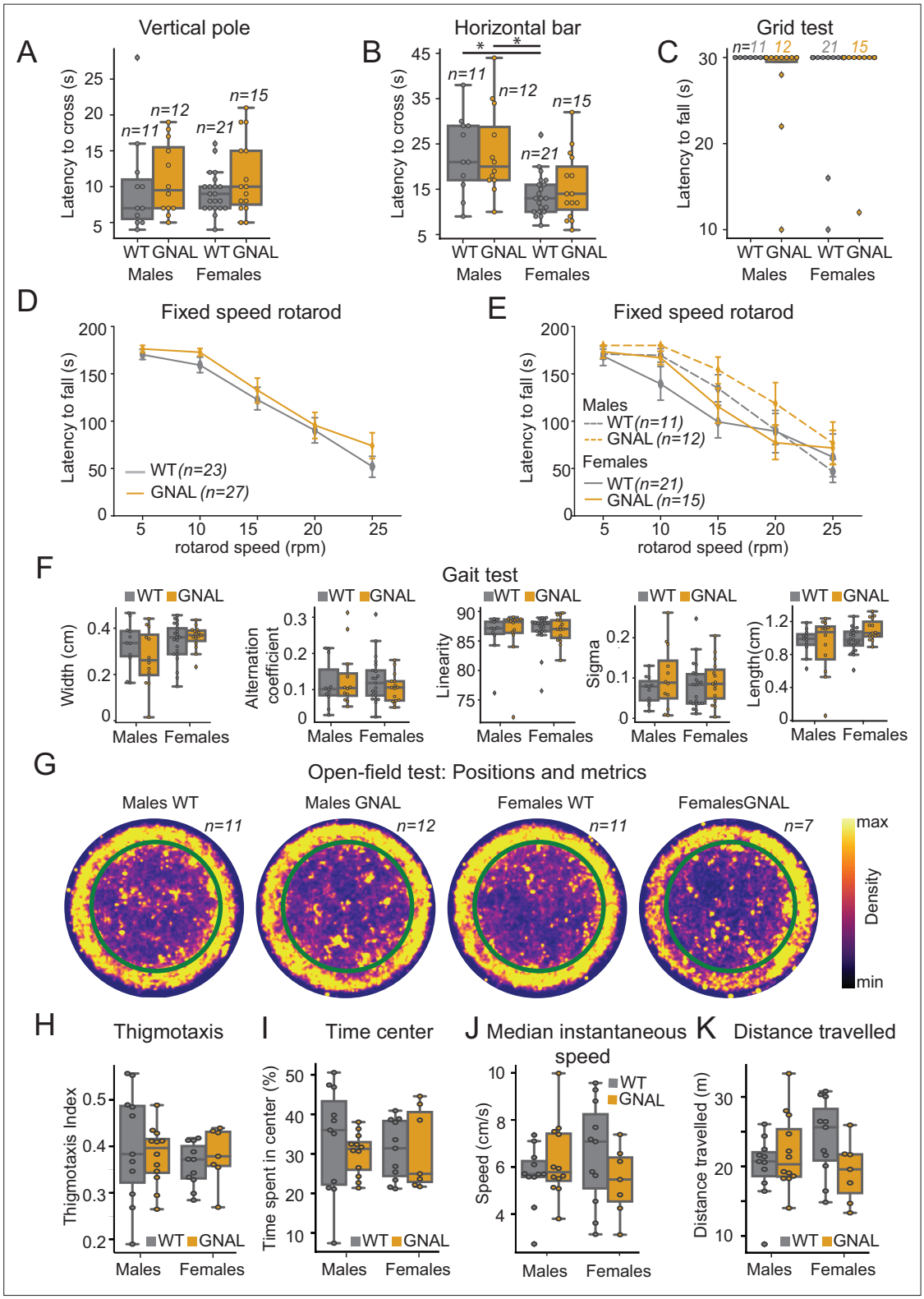

Figure 1. Young male and female *Gnal*$^{+/-}$ mice do not display motor coordination impairments. (**A**) Latency to climb down the vertical pole in male and female *Gnal*$^{+/-}$ (GNAL) and wildtype (WT) mice. (**B**) Latency to cross the horizontal bar. (**C**) Latency to fall during the grid test (30 s cutoff). (**D**) Latency to fall during the fixed-speed rotarod test separated by genotype, and (**E**) by gender and genotype. (**F**) Gait width, alternation coefficient, movement linearity, sigma, and stride length during the gait test. (**G**) Two-dimensional histograms showing the density of position of mice during open-field

Figure 1 continued on next page

Figure 1 continued

sessions, separated by gender and genotype. Thigmotaxis index (**H**), percentage of time spent in center (**I**), median instantaneous speed (**J**), and total distance traveled (**K**) during the open-field test. Reported statistics are the comparison of groups separated by gender and genotype using a Kruskal–Wallis test, followed by a Dunn's post-hoc test corrected using Holm–Sidak method. *p<0.05.

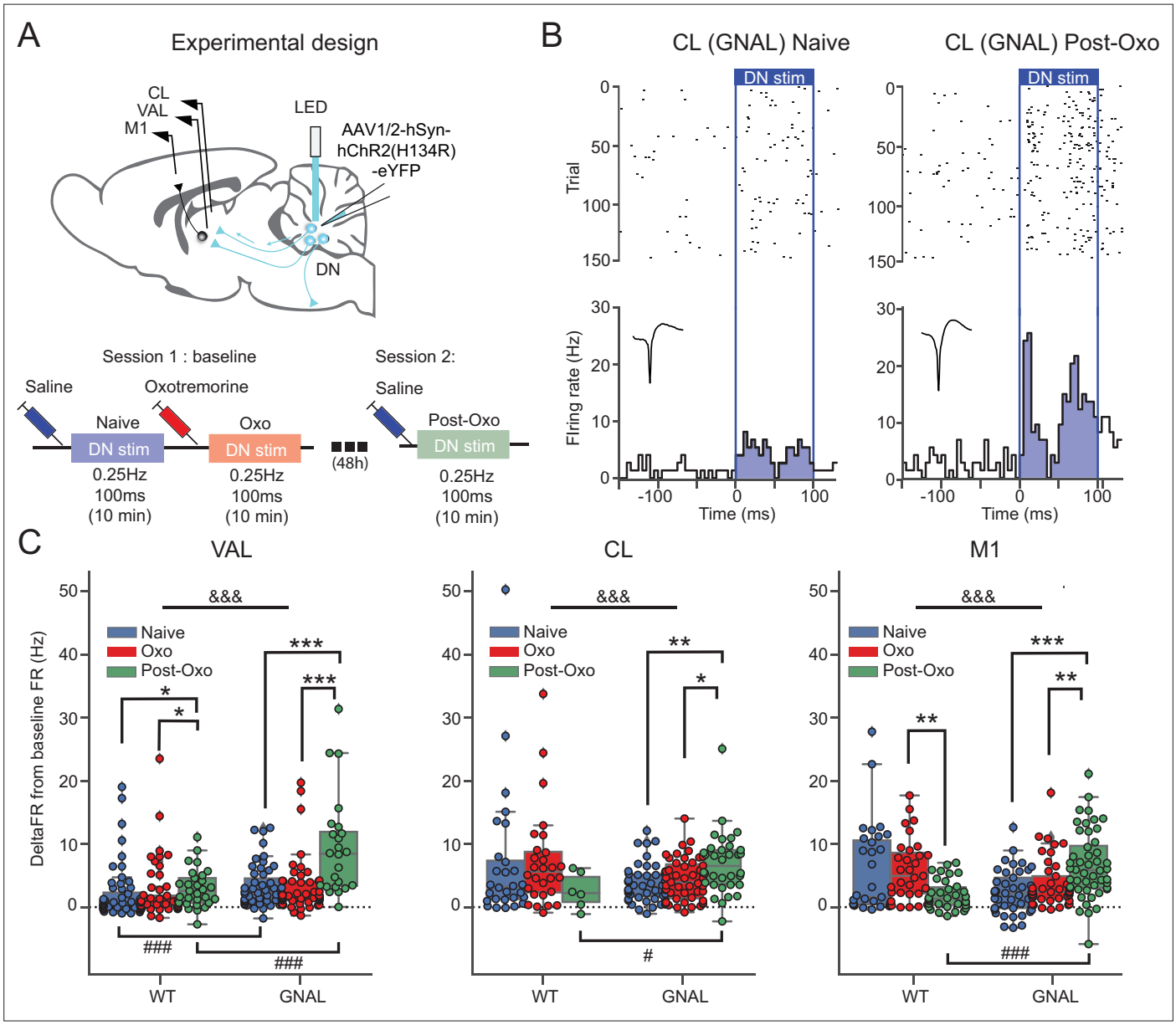

Figure 2. Exposure to oxotremorine causes a long-lasting increase in thalamic and cortical response to dentate nucleus (DN) stimulation in *Gnal*$^{+/-}$ mice. (**A**) Schematics describing the experimental design of thalamo-cortical recordings coupled with DN stimulation (top) and experimental timeline (bottom). (**B**) Examples of peristimulus time histogram (PSTH) and corresponding raster plot, centered on the onset of the cerebellar stimulation, of centrolateral thalamus (CL) neurons from the same recording site in a *Gnal*$^{+/-}$ mouse under saline condition, before being exposed to oxotremorine ('naive,' left) and 48–72 hr after being exposed to oxotremorine ('Post-Oxo,' right). Inset represents the average waveforms of the recorded neuron. (**C**) Distributions of responses to DN stimulations in naive condition (blue), under the acute effect of oxotremorine (red) and in saline post-oxo condition (green). Two-way ANOVA, with state and genotype as factors, followed by a Dunn's post-hoc test corrected using Holm–Sidak method to compare states within genotype. *p<0.05, **p<0.01, ***p<0.001; &&&p<0.001 for ANOVA interaction term between states and genotype.

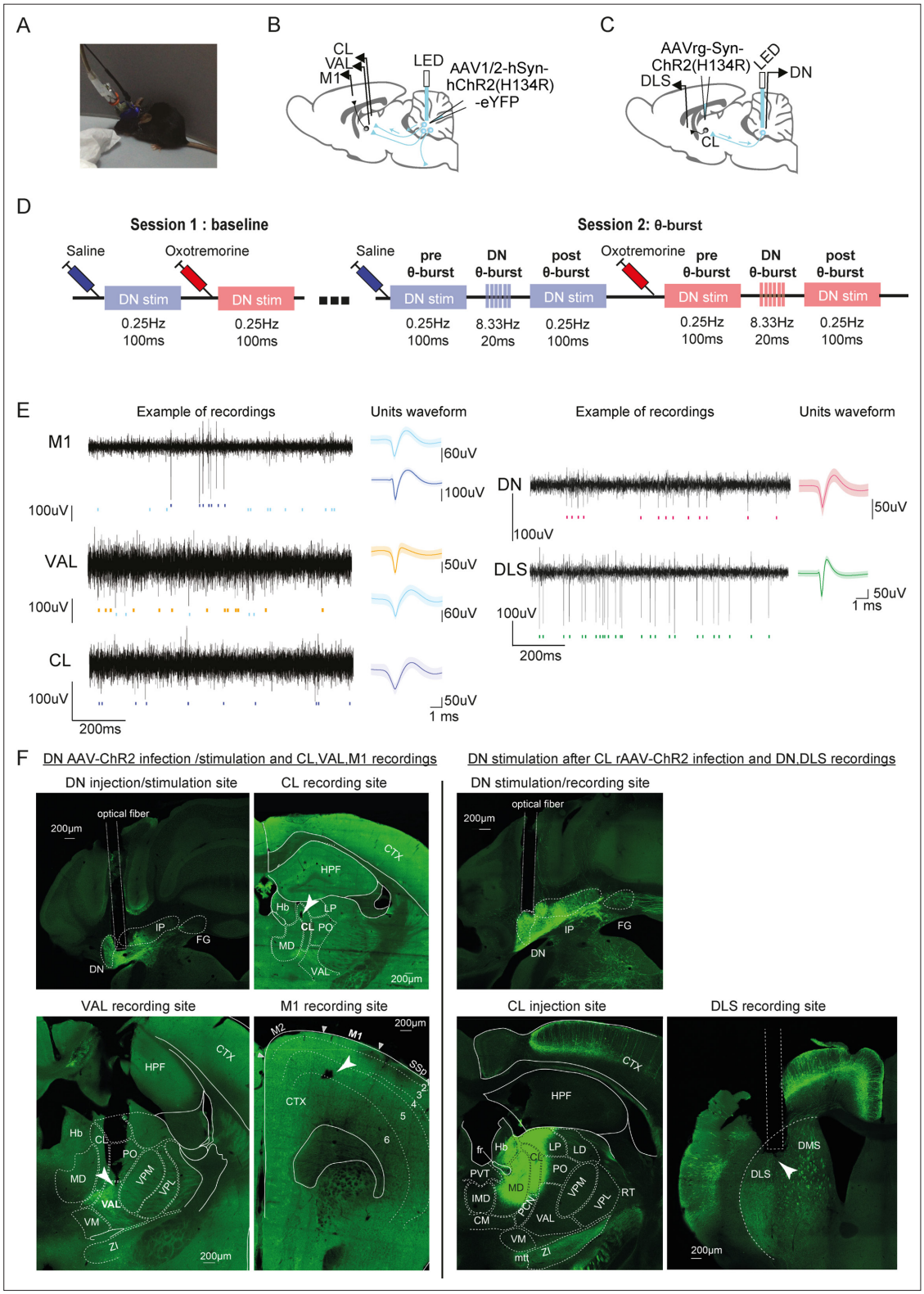

Figure 2—figure supplement 1. Electrophysiology recordings in thalamo-cortical and cerebello-striatal networks. (**A**) Picture of a freely moving mouse during a recording coupled with optogenetic DN stimulation. (**B**) Schematics describing the experimental design of thalamo-cortical recordings coupled with DN stimulation. Guide cannulas with bundles of electrodes were inserted into left motor (M1), CL, and VAL. (**C**) Schematics describing the experimental design of cerebello-striatal recordings coupled with dentate-CL (DN-CL) stimulation. Guide cannulas with bundles of

Figure 2—figure supplement 1 continued on next page

Figure 2—figure supplement 1 continued

electrodes were inserted into the DN and DLS; an optic fiber was inserted in the right DN. (**D**) Experimental timeline describing the protocol of two recording sessions: baseline (left) and θ-burst (right). (**E**) Example high-pass-filtered traces recorded in the M1, VAL, CL, DN, and DLS coupled with the corresponding spike-sorted units (left) and their average waveform (mean ± SD, right). (**F**) Example of cannula placement, optic fiber placement, and electrode position revealed by electrolytic lesions in M1, VAL, CL, DN, and DLS. The guide cannula for the electrodes is visible only when the angle of the brain slices was close enough to the angle of penetration. The localization of the targeted area and neighboring nuclei is outlined based on the Mouse Brain Allen Atlas (2011, version 2) (http://help.brain-map.org/download/attachments/2818169/AllenReferenceAtlas_v2_2011.pdf?version=1&modificationDate=1319667383440&api=v2) and adjusted manually to correspond to the landmarks. CL: centrolateral thalamus; CM: centromedial thalamus; CTX: cortex; DLS: dorsolateral striatum; DMS: dorsomedial striatum; DN: dentate nucleus; IMD: intermediodorsal thalamus; IP: interposed nucleus; FG: fastigial nucleus; Hb: habenula; HPF: hippocampal formation; LD: laterodorsal thalamus; LP: lateral posterior thalamus; MD: mediodorsal thalamus; M1: primary motor cortex; M2: secondary motor cortex; PO: posterior thalamus; PVT: paraventricular thalamus; RT: reticularis thalamus; VAL: ventral anterior lateral thalamus; VM: ventromedial thalamus; VPM/VPL: ventral posterior medial/lateral thalamus; ZI: zona incerta; fr: fasciculus retroflexus; mmt: mammillothalamic tract.

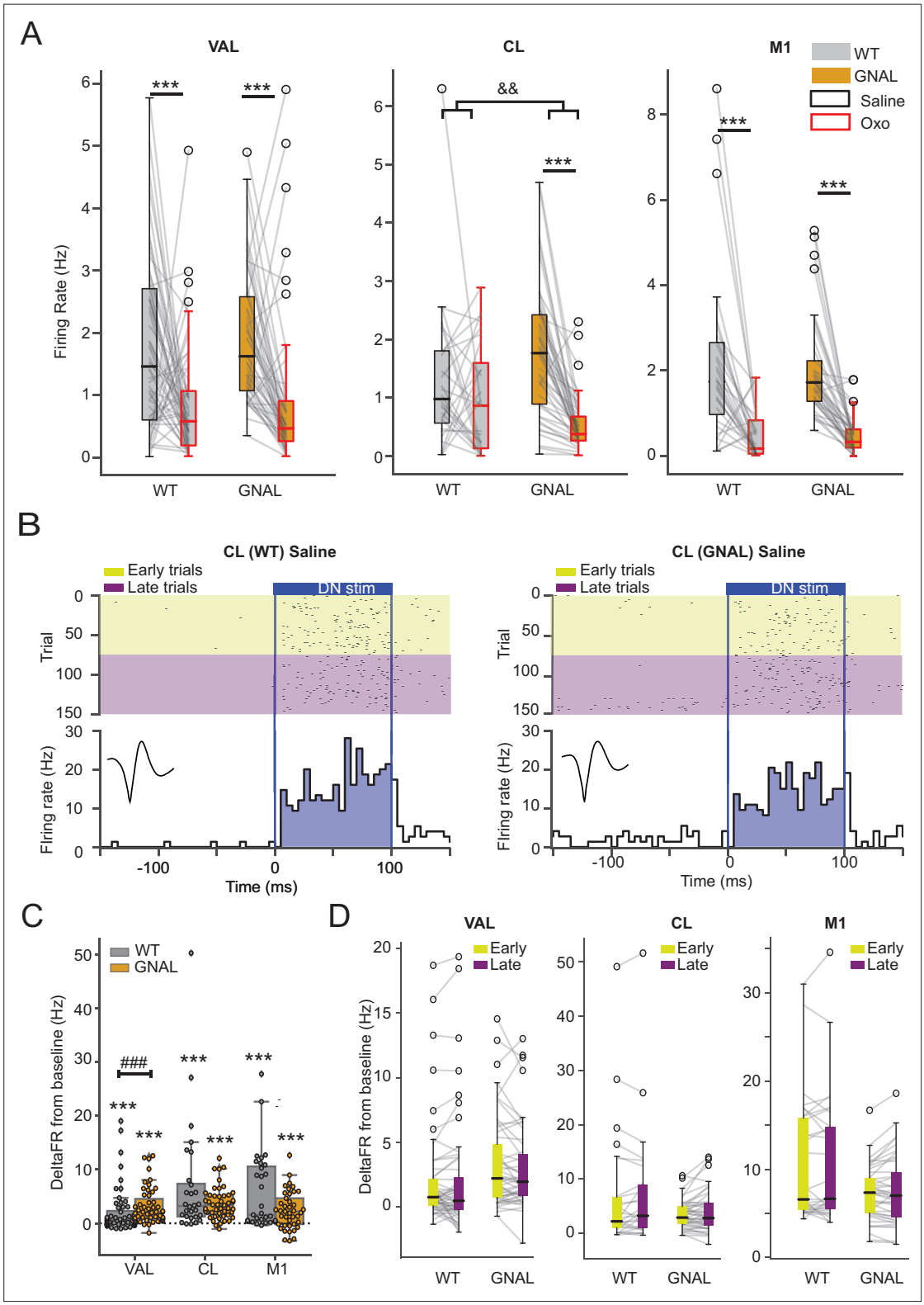

Figure 2—figure supplement 2. Effects of initial exposure to oxotremorine and dentate nucleus (DN) stimulation on the thalamo-cortical network in wildtype (WT) and *Gnal*$^{+/-}$ mice. (**A**) Comparison of mean firing rate under saline and oxotremorine conditions in ventrolateral thalamus (VAL), centrolateral thalamus (CL), and primary motor cortex (M1). *p<0.05, **p<0.01, ***p<0.001 paired difference between treatment for the cells, &&p<0.01 interaction between treatment and genotypes. (**B**) Example of peristimulus time histogram (PSTH) and corresponding raster plot, centered on the

Figure 2—figure supplement 2 continued on next page

Figure 2—figure supplement 2 continued

onset of the cerebellar stimulation, of a CL neuron under saline condition, from a WT mouse (left) and *Gnal*$^{+/-}$ mouse (right). Inset represents the average waveform of the neuron. The first half of the stimulations is categorized as early (yellow) and the second half as late (purple). (**C**) Distributions of responses to DN stimulation under saline condition in VAL, CL, M1 (same as ***Figure 2C***), here with comparisons between genotypes. Wilcoxon test for paired samples *p<0.05, **p<0.01, ***p<0.001 and Mann–Whitney test for independent samples ###p<0.001. (**D**) Comparison of the responses between early and late DN stimulation under saline condition, showing no evolution of responses due to low-frequency repetitive DN stimulation. No significant difference according to Wilcoxon test.

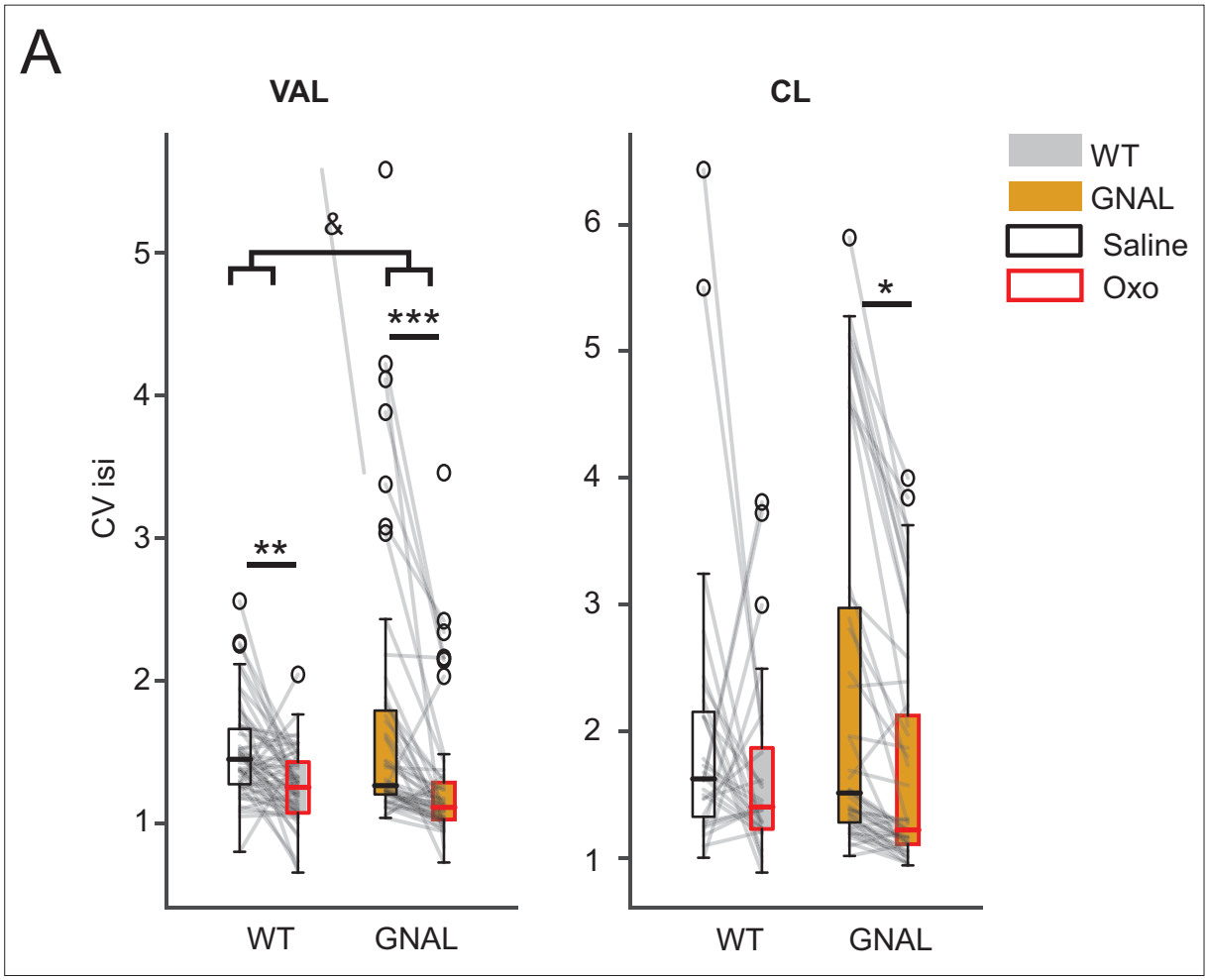

Figure 2—figure supplement 3. Effects of initial exposure to oxotremorine on the regularity of thalamic firing patterns in wildtype (WT) and *Gnal*$^{+/-}$ mice. (**A**) Comparison of CV_{isi} under saline and oxotremorine conditions in ventrolateral thalamus (VAL) and centrolateral thalamus (CL). *p<0.05, **p<0.01, ***p<0.001 paired difference between treatment for the cells, &p<0.05 interaction between treatment and genotypes.

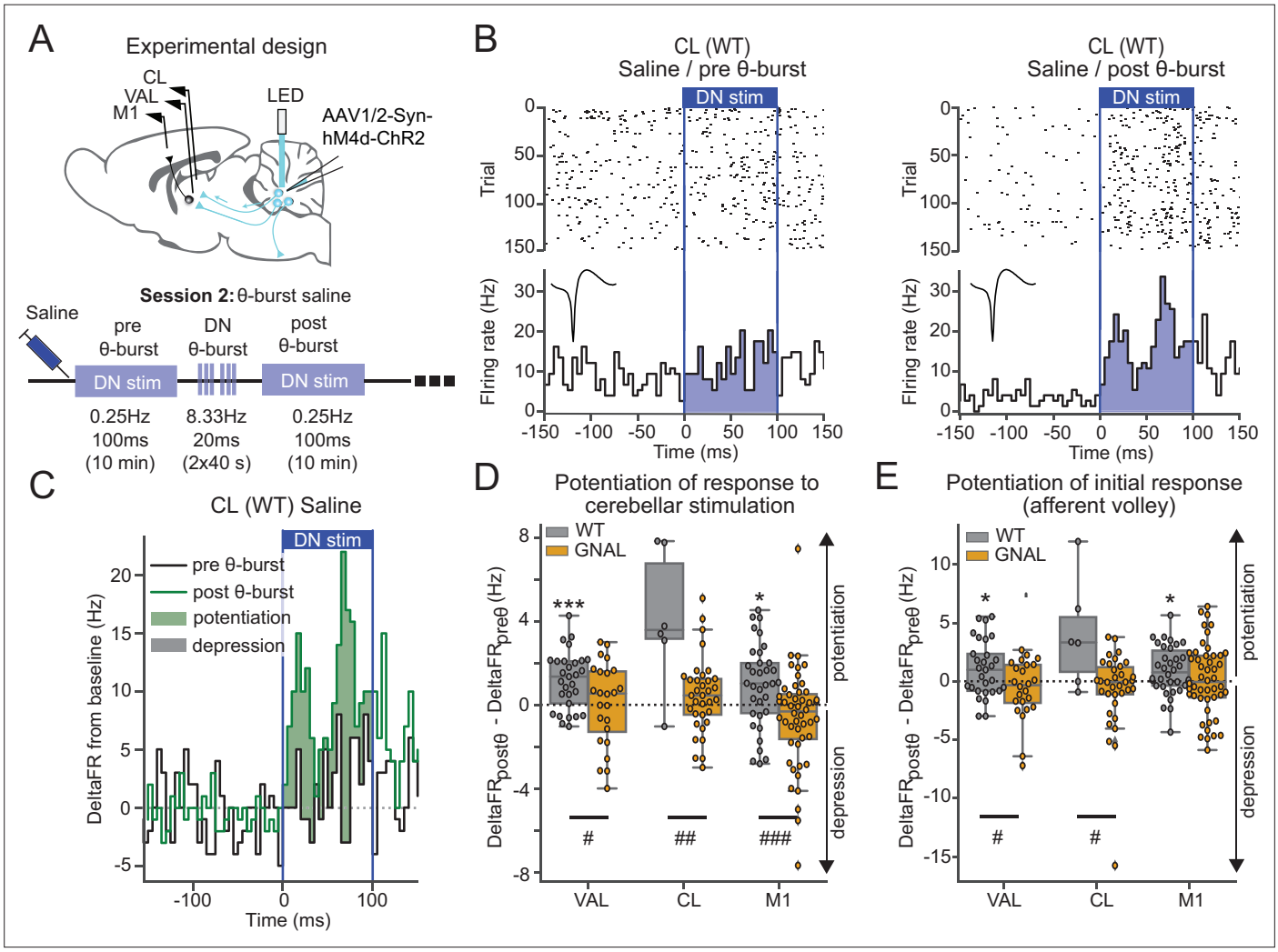

Figure 3. Asymptomatic *Gnal*$^{+/-}$ mice display an abnormal cerebello-thalamic plasticity induced by dentate nucleus (DN) θ -bursts. (**A**) Schematics describing the experimental design of thalamo-cortical recordings coupled with dentate nucleus-centrolateral thalamus (DN-CL) stimulation (top) and experimental timeline (bottom). All the mice received oxotremorine (0.1 mg/kg) in session 1, which took place 2–3 days before. (**B**) Example of peristimulus time histogram (PSTH) and corresponding raster plot, centered on the onset of the cerebellar stimulation, of a CL neuron from a wildtype (WT) mouse under saline condition, before θ -burst (left) and after θ -burst (right). Inset represents the average waveform of the neuron. (**C**) Overlay of PSTHs for the neuron shown in panel (**B**); the difference between the histograms is filled to highlight the potentiation or depression of the responses. (**D**) Impact of θ -burst stimulations administered in saline condition on the response to 100 ms DN stimulations. (**E**) Impact of θ -burst stimulations administered in saline condition on the afferent volley in response to 100 ms DN stimulation. Wilcoxon test for paired samples *p<0.05, **p<0.01, ***p<0.001. Mann–Whitney test for independent samples #p<0.05, ##p<0.01, ###p<0.001 difference between genotypes.

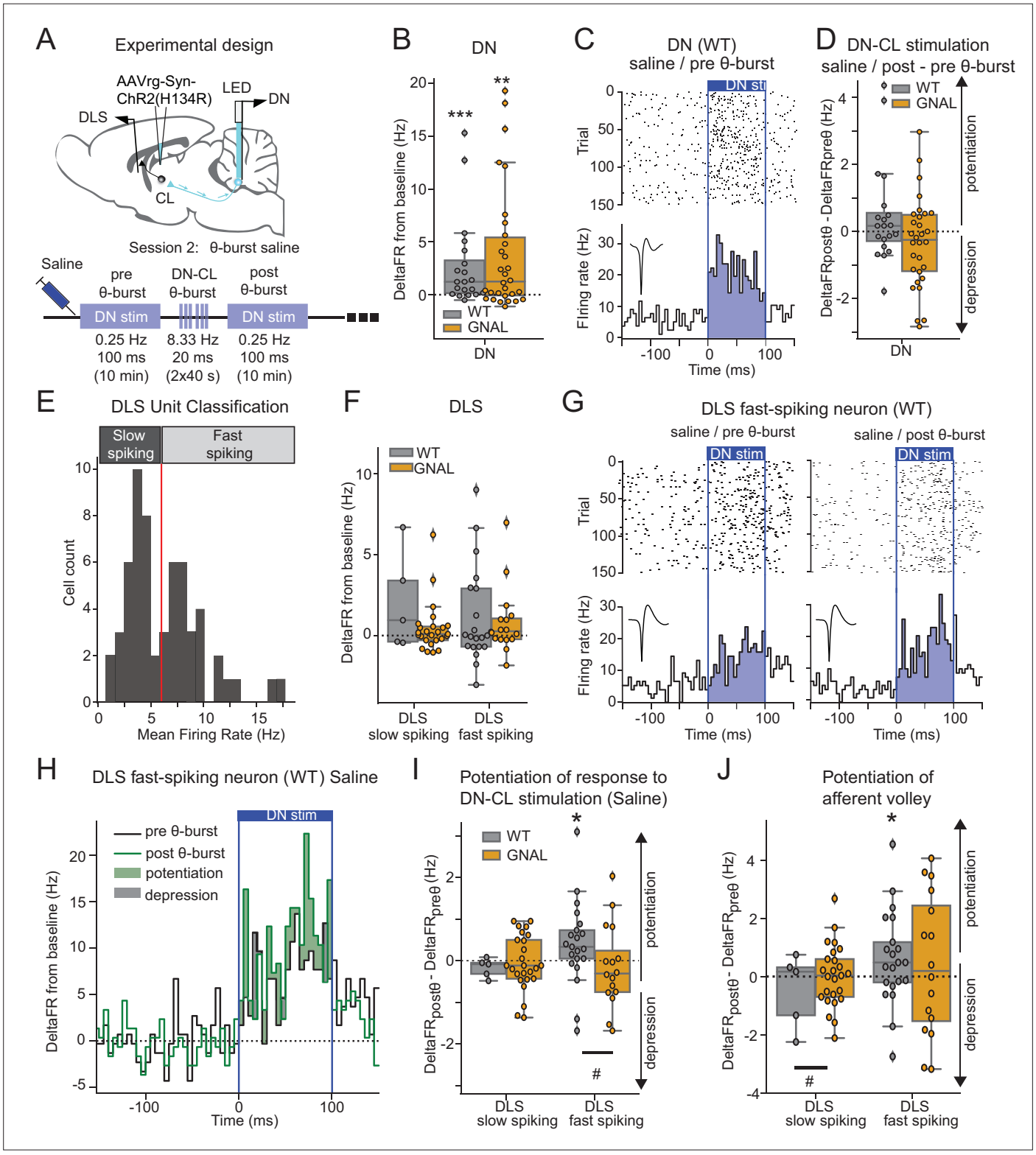

Figure 4. Dentate nucleus-centrolateral thalamus (DN-CL) θ -bursts potentiate the response of fast-spiking dorsolateral striatum (DLS) neurons to DN stimulation in WT wildtype (mice), but not in *Gnal*$^{+/-}$ mice. (**A**) Schematics describing the experimental design of cerebello-striatal recordings coupled with DN-CL stimulation (top) and experimental timeline (bottom). (**B**) Distributions of response amplitude in the DN to optogenetic stimulation in saline condition, before θ -bursts. (**C**) Example of peristimulus time histogram (PSTH) and corresponding raster plot, centered on the onset of the

Figure 4 continued on next page

Figure 4 continued

cerebellar stimulation, of a DN neuron from a WT mouse under saline condition, before θ-bursts. Inset represents the average waveform of the neuron. (**D**) Impact of θ-burst stimulations administered in saline condition on the amplitude of response to 100 ms DN-CL stimulation. (**E**) Illustration of the criteria used to classify DLS neurons as slow spiking and fast spiking based on their mean firing rate using a threshold of 6 Hz (red line). (**F**) Distributions of striatal responses to DN-CL stimulation in saline condition, before θ-burst. (**G**) Example of a PSTH and corresponding raster plot, centered on the onset of the DN-CL stimulation, of a DLS fast-spiking neuron from a WT mouse under saline condition, before θ-burst (left) and after θ-burst (right). Inset represents the average waveform of the neuron. (**H**) Overlay of the PSTHs from panel (**G**); the difference between the histograms is filled to highlight the potentiation or depression of responses. (**I**) Impact of θ-burst stimulations administered in saline condition on the response to 100 ms DN-CL stimulation. (**J**) Impact of θ-burst stimulations administered in saline condition on the afferent volley in response to 100 ms DN-CL stimulation. Wilcoxon test for paired samples *p<0.05, **p<0.01, ***p<0.001. Mann–Whitney test for independent samples #p<0.05, ##p<0.01, ###p<0.001 for differences between genotypes.

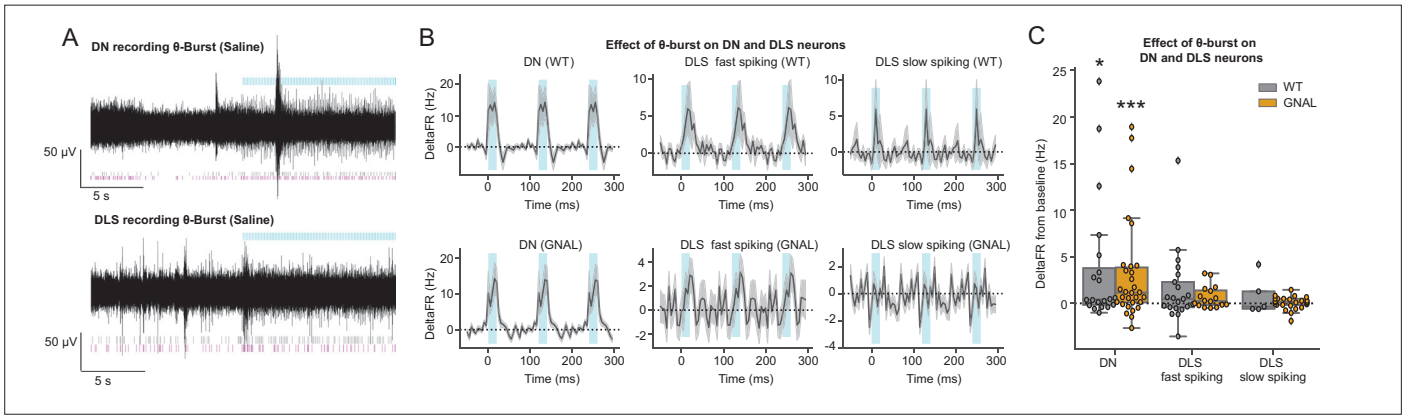

Figure 4—figure supplement 1. Dentate nucleus-centrolateral thalamus (DN-CL) θ -bursts elicit excitation in DN neurons and dorsolateral striatum (DLS) fast-spiking neurons. (**A**) Example high-pass-filtered traces recorded in the DN and DLS during θ -burst, with the corresponding spike-sorted units, showing an increased firing rate induced by θ -burst. θ -burst stimulations are represented by the blue lines. (**B**) Average peristimulus time histograms (PSTHs) (mean ± SD) of DN, DLS fast-spiking and slow-spiking neurons during DN-CL θ -burst for wildtype (WT) mice (top) and *Gnal*$^{+/-}$ (bottom). (**C**) Distributions of responses to DN-CL stimulation under saline condition in DN, DLS fast-spiking and slow-spiking neurons. Wilcoxon test for paired samples *p<0.05, **p<0.01, ***p<0.001. Mann–Whitney test for independent samples #p<0.05, ##p<0.01, ###p<0.001 difference between genotypes.

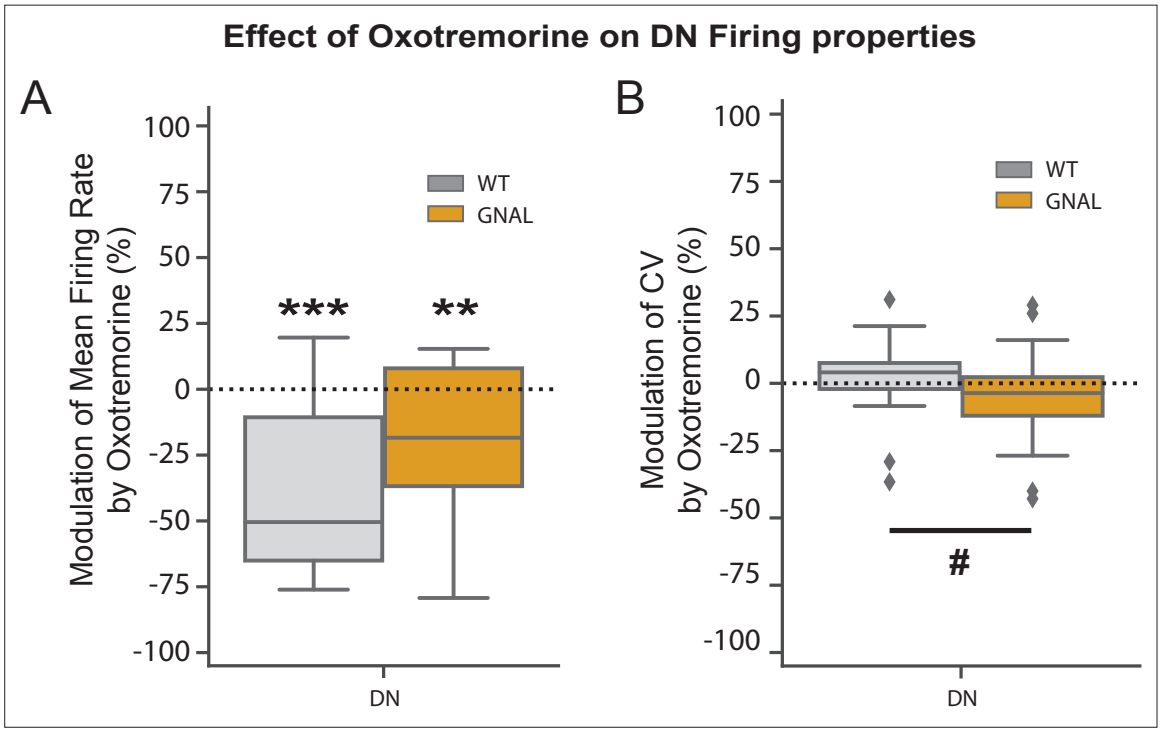

Figure 4—figure supplement 2. Effect of oxotremorine on the firing of the dentate nucleus (DN). (**A**) Modulation of mean firing rate and (**B**) CV in the DN caused by oxotremorine administration. Wilcoxon test for paired samples *p<0.05, **p<0.01, ***p<0.001. Mann–Whitney test for independent samples #p<0.05, ##p<0.01, ###p<0.001 difference between genotypes.

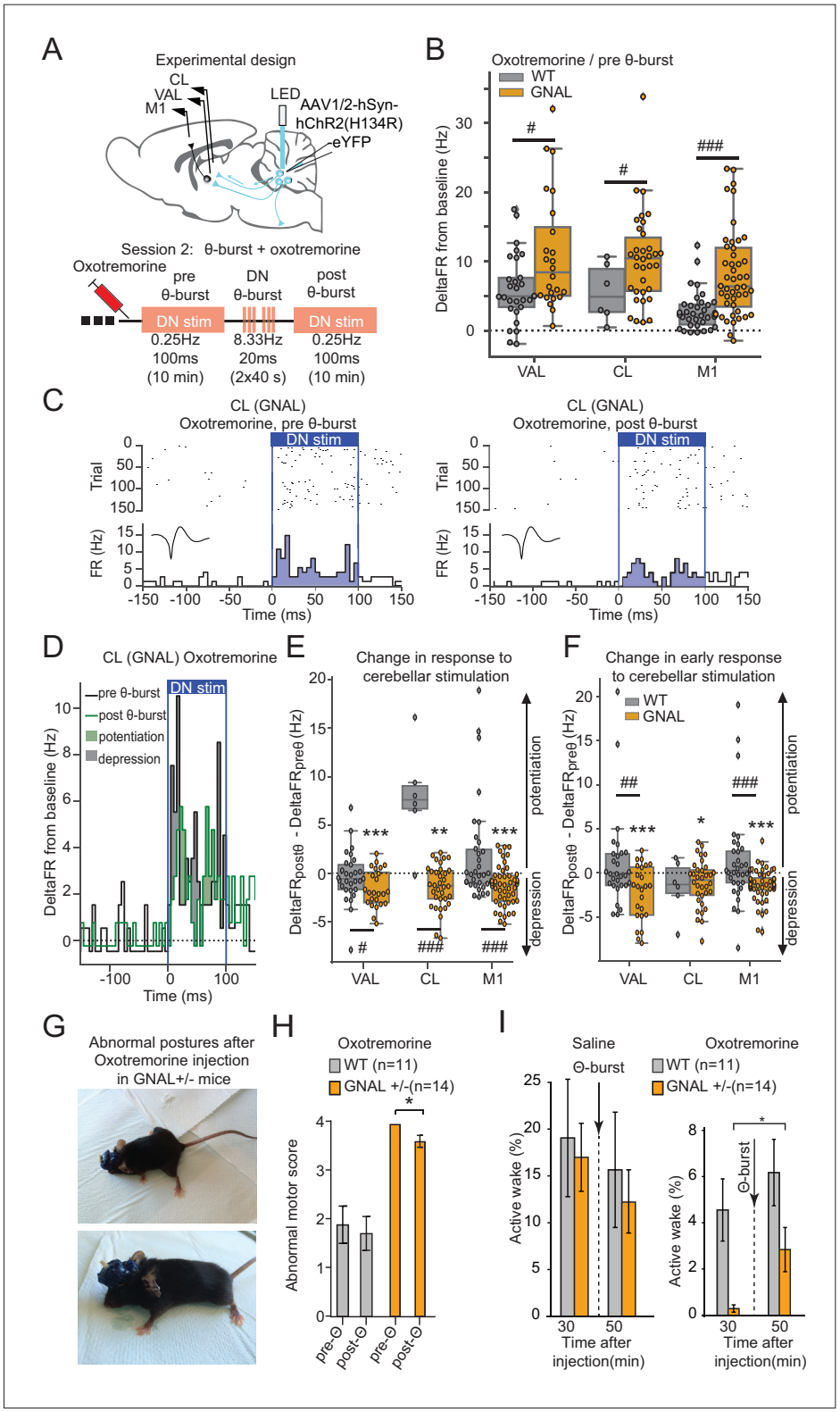

Figure 5. Dentate nucleus (DN) θ -bursts administered to symptomatic *Gnal*$^{+/-}$ mice induce a decreased response to DN stimulation and decrease motor symptoms of dystonia. (**A**) Schematics describing the experimental design of thalamo-cortical recordings coupled with DN stimulation (top) and experimental timeline (bottom). (**B**) Distributions of responses to DN stimulation in oxotremorine condition, before θ -burst. (**C**) Example peristimulus

Figure 5 continued on next page

Figure 5 continued

time histogram (PSTH) and corresponding raster plot, centered on the onset of the cerebellar stimulation of a centrolateral thalamus (CL) neuron from a *Gnal*$^{+/-}$ mouse under oxotremorine condition, before θ -burst (left) and after θ -burst (right). Inset represents the average waveform of the neuron. (**D**) Overlay of the PSTHs from panel (**C**); the difference between the histograms is filled to highlight the potentiation or depression of the responses. (**E**) Impact of θ -burst stimulations administered in oxotremorine condition on the response to +/-ms DN stimulation. (**F**) Impact of θ -burst stimulations administered in oxotremorine condition on the afferent volley in response to 100 ms DN stimulation. Wilcoxon test for paired samples *p<0.05, **p<0.01, ***p<0.001; Mann–Whitney test for independent samples #p<0.05, ##p<0.01, ###p<0.001 difference between genotypes. (**G**) Examples of dystonic postures in *Gnal*$^{+/-}$ mice following oxotremorine administration. (**H**) Average dystonia scores in *Gnal*$^{+/-}$ and wildtype (WT) mice following oxotremorine administration before and after DN θ -burst stimulations. (**I**) Change of average active wake percentage after one session of DN θ -burst stimulations in *Gnal*$^{+/-}$ and WT mice. Wilcoxon test *p<0.05 difference between pre- and post- θ -burst stimulations.

4

The cerebellum regulates fear extinction through thalamo-prefrontal cortex interactions in male mice

In this study, we used a combination of anatomical tracings, pathway-specfic chemogenetic inhibition and multi-site extracellular recordings in the medio-dorsal thamalamus (MD) and dorso-medial prefrontal cortex (dmPFC) during extinction of fear memory, in order to investigate the contribution of cerebello-thalamic projections to the medio-dorsal nucleus of the thalamus.

My contribution to this study was to analyze the extracellular recordings previously acquired during optogenetic stimulation of the fastigial nucleus (FN) and during the extinction of fear memory. I observed short latency increases of firing rate in the MD and dmPFC following optogenetic stimulations of FN neurons. Moreover, I revealed that the chemogenetic inhibition of FN-MD caused an increased bursting activity. Then, I discovered a cortico-thalamo-cortical coupling of fear-related 4Hz oscillations, entraining bursting activity in the MD, which in terms promotes a state of high oscillations in the system through. Ultimately, I revealed that the chemogenetic inhibition of FN-MD increased 4Hz oscillations in the dmPFC during extinction and enhanced the synchrony between the MD and the dmPFC, leading to

more bursting activity in the MD and more sustained oscillations in the dmPFC-MD circuit, overall impairing fear extinction.

nature communications

Article

https://doi.org/10.1038/s41467-023-36943-w

The cerebellum regulates fear extinction through thalamo-prefrontal cortex interactions in male mice

Received: 6 August 2022

Accepted: 22 February 2023

Published online: 17 March 2023

Check for updates

Jimena L. Frontera[1,2], Romain W. Sala[1,2], Ioana A. Georgescu[1], Hind Baba Aissa[1], Marion N. d'Almeida[1], Daniela Popa[1,3] & Clément Léna[1,3]

Fear extinction is a form of inhibitory learning that suppresses the expression of aversive memories and plays a key role in the recovery of anxiety and trauma-related disorders. Here, using male mice, we identify a cerebello-thalamo-cortical pathway regulating fear extinction. The cerebellar fastigial nucleus (FN) projects to the lateral subregion of the mediodorsal thalamic nucleus (MD), which is reciprocally connected with the dorsomedial prefrontal cortex (dmPFC). The inhibition of FN inputs to MD in male mice impairs fear extinction in animals with high fear responses and increases the bursting of MD neurons, a firing pattern known to prevent extinction learning. Indeed, this MD bursting is followed by high levels of the dmPFC 4 Hz oscillations causally associated with fear responses during fear extinction, and the inhibition of FN-MD neurons increases the coherence of MD bursts and oscillations with dmPFC 4 Hz oscillations. Overall, these findings reveal a regulation of fear-related thalamo-cortical dynamics by the cerebellum and its contribution to fear extinction.

Impaired emotion regulation is a growing concern in modern societies, and is responsible for major behavioral dysfunctions. Indeed, the failure to suppress fear responses underlies several anxiety disorders, such as the post-traumatic disorder (PTSD). The extinction of conditioned fear has been an essential paradigm to identify the brain networks and neural mechanisms involved in the suppression of fear[1,2]. Growing evidence indicates that the cerebellum has multiple connections with the fear network[3–5] review in ref. [6], and exhibits BOLD activations during emotion processing, notably in the medial part of the cerebellum[7–9]. Recent evidence showed that the cerebellum is also involved in fear extinction[10–12] and exhibits anomalous functional connectivity with the emotional network in PTSD[13,14]. However, little is known on how this structure regulates fear memories.

Fear extinction results from the formation of a new memory trace, and is known to heavily rely on the medial region of the prefrontal cortex (mPFC), composed of the dorsomedial (dmPFC) and ventromedial (vmPFC) subdivisions, which play complementary roles in fear extinction[15–18]. The mPFC is closely linked to other limbic structures (eg. amygdala, hippocampus)[19,20], and is reciprocally connected to the mediodorsal thalamic nucleus (MD)[21–24], known to have a substantial contribution in fear extinction learning[25–29]. Strikingly, dual firing patterns have been associated with extinction learning in MD thalamo-cortical neurons[27]. While the increase of tonic firing in MD facilitates fear extinction, burst firing in MD neurons prevents fear extinction learning.

Moreover, the interactions between the different structures of the limbic network in the course of emotional processing have been associated with neuronal synchronization[30–32]. Notably, the expression of conditioned fear memories has been associated with prominent synchronous 4 Hz oscillations within dmPFC-basolateral amygdala (BLA) circuit, which organize the spiking activity of local neuronal populations and cause fear memory expression[30,33,34].

[1]Neurophysiology of Brain Circuits Team, Institut de Biologie de l'Ecole Normale Supérieure (IBENS), Ecole Normale Supérieure, CNRS, INSERM, PSL Research University, 75005 Paris, France. [2]These authors contributed equally: Jimena L. Frontera, Romain W. Sala. [3]These authors jointly supervised this work: Daniela Popa, Clément Léna. e-mail: clement.lena@bio.ens.psl.eu

While the contributions of the mPFC, BLA, and MD to fear extinction have been studied in detail, much less is known about the contribution of the cerebellum. The cerebellum has been associated with fear learning and freezing behavior[35,36], review in ref. [37]. Associative fear learning triggers the long-term potentiation of synapses in the cerebellar cortex[38], and cerebellar vermis inactivation during consolidation phase weakens fear-related memories[39], suggesting that the cerebellar plasticity participates to fear processing (but see ref. [40]). Recently, we have described a role of the cerebellum in fear memories through its projections to the ventrolateral periaqueductal grey (vlPAG)[3]. However, little is known about the interconnections of the cerebellum with other limbic-related areas and their contributions to the neurophysiological mechanisms involved in fear extinction.

In this study, we address these questions with a combination of neuroanatomical tracing, chemogenetic manipulations, optogenetics and electrophysiology in freely moving mice, and we describe a pathway that links the cerebellum with the dmPFC via the MD and regulates fear extinction.

Results

The MD nucleus is a thalamic relay between the FN and the dmPFC

In order to examine the connectivity between the cerebellum and the thalamic MD nucleus, known to play an important role in fear extinction, we injected a retrograde adeno-associated virus (AAV) in MD to induce the expression of GFP in neurons projecting to this area (Fig. 1a). We found in the cerebellum a robust retrograde labeling in the cerebellar fastigial nucleus (FN) (Fig. 1b), notably in the caudal part (Fig. 1c), and more abundantly in the medial area of the FN (Fig. 1d). The distribution of retrogradely labeled neurons in FN were highly

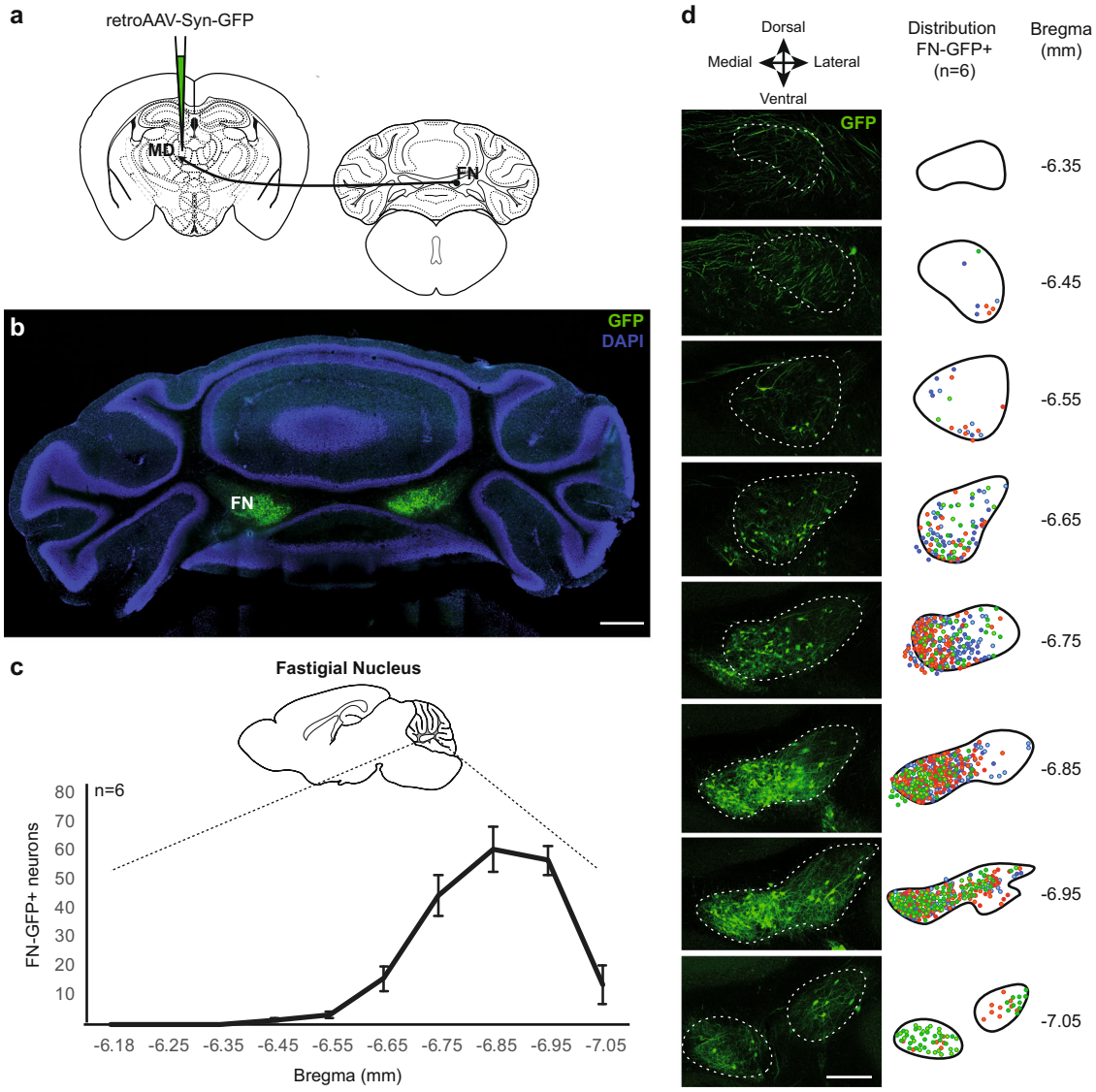

Fig. 1 | Cerebellar fastigial nucleus (FN) sends projections to the mediodorsal thalamic nucleus (MD). a Retrograde tracing strategy by injection of retrograde AAV-GFP in the MD. **b** Coronal cerebellar sections of FN with MD-projecting neurons expressing retrograde AAV-GFP (green), and cell nuclei labeled with DAPI (scale bar, 500 μm). **c** Quantification (mean +/− SEM) and antero-posterior distribution of retrograde GFP-labeled FN MD-projecting neurons (FN-GFP+) in coronal sections (data from 6 mice). AP position is reported relative to Bregma. **d** Distribution pattern of FN MD-projecting neurons (FN-GFP+) in coronal cerebellar sections across replicates ($n = 6$ mice, colors correspond to labeling from different animals). (scale bar, 250 μm). See also Supplementary Fig. 1. Brain schematic in panel **a** modified from the Allen Mouse Brain Atlas and Allen Reference Atlas – Mouse Brain[73,74] http://atlas.brain-map.org/atlas?atlas=1#atlas=1&plate=100960384, http://atlas.brain-map.org/atlas?atlas=1#atlas=1&plate=100960136, http://atlas.brain-map.org/atlas?atlas=1#atlas=1&plate=100960240.

https://doi.org/10.1038/s41467-023-36943-w

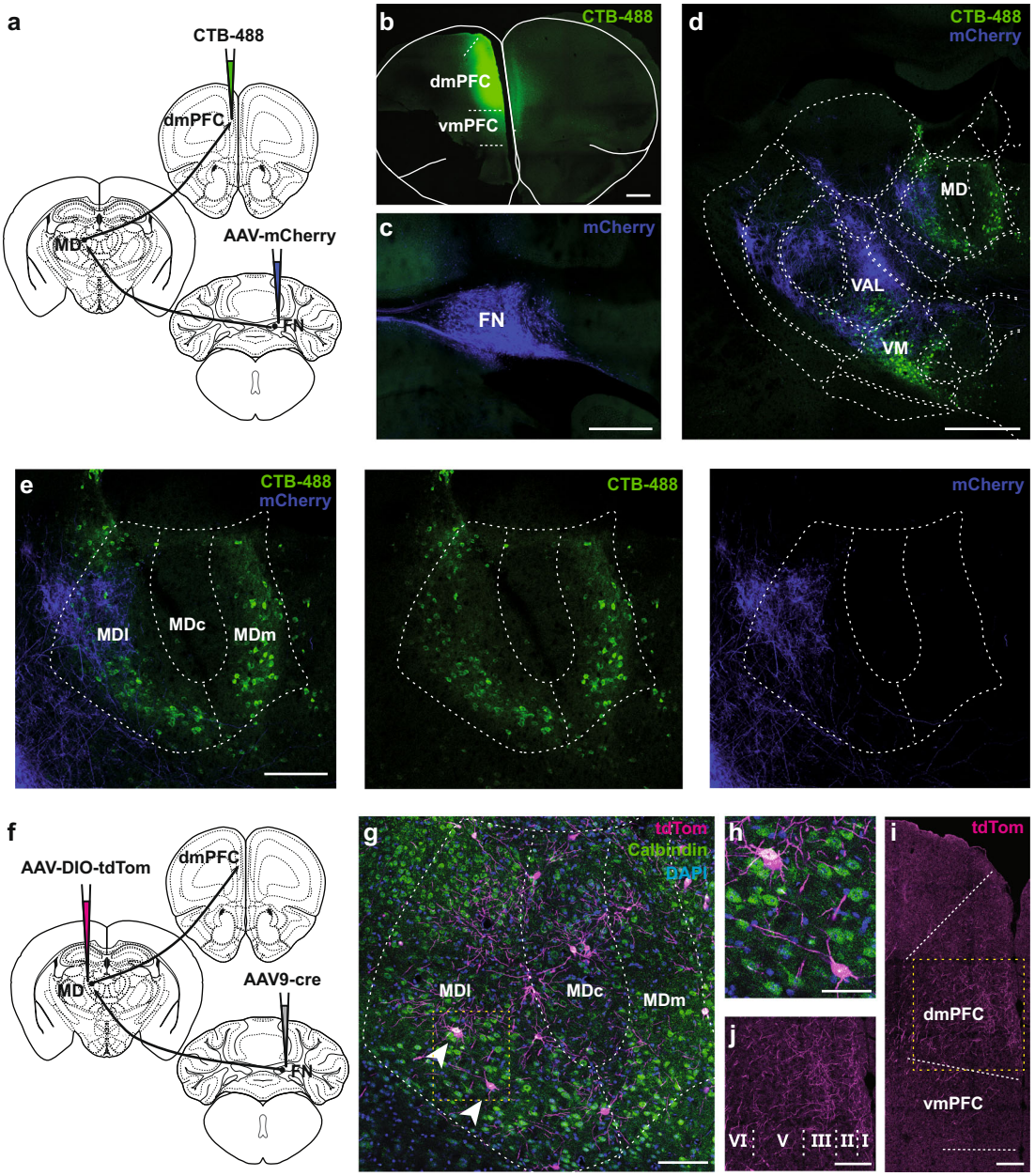

Fig. 2 | MD as a high-order thalamic relay between the FN and the dmPFC. **a** Strategy for neuroanatomical tracing by injections of anterograde AAV-mCherry in the FN and retrograde CTB-488 in the dmPFC ($n = 3$ replicates). **b** Example of CTB-488 injection site in the dmPFC (scale bar, 500 μm). **c** AAV-mCherry expression in the cerebellar FN (scale bar, 500 μm). **d** Thalamic section exhibiting contralateral FN projections (mCherry, blue) and thalamic dmPFC-projecting neurons (CTB-488, green) (scale bar, 500 μm). **e** Zoom-in from thalamus section in **d** (dotted line area), showing the FN projections to MD, preferentially into the lateral segment of the MD (MDl). MDc: central segment of MD, MDm: medial segment of MD. (scale bar, 100 μm). **f** Schematic representation of viral strategy to localize FN-post-synaptic neurons in MD. Anterograde trans-synaptic expression of cre by AAV9 and cre-dependent expression of td-Tomato in MD. ($n = 3$ replicates) **g** MD exhibiting FN-post-synaptic labeled neurons (arrow heads) with tdTom and co-localization of calbindin expression detected by immunostaining (green). Cell nuclei labeled with DAPI (blue). **h** Zoom-in from **g** (yellow dotted line area) exhibiting FN post-synaptic MD neurons. **i** dmPFC sections exhibiting FN-post-synaptic MD neuronal projections in different cortical layers (scale bar, 100 μm). **j** Zoom-in from dmPFC section in **i** (yellow dotted line area), cortical layers I-VI (scale bar, 100 μm). Brain schematics modified from the Allen Mouse Brain Atlas and Allen Reference Atlas – Mouse Brain[73,74] from http://atlas.brain-map.org/atlas?atlas=1#atlas=1&plate=100960136, http://atlas.brain-map.org/atlas?atlas=1#atlas=1&plate=100960240 in panels **a**, **f**, and from http://atlas.brain-map.org/atlas?atlas=1#atlas=1&plate=100960260 in panels **d**, **e**, **g**.

consistent across replicates ($n = 6$, Fig. 1d). Furthermore, we also found cortical retrograde-labeled neurons projecting to MD, localized principally in the dmPFC (composed by the anterior cingulate cortex (ACC) and the prelimbic area (PL)) and less in vmPFC (mainly infralimbic cortex (IL)) (Supplementary Fig. 1), consistent with previous studies showing mPFC projections to MD[21,41].

Since the MD is reciprocally connected with the dmPFC[21–24], we examined whether the areas of the MD that receive projections from the cerebellar FN correspond to MD areas projecting to the dmPFC. Using a combination of anterograde expression of AAV-mCherry in the FN (Fig. 2a, c) and the retrograde Cholera-Toxin subunit B (CTB) injection in the dmPFC (Fig. 2a, b), we found that the MD neurons projecting to the dmPFC were preferentially localized in the medial and the lateral MD (Fig. 2d, e), while the FN projections were principally localized contralaterally in the lateral MD, surrounding the MD neurons that project to the dmPFC (Fig. 2d, e). Thus, these

results suggest the existence of a di-synaptic FN-MD-dmPFC pathway.

To confirm the existence of this pathway, we used a trans-synaptic strategy combining injections of anterograde trans-synaptic AAV serotype 9 encoding cre-recombinase (cre) in the FN, with injections of anterograde cre-dependent AAV-DIO-tdTomato in the MD (Fig. 2f). We found tdTom-expression in MD neurons as a result of the anterograde trans-synaptic transport of AAV9-cre from FN terminals (Fig. 2g). Moreover, since MD dmPFC-projecting neurons have been reported to express calbindin, we examined calbindin-immunoreactivity and found that those tdTom-labeled MD neurons expressed calbindin (Fig. 2g, h). Finally, we observed the tdTom-labeled projections of MD neurons in the Layers I, III, V and VI of the dmPFC (Fig. 2i, j), confirming that the MD neurons receiving FN inputs project to the dmPFC. Taken together, our findings reveal the existence of a cerebello-dmPFC pathway through the lateral part of MD that also receives inputs from the dmPFC.

Optogenetic stimulations of FN induce short latency responses in the MD and dmPFC

To study whether the FN input can drive MD and dmPFC neuronal activity, we performed single-unit recordings in MD and dmPFC coupled with optogenetic stimulation of Channelrhodopsin-2 (ChR2)-expressing neurons in the FN in freely moving mice (Fig. 3a, b). Optogenetic stimulation (100 ms) of the FN induced an increase in firing rate during light pulses, both in MD and dmPFC (Fig. 3c), while FN illumination in absence of ChR2 expression did not induce variation of the firing rate at the population level (Supplementary Fig. 2, all statistics are detailed in the Supplementary File). During optogenetic stimulation of the FN, we found that 49% of the MD recorded cells (77/158 MD neurons, $n = 10$ mice) displayed a significant increase in firing, whereas in the dmPFC 47% of the population (17/36 dmPFC neurons, $n = 7$ mice) significantly increased their firing rate during the light stimulation. Furthermore, among the responsive neurons in the MD and the dmPFC, a smaller set (MD: 14 cells with latency <15 ms; dmPFC: 8 cells with latency <20 ms) displayed short latencies of response (Fig. 3d). While MD neurons showed an early and sustained response, dmPFC neurons exhibited an initial increase in firing rate that was further amplified around 50 ms of stimulation (Fig. 3e, f). These data suggest a potent excitatory effect of the FN input to MD and dmPFC involving direct and indirect pathways.

Then, to test the direct and specific contribution of FN input to MD neuronal responses, we combined retrograde AAV-cre injection in the MD with cre-dependent AAV-DIO-ChR2 injection in the FN (Fig. 3g, $n = 10$ mice). In these experiments, short illumination (10 ms) of the FN MD-projecting neurons expressing ChR2 produced short latency responses in MD neurons (9/90 with latency ≤ 15 ms, Fig. 3h). In contrast, no short latency responses were observed in the dmPFC but some neurons exhibited a late increase in discharge (9/48 with latencies >20 ms, Fig. 3h). Thus, these results indicate a monosynaptic excitatory connection between the FN and the MD, and in concordance with a modulatory role of the MD on dmPFC activity in vivo[42], the activation of this pathway did not elicit a potent short-latency activation of the dmPFC neurons.

Chemogenetic inhibition of the FN input to MD impairs fear extinction

Since the MD and the dmPFC are involved in fear extinction[15–18,27,28], we then investigated the contribution of the FN-MD pathway to this learning. For this purpose, mice were subjected to a Pavlovian fear conditioning protocol (FC), which consisted of 5 conditioned stimulus (CS, tone)-unconditioned stimulus (US, electrical foot-shock) paired presentations, followed by three consecutive days of fear extinction sessions (EXT), 25 unreinforced CS presentations per session (Fig. 4d).

We examined the contribution of the FN input to MD during fear extinction by specific chemogenetic inhibition of these projections. We selectively expressed inhibitory DREADD receptors in the FN neurons that target the MD, by injecting bilaterally retrograde CAV2-cre in the MD, and cre-dependent AAV- hM4Di (named Gi) in the FN (Fig. 4a–c). We then performed the FC and extinction sessions in these mice (Fig. 4d) and quantified the fear response as the percentage of time freezing during the CS.

After fear learning, control DREADD-expressing mice (saline-injected, CT + SAL) extinguished the freezing response over 3 days of extinction sessions (EXT1-3) (Fig. 4e). By contrast, mice under FN-MD input inhibition (Gi+CNO) during the first two days of extinction (EXT1 and EXT2), exhibited an impairment of fear extinction (Fig. 4e, Supplementary Fig. 3a, e). Both groups of mice had similar freezing levels at the beginning of EXT1 (median CT + SAL = 68.1%, Gi + CNO = 71.2%). Comparing mice expressing high levels of freezing during early EXT1 (above median) to mice expressing low levels freezing (below median) revealed that the impairment of extinction was only visible in the Gi+ CNO mice with the highest initial EXT1 freezing levels (Fig. 4e, top), in which little if any extinction occurred during EXT1 and EXT2. In contrast Gi + CNO mice with lower initial EXT1 freezing levels exhibited normal extinction suggesting that FN MD-projecting neurons primarily modulate extinction of high fear responses. During EXT3, without chemogenetic inhibition, both groups of mice showed a decrease in conditioned-fear response compared to EXT1 and EXT2, suggesting that the inhibition of FN MD-projecting neurons partially suppressed the expression of the learned extinction. Moreover, the basal freezing levels during the habituation to context A (before FC) or context B (before EXT1, EXT2 or EXT3, after SAL/CNO administration), were not significantly different between groups (Fig. 4f), indicating that chemogenetic inhibition did not induce general freezing behavior, but affected specifically the extinction of the freezing response to the CS. We verified that the dose of CNO used i.p. in our experiments had no effect per se on freezing or extinction learning, by performing FC and EXT sessions in sham mice (mice subjected to the same surgery procedure with infusion of AAV-mCherry instead of DREADD), injected with saline or CNO during EXT1 and EXT2. No differences were found between CNO and saline sham control mice, indicating that CNO had no effect in the absence of DREADD expression (Supplementary Fig. 3b, f). Altogether, these results indicate that FN neurons projecting to the MD modulate fear extinction.

To investigate if the effect observed by inhibition of FN MD-projecting neurons involves the FN inputs to the MD, we induced local inhibition of the DREADD-expressing FN terminals in MD, by intracranial local infusion of CNO in MD. In this set of experiments, mice expressing Gi in the FN-MD terminals received either SAL or CNO (0.5 mM) infusions, while another group of sham mice received the CNO (0.5 mM) infusion, 10 min before the EXT1 and EXT2. In concordance with the effect observed following the systemic administration of CNO, freezing levels were significantly higher in the Gi-CNO group at late EXT1, compared to both CT + SAL and CT + CNO control groups (Supplementary Fig. 3c, g). This effect was not observed in EXT2, but this may be due to the experimental limitations of repeated intracranial infusions. Overall, this result supports the hypothesis that FN influence on fear extinction is mediated by its input to MD.

The increased freezing observed during extinction following FN-MD inhibition could result from a disruption of the expression of conditioned fear (potentiation of fear expression, or disruption of fear suppression) rather than an effect on the extinction learning processes. If this was the case, FN-MD inhibition only during the EXT3 should result in an increased freezing. However, this experiment did not reveal significant differences between the FN-MD inhibited and control group (Supplementary Fig. 3d, h), indicating that this pathway does not simply modulate fear expression but also the extinction learning.

https://doi.org/10.1038/s41467-023-36943-w

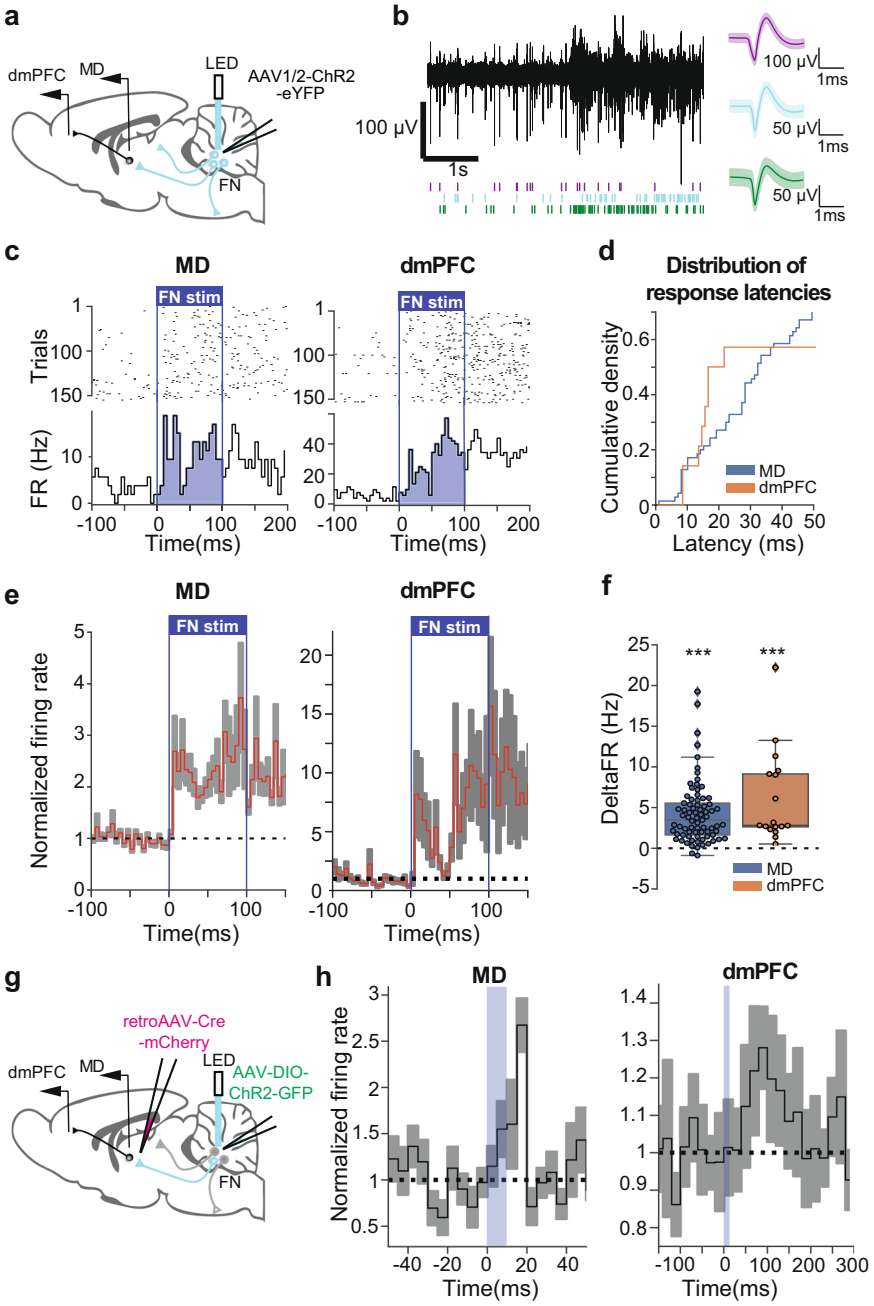

Fig. 3 | Optogenetic stimulation of FN input to MD induced responses in MD and dmPFC. a Strategy used for the specific optogenetic stimulation of FN neurons, representing the local injection of anterograde AAV-ChR2-eYFP in the FN and the implantation of recording electrodes in MD and dmPFC. **b** Example of high-passed filtered trace of a recording channel in MD (left) and spike shapes of single units from MD (average ± SD), after spike sorting (right). **c** Example PSTH (5 ms bins, bottom) and rasterplot (top) of a MD cell (left) and dmPFC cell (right) during 100 ms optogenetic stimulation of the FN. The light stimulation is represented by a blue rectangle. **d** Cumulative histograms showing the latency of neuronal response of responsive cells in MD and dmPFC triggered by 100 ms optogenetic stimulation of the FN. **e** PSTH (5 ms bins) displaying the change in firing rate (average ± SEM) of responsive cells during 100 ms optogenetic stimulation of the FN in MD (left), and in dmPFC (right). The light stimulation is represented by a blue rectangle. **f** Average change in firing rate of responsive cells during 100 ms optogenetic stimulation of the FN. Wilcoxon test, (77 MD neurons from 10 mice, 17 dmPFC neurons from 7 mice) $^{***}p < 0.001$. Boxplots represent quartiles and whiskers correspond to range; points are singled as outliers if they deviate more than 1.5 x interquartile range from the nearest quartile. **g** Strategy used for the specific optogenetic stimulation of the FN inputs in MD, by injection of retrograde AAV-cre-mCherry in the MD and anterograde cre-dependent AAV-DIO-ChR2-GFP in the FN, and the implantation of recording electrodes in MD and dmPFC. **h** PSTH displaying the change in firing rate (average ± SEM) of responsive cells following 10 ms optogenetic stimulation of the FN in MD (left, 5 ms bin), and in dmPFC (right, dmPFC, 20 ms bin). Data available at doi:10.5061/dryad.9kd51c5ng. Detailed statistical results are available in the Supplementary Tables referenced by panel numbers.

Overall, these data indicate that the FN input to MD modulates the fear extinction in normal conditions, and that inhibiting this input leads to a deficiency in the extinction of the fear response.

FN input to the MD is not involved in anxiety behavior or nociception sensitivity

The mPFC-limbic circuit is also recruited in anxiety[19]. Thus, in order to test whether the FN input to MD contributes to anxiety-like behavior, we

https://doi.org/10.1038/s41467-023-36943-w

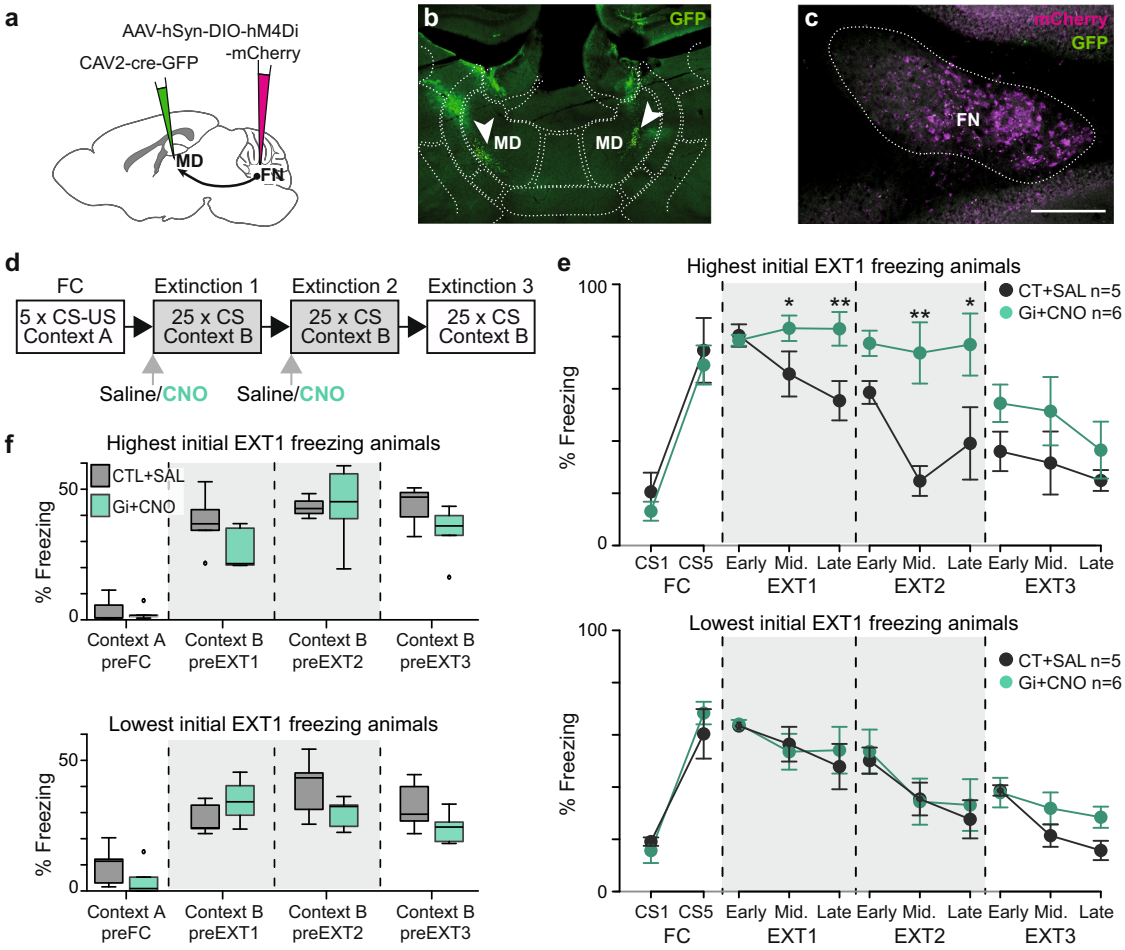

Fig. 4 | FN input to MD modulates fear extinction. a Chemogenetic strategy to inhibit specifically the activity of FN-MD input, bilateral retrograde expression of cre recombinase in MD by CAV2-cre-GFP infusion and anterograde cre-dependent expression of inhibitory DREADD (hM4Di (Gi)) in the cerebellar FN. **b** Injection site of CAV2-cre-GFP in the MD. **c** Cre-dependent expression of inhibitory DREADD reported by mCherry fluorescence in the FN (scale bar, 250 μm). **d** Classical fear conditioning and extinction protocol used. FN-MD projections were inhibited by CNO administration during extinction 1 and 2. **e** FN-MD input inhibition (Gi+CNO, $n = 12$) during extinction sessions 1 and 2 reduced extinction of fear response compared to the control group (CT + SAL, $n = 10$). The mice were separated in two groups of same size expressing respectively the highest and lowest freezing levels on the Early stage of EXT 1. Lines represent mean ± SEM. Post-hoc two-sided *t*-test Holm-Sidak corrected, $^*p < 0.05$. **f** FN-MD chemogenetic inhibition of FN-MD input did not affect basal levels of freezing during habituation to the context of fear conditioning (Context A) or extinction (Context B), compared to the control mice; same groups and statistics as in panel **e**. Boxplots represent quartiles and whiskers correspond to range; points are singled as outliers if they deviate more than 1.5 x interquartile range from the nearest quartile, $p > 0.05$. Data available at doi:10.5061/dryad.9kd51c5ng. Detailed statistical results are available in the Supplementary Tables referenced by panel numbers.

performed different anxiety tests under chemogenetic inhibition of FN-MD projections: open field (Supplementary Fig. 4a), elevated plus maze (Supplementary Fig. 4b) and dark-light box (Supplementary Fig. 4c). There were no differences between the control and the FN-MD inhibition groups. Overall, these results indicate that the inhibition of FN MD-projecting neurons do not significantly affect anxiety behavior.

Since the MD also receives spinal nociceptive inputs and it is involved in the processing of negative affective aspects of pain[43], we examined the sensitivity of the mice to painful stimuli, using hot plate and tail immersion tests (Supplementary Fig. 4d). The results showed no alteration in the sensitivity under inhibition of FN input to MD, indicating that the inhibition of FN-MD projections does not modulate nociception.

Overall, our behavioral results suggest that cerebellar FN-MD projections contribute more specifically to the fear extinction learning process than to other MD-dmPFC functions related to negative emotions, such as anxiety and nociception.

Inhibition of the FN input to MD increases thalamic bursting

Previous work showed that high-frequency bursts of action potentials in MD prevented fear extinction while an increased tonic firing in the MD promoted fear extinction learning[27]. Since inhibition of FN input to MD impaired fear extinction, an increased bursting in the MD could be a possible mechanism that explains our findings. Thus, we examined how the chemogenetic inhibition of the FN input to MD affects burst firing in the MD (Fig. 5). We used the Robust Gaussian Surprise method[44] (Fig. 5a, b) to detect bursts in the MD and quantify two bursting parameters: the burst occurrence (number of bursts per second) and firing rate within-bursts. All MD cells exhibited some bursting activity.

The inhibition of FN-MD input during EXT1 induced an increase in burst occurrence compared to the FC, both in the baseline (before first CS presentation) and during CS presentation (Fig. 5c, d). Notably, the burst occurrence in EXT1 was higher in the Gi + CNO group compared to the control, during baseline (when fear expression is enhanced, Fig. 4f right) and during CS presentation (Fig. 5c), and was reversed to values close to baseline during EXT3. While the burst occurrence was increased by the chemogenetic inhibition of FN-MD input, the firing rate within-burst was not different than the control mice, suggesting that bursting intensity in the MD was not altered by the disruption of FN-MD (Fig. 5d). Taken together, these data indicate that the FN-MD

https://doi.org/10.1038/s41467-023-36943-w

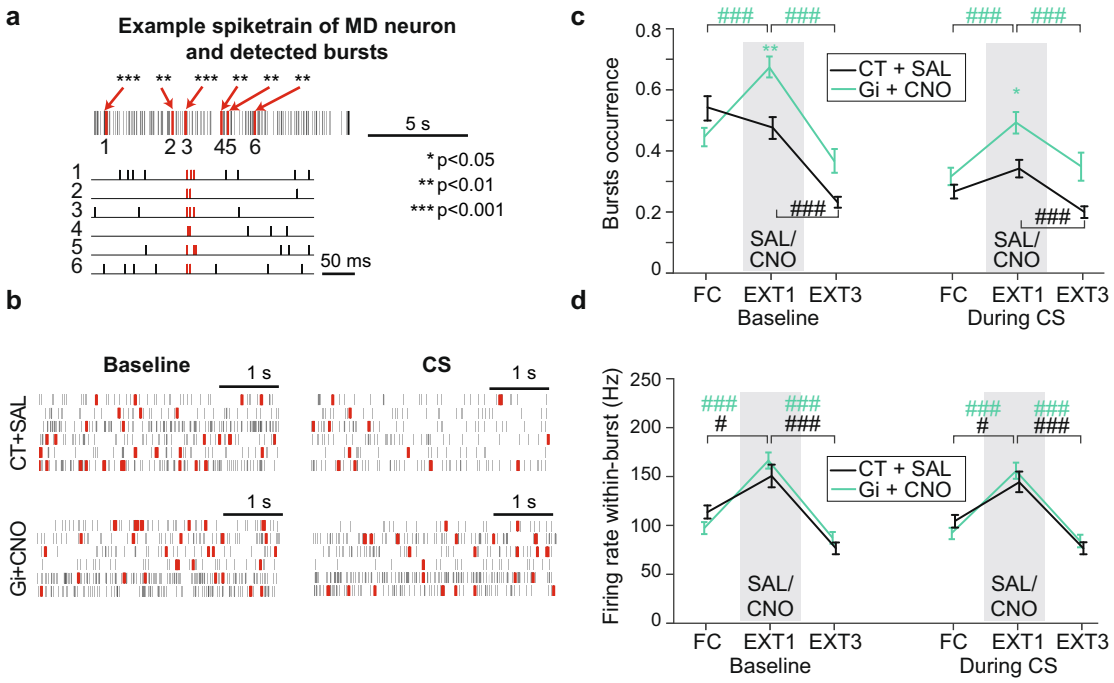

Fig. 5 | Chemogenetic inhibition of FN-MD input during EXT1 increases burst occurrence in the MD. a Example of burst detection in a spiketrain from a MD neuron, bursts are represented in red, and their associated *p*-values are reported. One sample *t*-test on ISI of burts compared to the local distribution of ISI. $^{*}p < 0.05$, $^{**}p < 0.01$, $^{***}p < 0.001$. **b** Example spiketrains of MD neurons during Baseline (left), and during CS (right), from a CT + SAL mouse (top), Gi + CNO mouse (bottom). Each line corresponds to a given neuron, bursts are represented in red. **c** Burst occurrence (number of bursts per second) during baseline (left), and during CS (right). **d** The average firing rate within a burst during baseline (left) and during CS (right). Comparisons between Gi + CNO (FC, EXT1, EXT3 $n = 49, 67, 51$ from 5 mice) and CT + SAL ($n = 36, 39, 22$ from 4 mice) for each phase are shown by colored stars on top of the corresponding phase Holm-Sidak corrected Mann–Whitney *U* test, $^{*}p < 0.05$, $^{**}p < 0.01$, $^{***}p < 0.001$. Comparisons between phases for each experimental group are shown by colored stars on top of line between two phases. Holm-Sidak corrected Mann–Whitney U test, $\#p < 0.05$, $\#\#p < 0.01$, $\#\#\#p < 0.001$. Data available at doi:10.5061/dryad.9kd51c5ng. Data are ploted as mean +/− SEM. All tests are two-sided. Detailed statistical results are available in the Supplementary Tables referenced by panel numbers.

input participates in the regulation of burst firing in MD neurons and its inhibition results in an increased MD bursting activity in periods where fear expression is higher.

dmPFC 4 Hz oscillations and neuronal dynamics in the MD

During fear extinction, the fear expression (conditioned-freezing) is associated with 4 Hz olfactory-entrained oscillations in the dmPFC and amygdala, anticipating and causing freezing occurrence[30,45]. To further investigate the interactions between MD and dmPFC during fear extinction, we studied how MD neuronal activity is related to the dmPFC 4 Hz local field potential (LFP) oscillations.

Consistently with the observations of Karalis et al.[30], we observed high levels of 4 Hz oscillations in the LFP of the dmPFC induced by the presentation of the CS in EXT1 (Fig. 6a), with peaks of Power Spectrum Density (PSD) in the 4 Hz range (2–6 Hz) (Fig. 6b). We found an increased fraction of the PSD associated to 4 Hz oscillations during CS compared to baseline in both experimental groups (Fig. 6c), consistent with the increase in fear responses during the CS. Moreover, the fraction of the PSD associated to 4 Hz oscillations during CS was increased under inhibition of FN input to MD, compared to control mice, consistent with the higher expression of fear response in this group.

Next, we examined the modulation of MD activity by dmPFC 4 Hz oscillations during CS presentations. MD neuronal activity exhibited a negative correlation with the amplitude of dmPFC 4 Hz oscillations during CS in both experimental groups, indicating a reduction of MD firing rate during high 4 Hz in most cells (Fig. 6d, e). We then identified episodes of high 4 Hz oscillations and found a significant reduction in burst occurrence in the MD during these episodes (Fig. 6f). However, the down-modulation of MD bursting by dmPFC 4 Hz oscillations was significantly milder during CS when the FN input to MD was inhibited (Fig. 6f), yielding an overall higher burst occurrence during episodes of high dmPFC 4 Hz oscillations during CS (Fig. 6g).

All together, these data indicate an inhibition of the MD by dmPFC 4 Hz oscillations associated with freezing during fear extinction, and that the disruption of the FN-MD pathway during extinction results in an increased bursting during CS-related freezing.

Phase-locking of MD bursting to dmPFC 4 Hz oscillations during fear extinction

Sustained fear expression relies on the maintenance of dmPFC 4 Hz oscillations[46]. We therefore examined how MD bursting is related to the dynamics of these oscillations. The average dmPFC LFP around MD bursts during episodes of high dmPFC 4 Hz revealed a slow oscillatory component centered on a positive peak in the dmPFC LFP, with a peak-to-peak latency compatible with a 4 Hz oscillation (Fig. 7a), suggesting that the MD bursting is organized around positive peaks of dmPFC 4 Hz oscillations. In agreement with this, the MD bursting (pooled across mice) displayed a significant phase-locking to dmPFC 4 Hz in both control and FN-MD inhibited mice, with a preferred phase close to the positive peaks of dmPFC 4 Hz oscillations (Fig. 7b), but the amplitude of modulation appeared larger following FN-MD inhibition. In concordance with this global MD observation, individual MD neurons showed phase-locking around a preferred phase close to the positive phase of dmPFC LFP (Fig. 7c), and a higher concentration of the individual preferred phases (measured by the distribution of angular distance between preferred bursting phases and dmPFC 4 Hz positive peak) was observed under FN-MD input inhibition indicating a more consistent phase locking of MD bursting to dmPFC 4 Hz oscillations in this condition (Fig. 7d, Supplementary Fig. 5a). These results

https://doi.org/10.1038/s41467-023-36943-w

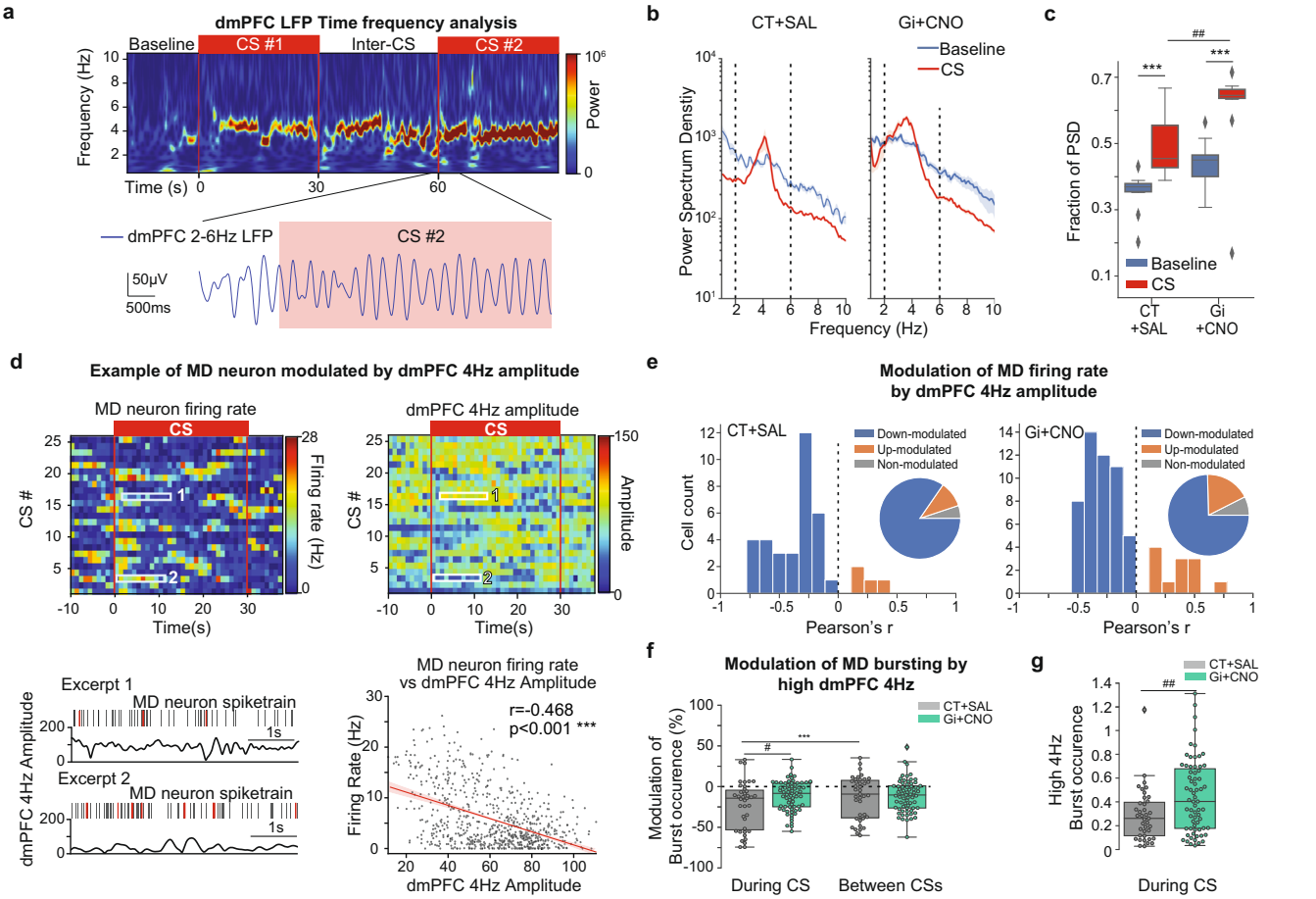

Fig. 6 | Neuronal activity in the MD is modulated by dmPFC 4 Hz LFP oscillations during EXT1. a Representative spectrogram of dmPFC LFP during EXT1 (top), displaying a 4 Hz component induced by the CS. 2–6 Hz filtered LFP traces from dmPFC (blue), showing the apparition of 4 Hz oscillations after the onset of the CS (red rectangle). **b** A 4 Hz component (2–6 Hz) is visible in the Power Spectrum Density (PSD) dmPFC LFP during EXT1 for CT + SAL (left) and Gi+CNO (right), average ± SEM, dashed lines represent the 4 Hz range (2–6 Hz). **c** The fraction of the PSD representing 2–6 Hz oscillations is increased during Extinction compared to Baseline. Wilcoxon test, $^{***}p < 0.001$. The fraction of the PSD during CS is increased in Gi + CNO compared to CT + SAL, Mann–Whitney *U* test, $\#\#p < 0.01$ (CT + SAL = 14 recording sites from 4 mice, Gi + CNO = 15 recording sites from 5 mice). **d** Average firing rate of a MD neuron during EXT1, centered on the onsets of CSs (top left), binned average amplitude 4 Hz oscillations in the dmPFC (top right). Example raster and corresponding trace of amplitude 4 Hz oscillations in the dmPFC, bursts are displayed in red (bottom left). Scatterplot displaying the averaged firing rate (1 s bins) as a function of the corresponding average amplitude 4 Hz oscillations, Linear regression line and confidence interval are shown in red (bottom right). Pearson's correlation coefficient, $^{***}p < 0.001$. **e** Distributions of Pearson's correlation coefficient of MD neurons firing rate and dmPFC 4 Hz amplitude for CT + SAL (top) and Gi + CNO (bottom). **f** Modulation of burst occurrence of MD neurons firing during episodes of high dmPFC 4 Hz. Mann–Whitney *U* test, $\#p < 0.05$. Wilcoxon test, $^{***}p < 0.001$. **g** Distributions of burst occurrence of MD neurons firing during episodes of high dmPFC 4 Hz during CS. Mann–Whitney *U* test, $\#\#\#p < 0.001$. (CT + SAL = 39 neurons recorded from 4 mice, Gi + CNO = 67 neurons recorded from 5 mice). Boxplots represent quartiles and whiskers correspond to range; points are singled as outliers if they deviate more than 1.5 x interquartile range from the nearest quartile. Data available at doi:10.5061/dryad.9kd51c5ng. All tests are two-sided. Detailed statistical results are available in the Supplementary Tables referenced by panel numbers.

show that the MD bursting is temporally organized by dmPFC 4 Hz oscillations during fear extinction, and that the inhibition of FN-MD pathway during extinction increases the phase locking of MD bursting to dmPFC 4 Hz oscillations.

While these results suggest that MD bursting is entrained by dmPFC 4 Hz oscillations, we investigated whether the occurrence MD bursting would reciprocally impact on the amplitude of the later dmPFC 4 Hz oscillations. The comparison of 4 Hz oscillation amplitude 500 ms before and after MD bursting during CS presentations revealed that the amplitude of dmPFC 4 Hz oscillations after MD bursting was significantly higher than before bursting if the bursting occurred during episodes of high dmPFC 4 Hz, in both experimental groups (Fig. 7d). Indeed, this increase in amplitude was higher if the bursting occurred during episodes of high dmPFC 4 Hz compared to episodes of low dmPFC 4 Hz, as displayed by an increased ratio of dmPFC 4 Hz amplitude after/before MD bursting (Fig. 7e). In the case of MD bursting occurring during episodes of low dmPFC 4 Hz, the amplitude after burst was not significantly different from the amplitude preceding the burst (Supplementary Fig. 5b). Thus, these data suggest that MD bursting during episodes of high dmPFC 4 Hz contributes in both groups to the maintenance of these oscillations.

dmPFC-MD 4 Hz coherence is modulated by the FN inputs to MD

Since our data showed that dmPFC 4 Hz oscillations can organize MD neuronal activity, we then investigated the presence of an oscillatory 4 Hz component in the MD LFP. Interestingly, similar to our previous observations in the dmPFC, the presentation of the CS during fear extinction resulted, in both experimental groups, in high levels of 4 Hz oscillations in the LFP of the MD synchronized with the dmPFC oscillations (Fig. 8a). This was evidenced by the presence of peaks in the Power Spectrum Density (PSD) in the 4 Hz range (2–6 Hz) (Fig. 8b), and by an increased fraction of the PSD associated to 4 Hz oscillations when compared to baseline (Fig. 8c).

https://doi.org/10.1038/s41467-023-36943-w

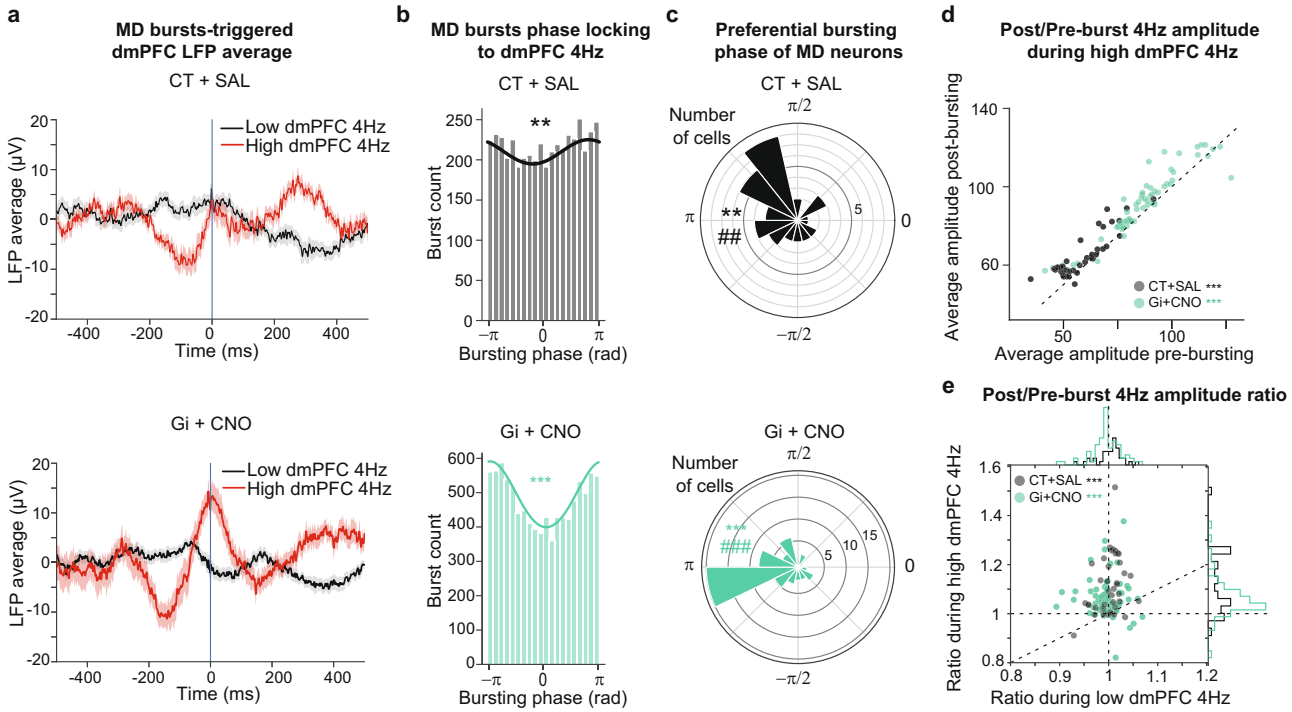

Fig. 7 | Phase-locking of MD bursting to dmPFC 4 Hz LFP oscillations during EXT1 is increased by chemogenetic inhibition of FN-MD. a Average of dmPFC LFP (average ± SEM), around MD bursts occurring during episodes of either high dmPFC 4 Hz (red) or low dmPFC 4 Hz) red, for CT + SAL (top) and Gi+CNO (bottom). **b** Phase histograms of MD bursting during episodes of high 4 Hz, for CT + SAL mice (top) and Gi + CNO mice (bottom). The solid line represents a Von Mises fit associated to the circular distribution. Rayleigh test $^{**}p < 0.01$, $^{***}p < 0.001$. **c** Distributions of preferential bursting phases of MD neurons during episodes of high 4 Hz, for CT + SAL mice (top) and Gi+CNO mice (bottom). Rayleigh test $^{**}p < 0.01$, $^{***}p < 0.001$. Circular V test, testing for a unimodal circular distribution centered on pi (which corresponds to positive peaks in dmPFC 4 Hz oscillations) $\#\#p < 0.01$, $\#\#\#p < 0.001$. **d** The average amplitude of dmPFC 4Hz oscillations during the 500 ms following MD bursting is increased compared to the 500 ms preceding the burst during high dmPFC 4 Hz episodes. **e** The ratios of the average 4 Hz amplitude during the 500 ms after and before MD bursting are higher during episodes of high dmPFC 4 Hz compared to episodes of low dmPFC 4 Hz, vertical and horizontal dotted lines are centered on 1, the diagonal dotted line corresponds to equal ratios in both conditions. Distributions of ratios in both conditions are displayed in the marginal histograms. Wilcoxon test, $^{***}p < 0.001$. (CT + SAL = 39 neurons recorded from 4 mice, Gi + CNO = 67 neurons recorded from 5 mice). Data available at doi:10.5061/dryad.9kd51c5ng. All tests are two-sided. Detailed statistical results are available in the Supplementary Tables referenced by panel numbers.

4 Hz filtered LFP traces (2–6 Hz) from the dmPFC and MD recording sites were strongly correlated in both control and FN-MD inhibited groups (Fig. 8e), with maxima in the cross-correlograms present at short negative lags (Fig. 8e), suggesting that dmPFC 4 Hz oscillations entrain MD 4 Hz oscillations. This observation was confirmed by the presence of a sharp 4 Hz peak in the Generalized Partial Directed Coherence (GPDC) in dmPFC-to-MD direction (Fig. 8f). Furthermore, the 4 Hz GPDC in the dmPFC-to-MD direction was increased in the FN-MD inhibition group compared to the control (Fig. 8g), indicating that the inhibition of the FN-MD pathway increases the contribution of dmPFC to MD 4 Hz oscillations.

Since our data showed that MD bursting was followed by an increase in dmPFC 4 Hz amplitude, we then investigated the effect of MD bursting on the coherence between the MD and dmPFC 4 Hz amplitude. Our study revealed a transient increase in MD-dmPFC 4 Hz coherence after MD bursting during periods of high dmPFC 4 Hz oscillations (Fig. 9a, b). Indeed, when comparing the average baseline coherence preceding the burst (1000–250 ms before the burst) between the two treatments, we observed higher levels of 4 Hz MD-dmPFC coherence in Gi + CNO mice compared to CT + SAL (Fig. 9c), but MD bursting was followed in both cases by a short-term increase in cortico-thalamic coupling for a duration of about one cycle of 4 Hz oscillations (Fig. 9d). Overall, these data further support that MD bursting participates to the maintenance of dmPFC 4 Hz oscillation via MD-dmPFC synchronization.

Discussion

The cerebellum has been known to influence fear learning and fear expression[3,35], review in ref. [37], and it may participate in a variety of other emotional processes[47] via the projections of the FN to multiple brain regions, including limbic structures such as the vlPAG, thalamus and hypothalamus[3,5,48,49]. Furthermore, recent evidence revealed that the cerebellum participates in fear extinction in humans and rodents[3,10–12]. However, the circuits relaying the cerebellar contributions to this emotional learning have remained elusive.

In the current study, we identified cerebellar mechanisms regulating fear extinction through a cerebello-thalamo-cortical pathway. Our findings reveal the existence of a functional disynaptic pathway from the cerebellum to the dmPFC through the thalamic MD: we showed that the cerebellar FN projects to the lateral subregion of thalamic MD, which is reciprocally connected to the dmPFC, and that trans-synaptic experiments from the FN results in labeling of calbindin-positive MD neurons that project to the dmPFC. In addition, optogenetic stimulations of FN input to MD elicit fast activation of MD, consistent with a direct pathway. Interestingly, while non-specific optogenetic stimulation of the FN triggered fast activation of some dmPFC neurons, we did not find fast responses when the stimulation was confined to the MD-projecting FN neurons. This absence (or scarcity) of fast mPFC response is consistent with previous results showing that MD activation may only increase the firing rate in fast-spiking mPFC neurons, and with a modulatory role of the MD inputs on

https://doi.org/10.1038/s41467-023-36943-w

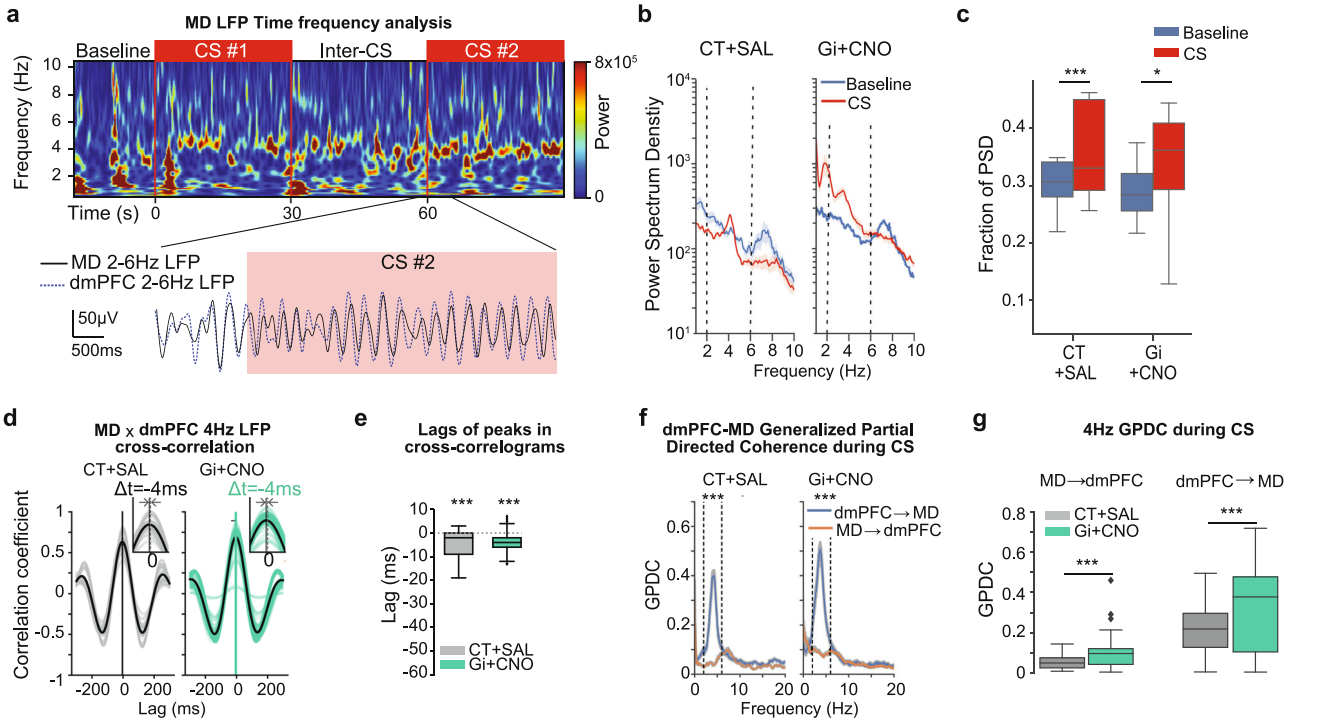

Fig. 8 | dmPFC-MD 4 Hz coherence is increased by chemogenetic inhibition of FN-MD. a Representative spectrogram of MD LFP during EXT1 (top), displaying a 4 Hz component induced by the CS. 2–6 Hz filtered LFP traces from dmPFC (blue), showing the apparition of 4 Hz oscillations after the onset of the CS (red rectangle). **b** A 4 Hz component (2–6 Hz) is visible in the Power Spectrum Density (PSD) MD LFP during EXT1 for CT + SAL (left) and Gi + CNO (right), average ± SEM, dashed lines represent the 4 Hz range (2–6 Hz). **c** The fraction of the PSD representing 2–6 Hz oscillations is increased during Extinction compared to Baseline. Wilcoxon test, $^{***}p < 0.001$ (CT + SAL = 28 recording sites from 4 mice, Gi + CNO = 30 recording sites from 5 mice). **d** Cross-correlation of 2–6 Hz filtered LFP in MD and in dmPFC display maxima at negative lags. Colored lines represent pairwise cross-correlations. Black lines represent averages. **e** Lags of maximum peaks in cross-correlations, Wilcoxon test $^{***}p < 0.001$. **f** Generalized Partial Directed Coherence (GPDC) between dmPFC and MD LFP during CS, Average ± SEM, Wilcoxon test on the 4 Hz GPDC dmPFC->MD versus MD->dmPFC, $^{*}p < 0.05$, $^{**}p < 0.01$, $^{***}p < 0.001$. **g**, 4 Hz GPDC dmPFC -> MD. Mann–Whitney *U* test, $^{*}p < 0.05$, $^{**}p < 0.01$, $^{***}p < 0.001$ (CT + SAL = 28 recording sites in MD and 14 recording sites in MD from 4 mice, Gi+CNO = 30 recording sites in MD and 15 recording sites in the dmPFC from 5 mice). Boxplots represent quartiles and whiskers correspond to range; points are singled as outliers if they deviate more than 1.5 x interquartile range from the nearest quartile. Data available at doi:10.5061/dryad.9kd51c5ng. All tests are two-sided. Detailed statistical results are available in the Supplementary Tables referenced by panel numbers.

mPFC activity in vivo[42]. Another pathway linking the cerebellum and mPFC via the ventral anterior lateral thalamus has been previously hypothesized to explain the cerebellar control of mPFC discharge associated with the conditioned responses in trace eyeblink conditioning[50]. More recently, functional connectivity between the cerebellum and the mPFC has been shown to influence social and repetitive/inflexible behaviors through the ventromedial (VM) thalamus[51]. Both VM and MD are matrix-type thalamus, but their contribution to mPFC activity is functionally distinct since inputs from these two thalamic nuclei target different cell types and layers in the mPFC[52,53].

Cerebellar projections to sub-regions of the MD seem to be conserved across mammalian species, reviewed in ref. [54], and have been proposed to contribute to the cerebello-prefrontal interactions, reviewed in ref. [55]. The FN-MD pathway described in our study is well-positioned to relay cerebellar influence on extinction learning, since cerebellar territories associated to fear have been found in the medial part of the cerebellum[7,8]. In addition, the MD has bidirectional connections with mPFC regions[21,41,56,57], specially the ACC, PL and IL, key brain structures for fear extinction[16–20,27–29], and MD controls dmPFC synaptic plasticity required for fear extinction[25,26].

A remarkable finding in our study is that the specific inhibition of FN input to the MD leads to an impairment of the extinction learning. This effect is primarily effective when starting extinction from high fear expression levels and does not reflect a simple prevention of the expression of fear extinction learning since it failed to affect the fear response when performed only in EXT3. These results suggest that the FN facilitates fear extinction when fear responses are high. Indeed, we found that inhibition of FN-MD projections affects the firing pattern of MD neurons, and notably increases the bursting activity during the CS. While MD bursting, also observed between CS, does not seem to cause freezing, it has been shown to prevent extinction learning. Moreover, while coordinated activities between limbic brain structures are important for fear extinction[33], our work reveals that MD bursting is regulated by the limbic 4 Hz oscillations that take place during fear expression. The dmPFC plays a central role in these oscillations[30], which are synchronized with respiration via the olfactory bulb[46], and regulated by the amygdala[33,45,58]. Interestingly, we also found that the inhibition of this cerebellar output enhances the entrainment of MD bursting to dmPFC 4 Hz oscillations. This is consistent with the role of the cerebellum in modulating brain oscillations and their coordination across different brain regions[59–61], review in ref. [62], as with a modulation of slow oscillations (<10 Hz) in the mPFC[63,64]. In addition, our data show that the amplitude of the dmPFC 4 Hz oscillations is increased after MD bursts, suggesting that the bursts exert a positive feedback participating in the maintenance of these oscillations.

In agreement with previous trans-synaptic work[5], we found that the FN preferentially targets the dmPFC rather the vmPFC via the MD. While extinction learning has been tightly linked to the vmPFC[16,17], failure to extinct fear responses is linked to enhanced dmPFC activity[65] and the dmPFC 4 Hz oscillations play a central role in the maintenance of the fear response[46,65]. Therefore, by dampening the entrainment of MD bursting by dmPFC oscillations, the cerebellum –under physiological conditions- may limit the positive feedback

https://doi.org/10.1038/s41467-023-36943-w

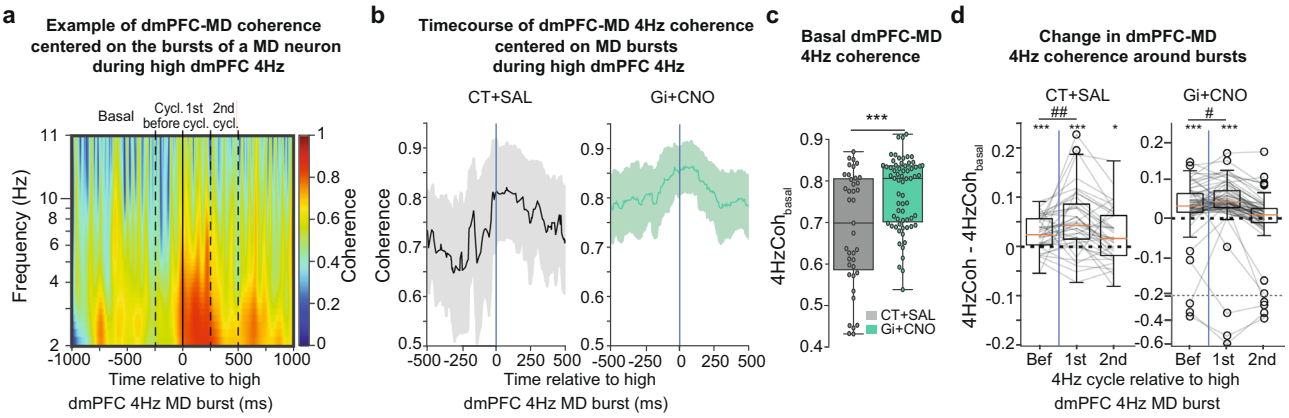

Fig. 9 | MD bursting is followed by high 4 Hz MD-mPFC coherence. a Example of time frequency coherence analysis between dmPFC and MD LFP, centered on the bursting of a MD neuron during episodes of high 4 Hz showing an increase of coherence in the 4 Hz range after the burst. **b**, Average 4 Hz coherence between dmPFC and MD LFP, centered on MD bursting during episode of high 4 Hz for CT + SAL mice (left) and Gi + CNO mice (right), showing an increase of coherence in the 4 Hz range after the burst. **c**, Distributions of basal coherence between dmPFC and MD LFP before MD bursting (−1000 ms to −250 ms) during episodes of high 4 Hz. Mann–Whitney *U* test, $^{***}p < 0.001$. **d** Distributions of increase in coherence between dmPFC and MD LFP during episodes of high 4 Hz, before MD bursting (−250 ms to 0 ms) and during the first and second 4 Hz cycle after bursting. One sample Wilcoxon test, $^{*}p < 0.05$, $^{***}p < 0.001$. Two samples Wilcoxon test, $\#p < 0.05$, $\#\#p < 0.01$ (CT + SAL = 39 neurons recorded from 4 mice, Gi + CNO = 67 neurons recorded from 5 mice). Boxplots represent quartiles and whiskers correspond to range; points are singled as outliers if they deviate more than 1.5 x interquartile range from the nearest quartile. Data available at doi:10.5061/dryad.9kd51c5ng. All tests are two-sided. Detailed statistical results are available in the Supplementary Tables referenced by panel numbers.

exerted by MD on dmPFC 4 Hz oscillations and hence on fear responses[30,46]. Indeed, the drop in freezing response observed in Fig. 4e (top panel) between the end of EXT 2 and beginning of EXT3 when releasing the inhibition of FN-MD projections suggest that this inhibition also promotes the expression of the learned fear response. Our results in high-freezing mice suggest that high MD bursting during high levels of fear expression (>70%) could be particularly effective at preventing the expression of extinction learning. Moreover, recent studies have revealed the importance of the neuronal connections and dynamical synchrony between the dmPFC and vmPFC in extinction learning[66,67]. Our data are therefore consistent with a modulatory role of the dmPFC in fear extinction learning, by which the cerebellum exerts a control over fear extinction.

Finally, our demonstration of the role of cerebellum in facilitating the extinction of the fear response is in concordance with the role of the cerebellum in rapidly adapting the behavior to unexpected situations[3,10,68]. Beyond the classical role of cerebellum in tuning motor behavior, our work provides an anatomo-functional substrate for its role in adapting the emotional behavior strategy. Overall, our work provides support for the role of the cerebellum in psychiatric conditions with deficiencies of fear extinction, such as PTSD, reviewed in ref. [14]. Targeting the lateral cerebellum have been recently shown as a relevant target for the treatment of autism-spectrum disorder[69], while stimulation of the medial cerebellum improved the negative symptoms in schizophrenia[70]. Our work may therefore motivate future research on therapeutic approaches targeting the cerebellum or its projections to the thalamus for the treatment of fear-related and anxiety disorders.

Methods

Animals

Adult male C57BL/6 N mice (Charles River, France,MSR Cat# CRL_27,RRID:IMSR_CRL:27), were housed in groups of 4 mice per cage, with free access to food and water, maintained at 21–22 °C, with a 12 h:12 h light/dark cycle with a constant humidity of 40%. Adult male wild-type mice 8–12 weeks of age were used for all the experiments. Male and female mice are equally suitable for fear conditioning analysis[71], but male mice are bigger and have therefore more strength to carry the implant and preamplifier in electrophysiological experiments. Animal care and experimental procedures followed the European Community Council Directives (authorization number APAFIS#1334-2015070818367911 v3 and APAFIS #29793-202102121752192).

Stereotactic surgeries

Surgeries for tracing, chemogenetic, optogenetic and electrophysiological experiments, were performed in 7–8 weeks-old mice, placed in a stereotaxic frame (Kopf Instruments) after buprenorphine administration, and anaesthetized with isoflurane 2% along the whole procedure. In addition, a local analgesia was administered subcutaneously above the skull with 0.02% of lidocaine. The body temperature was monitored and maintained at 36 °C with a heating pad and a rectal thermometer.

For viral injections and electrodes and optic fiber implantations, the stereotaxic coordinates used for FN (AP: −6.37, ML: ±0.70, DV: −2.12), MD (AP: −1.12, ML: ±0.65, DV: −3.15) and dmPFC (AP: +2.34, ML: ±0.25, DV: −1.5) were taken relative to the bregma, and the depth was considered from the brain surface. Glass capillaries used for viral infusions were kept at the injection site for 5 min after viral infusion before being slowly withdrawn.

Neuroanatomical tracing and histology

For neuroanatomical tracing a group of mice was injected with 100 nl of anterograde AAV1-CB7-CI-mCherry-WPRE-rBG (Upenn Vector) in the FN ($n = 6$), 100 nl CTB-alexa 488 (Invitrogen) in the dmPFC ($n = 6$), or retrograde AAV-Syn-eGFP (Addgene) were injected in the MD ($n = 6$). For trans-synaptic labeling, a group of mice was injected with 75 nl of AAV9-CMV-PI-Cre-rBG (Addgene) in the FN, and 100 nl of AAV1-CAG-Flex-tdTomato-WPRE-bGH in the MD ($n = 3$), and MD sections were used to perform Calbindin immunostaining.

Mice were deeply anesthetized with ketamine 80 mg kg^{-1} and xylazine 10 mg kg^{-1} i.p., and transcardially perfused with formalin (Sigma) 3–4 weeks after the surgery to assess the viral expression. Brains were dissected and kept overnight in formalin at 4 °C and then placed in PBS solution until slicing. Coronal brain sections of 50 or 90 µm were made using a vibratome (Leica VT 1000 S), then dried and mounted with Mowiol (Sigma) or Fluoroshield with DAPI medium (Sigma). The slices were analyzed and imaged using a confocal microscope (Leica TCS Sp8).

The same procedure was used to verify electrode and optic fiber implantation sites and viral expressions for each experiment, mice were perfused as detailed above, and mice with no viral expression or misplacement of the viral infusion, optic fiber or electrode were excluded from the analysis. Electrode placements are summarized in the Supplementary Fig. 6.

Immunohistochemistry

For the immunostaining, 50 μm slices containing MD were washed with PBS-0.3% Triton X-100, blockage of nonspecific sites was assessed by 2 h of incubation with 3% normal donkey serum (NDS). Sections were then incubated in a solution containing monoclonal mouse anti-Calbindin-D-28K (1:300, Sigma, C9848) in PBS-0.3% Triton X-100 with 1.5% NDS at 4 °C for 24 h. After first antibody incubation, slices were rinsed and sections were incubated at room temperature for 2 h with secondary antibody, donkey anti-mouse IgG conjugated to Alexa Fluor 488 (1:300, Invitrogen, R37114). Slices were mounted with Mowiol and analyzed with the confocal microscope.

Fear conditioning and extinction protocol

Previous to behavioral experiments, mice were daily handled during one week. Fear conditioning and extinction protocol were performed in two different chamber configurations (Context A or B), placed inside of a sound-attenuating box (Ugo Basile). The fear conditioning was performed in the Context A, which consisted in a rectangular-shaped Plexiglas chamber, 17 × 17 × 25 cm (L × W × H) dimension, with a grid floor and black and white checker walls, scented with peppermint soup. On fear conditioning day (day 1), mice were left for 5 min to habituate to context A, then they were exposed to 5 presentations of a tone (30 s, 80 dB, 2.7 kHz, representing the CS), that co-terminated with a mild foot-shock (0.5 sec, 0,4 mA, representing the US), and with an interval between CS-US presentations of 120 s. During the following 3 days, mice underwent the fear extinction training, which consisted in 3 days of extinction sessions (EXT1-3). Extinction sessions were performed in the Context B, composed by a yellow cylindrical chamber (17 cm diameter, 25 cm H), grey Plexiglas floor, and vanilla scented. Each extinction session started with 5 min of habituation period in the novel context B, followed by 25 consecutive un-reinforced 30s-long CS presentations, with an interval between CS of 30 s.

Mice were video-tracked using a high-definition video camera, positioned above the testing chambers. Stimuli administration was controlled by the EthoVision XT 14 software (Noldus Information Technology), which assessed also the freezing behavior during the experiments as inactive periods (the threshold of inactivity was set to not detect the breathing movements as active periods). All mice returned to their home cage after the experiments. Analysis of freezing levels in each session was performed by comparisons between groups of the first CS and CS5 for FC, and averaged of CS1-CS5 representing "early" EXT, CS10-CS14 as "middle" EXT, and CS21-CS25 as "late" EXT.

Anxiety tests

Open field, elevated plus maze and dark-light box tests were performed in order to analyze anxiety-like behavior. On week before subjecting the mice to fear conditioning, they were subjected on successive days to anxiety tests, starting with the less anxiogenic, open field test, followed by elevated plus maze and dark-light box. Open field test consisted in a 38 cm diameter circular arena (Noldus), under 40–50 lux luminosity. Each mouse was placed in the center of the arena and allowed to explore freely for 10 min. Frequency of entries to the center of the arena, time spent in center, distance moved in center, were measured. Elevated plus maze test was realized using an elevated (52 cm above the floor), plus-shaped apparatus (Noldus) with 2 open arms (36 ×6 cm L × W) and 2 closed arms (36 × 6 × 25 cm L × W × H), under 40–50 lux luminosity in the open arms. Mice were left to freely explore the arena for 5 min, while assessing the frequency of entries in open and closed arms, time spent in open arms, total distance moved. In the dark-light box test, each mouse was placed in the light zone (luminosity 500–600 lux, 40 × 20 × 20 cm L × W × H dimension) of the apparatus (Noldus) and left to freely explore for 5 min, while assessing the frequency of entries in light zone, time spent in light zone, latency to enter in dark zone (0 lux, 20 × 20 × 20 cm L × W × H dimension), and total distance moved. Mice were video tracked and behavior was analyzed using EthoVision XT 14.

Hot plate and tail immersion tests

Pain sensitivity was analyzed using hot plate and tail immersion assays performed two weeks after the end of the other experiments. Mice were placed on a hot plate (55 °C) (Harvard apparatus), until they jumped or licked their hind paw. The latency to the first reaction was measured. After the hot plate test, tail immersion test was performed. The mice tail tips were immersed in hot water (50 °C) and the latency of the tail flick or withdrawal was measured. All experiments were video tracked.

Chemogenetics

Specific chemogenetic inhibition of the FN neurons projecting to MD was carried out by bilateral injection of 250 nl of a retrograde virus expressing a cre-recombinase in the MD (CAV2-cre-GFP, from Platforme de Vectorologie de Montpellier) in combination with the infusion of 200 nl of inhibitory cre-dependent DREADD (AAV-hSyn-DIO-hM4Di-mCherry, Addgene) bilaterally in FN, adapted from previous works in our team[72] which demonstrated a strong reduction in cerebellar nuclei firing rate upon injection of CNO (1 mg/kg). The behavioral experiments started 10–14 days after the surgery, to ensure the expression of the receptors and the recovery of the mice. Transient inhibition of the FN MD-projecting neurons was assessed by intraperitoneal administration of the clozapine N-oxide (CNO, Tocris Bioscience) dissolved in saline solution (1.25 mg/kg), while a control group received only saline administration, 30 min before the first 2 extinction sessions (EXT1 and EXT2) or 30 min before anxiety or nociceptive tests.

Additional controls were performed to verify the specificity of the pathway inhibition and the DREADD-modulation effect. To corroborate that the CNO dose has not an effect per se in our experimental conditions, a batch of mice (named "Sham" mice) underwent the same surgical procedure with the injection of AAV-hSyn-mCherry instead of the DREADD vector. During behavioral experiments, the Sham mice received either an intraperitoneal injection of saline or CNO solution (1.25 mg/kg), 30 min before the tests, and freezing levels were analyzed in absence of DREADD expression. On the other hand, to verify that the effect observed under DREADD inhibition was specific of the FN terminals in MD, mice were implanted with 30 G cannulas bilaterally in the MD to allow the local infusion of 200 nl of CNO or saline intracranially. During extinction sessions, mice expressing inhibitory DREADD received either sterilized filtered PBS or CNO (0.5 mM) infusion, and another group of Sham mice received CNO (0.5 mM). The intracranial infusions were performed 10 min before the beginning of each session, by using a pump at an infusion speed of 100 nl/min, and a total volume of 250 nl. Freezing levels were analyzed and the positions of the cannulas were corroborated histologically.

Electrophysiological recordings

Extracellular recordings were assessed using standard 16 channels electrode interface boards (EIB-16; Neuralynx), to which 2 cannulas were attached, one for each recorded region, MD and dmPFC. The electrode bundles consisted of nickel chrome wires (16μm diameter, Coating ¼ Hard PAC, KANTHAL Precision Technology) twisted in groups of 6, gold-plated to 100–400 kΩ (cyanure-free gold solution, Sifco). Two bundles were inserted per cannula (stainless steel, 30 Gauge, Phymep). The recording electrodes were then progressively

lowered until they reached the targeted brain structures and the electrode interface boards were cemented to the skull (Dental Parkell Adhesive Resin Cement Super-Bond C&B). Miniature stainless steel screws were implanted on the left parieto-occipital suture, serving as electrical reference and ground. The skin ridges were sutured and mice were allowed to recover in their home cage for at least 10 days. Recordings were performed on a TDT system control by Synapse v95 (Tucker-Davis Technologies, Davis, CA) when no fear conditioning was involved, or on Multi-Channel System W2100 system with their recording software (v1.5.6)

Optogenetics and electrophysiological recordings

The neural activity in the MD and dmPFC was recorded during the optogenetic activation of the contralateral FN neurons. Expression of channelrhodopsin 2 (ChR2) was assessed by injection of an anterograde AAV8-Syn-ChR2-H134R-EYFP (Addgene) in the FN, and an optical was fiber implanted above (200 µm diameter, 0.22 aperture, fixed in a stainless steel ferula, Thor Labs) and contralateral to the recording sites. Electrodes were placed through cannulas in the MD and dmPFC and the EIB were fixed to the skull. The optical stimulations were performed three or four weeks after the surgery (to ensure the ChR2 expression), in freely moving mice. After a 5 min habituation period in an open field (38 cm diameter), the activation of the FN projections was done, using light pulses of 100 ms, at 0.25 Hz, 1 mW, for 30 min (with a 2 min break every 10 min block). The choice of light intensity to stimulate FN neurons was based on the calibration performed in our previous work[3]. The activation of MD and dmPFC neurons by optogenetic stimulation of FN neurons was assessed by computing the Peri-Stimulus Time Histogram (5 ms bins) around the optogenetic stimulation. This PSTH was then normalized using a classical Z-score (subtracting by the mean value of the PSTH during the 100 ms before the stimulation and dividing it by its standard deviation). Normalized PSTH reaching an absolute Z-score value superior to 3 during the 100 ms stimulation were considered responsive.

In another group of mice, the specific activation of the FN-MD pathway was assessed by injecting a cre-dependent anterograde adenovirus expressing ChR2 (AAV-Dio-ChR2-EYFP, Addgene) in the FN, together with a retrograde adenovirus expressing cre-recombinase (AAV-Cre-mCherry, Addgene) in the contralateral MD (left side). The implantation and surgical procedures were identical with the ones described above. The FN MD-projecting neurons were stimulated by pulses of 10 ms, at 0.5 Hz and 1 mW, during 10 min. Luminous stimuli were administered and neural signals were recorded using Tucker Davis Technology System 3 acquisition system (25 Hz sampling rate, RZ2, RV2, Tucker-Davis Technologies) and the spike sorting was performed using Matlab scripts. Viral infusions and implant positions were confirmed histologically when the experiment ended. Analysis of the spike sorted data was performed using Python. The specific activation of MD and dmPFC neurons by optogenetic stimulation of FN MD-projecting neurons was assessed by computing the Peri-Stimulus Time Histogram (5 ms bins) around the optogenetic stimulation. This PSTH was then normalized using a classical Z-score (subtracting by the mean value of the PSTH during the 100 ms before the stimulation and dividing it by its standard deviation). Normalized PSTH reaching an absolute Z-score value superior to 3.5 were considered responsive.

In order to assess the validity of the optostimulation experiments, we performed a control experiment to verify that FN illumination in absence of ChR2 expression does not affect spike firing in the areas recorded. We implanted an optic fiber in the FN together with electrodes in FN, MD and dmPFC, in mice injected with retrograde AAV-GFP (without the expression of ChR2) in the MD, and performed 100 ms illuminations at 0.25 Hz, 1 mW, for 30 min (with a 2 min break every 10 min block), while recording in the FN, MD and dmPFC (Supplementary Fig. 2A–B). There was no variation of firing rate at the population level in the FN, MD and dmPFC (Supplementary Fig. 2C), although we observed 1 neuron in the FN and 3 neurons in the MD reaching the threshold of significant variation of firing rate during the 100 ms of illumination (Supplementary Fig. 2D). However, the transient nature of the mild increase in firing rate suggests a coincidental classification as responsive cells.

Since the wireless transmitter used in the electrophysiological experiments represented a significant hindrance for the movement and was associated with atypical immobile postures (nose down and/or tilted head to rest the preamplifier on the floor or against the wall) which could indifferently reflect freezing or resting, we could not score freezing in these mice.

Chemogenetics and electrophysiological recordings

Mice expressing cre-dependent inhibitory DREADDs in FN MD-projecting neurons (see chemogenetics section) were implanted with electrodes in the MD and dmPFC (as described in "Electrophysiological recordings" section). The neuronal activity of the MD and dmPFC was examined during FC and extinction learning, under chemogenetic inhibition of the FN-MD projections during EXT1 and without manipulation during EXT3. After experiments were concluded, viral expression and electrode positions were confirmed by histology.

Quantification and statistical analysis

Behavioral data analysis. For freezing analysis, the data were analyzed by repeated-measure ANOVA computed with R 3.6.3 (lme package version 3.1-3) and posthoc tests were performed with the package emmeans (version 1.7.0) using Rstudio 4.1.2. During extinction, Early, Middle, Late values of freezing respectively correspond to the average of the 5 first, 5 middle and 5 last CS freezing scores. For other behavioral measures, *t*-test were used (Graph Pad Prism® version 7). All tests used are two-sided (when applicable).

Electrophysiological data analysis

Burst analysis. We quantified the occurrence of bursts in MD, detected using the Robust Gaussian surprise algorithm 1. Spike trains were processed in the following way: Inter-Spike Intervals (ISI) were calculated, then transformed to log (ISI). A central set of ISI was defined as the portion of this distribution lying under [E−1.64*MAD; E + 1.64*MAD], where E is the midpoint of top and bottom 100*p percentile of the log (ISI)s with $p = 0.05$. The central location of this distribution was defined as the median of the central set previously mentioned, and the distribution of log (ISI) was then normalized by subtracting the central location. This normalization process was performed on the entire spike train using a sliding window of half-width 0.2*N/2, where N is the number of spikes in the spike train. The burst-threshold is set as 0.5 percentile of the central distribution. Bursts seeds were defined as normalized ISI being below the burst-threshold. Those seeds were then extended by recursively trying to add the previous and the next normalized ISI, if the addition lead to an increase of the associated *p*-value, the concatenation process was stopped, otherwise it was continued. Overlapping bursts strings were cleaned by keeping the strings with the lowest associated *p*-value, thus making them mutually exclusive. Burst occurrence was computed as the number of bursts strings divided by the duration of the recorded spike trains. The average burst firing rate was calculated as the number of spikes contained within a burst divided by the total duration of burst strings in the spike train.

Local field potential, spectral analysis and phase locking. In order to process the LFP, the raw electrophysiological traces sampled at 25 KHz were filtered between 1 Hz and 200 Hz, then downsampled to 1 kHz. All signals were filtered using the filtfilt function from the package scipy, with zero-phase distortion 5th order Butterworth filters. Power Spectral Densities (PSD) were computed using the welch function from the scipy package. The fraction of the PSD representing 4 Hz

oscillations was defined the integral of the PSD in the 4 Hz range (2–6 Hz) divided by the integral of the PSD from 1 to 100 Hz. To assess the relationship between LFP in the dmPFC and in the MD, Generalized Partial Directed Coherence analysis was performed on the processed LFP traces using the package spectral_connectivity from Eden Kramer Lab (https://github.com/Eden-Kramer-Lab/spectral_connectivity). For the specific analysis of 4 Hz LFP, the processed LFP traces were filtered in the desired frequency band (2–6 Hz) using the filtfilt function from the scipy package, with zero-phase distortion 5th order Butterworth filters. To study the relationship between the timing of MD neuronal activity and the dmPFC 4 Hz oscillations, Hilbert's transform was performed using the function hilbert from the package scipy, allowing the extraction of the instantaneous phase and amplitude of envelope estimated at every sample point of the signal. Phases were expressed in radians, with a phase of 0 corresponding to a negative peak in the 4 Hz LFP. Phase locking analysis of bursting activity was performed by considering the first spike of each bursts. Considering spikes occurring in periods associated to weak 4 Hz oscillations would result in the inclusion of uninformative phases in the analysis. So, in order to prevent this bias, only burst occurring in periods of high 4 Hz were considered. Periods of high 4 Hz were defined as periods were the amplitude of envelope was superior to the median amplitude of envelope during the baseline before the Extinction session plus one median absolute deviation (MAD). In other words, we considered the periods where the Robust Z-score of the amplitude of envelope was superior to 1, creating a spike train corresponding to MD bursting during periods of high 4 Hz oscillations in dmPFC. Von Mises distributions fit on phase distributions were performed using the function vonmises from the package scipy, allowing the computation of the parameter Kappa, indicative of the concentration of a circular distribution. Rayleigh tests and circular V-tests with a preferred direction of pi were performed using the package pingouin, respectively using the functions circ_rayleigh and circ_vtest. In order to assess the relationship between MD bursting and the coherence between dmPFC and MD LFP, we used the function spectral_connectivity included in the package mne, For this, LFP snippets of 2000ms centered on the bursts of each individual MD neurons were extracted from the channels displaying the highest fraction of the PSD corresponding to 4 Hz oscillations in the MD and in the dmPFC, and the coherence between MD and dmPFC LFP was calculated using Morlet wavelets of the first order, yielding a time frequency coherence analysis centered on MD bursts.

Reporting summary

Further information on research design is available in the Nature Portfolio Reporting Summary linked to this article.

Data availability

The data generated during this study have been deposited on the Dryad database with the reference doi:10.5061/dryad.9kd51c5ng.

Code availability

The source code generated during this study have been deposited on the Dryad database with the reference https://doi.org/10.5281/zenodo.7603770.

Material availability

This study did not generate new unique reagents.

References

1. Milad, M. R. & Quirk, G. J. Fear extinction as a model for translational neuroscience: ten years of progress. *Physiol. Behav.* **63**, 129–151 (2012).
2. Maren, S. & Holmes, A. Stress and fear extinction. *Neuropsychopharmacology* **41**, 58–79 (2016).
3. Frontera, J. L. et al. Bidirectional control of fear memories by cerebellar neurons projecting to the ventrolateral periaqueductal grey. *Nat. Commun.* **11**, 5207 (2020).
4. Vaaga, C. E., Brown, S. T. & Raman, I. M. Cerebellar modulation of synaptic input to freezing-related neurons in the periaqueductal grey. *Elife* **9**, e54302 (2020).
5. Fujita, H., Kodama, T. & du Lac, S. Modular output circuits of the fastigial nucleus for diverse motor and nonmotor functions of the cerebellar vermis. *Elife* **9**, e58613 (2020).
6. Apps, R. & Strata, P. Neuronal circuits for fear and anxiety-the missing link. *Nat. Rev. Neurosci.* **16**, 642–643 (2015).
7. Baumann, O. & Mattingley, J. B. Functional topography of primary emotion processing in the human cerebellum. *Neuroimage* **61**, 805–811 (2012).
8. Damasio, A. R. et al. Subcortical and cortical brain activity during the feeling of self-generated emotions. *Nat. Neurosci.* **3**, 1049–1056 (2000).
9. Stoodley, C. J. & Schmahmann, J. D. Functional topography in the human cerebellum: a meta-analysis of neuroimaging studies. *Neuroimage* **44**, 489–501 (2009).
10. Ernst, T. M. et al. The cerebellum is involved in processing of predictions and prediction errors in a fear conditioning paradigm. *Elife* **8**, e46831 (2019).
11. Batsikadze, G. et al. The cerebellum contributes to context-effects during fear extinction learning: a 7T fMRI study. *Neuroimage* **253**, 119080 (2022).
12. Utz, A. et al. Cerebellar vermis contributes to the extinction of conditioned fear. *Neurosci. Lett.* **604**, 173–177 (2015).
13. Rabellino, D., Densmore, M., Theberge, J., McKinnon, M. C. & Lanius, R. A. The cerebellum after trauma: resting-state functional connectivity of the cerebellum in posttraumatic stress disorder and its dissociative subtype. *Hum. Brain Mapp.* **39**, 3354–3374 (2018).
14. Carletto, S. & Borsato, T. Neurobiological correlates of post-traumatic stress disorder: a focus on cerebellum role. *Eur. J. Trauma Dissociation* **1**, 153–157 (2017).
15. Shiba, Y., Santangelo, A. M. & Roberts, A. C. Beyond the medial regions of prefrontal cortex in the regulation of fear and anxiety. Frontiers in systems. *Neuroscience* **10**, 1–13 (2016).
16. Quirk, G. J. & Mueller, D. Neural mechanisms of extinction learning and retrieval. *Neuropsychopharmacology* **33**, 56–72 (2008).
17. Giustino, T. F. & Maren, S. The role of the medial prefrontal cortex in the conditioning and extinction of fear. *Front. Behav. Neurosci.* **9**, 298 (2015).
18. Vidal-Gonzalez, I., Vidal-Gonzalez, B., Rauch, S. L. & Quirk, G. J. Microstimulation reveals opposing influences of prelimbic and infralimbic cortex on the expression of conditioned fear. *Learn. Mem.* **13**, 728–733 (2006).
19. Likhtik, E., Stujenske, J. M., Topiwala, M. A., Harris, A. Z. & Gordon, J. A. Prefrontal entrainment of amygdala activity signals safety in learned fear and innate anxiety. *Nat. Neurosci.* **17**, 106–113 (2014).
20. Tovote, P., Fadok, J. P. & Luthi, A. Neuronal circuits for fear and anxiety. *Nat. Rev. Neurosci.* **16**, 317–331 (2015).
21. Alcaraz, F., Marchand, A. R., Courtand, G., Coutureau, E. & Wolff, M. Parallel inputs from the mediodorsal thalamus to the prefrontal cortex in the rat. *Eur. J. Neurosci.* **44**, 1972–1986 (2016).
22. Hunnicutt, B. J. et al. A comprehensive thalamocortical projection map at the mesoscopic level. *Physiol. Behav.* **176**, 139–148 (2014).
23. Morceau, S., Piquet, R., Wolff, M. & Parkes, S. L. Targeting reciprocally connected brain regions through CAV-2 mediated interventions. *Front. Mol. Neurosci.* **12**, 303 (2019).
24. de Kloet, S. F. et al. Bi-directional regulation of cognitive control by distinct prefrontal cortical output neurons to thalamus and striatum. *Nat. Commun.* **12**, 1994 (2021).

25. Herry, C. & Garcia, R. Prefrontal cortex long-term potentiation, but not long-term depression, is associated with the maintenance of extinction of learned fear in mice. *J. Neurosci.* **22**, 577–583 (2002).
26. Herry, C., Vouimba, R. M. & Garcia, R. Plasticity in the mediodorsal thalamo-prefrontal cortical transmission in behaving mice. *J. Neurophysiol.* **82**, 2827–2832 (1999).
27. Lee, S. et al. Bidirectional modulation of fear extinction by mediodorsal thalamic firing in mice. *Nat. Neurosci.* **15**, 308–314 (2012).
28. Lee, S. & Shin, H. S. The role of mediodorsal thalamic nucleus in fear extinction. *J. Anal. Sci. Technol.* **7**, 39 (2016).
29. Paydar, A. et al. Extrasynaptic GABAA receptors in mediodorsal thalamic nucleus modulate fear extinction learning. *Mol. Brain* **7**, 1–9 (2014).
30. Karalis, N. et al. 4-Hz oscillations synchronize prefrontal-amygdala circuits during fear behavior. *Nat. Neurosci.* **19**, 605–612 (2016).
31. Livneh, U. & Paz, R. Amygdala-prefrontal synchronization underlies resistance to extinction of aversive memories. *Neuron* **75**, 133–142 (2012).
32. Popa, D., Duvarci, S., Popescu, A. T., Lena, C. & Pare, D. Coherent amygdalocortical theta promotes fear memory consolidation during paradoxical sleep. *Proc. Natl Acad. Sci. USA* **107**, 6516–6519 (2010).
33. Ozawa, M. et al. Experience-dependent resonance in amygdalocortical circuits supports fear memory retrieval following extinction. *Nat. Commun.* **11**, 4358 (2020).
34. Dejean, C. et al. Prefrontal neuronal assemblies temporally control fear behaviour. *Nature* **535**, 420–424 (2016).
35. Koutsikou, S. et al. Neural substrates underlying fear-evoked freezing: the periaqueductal grey-cerebellar link. *J. Physiol.* **592**, 2197–2213 (2014).
36. Lawrenson, C. et al. Cerebellar modulation of memory encoding in the periaqueductal grey and fear behaviour. *Elife* **11**, e76278 (2022).
37. Strata, P. The emotional cerebellum. *Cerebellum* **14**, 570–577 (2015).
38. Sacchetti, B., Scelfo, B., Tempia, F. & Strata, P. Long-term synaptic changes induced in the cerebellar cortex by fear conditioning. *Neuron* **42**, 973–982 (2004).
39. Sacchetti, B., Baldi, E., Lorenzini, C. A. & Bucherelli, C. Cerebellar role in fear-conditioning consolidation. *Proc. Natl Acad. Sci. USA* **99**, 8406–8411 (2002).
40. Galliano, E. et al. Synaptic transmission and plasticity at inputs to murine cerebellar Purkinje cells are largely dispensable for standard nonmotor tasks. *J. Neurosci.* **33**, 12599–12618 (2013).
41. Kuramoto, E. et al. Individual mediodorsal thalamic neurons project to multiple areas of the rat prefrontal cortex: a single neuron-tracing study using virus vectors. *J. Comp. Neurol.* **525**, 166–185 (2017).
42. Schmitt, L. I. et al. Thalamic amplification of cortical connectivity sustains attentional control. *Nature* **545**, 219–223 (2017).
43. Jeon, D. et al. Observational fear learning involves affective pain system and Cav1.2 Ca2+ channels in ACC. *Nat. Neurosci.* **13**, 482–488 (2010).
44. Ko, D., Wilson, C. J., Lobb, C. J. & Paladini, C. A. Detection of bursts and pauses in spike trains. *J. Neurosci. Methods* **211**, 145–158 (2012).
45. Davis, P., Zaki, Y., Maguire, J. & Reijmers, L. G. Cellular and oscillatory substrates of fear extinction learning. *Nat. Neurosci.* **20**, 1624–1633 (2017).
46. Bagur, S. et al. Breathing-driven prefrontal oscillations regulate maintenance of conditioned-fear evoked freezing independently of initiation. *Nat. Commun.* **12**, 2605 (2021).
47. Schmahmann, J. D. In *Handbook of the Cerebellum and Cerebellar Disorders* (eds Manto, M. et al.) (Springer, 2013).
48. Teune, T. M., Van Der Burg, J., Van Der Moer, J., Voogd, J. & Ruigrok, T. J. H. Topography of cerebellar nuclear projections to the brain stem in the rat. *Prog. Brain Res.* **124**, 141–172 (2000).
49. Groenewegen, H. J. Organization of the afferent connections of the mediodorsal thalamic nucleus in the rat, related to the mediodorsal-prefrontal topography. *Neuroscience* **24**, 379–431 (1988).
50. Siegel, J. J. & Mauk, M. D. Persistent activity in prefrontal cortex during trace eyelid conditioning: dissociating responses that reflect cerebellar output from those that do not. *J. Neurosci.* **33**, 15272–15284 (2013).
51. Kelly, E. et al. Regulation of autism-relevant behaviors by cerebellar-prefrontal cortical circuits. *Nat. Neurosci.* **23**, 1102–1110 (2020).
52. Anastasiades, P. G., Collins, D. P. & Carter, A. G. Mediodorsal and ventromedial thalamus engage distinct L1 circuits in the prefrontal cortex. *Neuron* **109**, 314–330.e314 (2021).
53. Collins, D. P., Anastasiades, P. G., Marlin, J. J. & Carter, A. G. Reciprocal circuits linking the prefrontal cortex with dorsal and ventral thalamic nuclei. *Neuron* **98**, e364 (2018).
54. Hintzen, A., Pelzer, E. A. & Tittgemeyer, M. Thalamic interactions of cerebellum and basal ganglia. *Brain Struct. Funct.* **223**, 569–587 (2018).
55. Bostan, A. C., Dum, R. P. & Strick, P. L. Cerebellar networks with the cerebral cortex and basal ganglia. *Trends Cogn. Sci.* **17**, 241–254 (2013).
56. Parnaudeau, S., Bolkan, S. S. & Kellendonk, C. The Mediodorsal thalamus: an essential partner of the prefrontal cortex for cognition. *Biol. Psychiatry* **83**, 648–656 (2018).
57. Ray, J. P. & Price, J. L. The organization of the thalamocortical connections of the mediodorsal thalamic nucleus in the rat, related to the ventral forebrain–prefrontal cortex topography. *J. Comp. Neurol.* **323**, 167–197 (1992).
58. Hagihara, K. M. et al. Intercalated amygdala clusters orchestrate a switch in fear state. *Nature* **594**, 403–407 (2021).
59. Popa, D. et al. Functional role of the cerebellum in gamma-band synchronization of the sensory and motor cortices. *J. Neurosci.* **33**, 6552–6556 (2013).
60. Lindeman, S. et al. Cerebellar Purkinje cells can differentially modulate coherence between sensory and motor cortex depending on region and behavior. *Proc. Natl Acad. Sci. USA* **118**, e2015292118 (2021).
61. Lesting, J. et al. Directional theta coherence in prefrontal cortical to amygdalo-hippocampal pathways signals fear extinction. *PLoS ONE* **8**, e77707 (2013).
62. McAfee, S. S., Liu, Y., Sillitoe, R. V. & Heck, D. H. Cerebellar coordination of neuronal communication in cerebral cortex. *Front. Syst. Neurosci.* **15**, 781527 (2021).
63. Parker, K. L. et al. Delta-frequency stimulation of cerebellar projections can compensate for schizophrenia-related medial frontal dysfunction. *Mol. Psychiatry* **22**, 647–655 (2017).
64. McAfee, S. S., Liu, Y., Sillitoe, R. V. & Heck, D. H. Cerebellar Lobulus Simplex and Crus I differentially represent phase and phase difference of prefrontal cortical and hippocampal oscillations. *Cell Rep.* **27**, 2328–2334.e2323 (2019).
65. Burgos-Robles, A., Vidal-Gonzalez, I. & Quirk, G. J. Sustained conditioned responses in prelimbic prefrontal neurons are correlated with fear expression and extinction failure. *J. Neurosci.* **29**, 8474–8482 (2009).
66. Watanabe, M., Uematsu, A. & Johansen, J. P. Enhanced synchronization between prelimbic and infralimbic cortices during fear extinction learning. *Mol. Brain* **14**, 175 (2021).
67. Marek, R., Xu, L., Sullivan, R. K. P. & Sah, P. Excitatory connections between the prelimbic and infralimbic medial prefrontal cortex show a role for the prelimbic cortex in fear extinction. *Nat. Neurosci.* **21**, 654–658 (2018).
68. Ohmae, S. & Medina, J. F. Climbing fibers encode a temporal-difference prediction error during cerebellar learning in mice. *Nat. Neurosci.* **18**, 1798–1803 (2015).

69. Stoodley, C. J. et al. Altered cerebellar connectivity in autism and cerebellar-mediated rescue of autism-related behaviors in mice. *Nat. Neurosci.* **20**, 1744–1751 (2017).
70. Brady, R. O. Jr. et al. Cerebellar-prefrontal network connectivity and negative symptoms in schizophrenia. *Am. J. Psychiatry* **176**, 512–520 (2019).
71. Kaluve, A. M., Le, J. T. & Graham, B. M. Female rodents are not more variable than male rodents: a meta-analysis of preclinical studies of fear and anxiety. *Neurosci. Biobehav Rev.* **143**, 104962 (2022).
72. Varani, A. P. et al. Dual contributions of cerebellar-thalamic networks to learning and offline consolidation of a complex motor task. Preprint at *bioRxiv*. https://doi.org/10.1101/2020.08.27.270330 (2020).
73. Allen Institute for Brain Science (2004). Allen Mouse Brain Atlas [dataset]. http://mouse.brain-map.org/ Allen Institute for Brain Science (2011).
74. Lein, E. S. et al. Genome-wide atlas of gene expression in the adult mouse brain. *Nature* **445**, 168–176 (2007).

Acknowledgements

This work was supported by Fondation pour la Recherche Medicale (FRM DPP20151033983 to D.P. and FRM FRM-EQU202103012770 to C.L.) and by Agence Nationale de Recherche to D.P. (ANR-21-CE37-0025 CerebellEmo) and to C.L. (ANR-17-CE37-0009 Mopla, ANR-17-CE16-0019 Synpredict, ANR-21-CE16-0017 PomPom) and by the Labex Memolife and the Institut National de la Santé et de la Recherche Médicale (France). This work was supported by University of Medicine and Pharmacy "Carol Davila", a project number 819/11.01.2019 corresponding to the salary to I.A.G. We thank the Imaging Facility at IBENS (IMACHEM-IBiSA, France-BioImaging ANR-10-INBS-04, FRC Rotary International France, Investments for the future, ANR-10-LABX-54 MEMOLIFE). The authors are grateful to Dagmar Timmann and Thomas Watson for critical reading of the manuscript.

Author contributions

C.L. and D.P. acquired the funding, designed and supervised the project; J.L.F. performed and analyzed the anatomical and chemogenetic behavioral experiments; R.W.S., I.A.G., H.B.A., and M.A. performed the electrophysiological experiments and data curation (spike sorting, histological verification). R.W.S. and C.L. analyzed the electrophysiological experiments. All authors interpreted results, participated to the writing and approved the final manuscript.

Competing interests

The authors declare no competing interests.

Additional information

Supplementary information The online version contains supplementary material available at https://doi.org/10.1038/s41467-023-36943-w.

Correspondence and requests for materials should be addressed to Clément Léna.

Peer review information *Nature Communications* thanks Erik Carlson, Dagmar Timmann and the other, anonymous, reviewer(s) for their contribution to the peer review of this work. Peer reviewer reports are available.

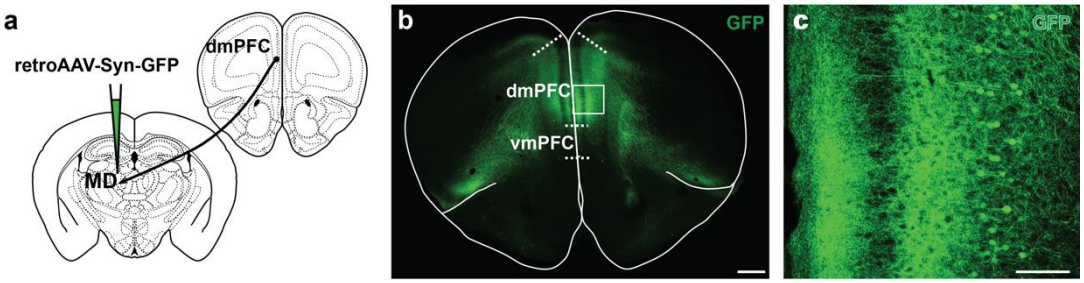

Supplementary Fig. 1. dmPFC neurons project to the MD. a, Retrograde tracing strategy by injection of retrograde AAV-GFP in the MD. **b,** dmPFC-MD projecting neurons expressing retrograde AAV-GFP (green, scale bar, 500 µm). **c,** Zoom-in of dmPFC section from (**b**), GFP+ neurons in cortical layers of the dmPFC projecting to MD (scale bar, 100 µm). n=3 replicates. Brain schematic in panel (a) modified from the Allen Mouse Brain Atlas and Allen Reference Atlas – Mouse Brain[73,74] http://atlas.brain-map.org/atlas?atlas=1#atlas=1&plate=100960384, http://atlas.brain-map.org/atlas?atlas=1#atlas=1&plate=100960136, http://atlas.brain-map.org/atlas?atlas=1#atlas=1&plate=100960240.

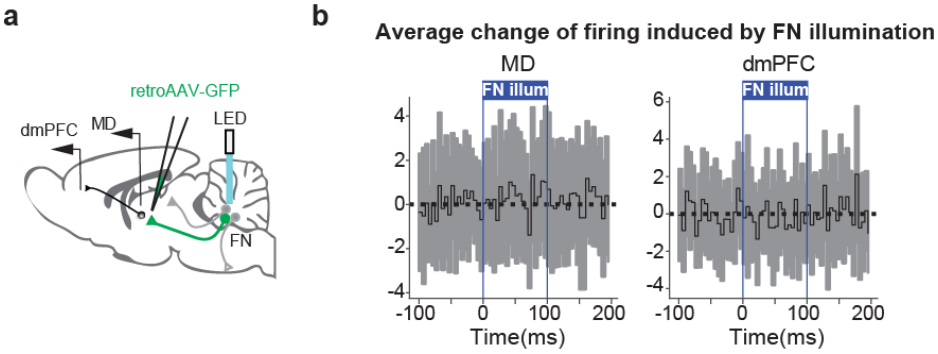

Supplementary Fig. 2. Cell responses to FN illumination in absence of ChR2 expression. a, Strategy used for the FN illumination control experiment, representing the local injection of retrograde AAV-eGFP in the MD and implantation of recording electrodes in MD and dmPFC. **b**, PSTH (5 ms bins) displaying the change in firing rate (average ± SD) during 100 ms illumination of the FN in MD (left), and in dmPFC (right). The light stimulation is represented by a blue rectangle.

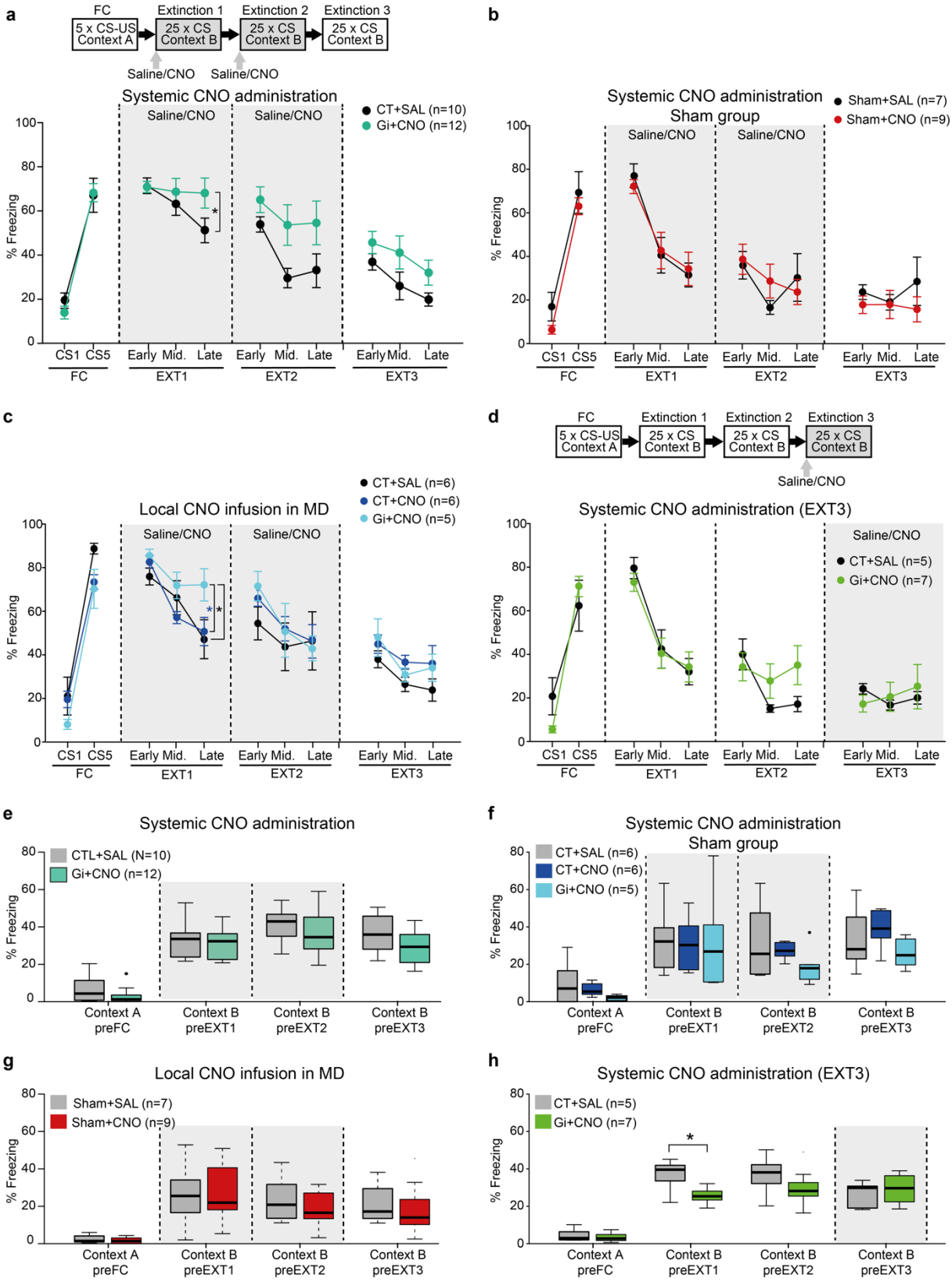

Supplementary Fig. 3. Specific chemogenetic inhibition of FN terminals in MD modulates fear extinction learning. a, Top panel: classical fear conditioning and extinction protocol used, with Saline or CNO administration during extinctions 1 and 2. Bottom: same data as Fig. 4e without separating high-freezing and low-freezing mice; a reduction of fear extinction is still visible in EXT1. Lines represent mean ± SEM. Posthoc t-test, * $p<0.05$. **b**, Verification that the CNO dose used has not effect on freezing in absence of DREADD-Gi expression (Sham mice); no differences in freezing levels were found between sham mice injected i.p. with CNO or saline (Sham+SAL, n = 7; Sham+CNO, n = 9). Posthoc t-test, $p > 0.5$. **c,** Specific inhibition of FN-terminals in MD by intracranial CNO infusion in EXT1 and EXT2 sessions (Gi+CNO, n = 5) reduced extinction of fear

response compared to the control groups (CT+SAL, n = 6; CT+CNO, n = 6). **d,** Top panel: fear conditioning and extinction protocol with Saline or CNO administration in EXT3 in mice expressing inhibitory DREADD in FN neurons projecting to MD. Inhibition of FN input to MD during EXT3 (Gi+CNO, n = 7) did not affect the expression of CS-freezing response compared to control group (CT+SAL, n = 5). Lines represent mean ± SEM. Posthoc t-test, p>0.5 Holm-Sidak corrected. **e-h** baseline freezing levels before FC (context A) and before each extinction session (context B). A small difference between groups was observed in the EXT1 baseline freezing for the late inhibition experiment (**h**); this reveals a small heterogeneity between the groups of animals which, at that time of the protocol received both the same treatment; however the inter-group difference in baseline freezing fell below significance during EXT2 (and EXT3). Posthoc t-test, * p<0.05. Boxplots represent quartiles and whiskers correspond to range; points are singled as outliers if they deviate more than 1.5 x interquartile range from the nearest quartile. Data available at doi:10.5061/dryad.9kd51c5ng All tests are two-sided. Detailed statistical results are available in the Supplementary Tables.

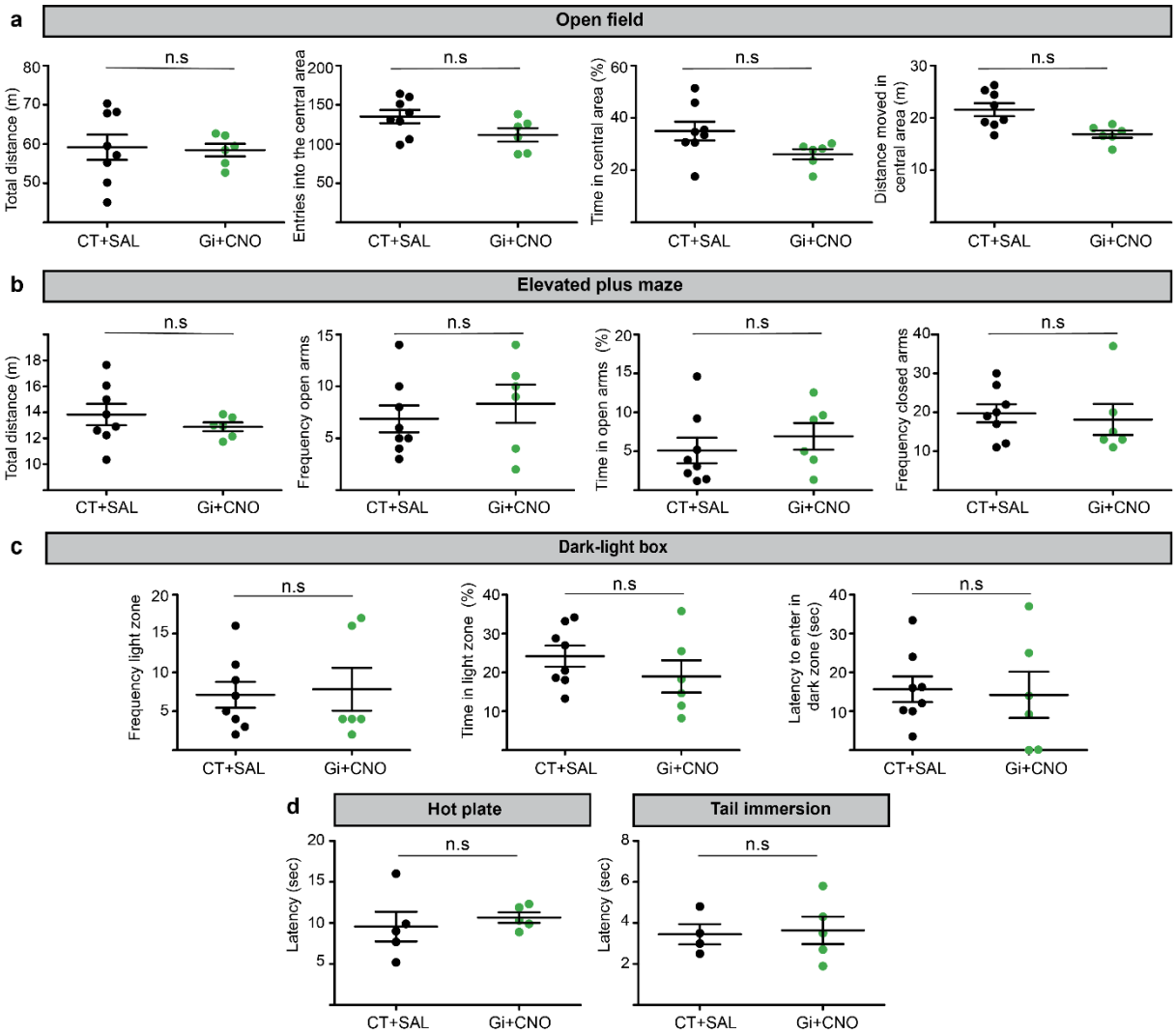

Supplementary Fig. 4. FN input to MD does not contribute either to anxiety like behavior or nociception. a-c, FN-MD chemogenetic inhibition (Gi+CNO, n = 6) had no effect on anxiety like behavior compared to the control mice (CT+SAL, n = 8) in the open field (**a**), in the elevated plus maze (**b**), or in the dark-light box (**c**). **d,** Inhibition of FN-MD projections had not significant effect on hot plate (Gi+CNO, n = 5; CT+SAL, n = 5) (left) or tail immersion (Gi+CNO, n = 4; CT+SAL, n = 4) (right) tests compared to the control. Scatter dot plot with mean ± SEM, n.s.: Mann-Whitney U test, p > 0.05. Data available at doi:10.5061/dryad.9kd51c5ng . All tests are two-sided. Detailed statistical results are available in the Supplementary Tables.

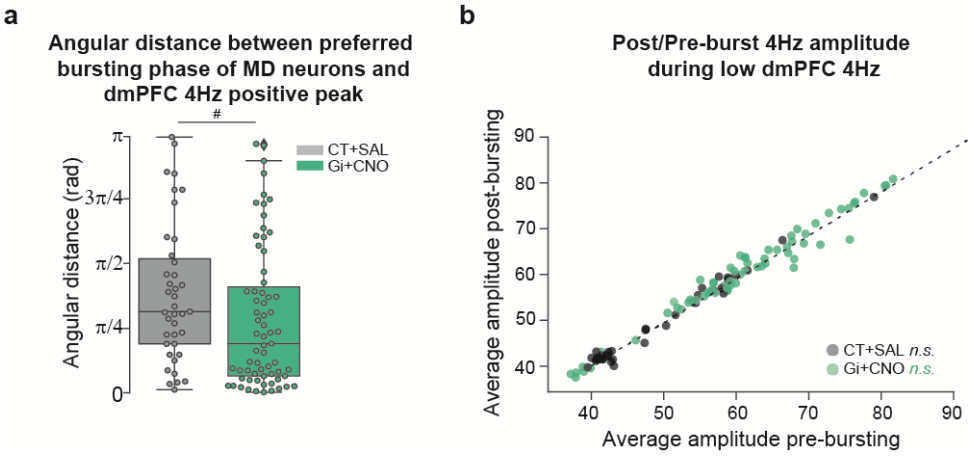

Supplementary Fig. 5. The inhibition of FN inputs to MD induces a greater phase locking to dmPFC 4Hz positive peaks and MD bursting is not associated to an increase in 4Hz amplitude during periods of low dmPFC 4Hz. a, Distributions of angular distance between referential bursting phases of MD neurons and pi (positive peaks in dmPFC 4Hz oscillations). Mann-Whitney U test, #p=0.01. **b**, The average 4 Hz amplitude of the 500 ms following MD bursting is not increased during episodes of low 4 Hz compared to the 500 ms preceding the burst. Wilcoxon test. All tests are two-sided. Detailed statistical results are available in the Supplementary Tables. Data available at doi:10.5061/dryad.9kd51c5ng

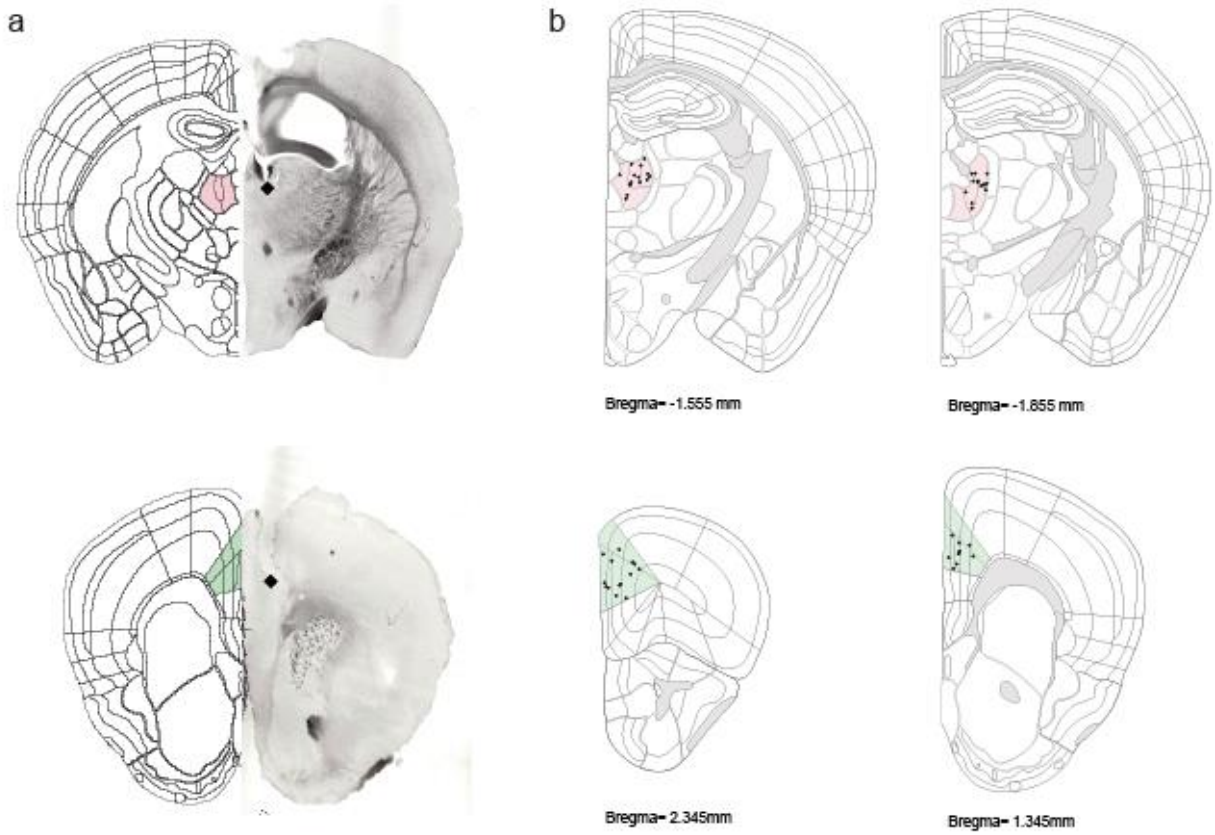

Supplementary Figure 6. Histological placement of the electrodes. a, example brain slices of MD (top) and dmPFC (bottom). An atlas schematic is provided on the left, where the the MD (pink) and dmPFC (green) are highlighted. The estimated tip of the bundle is labeled by the black losange. **b,** summary of the electrode position within the MD and dmPFC. All brain schematics are modified from the Allen Mouse Brain Atlas and Allen Reference Atlas – Mouse Brain[73,74] https://atlas.brain-map.org/atlas?atlas=1&plate=100960260 and http://atlas.brain-map.org/atlas?atlas=1#atlas=1&plate=100960365 for panel a, and https://atlas.brain-map.org/atlas?atlas=1&plate=100960244, https://atlas.brain-map.org/atlas?atlas=1&plate=100960232 https://atlas.brain-map.org/atlas?atlas=1&plate=100960360 https://atlas.brain-map.org/atlas?atlas=1&plate=100960360 for panel b.

Experiment	region	n cells	N mice
FN stimulation	MD	158.00	10.00
	dmPFC	36.00	7.00
FN-MD stimulation	MD	90.00	8.00
	dmPFC	48.00	8.00

Supplementary Table 1: Statistics for Optogenetic recordings.

Group	Group	Phase	region	n cells	N mice
Recorded neuron	CT+SAL	FC	MD	36.00	4.00
		EXT1	MD	39.00	4.00
		EXT3	MD	22.00	4.00
	Gi+CNO	FC	MD	49.00	5.00
		EXT1	MD	67.00	5.00
		EXT3	MD	51.00	5.00

Supplementary Table 2: Statistics for Chemogenetic recordings.

Group	Phase	region	n channels	N mice
CT+SAL	EXT1	MD	28.00	4.00
		dmPFC	14.00	4.00
Gi+CNO	EXT1	MD	30.00	5.00
		dmPFC	15.00	5.00

Supplementary Table 3: Statistics for LFP channels.

Value	Test	Structure	Statistic	p-value	Sig.
DeltaFR	One sample Wilcoxon test	MD	14.00	<0.001	***
DeltaFR	One sample Wilcoxon test	dmPFC	0.00	<0.001	***

Supplementary Table 4: Statistics for Fig 3f.

Mice	Phase	Effect	ANOVA	p-value	Sig.
High-freezing mice	FC	CS	F(1,8)=51.04	9.156e-05	***
		Treatment	F(1,8)=0.7107	0.4234	n.s.
		CS:Treatment	F(1,8)=0.01367	0.9098	n.s.
	EXT1	CS	F(2,18)=2.067	0.1556	n.s.
		Treatment	F(1,9)=5.952	0.03739	*
		CS:Treatment	F(2,18)=4.346	0.02884	*
	EXT2	CS	F(2,18)=4.637	0.02376	*
		Treatment	F(1,9)=8.956	0.01514	*
		CS:Treatment	F(2,18)=3.06	0.07178	n.s.
	EXT3	CS	F(2,18)=3.715	0.04459	*
		Treatment	F(1,9)=1.757	0.2177	n.s.
		CS:Treatment	F(2,18)=0.3146	0.734	n.s.
Low-freezing mice	FC	CS	F(1,8)=94.43	1.051e-05	***
		Treatment	F(1,8)=0.1369	0.721	n.s.
		CS:Treatment	F(1,8)=1.389	0.2725	n.s.
	EXT1	CS	F(218)=4.472	0.0265	*
		Treatment	F(19)=0.03038	0.8655	n.s.
		CS:Treatment	F(218)=0.5615	0.58	n.s.
	EXT2	CS	F(218)=12.88	0.0003373	***
		Treatment	F(19)=0.06678	0.8019	n.s.
		CS:Treatment	F(218)=0.2771	0.7611	n.s.
	EXT3	CS	F(218)=18.59	4.184e-05	*
		Treatment	F(19)=1.609	0.2365	n.s.
		CS:Treatment	F(218)=3.51	0.05161	n.s.

Supplementary Table 5: Statistics for Fig 4e ANOVAs.

Mice	Group 1	Group 2	Phase	CS period	Estimate (Grp1-Grp2)	SE	df	t	p-value	sig
High-freezing mice	Gi+CNO	CT+SAL	FC	CS1	7.41	10.91	16.00	0.68	0.51	n.s.
				CS5	5.60	10.91	16.00	0.51	0.61	n.s.
			EXT1	Early	1.83	8.30	23.84	0.22	0.83	n.s.
				Middle	-17.50	8.30	23.84	-2.11	0.05	*
				Late	-27.52	8.30	23.84	-3.31	0.00	**
			EXT2	Early	-18.81	13.76	15.75	-1.37	0.19	n.s.
				Middle	-49.02	13.76	15.75	-3.56	0.00	**
				Late	-37.85	13.76	15.75	-2.75	0.01	*
			EXT3	Early	-18.43	14.09	13.81	-1.31	0.21	n.s.
				Middle	-19.85	14.09	13.81	-1.41	0.18	n.s.
				Late	-11.63	14.09	13.81	-0.83	0.42	n.s.
Low-freezing mice	Gi+CNO	CT+SAL	FC	CS1	3.42	7.82	15.15	0.44	0.67	n.s.
				CS5	-7.97	7.82	15.15	-1.02	0.32	n.s.
			EXT1	Early	-0.67	9.26	16.69	-0.07	0.94	n.s.
				Middle	2.89	9.26	16.69	0.31	0.76	n.s.
				Late	-6.28	9.26	16.69	-0.68	0.51	n.s.
			EXT2	Early	-3.52	11.50	13.65	-0.31	0.76	n.s.
				Middle	1.01	11.50	13.65	0.09	0.93	n.s.
				Late	-5.46	11.50	13.65	-0.47	0.64	n.s.
			EXT3	Early	0.83	6.68	14.37	0.12	0.90	n.s.
				Middle	-10.47	6.68	14.37	-1.57	0.14	n.s.
				Late	-12.72	6.68	14.37	-1.91	0.08	n.s.

9.00

Supplementary Table 6: Statistics for Fig 4e contrasts.

Mice	Effect	ANOVA	p-value	Sig.
High-freezing mice	Treatment	F(1,9)=0.00802	0.93	n.s.
	Context	F(3,21)=63.65	0.00	***
	Treatment:Context	F(3,21)=1.607	0.22	n.s.
Low-freezing mice	Treatment	F(1,9)=2.532	0.15	n.s.
	Context	F(3,27)=36.52	0.00	***
	Treatment:Context	F(3,27)=3.189	0.04	*

Supplementary Table 7: Statistics for Fig 4f ANOVAs.

Mice	context	Group1	Group2	Estimate (Grp1-Grp2)	SE	df	t.ratio	p.value	Sig.
High-freezing mice	context A	CNO	SAL	-4.01	6.27	9.00	-0.64	0.54	n.s.
	context B preEXT1	CNO	SAL	-13.28	6.27	9.00	-2.12	0.06	n.s.
	context B preEXT2	CNO	SAL	0.87	6.79	9.00	0.13	0.90	n.s.
	context B preEXT3	CNO	SAL	-8.94	6.79	9.00	-1.32	0.22	n.s.
Low-freezing mice	context A	CNO	SAL	-6.02	4.56	9.00	-1.32	0.22	n.s.
	context B preEXT1	CNO	SAL	6.79	4.56	9.00	1.49	0.17	n.s.
	context B preEXT2	CNO	SAL	-9.77	4.56	9.00	-2.14	0.06	n.s.
	context B preEXT3	CNO	SAL	-8.24	4.56	9.00	-1.81	0.10	n.s.

Supplementary Table 8: Statistics for Fig 4f Contrasts.

Experiment	Phase	Effect	ANOVA	p-value	Sig.
EXT1 EXT2 systemic	FC	CS	F(1,18)=133.7	<0.001	***
		Treatment	F(1,18)=0.1936	0.665	n.s.
		CS:Treatment	F(1,18)=0.5587	0.464	n.s.
	EXT1	CS	F(2,40)=5.935	0.006	**
		Treatment	F(1,20)=1.538	0.2308	n.s.
		CS:Treatment	F(2,40)=3.38	0.04401	*
	EXT2	CS	F(2,40)=11.73	<0.001	***
		Treatment	F(1,20)=3.982	0.0598	n.s.
		CS:Treatment	F(2,40)=1.439	0.2492	n.s.
	EXT3	CS	F(2,40)=12.22	<0.001	***
		Treatment	F(1,20)=2.908	0.1036	n.s.
		CS:Treatment	F(2,40)=0.5247	0.5958	n.s.
EXT1 EXT2 systemic SHAM	FC	CS	F(1,28)=93.32	<0.001	***
		Treatment	F(1,28)=2.245	0.1452	n.s.
		CS:Treatment	F(1,28)=0.1467	0.7046	n.s.
	EXT1	CS	F(2,28)=40.45	<0.001	***
		Treatment	F(1,14)=8.389e-06	0.9977	n.s.
		CS:Treatment	F(2,28)=0.3898	0.6808	n.s.
	EXT2	CS	F(2,28)=3.663	0.03862	*
		Treatment	F(1,14)=0.1186	0.7357	n.s.
		CS:Treatment	F(2,28)=1.427	0.257	n.s.
	EXT3	CS	F(2,28)=0.3484	0.7088	n.s.
		Treatment	F(1,14)=0.8528	0.3714	n.s.
		CS:Treatment	F(2,28)=0.89	0.4219	n.s.
Local infusion in MD	FC	CS	F(1,28)=180.6	<0.001	***
		Treatment	F(2,28)=3.891	0.03228	*
		CS:Treatment	F(2,28)=0.8224	0.4497	n.s.
	EXT1	CS	F(2,28)=28.78	<0.001	***
		Treatment	F(2,14)=2.142	0.1543	n.s.
		CS:Treatment	F(4,28)=2.719	0.0497	*
	EXT2	CS	F(2,28)=8.082	0.001	**
		Treatment	F(2,14)=0.2967	0.7479	n.s.
		CS:Treatment	F(4,28)=0.7401	0.5726	n.s.
	EXT3	CS	F(2,28)=6.821	0.0038	**
		Treatment	F(2,14)=2.013	0.1705	n.s.
		CS:Treatment	F(4,28)=0.2776	0.89	n.s.
EXT3 systemic	FC	CS	F(1,12)=75.87	<0.001	***
		Treatment	F(1,12)=0.2627	0.6175	n.s.
		CS:Treatment	F(1,12)=3.799	0.07506	n.s.
	EXT1	CS	F(2,24)=38.94	<0.001	***
		Treatment	F(1,12)=0.07624	0.7872	n.s.
		CS:Treatment	F(2,24)=0.3532	0.7061	n.s.
	EXT2	CS	F(2,24)=3.517	0.04576	*
		Treatment	F(1,12)=0.8919	0.3636	n.s.
		CS:Treatment	F(2,24)=2.072	0.1479	n.s.
	EXT3	CS	F(2,24)=0.3027	0.7416	n.s.
		Treatment	F(1,12)=0.007115	0.9342	n.s.
		CS:Treatment	F(2,24)=0.8221	0.4515	n.s.

Supplementary Table 9: Statistics for SupFig 3a-d ANOVAs.

Experiment	Group 1	Group 2	Phase	CS period	Estimate	SE	df	t	p-value	Sig.
EXT1 EXT2 systemic	Gi+CNO	CT+SAL	FC	CS1	5.41	6.52	35.74	0.83	0.41	n.s.
				CS5	-1.18	6.52	35.74	-0.18	0.86	n.s.
			EXT1	Early	0.58	7.44	35.33	0.08	0.94	n.s.
				Middle	-5.50	7.44	35.33	-0.74	0.46	n.s.
				Late	-16.90	7.44	35.33	-2.27	0.03	*
			EXT2	Early	-11.17	10.57	29.90	-1.06	0.30	n.s.
				Middle	-24.00	10.57	29.90	-2.27	0.03	*
				Late	-21.66	10.57	29.90	-2.05	0.05	*
			EXT3	Early	-8.80	7.92	30.63	-1.11	0.28	n.s.
				Middle	-15.16	7.92	30.63	-1.91	0.07	n.s.
				Late	-12.18	7.92	30.63	-1.54	0.13	n.s.
EXT1 EXT2 systemic SHAM	SHAM+CNO	SHAM+SAL	FC	CS1	10.62	7.98	28.00	1.33	0.19	n.s.
				CS5	6.30	7.98	28.00	0.79	0.44	n.s.
			EXT1	Early	4.99	9.62	28.58	0.52	0.61	n.s.
				Middle	-2.14	9.62	28.58	-0.22	0.83	n.s.
				Late	-2.78	9.62	28.58	-0.29	0.77	n.s.
			EXT2	Early	-2.77	10.23	31.52	-0.27	0.79	n.s.
				Middle	-12.12	10.23	31.52	-1.19	0.24	n.s.
				Late	6.68	10.23	31.52	0.65	0.52	n.s.
			EXT3	Early	5.76	8.77	28.79	0.66	0.52	n.s.
				Middle	1.00	8.77	28.79	0.11	0.91	n.s.
				Late	12.88	8.77	28.79	1.47	0.15	n.s.
Local infusion in MD	CT+SAL	Gi+CNO	FC	CS1	13.02	8.02	28.00	1.62	0.25	n.s.
				CS5	18.46	8.02	28.00	2.30	0.07	n.s.
			EXT1	Early	-9.18	8.60	26.25	-1.07	0.54	n.s.
				Middle	-5.64	8.60	26.25	-0.66	0.79	n.s.
				Late	-24.95	8.60	26.25	-2.90	0.02	*
			EXT2	Early	-17.08	12.65	27.10	-1.35	0.38	n.s.
				Middle	-7.57	12.65	27.10	-0.60	0.82	n.s.
				Late	3.72	12.65	27.10	0.29	0.95	n.s.
			EXT3	Early	-10.01	7.76	37.80	-1.29	0.41	n.s.
				Middle	-4.30	7.76	37.80	-0.55	0.84	n.s.
				Late	-10.21	7.76	37.80	-1.32	0.40	n.s.
	CT+SAL	CT+CNO	FC	CS1	1.56	7.64	28.00	0.20	0.98	n.s.
				CS5	15.33	7.64	28.00	2.01	0.13	n.s.
			EXT1	Early	-6.66	8.20	26.25	-0.81	0.70	n.s.
				Middle	9.11	8.20	26.25	1.11	0.52	n.s.
				Late	-3.52	8.20	26.25	-0.43	0.90	n.s.
			EXT2	Early	-11.52	12.06	27.10	-0.96	0.61	n.s.
				Middle	-8.29	12.06	27.10	-0.69	0.77	n.s.
				Late	0.20	12.06	27.10	0.02	1.00	n.s.
			EXT3	Early	-6.96	7.40	37.80	-0.94	0.62	n.s.
				Middle	-10.15	7.40	37.80	-1.37	0.37	n.s.
				Late	-12.18	7.40	37.80	-1.65	0.24	n.s.
	Gi+CNO	CT+CNO	FC	CS1	-11.46	8.02	28.00	-1.43	0.34	n.s.
				CS5	-3.13	8.02	28.00	-0.39	0.92	n.s.
			EXT1	Early	2.51	8.60	26.25	0.29	0.95	n.s.
				Middle	14.74	8.60	26.25	1.71	0.22	n.s.
				Late	21.43	8.60	26.25	2.49	0.05	*
			EXT2	Early	5.57	12.65	27.10	0.44	0.90	n.s.
				Middle	-0.72	12.65	27.10	-0.06	1.00	n.s.
				Late	-3.52	12.65	27.10	-0.28	0.96	n.s.
			EXT3	Early	3.05	7.76	37.80	0.39	0.92	n.s.
				Middle	-5.85	7.76	37.80	-0.75	0.73	n.s.
				Late	-1.98	7.76	37.80	-0.25	0.96	n.s.
EXT3 systemic	CT+SAL	Gi+CNO	FC	CS1	15.19	8.77	23.99	1.73	0.10	n.s.
				CS5	-8.78	8.77	23.99	-1.00	0.33	n.s.
			EXT1	Early	6.54	9.70	26.38	0.67	0.51	n.s.
				Middle	1.95	9.70	26.38	0.20	0.84	n.s.
				Late	-2.18	9.70	26.38	-0.22	0.82	n.s.
			EXT2	Early	5.69	11.22	26.84	0.51	0.62	n.s.
				Middle	-12.62	11.22	26.84	-1.12	0.27	n.s.
				Late	-17.87	11.22	26.84	-1.59	0.12	n.s.
			EXT3	Early	6.78	10.24	23.75	0.66	0.51	n.s.
				Middle	-3.79	10.24	23.75	-0.37	0.71	n.s.
				Late	-5.11	10.24	23.75	-0.50	0.62	n.s.

Supplementary Table 10: Statistics for SupFig 3a-d contrasts.

Experiment	Effect	ANOVA	p-value	Sig.
EXT1 EXT2 systemic	Group	F(1,20)=1.315,	0.27	n.s.
	Context	F(3,54)=62.02,	0.00	***
	Group:Context	F(3,54)=0.3499,	0.79	n.s.
EXT1 EXT2 systemic SHAM	Group	F(2,14)=0.5874,	0.57	n.s.
	Context	F(3,42)=25.29,	0.00	***
	Group:Context	F(6,42)=0.7821,	0.59	n.s.
Local infusion in MD	Group	F(1,14)=0.147,	0.71	n.s.
	Context	F(3,42)=22.59,	0.00	***
	Group:Context	F(3,42)=0.6034,	0.62	n.s.
EXT3 systemic	Group	F(1,10)=1.364,	0.27	n.s.
	Context	F(3,30)=64.24,	0.00	***
	Group:Context	F(3,30)=3.188,	0.04	*

Supplementary Table 11: Statistics for SupFig 3e-h ANOVAs.

group	context	Group 1	Group 2	Estimate	SE	df	t.ratio	p.value	Sig.
EXT1 EXT2 systemic	CONTEXT A	CT+SAL	Gi+CNO	3.81	4.01	20.00	0.95	0.35	n.s.
	CONTEXT B preEXT1	CT+SAL	Gi+CNO	1.76	4.01	20.00	0.44	0.67	n.s.
	CONTEXT B preEXT2	CT+SAL	Gi+CNO	4.15	4.19	20.00	0.99	0.33	n.s.
	CONTEXT B preEXT3	CT+SAL	Gi+CNO	7.38	4.19	20.00	1.76	0.09	n.s.
EXT1 EXT2 systemic SHAM	CONTEXT A	SHAM+SAL	SHAM+CNO	0.71	5.90	14.00	0.12	0.91	n.s.
	CONTEXT B preEXT1	SHAM+SAL	SHAM+CNO	-2.78	5.90	14.00	-0.47	0.64	n.s.
	CONTEXT B preEXT2	SHAM+SAL	SHAM+CNO	5.54	5.90	14.00	0.94	0.36	n.s.
	CONTEXT B preEXT3	SHAM+SAL	SHAM+CNO	3.21	5.90	14.00	0.54	0.59	n.s.
Local infusion in MD	CONTEXT A	Gi+CNO	Gi+SAL	-8.00	8.62	14.00	-0.93	0.63	n.s.
	CONTEXT A	Gi+CNO	SHAM+CNO	-4.41	8.62	14.00	-0.51	0.87	n.s.
	CONTEXT A	Gi+SAL	SHAM+CNO	3.59	8.22	14.00	0.44	0.90	n.s.
	CONTEXT B preEXT1	Gi+CNO	Gi+SAL	0.05	8.62	14.00	0.01	1.00	n.s.
	CONTEXT B preEXT1	Gi+CNO	SHAM+CNO	2.29	8.62	14.00	0.27	0.96	n.s.
	CONTEXT B preEXT1	Gi+SAL	SHAM+CNO	2.24	8.22	14.00	0.27	0.96	n.s.
	CONTEXT B preEXT2	Gi+CNO	Gi+SAL	-12.61	8.62	14.00	-1.46	0.34	n.s.
	CONTEXT B preEXT2	Gi+CNO	SHAM+CNO	-8.00	8.62	14.00	-0.93	0.63	n.s.
	CONTEXT B preEXT2	Gi+SAL	SHAM+CNO	4.62	8.22	14.00	0.56	0.84	n.s.
	CONTEXT B preEXT3	Gi+CNO	Gi+SAL	-7.09	8.62	14.00	-0.82	0.70	n.s.
	CONTEXT B preEXT3	Gi+CNO	SHAM+CNO	-12.72	8.62	14.00	-1.48	0.33	n.s.
	CONTEXT B preEXT3	Gi+SAL	SHAM+CNO	-5.63	8.22	14.00	-0.68	0.78	n.s.
EXT3 systemic	CONTEXT A	CT+SAL	Gi+CNO	1.23	4.46	10.00	0.28	0.79	n.s.
	CONTEXT B preEXT1	CT+SAL	Gi+CNO	10.81	4.46	10.00	2.42	0.04	*
	CONTEXT B preEXT2	CT+SAL	Gi+CNO	6.62	4.46	10.00	1.48	0.17	n.s.
	CONTEXT B preEXT3	CT+SAL	Gi+CNO	-2.90	4.46	10.00	-0.65	0.53	n.s.

Supplementary Table 12: Statistics for SupFig3e-h Contrasts.

Parameter	Kruskal	p-value	Sig.	Group1	Group2	p-value	Sig.
Total Distance	1.04	0.59	n.s.	CT+SAL	Gi+CNO	0.94	n.s.
Entries Central Area	3.37	0.18	n.s.	CT+SAL	Gi+CNO	0.21	n.s.
Percentage time Central Area	4.61	0.10	n.s.	CT+SAL	Gi+CNO	0.10	n.s.
Distance moved Central Area	5.30	0.07	n.s.	CT+SAL	Gi+CNO	0.06	n.s.

Supplementary Table 13: Statistics for SupFig 4a.

Parameter	Kruskal	p-value	Sig.	Group1	Group2	p-value	Sig.
Distance moved	0.71	0.70	n.s.	CT+SAL	Gi+CNO	0.83	n.s.
Frequency open arms	0.79	0.67	n.s.	CT+SAL	Gi+CNO	0.82	n.s.
Percentage time opened arms	1.16	0.56	n.s.	CT+SAL	Gi+CNO	0.70	n.s.
Frequency closed arms	2.51	0.28	n.s.	CT+SAL	Gi+CNO	0.64	n.s.

Supplementary Table 14: Statistics for SupFig 4b.

Parameter	Kruskal	p-value	Sig.	Group1	Group2	p-value	Sig.
Frequency Light zone	1.71	0.43	n.s.	CT+SAL	Gi+CNO	0.96	n.s.
Percentage time Light zone	1.67	0.43	n.s.	CT+SAL	Gi+CNO	0.48	n.s.
Latency to enter Dark Zone	0.28	0.87	n.s.	CT+SAL	Gi+CNO	0.95	n.s.

Supplementary Table 15: Statistics for SupFig 4c.

Parameter	Kruskal	p-value	Sig.	Group1	Group2	p-value	Sig.
Hot plate Latency	1.37	0.50	n.s.	CT+SAL	Gi+CNO	0.64	n.s.
Tail immersion Latency	0.03	0.98	n.s.	CT+SAL	Gi+CNO	1.00	n.s.

Supplementary Table 16: Statistics for SupFig 4d.

Parameter	Phase	Group 1	Group 2	Test	Stat	p-value	Sig.
Bursts per second baseline	FC	CT+SAL	Gi+CNO	Mann Whitney U	698.00	0.10	n.s.
	EXT1	CT+SAL	Gi+CNO	Mann Whitney U	819.00	0.00	**
	EXT3	CT+SAL	Gi+CNO	Mann Whitney U	440.00	0.10	n.s.
Bursts per second CS	FC	CT+SAL	Gi+CNO	Mann Whitney U	771.00	0.16	n.s.
	EXT1	CT+SAL	Gi+CNO	Mann Whitney U	899.50	0.01	*
	EXT3	CT+SAL	Gi+CNO	Mann Whitney U	439.00	0.14	n.s.
Average burst firing rate baseline	FC	CT+SAL	Gi+CNO	Mann Whitney U	697.00	0.14	n.s.
	EXT1	CT+SAL	Gi+CNO	Mann Whitney U	1154.00	0.29	n.s.
	EXT3	CT+SAL	Gi+CNO	Mann Whitney U	504.00	0.29	n.s.
Average burst firing rate CS	FC	CT+SAL	Gi+CNO	Mann Whitney U	733.00	0.25	n.s.
	EXT1	CT+SAL	Gi+CNO	Mann Whitney U	1145.00	0.27	n.s.
	EXT3	CT+SAL	Gi+CNO	Mann Whitney U	547.00	0.43	n.s.

Supplementary Table 17: Statistics for Fig 5.

Parameter	Group	Phase 1	Phase 2	Test	Stat	p-value	Sig.
Bursts per second baseline	CT+SAL	FC	EXT1	Mann Whitney U	625.00	0.208	n.s.
		EXT1	EXT3	Mann Whitney U	128.00	<0.001	###
	Gi+CNO	FC	EXT3	Mann Whitney U	904.00	<0.001	###
		EXT1	EXT3	Mann Whitney U	613.00	<0.001	###
Bursts per second CS	CT+SAL	FC	EXT1	Mann Whitney U	539.00	0.803	n.s.
		EXT1	EXT3	Mann Whitney U	197.00	<0.001	###
	Gi+CNO	FC	EXT3	Mann Whitney U	1042.50	<0.001	###
		EXT1	EXT3	Mann Whitney U	1121.00	<0.001	###
Average burst firing rate baseline	CT+SAL	FC	EXT1	Mann Whitney U	501.00	0.018	#
		EXT1	EXT3	Mann Whitney U	162.00	<0.001	###
	Gi+CNO	FC	EXT3	Mann Whitney U	712.00	<0.001	###
		EXT1	EXT3	Mann Whitney U	586.00	<0.001	###
Average burst firing rate CS	CT+SAL	FC	EXT1	Mann Whitney U	478.00	0.018	#
		EXT1	EXT3	Mann Whitney U	163.00	<0.001	###
	Gi+CNO	FC	EXT3	Mann Whitney U	779.00	<0.001	###
		EXT1	EXT3	Mann Whitney U	650.00	<0.001	###

Supplementary Table 18: Statistics for Fig 5 bis.

Variable	Group	Test	Condition 1	Condition 2	Statistic	p-value	Sig.
Fraction of PSD	CT+SAL	Wilcoxon	Baseline	CS	0.00	<0.001	***
	Gi+CNO	Wilcoxon	Baseline	CS	1.00	<0.001	***

Supplementary Table 19: Statistics for Fig 6c.

Variable	Condition	Test	Condition 1	Condition 2	Statistic	p-value	Sig.
Fraction of PSD	CS	Mann Whitney U	CT+SAL	Gi+CNO	22.00	0.00	##

Supplementary Table 20: Statistics for Fig 6c bis.

Group	Test	Statistic	p-value	Sig.
CT+SAL during CS	One sample Wilcoxon test	100.00	<0.001	***
Gi+CNO during CS	One sample Wilcoxon test	460.00	<0.001	***
CT+SAL between CSs	One sample Wilcoxon test	212.00	0.0129	*
Gi+CNO between CSs	One sample Wilcoxon test	467.00	<0.001	***

Supplementary Table 21: Statistics for Fig 6f.

Condition 1	Condition 2	Test	Statistic	p-value	Sig.
CT+SAL during CS	Gi+CNO during CS	Mann Whitney U	1013.00	0.0274	#
CT+SAL between CSs	Gi+CNO between CSs	Mann Whitney U	1295.00	0.4712	n.s.
CT+SAL during CS	CT+SAL between CSs	Wilcoxon	136.00	<0.001	***
Gi+CNO during CS	Gi+CNO between CSs	Wilcoxon	990.00	0.3519	n.s.

Supplementary Table 22: Statistics for Fig 6f bis.

Variable	Test	Condition 1	Condition 2	Statistic	p-value	Sig.
Burst occurence	Mann Whitney U	CT+SAL	Gi+CNO	890.00	0.00	##

Supplementary Table 23: Statistics for Fig 6g.

Value	Test	Group	Z	p-value	Sig.
MD bursting phase	Rayleigh test	CT+SAL	5.67	0.0034	**
	Rayleigh test	Gi+CNO	90.56	<0.001	***

Supplementary Table 24: Statistics for Fig 7b.

Value	Test	Group	Z	p-value	Sig.
MD neurons preferential bursting phase	Rayleigh test	CT+SAL	4.67	0.0085	**
	Circular V-test (dir=pi)	CT+SAL	12.50	0.0023	##
	Rayleigh test	Gi+CNO	17.98	<0.001	***
	Circular V-test (dir=pi)	Gi+CNO	33.94	<0.001	###

Supplementary Table 25: Statistics for Fig 7c.

Value	Category	Test	Group	Statistic	p-value	Sig.
Average dmPFC 4Hz relative to MD bursting (prior vs post bursting)	High 4Hz episode	Wilcoxon	CT+SAL	35.00	<0.001	***
		Wilcoxon	Gi+CNO	143.00	<0.001	***

Supplementary Table 26: Statistics for Fig 7d.

Value	Test	Group	Statistic	p-value	Sig.
Ratio Post/Pre-burst 4Hz amplitude (low vs high 4Hz episode)	Wilcoxon	CT+SAL	31.00	<0.001	***
	Wilcoxon	Gi+CNO	215.00	<0.001	***

Supplementary Table 27: Statistics for Fig 7e.

Variable	Test	Condition 1	Condition 2	Statistic	p-value	Sig.
Angular distance	Mann Whitney U	CT+SAL	Gi+CNO	973.00	0.01	#

Supplementary Table 28: Statistics for SupFig 5a.

Value	Category	Test	Group	Statistic	p-value	Sig.
Average dmPFC 4Hz relative to MD bursting (prior vs post bursting)	Low 4Hz episode	Wilcoxon	CT+SAL	338.00	0.47	n.s.
		Wilcoxon	Gi+CNO	953.00	0.25	n.s.

Supplementary Table 29: Statistics for SupFig 5b.

Variable	Group	Test	Condition 1	Condition 2	Statistic	p-value	Sig.
Fraction of PSD	CT+SAL	Wilcoxon	Baseline	CS	0.00	<0.001	***
	Gi+CNO	Wilcoxon	Baseline	CS	68.00	0.0326	*

Supplementary Table 30: Statistics for Fig 8c.

Variable	Group	Test	Statistic	p-value	Sig.
Lag of peak cross-correlation	CT+SAL	Wilcoxon	456.00	<0.001	***
dmPFC - MD 4Hz LFP	Gi+CNO	Wilcoxon	351.00	<0.001	***

Supplementary Table 31: Statistics for Fig 8e.

Variable	Group	Test	Direction 1	Direction 2	Statistic	p-value	Sig.
4Hz range GPDC EXT1	CT+SAL	Wilcoxon	dmPFC->MD	MD->dmPFC	87.00	<0.001	***
	Gi+CNO	Wilcoxon	dmPFC->MD	MD->dmPFC	925.00	<0.001	***

Supplementary Table 32: Statistics for Fig 8f.

Value	Test	Group 1	Group 2	Statistic	p-value	Sig.
4Hz GPDC dmPFC->MD	Mann Whitney U	CT+SAL	Gi+CNO	8045.00	<0.001	***
4Hz GPDC MD->dmPFC	Mann Whitney U	CT+SAL	Gi+CNO	5894.00	<0.001	***

Supplementary Table 33: Statistics for Fig 8g.

Value	Test	Group 1	Group 2	Statistic	p-value	Sig.
Basal dmPFC-MD 4Hz coherence before MD bursting	Mann Whitney U	CT+SAL	Gi+CNO	809.00	<0.001	***

Supplementary Table 34: Statistics for Fig 9c.

Test	Group	Value 1	Value 2	Statistic	p-value	Sig.
Wilcoxon test	CT+SAL	4HzCohbasal	4HzCoh 1st cycle before burst	98.00	<0.001	***
		4HzCohbasal	4HzCoh 1st cycle after burst	95.00	<0.001	***
		4HzCohbasal	4HzCoh 2nd cycle after burst	223.00	0.0197	*
	Gi+SAL	4HzCohbasal	4HzCoh 1st cycle before burst	366.00	<0.001	***
		4HzCohbasal	4HzCoh 1st cycle after burst	247.00	<0.001	***
		4HzCohbasal	4HzCoh 2nd cycle after burst	842.00	0.0635	n.s.

Supplementary Table 35: Statistics for Fig 9d.

Test	Group	Value 1	Value 2	Statistic	p-value	Sig.
Wilcoxon test	CT+SAL	4HzCoh 1st cycle before burst	4HzCoh 1st cycle after burst	202.00	0.01	##
	Gi+SAL	4HzCoh 1st cycle before burst	4HzCoh 1st cycle after burst	761.00	0.02	#

Supplementary Table 36: Statistics for Fig 9d bis.

5 Discussion

5.1 Limitations of the studies

5.1.1 Diversity of cerebellar nuclei neurons

In our studies, we typically consider the output of the cerebellum as partitioned into the 3 main cerebellar nuclei, being the fastigial nucleus (FN), the interposed nucleus (IN) and the dentate nucleus (DN). However, many evidences tend to point towards an anatomical and functional heterogeneity between the neurons from a same cerebellar nucleus (Fujita et al. 2020; Kebschull, Richman, et al. 2020; Kebschull, Casoni, et al. 2023).

Targeting cerebellar nuclei neurons is a powerful way to investigate cerebellar function. As an example, one of our studies is particularly interested in cerebello-thalamic projections originating from the cerebellar fastigial nucleus projecting to the medio-dorsal thalamus involved in the regulation of cortico-thalamo-cortical synchrony and extinction of fear memory (Frontera, Sala, et al. 2023). It was recently showed that the FN was composed of distinct sub-populations of projection neurons, having different anatomical characteristics, gene expression and projection targets (Fujita et al. 2020). Although this study revealed that MD-projecting FN neurons belong to a single sub-population of neurons named F4, which also projects to several

other targets such as the ventro-medial and centro-lateral thalamus, it is possible that the F4 sub-population is itself heterogeneous. Indeed, a recent study revealed that glutamatergic projection neurons of the cerebellar nuclei were composed of intermingled clusters of sub-populations named class-A and class-B projection neurons (Kebschull, Richman, et al. 2020; Kebschull, Casoni, et al. 2023). In the case of PAG-projecting neurons, collaterals were visible in several structures including the MD and PF thalamic nuclei.

Although the pathways that we study may be restricted to one of these sub-populations of cerebellar nuclei neurons, we cannot rule out the possibility that there can be different sub-populations contributing to cerebello-thalamic pathways having different functions and computations either via the same thalamic nucleus or via differential collateralization to other structures.

5.1.2 Perturbation of cerebellar output

The neurons of the cerebellar nuclei were described as spontaneously regular spiking (Jahnsen 1986), with firing rates as high as several tens of Hz in slices (Raman, Gustafson, et al. 2000) as well as in-vivo (Özcan et al. 2020). In particular, glutamatergic neurons of the cerebellar nuclei display high regularity, and higher average firing rate compared to GABAergic neurons (Özcan et al. 2020).

This suggests that projection neurons from the cerebellar neurons are intrinsically tonically active and fast spiking. This tonic activity has some implications for the interpretation of experiments of perturbation of the cerebellar output. Indeed, if the modulation of the activity of cerebellar projection neurons is responsible for the support of a brain function, the ideal perturbation would be to prevent these modulations while maintaining the spontaneous behaviour of the cell. However, this is impossible with the current optogenetic and chemogenetic silencing, as they alter neuronal activity beyond this point. Indeed, most commonly used optogenetic silencing tools can lead to a complete silencing of neuronal activity during illumination (Wiegert et al. 2017). In the case of inhibitory DREADDs, the binding with CNO leads to a decreased excitability of the neuron, which in our study did not completely silence neuronal activity, and only down-modulated it by 50% (Varani et al. 2020).

In the case of the cerebello-thalamic pathway, the reduction of a tonic excitatory input to the thalamus, even incomplete, could have dramatic consequences. More specifically, it could contribute to a hyperpolarization which would favor de-inactivation of low-threshold calcium channel-driven and then favor bursts of activity

(Destexhe et al. 2002). A reduction of excitator inputs could thus somewhat paradoxically favor higher frequency activity through bursting. Moreover, shifting the baseline state of neurones could not only disrupt its firing patterns but also create highly non-physiological shifts of activity, and create behavioral consequences beyond the physiological functions of the cerebellum. In the particular case of our MD study, the reduced excitator drive applied to the MD neurons by inhibitory DREADD in the afferent cerebellar inputs could explain the increased bursting activity (Frontera, Sala, et al. 2023), which incidentally is known to influence extinction learning (Lee, Ahmed, et al. 2012). Nonetheless, the fact that the inhibition of the pathway leads to an increased oscillatory coupling between the thalamus and the cortex is an indication that the cerebellum actively controls cortico-thalamic synchronization, and is not just providing an excitatory tone to the thalamus.

Moreover, both optogenetic and chemotogenetic tools have temporal and/or spatial specificity limitations which can impair their use. Typically, optogenetics tools have a great spatial and temporal specificity, as their spatial specificity is limited by the extent of the illumination pattern and their temporal specificity is limited by the activation and deactivation kinetics of the opsin used (Wiegert et al. 2017; Dugué, Akemann, et al. 2012; Dugué, Lörincz, et al. 2014). However, specifically in the case of optogenetic silencing, the properties of the opsins lead to instabilities if opened for more than few seconds, especially in the case of ion pumps which can alter ionic homoeostasis, limiting their use for long-lasting inhibitions (Wiegert et al. 2017; Zhang, Yang, et al. 2019).

On the other hand, chemogenetic tools display a lower temporal and spatial specificity, but are overall more suited for longer-term perturbation of neuronal activity (Roth 2016; White et al. 2017), which makes it a great tool for behavioural perturbations (Whissell et al. 2016; Roth 2016). However, both temporal and spatial specificity of chemogenetic perturbations are going to be heavily dependent not only on the accuracy of the targeted expression of the DREADD but also on the mode of administration of CNO. Indeed, CNO is usually administered either systemically or with intra-cranial micro-injections, with systemic injections leading to slow onset time and brain-wide presence of CNO, while intra-cranial micro-injections lead to a fast onset and more restricted activation of DREADDs receptors, limited by the spread of the CNO injection. Nonetheless, the effect of chemogenetic manipulation can persists for up to 6 hours (Whissell et al. 2016), as its offset is dependent on the systemic elimination of CNO. Thus, using chemogenetic tools to reversibly perturb neuronal activity during short periods is impossible in-vivo.

These properties of optogenetic and chemogenetic tools prevented us to reliably perturb neuronal activity only during trials or only during resting periods in the accelerating rotarod protocol, and lead to potential mixed effects of chemogenetic inhibition during the rotarod session. Similarly, the chemogenetic inhibition of the FN-MD pathway during extinction of fear memory (Frontera, Sala, et al. 2023) was not restricted to the extinction session and persisted during the hours following the end of the session, which could potentially alter memory consolidation mechanisms.

Furthermore, as silencing neuronal activity implies constant function of the silencing tool, it may lead to a plethora of undesired effects in the long term (Wiegert et al. 2017). Specifically, a prolonged optogenetic stimulation or inhibition can lead to tissue heating, and chronic chemogenetic inhibition could induce desensitization, homeostatic adaptations and intrinsic plasticity (Wiegert et al. 2017). Nonetheless, for the cerebellar nuclei, observations from our lab suggest that the repeated administration of CNO does not induce massive shift of baseline firing of cerebellar nuclei neurons expressing an inhibitory DREADD (Varani et al. 2020).

5.1.3 Potential involvement of cerebello-thalamic collaterals

The cerebellum projects to a wide variety of targets in the brain, including the diencephalon, mesencephalon and medulla oblongata (Novello et al. 2022). Strikingly, the thalamus is a profuse diencephalic target of the cerebellum, as many thalamic nuclei receive projections from the cerebellar nuclei (Ichinohe et al. 2000; Teune et al. 2000; Fujita et al. 2020; Novello et al. 2022).

However, single cerebellar nuclei neurons were shown to project to multiple targets, emitting collaterals not only to the thalamus, but also to other structures such as the tectum, the midbrain, the medulla oblongata and the spinal cord (Bharos et al. 1981; Bentivoglio, and Kuypers 1982; Sathyamurthy et al. 2020; Streng et al. 2021).

In addition, cerebellar nuclei neurons targeting the ventro-lateral thalamus send collateral branches to the granular layer of the cerebellar cortex where they contact both granule and Golgi cells (Houck et al. 2015), suggesting that a corollary discharge is sent to the cerebellar cortex, potentially leading to a feedback inhibition of the cerebellar nuclei.

Quite strikingly, neurons in the fastigial nucleus (FN) projecting to the superior colliculus also send collaterals to several thalamic and midbrain targets (Streng et al. 2021). This includes the medio-dorsal (MD), ventro-lateral (VAL), ventro-

medial (VM) and parafascicular (PF) thalamic nuclei, as well as the ventro-lateral periaqueductal gray (vlPAG). These findings potentially support the existence of a neuronal population in the fastigial nucleus projecting simultaneously to the MD and to vlPAG. And indeed, it was already observed that FN-vlPAG neurons send collaterals to several thalamic nuclei including the MD, the PF and the VAL (Frontera, Baba Aissa, et al. 2020), confirming that a neuronal population projecting to both vlPAG and MD exists in the FN.

The presence of collaterals to the MD and vlPAG from single axons indicates that the chemogenetic inhibition of FN-vlPAG neurons (Frontera, Baba Aissa, et al. 2020) and FN-MD neurons (Frontera, Sala, et al. 2023), target overlapping populations of the FN neurons. Yet in the case of systemic administration of CNO during extinction, the impact of inhibition between the two structures differ, the expression of fear during presentation of CS on the third day of extinction when CNO was not administered remained higher when vlPAG-projecting neurons were targeted while the effect was milder for MD-projecting neurons. Therefore the effects do not seem identical in the two experiments. The contribution of the MD could be anyway singled out by using intra-cranial micro-injections of CNO in the MD -which shall only decrease the activity of FN terminals in the MD-. These local injections produced similar, although weaker, effect than systemic injections (Frontera, Sala, et al. 2023) is a strong indication that the FN-MD projections are modulating the extinction of fear memory via the MD. However, an experiment involving intra-cranial micro-injections of CNO in the vlPAG might be necessary to clarify the involvement of FN-vlPAG projections in the extinction of fear memory.

Similarly, neurons of the cerebellar nuclei projecting to the spinal cord emit projections to the ventral thalamus and to the red nucleus (Sathyamurthy et al. 2020). This reveals that a population of cerebellar nuclei neurons projecting to the VAL also projects to the spinal cord and to the red nucleus. More interestingly, the chemogenetic inhibition of spinal cord-projecting CN neurons during the accelerating rotarod task impairs performances in motor skill learning (Sathyamurthy et al. 2020). This study however did not investigate the impact of the inhibition on motor abilities, and this prevents the disambiguation of motor defects vs motor learning defect.

Our results investigating the impact of inhibition of CN-VAL neurons during the learning of the accelerating rotarod task also showed an impairment of motor learning . Thus, the effect that we observed in our study could be mediated by any of the different potential targets that these neurons target, since we performed

intra-peritoneal injections of CNO.

However, some key differences between our results and the observations of this study should be noted. Indeed, we observe that the inhibition of CN-VAL neurons during the task doesn't initially induce a consistent deficit in performances during the first days of learning, and that the late inhibition of these neurons after learning (during the treatment reversal experiments) induce a strong decrease in performance . On the other hand, this study reveals that the inhibition of spinal cord-projecting CN neurons leads to a strong deficit, present even in early phases of learning (which could result from a direct motor impairment) and, that the inhibition of these neurons post-learning (on day 4) does not affect performances (Sathyamurthy et al. 2020). This suggests that although there is an intersection between the neuronal populations inhibited in both studies (as collateralization was observed), there may be a strong contingent of non-spinal cord-projecting CN-VAL neurons, and non-VAL-projecting spinal cord-projecting CN neurons carrying different functions, the former being more involved in the expression of a previously learned skill, whereas the latter is more involved in the acquisition of a motor skill.

Moreover, it was observed that CN neurons could emit collaterals in the VAL and CL simultaneously (Sakayori et al. 2019), suggesting a possible divergent transfer of information between the cerebellum and these two thalamic nuclei. This observation implies that at least a neuronal population in the CN would be inhibited in both of our experimental design of CN-VAL and CN-CL inhibition.

All together, these observations highlight the fact that performing intra-cranial micro-injections of CNO may be necessary to clearly unravel the phenotypes inducible by the inhibition of CN-VAL and CN-CL projections, as well as their functions. Nonetheless, the clear differences between the phenotypes induced by the chemogenetic inhibition CN-VAL and CN-CL neurons, as well as the dichotomy observed between cerebello-cortical and cerebello-striatal coupling are strong evidences that distinct pathways exist between the cerebellum, motor cortex and striatum, supporting different functions.

5.1.4 Assessment of synaptic plasticity in-vivo

In some of our studies, we compare the response of single neurons to optogenetic stimulations of cerebellar nuclei neurons at different stages of learning or pathology and treatment development to extrapolate a change in coupling between the cerebellum and other structures such as the thalamus, the motor cortex and the striatum (Aïssa et al. 2022). The underlying rational is that an increased response would reflect a long term potentiation of synapses between the stimulated cerebellar nuclei

neurons and the target neuron. On the other hand, a decreased response would reflect a synaptic long term depression.

More specifically, our investigation of the effect of cerebellar theta-bursts stimulations on cerebello-thalamo-cortical plasticity was supported by a comparison of the response of single neurons to optogenetic stimulations of cerebellar nuclei before and after the application of cerebellar theta-bursts stimulations (Aïssa et al. 2022). Our observed change in response could be due to multiple factors, including possible changes in intrinsic plasiticity (Shim, Lee, et al. 2018; Gao, van Beugen, et al. 2012; Frick et al. 2004; Kim, and Jung 2006; Zhang, and Linden 2003; Gittis et al. 2006). This is process is not restricted to synaptic plasticity and encompasses non-synaptic and more global changes (Shim, Lee, et al. 2018; Belmeguenai et al. 2010). Interestingly, it was reported to act alongside synaptic potentiation and depression (Hyun et al. 2013; Shim, Jang, et al. 2017), suggesting an interaction between both forms of plasticities. However, incongruence between synaptic and intrinsic plasticities were reported (Brager et al. 2007), where an increased excitability was observed alongside a long term depression of synaptic inputs, suggesting that the duality between synaptic and intrinsic plasticities could support homoeostasis in neuronal networks. Thus, an observed change in response could both reflect changes in synaptic and instrinsic plasticities, as these two are intertwined.

Synaptic plasticity has been shown to be a heterogeneous process, spreading over different timescales and mechanisms (Frey et al. 1998; Baltaci et al. 2019). As an example, it has been shown in hippocampal neurons that long term potentiation can be broken down into different components, as a short latency mechanism considered as "early-LTP" occurs prematurely, and can be later stabilized during the "late-LTP" phase (Frey et al. 1998). While early-LTP is dependent on the activation CaMKII to perform intra-cellular protein trafficking, the late-LTP requires gene expression and protein synthesis (Baltaci et al. 2019), occurring in the following tens of minutes up to hours following the plasticity-inducing stimulation. Subsequently, this stabilized LTP will be maintained by different cellular mechanisms (Baltaci et al. 2019). In our study, we compare responses before and after application of cerebellar theta-bursts stimulations. Knowing that the average response measured after stimulation occurs in the following 10-20 minutes following theta-bursts, it may reflect a mix of both early and late-LTP, and may not be completely indicative of the stability of the change, as it may not be fully consolidated yet. This is critical, as weak stimulations leading to solely early-LTP induce changes which can typically last for 1 to 3 hours, whereas late-LTP induces changes lasting for a day (Baltaci

et al. 2019).

In order to properly delineate the contribution of the different forms of plasticity on the change of response that we observed, as well as the stability of the change measured, a complementation by ex-vivo studies would have beenb necessary. Nonetheless, it should be noted that the long-term increases or decreases in firing rate observed during our experiments are still strong evidence that changes of coupling between the cerebellum and downstream structures are occurring during learning or after performing cerebellar theta-bursts stimulations, and thus have important functional implications.

5.2 Cerebellum as a coordinator of brain oscillations during learning

In our studies, we revealed that the cerebellum actively participates to the regulation of learning mechanisms depending on brain oscillations, whether through the presence of cerebellar spindles reactivating cortical populations during motor learning, or through the regulation of cortico-thalamo-cortical coupling of fear-related 4Hz oscillations between the MD and the dmPFC during extinction of fear memory (Frontera, Sala, et al. 2023).

5.2.1 Fear related 4Hz oscillations

As evidenced in previous studies, the expression of a conditioned fear behaviour is associated to particular patterns of activity in the dmPFC. Indeed, oscillations are visible in the LFP of the dmPFC during the expression of freezing following fear conditioning, at frequency of ~4Hz in rodents and corresponding to the breathing rhythm (Karalis et al. 2016a; Dejean et al. 2016; Bagur et al. 2021). These oscillations propagate to the amygdala, where they were also observed (Lesting et al. 2013; Karalis et al. 2016b; Davis et al. 2017; Ozawa et al. 2020; Hagihara et al. 2021), consistently with a high degree of interconnection with the prefrontal cortex. Knowing the importance of coordinated activity in the limbic circuits for the support emotional learning, it was critical to investigate the extent to which these oscillatory patterns of activity can affect neuronal dynamics in the limbic circuits.

We revealed that fear related oscillations are present in the medio-dorsal thalamus (MD), a central hub of the limbic system (Georgescu, Popa, et al. 2020). More importantly, these oscillations can participate to bursting activity in the MD,

which was shown to regulate the extinction of fear memory (Lee, Ahmed, et al. 2012). Thus, the presence of 4Hz oscillations in the dmPFC promotes synchronous bursting in the MD, which in turn impairs extinction.

Critically, we also observed that MD bursting nested within 4Hz oscillations could contribute to the persistence of these oscillations, increasing both their amplitudes and their cortico-thalamic coupling. This is consistent with the notion that bursting activity, particularly if engaging large populations of neurons, could contribute to oscillatory processes in the brain (Cunningham et al. 2004; Constantinou et al. 2015; Tal et al. 2020; Scherer et al. 2022).

Strikingly, we observed that the chemogenetic inhibition of FN-MD pathway during extinction learning leads to an increased coherence of 4Hz oscillations between the dmPFC and the MD, as well as more bursting activity in the MD and an enhanced entrainment of MD bursting by dmPFC 4Hz oscillations. This increased synchrony between the MD and the dmPFC following a cerebellar nuclei inhibition is consistent with the role of the cerebellum in modulating brain oscillations and coordinating brain structures (Popa et al. 2013; Lindeman et al. 2021; McAfee et al. 2019; McAfee et al. 2021; Heck et al. 2023).

Interestingly, this is the first report suggesting that the cerebellum could contribute to the desynchronization of distant structures' activities, as it was usually observed that perturbing the cerebellum would lead to a decreased synchrony between brain areas (Popa et al. 2013; Lindeman et al. 2021; Georgescu Margarint et al. 2020; Heck et al. 2023), rather implying a role of the cerebellum in promoting coherent oscillatory oscillations between distant structures. However, the mechanism underlying this desynchronization remains unknown and needs to be investigated. A simple hypothesis explaining this phenomenon, supported by preliminary results, will be discussed in a later section.

Altogether, our observations support the fact that the degree of synchrony of 4Hz oscillations in the limbic circuit is critical in regulating the expression of conditioned fear behaviour and extinction learning, and that this synchrony is actively controlled by the cerebellum, which, in normal conditions, promotes a desynchronization of the dmPFC-MD reciprocal network, reducing the bursting behaviour of the MD, limiting the maintenance of dmPFC 4Hz oscillations, which in term facilitates extinction learning.

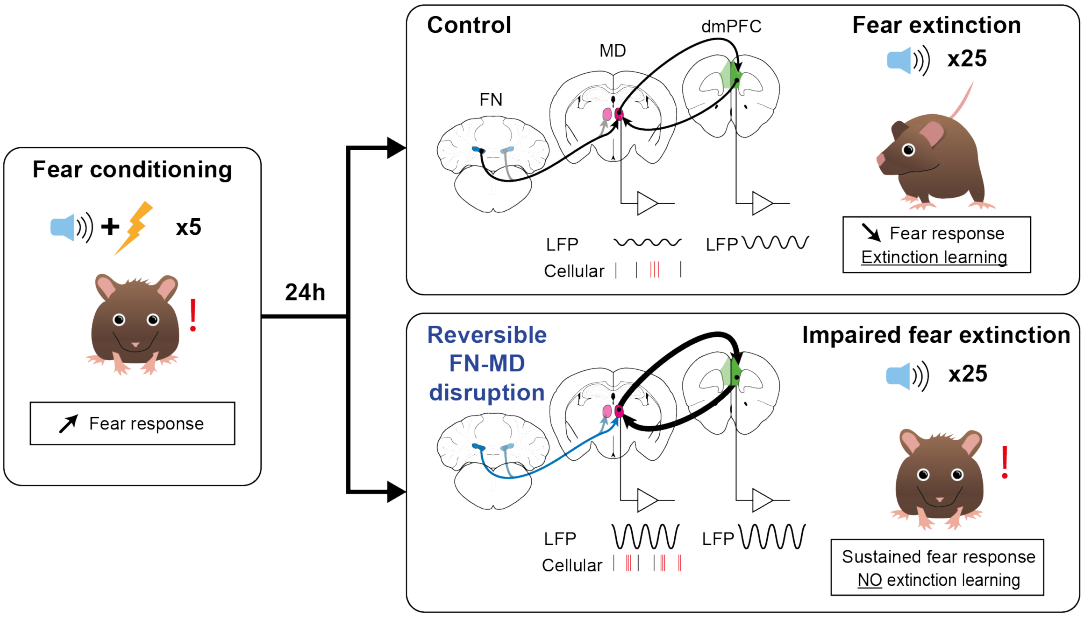

Figure 5.1: The cerebellum controls fear extinction through the synchrony of cortico-thalamic fear-related oscillations. Following fear conditioning, the exposition to the CS elicits a fear response. In normal extinction of fear memory, freezing is associated to fear-related oscillations in the dmPFC, which propagate to the MD where they can organize local bursting activity. The bursting of neurons in the MD is associated to persistent and more synchronous oscillations in the system. However, under physiological conditions these oscillations get weaker through extinction, the phase locking of MD bursting is mild and the fear response decreases. In contrast, the inhibition of FN-MD pathway leads to an enhance synchrony of fear-related oscillations between dmPFC and MD, with an increased bursting activity which is more entrained by these oscillations, and higher and more persistent levels of freezing.

5.2.2 Sleep spindles

In the past, a strong correlative link has been made between sleep spindles and learning. However, a potential causal role of these rhythms in the consolidation of an engram has yet to be determined. Indeed, many studies support the fact that the frequency of sleep spindles in the motor cortex is increased following motor learning (Fogel et al. 2007; Morin et al. 2008; Barakat, Doyon, et al. 2011), and that a correlation between the properties of sleep spindles and the learning rate of a given task can be observed (Barakat, Doyon, et al. 2011; Nishida et al. 2007; Barakat, Carrier, et al. 2013).

Interestingly, we were able to observe spindles during the resting periods in-between rotarod trials, which is consistent with the fact that spindles can also be observed during day-time naps (Nishida et al. 2007).

Remarkably, we observed that cerebellar spindles during NREM sleep following motor learning can synchronously reactivate neurons of the motor cortex, particu-

larly the neurons that were engaged in directional connectivity with the cerebellum during the task. This is consistent with the observations that sleep spindles can be recorded in the cerebellum and that the cerebellum contributes to sleep-dependent memory processes (Xu, De Carvalho, Clarke, et al. 2021; Jackson et al. 2023).

Within cerebellar sleep spindles, the preferred firing phase of cerebellar neurons anticipates the preferred firing phase of cortical neurons, suggesting that cerebellar neurons are entraining cortical neurons. Consistently with this, it was revealed that, although the cerebellum does not seem to initiate sleep spindles, a directional influence from the cerebellum to the motor cortex through the thalamus was observable during these events (Xu, De Carvalho, Clarke, et al. 2021; Jackson et al. 2023). How to reconcile these observations with the classical view of a thalamic origin of spindles remains unclear.

Interestingly, little overlap between spindles detected in the cerebellar nuclei and spindles detected in the motor cortex was observed, eventhough cerebellar spindles do entrain cortical activity. This may suggest that, if sleep spindles originate from thalamo-cortical networks as the current models imply, the spindles detected in the cerebellum but not in the motor cortex may arise from other cortical areas and propagate to the cerebellum through the mossy fibers system, entraining activity in the cerebellar cortex and cerebellar nuclei. Then, the cerebellar output neurons entrained by the spindle activity will activate the downstream thalamic and cortical neurons which were previously co-activated during the task. Thus, this mechanism may allow to selectively reactivate sub-networks from the cerebello-thalamo-cortical circuits which were previously engaged during the learning process and consolidate them.

In line with this idea, sleep spindles have been shown to affect functional connectivity in cortico-striatal networks (Lemke et al. 2021). Indeed, pairs of cortical and striatal neurons entrained by cortical spindles display a maintained connectivity, while pairs that are not entrained would rather display a decreased connectivity.

Consistently, we observed that pairs of cerebellar and cortical neurons entrained by cerebellar spindles during resting periods between trials display a maintained connectivity during a training session, and other pairs showed a tendency to have a decreased coupling. This, taken together with the fact that inhibiting CN-VAL neurons after the training session impairs the next rotarod trial, further suggest that cerebellar spindles are involved in the off-line consolidation of a motor skill and contribute shaping cerebello-cortical networks.

5.3 Cerebello-cortical-striatal networks during motor learning

While the roles of the cerebellum, motor cortex and basal ganglia in motor learning have been extensively studied in the past, little attention was brought to their potential interactions as they have been considered as separated learning devices having different contributions to sequence learning and motor adaptation (Doya 1999; Doya 2000; Krakauer et al. 2019).

However, we know that the cerebellum and the neo-cortex, in particular the motor cortex, are heavily interconnected (Middleton et al. 1997; Middleton et al. 1998; Kelly et al. 2003; Bostan, Dum, et al. 2013). Moreover, cerebellar activity can influence cortical activity (Popa et al. 2013; Proville et al. 2014; Chabrol et al. 2019; Dacre et al. 2021), and conversely the cortex can modulate cerebellar activity (Guo, Sauerbrei, et al. 2022).

Similarly, several pathways linking the basal ganglia and the cerebellum have been discovered, mainly involving intralaminar thalamic nuclei such as the centrolateral and parafascicular nuclei (Middleton et al. 1994; Bostan, Dum, et al. 2013; Bostan, and Strick 2018; Ichinohe et al. 2000; Chen, Fremont, et al. 2014; Xiao et al. 2018).

Thus, taking this in consideration along with the fact that interactions exist between sequence learning and sensorimotor adaptation (Liu, and Block 2021), interactions between the cerebellum, the basal ganglia and the motor cortex are likely to occur during motor learning.

5.3.1 Cerebellar connectivity with the motor cortex

In our study, we revealed that the cerebellum was profusely connected with both the contralateral and ipsilateral primary motor cortices, which suggest that cerebellar processing can propagate bilaterally. Even more interestingly, this statement holds true for both directions of communication, as we observed pairs of cerebellar and cortical neurons displaying a directional connectivity in the cerebello-cortical and cortico-cerebellar directions.

This is consistent with the observations that, cerebellar nuclei may emit both contralateral and (mild) ipsilateral projections (Sakai 2013), which is also the case for thalamo-cortical projections (Carretta et al. 1996; Dermon et al. 1994). Moreover, an extensive inter-hemispheric communication between cortices through the corpus callosum as been shown to exist and to support bi-manual movements (Jeong et al.

2021; Charalambous et al. 2016). In addition, cortico-cerebellar projections were shown to be bilateralized (Karavasilis et al. 2019; Zhu et al. 2023), as the cortex of one hemisphere contributes to both ipsilateral and contralateral mossy fibers systems (Zhu et al. 2023).

Thus, eventhough the majority of cerebello-cortical loops link the cerebellum with the contralateral motor cortex, the cerebellum has many potential pathways through which it could display a functional connectivity with the ipsilateral motor cortex, each of them having variable numbers of synapses and different integrative properties.

Interestingly, the cerebellar nuclei from one hemisphere were shown to represent movement from both sides of the body (Soteropoulos et al. 2008), and altering cerebellar function unilaterally with kainate infusion in the cerebellar cortex leads to a decreased inter-hemispheric cortical coherence (Georgescu Margarint et al. 2020), further suggesting that the cerebellum can functionally interact with the motor cortices of both hemispheres, which is consistent with the profuse open-loop connectivity recently observed between cerebellum and cortex (Zhu et al. 2023).

5.3.2 Plastic changes in cerebello-cortical and cerebello-striatal networks

We observed dynamic changes in the connectivity between the cerebellum and the cortex during the process of accelerating rotarod learning. During the course of motor learning, the occurrence of putative oligosynaptically-connected pairs (pairs of cells exhibiting short-term asymmetry in their crosscorrelogram) between the cerebellum the motor cortex and the striatum increased, particularly in the cerebello-cortical and cerebello-striatal directions, and the magnitude of response to cerebellar stimulation increased in both motor cortex and striatum. These observations suggest that motor learning triggers plastic changes in the cerebello-thalamo-cortical tracts, leading to an increased drive of the cerebellar nuclei neurons on cortical activity.

Consistently, we also observed in our studies that long term potentiation of the cerebello-thalamo-cortical and cerebello-thalamo-striatal tracts was inducible, as the application of theta-bursts stimulation in the deep cerebellar nuclei leads to an increase in response to cerebellar stimulations in the thalamus and motor cortex of wild-type mice, as well as in the fast-spiking neurons of the striatum (Aïssa et al. 2022). In addition, the ability of cerebello-thalamic synapses to undergo long-term potentiation has been observed in the past (Aumann 2002; Aumann, Redman, et al. 2000), and can occur spontaneously during motor adaptation (Aumann, and Horne

1999). Similarly, long-term potentiation was discovered in the thalamo-cortical systems (Aumann 2002; Baranyi et al. 1991; Iriki et al. 1991), along with changes of cerebello-cortical plasticity associated to motor adaptation (Rispal-Padel et al. 1992; Meftah et al. 1994).

Previous studies have shown that motor learning was associated to a long-term depression of the parallel fiber to Purkinje cell synapse and an increased excitability in the primary motor cortex (Spampinato et al. 2017). A recent study revealed that progressive changes occur in the cerebello-cortical tract during motor learning, as variations of cerebellar brain inhibition can be observed early during learning, and an occlusion of LTP in the motor cortex could be observed in later learning stages (Spampinato et al. 2017).

Moreover, it was recently observed that cerebello-cortical connectivity was increased following motor learning (Mehrkanoon et al. 2016), consistently with our observations. Strikingly, our results revealed the existence of an enhancement of cerebello-striatal connectivity induced by motor learning, along with an increased collaboration of cerebellar and striatal inputs to the motor cortex during the execution of a learned task, which was not reported before.

5.3.3 Offline refinement and consolidation of a motor skill

Motor learning is associated to a wide variety of sleep-dependent processes, and it was shown that every form of sleep, including day-time naps, could contribute to consolidation of motor skill (Doyon, Korman, et al. 2009; Nishida et al. 2007). Thus, we sought to investigate the neuronal activity in the cerebello-cortico-striatal networks during the resting periods in-between the rotarod trials, during which mice exhibit inactivity and can fall asleep. This led us to make three critical discoveries:

- Cerebello-cortical connectivity, but not cerebello-striatal, is maintained during resting periods
- Cerebellar spindles during NREM sleep reactivate cortical neurons and shape cerebello-cortical connectivity
- Replays of neuronal activity predict the refinement of motor strategy during rotarod learning

Knowing that cerebellar sleep spindles were discussed in a previous section of this discussion, we will focus on the connectivity between cerebellum, striatum and

motor cortex, as well as on the presence of replays of neuronal activity during the resting periods between rotarod trials.

Cerebello-cortical and cerebello-striatal connectivity

Strikingly, a strong difference was observed between cerebello-cortical and cerebello-striatal ascending connectivities during resting periods. The pairs of cerebellar and cortical neurons exhibiting directional connectivity during the task would display similar connectivity patterns during resting periods, suggesting that cerebello-cortical connectivity is still engaged even outside of the task, when the animal is resting. Consistently with this, not only the cerebellum was shown to display an increased activity during sleep following motor learning, but the magnitude of this activity was directly correlated to the savings of the motor skill (Debas et al. 2010).

Furthermore, the maintained cerebello-cortical connectivity that we observed is consistent with the reports of maintained interactions between the cerebellum and the motor cortex during sleep (Xu, De Carvalho, Clarke, et al. 2021; Jackson et al. 2023), which also revealed that the directional connectivity was maintained between cerebellar and cortical neurons (Xu, De Carvalho, Clarke, et al. 2021; Xu, De Carvalho, and Jackson 2022).

On the other hand, we observed that directional connectivity between the cerebellum and the striatum was altered during resting periods, as pairs of cerebellar and striatal neurons exhibiting directional connectivity during the task would not conserve this relationship during resting periods. Consistently with this, no report was made of a potential involvement of cerebello-striatal loops in the consolidation of a motor skill. Interestingly, this difference between cerebello-cortical and cerebello-striatal ascending connectivities is in line with the previous expectations that cerebello-cortical and cerebello-striatal loops may contribute differentially to motor learning (Doyon, Penhune, et al. 2003).

Replays and refinement of motor strategy

We observed that mice typically use a discrete set of strategies on the rotarod, either jumping or adapting a gait-like strategy, alternating hind-paws. Moreover, we revealed the fact that expert mice tend to jump less than naive mice, suggesting that they favor a gait-like strategy, which correlates directly with the overall performances of the mice. Altogether, this suggests that the accelerating rotarod is a complex

problem to solve for mice with multiple solutions, and that the learning process corresponds to choosing the optimal strategy and correctly executing it.

These results strongly contrast with the observations of Nguyen et al, which showed that while learning was associated to changes in kinematics and inter-limb coordination, mice tend to favor a gait-like strategy relatively early without any change in coordination between hind-paws (Nguyen et al. 2021). However, many factors are known to influence the performance on the rotarod task, including the device used, the protocol, the gender, the age and the weight of the mice (Rustay et al. 2003; Kovács et al. 2013; Eltokhi et al. 2021). Interestingly, the diameter of the cylinder used by Nguyen et al is much larger (5.08cm, 2inch) than the one used in our studies (3cm, 1.18inch), and their acceleration protocol (15rpm to 40rpm in 80s) is different than the one used during our recordings (10rpm to 45rpm in 300s).

These larger cylinders diameter, coupled to the higher starting speed, may explain that jumping is less frequent in their study, as for a similar rotation speed, the mice of their study had to perform a much longer distance (1.69 times longer) on a rod that is closer to a plane due to its larger diameter.

While reactivations of neuronal activity during sleep were already observed in the motor cortex (Xu, de Carvalho, et al. 2019), particularly following motor learning (Eichenlaub et al. 2020; Rubin et al. 2022), little was known on the extent to which these replays could be present in other structures of the motor networks such as the cerebellum, thalamus and basal ganglia.

In our recordings, we were able to specifically detect replays of motor patterns (individual steps), which engage neurons not only in the motor cortex, but also in the cerebellar nuclei, motor thalamus, centrolateral thalamus and striatum bilaterally. This suggests that replays of activities are coordinated events widely distributed in the motor network, which is in line with the previous observations of coordinated replays between hippocampus, cortices and amygdala (Ji, and Wilson 2007; Girardeau, Inema, et al. 2017). However, this is the first report of replays of activity in the cerebellum, thalamus and striatum. We were able to detect such replays of neuronal activity throughout the resting periods, which is consistent with the observations that replays of neuronal activity can happen even during wakefulness (Karlsson et al. 2009; Rubin et al. 2022).

Strikingly, we observed that the structure of the replay activity during resting periods was predictive of the variations in motor strategies. Surprisingly, no link was previously made between the occurrence of these replay and the refinement of a strategy during a motor task, with no suggestion that the execution of a partic-

ular replay would influence the next motor sequences performed. However, it was proposed that the prioritization of hippocampal replays was correlated with later choices in a spatial navigation task (Mattar et al. 2018), which would be somewhat consistent with our observation that the relative frequency of replays influences trial-to-trial variations in the motor strategy used on the rotarod.

Although we observed that the cerebellum contributes to replays of activity, its functional role in generating or maintaining these replays remains unknown. However, it was previously shown that the cerebellum is needed for preparatory activity in the motor cortices (Gao, Davis, et al. 2018; Chabrol et al. 2019; Zhu et al. 2023), and that perturbing cerebellar activity before the onset of a movement could collapse cortical dynamics and lead to a decrease in performance during a sensorimotor task (Gao, Davis, et al. 2018).

The cerebellum may very well play a similar role during the replays of neuronal activity. If it is the case, cerebellar activity might be necessary to stabilize the replay and guarantee the correct execution of the replay of a particular sequence. This hypothesis may explain why the offline perturbation of CN-VAL neurons after the session leads to an impairment of the performances during the first trial of the subsequent day with a fast recovery on the second and third trials, as perturbing cerebellar activity during replay may bias the mouse towards the expression of a sub-optimal strategy, which will be corrected during the next unperturbed resting periods.

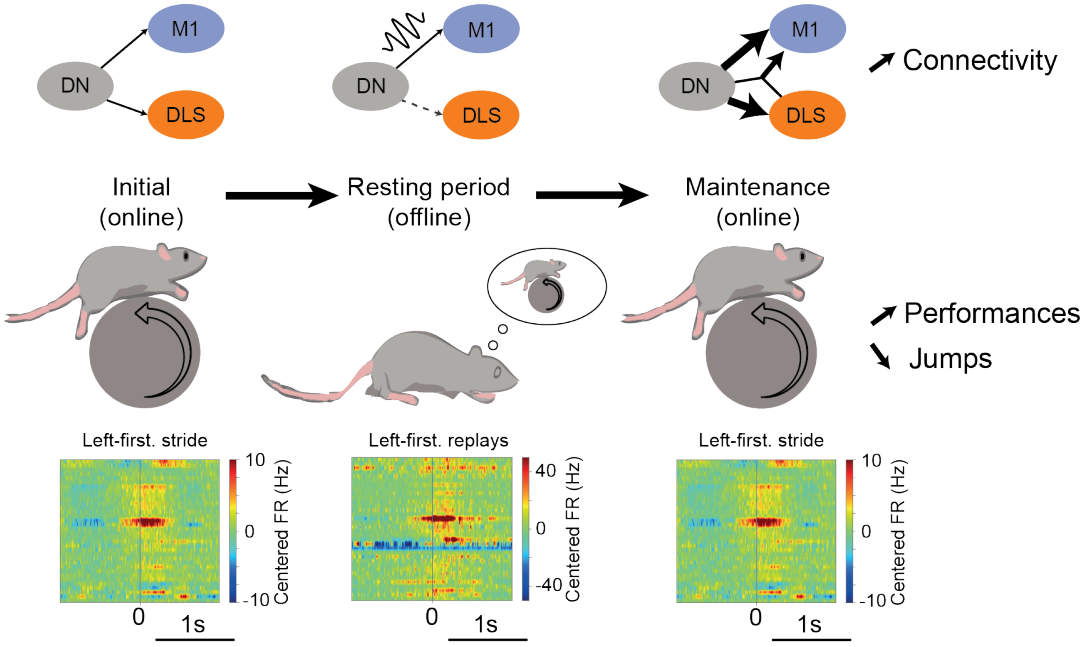

Figure 5.2: The offline consolidation of a motor skill differentially involve cerebello-cortical and cerebello-striatal networks. Undergoing accelerating rotarod training is associated to a long lasting increase of connectivity in cerebello-cortical and cerebello-striatal networks. During the resting periods in-between rotarod trials, the presence of cerebellar spleep spindles during NREM sleep reactivates cortical neurons and shapes cerebello-cortical connectivity. Resting periods are also associated to sequential replays of neuronal activity corresponding to the different motor patterns used on the rotarod, which are predictive of the trial-to-trial refinement of the motor strategy during the task.

5.4 Cerebello-thalamic pathways in dystonia

Mutations in Gnal (DYT25) and their association with a dystonic phenotype were first identified in 2012 (Fuchs et al. 2013). DYT25 is known to be an adult-onset dystonia, with an age at onset ranging from 7 to 63 years depending on the cases. In terms of body distribution, although the onset is mainly cervical (80% of cases), DYT25 can affect many body parts, and can be generalized through the progression of the disease, even though it is a relatively rare occurrence (Fuchs et al. 2013; Miao et al. 2020; Vemula et al. 2013; Dufke et al. 2014; Kumar et al. 2014; Ziegan et al. 2014; Saunders-Pullman et al. 2014; Carecchio et al. 2016). Considering the heterogeneity of phenotypes, the late age of onset observed in DYT25 patients, and the fact that an incomplete penetrance of the disease was reported (Vemula et al. 2013), may suggest that the mutation of Gnal leads to sub-threshold alterations in the motor networks of non-manifesting mutations carriers, which can progress with time and/or external factors, eventually triggering the disease onset.

5.4.1 Constitutive alteration and pathological switch

Consistently with this hypothesis, we revealed that, although Gnal+/- mice do not display motor symptoms in the absence of cholinergic agonist, they exhibit a constitutive alteration in cerebello-thalamic connectivity (Aïssa et al. 2022). Indeed, the neuronal response to stimulations of the dentate nucleus is increased in the motor thalamus of Gnal+/- mice compared to wild type animals, but not in the centro-lateral thalamus nor in the motor cortex. This is consistent with the reports of alterations of cerebello-thalamic pathways in another hereditary dystonia, DYT1, caused by a mutation of the torsinA gene (Argyelan et al. 2009; Uluğ et al. 2011).

Interestingly, regarding the ascending cerebello-thalamo-cortical tracts, non-manifesting carrieres of torsinA mutation (known to cause DYT1), whether human or mice, exhibit strong alterations of thalamo-cortical axis, and milder connectivity impairments in the cerebello-thalamic tracts (Argyelan et al. 2009; Uluğ et al. 2011). On the other hand, symptomatic DYT1 patients display even deeper cerebello-thalamic alterations (Argyelan et al. 2009; Uluğ et al. 2011), suggesting that the integrity of cerebello-thalamic tracts is a key factor influencing the penetrance of the disease.

Knowing that non-manifesting DYT1 mice display an increased cerebellar activity (Uluğ et al. 2011), this could be compatible with a role of the cerebellum in actively compensating the alterations of cortical and thalamo-cortical networks in the presymptomatic state until cerebello-thalamic network becomes so severely altered than this compensation cannot occur anymore, leading to the pathological state.

However, it was also shown that performing an acute knock down of torsinA in the cerebellum in mice is sufficient to induce an aberrant cerebellar activity and a dystonic phenotype (Fremont, Tewari, et al. 2017), rather suggesting a role of the cerebellum in pathophysiology of the disease.

We observed an evolution of cerebello-thalamic alterations with the progression of the disease in Gnal+/- mice. Indeed, while presymptomatic Gnal+/- mice only displayed an increased response to cerebellar stimulations in the motor thalamus compared to wild-type animals, the initial exposure to oxotremorine lead to long-lasting increases of responses to cerebellar stimulations in the centro-lateral thalamus, the motor cortex, and further exaggerated to the response in the motor thalamus. However, the exposure to oxotremorine doesn't produce long-lasting symptoms, as Gnal+/- mice later come back to an asymptomatic state. Then, the increased response observed in the thalamus and motor cortex in an asymptomatic

could either contribute to enhance a compensatory action of the cerebellum on the motor network, or on the other hand create an imbalanced connectivity in the motor network, later leading to a persistent symptomatic state.

Interestingly, an increased connectivity between the cerebellum and the motor cortex has also been reported in dystonic patients (Zito et al. 2022), along with an impaired GABAergic transmission in the cerebellum and in the sensorimotor cortex (Gallea et al. 2016). These findings are consistent with the heightened response to cerebellar stimulations observed in the motor cortex of Gnal+/- mice, and suggests that dystonia can arise from the promotion of excitation in the motor cortex.

5.4.2 Aberrant plasticity

In addition of showing an increased cerebello-thalamic functional connectivity in asymptomatic Gnal+/- mice, we also revealed that these mice display an aberrant cerebello-thalamic and cerebello-cortical plasticity (Aïssa et al. 2022). Indeed, while wild-type mice receiving theta-burst stimulations of the dentate nucleus later exhibit an increase in response to cerebellar stimulations in the thalamus and the motor cortex, suggesting a long-term potentiation of the cerebello-thalamo-cortical pathway, asymptomatic Gnal+/- mice do not display a consistent change in response to cerebellar stimulations (Aïssa et al. 2022). Considering the fact that the response to cerebellar stimulations of Gnal+/- mice was already potentiated following the exposure to oxotremorine, this absence of further potentiation could reflect an occlusion of LTP-like behaviour, which is a process shown to be inducible or to appear spontaneously during learning processes (Stefan et al. 2006; Delvendahl et al. 2010). Interestingly, dysfunctional plasticity is a hallmark of dystonia, specifically in the motor cortical plasticity (Calabresi, Pisani, et al. 2016; Quartarone, Bagnato, et al. 2003; Quartarone, Rizzo, Bagnato, et al. 2005; Quartarone, Morgante, et al. 2008; Gilio et al. 2007; Quartarone, and Hallett 2013), present even in non-manifesting mutation carriers of hereditary dystonia (Edwards et al. 2006).

In addition, defects of cortico-striatal plasticity have been described in hereditary dystonias, as cortico-striatal synapses of DYT1 and DYT25 mice can undergo LTP but not LTD (Maltese et al. 2014; Yu-Taeger et al. 2020; Martella et al. 2021). Consistently with an abnormal striatal plasticity in DYT25, we observed that, while the fast-spiking neurons in the dorsolateral striatum (DLS) of wild-type mice could display an increased response to cerebellar stimulation following cerebellar theta bursts stimulations, fast-spiking DLS neurons of Gnal+/- mice did not responses to cerebellar stimulations (Aïssa et al. 2022). Although this lack of potentiation may seem similar to the one observed in the thalamus and motor cortex, it is important

to note that in contrary to these structures, the basal response of fast-spiking DLS neurons to cerebellar stimulations was not higher in Gnal+/- mice compared to the wild type mice. Thus, the hypothesis of an occlusion of cerebello-striatal LFP due to a saturation of potentiation seems less likely.

5.5 Future perspectives

5.5.1 FN-MD and the control of fear-related 4Hz oscillations

As described previously, we demonstrated that disrupting cerebellar output to the medio-dorsal thalamus during the extinction of fear memory enhanced the synchrony of fear-related 4Hz oscillations in the cortico-thalamo-cortical circuit between the dmPFC and the MD, along with an impairment of fear extinction (Frontera, Sala, et al. 2023).

The increased synchrony observed in absence of a functional cerebellar output suggests that, in normal condition, the cerebellum desynchronizes the cortico-thalamo-cortical loop. However, the actual mechanisms allowing the cerebellum to promote the desynchronization of two distant structures are not known yet.

A simple hypothesis could be that, since brain oscillations require the synchronous activation of large populations of neurons intercalated with periods of silence (Buzsáki 2006; Harris, Csicsvari, et al. 2003), the presence of an oscillatory input with a similar frequency but in opposition of phase could lead to an attenuation of these brain oscillations, as an activity would arise during periods of silence and disappear during the periods of synchronous activity in the system. In this view, the system would be composed of two oscillators being the dmPFC and the cerebellum, coupled at the level of the MD where they dynamically affect local neuronal dynamics and tune the measured degree of synchrony between the dmPFC and the MD.

However, this hypothesis holds some requirements. In order for the cerebellum to generate an output signal phase-opposed to the 4Hz oscillations of the dmPFC, the cerebellum will need to receive an input from the dmPFC, whether direct or indirect. Then, the cerebellum needs to be able to perform a phase transform on this input signal, yielding to an output signal which will be a phase- and amplitude -modulated version of the 4Hz oscillations in the dmPFC. Finally, there should be a possible convergence of inputs from the dmPFC and from the cerebellum in the

MD, allowing for a local integration of both signals.

Descending pathways from the prefrontal cortex to the cerebellum involving precerebellar nuclei and the mossy fibers system have been previously described (Kelly et al. 2003). Moreover, it was observed that coherent oscillations could exist between the neocortex and the cerebellum (Roš et al. 2009; McAfee et al. 2019). In addition, populations of Purkinje cells in lobulus simplex and Crus I have been shown to not only be tuned to prefrontal oscillations, but to be able to represent the phase difference between prefrontal and hippocampal oscillations (McAfee et al. 2019), suggesting that the cerebellum could be involved in synchronizing these two structures. Thus, the presence of a cerebellar tuning to dmPFC 4Hz oscillations, as well as a phase and amplitude modulation of this signal by cerebellar circuits is a possibility.

Furthermore, we demonstrated that the FN targets the lateral compartment of the MD, and that the MD received direct projections from the dmPFC (Frontera, Sala, et al. 2023), confirming that the medio-dorsal thalamus is a potential interaction site between dmPFC and FN 4Hz oscillations.

In order to investigate the hypothesis of the cerebellum providing a negative interference dampening the propagation of dmPFC 4Hz oscillations to the MD, we performed simultaneous recordings in the FN, MD and dmPFC during extinction. We made critical observations in line with the previously mentioned hypothesis.

Notably, the relationship between 4Hz oscillations in the dmPFC and in the MD was dynamical, as the extinction session was populated by both periods of high synchrony and low synchrony between the MD and the dmPFC. During periods of high synchrony, the amplitude of the oscillations was high in both structures and the phase difference between signals was low. On the other hand, periods of low synchrony could arise, even in the presence of high dmPFC 4Hz oscillations, where the amplitude of the oscillation was low in the MD and the phase relationship between both signals was inconsistent.

Strikingly, periods of high synchrony between MD and dmPFC occurred when the FN was synchronous with the dmPFC, displaying a low phase difference. In contrast, when the phase of the 4Hz oscillations in FN was opposed to the phase in the dmPFC, the amplitude of oscillation in the MD was decreased. Ultimately, the amplitude of the oscillation in the MD was directly correlated to the phase difference between the 4Hz oscillations in the dmPFC and in the FN, consistently with the hypothesis that the FN provides a negative interference to the MD, facilitating fear extinction.

In addition, the persistent interference of FN leads to a decreased amplitude in the dmPFC after few oscillatory cycles, in line with the MD potentially having a positive feedback effect on dmPFC 4Hz (Frontera, Sala, et al. 2023), suggesting that dmPFC and the cerebellum are two oscillators coupled in a dynamical system.

Although a strong correlative relationship was observed between the state of 4Hz oscillations in the cortico-cerebellar and cortico-thalamic circuits, further analysis and experiments are required to demonstrate this hypothesis.

Notably, performing optogenetic closed loop manipulations of the FN-MD pathway during extinction, either forcing the cerebellar output to be in phase or phase-opposed with the 4Hz oscillations in the dmPFC, would be a solid demonstration of the ability of the cerebellum to modulate fear extinction through the regulation of cortico-thalamo-cortical synchrony.

5.5.2 Motor learning and memory consolidation

In our studies, we provided evidence supporting the fact that the consolidation and the refinement of motor learning depend on several neuronal mechanisms occurring during resting following practice.

Notably, this included the occurrence of cerebellar sleep spindles during NREM sleep, selectively reactivating cortical neurons engaged with cerebellar neurons during the task. Cortical neurons entrained by cerebellar spindles maintained their connectivity with the cerebellum, while other neurons tended to display a decrease in connectivity. This suggests that, at least within a training session, cerebellar spindle contribute in shaping cerebello-cortical networks.

However, we do not know the extent to which cerebellar spindles contribute to the increase in cerebello-cortical connectivity that we observed between training sessions, nor to the refinement of the motor strategy during accelerating rotarod learning. In order to elucidate these points, a selective perturbation of the cerebellar output during NREM cerebellar sleep spindles could be performed. Indeed, a retrograde virus expressing an inhibitory opsin could be injected in the motor thalamus, and an optic fiber could be implanted in the cerebellar nuclei, while performing simultaneous recordings in the cerebellar nuclei and in the motor cortex. This construct, in addition of being feasible and quite similar to our previous experimental construct, would allow to perform closed loop perturbations of the cerebellar pathway to the motor cortex. While the electrodes in the motor cortex should allow for sleep stage classification and the detection of NREM sleep, the electrodes in the

cerebellar nuclei would serve for the online detection of cerebellar sleep spindles, using a simple online bandpass filter at 10-16Hz and an amplitude threshold. Then, the functional consequences of these perturbations should be assessed using the same cross-correlogram based metrics used in our study, the measure of the latency to fall and the evolution of motor strategy during learning.

An appealing prediction would be that perturbing cerebellar sleep spindles will hinder the increase in cerebello-cortical connectivity that we observed in our study, making these networks more stationary. In addition, it could also prevent the gradual shift observed between jumping and performing a gait-like strategy on the rotarod, impairing the learning.

Moreover, it has been shown that the nesting of sleep spindles in slow oscillations was of particular interest for learning (Kam et al. 2019; Hahn et al. 2022), as well as for connectivity (Lemke et al. 2021). Thus, studying slow oscillations along with the spindles may be more indicative of connectivity and learning changes occurring during accelerating rotarod learning.

Similarly, we observed that strategy-specific replays of neuronal activity occurred in the motor network following the execution of the task, and that the temporal structure of these replays was predictive of the refinement of the motor strategy on the rotarod. Although the cerebellum is reactivated during replays, we do not know to which extent cerebellar activity is necessary for replays to arise or to be maintained, or if the cerebellum is actually needed for the update the motor strategy.

A similar experimental than the one exposed above for the specific perturbation of cerebellar output during sleep spindles could be used. However, the online detection of replays may be more complex. As reported, replays arise during periods of high gamma oscillations in the motor cortex [[Rubin et al 2022]], thus, one possibility will be to perturb cerebellar output during periods of high cortical gamma oscillations. But, because the bursts of gamma oscillations in the motor cortex could be an event non-specific to replays of activity, the link between periods of high cortical gamma and replays needs to be assessed before performing such experiments. Fortunately, this analysis can be made on our already acquired dataset.

Our prediction would be that specifically perturbing such replays of activity during resting will alter the motor strategy used during the next trial, but that impairment will be recovered after the next unperturbed resting period.

A simpler experiment would be to reproduce the chemogenetic inhibitions of CN-VAL and CN-CL neurons, both during the execution of the task and offline, while performing multisite neuronal recording and classification of the behavioral motor

strategy. These experiments should reveal the consequences of these inhibitions of cerebellar activity and on the execution of the task. Notably, this approach may elucidate the mystery surrounding the reasons behind the impairment of performances observed during the first trial of the subsequent day following the offline inhibition of CN-VAL neurons.

5.5.3 Cerebellar nuclei theta-burst stimulations as a treatment

In our study, we revealed the potential use of cerebellar theta-burst stimulations as a treatment of DYT25 (Aïssa et al. 2022). Surprisingly, while performing cerebellar theta-burst stimulations on asymptomatic Gnal+/- mice failed to induce any change in response to cerebellar stimulations in the thalamus, striatum and motor cortex, the same operation performed on symptomatic Gnal+/- mice not only induced a depression of the response to cerebellar stimulation in the thalamus and the motor cortex (so a normalization of the response), but also reduced the severity of dystonic symptoms (Aïssa et al. 2022). This observation is consistent with the previous studies showing a potential for TMS based protocols to treat dystonia (Koch, Porcacchia, et al. 2014; Lozeron et al. 2016), and is in line with the notion that hyperkinetic disorders arise from an over excitability of the motor cortex leading to involuntary movements (Calabresi, Pisani, et al. 2016), and suggests that inducing LTD in the motor network may be a potent mechanism for treating such disorders.

Strikingly, while the results of cerebellar theta-bursts stimulations in the treatment of dystonia have been shown to be highly variable, several parameters could potentially explain this variability (Quartarone, Rizzo, Terranova, et al. 2017). Notably, protocols involving repeated administration of theta-bursts, as well as bilateral stimulations, seem to yield better results (Koch, Porcacchia, et al. 2014; Quartarone, Rizzo, Terranova, et al. 2017). In our study, we observed a minor effect of cerebellar theta bursts stimulations on dystonic symptoms. However, we only performed one session of unilateral cerebellar theta-bursts stimulations, suggesting that we could improve these results by performing multiple sessions and implementing bilateral theta-burst stimulations.

Similarly, the results of theta-burst stimulations are influenced by the protocol used (cTBS or iTBS) and by the amplitude of stimulations (Harrington et al. 2015). Indeed, applying cTBS induces a reduction of the N100 amplitude, an indicator of GABAergic transmission, and reduces the amplitude of movement evoked potential, but only when performed at low intensity (Harrington et al. 2015). In contrast,

iTBS can induce an increase of the N100 amplitude, but only when the iTSB is performed at high intensity (Harrington et al. 2015). Thus, lowering the intensity of stimulations during our protocol, which in practice are closer to cTBS, could improve the efficiency of the treatment.

Interestingly, defects of cortico-striatal plasticity have been described in hereditary dystonias. Indeed, cortico-striatal synapses of DYT1 and DYT25 mice models can undergo LTP but not LTD (Maltese et al. 2014; Yu-Taeger et al. 2020; Martella et al. 2021). However, the LTD of cortico-striatal synapses can be rescued in these mice models of DYT1 and DYT25 by the chronic administration of dipraglurant, an mGluR5 antagonist, prior to the execution of an LTD inducing protocol (Yu-Taeger et al. 2020). Thus, the priming of Gnal+/- mice by daily injections of dipraglurant could allow for a deeper depression of the response to cerebellar stimulations in the motor network induced by cerebellar theta-burst stimulations.

If the beneficent effect of cerebellar theta-burst stimulation is obtained through the depression of the cerebello-cortical tract, an interesting perspective to explore would be the optimization of the treatment by either experimenting on protocols where both the cerebellum and the cortex are stimulated at a delay (similarly to paired associated stimuli protocols), or a protocol exploiting spontaneous cortical rhythms.

Bibliography

(1) Aggleton, J. P., and Mishkin, M. (1984). Projections of the amygdala to the thalamus in the cynomolgus monkey. *The Journal of Comparative Neurology 222*, 56–68, DOI: 10.1002/cne.902220106, PubMed ID: 6321564.

(2) Aïssa, H. B., Sala, R. W., Georgescu Margarint, E. L., Frontera, J. L., Varani, A. P., Menardy, F., Pelosi, A., Hervé, D., Léna, C., and Popa, D. (2022). Functional abnormalities in the cerebello-thalamic pathways in a mouse model of DYT25 dystonia. *eLife 11*, ed. by Carey, M. R., Behrens, T. E., and Hoebeek PhD, F., Publisher: eLife Sciences Publications, Ltd, e79135, DOI: 10.7554/eLife.79135.

(3) Aizenman, C. D., and Linden, D. J. (2000). Rapid, synaptically driven increases in the intrinsic excitability of cerebellar deep nuclear neurons. *Nature Neuroscience 3*, 109–111, DOI: 10.1038/72049, PubMed ID: 10649564.

(4) Aizenman, C. D., and Linden, D. J. (1999). Regulation of the rebound depolarization and spontaneous firing patterns of deep nuclear neurons in slices of rat cerebellum. *Journal of Neurophysiology 82*, 1697–1709, DOI: 10.1152/jn.1999.82.4.1697, PubMed ID: 10515960.

(5) Aizenman, C. D., Manis, P. B., and Linden, D. J. (1998). Polarity of long-term synaptic gain change is related to postsynaptic spike firing at a cerebellar inhibitory synapse. *Neuron 21*, 827–835, DOI: 10.1016/s0896-6273(00)80598-x, PubMed ID: 9808468.

(6) Albin, R. L., Young, A. B., and Penney, J. B. (1989). The functional anatomy of basal ganglia disorders. *Trends in Neurosciences 12*, 366–375, DOI: 10.1016/0166-2236(89)90074-x, PubMed ID: 2479133.

(7) Albus, J. S. (1971). A theory of cerebellar function. *Mathematical Biosciences 10*, 25–61, DOI: 10.1016/0025-5564(71)90051-4.

(8) Alonso-Martínez, C., Rubio-Teves, M., Porrero, C., and Clascá, F. (2023). Cerebellar and basal ganglia inputs define three main nuclei in the mouse ventral motor thalamus. *Frontiers in Neuroanatomy 17*, 1242839, DOI: 10.3389/fnana.2023.1242839, PubMed ID: 37645018.

(9) Alviña, K., Ellis-Davies, G., and Khodakhah, K. (2009). T-type calcium channels mediate rebound firing in intact deep cerebellar neurons. *Neuroscience 158*, 635–641, DOI: 10.1016/j.neuroscience.2008.09.052, PubMed ID: 18983899.

(10) Alviña, K., Walter, J. T., Kohn, A., Ellis-Davies, G., and Khodakhah, K. (2008). Questioning the role of rebound firing in the cerebellum. *Nature Neuroscience 11*, 1256–1258, DOI: 10.1038/nn.2195, PubMed ID: 18820695.

(11) Aman, T. K., and Raman, I. M. (2007). Subunit dependence of Na channel slow inactivation and open channel block in cerebellar neurons. *Biophysical Journal 92*, 1938–1951, DOI: 10.1529/biophysj.106.093500, PubMed ID: 17189307.

(12) Andre, P., Zaccaroni, M., Fiorenzani, P., Della Seta, D., Menzocchi, M., and Farabollini, F. (2019). Offline consolidation of spatial memory: Do the cerebellar output circuits play a role? A study utilizing a Morris water maze protocol in male Wistar rats. *Brain Research 1718*, 148–158, DOI: 10.1016/j.brainres.2019.05.010, PubMed ID: 31075262.

(13) Angaut, P., and Cicirata, F. (1994). [Anatomo-functional organization of the neocerebellar control pathways on the cerebral motor cortex]. *Revue Neurologique 150*, 39–45, PubMed ID: 7801039.

(14) Angaut, P., and Cicirata, F. (1990). Dentate control pathways of cortical motor activity. Anatomical and physiological studies in rat: comparative considerations. *Archives Italiennes De Biologie 128*, 315–330, PubMed ID: 2268184.

(15) Angaut, P., Cicirata, F., and Serapide, F. (1985). Topographic organization of the cerebellothalamic projections in the rat. An autoradiographic study. *Neuroscience 15*, 389–401, DOI: 10.1016/0306-4522(85)90221-0, PubMed ID: 4022330.

(16) Angaut, P., and Sotelo, C. (1989). Synaptology of the cerebello-olivary pathway. Double labelling with anterograde axonal tracing and GABA immunocytochemistry in the rat. *Brain Research 479*, 361–365, DOI: 10.1016/0006-8993(89)91641-7, PubMed ID: 2466540.

(17) Angaut, P., and Sotelo, C. (1987). The dentato-olivary projection in the rat as a presumptive GABAergic link in the olivo-cerebello-olivary loop. An ultrastructural study. *Neuroscience Letters 83*, 227–231, DOI: 10.1016/0304-3940(87)90090-5, PubMed ID: 3441304.

(18) Ankri, L., Husson, Z., Pietrajtis, K., Proville, R., Léna, C., Yarom, Y., Dieudonné, S., and Uusisaari, M. Y. (2015). A novel inhibitory nucleo-cortical circuit controls cerebellar Golgi cell activity. *eLife 4*, e06262, DOI: 10.7554/eLife.06262, PubMed ID: 25965178.

(19) Apps, R., and Hawkes, R. (2009). Cerebellar cortical organization: a one-map hypothesis. *Nature Reviews Neuroscience 10*, Number: 9 Publisher: Nature Publishing Group, 670–681, DOI: 10.1038/nrn2698.

(20) Apps, R., Hawkes, R., Aoki, S., Bengtsson, F., Brown, A. M., Chen, G., Ebner, T. J., Isope, P., Jörntell, H., Lackey, E. P., Lawrenson, C., Lumb, B., Schonewille, M., Sillitoe, R. V., Spaeth, L., Sugihara, I., Valera, A., Voogd, J., Wylie, D. R., and Ruigrok, T. J. H. (2018). Cerebellar Modules and Their Role as Operational Cerebellar Processing Units. *Cerebellum (London, England) 17*, 654–682, DOI: 10.1007/s12311-018-0952-3, PubMed ID: 29876802.

(21) Argyelan, M., Carbon, M., Niethammer, M., Ulug, A. M., Voss, H. U., Bressman, S. B., Dhawan, V., and Eidelberg, D. (2009). Cerebellothalamocortical connectivity regulates penetrance in dystonia. *The Journal of Neuroscience: The Official Journal of the Society for Neuroscience 29*, Number: 31, 9740–9747, DOI: 10.1523/JNEUROSCI.2300-09.2009, PubMed ID: 19657027.

(22) Armano, S., Rossi, P., Taglietti, V., and D'Angelo, E. (2000). Long-term potentiation of intrinsic excitability at the mossy fiber-granule cell synapse of rat cerebellum. *The Journal of Neuroscience: The Official Journal of the Society for Neuroscience 20*, 5208–5216, DOI: 10.1523/JNEUROSCI.20-14-05208.2000, PubMed ID: 10884304.

(23) Arruda-Carvalho, M., and Clem, R. L. (2015). Prefrontal-amygdala fear networks come into focus. *Frontiers in Systems Neuroscience 9*, https://www.frontiersin.org/articles/10.3389/fnsys.2015.00145.

(24) Arshavsky, Y. I., Berkinblit, M. B., Fukson, O. I., Gelfand, I. M., and Orlovsky, G. N. (1972). Recordings of neurones of the dorsal spinocerebellar tract during evoked locomotion. *Brain Research 43*, 272–275, DOI: 10.1016/0006-8993(72)90295-8, PubMed ID: 5050195.

(25) Arshavsky, Y. I., Gelfand, I. M., Orlovsky, G. N., and Pavlova, G. A. (1978). Messages conveyed by spinocerebellar pathways during scratching in the cat. II. Activity of neurons of the ventral spinocerebellar tract. *Brain Research 151*, 493–506, DOI: 10.1016/0006-8993(78)91082-x, PubMed ID: 667627.

(26) Arshavsky, Y. I., Gelfand, I. M., and Orlovsky, G. N. (1983). The cerebellum and control of rhythmical movements. *Trends in Neurosciences 6*, Publisher: Elsevier, 417–422, DOI: 10.1016/0166-2236(83)90191-1.

(27) Arshavsky YuI, n., Gelfand, I. M., Orlovsky, G. N., Pavlova, G. A., and Popova, L. B. (1984). Origin of signals conveyed by the ventral spino-cerebellar tract and spino-reticulo-cerebellar pathway. *Experimental Brain Research 54*, 426–431, DOI: 10.1007/BF00235467, PubMed ID: 6723862.

(28) Artola, A., Bröcher, S., and Singer, W. (1990). Different voltage-dependent thresholds for inducing long-term depression and long-term potentiation in slices of rat visual cortex. *Nature 347*, 69–72, DOI: 10.1038/347069a0, PubMed ID: 1975639.

(29) Aumann, T. D. (2002). Cerebello-thalamic synapses and motor adaptation. *Cerebellum (London, England) 1*, 69–77, DOI: 10.1080/147342202753203104, PubMed ID: 12879975.

(30) Aumann, T. D., and Horne, M. K. (1999). Ultrastructural change at rat cerebellothalamic synapses associated with volitional motor adaptation. *The Journal of Comparative Neurology 409*, 71–84, DOI: 10.1002/(sici)1096-9861(19990621)409:1<71::aid-cne6>3.0.co;2-c, PubMed ID: 10363712.

(31) Aumann, T. D., Rawson, J. A., Finkelstein, D. I., and Horne, M. K. (1994). Projections from the lateral and interposed cerebellar nuclei to the thalamus of the rat: a light and electron microscopic study using single and double anterograde labelling. *The Journal of Comparative Neurology 349*, 165–181, DOI: 10.1002/cne.903490202, PubMed ID: 7860776.

(32) Aumann, T. D., Redman, S. J., and Horne, M. K. (2000). Long-term potentiation across rat cerebello-thalamic synapses in vitro. *Neuroscience Letters 287*, 151–155, DOI: 10.1016/s0304-3940(00)01162-9, PubMed ID: 10854734.

(33) Azim, E., Jiang, J., Alstermark, B., and Jessell, T. M. (2014). Skilled reaching relies on a V2a propriospinal internal copy circuit. *Nature 508*, 357–363, DOI: 10.1038/nature13021, PubMed ID: 24487617.

(34) Bagur, S., Lefort, J. M., Lacroix, M. M., de Lavilléon, G., Herry, C., Chouvaeff, M., Billand, C., Geoffroy, H., and Benchenane, K. (2021). Breathing-driven prefrontal oscillations regulate maintenance of conditioned-fear evoked freezing independently of initiation. *Nature Communications 12*, Number: 1, 2605, DOI: 10.1038/s41467-021-22798-6, PubMed ID: 33972521.

(35) Baik, J. S. (2012). Neurological picture. Isolated cerebellar hemiatrophy related with focal dystonia. *Journal of Neurology, Neurosurgery, and Psychiatry 83*, 948, DOI: 10.1136/jnnp-2012-303049, PubMed ID: 22842205.

(36) Balint, B., Mencacci, N. E., Valente, E. M., Pisani, A., Rothwell, J., Jankovic, J., Vidailhet, M., and Bhatia, K. P. (2018). Dystonia. *Nature Reviews Disease Primers 4*, Number: 1 Publisher: Nature Publishing Group, 1–23, DOI: 10.1038/s41572-018-0023-6.

(37) Baltaci, S. B., Mogulkoc, R., and Baltaci, A. K. (2019). Molecular Mechanisms of Early and Late LTP. *Neurochemical Research 44*, 281–296, DOI: 10.1007/s11064-018-2695-4, PubMed ID: 30523578.

(38) Bana, C., Nascimbene, C., Vanotti, A., Zardoni, M., Mariani, C., and Osio, M. (2015). A Case of Masticatory Dystonia Following Cerebellar Haemorrhage. *Cerebellum (London, England) 14*, 723–727, DOI: 10.1007/s12311-015-0655-y, PubMed ID: 25700680.

(39) Barakat, M., Doyon, J., Debas, K., Vandewalle, G., Morin, A., Poirier, G., Martin, N., Lafortune, M., Karni, A., Ungerleider, L. G., Benali, H., and Carrier, J. (2011). Fast and slow spindle involvement in the consolidation of a new motor sequence. *Behavioural Brain Research 217*, 117–121, DOI: 10.1016/j.bbr.2010.10.019, PubMed ID: 20974183.

(40) Barakat, M., Carrier, J., Debas, K., Lungu, O., Fogel, S., Vandewalle, G., Hoge, R. D., Bellec, P., Karni, A., Ungerleider, L. G., Benali, H., and Doyon, J. (2013). Sleep spindles predict neural and behavioral changes in motor sequence consolidation. *Human Brain Mapping 34*, 2918–2928, DOI: 10.1002/hbm.22116, PubMed ID: 22674673.

(41) Baranyi, A., Szente, M. B., and Woody, C. D. (1991). Properties of associative long-lasting potentiation induced by cellular conditioning in the motor cortex of conscious cats. *Neuroscience 42*, 321–334, DOI: 10.1016/0306-4522(91)90378-2, PubMed ID: 1896132.

(42) Barash, S., Melikyan, A., Sivakov, A., Zhang, M., Glickstein, M., and Thier, P. (1999). Saccadic dysmetria and adaptation after lesions of the cerebellar cortex. *The Journal of Neuroscience: The Official Journal of the Society for Neuroscience 19*, 10931–10939, DOI: 10.1523/JNEUROSCI.19-24-10931.1999, PubMed ID: 10594074.

(43) Barbera, G., Liang, B., Zhang, L., Gerfen, C. R., Culurciello, E., Chen, R., Li, Y., and Lin, D.-T. (2016). Spatially Compact Neural Clusters in the Dorsal Striatum Encode Locomotion Relevant Information. *Neuron 92*, 202–213, DOI: 10.1016/j.neuron.2016.08.037, PubMed ID: 27667003.

(44) Barrett, D., Shumake, J., Jones, D., and Gonzalez-Lima, F. (2003). Metabolic Mapping of Mouse Brain Activity after Extinction of a Conditioned Emotional Response. *The Journal of Neuroscience 23*, 5740–5749, DOI: 10.1523/JNEUROSCI.23-13-05740.2003, PubMed ID: 12843278.

(45) Batini, C., Compoint, C., Buisseret-Delmas, C., Daniel, H., and Guegan, M. (1992). Cerebellar nuclei and the nucleocortical projections in the rat: retrograde tracing coupled to GABA and glutamate immunohistochemistry. *The Journal of Comparative Neurology 315*, 74–84, DOI: 10.1002/cne.903150106, PubMed ID: 1371781.

(46) Batla, A. (2018). Dystonia: A review. *Neurology India 66*, S48–S58, DOI: 10.4103/0028-3886.226439, PubMed ID: 29503327.

(47) Bédard, P., and Sanes, J. N. (2011). Basal ganglia-dependent processes in recalling learned visual-motor adaptations. *Experimental Brain Research 209*, 385–393, DOI: 10.1007/s00221-011-2561-y, PubMed ID: 21311878.

(48) Belluscio, L., Gold, G. H., Nemes, A., and Axel, R. (1998). Mice deficient in G(olf) are anosmic. *Neuron 20*, Number: 1, 69–81, DOI: 10.1016/s0896-6273(00)80435-3, PubMed ID: 9459443.

(49) Belmeguenai, A., Hosy, E., Bengtsson, F., Pedroarena, C. M., Piochon, C., Teuling, E., He, Q., Ohtsuki, G., De Jeu, M. T. G., Elgersma, Y., De Zeeuw, C. I., Jörntell, H., and Hansel, C. (2010). Intrinsic plasticity complements long-term potentiation in parallel fiber input gain control in cerebellar Purkinje cells. *The Journal of Neuroscience: The Official Journal of the Society for Neuroscience 30*, 13630–13643, DOI: 10.1523/JNEUROSCI.3226-10.2010, PubMed ID: 20943904.

(50) Benazzouz, A., Breit, S., Koudsie, A., Pollak, P., Krack, P., and Benabid, A.-L. (2002). Intraoperative microrecordings of the subthalamic nucleus in Parkinson's disease. *Movement Disorders: Official Journal of the Movement Disorder Society 17 Suppl 3*, S145–149, DOI: 10.1002/mds.10156, PubMed ID: 11948769.

(51) Benninger, D. H., Lomarev, M., Lopez, G., Wassermann, E. M., Li, X., Considine, E., and Hallett, M. (2010). Transcranial direct current stimulation for the treatment of Parkinson's disease. *Journal of Neurology, Neurosurgery, and Psychiatry 81*, 1105–1111, DOI: 10.1136/jnnp.2009.202556, PubMed ID: 20870863.

(52) Bentivoglio, M., and Kuypers, H. G. (1982). Divergent axon collaterals from rat cerebellar nuclei to diencephalon, mesencephalon, medulla oblongata and cervical cord. A fluorescent double retrograde labeling study. *Experimental Brain Research 46*, 339–356, DOI: 10.1007/BF00238629, PubMed ID: 7095042.

(53) Bentivoglio, M., and Molinari, M. (1986). Crossed divergent axon collaterals from cerebellar nuclei to thalamus and lateral medulla oblongata in the rat. *Brain Research 362*, 180–184, DOI: 10.1016/0006-8993(86)91414-9.

(54) Berardelli, A., Inghilleri, M., Rothwell, J. C., Romeo, S., Currà, A., Gilio, F., Modugno, N., and Manfredi, M. (1998). Facilitation of muscle evoked responses after repetitive cortical stimulation in man. *Experimental Brain Research 122*, 79–84, DOI: 10.1007/s002210050493, PubMed ID: 9772114.

(55) Bergman, H., Wichmann, T., Karmon, B., and DeLong, M. R. (1994). The primate subthalamic nucleus. II. Neuronal activity in the MPTP model of parkinsonism. *Journal of Neurophysiology 72*, 507–520, DOI: 10.1152/jn.1994.72.2.507, PubMed ID: 7983515.

(56) Bernard, J., and Seidler, R. (2013). Cerebellar contributions to visuomotor adaptation and motor sequence learning: an ALE meta-analysis. *Frontiers in Human Neuroscience 7*, https://www.frontiersin.org/articles/10.3389/fnhum.2013.00027.

(57) Bharos, T. B., Kuypers, H. G., Lemon, R. N., and Muir, R. B. (1981). Divergent collaterals from deep cerebellar neurons to thalamus and tectum, and to medulla oblongata and spinal cord: retrograde fluorescent and electrophysiological studies. *Experimental Brain Research 42*, 399–410, DOI: 10.1007/BF00237505, PubMed ID: 6165608.

(58) Bhattacharjee, S., Kashyap, R., Abualait, T., Annabel Chen, S.-H., Yoo, W.-K., and Bashir, S. (2021). The Role of Primary Motor Cortex: More Than Movement Execution. *Journal of Motor Behavior 53*, 258–274, DOI: 10.1080/00222895.2020.1738992, PubMed ID: 32194004.

(59) Blanchard, D. C., and Blanchard, R. J. (1988). Ethoexperimental approaches to the biology of emotion. *Annual Review of Psychology 39*, 43–68, DOI: 10.1146/annurev.ps.39.020188.000355, PubMed ID: 2894198.

(60) *Handbook of anxiety and fear*; Blanchard, R. J., Blanchard, D. C., Griebel, G., and Nutt, D., Eds.; Handbook of anxiety and fear, Pages: xv, 517; Elsevier Academic Press: San Diego, CA, US, 2008.

(61) Bloodgood, D. W., Sugam, J. A., Holmes, A., and Kash, T. L. (2018). Fear extinction requires infralimbic cortex projections to the basolateral amygdala. *Translational Psychiatry 8*, 60, DOI: 10.1038/s41398-018-0106-x, PubMed ID: 29507292.

(62) Blot, A., de Solages, C., Ostojic, S., Szapiro, G., Hakim, V., and Léna, C. (2016). Time-invariant feed-forward inhibition of Purkinje cells in the cerebellar cortex in vivo. *The Journal of Physiology 594*, 2729–2749, DOI: 10.1113/JP271518, PubMed ID: 26918702.

(63) Blum, S., Hebert, A. E., and Dash, P. K. (2006). A role for the prefrontal cortex in recall of recent and remote memories. *Neuroreport 17*, 341–344, DOI: 10.1097/01.wnr.0000201509.53750.bc, PubMed ID: 16462609.

(64) Bodranghien, F., Bastian, A., Casali, C., Hallett, M., Louis, E. D., Manto, M., Mariën, P., Nowak, D. A., Schmahmann, J. D., Serrao, M., Steiner, K. M., Strupp, M., Tilikete, C., Timmann, D., and van Dun, K. (2016). Consensus Paper: Revisiting the Symptoms and Signs of Cerebellar Syndrome. *Cerebellum (London, England) 15*, 369–391, DOI: 10.1007/s12311-015-0687-3, PubMed ID: 26105056.

(65) Bogenpohl, J. W., Ritter, S. L., Hall, R. A., and Smith, Y. (2012). Adenosine A2A Receptor in the Monkey Basal Ganglia: Ultrastructural Localization and Colocalization With the Metabotropic Glutamate Receptor 5 in the Striatum. *The Journal of comparative neurology 520*, 570–589, DOI: 10.1002/cne.22751, PubMed ID: 21858817.

(66) Boisen, E. (1979). Torticollis caused by an infratentorial tumour: three cases. *The British Journal of Psychiatry: The Journal of Mental Science 134*, 306–307, DOI: 10.1192/bjp.134.3.306, PubMed ID: 509012.

(67) Bolam, J. P., Izzo, P. N., and Graybiel, A. M. (1988). Cellular substrate of the histochemically defined striosome/matrix system of the caudate nucleus: a combined Golgi and immunocytochemical study in cat and ferret. *Neuroscience 24*, 853–875, DOI: 10.1016/0306-4522(88)90073-5, PubMed ID: 2454418.

(68) Bologna, M., and Berardelli, A. (2017). Cerebellum: An explanation for dystonia? *Cerebellum & Ataxias 4*, 6, DOI: 10.1186/s40673-017-0064-8, PubMed ID: 28515949.

(69) Bonjean, M., Baker, T., Lemieux, M., Timofeev, I., Sejnowski, T., and Bazhenov, M. (2011). Corticothalamic feedback controls sleep spindle duration in vivo. *The Journal of Neuroscience: The Official Journal of the Society for Neuroscience 31*, 9124–9134, DOI: 10.1523/JNEUROSCI.0077-11.2011, PubMed ID: 21697364.

(70) Bosco, G., and Poppele, R. E. (2001). Proprioception from a spinocerebellar perspective. *Physiological Reviews 81*, 539–568, DOI: 10.1152/physrev.2001.81.2.539, PubMed ID: 11274339.

(71) Bostan, A. C., Dum, R. P., and Strick, P. L. (2013). Cerebellar networks with the cerebral cortex and basal ganglia. *Trends in cognitive sciences 17*, Number: 5, 241–254, DOI: 10.1016/j.tics.2013.03.003, PubMed ID: 23579055.

(72) Bostan, A. C., Dum, R. P., and Strick, P. L. (2010). The basal ganglia communicate with the cerebellum. *Proceedings of the National Academy of Sciences of the United States of America 107*, 8452–8456, DOI: 10.1073/pnas.1000496107, PubMed ID: 20404184.

(73) Bostan, A. C., and Strick, P. L. (2018). The basal ganglia and the cerebellum: nodes in an integrated network. *Nature reviews. Neuroscience 19*, Number: 6, 338–350, DOI: 10.1038/s41583-018-0002-7, PubMed ID: 29643480.

(74) Bouton, M. E., and Bolles, R. C. (1979). Contextual control of the extinction of conditioned fear. *Learning and Motivation 10*, 445–466, DOI: 10.1016/0023-9690(79)90057-2.

(75) Bracke-Tolkmitt, R., Linden, A., Canavan, A. G. M., Rockstroh, B., Scholz, E., Wessel, K., and Diener, H.-C. (1989). The cerebellum contributes to mental skills. *Behavioral Neuroscience 103*, Place: US Publisher: American Psychological Association, 442–446, DOI: 10.1037/0735-7044.103.2.442.

(76) Bradnam, L. V., Graetz, L. J., McDonnell, M. N., and Ridding, M. C. (2015). Anodal transcranial direct current stimulation to the cerebellum improves handwriting and cyclic drawing kinematics in focal hand dystonia. *Frontiers in Human Neuroscience 9*, 286, DOI: 10.3389/fnhum.2015.00286, PubMed ID: 26042019.

(77) Bradnam, L. V., McDonnell, M. N., and Ridding, M. C. (2016). Cerebellar Intermittent Theta-Burst Stimulation and Motor Control Training in Individuals with Cervical Dystonia. *Brain Sciences 6*, 56, DOI: 10.3390/brainsci6040056, PubMed ID: 27886079.

(78) Brager, D. H., and Johnston, D. (2007). Plasticity of intrinsic excitability during long-term depression is mediated through mGluR-dependent changes in I(h) in hippocampal CA1 pyramidal neurons. *The Journal of Neuroscience: The Official Journal of the Society for Neuroscience 27*, 13926–13937, DOI: 10.1523/JNEUROSCI.3520-07.2007, PubMed ID: 18094230.

(79) Braitenberg, V., and Atwood, R. P. (1958). Morphological observations on the cerebellar cortex. *The Journal of Comparative Neurology 109*, 1–33, DOI: 10.1002/cne.901090102, PubMed ID: 13563670.

(80) Broca, P. (1878). Anatomie comparée des circonvolutions cérébrales. Le grand lobe limbique et la scissure limbique dans la série des mammifères. *Rev Anthrop 1*, 385–498.

(81) Brown, A. M., van der Heijden, M. E., Jinnah, H. A., and Sillitoe, R. V. (2022). Cerebellar Dysfunction as a Source of Dystonic Phenotypes in Mice. *Cerebellum (London, England)*, DOI: 10.1007/s12311-022-01441-0, PubMed ID: 35821365.

(82) Brown, A. M., van der Heijden, M. E., Jinnah, H. A., and Sillitoe, R. V. (2023). Cerebellar Dysfunction as a Source of Dystonic Phenotypes in Mice. *Cerebellum (London, England) 22*, 719–729, DOI: 10.1007/s12311-022-01441-0, PubMed ID: 35821365.

(83) Brown, E. G., Bledsoe, I. O., Luthra, N. S., Miocinovic, S., Starr, P. A., and Ostrem, J. L. (2020). Cerebellar Deep Brain Stimulation for Acquired Hemidystonia. *Movement Disorders Clinical Practice 7*, _eprint: https://onlinelibrary.wiley.com/doi/pdf/10.1002/mdc3.12876, 188–193, DOI: 10.1002/mdc3.12876.

(84) Buch, E. R., Claudino, L., Quentin, R., Bönstrup, M., and Cohen, L. G. (2021). Consolidation of human skill linked to waking hippocampo-neocortical replay. *Cell Reports 35*, 109193, DOI: 10.1016/j.celrep.2021.109193.

(85) Bukalo, O., Nonaka, M., Weinholtz, C. A., Mendez, A., Taylor, W. W., and Holmes, A. (2021). Effects of optogenetic photoexcitation of infralimbic cortex inputs to the basolateral amygdala on conditioned fear and extinction. *Behavioural Brain Research 396*, 112913, DOI: 10.1016/j.bbr.2020.112913, PubMed ID: 32950607.

(86) Bürk, K. (2017). Friedreich Ataxia: current status and future prospects. *Cerebellum & Ataxias 4*, 4, DOI: 10.1186/s40673-017-0062-x, PubMed ID: 28405347.

(87) Burroughs, A., Wise, A. K., Xiao, J., Houghton, C., Tang, T., Suh, C. Y., Lang, E. J., Apps, R., and Cerminara, N. L. (2017). The dynamic relationship between cerebellar Purkinje cell simple spikes and the spikelet number of complex spikes. *The Journal of Physiology 595*, 283–299, DOI: 10.1113/JP272259, PubMed ID: 27265808.

(88) Busch, S. E., and Hansel, C. (2023). Climbing fiber multi-innervation of mouse Purkinje dendrites with arborization common to human. *Science (New York, N.Y.) 381*, 420–427, DOI: 10.1126/science.adi1024, PubMed ID: 37499000.

(89) Buttkus, F., Baur, V., Jabusch, H.-C., de la Cruz Gomez-Pellin, M., Paulus, W., Nitsche, M. A., and Altenmüller, E. (2011). Single-session tDCS-supported retraining does not improve fine motor control in musician's dystonia. *Restorative Neurology and Neuroscience 29*, 85–90, DOI: 10.3233/RNN-2011-0582, PubMed ID: 21701060.

(90) Buzsáki, G. (1989). Two-stage model of memory trace formation: a role for "noisy" brain states. *Neuroscience 31*, 551–570, DOI: 10.1016/0306-4522(89)90423-5, PubMed ID: 2687720.

(91) Buzsáki, G., *Rhythms of the Brain*; Oxford University Press: 2006, DOI: 10.1093/acprof:oso/9780195301069.001.0001.

(92) Calabresi, P., Picconi, B., Tozzi, A., Ghiglieri, V., and Di Filippo, M. (2014). Direct and indirect pathways of basal ganglia: a critical reappraisal. *Nature Neuroscience 17*, 1022–1030, DOI: 10.1038/nn.3743.

(93) Calabresi, P., Pisani, A., Rothwell, J., Ghiglieri, V., Obeso, J. A., and Picconi, B. (2016). Hyperkinetic disorders and loss of synaptic downscaling. *Nature Neuroscience 19*, Number: 7, 868–875, DOI: 10.1038/nn.4306, PubMed ID: 27351172.

(94) Calderon, D. P., Fremont, R., Kraenzlin, F., and Khodakhah, K. (2011). The neural substrates of Rapid-Onset Dystonia-Parkinsonism. *Nature neuroscience 14*, 357–365, DOI: 10.1038/nn.2753, PubMed ID: 21297628.

(95) Carecchio, M., Panteghini, C., Reale, C., Barzaghi, C., Monti, V., Romito, L., Sasanelli, F., and Garavaglia, B. (2016). Novel GNAL mutation with intra-familial clinical heterogeneity: Expanding the phenotype. *Parkinsonism & Related Disorders 23*, 66–71, DOI: 10.1016/j.parkreldis.2015.12.012.

(96) Carretta, D., Sbriccoli, A., Santarelli, M., Pinto, F., Granato, A., and Minciacchi, D. (1996). Crossed thalamo-cortical and cortico-thalamic projections in adult mice. *Neuroscience Letters 204*, 69–72, DOI: 10.1016/0304-3940(96)12319-3.

(97) Castle, M., Aymerich, M. S., Sanchez-Escobar, C., Gonzalo, N., Obeso, J. A., and Lanciego, J. L. (2005). Thalamic innervation of the direct and indirect basal ganglia pathways in the rat: Ipsi- and contralateral projections. *The Journal of Comparative Neurology 483*, 143–153, DOI: 10.1002/cne.20421, PubMed ID: 15678473.

(98) Castro, L. R. V., Brito, M., Guiot, E., Polito, M., Korn, C. W., Hervé, D., Girault, J.-A., Paupardin-Tritsch, D., and Vincent, P. (2013). Striatal neurones have a specific ability to respond to phasic dopamine release. *The Journal of Physiology 591*, 3197–3214, DOI: 10.1113/jphysiol.2013.252197, PubMed ID: 23551948.

(99) Catani, M. (2017). A little man of some importance. *Brain: A Journal of Neurology 140*, 3055–3061, DOI: 10.1093/brain/awx270, PubMed ID: 29088352.

(100) Cavdar, S., San, T., Aker, R., Sehirli, U., and Onat, F. (2001). Cerebellar connections to the dorsomedial and posterior nuclei of the hypothalamus in the rat. *Journal of Anatomy 198*, 37–45, DOI: 10.1046/j.1469-7580.2001.19810037.x, PubMed ID: 11215766.

(101) Çavdar, S., Onat, F. Y. l., Yananli, H. R., Şehirli, Ü. S., Tulay, C., Saka, E., and Gürdal, E. (2002). Cerebellar connections to the rostral reticular nucleus of the thalamus in the rat. *Journal of Anatomy 201*, 485–491, DOI: 10.1046/j.1469-7580.2002.00119.x, PubMed ID: 12489760.

(102) Cesana, E., Pietrajtis, K., Bidoret, C., Isope, P., D'Angelo, E., Dieudonné, S., and Forti, L. (2013). Granule cell ascending axon excitatory synapses onto Golgi cells implement a potent feedback circuit in the cerebellar granular layer. *The Journal of Neuroscience: The Official Journal of the Society for Neuroscience 33*, 12430–12446, DOI: 10.1523/JNEUROSCI.4897-11.2013, PubMed ID: 23884948.

(103) Chabrol, F. P., Blot, A., and Mrsic-Flogel, T. D. (2019). Cerebellar Contribution to Preparatory Activity in Motor Neocortex. *Neuron 103*, 506–519.e4, DOI: 10.1016/j.neuron.2019.05.022, PubMed ID: 31201123.

(104) Chail, A., Saini, R. K., Bhat, P. S., Srivastava, K., and Chauhan, V. (2018). Transcranial magnetic stimulation: A review of its evolution and current applications. *Industrial Psychiatry Journal 27*, 172–180, DOI: 10.4103/ipj.ipj_88_18, PubMed ID: 31359968.

(105) Charalambous, C. C., Bowden, M. G., and Adkins, D. L. (2016). Motor cortex and motor cortical interhemispheric communication in walking afterstroke – the roles of TMS and animal models in our current and future understanding. *Neurorehabilitation and neural repair 30*, 94–102, DOI: 10.1177/1545968315581418, PubMed ID: 25878201.

(106) Chen, C. H., Fremont, R., Arteaga-Bracho, E. E., and Khodakhah, K. (2014). Short latency cerebellar modulation of the basal ganglia. *Nature neuroscience 17*, Number: 12, 1767–1775, DOI: 10.1038/nn.3868, PubMed ID: 25402853.

(107) Chen, M., and Bi, L.-L. (2019). Optogenetic Long-Term Depression Induction in the PVT-CeL Circuitry Mediates Decreased Fear Memory. *Molecular Neurobiology 56*, 4855–4865, DOI: 10.1007/s12035-018-1407-z, PubMed ID: 30406427.

(108) Chen, S., and Hillman, D. E. (1993). Colocalization of neurotransmitters in the deep cerebellar nuclei. *Journal of Neurocytology 22*, 81–91, DOI: 10.1007/BF01181572, PubMed ID: 8095297.

(109) Chen, W., de Hemptinne, C., Miller, A. M., Leibbrand, M., Little, S. J., Lim, D. A., Larson, P. S., and Starr, P. A. (2020). Prefrontal-Subthalamic Hyperdirect Pathway Modulates Movement Inhibition in Humans. *Neuron 106*, 579–588.e3, DOI: 10.1016/j.neuron.2020.02.012, PubMed ID: 32155442.

(110) Chouinard, P. A., and Paus, T. (2006). The primary motor and premotor areas of the human cerebral cortex. *The Neuroscientist: A Review Journal Bringing Neurobiology, Neurology and Psychiatry 12*, 143–152, DOI: 10.1177/1073858405284255, PubMed ID: 16514011.

(111) Clark, E., Johnson, J., Dong, Y. N., Mercado-Ayon, E., Warren, N., Zhai, M., McMillan, E., Salovin, A., Lin, H., and Lynch, D. R. (2018). Role of frataxin protein deficiency and metabolic dysfunction in Friedreich ataxia, an autosomal recessive mitochondrial disease. *Neuronal Signaling 2*, NS20180060, DOI: 10.1042/NS20180060, PubMed ID: 32714592.

(112) Classen, J. In *Handbook of Clinical Neurology*; Elsevier: 2013; Vol. 116, pp 525–534.

(113) Coesmans, M., Weber, J. T., De Zeeuw, C. I., and Hansel, C. (2004). Bidirectional parallel fiber plasticity in the cerebellum under climbing fiber control. *Neuron 44*, 691–700, DOI: 10.1016/j.neuron.2004.10.031, PubMed ID: 15541316.

(114) Cohen, D. A., Pascual-Leone, A., Press, D. Z., and Robertson, E. M. (2005). Off-line learning of motor skill memory: A double dissociation of goal and movement. *Proceedings of the National Academy of Sciences 102*, Publisher: Proceedings of the National Academy of Sciences, 18237–18241, DOI: 10.1073/pnas.0506072102.

(115) Collins, D. P., Anastasiades, P. G., Marlin, J. J., and Carter, A. G. (2018). Reciprocal circuits linking the prefrontal cortex with dorsal and ventral thalamic nuclei. *Neuron 98*, Number: 2, 366–379.e4, DOI: 10.1016/j.neuron.2018.03.024, PubMed ID: 29628187.

(116) Coltz, J. D., Johnson, M. T., and Ebner, T. J. (1999). Cerebellar Purkinje cell simple spike discharge encodes movement velocity in primates during visuomotor arm tracking. *The Journal of Neuroscience: The Official Journal of the Society for Neuroscience 19*, 1782–1803, DOI: 10.1523/JNEUROSCI.19-05-01782.1999, PubMed ID: 10024363.

(117) Constantinou, M., Elijah, D. H., Squirrell, D., Gigg, J., and Montemurro, M. A. (2015). Phase-locking of bursting neuronal firing to dominant LFP frequency components. *Bio Systems 136*, Publisher: Elsevier, 73, DOI: 10.1016/j.biosystems.2015.08.004, PubMed ID: 26305338.

(118) Conti, A. M., Pullman, S., and Frucht, S. J. (2008). The hand that has forgotten its cunning–lessons from musicians' hand dystonia. *Movement Disorders: Official Journal of the Movement Disorder Society 23*, 1398–1406, DOI: 10.1002/mds.21976, PubMed ID: 18398917.

(119) Contreras, D., and Steriade, M. (1996). Spindle oscillation in cats: the role of corticothalamic feedback in a thalamically generated rhythm. *The Journal of Physiology 490 (Pt 1)*, 159–179, DOI: 10.1113/jphysiol.1996.sp021133, PubMed ID: 8745285.

(120) Contreras-López, R., Alatriste-León, H., Díaz-Hernández, E., Ramírez-Jarquín, J. O., and Tecuapetla, F. (2023). The deep cerebellar nuclei to striatum disynaptic connection contributes to skilled forelimb movement. *Cell Reports 42*, 112000, DOI: 10.1016/j.celrep.2023.112000.

(121) Corcoran, K. A., and Quirk, G. J. (2007). Activity in Prelimbic Cortex Is Necessary for the Expression of Learned, But Not Innate, Fears. *The Journal of Neuroscience 27*, 840–844, DOI: 10.1523/JNEUROSCI.5327-06.2007, PubMed ID: 17251424.

(122) Corvol, J. C., Studler, J. M., Schonn, J. S., Girault, J. A., and Hervé, D. (2001). Galpha(olf) is necessary for coupling D1 and A2a receptors to adenylyl cyclase in the striatum. *Journal of Neurochemistry 76*, Number: 5, 1585–1588, DOI: 10.1046/j.1471-4159.2001.00201.x, PubMed ID: 11238742.

(123) Corvol, J.-C., Valjent, E., Pascoli, V., Robin, A., Stipanovich, A., Luedtke, R. R., Belluscio, L., Girault, J.-A., and Hervé, D. (2007). Quantitative changes in Galphaolf protein levels, but not D1 receptor, alter specifically acute responses to psychostimulants. *Neuropsychopharmacology: Official Publication of the American College of Neuropsychopharmacology 32*, 1109–1121, DOI: 10.1038/sj.npp.1301230, PubMed ID: 17063155.

(124) Coutant, B., Frontera, J. L., Perrin, E., Combes, A., Tarpin, T., Menardy, F., Mailhes-Hamon, C., Perez, S., Degos, B., Venance, L., Léna, C., and Popa, D. (2022). Cerebellar stimulation prevents Levodopa-induced dyskinesia in mice and normalizes activity in a motor network. *Nature Communications 13*, 3211, DOI: 10.1038/s41467-022-30844-0, PubMed ID: 35680891.

(125) Criscimagna-Hemminger, S. E., Bastian, A. J., and Shadmehr, R. (2010). Size of error affects cerebellar contributions to motor learning. *Journal of Neurophysiology 103*, 2275–2284, DOI: 10.1152/jn.00822.2009, PubMed ID: 20164398.

(126) Cui, G., Jun, S. B., Jin, X., Pham, M. D., Vogel, S. S., Lovinger, D. M., and Costa, R. M. (2013). Concurrent activation of striatal direct and indirect pathways during action initiation. *Nature 494*, 238–242, DOI: 10.1038/nature11846, PubMed ID: 23354054.

(127) Cunningham, M. O., Whittington, M. A., Bibbig, A., Roopun, A., LeBeau, F. E. N., Vogt, A., Monyer, H., Buhl, E. H., and Traub, R. D. (2004). A role for fast rhythmic bursting neurons in cortical gamma oscillations in vitro. *Proceedings of the National Academy of Sciences 101*, Publisher: Proceedings of the National Academy of Sciences, 7152–7157, DOI: 10.1073/pnas.0402060101.

(128) D'Angelo, E. In *Progress in Brain Research*, Ramnani, N., Ed.; Cerebellar Learning, Vol. 210; Elsevier: 2014, pp 31–58, DOI: 10.1016/B978-0-444-63356-9.00002-9.

(129) D'Angelo, E., Mapelli, L., Casellato, C., Garrido, J. A., Luque, N., Monaco, J., Prestori, F., Pedrocchi, A., and Ros, E. (2016). Distributed Circuit Plasticity: New Clues for the Cerebellar Mechanisms of Learning. *The Cerebellum 15*, 139–151, DOI: 10.1007/s12311-015-0711-7.

(130) Dacre, J., Colligan, M., Clarke, T., Ammer, J. J., Schiemann, J., Chamosa-Pino, V., Claudi, F., Harston, J. A., Eleftheriou, C., Pakan, J. M., Huang, C.-C., Hantman, A. W., Rochefort, N. L., and Duguid, I. (2021). A cerebellar-thalamocortical pathway drives behavioral context-dependent movement initiation. *Neuron 109*, Number: 14, 2326–2338.e8, DOI: 10.1016/j.neuron.2021.05.016, PubMed ID: 34146469.

(131) Dahlström, A., and Fuxe, K. (1964). Localization of monoamines in the lower brain stem. *Experientia 20*, 398–399, DOI: 10.1007/BF02147990, PubMed ID: 5856530.

(132) Dang, M. T., Yokoi, F., McNaught, K. S. P., Jengelley, T.-A., Jackson, T., Li, J., and Li, Y. (2005). Generation and characterization of Dyt1 DeltaGAG knock-in mouse as a model for early-onset dystonia. *Experimental Neurology 196*, 452–463, DOI: 10.1016/j.expneurol.2005.08.025, PubMed ID: 16242683.

(133) Davidson, T. J., Kloosterman, F., and Wilson, M. A. (2009). Hippocampal replay of extended experience. *Neuron 63*, 497–507, DOI: 10.1016/j.neuron.2009.07.027, PubMed ID: 19709631.

(134) Davis, P., Zaki, Y., Maguire, J., and Reijmers, L. G. (2017). Cellular and Oscillatory Substrates of Fear Extinction Learning. *Nature neuroscience 20*, 1624–1633, DOI: 10.1038/nn.4651, PubMed ID: 28967909.

(135) De Zeeuw, C. I., Lisberger, S. G., and Raymond, J. L. (2021). Diversity and dynamism in the cerebellum. *Nature Neuroscience 24*, 160–167, DOI: 10.1038/s41593-020-00754-9.

(136) Dean, P. (1995). Modelling the role of the cerebellar fastigial nuclei in producing accurate saccades: the importance of burst timing. *Neuroscience 68*, 1059–1077, DOI: 10.1016/0306-4522(95)00239-f, PubMed ID: 8544982.

(137) Dean, P., and Porrill, J. (2008). Adaptive-filter models of the cerebellum: computational analysis. *Cerebellum (London, England) 7*, 567–571, DOI: 10.1007/s12311-008-0067-3, PubMed ID: 18972182.

(138) Debas, K., Carrier, J., Orban, P., Barakat, M., Lungu, O., Vandewalle, G., Hadj Tahar, A., Bellec, P., Karni, A., Ungerleider, L. G., Benali, H., and Doyon, J. (2010). Brain plasticity related to the consolidation of motor sequence learning and motor adaptation. *Proceedings of the National Academy of Sciences of the United States of America 107*, 17839–17844, DOI: 10.1073/pnas.1013176107, PubMed ID: 20876115.

(139) Dejean, C., Courtin, J., Karalis, N., Chaudun, F., Wurtz, H., Bienvenu, T. C. M., and Herry, C. (2016). Prefrontal neuronal assemblies temporally control fear behaviour. *Nature 535*, Number: 7612, 420–424, DOI: 10.1038/nature18630, PubMed ID: 27409809.

(140) DeLong, M. R. (1990). Primate models of movement disorders of basal ganglia origin. *Trends in Neurosciences 13*, 281–285, DOI: 10.1016/0166-2236(90)90110-v, PubMed ID: 1695404.

(141) Delvendahl, I., Jung, N. H., Mainberger, F., Kuhnke, N. G., Cronjaeger, M., and Mall, V. (2010). Occlusion of bidirectional plasticity by preceding low-frequency stimulation in the human motor cortex. *Clinical Neurophysiology: Official Journal of the International Federation of Clinical Neurophysiology 121*, 594–602, DOI: 10.1016/j.clinph.2009.09.034, PubMed ID: 20074998.

(142) Dermon, C. R., and Barbas, H. (1994). Contralateral thalamic projections predominantly reach transitional cortices in the rhesus monkey. *The Journal of Comparative Neurology 344*, 508–531, DOI: 10.1002/cne.903440403, PubMed ID: 7523458.

(143) Destexhe, A., and Sejnowski, T. J. (2002). The initiation of bursts in thalamic neurons and the cortical control of thalamic sensitivity. *Philosophical Transactions of the Royal Society B: Biological Sciences 357*, 1649–1657, DOI: 10.1098/rstb.2002.1154, PubMed ID: 12626001.

(144) Dieudonné, S., and Dumoulin, A. (2000). Serotonin-driven long-range inhibitory connections in the cerebellar cortex. *The Journal of Neuroscience: The Official Journal of the Society for Neuroscience 20*, 1837–1848, DOI: 10.1523/JNEUROSCI.20-05-01837.2000, PubMed ID: 10684885.

(145) Donoghue, J. P., and Herkenham, M. (1986). Neostriatal projections from individual cortical fields conform to histochemically distinct striatal compartments in the rat. *Brain Research 365*, 397–403, DOI: 10.1016/0006-8993(86)91658-6, PubMed ID: 3004664.

(146) Douglas, R. J., and Martin, K. A. (1991). A functional microcircuit for cat visual cortex. *The Journal of Physiology 440*, 735–769, DOI: 10.1113/jphysiol.1991.sp018733, PubMed ID: 1666655.

(147) Douglas, R. J., and Martin, K. A. C. (2004). Neuronal circuits of the neocortex. *Annual Review of Neuroscience 27*, 419–451, DOI: 10.1146/annurev.neuro.27.070203.144152, PubMed ID: 15217339.

(148) Doya, K. (1999). What are the computations of the cerebellum, the basal ganglia and the cerebral cortex? *Neural Networks: The Official Journal of the International Neural Network Society 12*, 961–974, DOI: 10.1016/s0893-6080(99)00046-5, PubMed ID: 12662639.

(149) Doya, K. (2000). Complementary roles of basal ganglia and cerebellum in learning and motor control. *Current Opinion in Neurobiology 10*, 732–739, DOI: 10.1016/S0959-4388(00)00153-7.

(150) Doyon, J., Korman, M., Morin, A., Dostie, V., Hadj Tahar, A., Benali, H., Karni, A., Ungerleider, L. G., and Carrier, J. (2009). Contribution of night and day sleep vs. simple passage of time to the consolidation of motor sequence and visuomotor adaptation learning. *Experimental Brain Research 195*, 15–26, DOI: 10.1007/s00221-009-1748-y, PubMed ID: 19277618.

(151) Doyon, J., Penhune, V., and Ungerleider, L. G. (2003). Distinct contribution of the cortico-striatal and cortico-cerebellar systems to motor skill learning. *Neuropsychologia 41*, 252–262, DOI: 10.1016/s0028-3932(02)00158-6, PubMed ID: 12457751.

(152) Drinnan, S. L., Hope, B. T., Snutch, T. P., and Vincent, S. R. (1991). G(olf) in the basal ganglia. *Molecular and Cellular Neurosciences 2*, 66–70, DOI: 10.1016/1044-7431(91)90040-u, PubMed ID: 19912784.

(153) Dubois, C. J., Fawcett-Patel, J., Katzman, P. A., and Liu, S. J. (2020). Inhibitory neurotransmission drives endocannabinoid degradation to promote memory consolidation. *Nature Communications 11*, 6407, DOI: 10.1038/s41467-020-20121-3, PubMed ID: 33335094.

(154) Dubois, C. J., and Liu, S. J. (2021). GluN2D NMDA Receptors Gate Fear Extinction Learning and Interneuron Plasticity. *Frontiers in Synaptic Neuroscience 13*, 681068, DOI: 10.3389/fnsyn.2021.681068, PubMed ID: 34108872.

(155) Dufke, C., Sturm, M., Schroeder, C., Moll, S., Ott, T., Riess, O., Bauer, P., and Grundmann, K. (2014). Screening of mutations in GNAL in sporadic dystonia patients. *Movement Disorders: Official Journal of the Movement Disorder Society 29*, 1193–1196, DOI: 10.1002/mds.25794, PubMed ID: 24408567.

(156) Dugué, G. P., Akemann, W., and Knöpfel, T. (2012). A comprehensive concept of optogenetics. *Progress in Brain Research 196*, 1–28, DOI: 10.1016/B978-0-444-59426-6.00001-X, PubMed ID: 22341318.

(157) Dugué, G. P., Lörincz, M. L., Lottem, E., Audero, E., Matias, S., Correia, P. A., Léna, C., and Mainen, Z. F. (2014). Optogenetic recruitment of dorsal raphe serotonergic neurons acutely decreases mechanosensory responsivity in behaving mice. *PloS One 9*, e105941, DOI: 10.1371/journal.pone.0105941, PubMed ID: 25148042.

(158) Dum, R. P., and Strick, P. L. (1991). The origin of corticospinal projections from the premotor areas in the frontal lobe. *The Journal of Neuroscience: The Official Journal of the Society for Neuroscience 11*, 667–689, DOI: 10.1523/JNEUROSCI.11-03-00667.1991, PubMed ID: 1705965.

(159) Dumoulin, A., Triller, A., and Dieudonné, S. (2001). IPSC kinetics at identified GABAergic and mixed GABAergic and glycinergic synapses onto cerebellar Golgi cells. *The Journal of Neuroscience: The Official Journal of the Society for Neuroscience 21*, 6045–6057, DOI: 10.1523/JNEUROSCI.21-16-06045.2001, PubMed ID: 11487628.

(160) Ebner, T. J., and Pasalar, S. (2008). Cerebellum predicts the future motor state. *Cerebellum (London, England) 7*, 583–588, DOI: 10.1007/s12311-008-0059-3, PubMed ID: 18850258.

(161) Eccles, J., Llinas, R., and Sasaki, K. (1964). GOLGI CELL INHIBITION IN THE CEREBELLAR CORTEX. *Nature 204*, 1265–1266, DOI: 10.1038/2041265a0, PubMed ID: 14254404.

(162) Eccles, J. C., *The cerebellum as a neuronal machine*; Springer Science & Business Media: 1967.

(163) Edwards, M. J., Huang, Y.-Z., Mir, P., Rothwell, J. C., and Bhatia, K. P. (2006). Abnormalities in motor cortical plasticity differentiate manifesting and nonmanifesting DYT1 carriers. *Movement Disorders: Official Journal of the Movement Disorder Society 21*, 2181–2186, DOI: 10.1002/mds.21160, PubMed ID: 17078060.

(164) Ego-Stengel, V., and Wilson, M. A. (2010). Disruption of ripple-associated hippocampal activity during rest impairs spatial learning in the rat. *Hippocampus 20*, 1–10, DOI: 10.1002/hipo.20707, PubMed ID: 19816984.

(165) Eichenlaub, J.-B., Jarosiewicz, B., Saab, J., Franco, B., Kelemen, J., Halgren, E., Hochberg, L. R., and Cash, S. S. (2020). Replay of Learned Neural Firing Sequences during Rest in Human Motor Cortex. *Cell Reports 31*, Number: 5, 107581, DOI: 10.1016/j.celrep.2020.107581, PubMed ID: 32375031.

(166) Eisen, A., and Weber, M. (2001). The motor cortex and amyotrophic lateral sclerosis. *Muscle & Nerve 24*, 564–573, DOI: 10.1002/mus.1042, PubMed ID: 11268031.

(167) Eltokhi, A., Kurpiers, B., and Pitzer, C. (2021). Comprehensive characterization of motor and coordination functions in three adolescent wild-type mouse strains. *Scientific Reports 11*, Number: 1 Publisher: Nature Publishing Group, 6497, DOI: 10.1038/s41598-021-85858-3.

(168) Enderle, J. D. (2002). Neural control of saccades. *Progress in Brain Research 140*, 21–49, DOI: 10.1016/S0079-6123(02)40040-4, PubMed ID: 12508580.

(169) Engbers, J. D. T., Anderson, D., Tadayonnejad, R., Mehaffey, W. H., Molineux, M. L., and Turner, R. W. (2011). Distinct roles for I(T) and I(H) in controlling the frequency and timing of rebound spike responses. *The Journal of Physiology 589*, 5391–5413, DOI: 10.1113/jphysiol.2011.215632, PubMed ID: 21969455.

(170) Fafara-Leś, A., Kwiatkowski, S., Maryńczak, L., Kawecki, Z., Adamek, D., Herman-Sucharska, I., and Kobylarz, K. (2014). Torticollis as a first sign of posterior fossa and cervical spinal cord tumors in children. *Child's Nervous System: ChNS: Official Journal of the International Society for Pediatric Neurosurgery 30*, 425–430, DOI: 10.1007/s00381-013-2255-9, PubMed ID: 23955178.

(171) Falls, W. A., Miserendino, M. J., and Davis, M. (1992). Extinction of fear-potentiated startle: blockade by infusion of an NMDA antagonist into the amygdala. *The Journal of Neuroscience: The Official Journal of the Society for Neuroscience 12*, 854–863, DOI: 10.1523/JNEUROSCI.12-03-00854.1992, PubMed ID: 1347562.

(172) Farley, S. J., Radley, J. J., and Freeman, J. H. (2016). Amygdala Modulation of Cerebellar Learning. *The Journal of Neuroscience: The Official Journal of the Society for Neuroscience 36*, 2190–2201, DOI: 10.1523/JNEUROSCI.3361-15.2016, PubMed ID: 26888929.

(173) Fernandez, L. M. J., and Lüthi, A. (2020). Sleep Spindles: Mechanisms and Functions. *Physiological Reviews 100*, 805–868, DOI: 10.1152/physrev.00042.2018, PubMed ID: 31804897.

(174) Ferraris, M., Ghestem, A., Vicente, A. F., Nallet-Khosrofian, L., Bernard, C., and Quilichini, P. P. (2018). The Nucleus Reuniens Controls Long-Range Hippocampo–Prefrontal Gamma Synchronization during Slow Oscillations. *The Journal of Neuroscience 38*, 3026–3038, DOI: 10.1523/JNEUROSCI.3058-17.2018, PubMed ID: 29459369.

(175) Ferrucci, R., Bocci, T., Cortese, F., Ruggiero, F., and Priori, A. (2016). Cerebellar transcranial direct current stimulation in neurological disease. *Cerebellum & Ataxias 3*, 16, DOI: 10.1186/s40673-016-0054-2, PubMed ID: 27595007.

(176) Fogel, S. M., Smith, C. T., and Cote, K. A. (2007). Dissociable learning-dependent changes in REM and non-REM sleep in declarative and procedural memory systems. *Behavioural Brain Research 180*, 48–61, DOI: 10.1016/j.bbr.2007.02.037, PubMed ID: 17400305.

(177) Foster, A. C., Mena, E. E., Monaghan, D. T., and Cotman, C. W. (1981). Synaptic localization of kainic acid binding sites. *Nature 289*, 73–75, DOI: 10.1038/289073a0, PubMed ID: 6256647.

(178) Foster, D. J., and Wilson, M. A. (2006). Reverse replay of behavioural sequences in hippocampal place cells during the awake state. *Nature 440*, 680–683, DOI: 10.1038/nature04587, PubMed ID: 16474382.

(179) Fraioli, B., and Guidetti, n. (1975). Effects of stereotactic lesions of the dentate nucleus of the cerebellum in man. *Applied Neurophysiology 38*, 81–90, DOI: 10.1159/000102647, PubMed ID: 769688.

(180) Fredette, B. J., and Mugnaini, E. (1991). The GABAergic cerebello-olivary projection in the rat. *Anatomy and Embryology 184*, 225–243, DOI: 10.1007/BF01673258, PubMed ID: 1793166.

(181) Fremont, R., Calderon, D. P., Maleki, S., and Khodakhah, K. (2014). Abnormal High-Frequency Burst Firing of Cerebellar Neurons in Rapid-Onset Dystonia-Parkinsonism. *Journal of Neuroscience 34*, Number: 35, 11723–11732, DOI: 10.1523/JNEUROSCI.1409-14.2014.

(182) Fremont, R., and Khodakhah, K. (2012). Alternative Approaches to Modeling Hereditary Dystonias. *Neurotherapeutics 9*, 315–322, DOI: 10.1007/s13311-012-0113-1, PubMed ID: 22422472.

(183) Fremont, R., Tewari, A., Angueyra, C., and Khodakhah, K. (2017). A role for cerebellum in the hereditary dystonia DYT1. *eLife 6*, e22775, DOI: 10.7554/eLife.22775, PubMed ID: 28198698.

(184) Frey, U., and Morris, R. G. (1998). Weak before strong: dissociating synaptic tagging and plasticity-factor accounts of late-LTP. *Neuropharmacology 37*, 545–552, DOI: 10.1016/s0028-3908(98)00040-9, PubMed ID: 9704995.

(185) Frick, A., Magee, J., and Johnston, D. (2004). LTP is accompanied by an enhanced local excitability of pyramidal neuron dendrites. *Nature Neuroscience 7*, 126–135, DOI: 10.1038/nn1178, PubMed ID: 14730307.

(186) Friedman, N. P., and Robbins, T. W. (2022). The role of prefrontal cortex in cognitive control and executive function. *Neuropsychopharmacology 47*, Number: 1 Publisher: Nature Publishing Group, 72–89, DOI: 10.1038/s41386-021-01132-0.

(187) Frings, M., Maschke, M., Erichsen, M., Jentzen, W., Müller, S. P., Kolb, F. P., Diener, H.-C., and Timmann, D. (2002). Involvement of the human cerebellum in fear-conditioned potentiation of the acoustic startle response: a PET study. *Neuroreport 13*, 1275–1278, DOI: 10.1097/00001756-200207190-00012, PubMed ID: 12151786.

(188) Frontera, J. L., Sala, R. W., Georgescu, I. A., Baba Aissa, H., d'Almeida, M. N., Popa, D., and Léna, C. (2023). The cerebellum regulates fear extinction through thalamo-prefrontal cortex interactions in male mice. *Nature Communications 14*, Number: 1 Publisher: Nature Publishing Group, 1508, DOI: 10.1038/s41467-023-36943-w.

(189) Frontera, J. L., Baba Aissa, H., Sala, R. W., Mailhes-Hamon, C., Georgescu, I. A., Léna, C., and Popa, D. (2020). Bidirectional control of fear memories by cerebellar neurons projecting to the ventrolateral periaqueductal grey. *Nature Communications 11*, Number: 1 Publisher: Nature Publishing Group, 5207, DOI: 10.1038/s41467-020-18953-0.

(190) Fu, Y., Yuan, Y., Halliday, G., Rusznák, Z., Watson, C., and Paxinos, G. (2012). A cytoarchitectonic and chemoarchitectonic analysis of the dopamine cell groups in the substantia nigra, ventral tegmental area, and retrorubral field in the mouse. *Brain Structure & Function 217*, 591–612, DOI: 10.1007/s00429-011-0349-2, PubMed ID: 21935672.

(191) Fuchs, T., Saunders-Pullman, R., Masuho, I., Luciano, M. S., Raymond, D., Factor, S., Lang, A. E., Liang, T.-W., Trosch, R. M., White, S., Ainehsazan, E., Hervé, D., Sharma, N., Ehrlich, M. E., Martemyanov, K. A., Bressman, S. B., and Ozelius, L. J. (2013). Mutations in GNAL cause primary torsion dystonia. *Nature Genetics 45*, Number: 1, 88–92, DOI: 10.1038/ng.2496, PubMed ID: 23222958.

(192) Fujita, H., Kodama, T., and du Lac, S. (2020). Modular output circuits of the fastigial nucleus for diverse motor and nonmotor functions of the cerebellar vermis. *eLife 9*, DOI: 10.7554/eLife.58613, PubMed ID: 32639229.

(193) Fujita, M. (1982). Adaptive filter model of the cerebellum. *Biological Cybernetics 45*, 195–206, DOI: 10.1007/BF00336192, PubMed ID: 7171642.

(194) Fujiyama, F., Sohn, J., Nakano, T., Furuta, T., Nakamura, K. C., Matsuda, W., and Kaneko, T. (2011). Exclusive and common targets of neostriatofugal projections of rat striosome neurons: a single neuron-tracing study using a viral vector. *The European Journal of Neuroscience 33*, 668–677, DOI: 10.1111/j.1460-9568.2010.07564.x, PubMed ID: 21314848.

(195) Fukaya, C., Katayama, Y., Kano, T., Nagaoka, T., Kobayashi, K., Oshima, H., and Yamamoto, T. (2007). Thalamic deep brain stimulation for writer's cramp. *Journal of Neurosurgery 107*, 977–982, DOI: 10.3171/JNS-07/11/0977, PubMed ID: 17977270.

(196) Furlong, T. M., Richardson, R., and McNally, G. P. (2016). Habituation and extinction of fear recruit overlapping forebrain structures. *Neurobiology of Learning and Memory 128*, 7–16, DOI: 10.1016/j.nlm.2015.11.013, PubMed ID: 26690954.

(197) Gabbott, P. L. A., Warner, T. A., Jays, P. R. L., Salway, P., and Busby, S. J. (2005). Prefrontal cortex in the rat: projections to subcortical autonomic, motor, and limbic centers. *The Journal of Comparative Neurology 492*, 145–177, DOI: 10.1002/cne.20738, PubMed ID: 16196030.

(198) Gagnon, D., Petryszyn, S., Sanchez, M. G., Bories, C., Beaulieu, J. M., De Koninck, Y., Parent, A., and Parent, M. (2017). Striatal Neurons Expressing D1 and D2 Receptors are Morphologically Distinct and Differently Affected by Dopamine Denervation in Mice. *Scientific Reports 7*, 41432, DOI: 10.1038/srep41432, PubMed ID: 28128287.

(199) Galea, J. M., Vazquez, A., Pasricha, N., de Xivry, J.-J. O., and Celnik, P. (2011). Dissociating the roles of the cerebellum and motor cortex during adaptive learning: the motor cortex retains what the cerebellum learns. *Cerebral Cortex (New York, N.Y.: 1991) 21*, 1761–1770, DOI: 10.1093/cercor/bhq246, PubMed ID: 21139077.

(200) Gallea, C., Horovitz, S. G., Najee-Ullah, M. '., and Hallett, M. (2016). Impairment of a parieto-premotor network specialized for handwriting in writer's cramp. *Human Brain Mapping 37*, 4363–4375, DOI: 10.1002/hbm.23315, PubMed ID: 27466043.

(201) Gao, Z., Davis, C., Thomas, A. M., Economo, M. N., Abrego, A. M., Svoboda, K., De Zeeuw, C. I., and Li, N. (2018). A cortico-cerebellar loop for motor planning. *Nature 563*, Number: 7729, 113–116, DOI: 10.1038/s41586-018-0633-x, PubMed ID: 30333626.

(202) Gao, Z., Proietti-Onori, M., Lin, Z., ten Brinke, M. M., Boele, H.-J., Potters, J.-W., Ruigrok, T. J. H., Hoebeek, F. E., and De Zeeuw, C. I. (2016). Excitatory Cerebellar Nucleocortical Circuit Provides Internal Amplification during Associative Conditioning. *Neuron 89*, 645–657, DOI: 10.1016/j.neuron.2016.01.008.

(203) Gao, Z., van Beugen, B. J., and De Zeeuw, C. I. (2012). Distributed synergistic plasticity and cerebellar learning. *Nature Reviews. Neuroscience 13*, 619–635, DOI: 10.1038/nrn3312, PubMed ID: 22895474.

(204) Georgescu, E. L., Georgescu, I. A., Zahiu, C. D. M., Şteopoaie, A. R., Morozan, V. P., Pană, A. Ş., Zăgrean, A.-M., and Popa, D. (2018). Oscillatory Cortical Activity in an Animal Model of Dystonia Caused by Cerebellar Dysfunction. *Frontiers in Cellular Neuroscience 12*, 390, DOI: 10.3389/fncel.2018.00390, PubMed ID: 30459559.

(205) Georgescu, I. A., Popa, D., and Zagrean, L. (2020). The Anatomical and Functional Heterogeneity of the Mediodorsal Thalamus. *Brain Sciences 10*, 624, DOI: 10.3390/brainsci10090624, PubMed ID: 32916866.

(206) Georgescu Margarint, E. L., Georgescu, I. A., Zahiu, C.-D.-M., Șteopoaie, A. R., Tirlea, S.-A., Popa, D., Zagrean, A.-M., and Zagrean, L. (2020). Reduced Interhemispheric Coherence after Cerebellar Vermis Output Perturbation. *Brain Sciences 10*, 621, DOI: 10.3390/brainsci10090621, PubMed ID: 32911623.

(207) Gerfen, C. R., Baimbridge, K. G., and Miller, J. J. (1985). The neostriatal mosaic: compartmental distribution of calcium-binding protein and parvalbumin in the basal ganglia of the rat and monkey. *Proceedings of the National Academy of Sciences of the United States of America 82*, 8780–8784, PubMed ID: 3909155, https://www.ncbi.nlm.nih.gov/pmc/articles/PMC391521/.

(208) Gerfen, C. R. (1984). The neostriatal mosaic: compartmentalization of corticostriatal input and striatonigral output systems. *Nature 311*, 461–464, DOI: 10.1038/311461a0, PubMed ID: 6207434.

(209) Gerfen, C. R., Staines, W. A., Arbuthnott, G. W., and Fibiger, H. C. (1982). Crossed connections of the substantia nigra in the rat. *The Journal of Comparative Neurology 207*, 283–303, DOI: 10.1002/cne.902070308, PubMed ID: 7107988.

(210) Gerfen, C. R., and Surmeier, D. J. (2011). Modulation of striatal projection systems by dopamine. *Annual Review of Neuroscience 34*, 441–466, DOI: 10.1146/annurev-neuro-061010-113641, PubMed ID: 21469956.

(211) Gibo, T. L., Criscimagna-Hemminger, S. E., Okamura, A. M., and Bastian, A. J. (2013). Cerebellar motor learning: are environment dynamics more important than error size? *Journal of Neurophysiology 110*, 322–333, DOI: 10.1152/jn.00745.2012, PubMed ID: 23596337.

(212) Gilio, F., Suppa, A., Bologna, M., Lorenzano, C., Fabbrini, G., and Berardelli, A. (2007). Short-term cortical plasticity in patients with dystonia: a study with repetitive transcranial magnetic stimulation. *Movement Disorders: Official Journal of the Movement Disorder Society 22*, 1436–1443, DOI: 10.1002/mds.21465, PubMed ID: 17516450.

(213) Giménez-Amaya, J. M., and Graybiel, A. M. (1990). Compartmental origins of the striatopallidal projection in the primate. *Neuroscience 34*, 111–126, DOI: 10.1016/0306-4522(90)90306-o, PubMed ID: 1691462.

(214) Gioanni, Y., Rougeot, C., Clarke, P. B., Lepousé, C., Thierry, A. M., and Vidal, C. (1999). Nicotinic receptors in the rat prefrontal cortex: increase in glutamate release and facilitation of mediodorsal thalamo-cortical transmission. *The European Journal of Neuroscience 11*, 18–30, DOI: 10.1046/j.1460-9568.1999.00403.x, PubMed ID: 9987008.

(215) Girardeau, G., Benchenane, K., Wiener, S. I., Buzsáki, G., and Zugaro, M. B. (2009). Selective suppression of hippocampal ripples impairs spatial memory. *Nature Neuroscience 12*, 1222–1223, DOI: 10.1038/nn.2384, PubMed ID: 19749750.

(216) Girardeau, G., Inema, I., and Buzsáki, G. (2017). Reactivations of emotional memory in the hippocampus–amygdala system during sleep. *Nature Neuroscience 20*, Number: 11 Publisher: Nature Publishing Group, 1634–1642, DOI: 10.1038/nn.4637.

(217) Gittis, A. H., and du Lac, S. (2006). Intrinsic and synaptic plasticity in the vestibular system. *Current Opinion in Neurobiology 16*, 385–390, DOI: 10.1016/j.conb.2006.06.012, PubMed ID: 16842990.

(218) Golgi, C., *Sulla fina anatomia del cervelletto umano*; Stabilimento dei fratelli Rechiedei: 1874.

(219) Gómez-González, G. B., and Martínez-Torres, A. (2021). Inter-fastigial projections along the roof of the fourth ventricle. *Brain Structure and Function 226*, 901–917, DOI: 10.1007/s00429-021-02217-8.

(220) Gonzalo-Ruiz, A., Leichnetz, G. R., and Smith, D. J. (1988). Origin of cerebellar projections to the region of the oculomotor complex, medial pontine reticular formation, and superior colliculus in New World monkeys: a retrograde horseradish peroxidase study. *The Journal of Comparative Neurology 268*, 508–526, DOI: 10.1002/cne.902680404, PubMed ID: 3356803.

(221) Goodchild, R. E., Kim, C. E., and Dauer, W. T. (2005). Loss of the dystonia-associated protein torsinA selectively disrupts the neuronal nuclear envelope. *Neuron 48*, 923–932, DOI: 10.1016/j.neuron.2005.11.010, PubMed ID: 16364897.

(222) Gordon, E. M., Chauvin, R. J., Van, A. N., Rajesh, A., Nielsen, A., Newbold, D. J., Lynch, C. J., Seider, N. A., Krimmel, S. R., Scheidter, K. M., Monk, J., Miller, R. L., Metoki, A., Montez, D. F., Zheng, A., Elbau, I., Madison, T., Nishino, T., Myers, M. J., Kaplan, S., Badke D'Andrea, C., Demeter, D. V., Feigelis, M., Ramirez, J. S. B., Xu, T., Barch, D. M., Smyser, C. D., Rogers, C. E., Zimmermann, J., Botteron, K. N., Pruett, J. R., Willie, J. T., Brunner, P., Shimony, J. S., Kay, B. P., Marek, S., Norris, S. A., Gratton, C., Sylvester, C. M., Power, J. D., Liston, C., Greene, D. J., Roland, J. L., Petersen, S. E., Raichle, M. E., Laumann, T. O., Fair, D. A., and Dosenbach, N. U. F. (2023). A somato-cognitive action network alternates with effector regions in motor cortex. *Nature 617*, Number: 7960 Publisher: Nature Publishing Group, 351–359, DOI: 10.1038/s41586-023-05964-2.

(223) Gornati, S. V., Schäfer, C. B., Eelkman Rooda, O. H., Nigg, A. L., De Zeeuw, C. I., and Hoebeek, F. E. (2018). Differentiating Cerebellar Impact on Thalamic Nuclei. *Cell Reports 23*, Number: 9, 2690–2704, DOI: 10.1016/j.celrep.2018.04.098, PubMed ID: 29847799.

(224) Grafman, J., Litvan, I., Massaquoi, S., Stewart, M., Sirigu, A., and Hallett, M. (1992). Cognitive planning deficit in patients with cerebellar atrophy. *Neurology 42*, 1493–1496, DOI: 10.1212/wnl.42.8.1493, PubMed ID: 1641142.

(225) Grafton, S. T., Salidis, J., and Willingham, D. B. (2001). Motor Learning of Compatible and Incompatible Visuomotor Maps. *Journal of Cognitive Neuroscience 13*, 217–231, DOI: 10.1162/089892901564270.

(226) Graybiel, A. M., and Ragsdale, C. W. (1978). Histochemically distinct compartments in the striatum of human, monkeys, and cat demonstrated by acetylthiocholinesterase staining. *Proceedings of the National Academy of Sciences of the United States of America 75*, 5723–5726, PubMed ID: 103101, https://www.ncbi.nlm.nih.gov/pmc/articles/PMC393041/.

(227) Graybiel, A. M. (1984). Correspondence between the dopamine islands and striosomes of the mammalian striatum. *Neuroscience 13*, 1157–1187, DOI: 10.1016/0306-4522(84)90293-8, PubMed ID: 6152035.

(228) Graybiel, A. M. (1990). Neurotransmitters and neuromodulators in the basal ganglia. *Trends in Neurosciences 13*, 244–254, DOI: 10.1016/0166-2236(90)90104-i, PubMed ID: 1695398.

(229) Graybiel, A. M., Ragsdale, C. W., Yoneoka, E. S., and Elde, R. P. (1981). An immunohistochemical study of enkephalins and other neuropeptides in the striatum of the cat with evidence that the opiate peptides are arranged to form mosaic patterns in register with the striosomal compartments visible by acetylcholinesterase staining. *Neuroscience 6*, 377–397, DOI: 10.1016/0306-4522(81)90131-7, PubMed ID: 6164013.

(230) Groenewegen, H. J. (1988). Organization of the afferent connections of the mediodorsal thalamic nucleus in the rat, related to the mediodorsal-prefrontal topography. *Neuroscience 24*, 379–431, DOI: 10.1016/0306-4522(88)90339-9, PubMed ID: 2452377.

(231) Groenewegen, H. J., and Voogd, J. (1977). The parasagittal zonation within the olivocerebellar projection. I. Climbing fiber distribution in the vermis of cat cerebellum. *The Journal of Comparative Neurology 174*, 417–488, DOI: 10.1002/cne.901740304, PubMed ID: 903414.

(232) Guo, J.-Z., Sauerbrei, B. A., Cohen, J. D., Mischiati, M., Graves, A. R., Pisanello, F., Branson, K. M., and Hantman, A. W. (2022). Disrupting cortico-cerebellar communication impairs dexterity. *eLife 10*, e65906, DOI: 10.7554/eLife.65906, PubMed ID: 34324417.

(233) Guo, K., Yamawaki, N., Svoboda, K., and Shepherd, G. M. (2018). Anterolateral Motor Cortex Connects with a Medial Subdivision of Ventromedial Thalamus through Cell Type-Specific Circuits, Forming an Excitatory Thalamo-Cortico-Thalamic Loop via Layer 1 Apical Tuft Dendrites of Layer 5B Pyramidal Tract Type Neurons. *The Journal of Neuroscience 38*, 8787–8797, DOI: 10.1523/JNEUROSCI.1333-18.2018, PubMed ID: 30143573.

(234) Hagihara, K. M., Bukalo, O., Zeller, M., Aksoy-Aksel, A., Karalis, N., Limoges, A., Rigg, T., Campbell, T., Mendez, A., Weinholtz, C., Mahn, M., Zweifel, L. S., Palmiter, R. D., Ehrlich, I., Lüthi, A., and Holmes, A. (2021). Intercalated amygdala clusters orchestrate a switch in fear state. *Nature 594*, 403–407, DOI: 10.1038/s41586-021-03593-1, PubMed ID: 34040259.

(235) Hahn, M. A., Bothe, K., Heib, D., Schabus, M., Helfrich, R. F., and Hoedlmoser, K. (2022). Slow oscillation-spindle coupling strength predicts real-life gross-motor learning in adolescents and adults. *eLife 11*, e66761, DOI: 10.7554/eLife.66761, PubMed ID: 35188457.

(236) Haines, D. E., Dietrichs, E., Mihailoff, G. A., and McDonald, E. F. (1997). The cerebellar-hypothalamic axis: basic circuits and clinical observations. *International Review of Neurobiology 41*, 83–107, DOI: 10.1016/s0074-7742(08)60348-7, PubMed ID: 9378614.

(237) Haines, D. E., May, P. J., and Dietrichs, E. (1990). Neuronal connections between the cerebellar nuclei and hypothalamus in Macaca fascicularis: cerebello-visceral circuits. *The Journal of Comparative Neurology 299*, 106–122, DOI: 10.1002/cne.902990108, PubMed ID: 1698835.

(238) Hampson, D. R., and Manalo, J. L. (1998). The activation of glutamate receptors by kainic acid and domoic acid. *Natural Toxins 6*, 153–158, DOI: 10.1002/(sici)1522-7189(199805/08)6:3/4<153::aid-nt16>3.0.co;2-1, PubMed ID: 10223631.

(239) Hansel, C., and Linden, D. J. (2000). Long-term depression of the cerebellar climbing fiber–Purkinje neuron synapse. *Neuron 26*, 473–482, DOI: 10.1016/s0896-6273(00)81179-4, PubMed ID: 10839365.

(240) Hansel, C., Linden, D. J., and D'Angelo, E. (2001). Beyond parallel fiber LTD: the diversity of synaptic and non-synaptic plasticity in the cerebellum. *Nature Neuroscience 4*, 467–475, DOI: 10.1038/87419, PubMed ID: 11319554.

(241) Harrington, A., and Hammond-Tooke, G. D. (2015). Theta Burst Stimulation of the Cerebellum Modifies the TMS-Evoked N100 Potential, a Marker of GABA Inhibition. *PLoS ONE 10*, e0141284, DOI: 10.1371/journal.pone.0141284, PubMed ID: 26529225.

(242) Harris, K. D., Csicsvari, J., Hirase, H., Dragoi, G., and Buzsáki, G. (2003). Organization of cell assemblies in the hippocampus. *Nature 424*, 552–556, DOI: 10.1038/nature01834, PubMed ID: 12891358.

(243) Harris, K. D., and Shepherd, G. M. G. (2015). The neocortical circuit: themes and variations. *Nature neuroscience 18*, 170–181, DOI: 10.1038/nn.3917, PubMed ID: 25622573.

(244) Hashimoto, K., Yoshida, T., Sakimura, K., Mishina, M., Watanabe, M., and Kano, M. (2009). Influence of parallel fiber-Purkinje cell synapse formation on postnatal development of climbing fiber-Purkinje cell synapses in the cerebellum. *Neuroscience 162*, 601–611, DOI: 10.1016/j.neuroscience.2008.12.037, PubMed ID: 19166909.

(245) Hashimoto, K., and Kano, M. (2013). Synapse elimination in the developing cerebellum. *Cellular and molecular life sciences: CMLS 70*, 4667–4680, DOI: 10.1007/s00018-013-1405-2, PubMed ID: 23811844.

(246) Hashimoto, M., Yamanaka, A., Kato, S., Tanifuji, M., Kobayashi, K., and Yaginuma, H. (2018). Anatomical Evidence for a Direct Projection from Purkinje Cells in the Mouse Cerebellar Vermis to Medial Parabrachial Nucleus. *Frontiers in Neural Circuits 12*, 6, DOI: 10.3389/fncir.2018.00006, PubMed ID: 29467628.

(247) Häusser, M., and Clark, B. A. (1997). Tonic Synaptic Inhibition Modulates Neuronal Output Pattern and Spatiotemporal Synaptic Integration. *Neuron 19*, 665–678, DOI: 10.1016/S0896-6273(00)80379-7.

(248) He, S. Q., Dum, R. P., and Strick, P. L. (1995). Topographic organization of corticospinal projections from the frontal lobe: motor areas on the medial surface of the hemisphere. *The Journal of Neuroscience: The Official Journal of the Society for Neuroscience 15*, 3284–3306, DOI: 10.1523/JNEUROSCI.15-05-03284.1995, PubMed ID: 7538558.

(249) Heck, D. H., Fox, M. B., Correia Chapman, B., McAfee, S. S., and Liu, Y. (2023). Cerebellar control of thalamocortical circuits for cognitive function: A review of pathways and a proposed mechanism. *Frontiers in Systems Neuroscience 17*, https://www.frontiersin.org/articles/10.3389/fnsys.2023.1126508.

(250) Heckroth, J. A. (1994). Quantitative morphological analysis of the cerebellar nuclei in normal and lurcher mutant mice. I. Morphology and cell number. *Journal of Comparative Neurology 343*, _eprint: https://onlinelibrary.wiley.com/doi/pdf/10.1002/cne.903430113, 173–182, DOI: 10.1002/cne.903430113.

(251) Heidbreder, C. A., and Groenewegen, H. J. (2003). The medial prefrontal cortex in the rat: evidence for a dorso-ventral distinction based upon functional and anatomical characteristics. *Neuroscience & Biobehavioral Reviews 27*, 555–579, DOI: 10.1016/j.neubiorev.2003.09.003.

(252) Heimburger, R. F. (1967). Dentatectomy in the treatment of dyskinetic disorders. *Confinia Neurologica 29*, 101–106, DOI: 10.1159/000103686, PubMed ID: 4231821.

(253) Herrick, C. J. (1933). Morphogenesis of the brain. *Journal of Morphology 54*, 233–258.

(254) Herry, C., and Garcia, R. (2002). Prefrontal cortex long-term potentiation, but not long-term depression, is associated with the maintenance of extinction of learned fear in mice. *The Journal of Neuroscience: The Official Journal of the Society for Neuroscience 22*, Number: 2, 577–583, PubMed ID: 11784805.

(255) Herry, C., Trifilieff, P., Micheau, J., Lüthi, A., and Mons, N. (2006). Extinction of auditory fear conditioning requires MAPK/ERK activation in the basolateral amygdala. *The European Journal of Neuroscience 24*, 261–269, DOI: 10.1111/j.1460-9568.2006.04893.x, PubMed ID: 16882022.

(256) Herry, C., Vouimba, R.-M., and Garcia, R. (1999). Plasticity in the Mediodorsal Thalamo-Prefrontal Cortical Transmission in Behaving Mice. *Journal of Neurophysiology 82*, Number: 5 Publisher: American Physiological Society, 2827–2832, DOI: 10.1152/jn.1999.82.5.2827.

(257) Herve, D., Levi-Strauss, M., Marey-Semper, I., Verney, C., Tassin, J., Glowinski, J., and Girault, J. (1993). G(olf) and Gs in rat basal ganglia: possible involvement of G(olf) in the coupling of dopamine D1 receptor with adenylyl cyclase. *The Journal of Neuroscience 13*, 2237–2248, DOI: 10.1523/JNEUROSCI.13-05-02237.1993, PubMed ID: 8478697.

(258) Hervé, D., Moine, C. L., Corvol, J.-C., Belluscio, L., Ledent, C., Fienberg, A. A., Jaber, M., Studler, J.-M., and Girault, J.-A. (2001). Golf Levels Are Regulated by Receptor Usage and Control Dopamine and Adenosine Action in the Striatum. *Journal of Neuroscience 21*, Number: 12 Publisher: Society for Neuroscience Section: ARTICLE, 4390–4399, DOI: 10.1523/JNEUROSCI.21-12-04390.2001, PubMed ID: 11404425.

(259) Herzfeld, D. J., Pastor, D., Haith, A. M., Rossetti, Y., Shadmehr, R., and O'Shea, J. (2014). Contributions of the cerebellum and the motor cortex to acquisition and retention of motor memories. *NeuroImage 98*, 147–158, DOI: 10.1016/j.neuroimage.2014.04.076, PubMed ID: 24816533.

(260) Herzfeld, D. J., Vaswani, P. A., Marko, M. K., and Shadmehr, R. (2014). A memory of errors in sensorimotor learning. *Science (New York, N.Y.) 345*, 1349–1353, DOI: 10.1126/science.1253138, PubMed ID: 25123484.

(261) Hira, R., Ohkubo, F., Tanaka, Y. R., Masamizu, Y., Augustine, G. J., Kasai, H., and Matsuzaki, M. (2013). In vivo optogenetic tracing of functional corticocortical connections between motor forelimb areas. *Frontiers in Neural Circuits 7*, 55, DOI: 10.3389/fncir.2013.00055, PubMed ID: 23554588.

(262) Hitchcock, E. (1973). Dentate lesions for involuntary movement. *Proceedings of the Royal Society of Medicine 66*, 877–879, PubMed ID: 4616241.

(263) Ho, S., Lajaunie, R., Lerat, M., Le, M., Crépel, V., Loulier, K., Livet, J., Kessler, J.-P., and Marcaggi, P. (2021). A stable proportion of Purkinje cell inputs from parallel fibers are silent during cerebellar maturation. *Proceedings of the National Academy of Sciences of the United States of America 118*, e2024890118, DOI: 10.1073/pnas.2024890118, PubMed ID: 34740966.

(264) Hoebeek, F. E., Witter, L., Ruigrok, T. J. H., and De Zeeuw, C. I. (2010). Differential olivo-cerebellar cortical control of rebound activity in the cerebellar nuclei. *Proceedings of the National Academy of Sciences of the United States of America 107*, 8410–8415, DOI: 10.1073/pnas.0907118107, PubMed ID: 20395550.

(265) Hooks, B. M., Mao, T., Gutnisky, D. A., Yamawaki, N., Svoboda, K., and Shepherd, G. M. G. (2013). Organization of cortical and thalamic input to pyramidal neurons in mouse motor cortex. *The Journal of Neuroscience: The Official Journal of the Society for Neuroscience 33*, 748–760, DOI: 10.1523/JNEUROSCI.4338-12.2013, PubMed ID: 23303952.

(266) Horisawa, S., Kohara, K., Nonaka, T., Mochizuki, T., Kawamata, T., and Taira, T. (2021). Case Report: Deep Cerebellar Stimulation for Tremor and Dystonia. *Frontiers in Neurology 12*, 642904, DOI: 10.3389/fneur.2021.642904, PubMed ID: 33746894.

(267) Horisawa, S., Taira, T., Goto, S., Ochiai, T., and Nakajima, T. (2013). Long-term improvement of musician's dystonia after stereotactic ventro-oral thalamotomy. *Annals of Neurology 74*, 648–654, DOI: 10.1002/ana.23877, PubMed ID: 23463596.

(268) Hoshi, E., Tremblay, L., Féger, J., Carras, P. L., and Strick, P. L. (2005). The cerebellum communicates with the basal ganglia. *Nature Neuroscience 8*, 1491–1493, DOI: 10.1038/nn1544, PubMed ID: 16205719.

(269) Hoshino, M., Miyashita, S., Seto, Y., and Yamada, M. In *Handbook of the Cerebellum and Cerebellar Disorders*, Manto, M., Gruol, D., Schmahmann, J., Koibuchi, N., and Sillitoe, R., Eds.; Springer International Publishing: Cham, 2019, pp 1–15, DOI: 10.1007/978-3-319-97911-3_5-2.

(270) Houck, B. D., and Person, A. L. (2015). Cerebellar Premotor Output Neurons Collateralize to Innervate the Cerebellar Cortex. *The Journal of Comparative Neurology 523*, 2254–2271, DOI: 10.1002/cne.23787, PubMed ID: 25869188.

(271) Hu, H., and Agmon, A. (2016). Differential Excitation of Distally versus Proximally Targeting Cortical Interneurons by Unitary Thalamocortical Bursts. *The Journal of Neuroscience: The Official Journal of the Society for Neuroscience 36*, 6906–6916, DOI: 10.1523/JNEUROSCI.0739-16.2016, PubMed ID: 27358449.

(272) Huang, Y.-Z., Chen, R.-S., Rothwell, J. C., and Wen, H.-Y. (2007). The after-effect of human theta burst stimulation is NMDA receptor dependent. *Clinical Neurophysiology: Official Journal of the International Federation of Clinical Neurophysiology 118*, 1028–1032, DOI: 10.1016/j.clinph.2007.01.021, PubMed ID: 17368094.

(273) Huang, Y.-Z., Edwards, M. J., Rounis, E., Bhatia, K. P., and Rothwell, J. C. (2005). Theta Burst Stimulation of the Human Motor Cortex. *Neuron 45*, Number: 2, 201–206, DOI: 10.1016/j.neuron.2004.12.033.

(274) Hull, C., and Regehr, W. G. (2012). Identification of an inhibitory circuit that regulates cerebellar Golgi cell activity. *Neuron 73*, 149–158, DOI: 10.1016/j.neuron.2011.10.030, PubMed ID: 22243753.

(275) Hunnicutt, B. J., Long, B. R., Kusefoglu, D., Gertz, K. J., Zhong, H., and Mao, T. (2014). A comprehensive thalamocortical projection map at the mesoscopic level. *Nature Neuroscience 17*, 1276–1285, DOI: 10.1038/nn.3780, PubMed ID: 25086607.

(276) Hutchinson, M., Kimmich, O., Molloy, A., Whelan, R., Molloy, F., Lynch, T., Healy, D. G., Walsh, C., Edwards, M. J., Ozelius, L., Reilly, R. B., and O'Riordan, S. (2013). The endophenotype and the phenotype: temporal discrimination and adult-onset dystonia. *Movement Disorders: Official Journal of the Movement Disorder Society 28*, 1766–1774, DOI: 10.1002/mds.25676, PubMed ID: 24108447.

(277) Hwang, K.-D., Kim, S. J., and Lee, Y.-S. (2022). Cerebellar Circuits for Classical Fear Conditioning. *Frontiers in Cellular Neuroscience 16*, https://www.frontiersin.org/articles/10.3389/fncel.2022.836948.

(278) Hyun, J. H., Eom, K., Lee, K.-H., Ho, W.-K., and Lee, S.-H. (2013). Activity-dependent downregulation of D-type K+ channel subunit Kv1.2 in rat hippocampal CA3 pyramidal neurons. *The Journal of Physiology 591*, 5525–5540, DOI: 10.1113/jphysiol.2013.259002, PubMed ID: 23981714.

(279) Ichinohe, N., Mori, F., and Shoumura, K. (2000). A di-synaptic projection from the lateral cerebellar nucleus to the laterodorsal part of the striatum via the central lateral nucleus of the thalamus in the rat. *Brain Research 880*, 191–197, DOI: 10.1016/S0006-8993(00)02744-X.

(280) Ilinsky, I. A., and Kultas-Ilinsky, K. (1987). Sagittal cytoarchitectonic maps of the Macaca mulatta thalamus with a revised nomenclature of the motor-related nuclei validated by observations on their connectivity. *The Journal of Comparative Neurology 262*, 331–364, DOI: 10.1002/cne.902620303, PubMed ID: 2821085.

(281) Iriki, A., Pavlides, C., Keller, A., and Asanuma, H. (1991). Long-term potentiation of thalamic input to the motor cortex induced by coactivation of thalamocortical and corticocortical afferents. *Journal of Neurophysiology 65*, 1435–1441, DOI: 10.1152/jn.1991.65.6.1435, PubMed ID: 1875252.

(282) Isope, P., and Barbour, B. (2002). Properties of Unitary Granule Cell→Purkinje Cell Synapses in Adult Rat Cerebellar Slices. *The Journal of Neuroscience 22*, 9668–9678, DOI: 10.1523/JNEUROSCI.22-22-09668.2002, PubMed ID: 12427822.

(283) Ito, M. (1989). Long-Term Depression. *Annual Review of Neuroscience 12*, _eprint: https://doi.org/10.1146/ann 85–102, DOI: 10.1146/annurev.ne.12.030189.000505, PubMed ID: 2648961.

(284) Ito, M. (1983). Evidence for synaptic plasticity in the cerebellar cortex. *Acta Morphologica Hungarica 31*, 213–218, PubMed ID: 6312772.

(285) Ito, M. (1982). Experimental verification of Marr-Albus' plasticity assumption for the cerebellum. *Acta Biologica Academiae Scientiarum Hungaricae 33*, 189–199, PubMed ID: 6129762.

(286) Ito, M., and Kano, M. (1982). Long-lasting depression of parallel fiber-Purkinje cell transmission induced by conjunctive stimulation of parallel fibers and climbing fibers in the cerebellar cortex. *Neuroscience Letters 33*, 253–258, DOI: 10.1016/0304-3940(82)90380-9, PubMed ID: 6298664.

(287) Iwakura, A., Uchigashima, M., Miyazaki, T., Yamasaki, M., and Watanabe, M. (2012). Lack of molecular-anatomical evidence for GABAergic influence on axon initial segment of cerebellar Purkinje cells by the pinceau formation. *The Journal of Neuroscience: The Official Journal of the Society for Neuroscience 32*, 9438–9448, DOI: 10.1523/JNEUROSCI.1651-12.2012, PubMed ID: 22764252.

(288) Iyer, M. B., Schleper, N., and Wassermann, E. M. (2003). Priming stimulation enhances the depressant effect of low-frequency repetitive transcranial magnetic stimulation. *The Journal of Neuroscience: The Official Journal of the Society for Neuroscience 23*, 10867–10872, DOI: 10.1523/JNEUROSCI.23-34-10867.2003, PubMed ID: 14645480.

(289) Jackson, A., and Xu, W. (2023). Role of cerebellum in sleep-dependent memory processes. *Frontiers in Systems Neuroscience 17*, 1154489, DOI: 10.3389/fnsys.2023.1154489, PubMed ID: 37143709.

(290) Jager, P., Moore, G., Calpin, P., Durmishi, X., Salgarella, I., Menage, L., Kita, Y., Wang, Y., Kim, D. W., Blackshaw, S., Schultz, S. R., Brickley, S., Shimogori, T., and Delogu, A. Dual midbrain and forebrain origins of thalamic inhibitory interneurons. *eLife 10*, e59272, DOI: 10.7554/eLife.59272, PubMed ID: 33522480.

(291) Jahnsen, H. (1986). Extracellular activation and membrane conductances of neurones in the guinea-pig deep cerebellar nuclei in vitro. *The Journal of Physiology 372*, 149–168, DOI: 10.1113/jphysiol.1986.sp016002, PubMed ID: 2425083.

(292) Jakob, C. (1906). Nueva contribución á la fisio-patología de los lóbulos frontales. *La Semana Médica 13*, 1325–1329.

(293) Jenkins, I. H., Brooks, D. J., Nixon, P. D., Frackowiak, R. S., and Passingham, R. E. (1994). Motor sequence learning: a study with positron emission tomography. *The Journal of Neuroscience: The Official Journal of the Society for Neuroscience 14*, 3775–3790, DOI: 10.1523/JNEUROSCI.14-06-03775.1994, PubMed ID: 8207487.

(294) Jeon, D., Kim, S., Chetana, M., Jo, D., Ruley, H. E., Lin, S.-Y., Rabah, D., Kinet, J.-P., and Shin, H.-S. (2010). Observational fear learning involves affective pain system and Cav1.2 Ca2+ channels in ACC. *Nature neuroscience 13*, 482–488, DOI: 10.1038/nn.2504, PubMed ID: 20190743.

(295) Jeong, M., Lee, H., Kim, Y., Wang, E. H.-J., Paik, S.-B., Lim, B. K., and Kim, D. (2021). Interhemispheric Cortico-Cortical Pathway for Sequential Bimanual Movements in Mice. *eNeuro 8*, ENEURO.0200–21.2021, DOI: 10.1523/ENEURO.0200-21.2021, PubMed ID: 34348983.

(296) Ji, D., and Wilson, M. A. (2007). Coordinated memory replay in the visual cortex and hippocampus during sleep. *Nature Neuroscience 10*, 100–107, DOI: 10.1038/nn1825, PubMed ID: 17173043.

(297) Ji, J., and Maren, S. (2007). Hippocampal involvement in contextual modulation of fear extinction. *Hippocampus 17*, 749–758, DOI: 10.1002/hipo.20331, PubMed ID: 17604353.

(298) Jin, X., and Costa, R. M. (2015). Shaping Action Sequences in Basal Ganglia Circuits. *Current opinion in neurobiology 33*, 188–196, DOI: 10.1016/j.conb.2015.06.011, PubMed ID: 26189204.

(299) Jinnah, H. A. (2015). Diagnosis & Treatment of Dystonia. *Neurologic clinics 33*, 77–100, DOI: 10.1016/j.ncl.2014.09.002, PubMed ID: 25432724.

(300) Jinnai, K., Nambu, A., Tanibuchi, I., and Yoshida, S. (1993). Cerebello- and pallido-thalamic pathways to areas 6 and 4 in the monkey. *Stereotactic and Functional Neurosurgery 60*, 70–79, DOI: 10.1159/000100591, PubMed ID: 8511435.

(301) Joel, D., and Weiner, I. (1994). The organization of the basal ganglia-thalamocortical circuits: open interconnected rather than closed segregated. *Neuroscience 63*, 363–379, DOI: 10.1016/0306-4522(94)90536-3, PubMed ID: 7891852.

(302) Johansen, J. P., Hamanaka, H., Monfils, M. H., Behnia, R., Deisseroth, K., Blair, H. T., and LeDoux, J. E. (2010). Optical activation of lateral amygdala pyramidal cells instructs associative fear learning. *Proceedings of the National Academy of Sciences 107*, Publisher: Proceedings of the National Academy of Sciences, 12692–12697, DOI: 10.1073/pnas.1002418107.

(303) Joho, R. H., and Hurlock, E. C. (2009). The role of Kv3-type potassium channels in cerebellar physiology and behavior. *Cerebellum (London, England) 8*, 323–333, DOI: 10.1007/s12311-009-0098-4, PubMed ID: 19247732.

(304) Jones, D. T., and Reed, R. R. (1989). Golf: an olfactory neuron specific-G protein involved in odorant signal transduction. *Science (New York, N.Y.) 244*, 790–795, DOI: 10.1126/science.2499043, PubMed ID: 2499043.

(305) Jones, E. G. (1975). Some aspects of the organization of the thalamic reticular complex. *The Journal of Comparative Neurology 162*, 285–308, DOI: 10.1002/cne.901620302, PubMed ID: 1150923.

(306) Jung, S. J., Vlasov, K., D'Ambra, A. F., Parigi, A., Baya, M., Frez, E. P., Villalobos, J., Fernandez-Frentzel, M., Anguiano, M., Ideguchi, Y., Antzoulatos, E. G., and Fioravante, D. (2022). Novel Cerebello-Amygdala Connections Provide Missing Link Between Cerebellum and Limbic System. *Frontiers in Systems Neuroscience 16*, 879634, DOI: 10.3389/fnsys.2022.879634, PubMed ID: 35645738.

(307) Kagerer, F. A., Contreras-Vidal, J. L., and Stelmach, G. E. (1997). Adaptation to gradual as compared with sudden visuo-motor distortions. *Experimental Brain Research 115*, 557–561, DOI: 10.1007/pl00005727, PubMed ID: 9262212.

(308) Kam, K., Pettibone, W. D., Shim, K., Chen, R. K., and Varga, A. W. (2019). Dynamics of Sleep Spindles and Coupling to Slow Oscillations Following Motor Learning in Adult Mice. *Neurobiology of learning and memory 166*, 107100, DOI: 10.1016/j.nlm.2019.107100, PubMed ID: 31622665.

(309) Karalis, N., Dejean, C., Chaudun, F., Khoder, S., Rozeske, R. R., Wurtz, H., Bagur, S., Benchenane, K., Sirota, A., Courtin, J., and Herry, C. (2016). 4 Hz oscillations synchronize prefrontal-amygdala circuits during fear behaviour. *Nature neuroscience 19*, Number: 4, 605–612, DOI: 10.1038/nn.4251, PubMed ID: 26878674.

(310) Karalis, N., Dejean, C., Chaudun, F., Khoder, S., Rozeske, R. R., Wurtz, H., Bagur, S., Benchenane, K., Sirota, A., Courtin, J., and Herry, C. (2016). 4-Hz oscillations synchronize prefrontal-amygdala circuits during fear behavior. *Nature Neuroscience 19*, Number: 4, 605–612, DOI: 10.1038/nn.4251, PubMed ID: 26878674.

(311) Karavasilis, E., Christidi, F., Velonakis, G., Giavri, Z., Kelekis, N. L., Efstathopoulos, E. P., Evdokimidis, I., and Dellatolas, G. (2019). Ipsilateral and contralateral cerebro-cerebellar white matter connections: A diffusion tensor imaging study in healthy adults. *Journal of Neuroradiology = Journal De Neuroradiologie 46*, 52–60, DOI: 10.1016/j.neurad.2018.07.004, PubMed ID: 30098370.

(312) Karlsson, M. P., and Frank, L. M. (2009). Awake replay of remote experiences in the hippocampus. *Nature Neuroscience 12*, 913–918, DOI: 10.1038/nn.2344, PubMed ID: 19525943.

(313) Karni, A., Meyer, G., Rey-Hipolito, C., Jezzard, P., Adams, M. M., Turner, R., and Ungerleider, L. G. (1998). The acquisition of skilled motor performance: Fast and slow experience-driven changes in primary motorcortex. *Proceedings of the National Academy of Sciences 95*, Publisher: Proceedings of the National Academy of Sciences, 861–868, DOI: 10.1073/pnas.95.3.861.

(314) Kattoor, J., Thürling, M., Gizewski, E. R., Forsting, M., Timmann, D., and Elsenbruch, S. (2014). Cerebellar contributions to different phases of visceral aversive extinction learning. *Cerebellum (London, England) 13*, 1–8, DOI: 10.1007/s12311-013-0512-9, PubMed ID: 23925594.

(315) Kawaguchi, Y. (1997). Neostriatal cell subtypes and their functional roles. *Neuroscience Research 27*, 1–8, DOI: 10.1016/s0168-0102(96)01134-0, PubMed ID: 9089693.

(316) Kawaguchi, Y., Wilson, C. J., Augood, S. J., and Emson, P. C. (1995). Striatal interneurones: chemical, physiological and morphological characterization. *Trends in Neurosciences 18*, 527–535, DOI: 10.1016/0166-2236(95)98374-8, PubMed ID: 8638293.

(317) Kawaguchi, Y., Wilson, C. J., and Emson, P. C. (1989). Intracellular recording of identified neostriatal patch and matrix spiny cells in a slice preparation preserving cortical inputs. *Journal of Neurophysiology 62*, 1052–1068, DOI: 10.1152/jn.1989.62.5.1052, PubMed ID: 2585039.

(318) Kawai, R., Markman, T., Poddar, R., Ko, R., Fantana, A. L., Dhawale, A. K., Kampff, A. R., and Ölveczky, B. P. (2015). Motor cortex is required for learning but not for executing a motor skill. *Neuron 86*, 800–812, DOI: 10.1016/j.neuron.2015.03.024, PubMed ID: 25892304.

(319) Kawato, M., Ohmae, S., Hoang, H., and Sanger, T. (2021). 50 Years Since the Marr, Ito, and Albus Models of the Cerebellum. *Neuroscience 462*, 151–174, DOI: 10.1016/j.neuroscience.2020.06.019.

(320) Kebschull, J. M., Casoni, F., Consalez, G. G., Goldowitz, D., Hawkes, R., Ruigrok, T. J. H., Schilling, K., Wingate, R., Wu, J., Yeung, J., and Uusisaari, M. Y. (2023). Cerebellum Lecture: the Cerebellar Nuclei—Core of the Cerebellum. *The Cerebellum*, DOI: 10.1007/s12311-022-01506-0, https://doi.org/10.1007/s12311-022-01506-0.

(321) Kebschull, J. M., Richman, E. B., Ringach, N., Friedmann, D., Albarran, E., Kolluru, S. S., Jones, R. C., Allen, W. E., Wang, Y., Cho, S. W., Zhou, H., Ding, J. B., Chang, H. Y., Deisseroth, K., Quake, S. R., and Luo, L. (2020). Cerebellar nuclei evolved by repeatedly duplicating a conserved cell-type set. *Science (New York, N.Y.) 370*, eabd5059, DOI: 10.1126/science.abd5059, PubMed ID: 33335034.

(322) Kelly, R. M., and Strick, P. L. (2000). Rabies as a transneuronal tracer of circuits in the central nervous system. *Journal of Neuroscience Methods 103*, 63–71, DOI: 10.1016/s0165-0270(00)00296-x, PubMed ID: 11074096.

(323) Kelly, R. M., and Strick, P. L. (2003). Cerebellar loops with motor cortex and prefrontal cortex of a nonhuman primate. *The Journal of Neuroscience: The Official Journal of the Society for Neuroscience 23*, 8432–8444, DOI: 10.1523/JNEUROSCI.23-23-08432.2003, PubMed ID: 12968006.

(324) Khilkevich, A., Zambrano, J., Richards, M.-M., and Mauk, M. D. Cerebellar implementation of movement sequences through feedback. *eLife 7*, e37443, DOI: 10.7554/eLife.37443, PubMed ID: 30063004.

(325) Khooshnoodi, M. A., Factor, S. A., and Jinnah, H. A. (2013). Secondary blepharospasm associated with structural lesions of the brain. *Journal of the Neurological Sciences 331*, 98–101, DOI: 10.1016/j.jns.2013.05.022, PubMed ID: 23747003.

(326) Kim, J. J., and Jung, M. W. (2006). Neural circuits and mechanisms involved in Pavlovian fear conditioning: a critical review. *Neuroscience and Biobehavioral Reviews 30*, 188–202, DOI: 10.1016/j.neubiorev.2005.06.005, PubMed ID: 16120461.

(327) Kim, O. A., Ohmae, S., and Medina, J. F. (2020). A cerebello-olivary signal for negative prediction error is sufficient to cause extinction of associative motor learning. *Nature Neuroscience 23*, Number: 12 Publisher: Nature Publishing Group, 1550–1554, DOI: 10.1038/s41593-020-00732-1.

(328) Kincaid, A. E., and Wilson, C. J. (1996). Corticostriatal innervation of the patch and matrix in the rat neostriatum. *The Journal of Comparative Neurology 374*, 578–592, DOI: 10.1002/(SICI)1096-9861(19961028)374:4<578::AID-CNE7>3.0.CO;2-Z, PubMed ID: 8910736.

(329) King, B. R., Fogel, S. M., Albouy, G., and Doyon, J. (2013). Neural correlates of the age-related changes in motor sequence learning and motor adaptation in older adults. *Frontiers in Human Neuroscience 7*, 142, DOI: 10.3389/fnhum.2013.00142, PubMed ID: 23616757.

(330) Kingma, A., Mooij, J. J., Metzemaekers, J. D., and Leeuw, J. A. (1994). Transient mutism and speech disorders after posterior fossa surgery in children with brain tumours. *Acta Neurochirurgica 131*, 74–79, DOI: 10.1007/BF01401456, PubMed ID: 7709788.

(331) Kish, S. J., Schut, L., Simmons, J., Gilbert, J., Chang, L.-J., and Rebbetoy, M. (1988). Brain acetylcholinesterase activity is markedly reduced in dominantly-inherited olivopontocerebellar atrophy. *Journal of Neurology, Neurosurgery & Psychiatry 51*, Place: United Kingdom Publisher: BMJ Publishing Group, 544–548, DOI: 10.1136/jnnp.51.4.544.

(332) Kita, H., Chang, H. T., and Kitai, S. T. (1983). The morphology of intracellularly labeled rat subthalamic neurons: a light microscopic analysis. *The Journal of Comparative Neurology 215*, 245–257, DOI: 10.1002/cne.902150302, PubMed ID: 6304154.

(333) Kita, H., and Kitai, S. T. (1987). Efferent projections of the subthalamic nucleus in the rat: light and electron microscopic analysis with the PHA-L method. *The Journal of Comparative Neurology 260*, 435–452, DOI: 10.1002/cne.902600309, PubMed ID: 2439552.

(334) Kita, T., and Kita, H. (2012). The subthalamic nucleus is one of multiple innervation sites for long-range corticofugal axons: a single-axon tracing study in the rat. *The Journal of Neuroscience: The Official Journal of the Society for Neuroscience 32*, 5990–5999, DOI: 10.1523/JNEUROSCI.5717-11.2012, PubMed ID: 22539859.

(335) Kitamura, T., and Yamada, J. (1989). Spinocerebellar tract neurons with axons passing through the inferior or superior cerebellar peduncles. A retrograde horseradish peroxidase study in rats. *Brain, Behavior and Evolution 34*, 133–142, DOI: 10.1159/000116499, PubMed ID: 2590830.

(336) Klomjai, W., Katz, R., and Lackmy-Vallée, A. (2015). Basic principles of transcranial magnetic stimulation (TMS) and repetitive TMS (rTMS). *Annals of Physical and Rehabilitation Medicine 58*, 208–213, DOI: 10.1016/j.rehab.2015.05.005, PubMed ID: 26319963.

(337) Koch, G., Brusa, L., Carrillo, F., Lo Gerfo, E., Torriero, S., Oliveri, M., Mir, P., Caltagirone, C., and Stanzione, P. (2009). Cerebellar magnetic stimulation decreases levodopa-induced dyskinesias in Parkinson disease. *Neurology 73*, 113–119, DOI: 10.1212/WNL.0b013e3181ad5387, PubMed ID: 19597133.

(338) Koch, G., Bonnì, S., Casula, E. P., Iosa, M., Paolucci, S., Pellicciari, M. C., Cinnera, A. M., Ponzo, V., Maiella, M., Picazio, S., Sallustio, F., and Caltagirone, C. (2019). Effect of Cerebellar Stimulation on Gait and Balance Recovery in Patients With Hemiparetic Stroke: A Randomized Clinical Trial. *JAMA neurology 76*, 170–178, DOI: 10.1001/jamaneurol.2018.3639, PubMed ID: 30476999.

(339) Koch, G., Mori, F., Marconi, B., Codecà, C., Pecchioli, C., Salerno, S., Torriero, S., Lo Gerfo, E., Mir, P., Oliveri, M., and Caltagirone, C. (2008). Changes in intracortical circuits of the human motor cortex following theta burst stimulation of the lateral cerebellum. *Clinical Neurophysiology: Official Journal of the International Federation of Clinical Neurophysiology 119*, Number: 11, 2559–2569, DOI: 10.1016/j.clinph.2008.08.008, PubMed ID: 18824403.

(340) Koch, G., Porcacchia, P., Ponzo, V., Carrillo, F., Cáceres-Redondo, M. T., Brusa, L., Desiato, M. T., Arciprete, F., Di Lorenzo, F., Pisani, A., Caltagirone, C., Palomar, F. J., and Mir, P. (2014). Effects of Two Weeks of Cerebellar Theta Burst Stimulation in Cervical Dystonia Patients. *Brain Stimulation 7*, Number: 4, 564–572, DOI: 10.1016/j.brs.2014.05.002.

(341) KOEPPEN, A. H. (2018). The neuropathology of the adult cerebellum. *Handbook of clinical neurology 154*, 129–149, DOI: 10.1016/B978-0-444-63956-1.00008-4, PubMed ID: 29903436.

(342) Koeppen, A. H. (2011). Friedreich's ataxia: Pathology, pathogenesis, and molecular genetics. *Journal of the neurological sciences 303*, 1–12, DOI: 10.1016/j.jns.2011.01.010, PubMed ID: 21315377.

(343) Koppelmans, V., Silvester, B., and Duff, K. (2022). Neural Mechanisms of Motor Dysfunction in Mild Cognitive Impairment and Alzheimer's Disease: A Systematic Review. *Journal of Alzheimer's Disease Reports 6*, Publisher: IOS Press, 307–344, DOI: 10.3233/ADR-210065.

(344) Korman, M., Doyon, J., Doljansky, J., Carrier, J., Dagan, Y., and Karni, A. (2007). Daytime sleep condenses the time course of motor memory consolidation. *Nature Neuroscience 10*, 1206–1213, DOI: 10.1038/nn1959, PubMed ID: 17694051.

(345) Kostadinov, D., Beau, M., Pozo, M. B., and Häusser, M. (2019). Predictive and reactive reward signals conveyed by climbing fiber inputs to cerebellar Purkinje cells. *Nature neuroscience 22*, 950–962, DOI: 10.1038/s41593-019-0381-8, PubMed ID: 31036947.

(346) Kovács, A. D., and Pearce, D. A. (2013). Location- and sex-specific differences in weight and motor coordination in two commonly used mouse strains. *Scientific Reports 3*, 2116, DOI: 10.1038/srep02116, PubMed ID: 23817037.

(347) Kozareva, V., Martin, C., Osorno, T., Rudolph, S., Guo, C., Vanderburg, C., Nadaf, N., Regev, A., Regehr, W., and Macosko, E. A transcriptomic atlas of the mouse cerebellum reveals regional specializations and novel cell types, en, Pages: 2020.03.04.976407 Section: New Results, 2020, DOI: 10.1101/2020.03.04.976407.

(348) Krakauer, J. W., Hadjiosif, A. M., Xu, J., Wong, A. L., and Haith, A. M. (2019). Motor Learning. *Comprehensive Physiology 9*, 613–663, DOI: 10.1002/cphy.c170043, PubMed ID: 30873583.

(349) Krauss, J. K., Seeger, W., and Jankovic, J. (1997). Cervical dystonia associated with tumors of the posterior fossa. *Movement Disorders: Official Journal of the Movement Disorder Society 12*, 443–447, DOI: 10.1002/mds.870120329, PubMed ID: 9159745.

(350) Krettek, J. E., and Price, J. L. (1977). The cortical projections of the mediodorsal nucleus and adjacent thalamic nuclei in the rat. *The Journal of Comparative Neurology 171*, 157–191, DOI: 10.1002/cne.901710204, PubMed ID: 64477.

(351) Kumandaş, S., Per, H., Gümüş, H., Tucer, B., Yikilmaz, A., Kontaş, O., Coşkun, A., and Kurtsoy, A. (2006). Torticollis secondary to posterior fossa and cervical spinal cord tumors: report of five cases and literature review. *Neurosurgical Review 29*, 333–338, discussion 338, DOI: 10.1007/s10143-006-0034-8, PubMed ID: 16924460.

(352) Kumar, K. R., Lohmann, K., Masuho, I., Miyamoto, R., Ferbert, A., Lohnau, T., Kasten, M., Hagenah, J., Brüggemann, N., Graf, J., Münchau, A., Kostic, V. S., Sue, C. M., Domingo, A. R., Rosales, R. L., Lee, L. V., Freimann, K., Westenberger, A., Mukai, Y., Kawarai, T., Kaji, R., Klein, C., Martemyanov, K. A., and Schmidt, A. (2014). Mutations in GNAL: a novel cause of craniocervical dystonia. *JAMA neurology 71*, Number: 4, 490–494, DOI: 10.1001/jamaneurol.2013.4677, PubMed ID: 24535567.

(353) Kuramoto, E., Furuta, T., Nakamura, K. C., Unzai, T., Hioki, H., and Kaneko, T. (2009). Two types of thalamocortical projections from the motor thalamic nuclei of the rat: a single neuron-tracing study using viral vectors. *Cerebral Cortex (New York, N.Y.: 1991) 19*, 2065–2077, DOI: 10.1093/cercor/bhn231, PubMed ID: 19174446.

(354) Kuramoto, E., Ohno, S., Furuta, T., Unzai, T., Tanaka, Y. R., Hioki, H., and Kaneko, T. (2015). Ventral medial nucleus neurons send thalamocortical afferents more widely and more preferentially to layer 1 than neurons of the ventral anterior-ventral lateral nuclear complex in the rat. *Cerebral Cortex (New York, N.Y.: 1991) 25*, 221–235, DOI: 10.1093/cercor/bht216, PubMed ID: 23968832.

(355) Kuypers, H. G. (1964). THE DESCENDING PATHWAYS TO THE SPINAL CORD, THEIR ANATOMY AND FUNCTION. *Progress in Brain Research 11*, 178–202, DOI: 10.1016/s0079-6123(08)64048-0, PubMed ID: 14300477.

(356) Kwakkel, G., Kollen, B. J., van der Grond, J., and Prevo, A. J. H. (2003). Probability of regaining dexterity in the flaccid upper limb: impact of severity of paresis and time since onset in acute stroke. *Stroke 34*, 2181–2186, DOI: 10.1161/01.STR.0000087172.16305.CD, PubMed ID: 12907818.

(357) Lacagnina, A. F., Brockway, E. T., Crovetti, C. R., Shue, F., McCarty, M. J., Sattler, K. P., Lim, S. C., Santos, S. L., Denny, C. A., and Drew, M. R. (2019). Distinct hippocampal engrams control extinction and relapse of fear memory. *Nature Neuroscience 22*, 753–761, DOI: 10.1038/s41593-019-0361-z.

(358) Lainé, J., and Axelrad, H. (1998). Lugaro cells target basket and stellate cells in the cerebellar cortex. *Neuroreport 9*, 2399–2403, DOI: 10.1097/00001756-199807130-00045, PubMed ID: 9694235.

(359) Lainé, J., and Axelrad, H. (1996). Morphology of the Golgi-impregnated Lugaro cell in the rat cerebellar cortex: a reappraisal with a description of its axon. *The Journal of Comparative Neurology 375*, 618–640, DOI: 10.1002/(SICI)1096-9861(19961125)375:4<618::AID-CNE5>3.0.CO;2-4, PubMed ID: 8930789.

(360) Lanciego, J. L., Luquin, N., and Obeso, J. A. (2012). Functional Neuroanatomy of the Basal Ganglia. *Cold Spring Harbor Perspectives in Medicine 2*, a009621, DOI: 10.1101/cshperspect.a009621, PubMed ID: 23071379.

(361) Lang, P. J., Davis, M., and Ohman, A. (2000). Fear and anxiety: animal models and human cognitive psychophysiology. *Journal of Affective Disorders 61*, 137–159, DOI: 10.1016/s0165-0327(00)00343-8, PubMed ID: 11163418.

(362) Langberg, T. (2016). Thalamic Bursts and Single Spikes Evoke Distinct Inhibitory States in the Primary Sensory Cortex. *The Journal of Neuroscience 36*, 11496–11497, DOI: 10.1523/JNEUROSCI.2676-16.2016, PubMed ID: 27911753.

(363) Lange, I., Kasanova, Z., Goossens, L., Leibold, N., De Zeeuw, C. I., van Amelsvoort, T., and Schruers, K. (2015). The anatomy of fear learning in the cerebellum: A systematic meta-analysis. *Neuroscience and Biobehavioral Reviews 59*, 83–91, DOI: 10.1016/j.neubiorev.2015.09.019, PubMed ID: 26441374.

(364) Laplane, D., Talairach, J., Meininger, V., Bancaud, J., and Bouchareine, A. (1977). Motor consequences of motor area ablations in man. *Journal of the Neurological Sciences 31*, 29–49, DOI: 10.1016/0022-510x(77)90004-1, PubMed ID: 833609.

(365) Latham, A., and Paul, D. H. (1971). Spontaneous activity of cerebellar Purkinje cells and their responses to impulses in climbing fibres. *The Journal of Physiology 213*, 135–156, PubMed ID: 5575334, https://www.ncbi.nlm.nih.gov/pmc/articles/PMC1331728/.

(366) Laurent, V., and Westbrook, R. F. (2009). Inactivation of the infralimbic but not the prelimbic cortex impairs consolidation and retrieval of fear extinction. *Learning & Memory (Cold Spring Harbor, N.Y.) 16*, 520–529, DOI: 10.1101/lm.1474609, PubMed ID: 19706835.

(367) Le Ber, I., Clot, F., Vercueil, L., Camuzat, A., Viémont, M., Benamar, N., De Liège, P., Ouvrard-Hernandez, A. M., Pollak, P., Stevanin, G., Brice, A., and Dürr, A. (2006). Predominant dystonia with marked cerebellar atrophy: a rare phenotype in familial dystonia. *Neurology 67*, 1769–1773, DOI: 10.1212/01.wnl.0000244484.60489.50, PubMed ID: 17130408.

(368) Lebrón, K., Milad, M. R., and Quirk, G. J. (2004). Delayed recall of fear extinction in rats with lesions of ventral medial prefrontal cortex. *Learning & Memory (Cold Spring Harbor, N.Y.) 11*, 544–548, DOI: 10.1101/lm.78604, PubMed ID: 15466306.

(369) LeDoux, J. E. Emotion Circuits in the Brain.

(370) Lee, A. K., and Wilson, M. A. (2002). Memory of sequential experience in the hippocampus during slow wave sleep. *Neuron 36*, 1183–1194, DOI: 10.1016/s0896-6273(02)01096-6, PubMed ID: 12495631.

(371) Lee, J.-H., Latchoumane, C.-F. V., Park, J., Kim, J., Jeong, J., Lee, K.-H., and Shin, H.-S. (2019). The rostroventral part of the thalamic reticular nucleus modulates fear extinction. *Nature Communications 10*, Number: 1 Publisher: Nature Publishing Group, 4637, DOI: 10.1038/s41467-019-12496-9.

(372) Lee, S., Ahmed, T., Lee, S., Kim, H., Choi, S., Kim, D.-S., Kim, S. J., Cho, J., and Shin, H.-S. (2012). Bidirectional modulation of fear extinction by mediodorsal thalamic firing in mice. *Nature Neuroscience 15*, Number: 2 Publisher: Nature Publishing Group, 308–314, DOI: 10.1038/nn.2999.

(373) Lee, S., and Shin, H.-S. (2016). The role of mediodorsal thalamic nucleus in fear extinction. *Journal of Analytical Science and Technology 7*, Number: 1, 13, DOI: 10.1186/s40543-016-0093-6.

(374) Leergaard, T. B., and Bjaalie, J. G. (2007). Topography of the complete corticopontine projection: from experiments to principal Maps. *Frontiers in Neuroscience 1*, 211–223, DOI: 10.3389/neuro.01.1.1.016.2007, PubMed ID: 18982130.

(375) Legg, C. R., Mercier, B., and Glickstein, M. (1989). Corticopontine projection in the rat: the distribution of labelled cortical cells after large injections of horseradish peroxidase in the pontine nuclei. *The Journal of Comparative Neurology 286*, 427–441, DOI: 10.1002/cne.902860403, PubMed ID: 2778100.

(376) Lemke, S. M., Ramanathan, D. S., Darevksy, D., Egert, D., Berke, J. D., and Ganguly, K. (2021). Coupling between motor cortex and striatum increases during sleep over long-term skill learning. *eLife 10*, e64303, DOI: 10.7554/eLife.64303, PubMed ID: 34505576.

(377) Léna, C., and Popa, D. In *The Neuronal Codes of the Cerebellum*; Elsevier: 2016, pp 135–153, DOI: 10.1016/B978-0-12-801386-1.00006-X.

(378) Leon, L. E. S., and Sillitoe, R. V. (2023). Disrupted sleep in dystonia depends on cerebellar function but not motor symptoms in mice. *bioRxiv: The Preprint Server for Biology*, 2023.02.09.527916, DOI: 10.1101/2023.02.09.527916, PubMed ID: 36798256.

(379) Lesting, J., Daldrup, T., Narayanan, V., Himpe, C., Seidenbecher, T., and Pape, H.-C. (2013). Directional Theta Coherence in Prefrontal Cortical to Amygdalo-Hippocampal Pathways Signals Fear Extinction. *PLoS ONE 8*, e77707, DOI: 10.1371/journal.pone.0077707, PubMed ID: 24204927.

(380) Leyton, A. S., and Sherrington, C. S. (1917). Observations on the excitable cortex of the chimpanzee, orang-utan, and gorilla. *Quarterly Journal of Experimental Physiology: Translation and Integration 11*, 135–222.

(381) Li, C. L., and Parker, L. O. (1969). Effect of dentate stimulation on neuronal activity in the globus pallidus. *Experimental Neurology 24*, 298–309, DOI: 10.1016/0014-4886(69)90023-5, PubMed ID: 5784137.

(382) Li, N., Daie, K., Svoboda, K., and Druckmann, S. (2016). Robust neuronal dynamics in premotor cortex during motor planning. *Nature 532*, 459–464, DOI: 10.1038/nature17643, PubMed ID: 27074502.

(383) Lin, S., and Xu, J. P., *Sunday Sparrows*; The Chinese University of Hong Kong Press: 2019, DOI: 10.2307/j.ctvzsmbnq.

(384) Lindeman, S., Hong, S., Kros, L., Mejias, J. F., Romano, V., Oostenveld, R., Negrello, M., Bosman, L. W. J., and De Zeeuw, C. I. (2021). Cerebellar Purkinje cells can differentially modulate coherence between sensory and motor cortex depending on region and behavior. *Proceedings of the National Academy of Sciences of the United States of America 118*, Number: 2, e2015292118, DOI: 10.1073/pnas.2015292118, PubMed ID: 33443203.

(385) Lingawi, N. W., Laurent, V., Westbrook, R. F., and Holmes, N. M. (2019). The role of the basolateral amygdala and infralimbic cortex in (re)learning extinction. *Psychopharmacology 236*, 303–312, DOI: 10.1007/s00213-018-4957-x, PubMed ID: 29959461.

(386) Lisberger, S., and Raymond, J. (1996). Neural recordings and behavioral observations in the monkey vestibulo-ocular reflex constrain the cellular mechanisms for cerebellum-dependent behavioral learning. *Journal of Physiology-Paris 90*, 381–382, DOI: 10.1016/S0928-4257(97)87923-5.

(387) Liu, C., Lee, C.-Y., Asher, G., Cao, L., Terakoshi, Y., Cao, P., Kobayakawa, R., Kobayakawa, K., Sakurai, K., and Liu, Q. (2021). Posterior subthalamic nucleus (PSTh) mediates innate fear-associated hypothermia in mice. *Nature Communications 12*, Number: 1 Publisher: Nature Publishing Group, 2648, DOI: 10.1038/s41467-021-22914-6.

(388) Liu, Y., and Block, H. J. (2021). The effect of sequence learning on sensorimotor adaptation. *Behavioural Brain Research 398*, 112979, DOI: 10.1016/j.bbr.2020.112979, PubMed ID: 33164864.

(389) Llinás, R., and Mühlethaler, M. (1988). Electrophysiology of guinea-pig cerebellar nuclear cells in the in vitro brain stem-cerebellar preparation. *The Journal of Physiology 404*, 241–258, DOI: 10.1113/jphysiol.1988.sp017288, PubMed ID: 2855348.

(390) Lopes, G., Nogueira, J., Dimitriadis, G., Menendez, J. A., Paton, J. J., and Kampff, A. R. (2023). A robust role for motor cortex. *Frontiers in Neuroscience 17*, https://www.frontiersin.org/articles/10.3389/fnins.2023.971980.

(391) Louis, E. D. (1994). Contralateral control: evolving concepts of the brain-body relationship from Hippocrates to Morgagni. *Neurology 44*, 2398–2400, DOI: 10.1212/wnl.44.12.2398, PubMed ID: 7991135.

(392) Lozeron, P., Poujois, A., Richard, A., Masmoudi, S., Meppiel, E., Woimant, F., and Kubis, N. (2016). Contribution of TMS and rTMS in the Understanding of the Pathophysiology and in the Treatment of Dystonia. *Frontiers in Neural Circuits 10*, 90, DOI: 10.3389/fncir.2016.00090, PubMed ID: 27891079.

(393) Lugaro, E. (1894). Sulle connessioni tra gli elemente nervosa della corteccia cerebellare con considerazioni generali sulsignificato fisiologico dei rapporti tra gli elementi nervosi. *Rivista Sperimentale di Freniatria 20*, 297.

(394) Luo, P., Moritani, M., and Dessem, D. (2001). Jaw-muscle spindle afferent pathways to the trigeminal motor nucleus in the rat. *The Journal of Comparative Neurology 435*, 341–353, DOI: 10.1002/cne.1034, PubMed ID: 11406816.

(395) MacLEAN, P. D. (1949). Psychosomatic disease and the visceral brain; recent developments bearing on the Papez theory of emotion. *Psychosomatic Medicine 11*, 338–353, DOI: 10.1097/00006842-194911000-00003, PubMed ID: 15410445.

(396) Maclean, P. D. (1952). Some psychiatric implications of physiological studies on frontotemporal portion of limbic system (visceral brain). *Electroencephalography and Clinical Neurophysiology 4*, 407–418, DOI: 10.1016/0013-4694(52)90073-4, PubMed ID: 12998590.

(397) Maltese, M., Martella, G., Madeo, G., Fagiolo, I., Tassone, A., Ponterio, G., Sciamanna, G., Burbaud, P., Conn, P., Bonsi, P., and Pisani, A. (2014). Anticholinergic drugs rescue synaptic plasticity in DYT1 dystonia: role of M1 muscarinic receptors. *Movement disorders : official journal of the Movement Disorder Society 29*, Number: 13, 1655–1665, DOI: 10.1002/mds.26009, PubMed ID: 25195914.

(398) Mao, T., Kusefoglu, D., Hooks, B. M., Huber, D., Petreanu, L., and Svoboda, K. (2011). Long-range neuronal circuits underlying the interaction between sensory and motor cortex. *Neuron 72*, 111–123, DOI: 10.1016/j.neuron.2011.07.029, PubMed ID: 21982373.

(399) Marek, R., Sun, Y., and Sah, P. (2019). Neural circuits for a top-down control of fear and extinction. *Psychopharmacology 236*, 313–320, DOI: 10.1007/s00213-018-5033-2, PubMed ID: 30215217.

(400) Marinelli, L., Crupi, D., Di Rocco, A., Bove, M., Eidelberg, D., Abbruzzese, G., and Felice Ghilardi, M. (2009). Learning and consolidation of visuo-motor adaptation in Parkinson's disease. *Parkinsonism & related disorders 15*, 6–11, DOI: 10.1016/j.parkreldis.2008.02.012, PubMed ID: 18424221.

(401) Marini, G., Pianca, L., and Tredici, G. (1999). Descending projections arising from the parafascicular nucleus in rats: trajectory of fibers, projection pattern and mapping of terminations. *Somatosensory & Motor Research 16*, 207–222, DOI: 10.1080/08990229970465, PubMed ID: 10527369.

(402) Marr, D. (1969). A theory of cerebellar cortex. *The Journal of Physiology 202*, 437–470, DOI: 10.1113/jphysiol.1969.sp008820, PubMed ID: 5784296.

(403) Martella, G., Bonsi, P., Imbriani, P., Sciamanna, G., Nguyen, H., Yu-Taeger, L., Schneider, M., Poli, S., Lütjens, R., and Pisani, A. (2021). Rescue of striatal long-term depression by chronic mGlu5 receptor negative allosteric modulation in distinct dystonia models. *Neuropharmacology 192*, 108608, DOI: 10.1016/j.neuropharm.2021.108608.

(404) Maschke, M., Gomez, C. M., Ebner, T. J., and Konczak, J. (2004). Hereditary cerebellar ataxia progressively impairs force adaptation during goal-directed arm movements. *Journal of Neurophysiology 91*, 230–238, DOI: 10.1152/jn.00557.2003, PubMed ID: 13679403.

(405) Masrori, P., and Van Damme, P. (2020). Amyotrophic lateral sclerosis: a clinical review. *European Journal of Neurology 27*, 1918–1929, DOI: 10.1111/ene.14393, PubMed ID: 32526057.

(406) Masuda, N., and Amari, S.-i. (2008). A computational study of synaptic mechanisms of partial memory transfer in cerebellar vestibulo-ocular-reflex learning. *Journal of Computational Neuroscience 24*, 137–156, DOI: 10.1007/s10827-007-0045-7, PubMed ID: 17616795.

(407) Matsushita, M., Gao, X., and Yaginuma, H. (1995). Spinovestibular projections in the rat, with particular reference to projections from the central cervical nucleus to the lateral vestibular nucleus. *The Journal of Comparative Neurology 361*, 334–334, DOI: 10.1002/cne.903610210, PubMed ID: 8543666.

(408) Mattar, M. G., and Daw, N. D. (2018). Prioritized memory access explains planning and hippocampal replay. *Nature Neuroscience 21*, Number: 11 Publisher: Nature Publishing Group, 1609–1617, DOI: 10.1038/s41593-018-0232-z.

(409) Maurice, N., Deniau, J.-M., Glowinski, J., and Thierry, A.-M. (1999). Relationships between the Prefrontal Cortex and the Basal Ganglia in the Rat: Physiology of the Cortico-Nigral Circuits. *The Journal of Neuroscience 19*, 4674–4681, DOI: 10.1523/JNEUROSCI.19-11-04674.1999, PubMed ID: 10341265.

(410) McAfee, S. S., Liu, Y., Sillitoe, R. V., and Heck, D. H. (2021). Cerebellar Coordination of Neuronal Communication in Cerebral Cortex. *Frontiers in Systems Neuroscience 15*, 781527, DOI: 10.3389/fnsys.2021.781527, PubMed ID: 35087384.

(411) McAfee, S. S., Liu, Y., Sillitoe, R. V., and Heck, D. H. (2019). Cerebellar Lobulus Simplex and Crus I Differentially Represent Phase and Phase Difference of Prefrontal Cortical and Hippocampal Oscillations. *Cell Reports 27*, Number: 8, 2328–2334.e3, DOI: 10.1016/j.celrep.2019.04.085, PubMed ID: 31116979.

(412) McAllister, W. R., McAllister, D. E., Scoles, M. T., and Hampton, S. R. (1986). Persistence of fear-reducing behavior: relevance for the conditioning theory of neurosis. *Journal of Abnormal Psychology 95*, 365–372, DOI: 10.1037//0021-843x.95.4.365, PubMed ID: 3805500.

(413) McCairn, K. W., and Turner, R. S. (2015). Pallidal stimulation suppresses pathological dysrhythmia in the parkinsonian motor cortex. *Journal of Neurophysiology 113*, 2537–2548, DOI: 10.1152/jn.00701.2014, PubMed ID: 25652922.

(414) McGregor, M. M., and Nelson, A. B. (2019). Circuit Mechanisms of Parkinson's Disease. *Neuron 101*, 1042–1056, DOI: 10.1016/j.neuron.2019.03.004.

(415) Medina, J. F., and Mauk, M. D. (1999). Simulations of cerebellar motor learning: computational analysis of plasticity at the mossy fiber to deep nucleus synapse. *The Journal of Neuroscience: The Official Journal of the Society for Neuroscience 19*, 7140–7151, DOI: 10.1523/JNEUROSCI.19-16-07140.1999, PubMed ID: 10436067.

(416) Medina, J. F., and Lisberger, S. G. (2008). Links from complex spikes to local plasticity and motor learning in the cerebellum of awake-behaving monkeys. *Nature Neuroscience 11*, 1185–1192, DOI: 10.1038/nn.2197, PubMed ID: 18806784.

(417) Medina, J. F., Nores, W. L., and Mauk, M. D. (2002). Inhibition of climbing fibres is a signal for the extinction of conditioned eyelid responses. *Nature 416*, 330–333, DOI: 10.1038/416330a, PubMed ID: 11907580.

(418) Meftah, E. M., and Rispal-Padel, L. (1994). Synaptic plasticity in the thalamo-cortical pathway as one of the neurobiological correlates of forelimb flexion conditioning: electrophysiological investigation in the cat. *Journal of Neurophysiology 72*, 2631–2647, DOI: 10.1152/jn.1994.72.6.2631, PubMed ID: 7897480.

(419) Mehrkanoon, S., Boonstra, T. W., Breakspear, M., Hinder, M., and Summers, J. J. (2016). Upregulation of cortico-cerebellar functional connectivity after motor learning. *NeuroImage 128*, 252–263, DOI: 10.1016/j.neuroimage.2015.12.052, PubMed ID: 26767943.

(420) Mendes, A., Vignoud, G., Perez, S., Perrin, E., Touboul, J., and Venance, L. (2020). Concurrent Thalamostriatal and Corticostriatal Spike-Timing-Dependent Plasticity and Heterosynaptic Interactions Shape Striatal Plasticity Map. *Cerebral Cortex (New York, N.Y.: 1991) 30*, Number: 8, 4381–4401, DOI: 10.1093/cercor/bhaa024, PubMed ID: 32147733.

(421) Meunier, S., Russmann, H., Shamim, E., Lamy, J.-C., and Hallett, M. (2012). Plasticity of cortical inhibition in dystonia is impaired after motor learning and Paired-Associative Stimulation. *The European Journal of Neuroscience 35*, 975–986, DOI: 10.1111/j.1460-9568.2012.08034.x, PubMed ID: 22429246.

(422) Meyer, G. (1987). Forms and spatial arrangement of neurons in the primary motor cortex of man. *The Journal of Comparative Neurology 262*, 402–428, DOI: 10.1002/cne.902620306, PubMed ID: 3655019.

(423) Miall, R. C., Weir, D. J., Wolpert, D. M., and Stein, J. F. (1993). Is the cerebellum a smith predictor? *Journal of Motor Behavior 25*, 203–216, DOI: 10.1080/00222895.1993.9942050, PubMed ID: 12581990.

(424) Miao, Q.-L., Herlitze, S., Mark, M. D., and Noebels, J. L. (2020). Adult loss of Cacna1a in mice recapitulates childhood absence epilepsy by distinct thalamic bursting mechanisms. *Brain 143*, Number: 1, 161–174, DOI: 10.1093/brain/awz365, PubMed ID: 31800012.

(425) Middleton, F. A., and Strick, P. L. (1994). Anatomical evidence for cerebellar and basal ganglia involvement in higher cognitive function. *Science (New York, N.Y.) 266*, 458–461, DOI: 10.1126/science.7939688, PubMed ID: 7939688.

(426) Middleton, F. A., and Strick, P. L. (1997). Cerebellar output channels. *International Review of Neurobiology 41*, 61–82, DOI: 10.1016/s0074-7742(08)60347-5, PubMed ID: 9378611.

(427) Middleton, F. A., and Strick, P. L. (1998). Cerebellar output: motor and cognitive channels. *Trends in Cognitive Sciences 2*, 348–354, DOI: 10.1016/S1364-6613(98)01220-0.

(428) Milad, M. R., and Quirk, G. J. (2002). Neurons in medial prefrontal cortex signal memory for fear extinction. *Nature 420*, Number: 6911 Publisher: Nature Publishing Group, 70–74, DOI: 10.1038/nature01138.

(429) Miller, W. C., and DeLong, M. R. (1988). Parkinsonian symptomatology. An anatomical and physiological analysis. *Annals of the New York Academy of Sciences 515*, 287–302, DOI: 10.1111/j.1749-6632.1988.tb32998.x, PubMed ID: 3364889.

(430) Mink, J. W. (1996). The basal ganglia: focused selection and inhibition of competing motor programs. *Progress in neurobiology 50*, 381–425.

(431) Mink, J. W., and Thach, W. T. (1993). Basal ganglia intrinsic circuits and their role in behavior. *Current opinion in neurobiology 3*, 950–957.

(432) Mittmann, W., Koch, U., and Häusser, M. (2005). Feed-forward inhibition shapes the spike output of cerebellar Purkinje cells. *The Journal of Physiology 563*, 369–378, DOI: 10.1113/jphysiol.2004.075028, PubMed ID: 15613376.

(433) Moini, J., and Piran, P. In *Functional and Clinical Neuroanatomy*, Moini, J., and Piran, P., Eds.; Academic Press: 2020, pp 497–517, DOI: 10.1016/B978-0-12-817424-1.00016-1.

(434) Molineux, M. L., McRory, J. E., McKay, B. E., Hamid, J., Mehaffey, W. H., Rehak, R., Snutch, T. P., Zamponi, G. W., and Turner, R. W. (2006). Specific T-type calcium channel isoforms are associated with distinct burst phenotypes in deep cerebellar nuclear neurons. *Proceedings of the National Academy of Sciences of the United States of America 103*, 5555–5560, DOI: 10.1073/pnas.0601261103, PubMed ID: 16567615.

(435) Molineux, M. L., Mehaffey, W. H., Tadayonnejad, R., Anderson, D., Tennent, A. F., and Turner, R. W. (2008). Ionic factors governing rebound burst phenotype in rat deep cerebellar neurons. *Journal of Neurophysiology 100*, 2684–2701, DOI: 10.1152/jn.90427.2008, PubMed ID: 18768644.

(436) Montague, P. R., Dayan, P., and Sejnowski, T. J. (1996). A framework for mesencephalic dopamine systems based on predictive Hebbian learning. *The Journal of Neuroscience: The Official Journal of the Society for Neuroscience 16*, 1936–1947, DOI: 10.1523/JNEUROSCI.16-05-01936.1996, PubMed ID: 8774460.

(437) Morceau, S., Piquet, R., Wolff, M., and Parkes, S. L. (2019). Targeting Reciprocally Connected Brain Regions Through CAV-2 Mediated Interventions. *Frontiers in Molecular Neuroscience 12*, https://www.frontiersin.org/articles/10.3389/fnmol.2019.00303.

(438) Morehead, J. R., Taylor, J. A., Parvin, D. E., and Ivry, R. B. (2017). Characteristics of Implicit Sensorimotor Adaptation Revealed by Task-irrelevant Clamped Feedback. *Journal of cognitive neuroscience 29*, Publisher: NIH Public Access, 1061, DOI: 10.1162/jocn_a_01108, PubMed ID: 28195523.

(439) Morin, A., Doyon, J., Dostie, V., Barakat, M., Tahar, A. H., Korman, M., Benali, H., Karni, A., Ungerleider, L. G., and Carrier, J. (2008). Motor Sequence Learning Increases Sleep Spindles and Fast Frequencies in Post-Training Sleep. *Sleep 31*, 1149–1156, PubMed ID: 18714787, https://www.ncbi.nlm.nih.gov/pmc/articles/PMC2542961/.

(440) Morton, S. M., and Bastian, A. J. (2006). Cerebellar contributions to locomotor adaptations during splitbelt treadmill walking. *The Journal of Neuroscience: The Official Journal of the Society for Neuroscience 26*, 9107–9116, DOI: 10.1523/JNEUROSCI.2622-06.2006, PubMed ID: 16957067.

(441) Muellbacher, W., Ziemann, U., Wissel, J., Dang, N., Kofler, M., Facchini, S., Boroojerdi, B., Poewe, W., and Hallett, M. (2002). Early consolidation in human primary motor cortex. *Nature 415*, 640–644, DOI: 10.1038/nature712, PubMed ID: 11807497.

(442) Mugnaini, E., Di˜o, M. R., and Jaarsma, D. In *Progress in Brain Research*, De Zeeuw, C. I., Strata, P., and Voogd, J., Eds.; The Cerebellum: From Structure to Control, Vol. 114; Elsevier: 1997, pp 131–150, DOI: 10.1016/S0079-6123(08)63362-2.

(443) Mugnaini, E., Sekerková, G., and Martina, M. (2011). The unipolar brush cell: a remarkable neuron finally receiving deserved attention. *Brain Research Reviews 66*, 220–245, DOI: 10.1016/j.brainresrev.2010.10.001, PubMed ID: 20937306.

(444) Muralidharan, A., Jensen, A. L., Connolly, A., Hendrix, C. M., Johnson, M. D., Baker, K. B., and Vitek, J. L. (2016). Physiological changes in the pallidum in a progressive model of Parkinson's disease: Are oscillations enough? *Experimental Neurology 279*, 187–196, DOI: 10.1016/j.expneurol.2016.03.002.

(445) Myers, K. M., and Davis, M. (2002). Behavioral and neural analysis of extinction. *Neuron 36*, 567–584, DOI: 10.1016/s0896-6273(02)01064-4, PubMed ID: 12441048.

(446) Nachev, P., Kennard, C., and Husain, M. (2008). Functional role of the supplementary and pre-supplementary motor areas. *Nature Reviews. Neuroscience 9*, 856–869, DOI: 10.1038/nrn2478, PubMed ID: 18843271.

(447) Nagai, H., de Vivo, L., Bellesi, M., Ghilardi, M. F., Tononi, G., and Cirelli, C. (2017). Sleep Consolidates Motor Learning of Complex Movement Sequences in Mice. *Sleep 40*, Number: 2, DOI: 10.1093/sleep/zsw059, PubMed ID: 28364506.

(448) Najac, M., and Raman, I. M. (2017). Synaptic excitation by climbing fibre collaterals in the cerebellar nuclei of juvenile and adult mice. *The Journal of Physiology 595*, 6703–6718, DOI: 10.1113/JP274598, PubMed ID: 28795396.

(449) Nam, S. C., and Hockberger, P. E. (1997). Analysis of spontaneous electrical activity in cerebellar Purkinje cells acutely isolated from postnatal rats. *Journal of Neurobiology 33*, _eprint: https://onlinelibrary.wiley.com/doi/pdf/10.1002/%28SICI%291097-4695%28199707%2933%3A1%3C1
NEU3%3E3.0.CO%3B2-G, 18–32, DOI: 10.1002/(SICI)1097-4695(199707)33:1<18::AID-NEU3>3.0.CO;2-G.

(450) Nambu, A., Takada, M., Inase, M., and Tokuno, H. (1996). Dual somatotopical representations in the primate subthalamic nucleus: evidence for ordered but reversed body-map transformations from the primary motor cortex and the supplementary motor area. *The Journal of Neuroscience: The Official Journal of the Society for Neuroscience 16*, 2671–2683, DOI: 10.1523/JNEUROSCI.16-08-02671.1996, PubMed ID: 8786443.

(451) Nambu, A., Tokuno, H., Hamada, I., Kita, H., Imanishi, M., Akazawa, T., Ikeuchi, Y., and Hasegawa, N. (2000). Excitatory cortical inputs to pallidal neurons via the subthalamic nucleus in the monkey. *Journal of Neurophysiology 84*, 289–300, DOI: 10.1152/jn.2000.84.1.289, PubMed ID: 10899204.

(452) Nambu, A., Yoshida, S., and Jinnai, K. (1990). Discharge patterns of pallidal neurons with input from various cortical areas during movement in the monkey. *Brain Research 519*, 183–191, DOI: 10.1016/0006-8993(90)90076-n, PubMed ID: 2397404.

(453) Nambu, A. (2004). A new dynamic model of the cortico-basal ganglia loop. *Progress in Brain Research 143*, 461–466, DOI: 10.1016/S0079-6123(03)43043-4, PubMed ID: 14653188.

(454) Napper, R. M., and Harvey, R. J. (1988). Number of parallel fiber synapses on an individual Purkinje cell in the cerebellum of the rat. *The Journal of Comparative Neurology 274*, 168–177, DOI: 10.1002/cne.902740204, PubMed ID: 3209740.

(455) Nauta, H. J., and Cole, M. (1978). Efferent projections of the subthalamic nucleus: an autoradiographic study in monkey and cat. *The Journal of Comparative Neurology 180*, 1–16, DOI: 10.1002/cne.901800102, PubMed ID: 418083.

(456) Nguyen, K. P., Sharma, A., Gil-Silva, M., Gittis, A. H., and Chase, S. M. (2021). Distinct Kinematic Adjustments over Multiple Timescales Accompany Locomotor Skill Development in Mice. *Neuroscience 466*, 260–272, DOI: 10.1016/j.neuroscience.2021.05.002.

(457) Nishida, M., and Walker, M. P. (2007). Daytime naps, motor memory consolidation and regionally specific sleep spindles. *PloS One 2*, e341, DOI: 10.1371/journal.pone.0000341, PubMed ID: 17406665.

(458) Noda, H. (1991). Cerebellar control of saccadic eye movements: its neural mechanisms and pathways. *The Japanese Journal of Physiology 41*, 351–368, DOI: 10.2170/jjphysiol.41.351, PubMed ID: 1960885.

(459) Novello, M., Bosman, L. W. J., and De Zeeuw, C. I. (2022). A Systematic Review of Direct Outputs from the Cerebellum to the Brainstem and Diencephalon in Mammals. *The Cerebellum*, DOI: 10.1007/s12311-022-01499-w, https://doi.org/10.1007/s12311-022-01499-w.

(460) O'Rourke, K., O'Riordan, S., Gallagher, J., and Hutchinson, M. (2006). Paroxysmal torticollis and blepharospasm following bilateral cerebellar infarction. *Journal of Neurology 253*, 1644–1645, DOI: 10.1007/s00415-006-0202-3, PubMed ID: 17219037.

(461) Öhman, A. In *Handbook of emotions*; The Guilford Press: New York, NY, US, 1993, pp 511–536.

(462) Ohtsuka, K., and Noda, H. (1995). Discharge properties of Purkinje cells in the oculomotor vermis during visually guided saccades in the macaque monkey. *Journal of Neurophysiology 74*, 1828–1840, DOI: 10.1152/jn.1995.74.5.1828, PubMed ID: 8592177.

(463) Ohtsuka, K., and Noda, H. (1991). Saccadic burst neurons in the oculomotor region of the fastigial nucleus of macaque monkeys. *Journal of Neurophysiology 65*, 1422–1434, DOI: 10.1152/jn.1991.65.6.1422, PubMed ID: 1875251.

(464) Ohtsuki, G., Piochon, C., and Hansel, C. (2009). Climbing fiber signaling and cerebellar gain control. *Frontiers in Cellular Neuroscience 3*, 4, DOI: 10.3389/neuro.03.004.2009, PubMed ID: 19597563.

(465) Olszyński, K. H., Polowy, R., Wardak, A. D., Grymanowska, A. W., and Filipkowski, R. K. (2021). Increased Vocalization of Rats in Response to Ultrasonic Playback as a Sign of Hypervigilance Following Fear Conditioning. *Brain Sciences 11*, 970, DOI: 10.3390/brainsci11080970, PubMed ID: 34439589.

(466) Orban, P., Peigneux, P., Lungu, O., Albouy, G., Breton, E., Laberenne, F., Benali, H., Maquet, P., and Doyon, J. (2010). The multifaceted nature of the relationship between performance and brain activity in motor sequence learning. *NeuroImage 49*, 694–702, DOI: 10.1016/j.neuroimage.2009.08.055.

(467) Osorno, T., Rudolph, S., Nguyen, T., Kozareva, V., Nadaf, N. M., Norton, A., Macosko, E. Z., Lee, W.-C. A., and Regehr, W. G. (2022). Candelabrum cells are ubiquitous cerebellar cortex interneurons with specialized circuit properties. *Nature Neuroscience 25*, 702–713, DOI: 10.1038/s41593-022-01057-x, PubMed ID: 35578131.

(468) Otsuka, S., Konno, K., Abe, M., Motohashi, J., Kohda, K., Sakimura, K., Watanabe, M., and Yuzaki, M. (2016). Roles of Cbln1 in Non-Motor Functions of Mice. *The Journal of Neuroscience: The Official Journal of the Society for Neuroscience 36*, 11801–11816, DOI: 10.1523/JNEUROSCI.0322-16.2016, PubMed ID: 27852787.

(469) Ozawa, M., Davis, P., Ni, J., Maguire, J., Papouin, T., and Reijmers, L. (2020). Experience-dependent resonance in amygdalo-cortical circuits supports fear memory retrieval following extinction. *Nature Communications 11*, Number: 1, 4358, DOI: 10.1038/s41467-020-18199-w, PubMed ID: 32868768.

(470) Özcan, O. O., Wang, X., Binda, F., Dorgans, K., De Zeeuw, C. I., Gao, Z., Aertsen, A., Kumar, A., and Isope, P. (2020). Differential Coding Strategies in Glutamatergic and GABAergic Neurons in the Medial Cerebellar Nucleus. *The Journal of Neuroscience: The Official Journal of the Society for Neuroscience 40*, Number: 1, 159–170, DOI: 10.1523/JNEUROSCI.0806-19.2019, PubMed ID: 31694963.

(471) Palay, S. L., and Chan-Palay, V., *Cerebellar cortex: cytology and organization*; Springer Science & Business Media: 1974.

(472) Palmer, L. M., Clark, B. A., Gründemann, J., Roth, A., Stuart, G. J., and Häusser, M. (2010). Initiation of simple and complex spikes in cerebellar Purkinje cells. *The Journal of Physiology 588*, 1709–1717, DOI: 10.1113/jphysiol.2010.188300, PubMed ID: 20351049.

(473) Papez, J. W. (1937). A proposed mechanism of emotion. *Archives of Neurology & Psychiatry 38*, 725–743.

(474) Park, J., Coddington, L. T., and Dudman, J. T. (2020). Basal Ganglia Circuits for Action Specification. *Annual Review of Neuroscience 43*, 485–507, DOI: 10.1146/annurev-neuro-070918-050452, PubMed ID: 32303147.

(475) Pasalar, S., Roitman, A. V., Durfee, W. K., and Ebner, T. J. (2006). Force field effects on cerebellar Purkinje cell discharge with implications for internal models. *Nature Neuroscience 9*, 1404–1411, DOI: 10.1038/nn1783, PubMed ID: 17028585.

(476) Pasquereau, B., DeLong, M. R., and Turner, R. S. (2016). Primary motor cortex of the parkinsonian monkey: altered encoding of active movement. *Brain: A Journal of Neurology 139*, 127–143, DOI: 10.1093/brain/awv312, PubMed ID: 26490335.

(477) Pasquereau, B., and Turner, R. S. (2011). Primary motor cortex of the parkinsonian monkey: differential effects on the spontaneous activity of pyramidal tract-type neurons. *Cerebral Cortex (New York, N.Y.: 1991) 21*, 1362–1378, DOI: 10.1093/cercor/bhq217, PubMed ID: 21045003.

(478) Pasquet, M. O., Tihy, M., Gourgeon, A., Pompili, M. N., Godsil, B. P., Léna, C., and Dugué, G. P. (2016). Wireless inertial measurement of head kinematics in freely-moving rats. *Scientific Reports 6*, 35689, DOI: 10.1038/srep35689, PubMed ID: 27767085.

(479) Paulson, H. L., Shakkottai, V. G., Clark, H. B., and Orr, H. T. (2017). Polyglutamine spinocerebellar ataxias - from genes to potential treatments. *Nature Reviews. Neuroscience 18*, 613–626, DOI: 10.1038/nrn.2017.92, PubMed ID: 28855740.

(480) Pavlov (1927), P. I. (2010). Conditioned reflexes: An investigation of the physiological activity of the cerebral cortex. *Annals of Neurosciences 17*, 136–141, DOI: 10.5214/ans.0972-7531.1017309, PubMed ID: 25205891.

(481) Paydar, A., Lee, B., Gangadharan, G., Lee, S., Hwang, E. M., and Shin, H.-S. (2014). Extrasynaptic GABAA receptors in mediodorsal thalamic nucleus modulate fear extinction learning. *Molecular Brain 7*, 39, DOI: 10.1186/1756-6606-7-39, PubMed ID: 24886120.

(482) Pedroarena, C. M. (2011). BK and Kv3.1 potassium channels control different aspects of deep cerebellar nuclear neurons action potentials and spiking activity. *Cerebellum (London, England) 10*, 647–658, DOI: 10.1007/s12311-011-0279-9, PubMed ID: 21750937.

(483) Pelosi, A., Menardy, F., Popa, D., Girault, J.-A., and Hervé, D. (2017). Heterozygous Gnal Mice Are a Novel Animal Model with Which to Study Dystonia Pathophysiology. *The Journal of Neuroscience 37*, Number: 26, 6253–6267, DOI: 10.1523/JNEUROSCI.1529-16.2017.

(484) Penfield, W., and Boldrey, E. (1937). Somatic motor and sensory representation in the cerebral cortex of man as studied by electrical stimulation. *Brain 60*, 389–443.

(485) Penny, G. R., Wilson, C. J., and Kitai, S. T. (1988). Relationship of the axonal and dendritic geometry of spiny projection neurons to the compartmental organization of the neostriatum. *The Journal of Comparative Neurology 269*, 275–289, DOI: 10.1002/cne.902690211, PubMed ID: 2833538.

(486) Penzo, M. A., Robert, V., Tucciarone, J., De Bundel, D., Wang, M., Van Aelst, L., Darvas, M., Parada, L. F., Palmiter, R. D., He, M., Huang, Z. J., and Li, B. (2015). The paraventricular thalamus controls a central amygdala fear circuit. *Nature 519*, 455–459, DOI: 10.1038/nature13978, PubMed ID: 25600269.

(487) Percheron, G., François, C., Talbi, B., Yelnik, J., and Fénelon, G. (1996). The primate motor thalamus. *Brain Research. Brain Research Reviews 22*, 93–181, PubMed ID: 8883918.

(488) Pert, C. B., Kuhar, M. J., and Snyder, S. H. (1976). Opiate receptor: autoradiographic localization in rat brain. *Proceedings of the National Academy of Sciences of the United States of America 73*, 3729–3733, PubMed ID: 185626, https://www.ncbi.nlm.nih.gov/pmc/articles/PMC431193/.

(489) Peters, A. J., Liu, H., and Komiyama, T. (2017). Learning in the Rodent Motor Cortex. *Annual review of neuroscience 40*, 77–97, DOI: 10.1146/annurev-neuro-072116-031407, PubMed ID: 28375768.

(490) Picard, N., and Strick, P. L. (2001). Imaging the premotor areas. *Current Opinion in Neurobiology 11*, 663–672, DOI: 10.1016/s0959-4388(01)00266-5, PubMed ID: 11741015.

(491) Pickford, J., and Apps, R. (2017). Collateral impact: a dual role for climbing fibre collaterals to the cerebellar nuclei? *The Journal of Physiology 595*, 6589–6590, DOI: 10.1113/JP275091, PubMed ID: 28895648.

(492) Pimentel-Farfan, A. K., Báez-Cordero, A. S., Peña-Rangel, T. M., and Rueda-Orozco, P. E. (2022). Cortico-striatal circuits for bilaterally coordinated movements. *Science Advances 8*, Number: 9, eabk2241, DOI: 10.1126/sciadv.abk2241, PubMed ID: 35245127.

(493) Pinault, D., and Deschênes, M. (1998). Projection and innervation patterns of individual thalamic reticular axons in the thalamus of the adult rat: a three-dimensional, graphic, and morphometric analysis. *The Journal of Comparative Neurology 391*, 180–203, DOI: 10.1002/(sici)1096-9861(19980209)391:2<180::aid-cne3>3.0.co;2-z, PubMed ID: 9518268.

(494) Pirot, S., Jay, T. M., Glowinski, J., and Thierry, A. M. (1994). Anatomical and electrophysiological evidence for an excitatory amino acid pathway from the thalamic mediodorsal nucleus to the prefrontal cortex in the rat. *The European Journal of Neuroscience 6*, 1225–1234, DOI: 10.1111/j.1460-9568.1994.tb00621.x, PubMed ID: 7524967.

(495) Pivetta, C., Esposito, M. S., Sigrist, M., and Arber, S. (2014). Motor-circuit communication matrix from spinal cord to brainstem neurons revealed by developmental origin. *Cell 156*, 537–548, DOI: 10.1016/j.cell.2013.12.014, PubMed ID: 24485459.

(496) Pizoli, C. E., Jinnah, H. A., Billingsley, M. L., and Hess, E. J. (2002). Abnormal cerebellar signaling induces dystonia in mice. *The Journal of Neuroscience: The Official Journal of the Society for Neuroscience 22*, 7825–7833, DOI: 10.1523/JNEUROSCI.22-17-07825.2002, PubMed ID: 12196606.

(497) Ploghaus, A., Tracey, I., Gati, J. S., Clare, S., Menon, R. S., Matthews, P. M., and Rawlins, J. N. (1999). Dissociating pain from its anticipation in the human brain. *Science (New York, N.Y.) 284*, 1979–1981, DOI: 10.1126/science.284.5422.1979, PubMed ID: 10373114.

(498) Poewe, W., Seppi, K., Tanner, C. M., Halliday, G. M., Brundin, P., Volkmann, J., Schrag, A.-E., and Lang, A. E. (2017). Parkinson disease. *Nature Reviews Disease Primers 3*, Number: 1 Publisher: Nature Publishing Group, 1–21, DOI: 10.1038/nrdp.2017.13.

(499) Pollack, I. F., Polinko, P., Albright, A. L., Towbin, R., and Fitz, C. (1995). Mutism and pseudobulbar symptoms after resection of posterior fossa tumors in children: incidence and pathophysiology. *Neurosurgery 37*, 885–893, DOI: 10.1227/00006123-199511000-00006, PubMed ID: 8559336.

(500) Popa, D., Spolidoro, M., Proville, R. D., Guyon, N., Belliveau, L., and Léna, C. (2013). Functional Role of the Cerebellum in Gamma-Band Synchronization of the Sensory and Motor Cortices. *The Journal of Neuroscience 33*, Number: 15, 6552–6556, DOI: 10.1523/JNEUROSCI.5521-12.2013, PubMed ID: 23575852.

(501) Porrill, J., and Dean, P. (2008). Silent synapses, LTP, and the indirect parallel-fibre pathway: computational consequences of optimal cerebellar noise-processing. *PLoS computational biology 4*, e1000085, DOI: 10.1371/journal.pcbi.1000085, PubMed ID: 18497864.

(502) Porrill, J., Dean, P., and Anderson, S. R. (2013). Adaptive filters and internal models: Multilevel description of cerebellar function. *Neural Networks 47*, 134–149, DOI: 10.1016/j.neunet.2012.12.005.

(503) Porter, R., and Lemon, R. (1995). Corticospinal function and voluntary movement.

(504) Prensa, L., Giménez-Amaya, J. M., and Parent, A. (1999). Chemical heterogeneity of the striosomal compartment in the human striatum. *The Journal of Comparative Neurology 413*, 603–618, PubMed ID: 10495446.

(505) Proville, R. D., Spolidoro, M., Guyon, N., Dugué, G. P., Selimi, F., Isope, P., Popa, D., and Léna, C. (2014). Cerebellum involvement in cortical sensorimotor circuits for the control of voluntary movements. *Nature Neuroscience 17*, Number: 9, 1233–1239, DOI: 10.1038/nn.3773, PubMed ID: 25064850.

(506) Pugh, J. R., and Raman, I. M. (2008). Mechanisms of potentiation of mossy fiber EPSCs in the cerebellar nuclei by coincident synaptic excitation and inhibition. *The Journal of Neuroscience: The Official Journal of the Society for Neuroscience 28*, 10549–10560, DOI: 10.1523/JNEUROSCI.2061-08.2008, PubMed ID: 18923031.

(507) Quartarone, A., and Hallett, M. (2013). Emerging Concepts in the Physiological Basis of Dystonia. *Movement disorders : official journal of the Movement Disorder Society 28*, 958–967, DOI: 10.1002/mds.25532, PubMed ID: 23893452.

(508) Quartarone, A., Morgante, F., Sant'Angelo, A., Rizzo, V., Bagnato, S., Terranova, C., Siebner, H. R., Berardelli, A., and Girlanda, P. (2008). Abnormal plasticity of sensorimotor circuits extends beyond the affected body part in focal dystonia. *Journal of Neurology, Neurosurgery & Psychiatry 79*, Number: 9 Publisher: BMJ Publishing Group Ltd Section: Research paper, 985–990, DOI: 10.1136/jnnp.2007.121632, PubMed ID: 17634214.

(509) Quartarone, A., Bagnato, S., Rizzo, V., Siebner, H. R., Dattola, V., Scalfari, A., Morgante, F., Battaglia, F., Romano, M., and Girlanda, P. (2003). Abnormal associative plasticity of the human motor cortex in writer's cramp. *Brain: A Journal of Neurology 126*, Number: Pt 12, 2586–2596, DOI: 10.1093/brain/awg273, PubMed ID: 14506068.

(510) Quartarone, A., Rizzo, V., Bagnato, S., Morgante, F., Sant'Angelo, A., Romano, M., Crupi, D., Girlanda, P., Rothwell, J. C., and Siebner, H. R. (2005). Homeostatic-like plasticity of the primary motor hand area is impaired in focal hand dystonia. *Brain: A Journal of Neurology 128*, 1943–1950, DOI: 10.1093/brain/awh527, PubMed ID: 15872016.

(511) Quartarone, A., Rizzo, V., Terranova, C., Cacciola, A., Milardi, D., Calamuneri, A., Chillemi, G., and Girlanda, P. (2017). Therapeutic Use of Non-invasive Brain Stimulation in Dystonia. *Frontiers in Neuroscience 11*, https://www.frontiersin.org/articles/10.3389/fnins.2017.00423.

(512) Quartarone, A., Siebner, H. R., and Rothwell, J. C. (2006). Task-specific hand dystonia: can too much plasticity be bad for you? *Trends in Neurosciences 29*, Number: 4, 192–199, DOI: 10.1016/j.tins.2006.02.007.

(513) Quirk, G. J., Garcia, R., and González-Lima, F. (2006). Prefrontal Mechanisms in Extinction of Conditioned Fear. *Biological Psychiatry 60*, 337–343, DOI: 10.1016/j.biopsych.2006.03.010.

(514) Quirk, G. J., Russo, G. K., Barron, J. L., and Lebron, K. (2000). The Role of Ventromedial Prefrontal Cortex in the Recovery of Extinguished Fear. *The Journal of Neuroscience 20*, 6225–6231, DOI: 10.1523/JNEUROSCI.20-16-06225.2000, PubMed ID: 10934272.

(515) Raman, I. M., and Bean, B. P. (1997). Resurgent sodium current and action potential formation in dissociated cerebellar Purkinje neurons. *The Journal of Neuroscience: The Official Journal of the Society for Neuroscience 17*, 4517–4526, DOI: 10.1523/JNEUROSCI.17-12-04517.1997, PubMed ID: 9169512.

(516) Raman, I. M., Gustafson, A. E., and Padgett, D. (2000). Ionic Currents and Spontaneous Firing in Neurons Isolated from the Cerebellar Nuclei. *The Journal of Neuroscience 20*, 9004–9016, DOI: 10.1523/JNEUROSCI.20-24-09004.2000, PubMed ID: 11124976.

(517) Ramanathan, K. R., and Maren, S. (2019). Nucleus reuniens mediates the extinction of contextual fear conditioning. *Behavioural Brain Research 374*, 112114, DOI: 10.1016/j.bbr.2019.112114, PubMed ID: 31351844.

(518) Ramo, S., and Cajal, S. (1911). Histologie du Systeme Nerveux de l'Homme et des Verte
bre
s.

(519) Rasmussen, A., and Hesslow, G. In *Progress in Brain Research*, Ramnani, N., Ed.; Cerebellar Learning, Vol. 210; Elsevier: 2014, pp 103–119, DOI: 10.1016/B978-0-444-63356-9.00005-4.

(520) Reinhold, K., Lien, A. D., and Scanziani, M. (2015). Distinct recurrent versus afferent dynamics in cortical visual processing. *Nature Neuroscience 18*, Number: 12 Publisher: Nature Publishing Group, 1789–1797, DOI: 10.1038/nn.4153.

(521) Rescorla, R. A. (1972). Classical Conditioning II: Current Research and Theory. *(No Title)*, 64, https://cir.nii.ac.jp/crid/1370285712430604164.

(522) Rico, A. J., Barroso-Chinea, P., Conte-Perales, L., Roda, E., Gómez-Bautista, V., Gendive, M., Obeso, J. A., and Lanciego, J. L. (2010). A direct projection from the subthalamic nucleus to the ventral thalamus in monkeys. *Neurobiology of Disease 39*, 381–392, DOI: 10.1016/j.nbd.2010.05.004, PubMed ID: 20452426.

(523) Rieubland, S., Roth, A., and Häusser, M. (2014). Structured connectivity in cerebellar inhibitory networks. *Neuron 81*, 913–929, DOI: 10.1016/j.neuron.2013.12.029, PubMed ID: 24559679.

(524) Rispal-Padel, L., and Meftah, E. M. (1992). Changes in motor responses induced by cerebellar stimulation during classical forelimb flexion conditioning in cat. *Journal of Neurophysiology 68*, 908–926, DOI: 10.1152/jn.1992.68.3.908, PubMed ID: 1432056.

(525) Rizzolatti, G., Fadiga, L., Gallese, V., and Fogassi, L. (1996). Premotor cortex and the recognition of motor actions. *Brain Research. Cognitive Brain Research 3*, 131–141, DOI: 10.1016/0926-6410(95)00038-0, PubMed ID: 8713554.

(526) Rizzolatti, G., Fogassi, L., and Gallese, V. (2002). Motor and cognitive functions of the ventral premotor cortex. *Current Opinion in Neurobiology 12*, 149–154, DOI: 10.1016/s0959-4388(02)00308-2, PubMed ID: 12015230.

(527) Robbins, S. J. (1990). Mechanisms underlying spontaneous recovery in autoshaping. *Journal of Experimental Psychology: Animal Behavior Processes 16*, Place: US Publisher: American Psychological Association, 235–249, DOI: 10.1037/0097-7403.16.3.235.

(528) Rocha, G. S., Freire, M. A. M., Britto, A. M., Paiva, K. M., Oliveira, R. F., Fonseca, I. A. T., Araújo, D. P., Oliveira, L. C., Guzen, F. P., Morais, P. L. A. G., and Cavalcanti, J. R. L. P. (2023). Basal ganglia for beginners: the basic concepts you need to know and their role in movement control. *Frontiers in Systems Neuroscience 17*, https://www.frontiersin.org/articles/10.3389/fnsys.2023.1242929.

(529) Rochefort, C., Lefort, J. M., and Rondi-Reig, L. (2013). The cerebellum: a new key structure in the navigation system. *Frontiers in Neural Circuits 7*, 35, DOI: 10.3389/fncir.2013.00035, PubMed ID: 23493515.

(530) Rodriguez, C. I., and Dymecki, S. M. (2000). Origin of the Precerebellar System. *Neuron 27*, 475–486, DOI: 10.1016/S0896-6273(00)00059-3.

(531) Roitman, A. V., Pasalar, S., Johnson, M. T. V., and Ebner, T. J. (2005). Position, direction of movement, and speed tuning of cerebellar Purkinje cells during circular manual tracking in monkey. *The Journal of Neuroscience: The Official Journal of the Society for Neuroscience 25*, 9244–9257, DOI: 10.1523/JNEUROSCI.1886-05.2005, PubMed ID: 16207884.

(532) Romano, V., De Propris, L., Bosman, L. W., Warnaar, P., Ten Brinke, M. M., Lindeman, S., Ju, C., Velauthapillai, A., Spanke, J. K., Middendorp Guerra, E., Hoogland, T. M., Negrello, M., D'Angelo, E., and De Zeeuw, C. I. (2018). Potentiation of cerebellar Purkinje cells facilitates whisker reflex adaptation through increased simple spike activity. *eLife 7*, e38852, DOI: 10.7554/eLife.38852, PubMed ID: 30561331.

(533) Roš, H., Sachdev, R. N. S., Yu, Y., Šestan, N., and McCormick, D. A. (2009). Neocortical Networks Entrain Neuronal Circuits in Cerebellar Cortex. *The Journal of Neuroscience 29*, 10309–10320, DOI: 10.1523/JNEUROSCI.2327-09.2009, PubMed ID: 19692605.

(534) Rosenblatt, F. (1958). The perceptron: A probabilistic model for information storage and organization in the brain. *Psychological Review 65*, Place: US Publisher: American Psychological Association, 386–408, DOI: 10.1037/h0042519.

(535) Rosin, D. L., Robeva, A., Woodard, R. L., Guyenet, P. G., and Linden, J. (1998). Immunohistochemical localization of adenosine A2A receptors in the rat central nervous system. *The Journal of Comparative Neurology 401*, 163–186, PubMed ID: 9822147.

(536) Roth, B. L. (2016). DREADDs for Neuroscientists. *Neuron 89*, 683–694, DOI: 10.1016/j.neuron.2016.01.040, PubMed ID: 26889809.

(537) Roy, A., Svensson, F. P., Mazeh, A., and Kocsis, B. (2017). Prefrontal-hippocampal coupling by theta rhythm and by 2-5 Hz oscillation in the delta band: The role of the nucleus reuniens of the thalamus. *Brain Structure & Function 222*, 2819–2830, DOI: 10.1007/s00429-017-1374-6, PubMed ID: 28210848.

(538) Royce, G. J., and Mourey, R. J. (1985). Efferent connections of the centromedian and parafascicular thalamic nuclei: an autoradiographic investigation in the cat. *The Journal of Comparative Neurology 235*, 277–300, DOI: 10.1002/cne.902350302, PubMed ID: 3998212.

(539) Rubin, D. B., Hosman, T., Kelemen, J. N., Kapitonava, A., Willett, F. R., Coughlin, B. F., Halgren, E., Kimchi, E. Y., Williams, Z. M., Simeral, J. D., Hochberg, L. R., and Cash, S. S. (2022). Learned Motor Patterns Are Replayed in Human Motor Cortex during Sleep. *The Journal of Neuroscience 42*, 5007–5020, DOI: 10.1523/JNEUROSCI.2074-21.2022, PubMed ID: 35589391.

(540) Ruigrok, T. J. (1997). Cerebellar nuclei: the olivary connection. *Progress in Brain Research 114*, 167–192, DOI: 10.1016/s0079-6123(08)63364-6, PubMed ID: 9193144.

(541) Ruigrok, T. J., de Zeeuw, C. I., van der Burg, J., and Voogd, J. (1990). Intracellular labeling of neurons in the medial accessory olive of the cat: I. Physiology and light microscopy. *The Journal of Comparative Neurology 300*, 462–477, DOI: 10.1002/cne.903000403, PubMed ID: 2273088.

(542) Ruigrok, T. J., and Voogd, J. (2000). Organization of projections from the inferior olive to the cerebellar nuclei in the rat. *The Journal of Comparative Neurology 426*, 209–228, DOI: 10.1002/1096-9861(20001016)426:2<209::aid-cne4>3.0.co;2-0, PubMed ID: 10982464.

(543) Ruigrok, T. J. H. In *Handbook of the Cerebellum and Cerebellar Disorders*, Manto, M., Schmahmann, J. D., Rossi, F., Gruol, D. L., and Koibuchi, N., Eds.; Springer Netherlands: Dordrecht, 2013, pp 497–528, DOI: 10.1007/978-94-007-1333-8_23.

(544) Ruigrok, T. J. H. In *Essentials of Cerebellum and Cerebellar Disorders: A Primer For Graduate Students*, Gruol, D. L., Koibuchi, N., Manto, M., Molinari, M., Schmahmann, J. D., and Shen, Y., Eds.; Springer International Publishing: Cham, 2016, pp 79–88, DOI: 10.1007/978-3-319-24551-5_9.

(545) Rumbach, L., Barth, P., Costaz, A., and Mas, J. (1995). Hemidystonia consequent upon ipsilateral vertebral artery occlusion and cerebellar infarction. *Movement Disorders: Official Journal of the Movement Disorder Society 10*, 522–525, DOI: 10.1002/mds.870100424, PubMed ID: 7565841.

(546) Rustay, N. R., Wahlsten, D., and Crabbe, J. C. (2003). Influence of task parameters on rotarod performance and sensitivity to ethanol in mice. *Behavioural Brain Research 141*, 237–249, DOI: 10.1016/s0166-4328(02)00376-5, PubMed ID: 12742261.

(547) Sacchetti, B., Baldi, E., Lorenzini, C. A., and Bucherelli, C. (2002). Cerebellar role in fear-conditioning consolidation. *Proceedings of the National Academy of Sciences of the United States of America 99*, Number: 12, 8406–8411, DOI: 10.1073/pnas.112660399, PubMed ID: 12034877.

(548) Sacchetti, B., Scelfo, B., Tempia, F., and Strata, P. (2004). Long-term synaptic changes induced in the cerebellar cortex by fear conditioning. *Neuron 42*, 973–982, DOI: 10.1016/j.neuron.2004.05.012, PubMed ID: 15207241.

(549) Sadikot, A. F., Parent, A., and François, C. (1992). Efferent connections of the centromedian and parafascicular thalamic nuclei in the squirrel monkey: a PHA-L study of subcortical projections. *The Journal of Comparative Neurology 315*, 137–159, DOI: 10.1002/cne.903150203, PubMed ID: 1372010.

(550) Sakai, S. T. Cerebellar Thalamic and Thalamocortical Projections — SpringerLink, 2013, https://link.springer.com/referenceworkentry/10.1007/978-94-007-1333-8_24.

(551) Sakayori, N., Kato, S., Sugawara, M., Setogawa, S., Fukushima, H., Ishikawa, R., Kida, S., and Kobayashi, K. (2019). Motor skills mediated through cerebellothalamic tracts projecting to the central lateral nucleus. *Molecular Brain 12*, 13, DOI: 10.1186/s13041-019-0431-x, PubMed ID: 30736823.

(552) Sakrison, D. (1963). Iterative design of optimum filters for non mean-square-error performance criteria. *IEEE Transactions on Information Theory 9*, Conference Name: IEEE Transactions on Information Theory, 161–167, DOI: 10.1109/TIT.1963.1057846.

(553) Salazar Leon, L. E., and Sillitoe, R. V. (2022). Potential interactions between cerebellar dysfunction and sleep disturbances in dystonia. *Dystonia 1*, 10691, DOI: 10.3389/dyst.2022.10691, PubMed ID: 37065094.

(554) Samaei, A., Ehsani, F., Zoghi, M., Hafez Yosephi, M., and Jaberzadeh, S. (2017). Online and offline effects of cerebellar transcranial direct current stimulation on motor learning in healthy older adults: a randomized double-blind sham-controlled study. *The European Journal of Neuroscience 45*, 1177–1185, DOI: 10.1111/ejn.13559, PubMed ID: 28278354.

(555) Sangrey, T., and Jaeger, D. (2010). Analysis of distinct short and prolonged components in rebound spiking of deep cerebellar nucleus neurons. *The European Journal of Neuroscience 32*, 1646–1657, DOI: 10.1111/j.1460-9568.2010.07408.x, PubMed ID: 21039958.

(556) Santini, E., Ge, H., Ren, K., de Ortiz, S. P., and Quirk, G. J. (2004). Consolidation of Fear Extinction Requires Protein Synthesis in the Medial Prefrontal Cortex. *The Journal of Neuroscience 24*, 5704–5710, DOI: 10.1523/JNEUROSCI.0786-04.2004, PubMed ID: 15215292.

(557) Sathyamurthy, A., Barik, A., Dobrott, C. I., Matson, K. J. E., Stoica, S., Pursley, R., Chesler, A. T., and Levine, A. J. (2020). Cerebellospinal Neurons Regulate Motor Performance and Motor Learning. *Cell Reports 31*, Number: 6, 107595, DOI: 10.1016/j.celrep.2020.107595, PubMed ID: 32402292.

(558) Sauerbrei, B. A., Guo, J.-Z., Cohen, J. D., Mischiati, M., Guo, W., Kabra, M., Verma, N., Mensh, B., Branson, K., and Hantman, A. W. (2020). Cortical pattern generation during dexterous movement is input-driven. *Nature 577*, Number: 7790, 386–391, DOI: 10.1038/s41586-019-1869-9, PubMed ID: 31875851.

(559) Saunders-Pullman, R., Fuchs, T., San Luciano, M., Raymond, D., Brashear, A., Ortega, R., Deik, A., Ozelius, L. J., and Bressman, S. B. (2014). Heterogeneity in primary dystonia: lessons from THAP1, GNAL, and TOR1A in Amish-Mennonites. *Movement Disorders: Official Journal of the Movement Disorder Society 29*, 812–818, DOI: 10.1002/mds.25818, PubMed ID: 24500857.

(560) Sawyer, S. F., Young, S. J., Groves, P. M., and Tepper, J. M. (1994). Cerebellar-responsive neurons in the thalamic ventroanterior-ventrolateral complex of rats: in vivo electrophysiology. *Neuroscience 63*, 711–724, DOI: 10.1016/0306-4522(94)90517-7, PubMed ID: 7898672.

(561) Scherer, M., Steiner, L. A., Kalia, S. K., Hodaie, M., Kühn, A. A., Lozano, A. M., Hutchison, W. D., and Milosevic, L. (2022). Single-neuron bursts encode pathological oscillations in subcortical nuclei of patients with Parkinson's disease and essential tremor. *Proceedings of the National Academy of Sciences of the United States of America 119*, e2205881119, DOI: 10.1073/pnas.2205881119, PubMed ID: 36018837.

(562) Schilling, K., Oberdick, J., Rossi, F., and Baader, S. L. (2008). Besides Purkinje cells and granule neurons: an appraisal of the cell biology of the interneurons of the cerebellar cortex. *Histochemistry and Cell Biology 130*, 601–615, DOI: 10.1007/s00418-008-0483-y, PubMed ID: 18677503.

(563) Schmahmann, J. D., and Sherman, J. C. (1998). The cerebellar cognitive affective syndrome. *Brain: A Journal of Neurology 121 (Pt 4)*, 561–579, DOI: 10.1093/brain/121.4.561, PubMed ID: 9577385.

(564) Schmolesky, M. T., Wang, Y., Hanes, D. P., Thompson, K. G., Leutgeb, S., Schall, J. D., and Leventhal, A. G. (1998). Signal timing across the macaque visual system. *Journal of Neurophysiology 79*, 3272–3278, DOI: 10.1152/jn.1998.79.6.3272, PubMed ID: 9636126.

(565) Schreurs, B. G., Gusev, P. A., Tomsic, D., Alkon, D. L., and Shi, T. (1998). Intracellular correlates of acquisition and long-term memory of classical conditioning in Purkinje cell dendrites in slices of rabbit cerebellar lobule HVI. *The Journal of Neuroscience: The Official Journal of the Society for Neuroscience 18*, 5498–5507, DOI: 10.1523/JNEUROSCI.18-14-05498.1998, PubMed ID: 9651230.

(566) Schultz, W. (1997). Dopamine neurons and their role in reward mechanisms. *Current Opinion in Neurobiology 7*, 191–197, DOI: 10.1016/s0959-4388(97)80007-4, PubMed ID: 9142754.

(567) Schultz, W. (1998). Predictive reward signal of dopamine neurons. *Journal of Neurophysiology 80*, 1–27, DOI: 10.1152/jn.1998.80.1.1, PubMed ID: 9658025.

(568) Schultz, W., Apicella, P., and Ljungberg, T. (1993). Responses of monkey dopamine neurons to reward and conditioned stimuli during successive steps of learning a delayed response task. *The Journal of Neuroscience: The Official Journal of the Society for Neuroscience 13*, 900–913, DOI: 10.1523/JNEUROSCI.13-03-00900.1993, PubMed ID: 8441015.

(569) Seidler, R. D. (2010). Neural correlates of motor learning, transfer of learning, and learning to learn. *Exercise and Sport Sciences Reviews 38*, 3–9, DOI: 10.1097/JES.0b013e3181c5cce7, PubMed ID: 20016293.

(570) Sekerková, G., Kim, J.-A., Nigro, M. J., Becker, E. B. E., Hartmann, J., Birnbaumer, L., Mugnaini, E., and Martina, M. (2013). Early onset of ataxia in moonwalker mice is accompanied by complete ablation of type II unipolar brush cells and Purkinje cell dysfunction. *The Journal of Neuroscience: The Official Journal of the Society for Neuroscience 33*, 19689–19694, DOI: 10.1523/JNEUROSCI.2294-13.2013, PubMed ID: 24336732.

(571) Senn, V., Wolff, S. B. E., Herry, C., Grenier, F., Ehrlich, I., Gründemann, J., Fadok, J. P., Müller, C., Letzkus, J. J., and Lüthi, A. (2014). Long-range connectivity defines behavioral specificity of amygdala neurons. *Neuron 81*, 428–437, DOI: 10.1016/j.neuron.2013.11.006, PubMed ID: 24462103.

(572) Shadmehr, R., and Mussa-Ivaldi, F. (1994). Adaptive representation of dynamics during learning of a motor task. *The Journal of Neuroscience 14*, 3208–3224, DOI: 10.1523/JNEUROSCI.14-05-03208.1994, PubMed ID: 8182467.

(573) Shadmehr, R., and Holcomb, H. H. (1997). Neural correlates of motor memory consolidation. *Science (New York, N.Y.) 277*, 821–825, DOI: 10.1126/science.277.5327.821, PubMed ID: 9242612.

(574) Shah, A., Jhawar, S. S., and Goel, A. (2012). Analysis of the anatomy of the Papez circuit and adjoining limbic system by fiber dissection techniques. *Journal of Clinical Neuroscience: Official Journal of the Neurosurgical Society of Australasia 19*, 289–298, DOI: 10.1016/j.jocn.2011.04.039, PubMed ID: 22209397.

(575) Sharott, A., Vinciati, F., Nakamura, K. C., and Magill, P. J. (2017). A Population of Indirect Pathway Striatal Projection Neurons Is Selectively Entrained to Parkinsonian Beta Oscillations. *The Journal of Neuroscience: The Official Journal of the Society for Neuroscience 37*, 9977–9998, DOI: 10.1523/JNEUROSCI.0658-17.2017, PubMed ID: 28847810.

(576) Shashidharan, P., Sandu, D., Potla, U., Armata, I. A., Walker, R. H., McNaught, K. S., Weisz, D., Sreenath, T., Brin, M. F., and Olanow, C. W. (2005). Transgenic mouse model of early-onset DYT1 dystonia. *Human Molecular Genetics 14*, 125–133, DOI: 10.1093/hmg/ddi012, PubMed ID: 15548549.

(577) Sheehy, M. P., and Marsden, C. D. (1982). Writers' cramp-a focal dystonia. *Brain: A Journal of Neurology 105 (Pt 3)*, 461–480, DOI: 10.1093/brain/105.3.461, PubMed ID: 7104663.

(578) Shim, H. G., Jang, D. C., Lee, J., Chung, G., Lee, S., Kim, Y. G., Jeon, D. E., and Kim, S. J. (2017). Long-Term Depression of Intrinsic Excitability Accompanied by Synaptic Depression in Cerebellar Purkinje Cells. *The Journal of Neuroscience: The Official Journal of the Society for Neuroscience 37*, 5659–5669, DOI: 10.1523/JNEUROSCI.3464-16.2017, PubMed ID: 28495974.

(579) Shim, H. G., Lee, Y.-S., and Kim, S. J. (2018). The Emerging Concept of Intrinsic Plasticity: Activity-dependent Modulation of Intrinsic Excitability in Cerebellar Purkinje Cells and Motor Learning. *Experimental Neurobiology 27*, 139–154, DOI: 10.5607/en.2018.27.3.139, PubMed ID: 30022866.

(580) Shima, K., and Tanji, J. (2000). Neuronal activity in the supplementary and presupplementary motor areas for temporal organization of multiple movements. *Journal of Neurophysiology 84*, 2148–2160, DOI: 10.1152/jn.2000.84.4.2148, PubMed ID: 11024102.

(581) Shink, E., Bevan, M. D., Bolam, J. P., and Smith, Y. (1996). The subthalamic nucleus and the external pallidum: two tightly interconnected structures that control the output of the basal ganglia in the monkey. *Neuroscience 73*, 335–357, DOI: 10.1016/0306-4522(96)00022-x, PubMed ID: 8783253.

(582) Sierra-Mercado, D., Padilla-Coreano, N., and Quirk, G. J. (2011). Dissociable Roles of Prelimbic and Infralimbic Cortices, Ventral Hippocampus, and Basolateral Amygdala in the Expression and Extinction of Conditioned Fear. *Neuropsychopharmacology 36*, Number: 2 Publisher: Nature Publishing Group, 529–538, DOI: 10.1038/npp.2010.184.

(583) Signoret-Genest, J., Schukraft, N., L. Reis, S., Segebarth, D., Deisseroth, K., and Tovote, P. (2023). Integrated cardio-behavioral responses to threat define defensive states. *Nature Neuroscience 26*, Number: 3 Publisher: Nature Publishing Group, 447–457, DOI: 10.1038/s41593-022-01252-w.

(584) Sillitoe, R. V., Fu, Y., and Watson, C. In *The Mouse Nervous System*; Elsevier: 2012, pp 360–397, DOI: 10.1016/B978-0-12-369497-3.10011-1.

(585) Sillitoe, R. V., and Joyner, A. L. (2007). Morphology, Molecular Codes, and Circuitry Produce the Three-Dimensional Complexity of the Cerebellum. *Annual Review of Cell and Developmental Biology 23*, _eprint: https://doi.org/10.1146/annurev.cellbio.23.090506.123237, 549–577, DOI: 10.1146/annurev.cellbio.23.090506.123237, PubMed ID: 17506688.

(586) Silva, B. A., Astori, S., Burns, A. M., Heiser, H., van den Heuvel, L., Santoni, G., Martinez-Reza, M. F., Sandi, C., and Gräff, J. (2021). A thalamo-amygdalar circuit underlying the extinction of remote fear memories. *Nature Neuroscience 24*, 964–974, DOI: 10.1038/s41593-021-00856-y, PubMed ID: 34017129.

(587) Silveri, M. C., Leggio, M. G., and Molinari, M. (1994). The cerebellum contributes to linguistic production: a case of agrammatic speech following a right cerebellar lesion. *Neurology 44*, 2047–2050, DOI: 10.1212/wnl.44.11.2047, PubMed ID: 7969957.

(588) Skaggs, W. E., and McNaughton, B. L. (1996). Replay of neuronal firing sequences in rat hippocampus during sleep following spatial experience. *Science (New York, N.Y.) 271*, 1870–1873, DOI: 10.1126/science.271.5257.1870, PubMed ID: 8596957.

(589) Soares, J., Kliem, M. A., Betarbet, R., Greenamyre, J. T., Yamamoto, B., and Wichmann, T. (2004). Role of external pallidal segment in primate parkinsonism: comparison of the effects of 1-methyl-4-phenyl-1,2,3,6-tetrahydropyridine-induced parkinsonism and lesions of the external pallidal segment. *The Journal of Neuroscience: The Official Journal of the Society for Neuroscience 24*, 6417–6426, DOI: 10.1523/JNEUROSCI.0836-04.2004, PubMed ID: 15269251.

(590) Somogyi, P., and Hámori, J. (1976). A quantitative electron microscopic study of the Purkinje cell axon initial segment. *Neuroscience 1*, 361–365, DOI: 10.1016/0306-4522(76)90127-5, PubMed ID: 1004711.

(591) Soteropoulos, D. S., and Baker, S. N. (2008). Bilateral representation in the deep cerebellar nuclei. *The Journal of Physiology 586*, 1117–1136, DOI: 10.1113/jphysiol.2007.144220, PubMed ID: 18187463.

(592) Sotres-Bayon, F., Bush, D. E. A., and LeDoux, J. E. (2007). Acquisition of fear extinction requires activation of NR2B-containing NMDA receptors in the lateral amygdala. *Neuropsychopharmacology: Official Publication of the American College of Neuropsychopharmacology 32*, 1929–1940, DOI: 10.1038/sj.npp.1301316, PubMed ID: 17213844.

(593) Sotres-Bayon, F., and Quirk, G. J. (2010). Prefrontal control of fear: more than just extinction. *Current Opinion in Neurobiology 20*, 231–235, DOI: 10.1016/j.conb.2010.02.005, PubMed ID: 20303254.

(594) Spaeth, L., Bahuguna, J., Gagneux, T., Dorgans, K., Sugihara, I., Poulain, B., Battaglia, D., and Isope, P. (2022). Cerebellar connectivity maps embody individual adaptive behavior in mice. *Nature Communications 13*, 580, DOI: 10.1038/s41467-022-27984-8, PubMed ID: 35102165.

(595) Spaeth, L., and Isope, P. (2023). What Can We Learn from Synaptic Connectivity Maps about Cerebellar Internal Models? *Cerebellum (London, England) 22*, 468–474, DOI: 10.1007/s12311-022-01392-6, PubMed ID: 35391650.

(596) Spampinato, D., and Celnik, P. (2017). Temporal dynamics of cerebellar and motor cortex physiological processes during motor skill learning. *Scientific Reports 7*, Number: 1 Publisher: Nature Publishing Group, 40715, DOI: 10.1038/srep40715.

(597) Stefan, K., Wycislo, M., Gentner, R., Schramm, A., Naumann, M., Reiners, K., and Classen, J. (2006). Temporary occlusion of associative motor cortical plasticity by prior dynamic motor training. *Cerebral Cortex (New York, N.Y.: 1991) 16*, 376–385, DOI: 10.1093/cercor/bhi116, PubMed ID: 15930370.

(598) Steriade, M. (2000). Corticothalamic resonance, states of vigilance and mentation. *Neuroscience 101*, 243–276, DOI: 10.1016/S0306-4522(00)00353-5.

(599) Steriade, M. (2006). Grouping of brain rhythms in corticothalamic systems. *Neuroscience 137*, 1087–1106, DOI: 10.1016/j.neuroscience.2005.10.029.

(600) Straub, C., Hunt, D. L., Yamasaki, M., Kim, K. S., Watanabe, M., Castillo, P. E., and Tomita, S. (2011). Unique functions of kainate receptors in the brain are determined by the auxiliary subunit Neto1. *Nature neuroscience 14*, 866–873, DOI: 10.1038/nn.2837, PubMed ID: 21623363.

(601) Streng, M. L., Tetzlaff, M. R., and Krook-Magnuson, E. (2021). Distinct Fastigial Output Channels and Their Impact on Temporal Lobe Seizures. *The Journal of Neuroscience 41*, 10091–10107, DOI: 10.1523/JNEUROSCI.0683-21.2021, PubMed ID: 34716233.

(602) Strick, P. L., Dum, R. P., and Fiez, J. A. (2009). Cerebellum and nonmotor function. *Annual Review of Neuroscience 32*, 413–434, DOI: 10.1146/annurev.neuro.31.060407.125606, PubMed ID: 19555291.

(603) Sugihara, I., Wu, H., and Shinoda, Y. (1999). Morphology of single olivocerebellar axons labeled with biotinylated dextran amine in the rat. *The Journal of Comparative Neurology 414*, 131–148, PubMed ID: 10516588.

(604) Sugihara, I., Wu, H.-S., and Shinoda, Y. (2001). The Entire Trajectories of Single Olivocerebellar Axons in the Cerebellar Cortex and their Contribution to Cerebellar Compartmentalization. *The Journal of Neuroscience 21*, 7715–7723, DOI: 10.1523/JNEUROSCI.21-19-07715.2001, PubMed ID: 11567061.

(605) Sugihara, I., and Shinoda, Y. (2007). Molecular, topographic, and functional organization of the cerebellar nuclei: analysis by three-dimensional mapping of the olivonuclear projection and aldolase C labeling. *The Journal of Neuroscience: The Official Journal of the Society for Neuroscience 27*, 9696–9710, DOI: 10.1523/JNEUROSCI.1579-07.2007, PubMed ID: 17804630.

(606) Sugimoto, T., and Hattori, T. (1983). Confirmation of thalamosubthalamic projections by electron microscopic autoradiography. *Brain Research 267*, 335–339, DOI: 10.1016/0006-8993(83)90885-5, PubMed ID: 6871679.

(607) Sullivan, R., Yau, W. Y., O'Connor, E., and Houlden, H. (2019). Spinocerebellar ataxia: an update. *Journal of Neurology 266*, 533–544, DOI: 10.1007/s00415-018-9076-4, PubMed ID: 30284037.

(608) Sultan, F., and Bower, J. M. (1998). Quantitative Golgi study of the rat cerebellar molecular layer interneurons using principal component analysis. *The Journal of Comparative Neurology 393*, 353–373, PubMed ID: 9548555.

(609) Yu-Taeger, L., Ott, T., Bonsi, P., Tomczak, C., Wassouf, Z., Martella, G., Sciamanna, G., Imbriani, P., Ponterio, G., Tassone, A., Schulze-Hentrich, J. M., Goodchild, R., Riess, O., Pisani, A., Grundmann-Hauser, K., and Nguyen, H. P. (2020). Impaired dopamine- and adenosine-mediated signaling and plasticity in a novel rodent model for DYT25 dystonia. *Neurobiology of Disease 134*, 104634, DOI: 10.1016/j.nbd.2019.104634.

(610) Tai, C.-H., and Tseng, S.-H. (2022). Cerebellar deep brain stimulation for movement disorders. *Neurobiology of Disease 175*, 105899, DOI: 10.1016/j.nbd.2022.105899, PubMed ID: 36265768.

(611) Takata, N. (2020). Thalamic reticular nucleus in the thalamocortical loop. *Neuroscience Research 156*, 32–40, DOI: 10.1016/j.neures.2019.12.004, PubMed ID: 31812650.

(612) Tal, I., Neymotin, S., Bickel, S., Lakatos, P., and Schroeder, C. E. (2020). Oscillatory Bursting as a Mechanism for Temporal Coupling and Information Coding. *Frontiers in Computational Neuroscience 14*, https://www.frontiersin.org/articles/10.3389/fncom.2020.00082.

(613) Tanaka, H., Ishikawa, T., and Kakei, S. (2019). Neural Evidence of the Cerebellum as a State Predictor. *Cerebellum (London, England) 18*, Number: 3, 349–371, DOI: 10.1007/s12311-018-0996-4, PubMed ID: 30627965.

(614) Tanji, J., and Shima, K. (1994). Role for supplementary motor area cells in planning several movements ahead. *Nature 371*, 413–416, DOI: 10.1038/371413a0, PubMed ID: 8090219.

(615) Tao, Y., Cai, C.-Y., Xian, J.-Y., Kou, X.-L., Lin, Y.-H., Qin, C., Wu, H.-Y., Chang, L., Luo, C.-X., and Zhu, D.-Y. (2020). Projections from Infralimbic Cortex to Paraventricular Thalamus Mediate Fear Extinction Retrieval. *Neuroscience Bulletin 37*, 229–241, DOI: 10.1007/s12264-020-00603-6, PubMed ID: 33180308.

(616) Tao, Y., Cai, C.-Y., Xian, J.-Y., Kou, X.-L., Lin, Y.-H., Qin, C., Wu, H.-Y., Chang, L., Luo, C.-X., and Zhu, D.-Y. (2021). Projections from Infralimbic Cortex to Paraventricular Thalamus Mediate Fear Extinction Retrieval. *Neuroscience Bulletin 37*, 229–241, DOI: 10.1007/s12264-020-00603-6, PubMed ID: 33180308.

(617) ten Brinke, M. M., Heiney, S. A., Wang, X., Proietti-Onori, M., Boele, H.-J., Bakermans, J., Medina, J. F., Gao, Z., and De Zeeuw, C. I. (2017). Dynamic modulation of activity in cerebellar nuclei neurons during pavlovian eyeblink conditioning in mice. *eLife 6*, ed. by Uchida, N., Publisher: eLife Sciences Publications, Ltd, e28132, DOI: 10.7554/eLife.28132.

(618) Teune, T. M., van der Burg, J., van der Moer, J., Voogd, J., and Ruigrok, T. J. (2000). Topography of cerebellar nuclear projections to the brain stem in the rat. *Progress in Brain Research 124*, 141–172, DOI: 10.1016/S0079-6123(00)24014-4, PubMed ID: 10943123.

(619) Timofeev, I., Bazhenov, M., Sejnowski, T. J., and Steriade, M. (2001). Contribution of intrinsic and synaptic factors in the desynchronization of thalamic oscillatory activity. *Thalamus & Related Systems 1*, 53–69, DOI: 10.1016/S1472-9288(01)00004-8.

(620) Timofeev, I., and Chauvette, S. (2013). The Spindles: Are They Still Thalamic? *Sleep 36*, 825–826, DOI: 10.5665/sleep.2702, PubMed ID: 23729924.

(621) Tinazzi, M., Farina, S., Bhatia, K., Fiaschi, A., Moretto, G., Bertolasi, L., Zarattini, S., and Smania, N. (2005). TENS for the treatment of writer's cramp dystonia: a randomized, placebo-controlled study. *Neurology 64*, 1946–1948, DOI: 10.1212/01.WNL.0000163851.70927.7E, PubMed ID: 15955950.

(622) Tolbert, D. L., Bantli, H., Hames, E. G., Ebner, T. J., McMullen, T. A., and Bloedel, J. R. (1980). A demonstration of the dentato-reticulospinal projection in the cat. *Neuroscience 5*, 1479–1488, DOI: 10.1016/0306-4522(80)90010-x, PubMed ID: 7402481.

(623) Tovote, P., Fadok, J. P., and Lüthi, A. (2015). Neuronal circuits for fear and anxiety. *Nature Reviews Neuroscience 16*, 317–331, DOI: 10.1038/nrn3945.

(624) Tozzi, A., de Iure, A., Di Filippo, M., Tantucci, M., Costa, C., Borsini, F., Ghiglieri, V., Giampà, C., Fusco, F. R., Picconi, B., and Calabresi, P. (2011). The distinct role of medium spiny neurons and cholinergic interneurons in the D/AA receptor interaction in the striatum: implications for Parkinson's disease. *The Journal of Neuroscience: The Official Journal of the Society for Neuroscience 31*, 1850–1862, DOI: 10.1523/JNEUROSCI.4082-10.2011, PubMed ID: 21289195.

(625) Travers, J. B., DiNardo, L. A., and Karimnamazi, H. (2000). Medullary reticular formation activity during ingestion and rejection in the awake rat. *Experimental Brain Research 130*, 78–92, DOI: 10.1007/s002219900223, PubMed ID: 10638444.

(626) Travis, A. M. (1955). Neurological deficiencies after ablation of the precentral motor area in Macaca mulatta. *Brain: A Journal of Neurology 78*, 155–173, DOI: 10.1093/brain/78.2.155, PubMed ID: 13239906.

(627) Tzvi, E., Loens, S., and Donchin, O. (2022). Mini-review: The Role of the Cerebellum in Visuomotor Adaptation. *Cerebellum (London, England) 21*, 306–313, DOI: 10.1007/s12311-021-01281-4, PubMed ID: 34080132.

(628) Ugolini, G. (2010). Advances in viral transneuronal tracing. *Journal of Neuroscience Methods 194*, 2–20, DOI: 10.1016/j.jneumeth.2009.12.001, PubMed ID: 20004688.

(629) Uluğ, A. M., Vo, A., Argyelan, M., Tanabe, L., Schiffer, W. K., Dewey, S., Dauer, W. T., and Eidelberg, D. (2011). Cerebellothalamocortical pathway abnormalities in torsinA DYT1 knock-in mice. *Proceedings of the National Academy of Sciences 108*, Number: 16 Publisher: National Academy of Sciences Section: Biological Sciences, 6638–6643, DOI: 10.1073/pnas.1016445108, PubMed ID: 21464304.

(630) Uno, M., Yoshida, M., and Hirota, I. (1970). The mode of cerebello-thalamic relay transmission investigated with intracellular recording from cells of the ventrolateral nucleus of cat's thalamus. *Experimental Brain Research 10*, 121–139, DOI: 10.1007/BF00234726.

(631) Urrutia Desmaison, J. D., Sala, R. W., Ayyaz, A., Nondhalee, P., Popa, D., and Léna, C. (2023). Cerebellar control of fear learning via the cerebellar nuclei-Multiple pathways, multiple mechanisms? *Frontiers in Systems Neuroscience 17*, 1176668, DOI: 10.3389/fnsys.2023.1176668, PubMed ID: 37229350.

(632) Usmani, N., Bedi, G. S., Sengun, C., Pandey, A., and Singer, C. (2011). Late onset of cervical dystonia in a 39-year-old patient following cerebellar hemorrhage. *Journal of Neurology 258*, 149–151, DOI: 10.1007/s00415-010-5685-2, PubMed ID: 20714744.

(633) Utz, A., Thürling, M., Ernst, T. M., Hermann, A., Stark, R., Wolf, O. T., Timmann, D., and Merz, C. J. (2015). Cerebellar vermis contributes to the extinction of conditioned fear. *Neuroscience Letters 604*, 173–177, DOI: 10.1016/j.neulet.2015.07.026, PubMed ID: 26219987.

(634) Uusisaari, M., and Knöpfel, T. (2010). GlyT2+ Neurons in the Lateral Cerebellar Nucleus. *The Cerebellum 9*, 42–55, DOI: 10.1007/s12311-009-0137-1.

(635) Uusisaari, M., Obata, K., and Knöpfel, T. (2007). Morphological and electrophysiological properties of GABAergic and non-GABAergic cells in the deep cerebellar nuclei. *Journal of Neurophysiology 97*, 901–911, DOI: 10.1152/jn.00974.2006, PubMed ID: 17093116.

(636) Uusisaari, M. Y., and Knöpfel, T. (2012). Diversity of neuronal elements and circuitry in the cerebellar nuclei. *Cerebellum (London, England) 11*, 420–421, DOI: 10.1007/s12311-011-0350-6, PubMed ID: 22278661.

(637) Valera, A. M., Binda, F., Pawlowski, S. A., Dupont, J.-L., Casella, J.-F., Rothstein, J. D., Poulain, B., and Isope, P. (2016). Stereotyped spatial patterns of functional synaptic connectivity in the cerebellar cortex. *eLife 5*, e09862, DOI: 10.7554/eLife.09862, PubMed ID: 26982219.

(638) Van Der Kooy, D., and Hattori, T. (1980). Single subthalamic nucleus neurons project to both the globus pallidus and substantia nigra in rat. *The Journal of Comparative Neurology 192*, 751–768, DOI: 10.1002/cne.901920409, PubMed ID: 7419753.

(639) Van der Want, J. J., Wiklund, L., Guegan, M., Ruigrok, T., and Voogd, J. (1989). Anterograde tracing of the rat olivocerebellar system with Phaseolus vulgaris leucoagglutinin (PHA-L). Demonstration of climbing fiber collateral innervation of the cerebellar nuclei. *The Journal of Comparative Neurology 288*, 1–18, DOI: 10.1002/cne.902880102, PubMed ID: 2794133.

(640) van der Heijden, M. E., Kizek, D. J., Perez, R., Ruff, E. K., Ehrlich, M. E., and Sillitoe, R. V. (2021). Abnormal cerebellar function and tremor in a mouse model for non-manifesting partially penetrant dystonia type 6. *The Journal of Physiology 599*, Number: 7, 2037–2054, DOI: 10.1113/JP280978, PubMed ID: 33369735.

(641) van der Want, J. J., and Voogd, J. (1987). Ultrastructural identification and localization of climbing fiber terminals in the fastigial nucleus of the cat. *The Journal of Comparative Neurology 258*, 81–90, DOI: 10.1002/cne.902580106, PubMed ID: 3571538.

(642) VanElzakker, M. B., Dahlgren, M. K., Davis, F. C., Dubois, S., and Shin, L. M. (2014). From Pavlov to PTSD: the extinction of conditioned fear in rodents, humans, and anxiety disorders. *Neurobiology of Learning and Memory 113*, 3–18, DOI: 10.1016/j.nlm.2013.11.014, PubMed ID: 24321650.

(643) Varani, A. P., Sala, R. W., Mailhes-Hamon, C., Frontera, J. L., Léna, C., and Popa, D. Dual contributions of cerebellar-thalamic networks to learning and offline consolidation of a complex motor task, en, Pages: 2020.08.27.270330 Section: New Results, 2020, DOI: 10.1101/2020.08.27.270330.

(644) Vemula, S. R., Puschmann, A., Xiao, J., Zhao, Y., Rudzińska, M., Frei, K. P., Truong, D. D., Wszolek, Z. K., and LeDoux, M. S. (2013). Role of G(olf) in familial and sporadic adult-onset primary dystonia. *Human Molecular Genetics 22*, Number: 12, 2510–2519, DOI: 10.1093/hmg/ddt102, PubMed ID: 23449625.

(645) Vertes, R. P. (2004). Differential projections of the infralimbic and prelimbic cortex in the rat. *Synapse (New York, N.Y.) 51*, 32–58, DOI: 10.1002/syn.10279, PubMed ID: 14579424.

(646) Vidal-Gonzalez, I., Vidal-Gonzalez, B., Rauch, S. L., and Quirk, G. J. (2006). Microstimulation reveals opposing influences of prelimbic and infralimbic cortex on the expression of conditioned fear. *Learning & Memory 13*, Number: 6, 728–733, DOI: 10.1101/lm.306106, PubMed ID: 17142302.

(647) Vidoni, E. D., Thomas, G. P., Honea, R. A., Loskutova, N., and Burns, J. M. (2012). Evidence of Altered Corticomotor System Connectivity in Early-Stage Alzheimer's Disease. *Journal of Neurologic Physical Therapy 36*, 8–16, DOI: 10.1097/NPT.0b013e3182462ea6, PubMed ID: 22333920.

(648) Voogd, J. (1967). Comparative aspects of the structure and fibre connexions of the mammalian cerebellum. *Progress in Brain Research 25*, 94–134, DOI: 10.1016/S0079-6123(08)60963-2, PubMed ID: 4866558.

(649) Voogd, J., and Ruigrok, T. J. H. In *The Human Nervous System (Third Edition)*, Mai, J. K., and Paxinos, G., Eds.; Academic Press: San Diego, 2012, pp 471–545, DOI: 10.1016/B978-0-12-374236-0.10015-X.

(650) Wagner, M. J., Kim, T. H., Savall, J., Schnitzer, M. J., and Luo, L. (2017). Cerebellar granule cells encode the expectation of reward. *Nature 544*, 96–100, DOI: 10.1038/nature21726, PubMed ID: 28321129.

(651) Walker, M. P. (2008). Sleep-dependent memory processing. *Harvard Review of Psychiatry 16*, 287–298, DOI: 10.1080/10673220802432517, PubMed ID: 18803104.

(652) Walker, M. P., Brakefield, T., Hobson, J. A., and Stickgold, R. (2003). Dissociable stages of human memory consolidation and reconsolidation. *Nature 425*, 616–620, DOI: 10.1038/nature01930, PubMed ID: 14534587.

(653) Walker, M. P., Brakefield, T., Morgan, A., Hobson, J. A., and Stickgold, R. (2002). Practice with sleep makes perfect: sleep-dependent motor skill learning. *Neuron 35*, 205–211, DOI: 10.1016/s0896-6273(02)00746-8, PubMed ID: 12123620.

(654) Walker, M. P., and Stickgold, R. (2006). Sleep, memory, and plasticity. *Annual Review of Psychology 57*, 139–166, DOI: 10.1146/annurev.psych.56.091103.070307, PubMed ID: 16318592.

(655) Wallesch, C. W., and Horn, A. (1990). Long-term effects of cerebellar pathology on cognitive functions. *Brain and Cognition 14*, 19–25, DOI: 10.1016/0278-2626(90)90057-u, PubMed ID: 2223042.

(656) Waln, O., and LeDoux, M. S. (2010). Delayed-onset oromandibular dystonia after a cerebellar hemorrhagic stroke. *Parkinsonism & Related Disorders 16*, 623–625, DOI: 10.1016/j.parkreldis.2010.07.010, PubMed ID: 20692865.

(657) Wang, C., Stratton, P. G., Sah, P., and Marek, R. (2022). Theta coupling within the medial prefrontal cortex regulates fear extinction and renewal. *iScience 25*, 105036, DOI: 10.1016/j.isci.2022.105036, PubMed ID: 36147953.

(658) Wang, V. Y., Rose, M. F., and Zoghbi, H. Y. (2005). Math1 expression redefines the rhombic lip derivatives and reveals novel lineages within the brainstem and cerebellum. *Neuron 48*, 31–43, DOI: 10.1016/j.neuron.2005.08.024, PubMed ID: 16202707.

(659) Wang, X., Liu, Z., Angelov, M., Feng, Z., Li, X., Li, A., Yang, Y., Gong, H., and Gao, Z. (2023). Excitatory nucleo-olivary pathway shapes cerebellar outputs for motor control. *Nature Neuroscience 26*, Number: 8 Publisher: Nature Publishing Group, 1394–1406, DOI: 10.1038/s41593-023-01387-4.

(660) Warnaar, P., Couto, J., Negrello, M., Junker, M., Smilgin, A., Ignashchenkova, A., Giugliano, M., Thier, P., and De Schutter, E. (2015). Duration of Purkinje cell complex spikes increases with their firing frequency. *Frontiers in Cellular Neuroscience 9*, https://www.frontiersin.org/articles/10.3389/fncel.2015.00122.

(661) Watanabe, M., and Kano, M. (2011). Climbing fiber synapse elimination in cerebellar Purkinje cells. *The European Journal of Neuroscience 34*, 1697–1710, DOI: 10.1111/j.1460-9568.2011.07894.x, PubMed ID: 22103426.

(662) Watson, T. C., Jones, M. W., and Apps, R. (2009). Electrophysiological Mapping of Novel Prefrontal – Cerebellar Pathways. *Frontiers in Integrative Neuroscience 3*, 18, DOI: 10.3389/neuro.07.018.2009, PubMed ID: 19738932.

(663) Weiler, N., Wood, L., Yu, J., Solla, S. A., and Shepherd, G. M. G. (2008). Top-down laminar organization of the excitatory network in motor cortex. *Nature neuroscience 11*, 360–366, DOI: 10.1038/nn2049, PubMed ID: 18246064.

(664) Whissell, P. D., Tohyama, S., and Martin, L. J. (2016). The Use of DREADDs to Deconstruct Behavior. *Frontiers in Genetics 7*, 70, DOI: 10.3389/fgene.2016.00070, PubMed ID: 27242888.

(665) White, J. J., and Sillitoe, R. V. (2017). Genetic silencing of olivocerebellar synapses causes dystonia-like behaviour in mice. *Nature Communications 8*, Number: 1 Publisher: Nature Publishing Group, 14912, DOI: 10.1038/ncomms14912.

(666) Widrow, B., Mantey, P., Griffiths, L., and Goode, B. (1967). Adaptive antenna systems. *Proceedings of the IEEE 55*, Conference Name: Proceedings of the IEEE, 2143–2159, DOI: 10.1109/PROC.1967.6092.

(667) Wiegert, J. S., Mahn, M., Prigge, M., Printz, Y., and Yizhar, O. (2017). Silencing Neurons: Tools, Applications, and Experimental Constraints. *Neuron 95*, 504–529, DOI: 10.1016/j.neuron.2017.06.050, PubMed ID: 28772120.

(668) Williams, D. R., and Litvan, I. (2013). Parkinsonian Syndromes. *Continuum : Lifelong Learning in Neurology 19*, 1189–1212, DOI: 10.1212/01.CON.0000436152.24038.e0, PubMed ID: 24092286.

(669) Wilson, M. A., and McNaughton, B. L. (1994). Reactivation of hippocampal ensemble memories during sleep. *Science (New York, N.Y.) 265*, 676–679, DOI: 10.1126/science.8036517, PubMed ID: 8036517.

(670) Wise, S. P. (1996). Corticospinal efferents of the supplementary sensorimotor area in relation to the primary motor area. *Advances in Neurology 70*, 57–69, PubMed ID: 8615231.

(671) Witter, L., Rudolph, S., Pressler, R. T., Lahlaf, S. I., and Regehr, W. G. (2016). Purkinje Cell Collaterals Enable Output Signals from the Cerebellar Cortex to Feed Back to Purkinje Cells and Interneurons. *Neuron 91*, 312–319, DOI: 10.1016/j.neuron.2016.05.037, PubMed ID: 27346533.

(672) Wöhr, M., Borta, A., and Schwarting, R. K. W. (2005). Overt behavior and ultrasonic vocalization in a fear conditioning paradigm: a dose-response study in the rat. *Neurobiology of Learning and Memory 84*, 228–240, DOI: 10.1016/j.nlm.2005.07.004, PubMed ID: 16115784.

(673) Wolpert, D. M., and Miall, R. C. (1996). Forward Models for Physiological Motor Control. *Neural Networks: The Official Journal of the International Neural Network Society 9*, 1265–1279, DOI: 10.1016/s0893-6080(96)00035-4, PubMed ID: 12662535.

(674) Woolsey, C. N. (1963). COMPARATIVE STUDIES ON LOCALIZATION IN PRECENTRAL AND SUPPLEMENTARY MOTOR AREAS. *International Journal of Neurology 4*, 13–20, PubMed ID: 14253338.

(675) Woolsey, C. N., Settlage, P. H., Meyer, D. R., Sencer, W., Pinto Hamuy, T., and Travis, A. M. (1952). Patterns of localization in precentral and "supplementary" motor areas and their relation to the concept of a premotor area. *Research Publications - Association for Research in Nervous and Mental Disease 30*, 238–264, PubMed ID: 12983675.

(676) Xiao, L., Bornmann, C., Hatstatt-Burklé, L., and Scheiffele, P. (2018). Regulation of striatal cells and goal-directed behavior by cerebellar outputs. *Nature Communications 9*, 3133, DOI: 10.1038/s41467-018-05565-y, PubMed ID: 30087345.

(677) Xu, W., De Carvalho, F., Clarke, A., and Jackson, A. (2021). Communication from the cerebellum to the neocortex during sleep spindles. *Progress in Neurobiology 199*, 101940, DOI: 10.1016/j.pneurobio.2020.101940, PubMed ID: 33161064.

(678) Xu, W., de Carvalho, F., and Jackson, A. (2019). Sequential Neural Activity in Primary Motor Cortex during Sleep. *The Journal of Neuroscience: The Official Journal of the Society for Neuroscience 39*, 3698–3712, DOI: 10.1523/JNEUROSCI.1408-18.2019, PubMed ID: 30842250.

(679) Xu, W., De Carvalho, F., and Jackson, A. (2022). Conserved Population Dynamics in the Cerebro-Cerebellar System between Waking and Sleep. *The Journal of Neuroscience: The Official Journal of the Society for Neuroscience 42*, 9415–9425, DOI: 10.1523/JNEUROSCI.0807-22.2022, PubMed ID: 36384678.

(680) Yakovlev, P. I. (1948). Motility, behavior and the brain; stereodynamic organization and neural coordinates of behavior. *The Journal of Nervous and Mental Disease 107*, 313–335, DOI: 10.1097/00005053-194810740-00001, PubMed ID: 18913439.

(681) Yamamoto, K., Kawato, M., Kotosaka, S., and Kitazawa, S. (2007). Encoding of movement dynamics by Purkinje cell simple spike activity during fast arm movements under resistive and assistive force fields. *Journal of Neurophysiology 97*, 1588–1599, DOI: 10.1152/jn.00206.2006, PubMed ID: 17079350.

(682) Yan, Z., and Surmeier, D. J. (1997). D5 dopamine receptors enhance Zn2+-sensitive GABA(A) currents in striatal cholinergic interneurons through a PKA/PP1 cascade. *Neuron 19*, 1115–1126, DOI: 10.1016/s0896-6273(00)80402-x, PubMed ID: 9390524.

(683) Yang, Y., and Lisberger, S. G. (2017). Modulation of Complex-Spike Duration and Probability during Cerebellar Motor Learning in Visually Guided Smooth-Pursuit Eye Movements of Monkeys. *eNeuro 4*, ENEURO.0115–17.2017, DOI: 10.1523/ENEURO.0115-17.2017, PubMed ID: 28698888.

(684) Yoshida, S., Nambu, A., and Jinnai, K. (1993). The distribution of the globus pallidus neurons with input from various cortical areas in the monkeys. *Brain Research 611*, 170–174, DOI: 10.1016/0006-8993(93)91791-p, PubMed ID: 8518946.

(685) Yu, B. M. (2016). Fault tolerance in the brain. *Nature 532*, Number: 7600 Publisher: Nature Publishing Group, 449–450, DOI: 10.1038/nature17886.

(686) Zadey, S., Buss, S. S., McDonald, K., Press, D. Z., Pascual-Leone, A., and Fried, P. J. (2021). Higher motor cortical excitability linked to greater cognitive dysfunction in Alzheimer's disease: results from two independent cohorts. *Neurobiology of Aging 108*, 24–33, DOI: 10.1016/j.neurobiolaging.2021.06.007.

(687) Zadro, I., Brinar, V. V., Barun, B., Ozretić, D., and Habek, M. (2008). Cervical dystonia due to cerebellar stroke. *Movement Disorders: Official Journal of the Movement Disorder Society 23*, 919–920, DOI: 10.1002/mds.21981, PubMed ID: 18361471.

(688) Zaki, Y., Mau, W., Cincotta, C., Monasterio, A., Odom, E., Doucette, E., Grella, S. L., Merfeld, E., Shpokayte, M., and Ramirez, S. (2022). Hippocampus and amygdala fear memory engrams re-emerge after contextual fear relapse. *Neuropsychopharmacology: Official Publication of the American College of Neuropsychopharmacology 47*, 1992–2001, DOI: 10.1038/s41386-022-01407-0, PubMed ID: 35941286.

(689) Zervas, N. T., Horner, F. A., and Pickren, K. S. (1967). The treatment of dyskinesia by stereotxic dentatectomy. *Confinia Neurologica 29*, 93–100, DOI: 10.1159/000103685, PubMed ID: 4968478.

(690) Zhang, C., Yang, S., Flossmann, T., Gao, S., Witte, O. W., Nagel, G., Holthoff, K., and Kirmse, K. (2019). Optimized photo-stimulation of halorhodopsin for long-term neuronal inhibition. *BMC biology 17*, Number: 1, 95, DOI: 10.1186/s12915-019-0717-6, PubMed ID: 31775747.

(691) Zhang, L., and Goldman, J. E. (1996). Generation of cerebellar interneurons from dividing progenitors in white matter. *Neuron 16*, 47–54, DOI: 10.1016/s0896-6273(00)80022-7, PubMed ID: 8562089.

(692) Zhang, W., and Linden, D. J. (2003). The other side of the engram: experience-driven changes in neuronal intrinsic excitability. *Nature Reviews. Neuroscience 4*, 885–900, DOI: 10.1038/nrn1248, PubMed ID: 14595400.

(693) Zhang, W., Shin, J. H., and Linden, D. J. (2004). Persistent changes in the intrinsic excitability of rat deep cerebellar nuclear neurones induced by EPSP or IPSP bursts. *The Journal of Physiology 561*, 703–719, DOI: 10.1113/jphysiol.2004.071696, PubMed ID: 15498810.

(694) Zheng, N., and Raman, I. M. (2010). Synaptic inhibition, excitation, and plasticity in neurons of the cerebellar nuclei. *Cerebellum (London, England) 9*, 56–66, DOI: 10.1007/s12311-009-0140-6, PubMed ID: 19847585.

(695) Zhu, J., Hasanbegović, H., Liu, L. D., Gao, Z., and Li, N. (2023). Activity map of a cortico-cerebellar loop underlying motor planning. *Nature Neuroscience*, Publisher: Nature Publishing Group, 1–13, DOI: 10.1038/s41593-023-01453-x.

(696) Zhuang, X., Belluscio, L., and Hen, R. (2000). GOLF Mediates Dopamine D1 Receptor Signaling. *The Journal of Neuroscience 20*, RC91, DOI: 10.1523/JNEUROSCI.20-16-j0001.2000, PubMed ID: 10924528.

(697) Ziegan, J., Wittstock, M., Westenberger, A., Dobričić, V., Wolters, A., Benecke, R., Klein, C., and Kamm, C. (2014). Novel GNAL mutations in two German patients with sporadic dystonia. *Movement Disorders: Official Journal of the Movement Disorder Society 29*, 1833–1834, DOI: 10.1002/mds.26066, PubMed ID: 25382112.

(698) Zito, G. A., Tarrano, C., Jegatheesan, P., Ekmen, A., Béranger, B., Rebsamen, M., Hubsch, C., Sangla, S., Bonnet, C., Delorme, C., Méneret, A., Degos, B., Bouquet, F., Brissard, M. A., Vidailhet, M., Gallea, C., Roze, E., and Worbe, Y. (2022). Somatotopy of cervical dystonia in motor-cerebellar networks: Evidence from resting state fMRI. *Parkinsonism & Related Disorders 94*, 30–36, DOI: 10.1016/j.parkreldis.2021.11.034.

Voies de communications parallèles cérébello-cérébrales et leur implication dans l'apprentissage implicite

Résumé :
Le cervelet est surtout connu pour être une structure clé dans la régulation des mouvements. Cependant, son haut degré d'interconnexion avec diverses structures corticales et sous-corticales soulève la question de son implication dans la régulation d'autres fonctions cérébrales, telles que les processus cognitifs. En particulier, les liens étroits entre le cervelet, les circuits moteurs et les circuits limbiques suggèrent une contribution du cervelet à l'apprentissage moteur et émotionnel.

En utilisant des traçage anatomiques, de l'électrophysiologie extracellulaire et du comportement, l'objectif de cette thèse est d'élucider l'implication du cervelet dans l'extinction de la mémoire de peur à travers le contrôle de la synchronisation thalamo-corticale des oscillations liées à la peur. Ensuite, cette thèse étudiera les contributions différentielles des réseaux cérébello-corticaux et cérébello-striataux à l'acquisition et à la consolidation d'une habileté motrice complexe. Enfin, elle se concentrera sur l'intégrité des réseaux cérébello-thalamiques et la fonctionnalité de la plasticité cérébello-thalamique dans un modèle murin de DYT25, une forme génétique de dystonie.

Parallel cerebello-cerebral pathways and their involvement in implicit learning

Abstract :

The cerebellum is mostly known to be a key structure in the regulation of movements. However, its high degree of inter-connectivity with various cortical and subcortical structures brings the question of its involvement in regulating other brain functions, such as cognitive processes. In particular, the tight links between the cerebellum, the motor circuits and the limbic circuits suggest a contribution of the cerebellum to both motor learning and emotional learning.

Using anatomical tracing, extracellular electrophysiology and behavior, the aim of this thesis is to unravel the involvement of the cerebellum in the extinction of fear memory through the control of thalamo-cortical synchrony of fear-related oscillations. Then, this thesis will investigate the differential contributions of cerebello-cortical and cerebello-striatal networks to the acquisition and the consolidation of a complex motor skill. Ultimately, it will focus on the integrity of cerebello-thalamic networks and the functionality of cerebello-thalamic plasticity in a mouse model of DYT25, a genetic form of dystonia.